GCAP SERVICES FOR THE CALFED BAY-DELTA PROGRAM/CALIFORNIA BAY-DELTA AUTHORITY (CBDA)
SACRAMENTO, CA
ERP-02D-P50

San Joaquin River Dissolved Oxygen Depletion Modeling

TASK 4 FINAL REPORT

3D San Joaquin River Water Quality Calibration 2000-2001

May 2006
GCAP0010

HydroQual
Environmental Engineers & Scientists

CONTENTS

FIGURES

Figure | Page

Follows Section 4

TABLES

SECTION 1

BACKGROUND

Dissolved oxygen (DO) concentrations in the San Joaquin River (SJR) Deep Water Ship Channel (DWSC) fall below the applicable water quality objective, which is 5 milligrams per liter (mg/L) December to August and 6 mg/L from September through November to protect migrating fall-run Chinook salmon. These low observed DO concentrations are believed to result from a combination of the City of Stockton Regional Wastewater Control Facility (RWCF) discharges; the upstream SJR load of algae and other oxygen-consuming organic materials (OCOM) such as biochemical oxygen demand (BOD), volatile suspended solids (VSS) and ammonia; a decrease in the SJR flow due to upstream diversions; and dredging of the Deep Water Ship Channel (DWSC). Formulating an efficient and cost-effective adaptive management strategy for the above water quality and SJR fish protection objective will require reliable models that can identify the major causes for the low DO episodes and evaluate potential management solutions.

The low DO problem area is generally identified as a 10-mile reach of the SJR in the DWSC downstream of Stockton. DO data in the SJR at Mossdale and Stockton highlight the DO problem in the DWSC with DO levels during March and July through October well below the water quality objectives at times. The effect of upstream algal growth can be inferred from the super-saturated DO levels observed at the Mossdale station that may indicate a high loading of algae. Concentrations measured at Vernalis or Mossdale indicate that a major fraction of the algae and oxygen-demanding load entering the DWSC may originate from the tributary and drainage sources upstream of Vernalis. Mossdale is just upstream of the Head of Old River (HOR), which is a major diversion from the SJR and the point where an operable tidal gate is expected to be constructed by the CBDA as part of the South Delta Improvement Plan. An adaptive management strategy that would balance the benefits of increased flow at the HOR against the DO impacts associated with increased river loading of organic materials into the DWSC is needed. The watershed sources of nutrients, algae and other organic materials (e.g., detritus, riparian vegetation) can be transported downstream by the SJR flow, but may also be diverted, settled or decayed within the river corridor. Each of these provides a pathway for increased oxygen demand in the DWSC. Nutrients may also be converted into algae and thereby increase the river load of organic materials that enter the DWSC and contribute to DO depletion.

HydroQual has conducted three-dimensional (3D) hydrodynamic and water quality modeling for the tidal SJR including the DWSC that will provide a scientifically defensible framework necessary to develop load allocations as part of the DO TMDL for the DWSC portion of the SJR. The 3D model extends from Vernalis at the upstream boundary to the downstream boundary near Jersey Point. The 3D DWSC model calibration period has been selected as the years 2000 and 2001

because data collected during this period in the DWSC as well as in the upstream SJR provide needed measurements for calibration to nutrients, algae, carbon, solids and dissolved oxygen measurements. Available data during this period also provide surface and bottom measurements during the summer and fall. These types of data will be used to verify processes affecting DO in the DWSC study area. In addition Figure 1 indicates that the 2000 to 2001 period encompasses a low flow period in the late summer and fall of 2001 so that a critical DO period is modeled.

As part of the development of the 3D DWSC water quality model, water quality simulations of the upstream SJR from Stevinson to Vernalis were conducted using the 1D DSM2 upper San Joaquin River Model developed by the California Department of Water Resources (DWR) for the same 2000-2001 period. The purpose for modeling the upper SJR was twofold: 1) to generate upper boundary loadings to the 3D DWSC model and 2) to develop a water quality model for the USJR where no model existed. The Delta Simulation Model Version 2 (DSM2-SJR) water quality model is able to reproduce observed chlorophyll-a, nutrient, BOD, DO, conductivity and temperature behavior in the 75 mile stretch of the upper SJR between Stevinson and Vernalis based on proper assignment of seasonal or summer conditions that include temperature, light, flow, loads and kinetic rates (HydroQual, 2005). However, this initial calibration showed that additional data (water quality and flow) for the various agricultural drains, groundwater, and inflows are needed to improve the calibration. It is for this reason that the 3D model upper boundary at Vernalis will be determined by the extensive set of data at Vernalis rather than 1D model outputs.

1.1 PURPOSE

This water quality modeling project was undertaken to provide a scientifically defensible framework necessary to develop load allocations as part of the DO TMDL for the DWSC portion of the SJR. The overall purpose of the project recognizes four major management areas: (1) control of watershed nonpoint nutrient sources; (2) control of wastewater point sources; (3) flow management into the DWSC (HOR tidal gate); and, (4) aeration of the DWSC during periods of low DO concentrations or high SJR algal loading. The selected hydrodynamic/water quality modeling framework is especially suited to provide quantitative information for the adaptive management implementation strategy to reduce the DO depletion that is observed in the DWSC.

The water quality model, consisting of an eutrophication model with a coupled sediment flux sub-model is capable of analyzing vertical and intra-tidal fluctuations of DO in the DWSC. In addition, the coupled sediment flux sub-model provides the ability to assess the impact of the SJR loading of algae and organic matter and the subsequent effect on sediment oxygen demand (SOD), sediment nutrient fluxes and water column DO levels. The 3D water quality model will allow the detailed effects of the DWSC geometry on the tidal flow and mixing patterns to be accurately simulated. The water quality processes that depend on the channel depth and flow velocity, such as the vertical settling and bottom resuspension of particulates, the vertical temperature stratification and reduced mixing during the day, and light-limited growth of algae, are simulated.

This report provides overviews of the hydrodynamic and water quality model frameworks. The modeling effort described in this report incorporates sources, such as upstream boundary inflows and the Stockton RWCF, and quantifies river water quality mechanisms operating in the DWSC. The report summarizes hydrodynamic and water quality model calibrations in the SJR DWSC for the 2000-2001 calibration period.

1.2 MODEL STUDY AREA

The general study area encompasses the upper SJR from Vernalis through its entrance into the DWSC and extends to Jersey Point. While this model area appears to extend far beyond the immediate DWSC where the DO levels are exceeding limits, important modeling issues were considered in selecting this study area. The selection of the downstream boundary location was done to eliminate effects from internal sources such as the Stockton RWCF, or the upstream or downstream boundaries. As one can imagine, this becomes important when the calibrated model is used for projections to determine impacts from internal sources under new loading conditions. The upstream boundary condition at Vernalis was selected because this location represents a location in the river where tidal influence is negligible. In this way the tidal modeling is within one framework (the DWSC model) and the nontidal upstream model in a separate framework (DSM2-SJR). This avoids the complication of adding in a downstream tidal boundary to the upstream DSM2-SJR model.

SECTION 2

THE HYDRODYNAMIC AND WATER QUALITY MODELS

2.1 SUMMARY OF MODELING

The SJR 3D DWSC model consists of two major components: the hydrodynamic model and the water quality model. In general, the hydrodynamic model computes the circulation of water due to tides, density variation, wind and freshwater flow. An important feature of the hydrodynamic model is the computation of transport and mixing processes within the tidal cycle. The water quality model represents the physical, chemical and biological processes that occur in the water and is directly coupled with the hydrodynamic model. The water quality model can calculate the effect of point and nonpoint source inputs on water quality parameters, such as dissolved oxygen, phytoplankton and nutrient levels. In addition, the water quality model includes a sediment component, which calculates sediment effects such as nutrient fluxes and oxygen demand on the water column resulting from carbon settling and decay.

The coupled hydrodynamic and water quality models were developed as a tool to simulate complex circulation and mixing, and effects of inputs and processes in the system that effect DO levels in the DWSC. The model is able to compute SJR flows influenced by both tides and upstream freshwater inflow. Specifically, the model is able to simulate varying tidal and geometry related impacts on flow in the DWSC in and outside of the Turning Basin as well as upstream of the SJR confluence with the DWSC. The model is able to compute phytoplankton (represented by chlorophyll-a), nutrient, and dissolved oxygen levels influenced by instream mechanisms as well upstream loadings. It will be shown that the model is capable of calculating dissolved oxygen levels based on seasonal instream algal growth patterns as well as seasonal upstream carbon and nutrient loadings. The study area extends from the upper SJR at Vernalis to Jersey Point and is shown in Figure 2.

2.1.1 Hydrodynamic Model

The hydrodynamic model used in this study is HydroQual's three-dimensional, time-dependent, estuarine and coastal circulation model, ECOMSED model developed by Blumberg and Mellor (1987). This model has been extensively used by over 1000 research groups around the world for simulations of various hydrodynamic systems; among them are works by Blumberg et al. (2004) on the Hudson estuary, Blumberg and Kim (2001) on St. Andrew Bay, Blumberg et al. (1999) on the New York Harbor, Ahsan and Blumberg (1999) on Onondaga Lake, NY, Mellor and Ezer (1991) on the Gulf Stream Region, Blumberg and Goodrich (1990) on Chesapeake Bay, Blumberg and Mellor (1985) on the Gulf of Mexico. In all these studies, model skill was assessed via extensive comparisons with data involving water surface elevations, currents, temperature, salinity, and pathogens. A confidence has been established that the predominant physics are realistically

reproduced by the model. The model has also been applied in an operational forecasting mode for the Great Lakes, the Gulf of Mexico, on the East Coast of the United States and in Norwegian coastal waters. An overview of ECOMSED framework is presented in Section 2.2 along with the SJR DWSC calibration. A more detailed discussion of the hydrodynamic model theory is presented in HydroQual's ECOMSED manual (HydroQual, 2004).

2.1.2 Water Quality Model

The water quality model used in the study is a state-of-the-art eutrophication model that includes a sediment submodel. The eutrophication modeling framework employed for the DWSC SJR system was developed during the Long Island Sound (HydroQual, Inc., 1991) and Chesapeake Bay (HydroQual, Inc., 1987, 1989) modeling studies. Since the 3D DWSC SJR water quality model is directly coupled with the hydrodynamic model, computation of water quality parameters also occurs within the tidal cycle. The coupled water quality/hydrodynamic model has been successfully applied in numerous studies, including those of the Hudson-Raritan Estuary (NY/NJ), Long Island Sound (NY/CT), Chesapeake Bay (MD/DE), Massachusetts Bay and Boston Harbor (MA), Jamaica Bay (NY), Tar-Pamlico Estuary (NC), and the Upper Mississippi River (MN). Discussions of the water quality model theory and the SJR DWSC calibration are presented in Sections 2.3 and 2.4, respectively. Appendix A contains a detailed discussion of the integrated eutrophication and sediment flux model.

2.2 HYDRODYNAMIC (ECOMSED) MODEL FRAMEWORK AND CALIBRATION

The transport and mixing of water quality constituents introduced to the downstream portion of the San Joaquin River (SJR) are controlled by estuarine circulation. At the same time, turbulent mixing created by tides, freshwater inflow and surface wind stress leads to horizontal and vertical dispersion in the water body. Coupled with turbulent mixing are heat exchange processes between the water column and the atmosphere. All of these mechanisms contained in the hydrodynamic model and coupled with an associated water quality model determine the distribution of water quality constituents throughout the study area.

The complexity of the physical processes governing the evolution of an introduced constituent, such as dissolved oxygen (DO) or pathogens, suggests the use of sophisticated hydrodynamic models. ECOMSED was applied to compute current, temperature and conservative tracer distributions in this portion of the San Joaquin River between Jersey Island and Vernalis.

2.2.1 Hydrodynamic Theory

The ECOMSED model incorporates the Mellor and Yamada (1982) level 2-1/2 turbulent closure model to provide a realistic representation of vertical mixing. A system of curvilinear coordinates is used in the horizontal direction, which allows for a smooth and accurate representation of variable shoreline geometry. In the vertical scale, the model uses a transformed

coordinate system known as the σ-coordinate transformation to permit better representation of bottom topography. Water surface elevation, three-dimensional water velocity, temperature, conservative tracer and water turbulence are calculated in response to weather conditions (wind and incident solar radiation), freshwater inflows, and tides and temperature at the open boundaries near Jersey Island. A more detailed discussion of ECOMSED framework is presented in the HydroQual's ECOMSED manual (HydroQual, 2004).

The model solves a coupled system of differential, prognostic equations describing the conservation of mass, momentum, temperature, salinity, turbulence energy and turbulence macroscale. The governing equations for velocity U_i = (u,v,w), temperature (T), salinity (S), and coordinate x_i = (x,y,z) are as follows:

$$\frac{\partial U_i}{\partial x_i} = 0 \tag{1}$$

$$\frac{\partial}{\partial t}(u,v)+\frac{\partial}{\partial x_i}\left[U_i(u,v)+f(-v,u)\right] = -\frac{1}{\rho_o}\left[\frac{\partial P}{\partial x},\frac{\partial P}{\partial y}\right]+\frac{\partial}{\partial z}\left[K_M\frac{\partial}{\partial z}(u,v)\right]+\left(F_u,F_v\right) \tag{2}$$

$$\frac{\partial T}{\partial t}+\frac{\partial}{\partial x_i}\left(U_i T\right) = \frac{\partial}{\partial z}\left[K_H\frac{\partial T}{\partial z}\right]+F_T \tag{3}$$

$$\frac{\partial S}{\partial t}+\frac{\partial}{\partial x_i}\left(U_i S\right) = \frac{\partial}{\partial z}\left[K_H\frac{\partial S}{\partial z}\right]+F_S \tag{4}$$

The horizontal diffusion terms, (F_u, F_v), F_T and F_S, in Equations 2 through 4 are calculated using a Smagorinsky (1963) horizontal diffusion formulation (Mellor and Blumberg, 1985). The hydrostatic approximation yields:

$$\frac{P}{\rho_o} = g(\eta - z)+\int_z^\eta g\frac{\rho-\rho_o}{\rho_o}dz' \tag{5}$$

where P is pressure, z is water depth, η(x,y) is the free surface elevation, ρ_o is a reference density, and ρ = ρ(T,S) is the density.

The vertical mixing coefficients, K_M and K_H, in Equations 2 through 4 are obtained by appealing to a $2^1/_2$ order turbulence closure scheme and are given by:

$$K_M = \hat{K}_M + \upsilon_M,\ K_H = \hat{K}_H + \upsilon_H \tag{6}$$

$$\hat{K}_M = q\ell S_M,\ \hat{K}_H = q\ell S_H \tag{7}$$

where $q^2/2$ is the turbulent kinetic energy, l is a turbulence length scale, S_M and S_H are stability functions defined by solutions to algebraic equations given by Mellor and Yamada (1982) as modified by Galperin et al. (1988), and υ_M and υ_H are constants. The variables q^2 and l are determined from the following equations:

$$\frac{\partial q^2}{\partial t} + \frac{\partial u q^2}{\partial x} + \frac{\partial v q^2}{\partial y} + \frac{\partial w q^2}{\partial z} = \frac{\partial}{\partial z}\left[K_q \frac{\partial q^2}{\partial z}\right] + 2K_M\left[\left(\frac{\partial u}{\partial z}\right)^2 + \left(\frac{\partial v}{\partial z}\right)^2\right] + \frac{2g}{\rho_o} K_H \frac{\partial \rho}{\partial z} - 2\frac{q^3}{B_1 \ell} + F_q \tag{8}$$

$$\frac{\partial q^2 \ell}{\partial t} + \frac{\partial u q^2 \ell}{\partial x} + \frac{\partial v q^2 \ell}{\partial y} + \frac{\partial w q^2 \ell}{\partial z} = \frac{\partial}{\partial z}\left[K_q \frac{\partial q^2 \ell}{\partial z}\right] + E_1 \ell\left\{K_M\left[\left(\frac{\partial u}{\partial z}\right)^2 + \left(\frac{\partial v}{\partial z}\right)^2\right] + \frac{g}{\rho_o} K_H \frac{\partial \rho}{\partial z}\right\} - 2\frac{q^3}{B_1 \ell} + F_\ell \tag{9}$$

where $K_q = 0.2ql$, the eddy diffusion coefficient for turbulent kinetic energy; F_q and F_l represent horizontal diffusion of the turbulent kinetic energy and turbulence length scale, and are parameterized in a manner analogous to either Equation 6 or 7; w is a wall proximity function defined as $w = 1 + E_2 (l/\kappa L)^2$, $(L)^{-1} = (\eta - z)^{-1} + (H + z)^{-1}$, κ is the von Karman constant, H is the water depth, η is the free surface elevation, and E_1, E_2 and B_1 are empirical constants set in the closure model.

The basic Equations 1 through 9 are transformed into a terrain following a σ-coordinate system in the vertical scale and an orthogonal curvilinear coordinate system in the horizontal scale. The resulting equations are vertically integrated to extract barotropic variable i.e., variables that are only a function of the x,y directions and independent of the z-direction, such as water elevation. A mode splitting technique is introduced such that the fast-moving, external (barotropic) mode and significantly slower internal (baroclinic) mode are calculated by prognostic equations with different time steps. Detailed solution techniques are described in Blumberg and Mellor (1987).

2.2.2 Model Configuration

The hydrodynamic model is developed to assess management options for improving the DWSC DO level. After obtaining the high-resolution shoreline data downstream of Stockton from the National Geophysical Data Center (NGDC), and the bathymetry data and the shoreline data between Stockton and Vernalis from California Department of Water Resources (DWR), we have designed an orthogonal, curvilinear modeling grid system, which encompasses the SJR from Vernalis to Blind Point on Jersey Island and discretizes the entire model domain including the SJR DWSC near Stockton (Figure 2). The model system consists of 168 × 15 grid cells in the horizontal plane and 11 equally spaced σ-levels in the vertical plane (i.e., 10 vertical segments). In the transformed σ-coordinate system, the model has an equal number of vertical segments in all the computational grid boxes. It should be noted that the curvilinear grid system would allow us to resolve the DWSC, the complex shoreline features and a number of sloughs/tributaries entering the SJR in the model domain, and, therefore, allows the design of an efficient and computationally time-effective modeling framework.

The bathymetry dataset and a data extraction scheme from HydroQual's grid generator were used to generate the SJR model depths. To evaluate the quality of this dataset and to verify the data extraction method, we selected four vertical sections at River Mile 33.0, 37.8, 38.5 and 40.6. These model cross-sectional areas were compared with the measured cross sections shown in Jones and Stokes' (2002). The average difference on the cross sections is only 220 ft^2, which is within 1% of the measured cross sectional areas.

2.2.3 Model Forcing Functions

Different types of input are needed to drive the model. Using the CA DWR DSM2-hydro, a one-dimensional hydrodynamic flow and salinity model, both DSM2 output and measured data were employed to develop the ECOMSED's forcing functions.

The hourly stage output from DSM2 (Segment 49) was applied at the downstream open boundary near Jersey Island as input to ECOMSED (Figure 2). In addition to the water surface elevation boundary conditions, the model open boundary was forced with measured daily temperature at Antioch.

The model is also driven by freshwater flow and temperature during the simulation periods. The river flows at 15 DSM2 segments, corresponding to the SJR flow at Vernalis and other 14 sloughs/tributaries, were obtained from the DSM2 simulations. The hourly DSM2 output was specified as input flows to ECOMSED. Measured daily temperatures at Vernalis, Mossdale, R&R Island and Antioch were assigned at the ECOMSED's river boundary locations since DSM2 temperature output was not available for the current simulation periods. For the specification of freshwater inflows, WWTP inputs are also accounted for in the hydrodynamic model with discharge

and temperature from the Stockton Regional Wastewater Control Facility (RWCF). Table 1 lists the boundary locations and DSM2 corresponding channels.

Table 1. Boundary Locations and DSM2 Channels

San Joaquin River Boundary	DSM2 Channel
SJR at Vernalis	17
Old River	54
Fourteenmile Slough	312
Turner Cut	172
Disappointment Slough	314
Columbia Cut	160
Little Connection Slough	319
Middle River	161
Potato Slough	328
Old River (Franks Tract)	124
Mokelumne River	349
Fishermans Cut	280
Thirteenmile Slough	310
False River	279
Paradise Cut	195
Downstream Boundary near Jersey Pt	49

Finally, the hydrodynamic model requires the input of wind speed and direction, air temperature, relative humidity, atmospheric pressure and solar radiation. The hourly data have included all the atmospheric parameters necessary for the simulations and were obtained from the meteorological station located at the Stockton Metropolitan Airport.

2.2.4 Model Calibration and Validation

The model calibration period was selected as October 1996. Using the DSM2 stage and flow output, ECOMSED simulations have been conducted. The ability of the hydrodynamic model to simulate advective and dispersive processes in the SJR was assessed by comparing the ECOMSED computed water surface elevations and volume fluxes against those by DSM2 at eight selected transects along the San Joaquin River (SJR) from Brandt Bridge to San Andreas Point (Figures 3 and 4). Figures 3 and 4 demonstrate reasonable agreement between the ECOMSED and the DSM2. However, at the Turning Basin, the ECOMSED shows that the range of volume flux variations through the cross section is about ± 30 m^3/s and the DSM2 gives a much smaller flux variation of about ± 10 m^3/s. With flows ranging from about 54 to 100 m^3/s at Vernalis and the stages from –0.6 to 1.2 m at Antioch, the computed flow velocity can reach to 2.5 m/s upstream of Stockton.

To evaluate the boundary impact on the Stockton RWCF discharge into the SJR, a tracer simulation has been set up for this calibration period. With an average flow rate of about 76 m^3/s at Vernalis and an effluent rate of 1.4 m^3/s from RWCF, it was found that the tracer concentration

near Turner Cut is about 2 % of and near Burns Reach less than 0.5 % of the initial concentration when tracer was released at RWCF.

2000-2001 was chosen as the validation period for ECOMSED. The survey data collected and the DSM2 output during this period were then used to verify the ECOMSED results. Water level calibration/validation demonstrated that the model bathymetry, geometry and hydraulics are properly configured and that the model dynamic processes are simulated correctly. For the validation period, computed water surface elevations were compared against the measurements and the DSM2 results at Vernalis (RSAN112), Mossdale (RSAN087), RWCF (RSAN063), DWSC near R5 (RSAN058), Fourteenmile Slough (RSAN052), Little Connection Slough (RSAN043), San Andreas Point (RSAN032), Threemile Slough (SLTRM004) and Jersey Island (RSAN018). Figure 5 presents these plots for July, August and September at the DWSC (RSAN058) for 2000 (5A) and 2001 (5B). All of the remaining comparisons are included in Appendix B. Based on those hourly model outputs and measurements, no tidal signals were detected near Vernalis. Both models properly reproduce the observed tidal signals from the upstream gage at Mossdale to the downstream gages on the SJR and the ECOMSED output matches the data and the DSM2 output well at those locations.

For the 2000-2001 validation period, 15-minute volume flux measurements were available at three locations. The first one is very close to Vernalis (RSAN112), the upstream inflow boundary of ECOMSED, the second is near the RWCF, Stockton (RSAN063) and the third is near our downstream open boundary (RSAN018). Figure 6 shows the daily averages of the observed, the DSM2 and the ECOMSED computed fluxes through those transects. Since the DSM2 output is employed as the input for ECOMSED, the latter matched the former better than the observations. During low flow summer months this difference could influence model calibrations. Therefore, an additional 15 cms was diverted to the Old River in June, July and August 2000 so that ECOMSED results were in good agreement with observations in the SJR near the Stockton RWCF. Though flow data is missing at Vernalis and near the RWCF in July and August of 2001, this same 15 cms adjustment was made for the same 3 month period so that ECOMSED and DSM2 results were in better agreement.

The model predicts temperature in response to the boundary and the meteorological conditions applied to the model as forcing functions. Daily average, maximum and minimum temperatures were available at Vernalis and hourly data at Mossdale, R&R Island (RSAN058) and Antioch (RSAN007) for the validation period. Time series of computed temperature were compared against the observed temperature at these four locations (Figure 7). As seen in Figure 7, the model captures the daily and seasonal temperature variations well, although these measurements have fairly large spatial and temporal extent covering the entire model domain over the 2-year simulation period. Generally, there is a good agreement between the model and observed temperature in the SJR. However, ECOMSED consistently underestimates the temperature by 2 to 3 ºC around the

DWSC at R&R Island location during the winter months. A number of sensitivity runs were conducted to understand the model-data discrepancies. A preliminary consideration would be given to incorporating the heat exchange between water and sediment into ECOMSED to improve the model performance. It should be noted that the summer period is the critical period for water quality simulations so that this winter temperature discrepancy would not effect summer water quality computations.

2.2.5 Simulated SJR Velocities

Tidally average velocities were computed based on simulated velocities at several locations in the SJR for years 2000 and 2001 and are listed in Table 2. SJR velocities at R3 show that velocities decrease upon entering the DWSC due to greater depth and width. Simulated velocity profiles at three locations (Turning Basin, R3 near Light 48, downstream of R5) in the SJR DWSC are shown in Figures 8, 9, and 10 for August and September of 2000 and show that not only does velocity vary longitudinally but there is a depth variability as well.. The tidally influenced velocities are given at depths of 0.1m, 2m, 4m, 8m and 10.5m depths. Lower bottom velocities are typical and are likely due to bottom shear stresses. Positive values represent flow in the upstream direction. Velocities at R5 range from maximums of 0.35 m/s at the surface to 0.10 m/sec at the bottom. At R3 velocities are approximately half of those at R5 with surface and bottom maximums of 0.2 m/s and 0.05 m/s respectively. In the Turning Basin flows are even further decreased with surface and bottom maximums of 0.075 ms/ and 0.015 m/s respectively. The fairly slow moving water upon entering the DWSC and downstream of R5 will allow for decreased travel times effecting water quality processes to have a greater impact on the river. These impacts will be further addressed in the remainder of the report.

Table 2. San Joaquin River Tidally Averaged Velocity (m/s), 2000 and 2001

Location	2000	2001
Vernalis	0.34	0.25
Downstream of Old River	0.35	0.26
R3	0.08	0.07
Turning Basin	0.01	0.01
Rough & Read Island Dock	0.07	0.07
R5	0.14	0.13
Turner Cut	0.10	0.10
Downstream Boundary	0.36	0.36

2.3 WATER QUALITY MODEL FRAMEWORK

The SJR DWSC eutrophication model includes the modeling of one phytoplankton group (summer assemblage), salinity, dissolved oxygen, total suspended solids and the various organic and inorganic forms of nitrogen, phosphorus, and carbon. Modeling of the exchanges of nutrients and oxygen between the water column and sediment was accomplished through the sediment flux submodel to compute nutrient fluxes and sediment oxygen demand. The diagrams presented in Figures 11 and 12 show the various kinetic pathways involved in the eutrophication and sediment modeling frameworks. A brief description of the 26 eutrophication and 14 sediment submodels state variables and their various kinetic pathways and important calibration constants appears below. Additional calibration constants are presented along with a detailed discussion of kinetics in Appendix A. The remainder of this section contains a general description of the model framework employed in this study and model calibration.

2.3.1 Phytoplankton - Winter and Summer Functional Groups

The eutrophication model includes three algal groups, a winter, summer, and fall population, represented by algal carbon in the model framework. The basic kinetics affecting phytoplankton growth and death are identical for the three groups, with a distinction in the assigned growth kinetic constants for each group. Phytoplankton growth is dependent upon temperature, ambient light and nutrient levels, which modify the maximum growth rate to ambient conditions. The growth rates of the three algal groups are controlled through the use of temperature optimums that maximize growth at a certain temperature and decrease growth above and below this temperature. In this manner, growth of winter, summer, and fall algal groups can peak at different times of the year or within different temperature regimes. In the DWSC SJR study, only one phytoplankton group was used because the data indicate a peak chlorophyll-a growth in the summer months.

Ambient surface light conditions are input externally and decrease with depth as a function of light extinction coefficients. Light extinction is a function of chlorophyll-a levels and solids levels. Typically the model requires a base extinction rate representing extinction due to solids and computes extinction due to changing algal levels. As part of this calibration the model was modified to calculate base light extinction due to total suspended solids levels thereby providing the capability for internal computation of temporal and spatial base light extinction based on solids. The surface light conditions are based upon ambient measurements of solar radiation measured within the day. Algal growth is further decreased when the ambient nutrients (phosphorus, nitrogen and silica) approach their respective limiting concentration. The model computes nutrient limitation factors, for phosphorus and nitrogen with the minimum factor chosen to adjust the growth rate. The silica system was not used in this calibration. The ambient growth rate, which is adjusted for temperature, light and nutrient limitations, is then used to determine the oxygen produced through photosynthesis during growth.

The model computes loss of biomass from the water column through respiration, zooplankton grazing and settling which is the same for the tree algal groups. The respiration formulation for each algal group uses a variable respiration rate, which is a function of the ambient growth rate plus a minimum basal rate. During respiration, dissolved oxygen is consumed and nutrients are recycled to the phosphorus, nitrogen and silica systems. Zooplankton grazing is accounted for through a temperature-dependent decay rate and recycles nutrients and carbon. Algal settling to the sediment is a temperature-dependent process that increases as the nutrient limitation factor decreases (nutrient-stressed settling).

2.3.2 Phosphorus

Particulate and dissolved organic phosphorus forms are included in the model, with further distinctions based upon reactivity. These reactivity distinctions, in turn, are based upon relative decay rates for the organics. A labile fraction describes organic material that decays on a time scale of several weeks to a month or two, while a refractory fraction accounts for decay processes lasting months to a year. The labile fractions decay primarily in the water column or else rapidly in the sediments; the refractory components mainly decompose in the sediments. The inorganic form of phosphorus, orthophosphate (PO_4), is also modeled, for a total of five state variables for phosphorus (Table 3).

Table 3. Phosphorus State Variables

Refractory Particulate Organic Phosphorus	(RPOP)
Labile Particulate Organic Phosphorus	(LPOP)
Refractory Dissolved Organic Phosphorus	(RDOP)
Labile Dissolved Organic Phosphorus	(LDOP)
Orthophosphate	(PO_4)

Particulate organic phosphorus, whether refractory or labile, decomposes to dissolved organic phosphorus through hydrolysis, which is a temperature- and bacterial biomass- mediated reaction. The size of the bacterial population involved in decomposing organic compounds in the water column affects the rate at which this process occurs. Because bacterial biomass is not directly modeled, algal biomass is used as a surrogate tracking variable for computational purposes. The particulate fraction of organic phosphorus settles within the water column at a temperature-dependent rate and is deposited to the sediment where it is further decomposed through anaerobic processes. The dissolved form of organic phosphorus further decomposes through mineralization into the inorganic form of phosphorus (PO_4), which is affected by the same factors controlling

hydrolysis. Inorganic phosphorus, PO_4, is lost through its utilization by algae as a nutrient essential for growth and is supplied from or lost to the sediment through sediment fluxes. All forms of phosphorus, organic and inorganic, are supplied as a consequence of algal respiration and zooplankton grazing, which is termed algal nutrient recycling. Inputs of organic and inorganic phosphorus from the atmosphere, boundaries, tributaries, nonpoint sources and point sources are also accounted for in the modeling framework.

2.3.3 Nitrogen

Organic nitrogen is divided into the same four components or state variables as organic phosphorus. The addition of two inorganic forms of nitrogen, ammonia (NH_3) and nitrite plus nitrate nitrogen (NO_3), produce a total of six state variables for nitrogen (Table 4).

Table 4. Nitrogen State Variables

Refractory Particulate Organic Nitrogen	(RPON)
Labile Particulate Organic Nitrogen	(LPON)
Refractory Dissolved Organic Nitrogen	(RDON)
Labile Dissolved Organic Nitrogen	(LDON)
Ammonia	(NH_3)
Nitrite plus Nitrate	(NO_3)

The particulate and dissolved forms of nitrogen decompose through the same reaction pathways as phosphorus, with the particulate fractions settling to the sediment. The dissolved organic forms mineralize to ammonia, which is subsequently nitrified to nitrite and nitrate via a reaction in which dissolved oxygen is consumed. Nitrification is an aerobic reaction; therefore, the reaction decreases as dissolved oxygen concentrations decrease below a certain value. The nitrification reaction is, therefore, dependent upon water column dissolved oxygen concentrations as well as temperature. The denitrification of nitrate to nitrogen gas is an anaerobic reaction that varies with temperature. Ammonia and nitrite plus nitrate are utilized by algae as nutrients for growth with ammonia being the preferred nutrient. A preference scheme for determining ammonia or nitrite plus nitrate preference at varying concentrations is presented in Appendix A. Algal nutrient recycling replenishes the four organic forms of nitrogen and ammonia during algal respiration and zooplankton grazing. Sediment fluxes of ammonia and nitrate are either a source of or sink for these nutrients in the water column. External inputs of all forms of nitrogen are also accounted for within the model.

2.3.4 Carbon

Organic carbon is divided into the same groups as organic nitrogen and phosphorus, with three additional state variables. Excretion of dissolved organic carbon by phytoplankton during photosynthesis is included as the fifth state variable, algal exudate. Algal exudate decays on a time scale similar to that for reactive dissolved organic carbon. Highly reactive particulate and dissolved organic material, such as carbonaceous inputs associated with sewage treatment plants or combined sewer outfalls which decay on a time scale of days to a week or two, is classified as reactive particulate or dissolved organic carbon and make up the remaining two carbon state variables. The seven state variables described for carbon are shown in Table 5.

Table 5. Carbon State Variables

Refractory Particulate Organic Carbon	(RPOC)
Labile Particulate Organic Carbon	(LPOC)
Refractory Dissolved Organic Carbon	(RDOC)
Labile Dissolved Organic Carbon	(LDOC)
Algal Exudate Dissolved Organic Carbon	(EXDOC)
Reactive Particulate Organic Carbon	(REPOC)
Reactive Dissolved Organic Carbon	(REDOC)

The particulate and dissolved forms of carbon decompose through the same reaction pathways as phosphorus and nitrogen, with the particulate fractions settling to the sediment. The dissolved forms of carbon oxidize to carbon dioxide, using dissolved oxygen during the process. Oxidation of dissolved organic carbon is aerobic and, therefore, reduced at low water column dissolved oxygen concentrations. The oxidation process is also modified by temperature and bacterial biomass levels, which are indirectly represented by algal biomass. Algal recycling due to zooplankton grazing is a source of both refractory and labile particulate and dissolved organic carbon. External inputs of organic carbon are also included in the modeling framework.

2.3.5 Silica

Two silica forms are included in the model: particulate biogenic silica, which is unavailable for algal growth, and silica, which is available for algal growth. Particulate biogenic silica is mineralized to available silica at a temperature- and bacterial biomass-dependent rate and can also settle to the sediment. Available silica is utilized as a nutrient during algal growth and can interact with the sediment through silica fluxes. Algal recycling supplies the particulate biogenic silica system through algal respiration and zooplankton grazing. The two state variables for silica are shown in

Table 6. However the silica system was not used for this study. Rather the biogenic silica system was reconfigured to represent total suspended solids (TSS). TSS is modeled as a conservative substance that is allowed to settle in the model.

Table 6. Silica State Variables	
Biogenic Silica – Unavailable	(BSI)
Silica – Available	(SI)

2.3.6 Dissolved Oxygen

Levels of dissolved oxygen are affected by the nitrification of ammonia, denitrification of nitrate, oxidation of dissolved organic carbon, algal oxygen production and respiration, sediment oxygen demand (SOD) and atmospheric reaeration. The sediment oxygen demand is assigned a temperature-dependent rate in the water quality model. Aqueous SOD, or the oxygen-demanding equivalent associated with sediment sulfide production, is included as an additional state variable (O2EQ). Dissolved oxygen saturation is computed from water column temperature and salinity obtained from the hydrodynamic model. The effects of algal photosynthesis and respiration on dissolved oxygen were briefly described in Section 2.3.1.

2.3.7 Sediment Interaction

A sediment model is coupled with the water quality model to define the interactions between the sediment and overlying water column. The sediment submodel used has three parts: the deposition of particulate organic matter (POM) to the sediment from the water column; the decay or diagenesis of the POM in the sediment; and the flux of the resulting end-products to the overlying water column.

The water column model state variables that are deposited to the sediment include: detrital algae, labile and refractory POC, labile and refractory PON, and labile and refractory POP. The fluxes of these state variables make up the incoming sources of particulate organic matter to the sediment. In the model the sediment bed is made up of two active layers; the layer directly below the water surface, which is typically anaerobic, and then the next layer, which is anaerobic. Soluble end products of diagenesis react in the aerobic and anaerobic layers of the sediment. The difference between the resulting aerobic layer dissolved concentration and the overlying water concentration determines the flux to or from the sediment. Figure 12 presents a schematic of these processes.

The multi-class G model (Westrich and Berner 1984) is used to model the diagenesis of POM. The multi-class G model more realistically recognizes that the pool of decomposable, sedimentary organic material is actually composed of various groups of compounds that have

different reactivities with regard to decomposition. The model framework assumes a 3-G model structure, i.e., POM is assumed to be comprised of a labile component, a refractory component and a slow refractory component. Each of these components is assumed to decay following different first-order reaction rates. It is further assumed that the reaction rates are temperature dependent. Table 7 presents the 14 state variables in the sediment submodel. Appendix A presents a more complete development of the of the sediment theory.

Table 7. Sediment Submodel State-Variables

State Variables
1. Temperature
2. Labile POP
3. Refractory POP
4. Slow Refractory POP
5. Labile PON
6. Refractory PON
7. Slow Refractory PON
8. Labile POC
9. Refractory POC
10. Slow Refractory POC
11. Ammonia Nitrogen
12. Nitrate Nitrogen
13. Inorganic Phosphorus
14. Hydrogen Sulfide

The importance of modeling an annual cycle when using a coupled sediment model is due to the storage capacity of the sediments and the subsequent effects on nutrient fluxes and sediment oxygen demand (SOD). Organic matter (nitrogen, phosphorus and carbon) deposited in the sediments during the winter and spring undergoes slower decay pathways due to the cooler temperatures. When the temperature increases during the summer months, stored organic matter decays at a faster rate, which results in different nutrient fluxes and SOD. Without the modeling of an annual cycle (i.e. modeling of summertime alone), summer nutrient fluxes and SOD would be under-computed because stored organic matter would not be included.

2.4 WATER QUALITY MODEL CALIBRATION

The water quality model calibration period covers a two year period from January, 2000 through December, 2001. Calibration requires the time-variable input of boundary condition data for all of the state variables. Hydrodynamic transport processes are directly coupled with the water quality model, so that water quality computations occur within the tidal cycle. The circulation obtained from the hydrodynamic model is averaged over a 2-hour period before transfer to the water quality model. Boundary condition locations are the same as for the hydrodynamic model.

The water quality model calibration compares model output and observed data found in the Data Atlas. The Data Atlas contains several types of data useful to the calibration process such as dissolved oxygen, organic nitrogen, ammonia nitrogen, nitrite plus nitrate nitrogen, organic phosphorus, orthophosphate, BOD_5, and chlorophyll-a. It will be shown that the water quality model calibration reasonably represents the observed distribution of phytoplankton (as represented by chlorophyll-a), nutrients and dissolved oxygen.

Details of the water quality model boundary conditions, inputs and constants are discussed in detail in the following subsections. The water quality model calibration section will present a summary of the calibration, highlighting important parameters and areas of the modeling study. While several of the calibration figures will be presented in these sections, the remainder of the figures are included in Appendix C.

2.4.1 Model Inputs

2.4.1.1 Solar Radiation

The ambient light level is a major factor controlling the growth of phytoplankton in an aquatic environment; therefore, it must be accurately represented in any modeling analysis. Ambient light levels can be determined directly from measurements of solar radiation near the water surface, or indirectly, from empirical relationships relating cloud cover to solar radiation. In this study, ambient light levels were obtained from direct measurement of daily solar radiation during the entire calibration period. These data were obtained from California, CIMIS Lodi West station for the years 2000 and 2001. The solar radiation data used for the calibration period is presented in Figure 13. Peak solar radiation values approach 700 langleys/day (ly/d) in the summer months and minimums of about 100 ly/d occurred in the winter months. Both panels of Figure 13 indicate typical seasonal ambient light patterns for the study area location. Each of the panels show periodic dips in light levels typically due to cloud cover and/or storm events. These tend to occur in winter and spring while periods with less cloud cover occur in the summer. Since daily solar values are input to the model these variations are represented in the model during computations of phytoplankton growth.

2.4.1.2 Light Attenuation

Another important factor controlling the growth of phytoplankton is the surface light attenuation with depth (light extinction). Available ambient light decreases with depth due to turbidity, which can be caused by suspended solids, color, and also phytoplankton. This total light extinction coefficient including effects of chlorophyll is denoted as K_{eT}. Since the water quality model internally computes the total light extinction coefficient (K_{eT}), generally only the base light extinction coefficient, $K_{eb,}$ is required. One of the goals of the DWSC modeling was to calculate light effects on algal growth based on water column algal levels and turbidity or solids. As part of this study the model code was revised to compute K_{eb} based on TSS. To accomplish this two changes had to be made. First, since TSS is not one of the state variables, it had to be incorporated into the

model. The silica state variables made the ideal system to use since, in this predominantly fresh water system, silica is not expected to be a limiting nutrient, so is not a necessary model component. Therefore the model code was amended so that the biogenic silica system was used for TSS where TSS is modeled as a conservative substance and is also able to settle. The available silica system is bypassed.

The second code change allows for the computation of time and spatially variable K_{eT} based on internally computed TSS and chlorophyll-a concentrations. Empirical equations to compute K_{eT} from secchi depth or solids and chlorophyll-a concentrations have been developed. The following analyses apply these equations to SJR DWSC secchi depth or solids and chlorophyll-a data to develop an equation to compute K_{eT} for use in the model.

The top three panels of Figure 14 present longitudinal secchi depth, chlorophyll-a and TSS concentrations along the SJR from Vernalis through the DWSC to station R8. The fourth panel of Figure 14 shows K_{eT} computed from secchi depth from the following equation:

$$K_{eT} = 1.8/depth; \quad (10)$$

(Sverdrup et al., 1942, Beeton, 1958), where depth is in meters and K_{eT} is in 1/m. Also presented on the fourth panel of Figure 14 is another estimate of K_{eT} (Di Toro, 1978) based on nonvolatile suspended solids (NVSS), organic detritus (volatile suspended solids, VSS), and chlorophyll-a:

$$K_{eT} = 0.052(NVSS) + 0.174(VSS) + 0.031(Chl\text{-}a); \quad (11)$$

where NVSS and VSS are in mg/L, chlorophyll-a is in μg/L and Ke_T is in 1/m. Based on SJR data, VSS is estimated to be approximately 20% of TSS, so that NVSS is approximately 80% of TSS. Using these estimates of NVSS and VSS, equation (11) reduces to:

$$K_{eT} = 0.0764(TSS) + 0.031(Chl\text{-}a); \quad (12)$$

with the first part of equation 12 represents the non-algal light extinction.

To summarize, secchi depths are between 1-2/ft in the SJR above the DWSC, then increase with decreasing chlorophyll-a, and TSS. The light extinction, K_{eT}, decreases from an average of approximately 1.5/ft above the DWSC to about 1.0- 0.5/ft in the DWSC. Light extinction follows the patterns of both secchi, algal and solids levels. That is, as secchi depth increases with decreases in algae and solids in the DWSC, a decrease in light extinction is computed. SJR turbidity data is shown in the bottom panel of Figure14 to demonstrate that TSS closely follows turbidity measurements. An interesting feature of the data is that solids, chlorophyll-a, and turbidity are lower in the Turning Basin than at Station R3 and equation 12 is able to capture this trend. Therefore equation 12 was added to the model code and along with model computed TSS and chlorophyll-a, was used to compute temporal and spatial K_{eT}s .

An alternate way to compute the total light extinction with depth in the water column, K_{eT}, applies the following equation (Thomann, 1987):

$$I=I_o e^{(-K_{eT}*z)} \quad (13)$$

where:

I=light intensity at depth z
I_o= surface light intensity
z=depth (m)
K_{eT} =light extinction coefficient (1/m)

Using this first order approximation, light intensity data with depth (Lehman, 2005) was used to verify light extinction computed by equation 12. Equation 13 was applied to LICOR Quantum meter readings at one location in the SJR (Channel Point) and four locations in the SJR DWSC (Turning Basin, Light 48, Rough & Ready Island, and Turner Cut) using a nonlinear least squares regression and the Excel Solver software. Figure 15 presents the data (symbols) and estimate (solid line) at each of the stations. Table 8 presents the K_{eT} based on the field light penetration data.

Table 8. Calculated Total Light Extinction Coefficients, July 18, 2001

Location	K_{eT} (1/ft)
Turning Basin	0.61
Channel Point	1.57
Light 48	0.95
Rough & Ready Island	0.63
Turner Cut	0.77

(Source: Lehman, 2005)

These independently computed total extinction coefficients match very well with those presented in Figure 14. Specifically a higher light extinction above the DWSC at Channel Point (K_{eT} of 1.57/ft) is computed, then decreasing extinction corresponding to decreasing chlorophyll-a and TSS at and downstream of R3 is computed.

2.4.1.3 Phytoplankton Stoichiometry

Phytoplankton stoichiometry (nutrient-to-biomass ratios) is another important factor controlling phytoplankton growth. Nutrient-to-biomass ratios determine the amount of a specific nutrient (nitrogen, phosphorus or silica) required to produce a specific amount of algal biomass (chl-a or carbon). Based on nitrogen and phosphorus data, there is not expected to be nutrient limited algal growth in the system. Typically, nutrient-to-biomass ratios are either determined from available data or reported literature values such as Redfield ratios (Redfield, 1963). Nutrient to

biomass ratios are presented in Figure 16 and represent data collected in the SJR at Vernalis by USGS (Kratzer, 2004) and UCD (Dahlgren, 2004). Data in the SJR below Vernalis and in the DWSC were not sufficient to calculate nutrient-to-biomass ratios so the below analysis of the SJR data at Vernalis serves as a guide and the typical literature Redfield ratios are applied in the model.

Typical Redfield ratios have been developed for the relationship of particulate organic carbon (POC) to chl-a, particulate organic nitrogen (PON) and particulate organic phosphorus (POP). The data show the relationships between POC and chl-a (C/Chl-a ratio), POC and PON (C/N ratio), and POC and POP (C/P ratio). The top panel shows that as algal biomass (chl-a) increases, POC also increases above some background, non-algal level. This relationship, the C/Chl-a ratio, is fundamental in phytoplankton modeling, since ambient algal levels are represented by measurements of chlorophyll-a. Also, this ratio represents the fact that algal carbon and chlorophyll-a are positively correlated. The solid line in the top panel represents a C/Chl-a ratio (slope) of 37.19, which is close to 40 taken from Lehman, 2004. Therefore a C/Chl-a ratio of 40 is used in the water quality model. The agreement between the data and the C/Chl ratio of 40 suggests that this ratio reasonably represents the phytoplankton population in the study area.

The nutrient-to-biomass ratios (C/N and C/P) are presented in the middle and bottom panels of Figure 16, respectively. Data in the SJR at Vernalis include only particulate nitrogen (PN) and particulate phosphorus (PP) but can be used to formulate N/C and P/C ratios assuming most of the particulate is in the organic form. Again these ratios are guides to confirm typical stoichiometric Redfield ratios of 5.68 for N/C and 41 for P/C that are applied in the model. The N/C ratio (slope) of 3.10 and P/C ratio (slope) of 31.99 in the middle and bottom panels of Figure are lower than the applied ratios, possibly the result of using PN and PP rather than PON and POP. The PN and PP data also exhibit a tendency to increase with increasing biomass (as represented by POC). In general, the nutrient ratios presented in the two panels along with Redfield ratios reasonably represent the increasing nutrient with increasing carbon trend observed in the SJR data.

2.4.1.4 Atmospheric Reaeration

Atmospheric reaeration is one of the two major sources supplying dissolved oxygen in many estuarine water bodies; the other source is phytoplankton oxygen production. In estuarine systems, atmospheric reaeration is usually accounted for through the specification of a constant oxygen transfer coefficient (K_L) in units of length/time (m/d). The oxygen transfer coefficient in open water bodies is usually controlled by the surface shear stress produced by the wind. Therefore, in the SJR DWSC water quality model, oxygen transfer coefficients inputs were based on both calculated K_L as a function of wind velocity and calibrations. The formulation used to calculate the oxygen transfer coefficients K_L in m/d, is based on the following equation by Banks (1975) and Banks and Herrera (1977):

$$K_L = 0.728U_w^{1/2} - 0.317U_w + 0.0372U_w^2 \quad (14)$$

where U_w = wind speed, m/s

Although this equation was developed for lakes and reservoirs, or large open bays, previous discussion indicating small average tidal velocities in the DWSC indicate that wind induced reaeration may be important. The following demonstrates this. If average tidal velocity, U, is in fps and average depth, H, in ft, then the O'Connor Dobbins formulation for rivers for the reaeration coefficient, K_a, is computed by the following equation:

$$K_a = 12.9U^{1/2}/H^{3/2} \quad (15)$$

where $K_a = K_L/H$

K_L (m/d) can then be computed from K_a and depth. Table 9 presents average tidal velocities, depths, velocity based K_a, velocity based K_L, and wind based K_L at various locations in the SJR study area. The last column of Table 9 gives the average K_L computed from an average wind speed of 2.9 m/s based on the reported 15 minute wind speed data at Rough and Ready Island (DWR). Comparison of the velocity based and wind based K_L indicates that reaeration under higher wind conditions in the critical section of the DWSC between R3 and R5 would be underestimated using the velocity based K_L.

Table 9. Comparison of Wind Speed Based and Velocity Based Reaeration in the San Joaquin River Model Area.

Location	Average Tidal Velocity m/s	Depth m	Average K_a* (1/d)	Velocity Based Average $K_L=K_a*H$ m/d	Wind Based Average K_L m/d
SJR at Vernalis	0.30	2.90	0.324	0.94	0.63
SJR DS of Old River	0.31	3.20	0.226	0.72	0.63
Turning Basin	0.01	10.93	0.012	0.13	0.63
Light48, R3	0.07	10.90	0.030	0.32	0.63
Rough & Ready Island	0.07	10.80	0.029	0.31	0.63
R5	0.13	10.80	0.041	0.44	0.63
Turner Cut	0.10	11.00	0.035	0.38	0.63
Downstream Boundary	0.36	9.00	0.088	0.79	0.63

Average Measured Wind Speed of 2.9 m/s, Minimum Measured Wind Speed of 1.1 m/s

*Ka (1/d) = 12.9*U^.5/H^3/2, where U in fps, H in ft

Figure 17 presents hourly average wind speed at Rough and Ready Island for 2000 and 2001 along with computed K_L using equation 14. Wind speed measurements were taken 27 feet above the RRI dock. Wind speeds range from a minimum of 1.1 m/s to highs of about 10 m/s. Computed K_Ls range from 0.5 m/d to maximums of about 4 m/d. Hourly wind speeds were input to the model to capture variations in wind speed such as higher winds in the late afternoon.

2.4.1.5 Settling and Resuspension

The net amount of material that settles through the water column is simulated in this model using 1) a settling rate from water column layer to water column layer and 2) a deposition rate from the bottom water column layer into the sediment bed. This net settling, or sedimentation, represents the sum of settling to and resuspension from the sediment. Hence, in the SJR DWSC water quality model, settling and resuspension rates are not individually specified. Instead, net settling and deposition rates are applied in the model to TSS, particulate organic material (POC, PON, POP) and phytoplankton systems. These net settling and deposition rates were used in the SJR DWSC model as one of the calibrating parameters. The model allows a single settling rate for the study area and spatially varying deposition rates for each algal group (chlorophyll-a), particulate organic matter, and TSS.

Table 10 lists the calibrated settling and deposition rates for the TSS, phytoplankton (representing chlorophyll-a), and particulate organic material (POC, PON, POP) systems. Water column settling and sediment deposition was first calibrated for TSS resulting in a settling rate of 2.5 m/d and spatially variable deposition rates from 0.05 to 0.5 m/d. Note that deposition rates in the SJR upstream of the confluence with the DWSC reflect a faster moving river where little deposition is expected. The TSS settling velocity of 2.5 m/d is in agreement with other literature settling velocities for silt of 2.4 – 24 m/d (Chapra, 1997). Recent studies in the SJR DWSC (Litton, 2003) result in average TSS settling velocities of 7.2 to 62.4 m/d and net settling rates, representing settling less resuspension, of 0.53 m/d between Light 48 and Light 43 and 0.336 m/d between light 43 and light 38 also in agreement with the model input TSS settling and deposition rates.

Water column chlorophyll-a and POM settling rates were then calibrated resulting in rates of 2.5 m/d and similar to TSS rates. Chlorophyll-a settling studies (Litton, 2003) also reported high settling rates of 2.4 to 9.5 m/d so that these values appear to be in agreement with the model input. Variable deposition rates were applied in the study area to reflect differences that would occur with different bottom velocities. Since the SJR upstream of the confluence with the DWSC is a narrow faster moving river, as compared to the DWSC, little deposition is expected resulting in negligible chlorophyll-a and POM deposition to Mossdale and as the river deepens some deposition appears to occur. The SJR in the DWSC slows down as the river deepens and widens. This would result in greater loss to the sediment as detention time increases with lower velocities. Therefore calibration of deposition in the SJR DWSC resulted in 0.25 m/d from R3 to the boundary and 0.5 m/d in the Turning Basin. A higher TSS deposition from Vernalis to Mossdale was needed with the thought

that TSS upstream of Vernalis comes from inflows, which may settle out. This will be further addressed in Section 2.5.2 during discussion of the calibration results

Table 10. SJR DWSC Model Settling and Deposition Rates for TSS, Chlorophyll-a and POM (POC, PON, POP) - Units in m/d

	TSS		Chlorophyll-a		POM (POC, PON, POP	
Model Area	Water Column Settling	Deposition to Sediment	Water Column Settling	Deposition to Sediment	Water Column Settling	Deposition to Sediment
SJR from Vernalis to Mossdale	2.5	0.2	2.5	0.001	2.5	0.05
SJR Mossdale to confluence with DWSC	2.5	0.05	2.5	0.05	2.5	0.05
SJR East of R3 (Turning Basin to Port of Stockton)	2.5	0.5	2.5	0.5	2.5	0.5
SJR DWSC Downstream of R3	2.5	0.25	2.5	0.25	2.5	0.25

2.4.1.6 Boundary Conditions

Model boundary locations have been discussed and were shown in Table 1. Upstream boundary concentrations at Vernalis were developed from the USGS (Kratzer, 2004) and UCD (Dahlgren, 2004) data sets along with limited data provided by Jones & Stokes and the Data Atlas. Table 11 lists and Figure 18 shows the model boundary locations and the sample locations where data was used to develop boundary inputs. Boundary concentrations were developed using dissolved oxygen, TSS, EC, ammonia, nitrate, organic nitrogen, orthophosphorus, organic phosphorus, particulate organic carbon, and dissolved organic carbon (DOC) data. Figure 19 shows the temporal data (symbols) and model input (solid lines) developed at the upstream location at Vernalis. Conductivity data was provided in the Data Atlas at Mossdale as these data did not exist at Vernalis. TSS data was also taken from the Data Atlas and originated from the California's BDAT data base.

The remaining nutrient and chlorophyll-a boundary conditions were developed from data in the Data Atlas and from UCD and USGS sources collected from June through October of 2000 and

June to December of 2001. Nutrient and chlorophyll-a boundary concentrations from January to June 2000 were therefore assigned at the initial June 2000 measurements and concentrations between October 2000 and May 2001 were assigned the last October 2000 measurements. As shown in Figure 19 the resulting temporal profiles provide a good representation of the data capturing important seasonal variations likely to effect the model calibration (i.e. elevated summer chlorophyll-a)

Table 11. Boundary Locations and SJR Data

San Joaquin River Boundary	Use SJR data at
SJR at Vernalis (Upstream Boundary)	SJR data at Vernalis & Mossdale
Paradise Cut	Mossdale
Old River	Mossdale
Fourteenmile Slough	R6
Turner Cut	R7
Disappointment Slough	R8
Columbia Cut	R8
Little Connection Slough	R8
Middle River	R8
Potato Slough	Potato Point, EC at RSAN032
Old River (Franks Tract)	Potato Point, EC at RSAN032
Mokelumne River	Potato Point, EC at RSAN032
Fishermans Cut	Potato Point, EC at RSAN032
Thirteenmile Slough	Potato Point, EC at RSAN032
False River	Potato Point, EC at RSAN032
SJR at Jersey Pt (Downstream Boundary)	Potato Point, EC at RSAN018

The remaining boundary locations were assigned instream concentrations since additional boundary data did not exit. Namely, instream data from seven locations (Mossdale, R6, R7, R8, Potato Point, RSAN032, RSAN018) were applied to the remaining model boundary locations as defined in Table 11. Figures 20 - 24 show the data (symbols) and model inputs (lines). For all but the downstream boundary, time variable inputs were formulated based on data. Similar to the upstream boundary only summer data exists so that early summer and late fall data were extrapolated to times with no data to develop temporal boundary conditions. Boundary conditions downstream of Potato Point including the downstream boundary near Jersey Point were input as constant values except for EC and DO, which were input as daily values. Constant inputs are TSS at 10 mg/l, chlorophyll-a at 2 μg/L, organic phosphorus at 0.04 mg/L, PO4 at 0.03 mg/L, organic

nitrogen at 0.25 mg/L, ammonia at 0.15 mg/L, nitrite plus nitrate at 0.30 mg/L, POC at 0.5 mg/L and DOC at 2.0 mg/L. DO boundary concentrations were computed as saturation minus 1. Though the data to develop boundary inputs are sparse, it is the upstream boundary at Vernalis for which there is sufficient data, and nutrients from the Stockton RWCF that will drive water quality in areas of the SJR DWSC that experience low DO such as the Turning Basin and near Rough and Ready Island. Therefore this method of assigning boundary conditions based on instream concentrations, though not ideal is acceptable.

The water quality model divides the organic nitrogen, phosphorus and carbon systems into two reactivity classes (labile and refractory) in addition to the particulate and dissolved splits. Specification of the labile and refractory fractions is dependent on the source of the organic constituents. River boundary inputs, as opposed to oceanic boundaries, are usually associated with point and nonpoint sources of more reactive organic material. Experimental determination of the reactivity splits is difficult to determine and, in many cases there is insufficient data to determine the splits. The POC splits in the past, have been estimated based on the results of long-term BOD studies. POC and DOC were assigned as labile carbon at Vernalis and as 75% refractory an 25% labile at all other boundaries. Since little or no information was available as to the particulate/dissolved or labile/refractory splits for both organic nitrogen and phosphorus data each was assigned to 50/50 particulate/dissolved with 50/50 labile/refractory reactivity split at Vernalis and 25/75 labile/refractory split at all other boundaries.

2.4.1.7 Point Sources

The Stockton Reclamation Wastewater Control Facility (RWCF) is the one major point source in the study area. Loadings for the Stockton RWCF were developed from data included in the Data Atlas that reflect both regular and special monitoring programs. The Stockton RWCF discharges flow from lagoons near the SJR above Rough & Ready Island (Figure 2). Point source loads were developed for ammonia, nitrite+nitrate, organic nitrogen, orthophosphate, TSS, chlorophyll-a, DO, organic carbon, and temperature. Figure 25 shows the temporal data for 2000 and 200 that were used to develop the point source loadings. The solid line through the data represents the concentrations and flow used to compute loads. Concentrations were interpolated for days with missing data. Varying daily loads were computed and used in the model. Daily EC loadings were computed from EC concentrations. EC concentrations were fairly consistent and averaged about 1200mS/cm. Seasonal temperatures were input via the hydrodynamic model. Nominal organic phosphorus of 0.3 mg/L was also input to the model. A typical ultimate to BOD_5 ratio of 4 was applied to the $CBOD_5$ data to compute ultimate CBOD loadings as dissolved organic carbon (DOC). Particulate organic carbon (POC) concentrations were estimated as 40% of VSS, where VSS was calculated as 85% of TSS from limited data. POC was input to the model less algal carbon. The data indicate that, at periods, nitrogen concentrations exceeded 25 mg/L, which can impact river nitrogen levels. Organic carbon as well as organic nitrogen and phosphorus were input

to the model as labile material subject to an instream labile decay rate. These rates were assigned as 0.11/d for CBOD and 0.07 for NBOD based on recent studies by Litton, 2003.

2.4.1.8 Constants

All of the water quality constants used in the model are tabulated in Appendix A along with a detailed discussion of the model theory. Table 12 presents a few of the more important constants used in the final calibration. The sediment submodel requires its own set of inputs. Sediment nutrient flux data were not available for this study. Instead, the sediment submodel inputs were based on previous studies and on the water quality model calibration of dissolved oxygen, chlorophyll-a, nitrogen and phosphorus. Table 13 presents the key sediment model coefficients used for the SJR DWSC model. Note that in order to simulate the increase in chlorophyll-a from Vernalis to Mossdale from 50 to over 80 μg/L in June of 2000 and 2001, the chlorophyll-a growth rate in that stretch of the SJR was artificially increased and death and grazing rates were turned off. This increase in chlorophyll-a between Vernalis and Mossdale due to growth alone is unlikely since the travel time in this 15-mile stretch, with a velocity of 0.30 m/s, is 1 day. With a potential growth rate of 2.2/day during the day resulting in an effective growth rate of 1.1/day, there would have to be no light limitation or losses to achieve this growth. Therefore, it is believed that there is an additional source of chlorophyll-a into the SJR between Vernalis and Mossdale.

Table 12. Summary of Eutrophication Model Constants

Parameter	Value at 20°C	Source
PHYTOPLANKTON*		
Growth Rate (1/d)	2.2	Calibrated & Upstream DSM2
Respiration Rate (1/d)	$0.02 + 0.20\mu_a$	Calibration
Zooplankton Grazing Rate (1/d)	0.10	Calibration
Carbon/Chlorophyll Ratio	40	Lehman, 2004
Nitrogen/Carbon Ratio	0.176	Typical Stoichiometry
Phosphorus/Carbon Ratio	0.024	Typical Stoichiometry
NITROGEN		
Hydrolysis Rate (1/d)	0.01 - Refractory	Other Studies
(Particulate-to-Dissolved Organic)	0.1 - Labile	
Mineralization Rate (1/d)	0.01 - Refractory	Other Studies
(Dissolved to Ammonia)	0.07 - Labile	
Nitrification Rate (1/d)	0.07	Litton, 2003
PHOSPHORUS		
Hydrolysis Rate (1/d)	0.01 - Refractory	Other Studies
(Particulate-to-Dissolved Organic)	0.05 - Labile	
Mineralization Rate (1/d)	0.01 - Refractory	Other Studies
(Dissolved to Orthophosphate)	0.07 - Labile	
CARBON		
Hydrolysis Rate (1/d)	0.01 - Refractory	Other Studies
(Particulate-to-Dissolved Organic)	0.05 - Labile	
Oxidation Rate (1/d)	0.11	Litton, 2003

*Phytoplankton rates apply below Mossdale

Table 13. Sediment Submodel Constants

Description	Notation	Value	Units
Physical Related			
Water column-sediment layer temperature diffusion coefficient	D	0.0018	cm2/sec
Depth of active sediment layer	H_2	10.	cm
Diagenesis Related			
G1 diagenesis decay rate at 20°C	k_{diag1}	0.035	day^{-1}
Temperature correction coefficient	θ_1	1.10	
G2 diagenesis decay rate at 20°C	k_{diag2}	0.0018	day^{-1}
Temperature correction coefficient	θ_2	1.15	
G3 diagenesis decay rate at 20°C	k_{diag3}	0.000001	day^{-1}
Temperature correction coefficient	θ_3	1.17	
	Labile	**Refractory**	**Slow Refractory**
G-Model Fraction Splits			
Phosphorus			
Phytoplankton group 1	0.65	0.20	0.15
Phytoplankton group 2	0.65	0.20	0.15
Non-phytoplankton POM	0.65`	0.20	0.15
Nitrogen			
Phytoplankton group 1	0.65	0.25	0.10
Phytoplankton group 2	0.65	0.25	0.10
Non-phytoplankton POM	0.65	0.25	0.10
Carbon			
Phytoplankton group 1	0.65	0.20	0.15
Phytoplankton group 2	0.65	0.20	0.15
Non-phytoplankton POM	0.65	0.20	0.15

2.4.2 Calibration Results

The ultimate goal of this project is to develop a mathematical model, which describes circulation, and the nutrient cycling and oxygen dynamics in the SJR DWSC. One method for judging the adequacy of the model in describing these processes is to compare the results of model computations to observed data. The SJR DWSC water quality model was calibrated using data from January 2000 to December 2001, where the bulk of the data used in the calibration was collected in June through October of both years. There is inherent variability when comparing measured concentrations of water quality variables to model output. This variability may be due to natural processes, for example, algal patchiness, spatial variability introduced when one compares the observed data from one location to the model output of a segment, or measurement variability. Therefore, given this variability, it is unrealistic to expect a model to exactly reproduce all observed water quality. However, it is realistic to expect that the model should reproduce seasonal and spatial trends in the data, as well as the interrelationships between variables. For example, it is expected that the model reproduce the annual cycle of phytoplankton biomass and primary productivity. For

the SJR DWSC, this should be reflected in high algal biomass during spring and summer, followed by decreasing algal biomass in the fall and winter, with highest productivity occurring during the summer months. Due to the variable geometry and flow between the USJR and the SJR DWSC and it's effect on water quality, this model should also be able to reproduce effects of settling and deposition on solids and phytoplankton biomass.

2.4.2.1 Water Column Calibration

Calibrating water quality models require the adjustment of certain parameters for site-specific conditions based on comparisons between observed data and model output. The method of model calibration begins with the selection of a set of parameters (kinetic constants) and coefficients based on other modeling studies and site-specific field studies. For the SJR DWSC model, many of the initial parameters and coefficients were originally derived from previous HydroQual studies (HydroQual, Inc., 1987, 1989, 1991 and 1992) or recent studies (Litton, 2003, Lehman 2004, Lehman, 2005). The remainder of the calibration phase involves the adjustment of key parameters and coefficients to obtain a reasonable representation of the water quality kinetics observed in the system. Adjustment of the model parameters is constrained by typical ranges as determined from the literature and other modeling studies.

The final calibration that is presented below is the result of many hydrodynamic and water quality model runs, which were made to obtain a consistent set of model coefficients that are reasonable and reproduce the observed data for all the state-variables considered. This involved performing sensitivities to key model parameters to determine their contribution to the overall results. For instance, model sensitivities were completed involving phytoplankton growth, respiration and grazing rates to assess the effects on calculated phytoplankton, DO and nutrient levels with the set of parameters that best reproduces the observed data. As discussed above, another very important aspect of the water quality model calibration is the specification of boundary conditions, meteorological conditions (wind and solar radiation), and most importantly, a hydrodynamic transport pattern that reasonably reproduces the observed conditions during the calibration period.

This section presents a comparison of the observed data and model output for the calibrated water quality model in four different formats:

- Temporal distributions of water column parameters at select stations for the full calibration period,
- Spatial distributions from Vernalis to Jersey Point,
- Vertical distributions of temperature and dissolved oxygen,
- Temporal distributions of sediment fluxes at select stations for the full calibration period.

Temporal comparisons of modeled and data temperature at several locations along the SJR study area are presented in Figure 26. The model is able to reproduce seasonal trends in the data well. Both model surface and bottom temperature is plotted, however the values are similar, which is an early indication that the system is not stratified.

The temporal distributions of observed data and model water quality parameters are presented in Figures 27 to 30 for SJR locations at Mossdale, R2, Turning Basin, and R5. The remain temporal calibration figures for Vernalis, R1, R3, R4, R6, R7, and R8 are included in Appendix C. The figures are in groups of three so that figures with A designations show temporal conductivity, TSS and TOC, figures with B designations show temporal nutrients, and figures designated with C show DO, chlorophyll-a and DOC. Figures 27A-30A show 2 year temporal conductivity and TSS from Mossdale to R5. Full 2 year data records were available at Mossdale for conductivity and at Vernalis for TSS but only summer 2000 and 2001 data were available at most of the sample locations. Conductivity is simulated in the model as a conservative substance. Model conductivity and data are in good agreement, a further indication beyond the hydrodynamic validation presented in Section 2.2.1.4 that the model flow pattern provides a good representation of the system during the 2000 to 2001 calibration period.

TSS is subject to settling and deposition in the model. Recall that a system wide TSS settling rate of 5 m/d was applied in the model with variable deposition rates through the system. TOC is represented in the model as nonalgal POC and DOC so that model TOC and phytoplankton carbon are added to plot total TOC as represented by the data. In general TOC measurements, though sparse remain relatively similar at about 4 mg/L. In general the model is able to reproduce both TSS and TOC at the various sample locations.

Figures 27B-30B show temporal NH_3, NO_2+NO_3, and PO_4 profiles from Mossdale to sampling location R5. Nitrogen and phosphorus model outputs match the data well. Note however there is no PO_4 data in 2001. Ammonia levels in the SJR from sample location R2 to R8 (see Appendix C) reflect the Stockton RWCF ammonia load as evidenced by high water column ammonia from October 2000 to March 2001. Although the Stockton RWCF is below sample location R2, its effect can be seen at R2 due to tidal influences. It is interesting to note that the model indicates that the Stockton RWCF load impacts nutrient levels as far away as R7 (see Appendix C). Though there is no ammonia data at R7 for most of the period of high RWCF load, concentrations at R7 in November indicate an increase. Nutrient concentrations throughout the model area are in ample supply so that a nutrient limitation is not expected to be a factor in algal growth.

The model captures seasonal chlorophyll-a growth and transport patterns in the SJR both before the confluence with the DWSC as well as within the DWSC as seen in Figures 27C to 30C. Dissolved oxygen profiles over the 2 year period are shown in the C series of figures along with DO saturation. DO concentrations in the USJR and in the DWSC follow seasonal variations with DO

near 10 mg/L in winter and near 7 mg/L in summer. Periods of supersaturation in the USJR are seen at Vernalis and Mossdale indicating that DO production due to chlorophyll-a growth is the dominant factor controlling oxygen levels. Summer DO levels downstream of Mossdale and in the DWSC are below saturation indicating that other oxygen demanding mechanism play a more important role. The following spatial graphs of model and data profiles will further discuss mechanisms and implications for the SJR DWSC.

The spatial distributions of observed data and model output are presented in Figures 31 to 34. The symbols represent the average concentrations and standard deviations at surface, mid and bottom depths as denoted in the figure legend in the top panel. Model output represents average model results from mid June through October for each of years 2000 and 2001 coinciding with the data, along with standard deviations shown as shaded areas. Spatial DO, chlorophyll-a, TSS, and conductivity are shown in Figures 31 and 33 for 2000 and 2001 respectively. Spatial NH_3, NO_2+NO_3 and PO_4 concentrations are shown in Figures 32 and 44 2000 and 2001 respectively.

TSS data show a decrease in concentration from Vernalis to Mossdale likely due to settling out of high solids from some of the inflows to the USJR. For example the USGS reports average TSS concentrations entering the USJR from Orestimba Creek, Hospital Creek and Spanish Grant Drain of 198 mg/L, 1,020 mg/L, and 491 mg/l respectively for data collected in June to November of 2000 and 2001 (Kratzer, 2004). Then from Mossdale to the confluence with the DWSC, TSS levels increase slightly, possibly due to chlorophyll-a die off as well less TSS settling. The Stockton RWCF is a source of TSS loading to the system and can contribute to TSS levels in the vicinity of R2. As mentioned above approximately 80% of TSS in the study area is VSS representing organic detritus that would result from chlorophyll-a die off and grazing.

Upon entering the DWSC, TSS concentrations at R3 drop and stratify indicating dilution as well as settling and deposition mechanisms. TSS shows surface and bottom differences in the SJR DWSC especially between the Turning Basin and sample location R4 where bottom TSS is almost double surface TSS. The model therefore is able to capture solids from the USJR entering the DWSC and settling in the water column as well as effects of resuspension. TSS concentrations in the Turning Basin are lower than at R3 indicating that a portion of solids from R3 tends to get caught in the Turning Basin and due to lower velocities can settle out of the water column.

Surface solids decrease downstream of R3, however bottom TSS at R4 shows an increase. This suggests that settling is occurring between sample locations R3 and R4 however deposition appears low possibly due to the nature of the solids (algal based) as well as mixing in the water column. This trend was suggested in sediment settling studies conducted in the SJR (Litton, 2003) where surface TSS concentrations entering the DWSC from the USJR decreased while bottom TSS concentrations increased between lights 43 and 38. Downstream of R4 both model and data TSS levels decrease. The model captures the trends seen in the TSS data.

Spatial profiles of chlorophyll-a indicate growth from Vernalis to Mossdale then a decrease in chlorophyll-a levels downstream of Mossdale and into the DWSC. What appear to be lower summer chlorophyll-a levels in the DWSC when compared to USJR levels may reflect a dilution effect as the SJR depths increase from 10-15ft in the USJR to about 35ft in the DWSC. Chlorophyll-a growth and die off rates between Vernalis and the DWSC are the same so that changes in chlorophyll-a concentrations reflect changes due to geometry. For example, the USJR is shallow and fast moving so that little net deposition is expected before the confluence with the DWSC. However, upon entering the DWSC, flows decrease and depths increase, allowing settling and net deposition to play a larger role in effecting chlorophyll-a levels. Also algal growth becomes light limited in the DWSC at greater depths so that concentrations are also the result of mixing over depth in the DWSC.

As seen in temporal figures, model and data DO spatial profiles show concentrations above saturation in the SJR from Vernalis to sample location R1 and at or below saturation from sample location R2 into the DWSC for both 2000 and 2001 summer periods. Again as water enters the DWSC and flows decrease processes that govern DO levels can have a greater effect on DO levels. Lower flows result in greater detention time for carbon to exert a demand on oxygen. Oxygen demand from the sediment due to chlorophyll-a and carbon settling and decay can also be greater with greater net deposition. DO levels in the DWSC tend to decrease on average 1.5 mg/L from R3 to R6 then level off and increase slightly towards sample location R8. These mechanisms are even greater in the Turning Basin where even lower velocities result in increased retention time allowing for greater oxygen demand due to both greater demand in the water column as well as from sediment oxygen demand. DO in the Turning Basin averages about 5.5 mg/L in 2000 and 2001.

Nitrogen and phosphorus spatial profiles in Figures 32 and 34 show the system is not nutrient limited as there is always greater than the minimum amounts of nutrients to allow chlorophyll-a growth, namely 10 ug/L available nitrogen (ammonia+nitrite+nitrate) and 1.0 ug/L available phosphorus (orthophosphorus). The impact of the Stockton RWCF ammonia discharge in 2001 is captured by the data and model. The Stockton RWCF ammonia discharge of about 10 mg N/L in 2001, as compared to about 3 mg N/L in 2000 in addition to 2001 having a lower summer flow causes a spike in ammonia between R3 and R5. As will be discussed subsequently the sediment contributes a small amount of nitrogen and phosphorus to the water column in the DWSC so that upstream sources and the Stockton RWCF are the more significant contributors to nitrogen in the system.

2.4.2.2 Sediment and Nutrient Fluxes

Figures 35, 36, and 37 show temporal sediment model computations for the calibration period at six locations (Mossdale, R2, Turning Basin, Lt. 43, R3-Lt. 48, and R6-Lt. 38). Computed and measured (when available) SOD is presented on the top panel. Measured SODs are taken from Littton, 2003. Fluxes between the sediment to the water column for NH_3 and NO_2 + NO_3 are

presented in the center panels and PO_4 is presented in the bottom panels of the figures. Model SOD of about 0.01 to 0.25 g/m^2-d in the USJR (Mossdale and R2, Figure 35) represents a nominal SOD in agreement with low deposition. Areas of higher deposition of organic matter to the sediment such as the Turning Basin and R3 (Figure 36) can be expected to have higher summer SOD. SODs in the Turning Basin and R3 are somewhat higher at 0.1 g/m^2-d and in general in agreement with the data. SOD at Lt 43 and R6 (Figure 37) are about 0.5 g/m^2-d indicating lesser amounts of carbon settling to the bottom.

Ammonia and nitrate flux from the sediment also tends to mirror deposition. Nitrogen and phosphorus fluxes are shown on a negative to positive scale meaning fluxes to the water are indicated as positive values and fluxes to the sediment are indicated as negative values. The nitrate flux is negative indicating a flux from the water column through the system. In the USJR ammonia fluxes are near zero while phosphorus fluxes are low also indicative of low deposition to the sediment. Summer ammonia and phosphorus fluxes are highest in the Turning Basin (200 mg/m^2-d, 30 mg/m^2-d respectively) then decreasing downstream. These fluxes add small amounts to the system. For example in the Turning Basin with depth of about 10 meters, an ammonia flux of 200 mg/m2-d converts to 0.02 mg/l-d and a phosphorus flux of 30 mg/m^2-d converts to 0.003 mg/l-d over the Turning Basin depth. In the Turning Basin ammonia concentrations average about 0.5 mg/L in 2000 and 0.25 mg/L in 2001 and phosphorus concentrations average about 0.15 mg/L for both years so that ammonia sediment fluxes contribute between 4 to 8 % and phosphorus fluxes contribute 2% of the water column concentrations. These percentage contributions are less downstream as nutrient levels are similar to the Turning Basin while sediment fluxes are less than in the Turing Basin.

2.4.2.3 Temperature and Dissolved Oxygen Vertical Profiles

Vertical profiles have been constructed of temperature and dissolved oxygen at the Turning Basin, and sample locations R3, R4, R5, R6, and R7 for 17 dates in each of summers of 2000 and 2001 from data provided by Jones and Stokes. For discussion purposes only the Turning Basin and R5 data in 2000 will be shown here in Figures 38 to 41. The remainder of figures are included in Appendix C. In general there is little to no temperature stratification in the Turning Basin and the sample locations for the 17 dates as seen in Figures 38 and 39. The few dates where temperature stratification is seen (for example, Aug 22, 2000, Sept 29, 2000) indicate differences in temperature of about 1-2 degrees C. The model is able to compute temperature with depth in agreement with the data. Note also that on occasion the surface model temperatures indicate daily ranges of up to 4 degrees C, which reflects daily heating and cooling.

Vertical profiles of dissolved oxygen data in the Turning Basin and at R5 for 2000 presented in Figures 40 and 41 show dates when there is both no stratification and other times when there is stratification. Sample location R5 indicates that there are little differences in surface and bottom DO. This is also true for the remaining locations shown in Appendix C. The lack of differences in

temperature and DO at and below SJR DWSC R3 indicate that there is good mixing in the SJR DWSC. The Turning Basin seems to experience less complete mixing and, due to very little movement, an opportunity for oxygen demanding processes to cause low DO in bottom layers while algal growth and reaeration in the surface layers lead to higher surface DO. Reasons for differences in stratification both at different times in the Turning Basin and when compared to downstream stations is explored further.

An important feature of the model is its ability to capture daily temperature and DO variability. Temperature changes reflect surface heating during the day and cooling at night along with effects of tidal and wind induced mixing. The top panels of Figures 42 and 43 show surface and bottom temperature during August and September in the Turning Basin and at R5 in 2000. Similar figures for 2001 are in Appendix C. The model computes daily heating and cooling in the surface layer. This diurnal change does not appear to occur in the bottom layer of the Turning Basin but does appear, though small, to occur at R5. Temperature stratification data collected at Rough & Ready Island in May to August, 2002 (Brown, 2003) and analyzed by HydroQual (HydroQual, 2004) also indicate greater surface diurnal changes and lesser bottom changes.

Diurnal DO changes reflect oxygen demanding processes such as sediment oxygen demand, organic algal die off, carbon decay, and nitrification along with oxygen production during the day as a result of algal growth and reaeration. These sources and sinks of DO can have different effects at surface and bottom levels. As algal growth occurs in the upper layers greater diurnal DO changes would be expected in the surface layers. Conversely, SOD would result in lower oxygen levels in bottom layers. The extent to which there are differences in DO levels between surface and bottom is determined by tidal and wind induced mixing. That is to say a system with greater mixing would result in less stratification. The second panels of Figures 42 and 43 present August and September surface and bottom DO in the Turning Basin and at R5. Similar figures for 2001 are in Appendix C. Again diurnal changes are clear in the surface layer and tend to dissipate towards the bottom layers. Surface DO peaks indicate effects of algal growth however what is more interesting is that there appears to be periods in the Turning Basin and at R5 with and with out stratification in the model as well as in the data over the two month period. This is trend is more pronounced in the Turning Basin. This would suggest that a different mixing pattern is occurring in the SJR DWSC at different times.

To examine mixing patterns in the SJR DWSC, temperature and DO data and model results are compared with elevation and wind speed at the Turning Basin and R5 for August and September of 2000 and 2001 using Figures 42 and 43. Shading in elevation panels of Figures 42 and 43 indicate spring tide periods and also tend to coincide with periods of greater stratification. While this is more pronounced in the Turning Basin, this pattern also occurs in the SJR at R5. Wind speed also contributes to stratification but it appears that its effects tend to enhanced or dampened stratification whereas tidal velocity has more influence.

2.4.2.4 Dissolved Oxygen Components

Dissolved oxygen levels in the SJR DWSC are effected by several oxygen sources and demands. Sources of oxygen are from surface reaeration and production during algal photosynthesis. Oxygen demand comes from algal respiration, nitrification, SOD and carbon decay. The 3D water quality model accounts for these oxygen sources and sinks so that at each model layer DO in mg/L-d can be output. As an example, depth profiles of daily average and ranges of oxygen sources and sinks are plotted for July 18, 2000 in the Turning Basin and at station R5 in Figure 44. Reaeration in the surface layer and SOD in the bottom layer are also given.

As expected the model computes algal related DO production in the surface layers and algal related DO demand in the surface and to a lesser degree in the bottom layers for both locations. DO production as a result of photosynthesis approaches 3 mg/L-d maximums in the Turning Basin and R5. Since algal respiration is linked to growth, a range of 0.1 to 0.6 mg/L-d in the surface reflects a daily variation as well. The fourth panel of Figure 44 indicates that nitrification is relatively similar over depth at about 0.1 mg/L-d in both the Turning Basin and R5. Ambient nitrogen is the result of upstream sources, the Stockton RWCF and as previously discussed, sediment fluxes. A slight increase in DO demand from bottom sediment nitrogen flux in the Turning Basin is seen for some of the days (not shown). This can reflect less movement in the Turning Basin as well as increases in sediment fluxes to the water column.

Since the SJR DWSC is generally a mixed system, depth averaged concentrations of the various DO source and demand components can be computed to assess contributions from these components. These calculations were done for the algal growth period of June to November for 2000 and 2001 for the Turning Basin and R5 and results are shown on Figures 45 and 46, respectively.. When oxygen sources and sinks are added, average net oxygen demand at the Turning Basin was 0.34 mg/L-d in 2000 and 0.29 mg/L-d in 2001. At R5 average net oxygen demand was 0.40 mg/L-d in 2000 and 0.30 mg/L-d in 2001. These values are in agreement with average losses of oxygen for similar time periods in 2000 and 2001 of 0.252 mg/L-d and 0.338 mg/L-d reported in Lehman et al., 2004. Model computations indicate that carbon is the greatest source of oxygen demand with 0.36 mg/L-d in 2000 and 0.43 mg/L-d in 2001 at R5. Oxygen demand from nitrification is 0.09 mg/L-d in 2000 and 0.1 mg/L-d in 2001 at R5. SOD exerted a depth averaged demand of 0.06 mg/L-d at R5 for both years. Respiration contributed about 0.05 mg/L-d to oxygen demand at R5.

2.4.3 Model Error Analysis

In order to quantitatively assess the level of model calibration, error analyses were completed. Typically, model calibrations are completed based on a weight of evidence approach. That is, model comparison to observed data is completed with the intent to achieve a best fit of the overall model to data at all monitoring stations for the parameters being analyzed. This approach

balances model comparison to data with the modeler's understanding of the physical, chemical and biological characteristics of the system. Ultimately, the goal of model calibration and validation is "not to curve fit model to data, but to describe the behavior of the data with a modeling framework of the principal mechanisms relevant to the problem" (Thomann, 1982). The following presents quantitative measures of the model goodness of fit.

There are number of measures that can be used to quantitatively assess model goodness of fit. Many of these measures are described in detail along with discussions of overall model verification assessments in a number of journal papers (Thomann, 1982; Ambrose and Roesch, 1982; Reckhow, et al., 1990). The following measures were computed for the SJR error analysis.

Absolute Mean Error, $\overline{E}$: $= \frac{1}{n}\sum_{i=1}^{n}(Y_i - X_i)$;

- Absolute Relative Mean Error: $= \frac{\overline{E}}{\overline{X}}$;
- Standard Error, SE: $= \left[\frac{1}{n}\sum_{i=1}^{n}(Y_i - X_i)^2\right]^{1/2}$;
- Coefficient of Variation, CV: $= \frac{SE}{\overline{X}}$;

where: Y = model, X = data, $\overline{X}$ = average of X, n = number of data points

Table 14 presents the results of the error analyses at several data collection locations in the upper SJR for TSS, conductivity, temperature, DIN (NH_3 and NO_2+NO_3), DIP (PO_4), DO, TOC, DOC, and chlorophyll-a. Daily average model results are compared to data except for DO. Since comparing grab samples of DO to daily average DO would not account for diurnal variations, statistics for DO were computed using average model DO from 8 am to 4 pm. This table presents the number of observations, data and model averages, along with the above statistics. The above statistics indicate model accuracy and precision. The absolute mean error indicates how close, on average the model reproduces the data. The absolute relative mean error normalizes the mean error to the average data. The standard error and coefficient of variation give information on the models ability to capture data variations. Table 14 gives averages of the relative absolute mean errors and CVs, in percent, for the above modeled parameters at Mossdale, R1 to R8, and in the Turning Basin. The average absolute relative mean error is 1.4% for temperature, 3.3% for conductivity, 12% for DIP, 20% for DIN, 41% for chlorophyll-a, 13% for TSS, 28% for TOC, 38% for DOC and 5% for DO. The coefficient of variation is 4% for temperature, 9% for conductivity, 19% for DIP, 33% for DIN, 108% for chlorophyll-a, 56% for TSS, 43% for TOC, 46% for DOC and 15% for DO.

Another way to view model-data comparisons is through probability distributions of model output and observed data. Probability distributions are useful for presenting the mean and variation

of a data set. The method for developing the distribution is to rank the data set from lowest to highest, calculate a percentage for each point (i/n-1) and to plot the transformed data on a probability scale, which implies a normal or log-normal distribution. The x-scale represents the percentage of data that are less than corresponding y-scale value (% less than or equal to) or conversely, 100 minus this percentage represents the percentage of the data exceeding the y-scale value. Probability distributions were computed at the ten data locations (Mossdale, R1 to R8, and in the Turning Basin) for TSS, conductivity, temperature, DIN, DIP, DO, DOC, TOC, and chlorophyll-a. Figures 47 and 48 present probability distributions in the Turning Basin and at R5. The remainder of probability plots are included in the Appendix as Figures C34 to C41. In these figures the model is represented as the filled circles and the data as the open diamonds.

Model DOC in the SJR above the DWSC matches the data but the data tends to be higher than the model in the DWSC. This could signify an external source of DOC such as from the sediment. Otherwise the model output captures the overall variability observed in the data in addition to the mean observed levels for temperature, conductivity DIN, DIP, DO, chlorophyll-a, and TSS.

Table 14. Comparison of Data and Model Results

						Error Statistics			
Parameter	SJR Location	Number of Data Points	Mean Data	Number of Model Points	Mean Model	Mean Error	Relative Mean Error (%)	Standard Error, SE	Coefficient of Variation, CV (%)
Temperature ©	Mossdale	34	22.8	34	22.7	0.14	0.61	0.54	2.36
	R1	51	21.0	51	21.1	0.14	0.65	0.83	3.98
	R2	63	19.7	63	19.8	0.08	0.39	0.85	4.31
	R3	62	20.3	62	20.1	0.18	0.88	0.74	3.66
	R4	63	20.3	63	19.9	0.33	1.65	0.82	4.07
	R5	58	20.2	58	19.6	0.58	2.86	1.12	5.54
	R6	52	21.8	52	21.2	0.61	2.81	0.91	4.18
	R7	51	21.9	51	21.5	0.36	1.65	0.88	4.01
	R8	52	21.5	52	21.7	0.26	1.21	0.94	4.36
	Turning Basin	34	23.3	34	23.7	0.37	1.59	0.79	3.38
						Average:	**1.43**		**3.99**
S. Cond (mS/cm)	Mossdale	34	640.0	34	600.1	39.93	6.24	47.43	7.41
	R1	34	632.2	34	598.1	34.06	5.39	43.56	6.89
	R2	34	589.3	34	611.8	22.51	3.82	56.79	9.64
	R3	68	617.1	68	636.4	19.29	3.13	51.27	8.31
	R4	68	628.3	68	636.8	8.50	1.35	47.42	7.55
	R5	68	632.1	68	635.0	2.96	0.47	48.05	7.60
	R6	68	633.3	68	626.3	7.07	1.12	46.23	7.30
	R7	66	586.1	66	558.7	27.38	4.67	73.57	12.55
	R8	34	389.6	34	417.4	27.72	7.11	60.62	15.56
	Turning Basin	68	639.7	68	640.1	0.48	0.08	73.83	11.54
						Average:	**3.34**		**9.44**
Chl-a (ug/L)	Mossdale	48	31.6	48	36.7	5.11	16.17	25.23	79.79
	R1	34	38.1	34	33.8	4.26	11.19	18.73	49.16
	R2	34	26.2	34	27.3	1.08	4.11	13.10	50.04
	R3	90	16.0	90	18.4	2.40	14.96	11.20	69.91
	R4	87	15.8	87	15.7	0.10	0.63	11.35	71.69
	R5	286	3.4	286	11.9	8.59	256.12	11.92	355.55
	R6	85	9.3	85	9.1	0.22	2.37	6.58	70.59
	R7	125	5.0	125	5.8	0.74	14.80	5.91	117.88
	R8	36	4.9	36	2.7	2.23	45.33	3.90	79.15
	Turning Basin	131	8.0	131	11.5	3.43	42.63	11.34	141.12
						Average:	**40.83**		**108.49**
DO (mg/L)	Mossdale	765	9.7	763	9.3	0.36	3.70	1.07	10.98
	R1	51	8.6	51	8.6	0.05	0.54	1.23	14.42
	R2	63	7.8	63	8.3	0.47	6.07	1.24	15.94
	R3	62	6.7	62	6.9	0.22	3.30	0.94	14.02
	R4	63	6.5	63	6.6	0.14	2.18	0.88	13.51
	R5	63	6.2	63	6.1	0.06	0.96	0.88	14.31
	R6	52	5.6	52	5.3	0.28	5.03	0.84	15.06
	R7	51	6.0	51	5.3	0.67	11.20	1.00	16.75
	R8	52	6.8	52	6.5	0.35	5.08	0.70	10.22
	Turning Basin	34	5.4	34	5.8	0.38	7.01	1.11	20.65
						Average:	**4.51**		**14.59**

Table 14 cont'd. Comparison of Data and Model Results

						Error Statistics			
Parameter	SJR Location	Number of Data Points	Mean Data	Number of Model Points	Mean Model	Mean Error	Relative Mean Error (%)	Standard Error, SE	Coefficient of Variation, CV (%)
DIN (mg/L)	Mossdale	50	1.4	50	1.9	0.52	36.54	1.22	86.31
	R1	34	1.8	34	1.9	0.09	4.75	0.30	16.73
	R2	34	1.8	34	2.1	0.22	11.95	0.41	22.25
	R3	68	2.0	68	2.4	0.40	19.91	0.62	30.67
	R4	68	2.0	68	2.4	0.39	19.23	0.52	25.61
	R5	68	1.9	68	2.3	0.44	23.62	0.55	29.27
	R6	68	1.9	68	2.3	0.40	21.56	0.55	29.47
	R7	66	1.7	66	1.9	0.26	15.81	0.41	24.64
	R8	34	1.0	34	1.2	0.22	21.11	0.35	33.63
	Turning Basin	68	1.8	68	2.3	0.44	24.07	0.60	32.85
						Average:	**19.86**		**33.14**
DIP (mg/L)	Mossdale	17	0.1	17	0.1	0.01	9.94	0.03	26.67
	R1	17	0.1	17	0.1	0.00	3.47	0.02	18.63
	R2	17	0.1	17	0.1	0.03	24.51	0.04	30.87
	R3	34	0.1	34	0.1	0.02	15.88	0.03	19.80
	R4	34	0.1	34	0.1	0.02	13.19	0.02	15.37
	R5	34	0.1	34	0.1	0.01	7.07	0.02	12.37
	R6	34	0.1	34	0.1	0.00	0.84	0.01	8.02
	R7	32	0.1	32	0.1	0.02	13.00	0.02	16.30
	R8	17	0.1	17	0.1	0.01	19.09	0.02	23.30
	Turning Basin	34	0.1	34	0.1	0.01	8.29	0.02	18.06
						Average:	**11.53**		**18.94**
DOC (mg/L)	Mossdale	17	3.4	17	3.0	0.41	11.84	0.72	21.08
	R1	17	3.5	17	2.8	0.78	21.90	1.18	33.28
	R2	17	3.5	17	2.6	0.95	27.16	1.19	34.04
	R3	34	3.6	34	2.2	1.41	39.61	1.63	45.74
	R4	34	3.3	34	2.0	1.31	39.22	1.56	46.67
	R5	34	3.5	34	1.7	1.79	50.70	2.04	57.78
	R6	34	3.4	34	1.6	1.88	54.65	2.22	64.33
	R7	32	3.5	32	1.5	1.94	55.85	2.13	61.21
	R8	17	3.1	17	2.3	0.78	25.14	1.01	32.81
	Turning Basin	34	3.4	34	1.4	1.93	57.11	2.09	61.86
						Average:	**38.32**		**45.88**
TOC (mg/L)	Mossdale	34	3.9	34	4.7	0.75	19.05	1.21	30.54
	R1	34	4.0	34	4.4	0.37	9.26	0.90	22.57
	R2	34	4.1	34	4.0	0.13	3.25	1.07	26.15
	R3	68	4.3	68	3.3	0.98	22.98	1.62	37.98
	R4	68	4.1	68	3.0	1.12	27.30	1.80	43.87
	R5	68	4.2	68	2.5	1.66	39.67	2.27	54.36
	R6	68	4.1	68	2.2	1.89	46.39	2.48	60.82
	R7	66	4.1	66	2.1	2.02	48.89	2.41	58.24
	R8	34	3.4	34	2.7	0.75	21.94	1.29	37.61
	Turning Basin	68	4.1	68	2.3	1.72	42.30	2.32	57.06
						Average:	**28.10**		**42.92**
TSS (mg/L)	Mossdale	34	35.0	34	53.1	18.09	51.72	20.25	57.92
	R1	34	48.1	34	51.6	3.47	7.21	19.11	39.70
	R2	34	50.5	34	45.5	4.98	9.86	23.79	47.14
	R3	85	34.6	85	36.4	1.79	5.18	16.99	49.13
	R4	85	36.2	85	33.5	2.65	7.34	25.94	71.74
	R5	85	29.4	85	31.0	1.55	5.28	15.33	52.13
	R6	85	26.4	85	27.3	0.93	3.52	11.97	45.37
	R7	83	22.8	83	20.5	2.34	10.27	10.80	47.39
	R8	34	15.8	34	15.4	0.40	2.54	5.62	35.68
	Turning Basin	85	17.6	85	23.1	5.51	31.25	19.45	110.26
						Average:	**13.42**		**55.65**

SECTION 3

SUMMARY AND CONCLUSIONS

The model calibration presented in this report is the result of many hydrodynamic, and coupled water quality and sediment model runs. Model runs were made to obtain a consistent set of model coefficients that are reasonable and reproduce the observed data for all the state-variables considered. The SJR from Vernalis through the DWSC represents a system with 2 distinct characteristics. Upstream of the DWSC, the SJR is shallow and narrow resulting in greater flows. There is less time for instream processes such as algal die off and carbon decay to negatively impact oxygen levels. Upon entering the DWSC, flows decrease due to geometry changes and organic material originating from upstream sources that have been carried through the river can negatively impact oxygen in the river. In addition algal growth in the DWSC also impacts DO in the DWSC. All of these processes appear to be affected by the tides.

An important aspect in developing the model is that the forcing functions, constants and rates in the model generally represent the true nature of the SJR and that the data used for model versus data comparisons are representative of the conditions in the SJR. The inputs and forcings in this model were taken from a number of sources over the 2 year calibration period so that it is believed that the true nature of mechanisms in the SJR have been applied. It has been shown that the varying characteristics of SJR between Vernalis and in the DWSC have been captured in this modeling effort through model comparisons to data.

The hydrodynamic model simulates tidal flows for the 2000-2001 period showing a tidal signal that extends to Vernalis, though its main effect is in the DWSC. Velocities in the DWSC at R3 are about half of those in the USJR showing the impact of geometry changes as flows enter the DWSC. Velocities in the Turning Basin are significantly reduced showing yet another unique feature of the system. Surface velocities throughout the DWSC are greater than bottom velocities reflecting bottom shear stresses.

Studies by others as well as this model indicate that there is significant settling of solids, POM, and algae as river waters enter the DWSC were the river deepens and widens. Model simulations of TSS show that deposition and resuspension represented as net settling in the model are able to reproduce the data. This is important as the water quality model was amended to compute light limitation for algal growth based on TSS. Analyses of TSS, secchi depth, and chlorophyll-a levels were done to formulate an equation to compute solids based algal light limited growth.

Nutrient levels throughout the study area are in ample supply to support chlorophyll-a growth. Nutrients in the study area originate from upstream agricultural sources, the Stockton RWCF, algal recycling and sediment sources. This modeling effort has shown that, indirectly in

supporting algal growth and directly through nitrification, nutrients contribute to an oxygen demand in the DWSC. The model is also able to simulate nutrients in the study area including the significant ammonia load from the Stockton RWCF.

Temporal and spatial profiles of simulated DO reproduce the data fairly well. DO levels are supersaturated in the SJR from Vernalis to Mossdale and at a deficit below Mossdale and through the DWSC. Summer and fall data and model DO concentrations are below the applicable water quality objectives of 5 mg/L December to August and 6 mg/L from September through November to protect migrating fall-run Chinook salmon. Vertical profiles of temperature indicate very little to no stratification in the DWSC. This indicates a generally well mixed system. Vertical profiles of DO indicate periods of stratification and no stratification in the Turning Basin but no stratification in the remainder of the DWSC. This indicates that lower velocities in the Turning Basin allow for components of oxygen demand to have an impact due to greater retention time. Instream carbon concentrations originate from upstream loads, instream algal die off and a carbon load from the Stockton RWCF. The model is able to simulate the decay of organic material in the water column as well as in the sediment, both resulting in oxygen demand in the water column.

Based on the application of reasonable model inputs and good comparisons to 2 years of data it is believed that this model can be used to assess management strategies. Some management strategies that can be considered would be to increase flow to the DWSC during the summer, to eliminate the Stockton RWCF load to determine impacts of RWCF nutrients, to simulate DO levels under aeration scenarios in the DWSC. It has been suggested that flow diversions at the HOR resulting in flows less than 1,500 cfs can lead to DO violations in the DWSC during late summer and early fall. (Lee, 2004). The impact of the planned installation of a tidal gate at the HOR in the DWSC can be simulated using HydroQual's 3D hydrodynamic and water quality model. This model can be used to simulate water quality conditions under varying flow diversions at the HOR It is expected that by limiting flow diversions to the HOR during summer and early fall DO levels show not go below the applicable water quality objectives. Nutrient loads, especially ammonia, from the Stockton RWCF can add significantly to nutrient levels in the USJR in the vicinity of the RWCF and in the DWSC. The impact of these loads on oxygen levels through allowing algal growth and by nitrification could be assessed. It is thought that ammonia from the RWCF is a major contributing factor to oxygen demand in the DWSC (Lehman, 2004). The model can be used to project algal growth and oxygen levels with the Stockton RWCF loads removed. Another important task underway is the installation of aeration devices in the DWSC in the vicinity of Rough and Ready Island. The model can be used to simulate oxygen levels under various aeration scenarios.

SECTION 4

REFERENCES

Ambrose, R.B. and S.E. Roesch, 1982. Dynamic Estuary Model Performance. Journal of Environmental Engineering, Vol. 108, pp. 51-71.

Ahsan, Q., and A. F. Blumberg, 1999. A Three-Dimensional Hydrothermal Model of Onondaga Lake, New York, Journal of Hydraulics, Vol. 125, No. 9, September 1999, ASCE.

Banks, R. B. 1975. Some Features of Wind Action on Shallow Lakes. Journal of the Environmental Engineering Division. ASCE, Vol. 101, No. EE5, Proc. Paper 11640, Oct., 1975, pp. 813-827.

Banks, R. B. , Herrera, F. F. 1977. Effect of Wnd and Rain on Surface Reaeration. Journal of the Environmental Engineering Division. ASCE, Vol. 103, No. EE3, Proc. Paper 13013, June, 1977, pp. 489-504.

Beeton, A.M. 1958. Relationship Between Secchi Disk Readings and Light Penetration in Lake Huron, *American Fisheries Society Trans*. 87:73-79.

Brown, R. T.. 2003. Evaluation of Aeration Technology for the Stockton Deep Water Ship Channel. Principle Investigator: Dr. Russ T. Brown, Jones & Stokes. Report to CALFED Bay-Delta Program. CALFED Project No. 01-N61-05.

Brown, L.C., and Barnwell, T.O. 1987. The Enhanced Stream Water Quality Models QUAL2E and QUAL2E-UNCAS, EPA/600/3-87-007, U.S. Environmental Protection Agency, Athens, GA, 189 pp.

Blumberg, A. F. and D. M. Goodrich, 1990. Modeling of Wind-Induced Destratification in Chesapeake Bay, Estuaries, Vol. 13, No. 3, 236-249.

Blumberg, A. F. and N. Kim, 2001. Flow Balances in St. Andrew Bay Revealed Through Hydrodynamic Simulations, Estuaries, Vol. 23, No. 1, 21-23.

Blumberg, A. F., and G. Mellor, 1985. A Simulation of the Circulation in the Gulf of Mexico, Israel Journal of Earth Sciences, Vol. 34, 122-144.

Blumberg, A.F., and G. L. Mellor. 1987. A Description of a Three-Dimensional Coastal Ocean Circulation Model. Three-dimensional coastal ocean models, N.S. Heaps, ed., American Geophysical Union, Washington, D.C., 1-16.

Blumberg, A. F., L. A. Khan and J. P. St. John, 1999. Three-Dimensional Hydrodynamic Model of New York harbor Region, Journal of Hydraulic Engineering, Vol. 125, No. 8, August 1999.

Blumberg, A. F., D. J. Dunning, H. Li, D. Heimbuch and W. R. Geyer, 2004. Use of a Particle-tracking Model for Predicting Entrainment at Power Plants on the Hudson River, Estuaries, Vol. 27, No. 3, 515-526.

Chapra, S. C. 1997. *Surface Water-Quality Modeling*, McGraw-Hill, New York.

Di Toro, D.M. 1978. Optics of Turbid Estuarine Waters: Approximations and Applications, *Water Research* 12:1059-1068.

Dahlgren, R. C. 2004. University of California at Davis (UCD), detailed sampling along the SJR and tributaries from water year 2000 to the present. Funded by the U.S. Fish and Wildlife Service.

Galperin, B., L. H. Kantha, S. Hassid and A. Rosati, 1988. A Quasi-Equilibrium Turbulent Energy Model for Geophysical Flows. Journal of Atmospheric Science, 45, 55-62.

HydroQual, Inc., 1987. "A Steady State Coupled Hydrodynamic/Water Quality Model of the Eutrophication and Anoxia Process in Chesapeake Bay," prepared for the USEPA Chesapeake Bay Program, Mahwah, New Jersey.

HydroQual, Inc., 1989. "Development and Calibration of a Coupled Hydrodynamic/Water Quality/Sediment Model of Chesapeake Bay," prepared for the USEPA Chesapeake Bay Program, Mahwah, New Jersey.

HydroQual, Inc., 1991. "Water Quality Modeling Analysis of Hypoxia in Long Island Sound," prepared for the Management Committee Long Island Sound Study and New England Interstate Water Pollution Control Commission, Mahwah, New Jersey.

HydroQual, Inc., 1992. "Elevenmile Creek and Perdido Bay Modeling Analysis," prepared for Champion International Corporation, Mahwah, New Jersey.

HydroQual, 2005. San Joaquin River Dissolved Oxygen Depletion Modeling, Task 5 Final Report – 1D Water Quality Calibration 2000 – 2001. Prepared for GCAP Services for the CALFED Bay – Delta Program/California Bay – Delta Authority (CBDA) Sacramento, CA. ERP-02D-P50.

HydroQual, 2004. A Primer for ECOMSED. HydroQual, Inc., Mahwah, New Jersey, pp 1-194.

Jones & Stokes, 2002. Stockton Deep Water Ship Channel Tidal Hydraulics and Downstream Tidal Exchange. Prepared for CALFED Bay-Delta Program.

Kratzer, C.R., Dileanis, P.D., Zamora, C., Silva, S.R., Kendall, C., Bergamaschi, B.A., and Dahlgren, R.A. 2004. Sources and Transport of Nutrients, Organic Carbon, and Chlorophyll-a in the San Joaquin River Upstream of Vernalis, California, during Summer and Fall, 2000 and 2001. U.S. Geological Survey, Water-Resources Investigations Report 03-4127. Prepared in

cooperation with CALFED Bay-Delta Program and CA. Dept. of Water Resources. Sacramento CA.

Lee, G.F. and Jones-Lee, Anne. 2005. Impact of SJR $ South Delta Flow Diversions on Water Quality. Presentation to the CA Water Resources Control Board, D1641 Water Rights Review, January 2005.

Lehman, 2005. Personal Communication.

Lehman, P.W., Sevier, J., Giulianotti, J. and Johnson, M. 2004. Sources of Oxygen Demand in the Lower San Joaquin River, California. Estuaries, Vol. 27, N0. 3, p. 405-418.

Litton, G.M. 2003. Deposition Rates and Oxygen Demands in the Stockton Deep Water Ship Channel of the San Joaquin River, June-November 2001. Prepared for the San Joaquin Dissolved Oxygen TMDL Steering Committee and CALFED.

Mellor, G. L. and T. Ezer, 1991. A Gulf Stream Model and an Altimetry Assimilation Scheme, Journal of Geophysical Research, Vol. 96, 8779-8797.

Mellor, G. L. and A. F. Blumberg, 1985. Modeling Vertical and Horizontal Viscosity and the Sigma Coordinate System. Monthly Weather Review, 113, 1379-1383.

Mellor, G. L. and T. Yamada, 1982, Development of a Turbulence Closure Model for Geophysical Fluid Problems, Rev. Geophys. Space Phys., 20, 851-875.

Reckhow, K.H., J.T. Clements and R.C. Dodd, 1990. Statistical Evaluation of Mechanistic Water-Quality Models. Journal of Environmental Engineering, Vol. 116, pp. 250-268.

Redfield, A.C., Ketchum, B.H. and Richards, F.A. 1963. The Influence of Organisms on the Composition of Seawater, in *The Sea*, M.N. Hill, ed. Vol. 2, pp. 27-46, Wiley-Interscience, NY.

Riley, G.A. 1956. Oceanography of Long Island Sound 1952-1954. II. Physical Oceanography, Bulletin Bingham. Oceanog. Collection 15, pp. 15-46.

Smagorinsky, J., 1963. General Circulation Experiments with the Primitive Equations, I, The Basic Experiment, Monthly Weather Review, 91, 99-164.

Sverdrup, H.U., M.W. Johnson, and R.H. Fleming. 1942. The Oceans, Prentice-Hall, Englewood Cliffs, NJ, 1087pp.

Thomann, R.V. and J. A. Mueller, 1987. Principles of Surface Water Quality Modeling and Control, Harper & Row, Publishers, Inc.

Thomann, R.V., 1982. Verification of Water Quality Models. Journal of Environmental Engineering, Vol. 108, pp. 923-940.

FIGURES

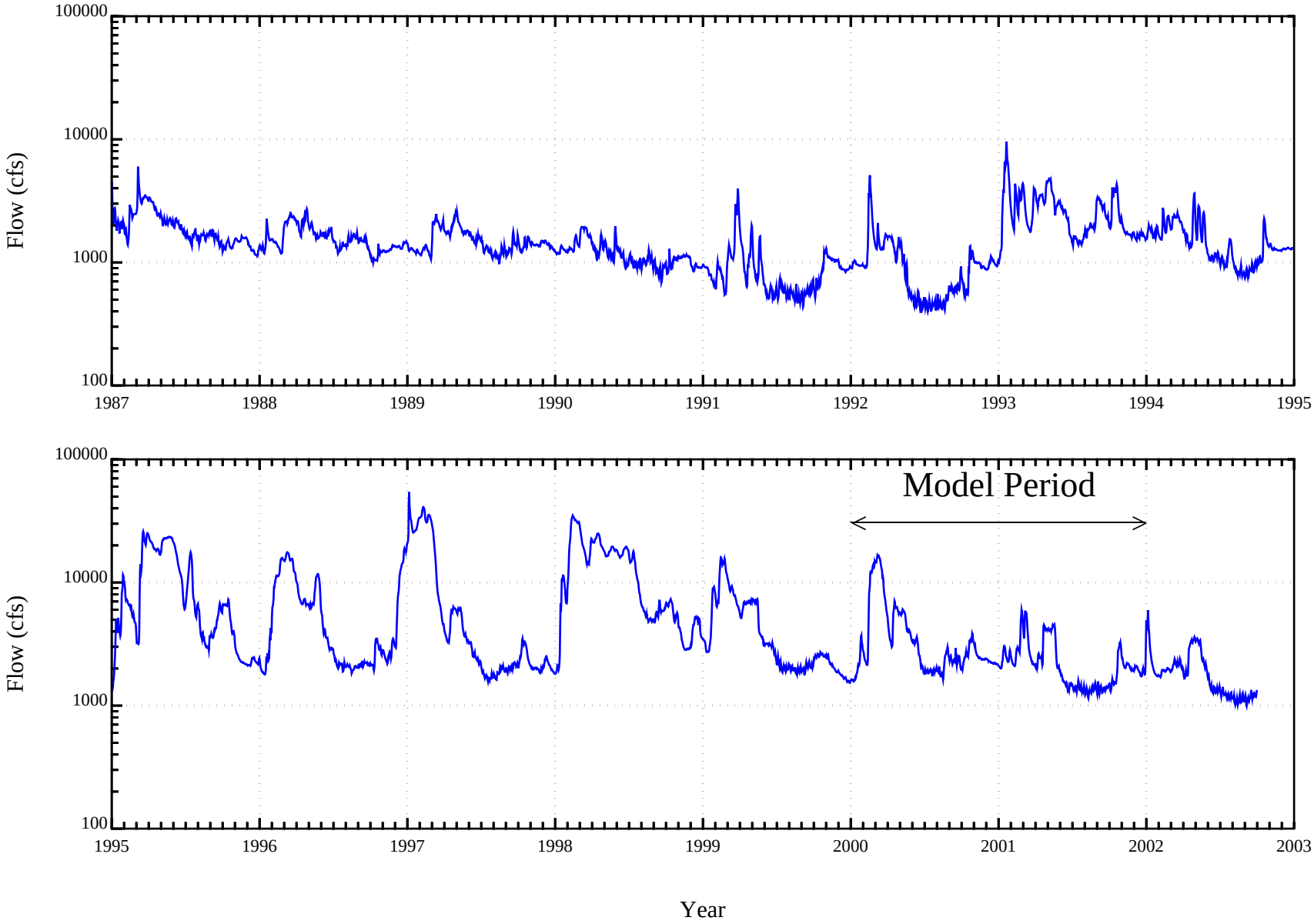

Figure 1. USGS Flow near Vernalis, CA (Gage #11303500)

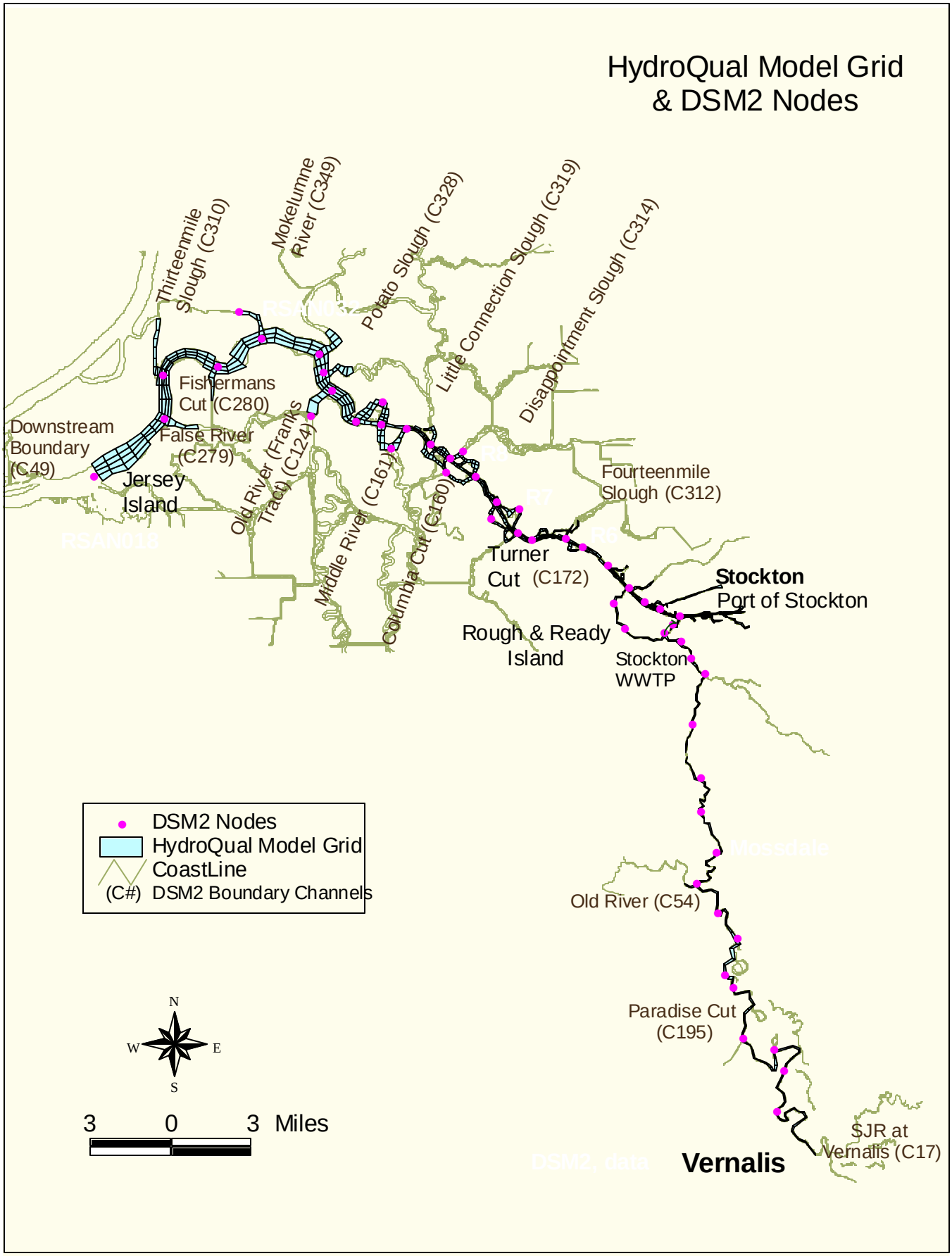

Figure 2. HydroQual 3D Hydrodynamic and Water Quality Model Grid and DSM2 Nodes

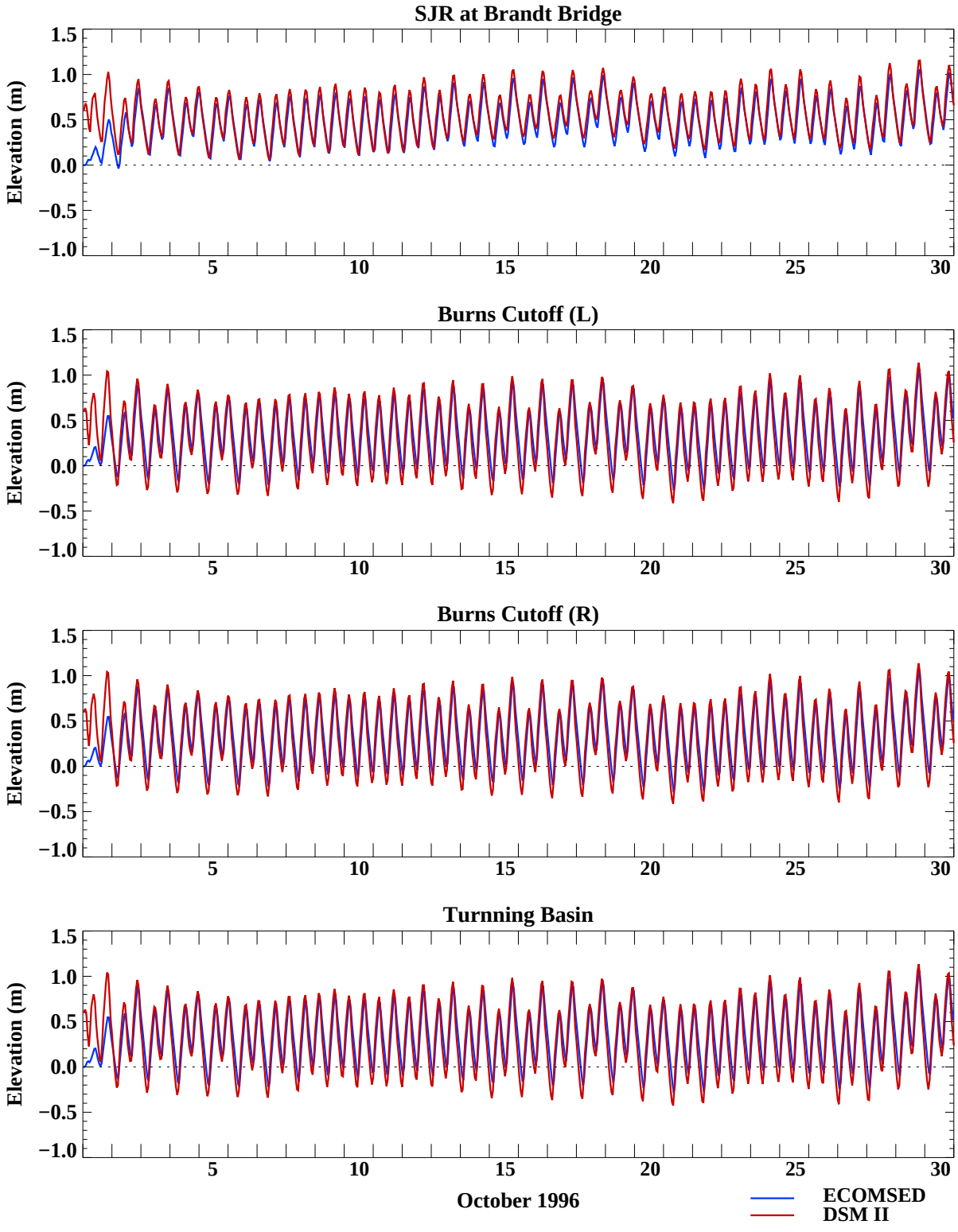

Figure 3. Comparison of ECOMSED and DSM2 Water Surface Elevations in the San Joaquin River, October 1996

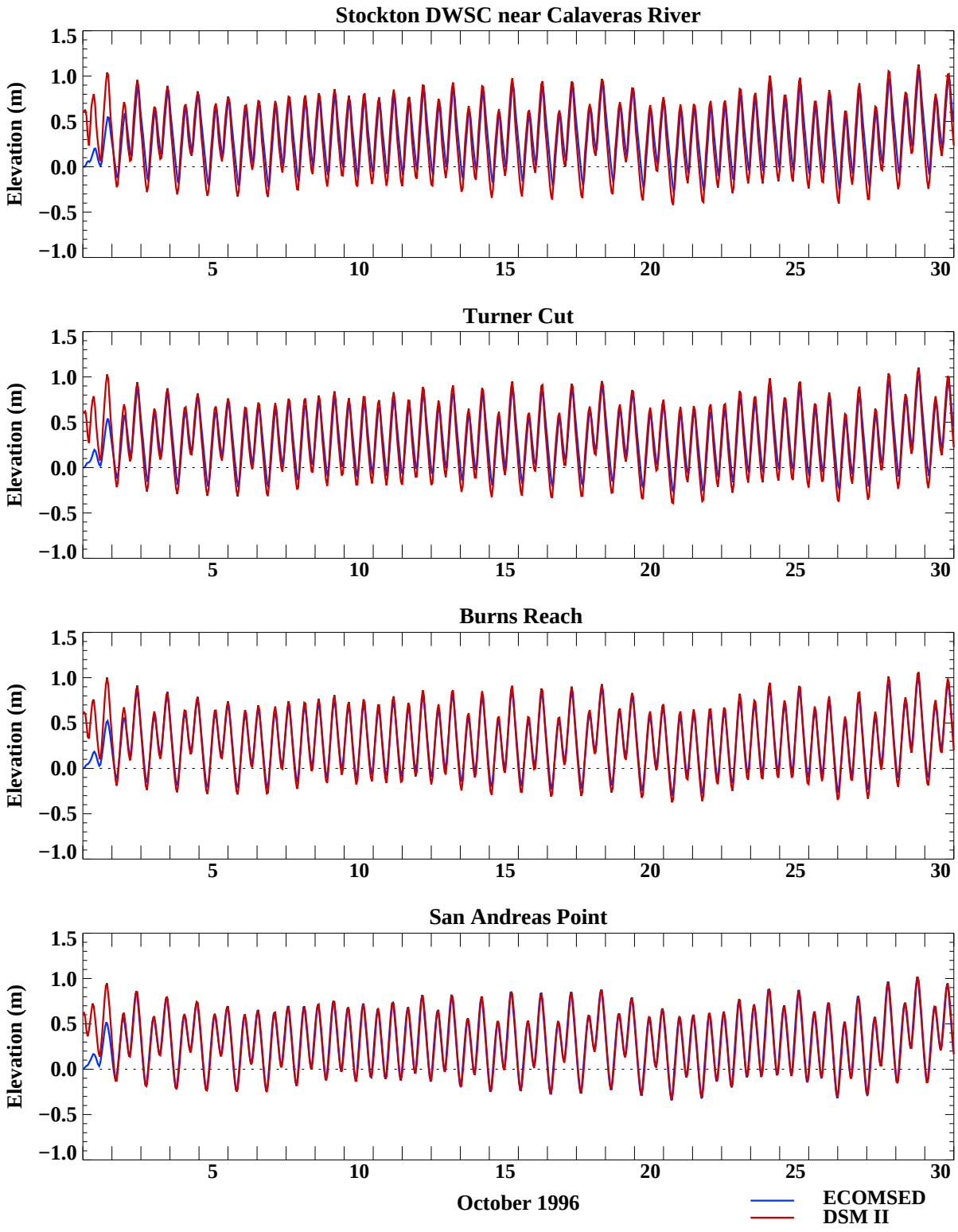

Figure 3. (Continued) Comparison of ECOMSED and DSM2 Water Surface Elevations in the San Joaquin River, October 1996

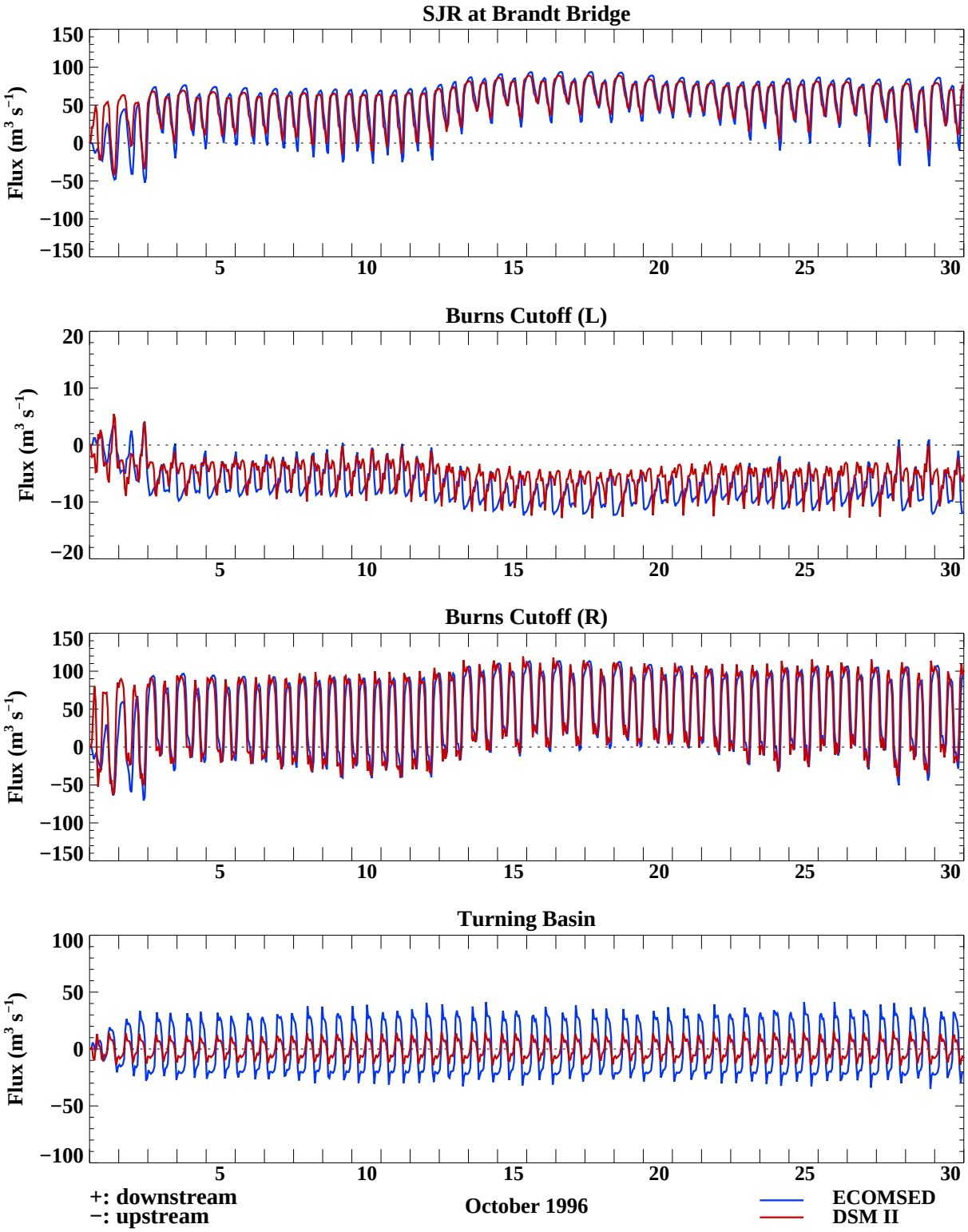

Figure 4. Comparison of ECOMSED and DSM2 Flux in the San Joaquin River, October 1996

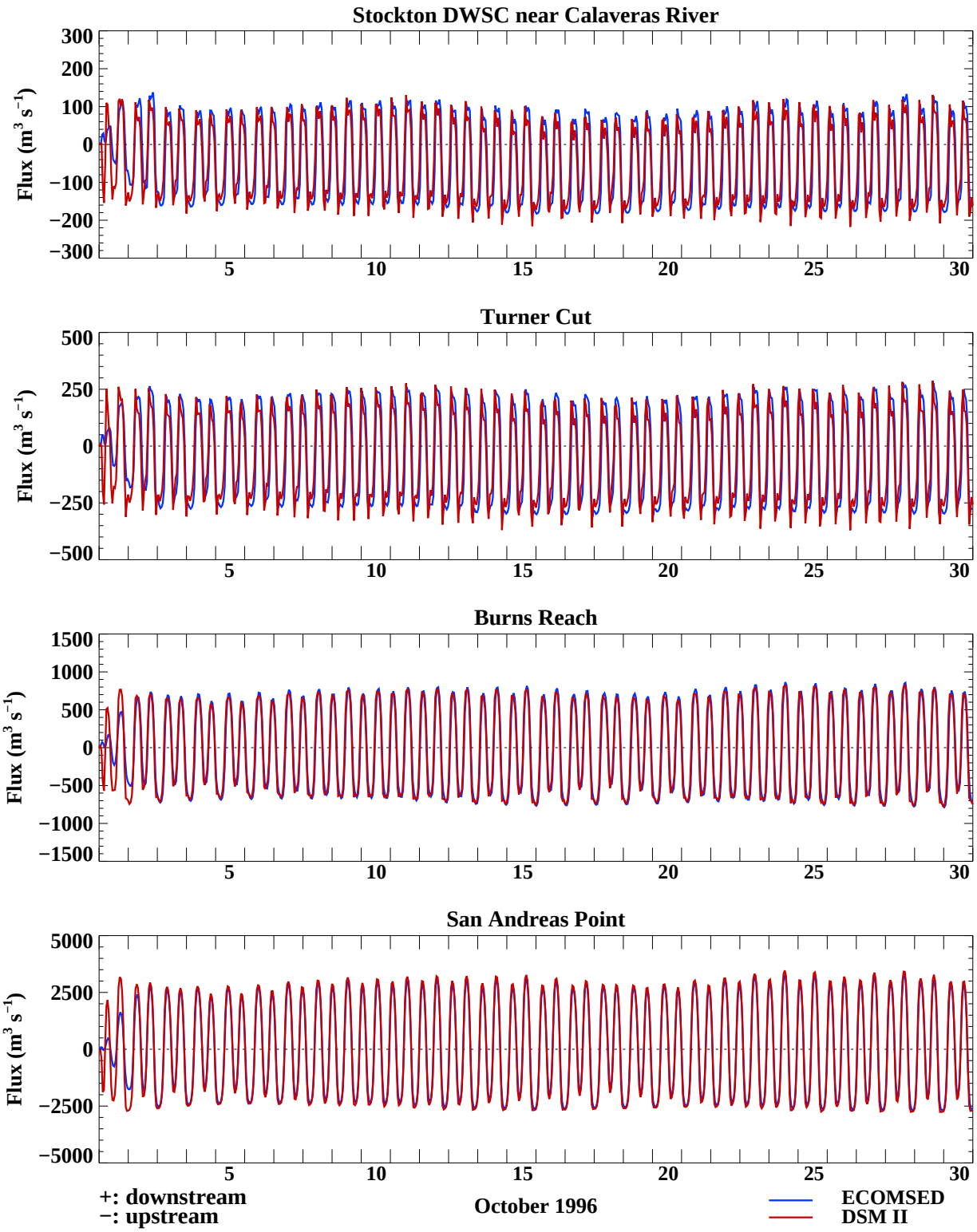

Figure 4. (Continued) Comparison of ECOMSED and DSM2 Flux in the San Joaquin River, October 1996

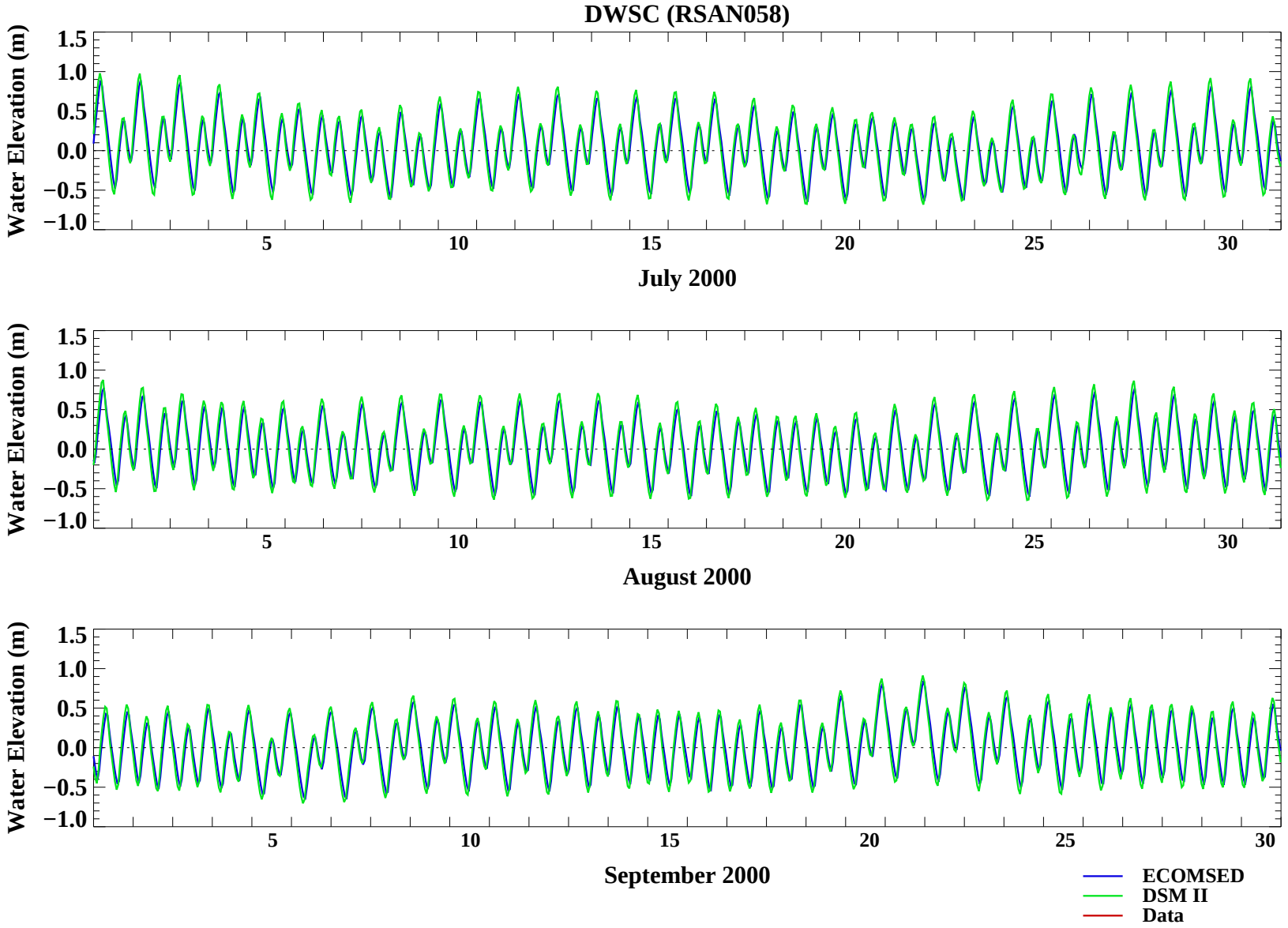

Figure 5A. Comparison of ECOMSED, DSM2, and Data Water Surface Elevations in the San Joaquin River DWSC Near R5, July to September, 2000

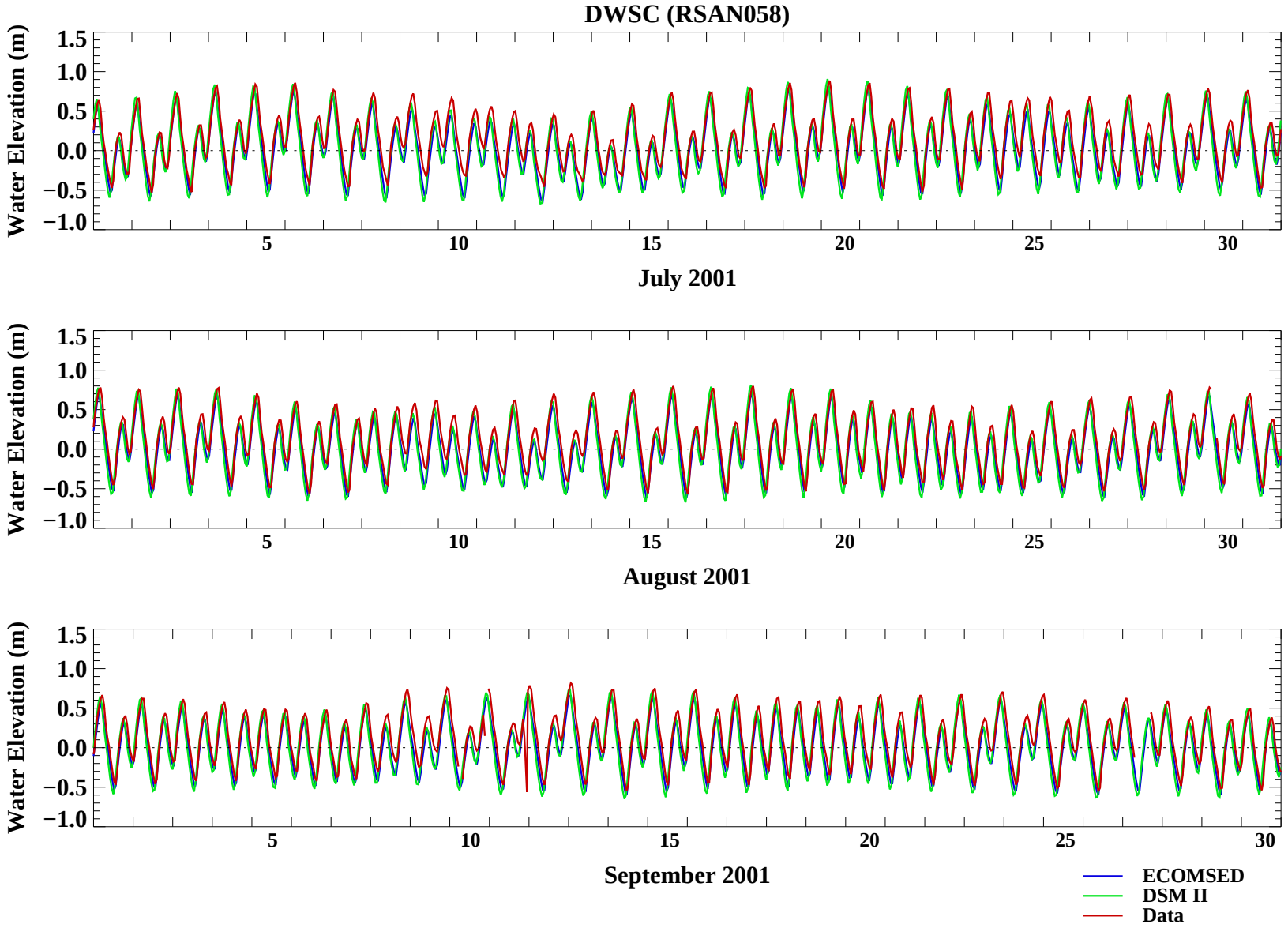

Figure 5B. Comparison of ECOMSED, DSM2, and Data Water Surface Elevations in the San Joaquin River DWSC Near R5, July to September, 2001

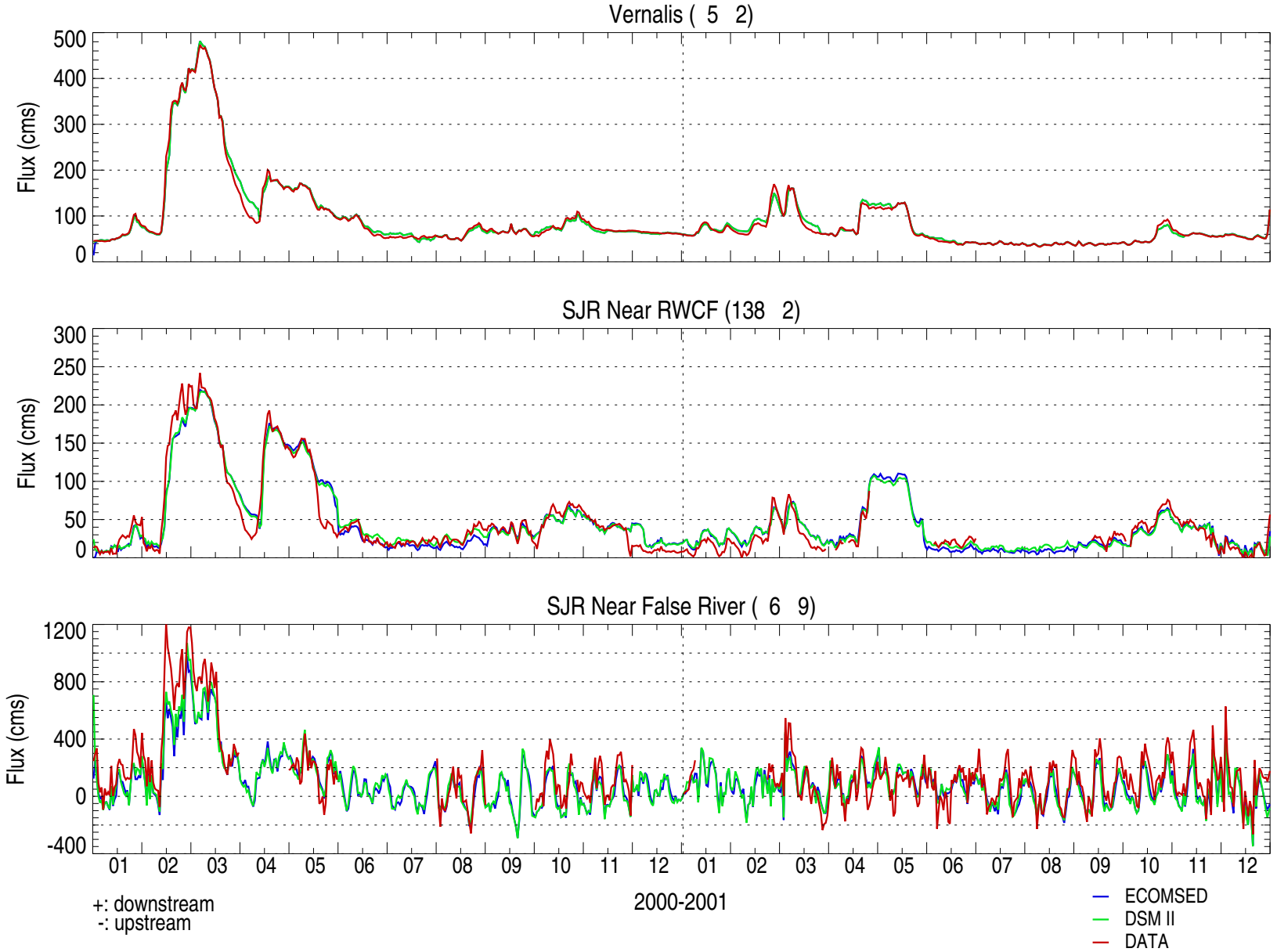

Figure 6. Comparison of ECOMSED, DSM2, and Data Water Surface Fluxes in the San Joaquin River at Vernalis, Stockton RWCF, and False River, 2000 and 2001

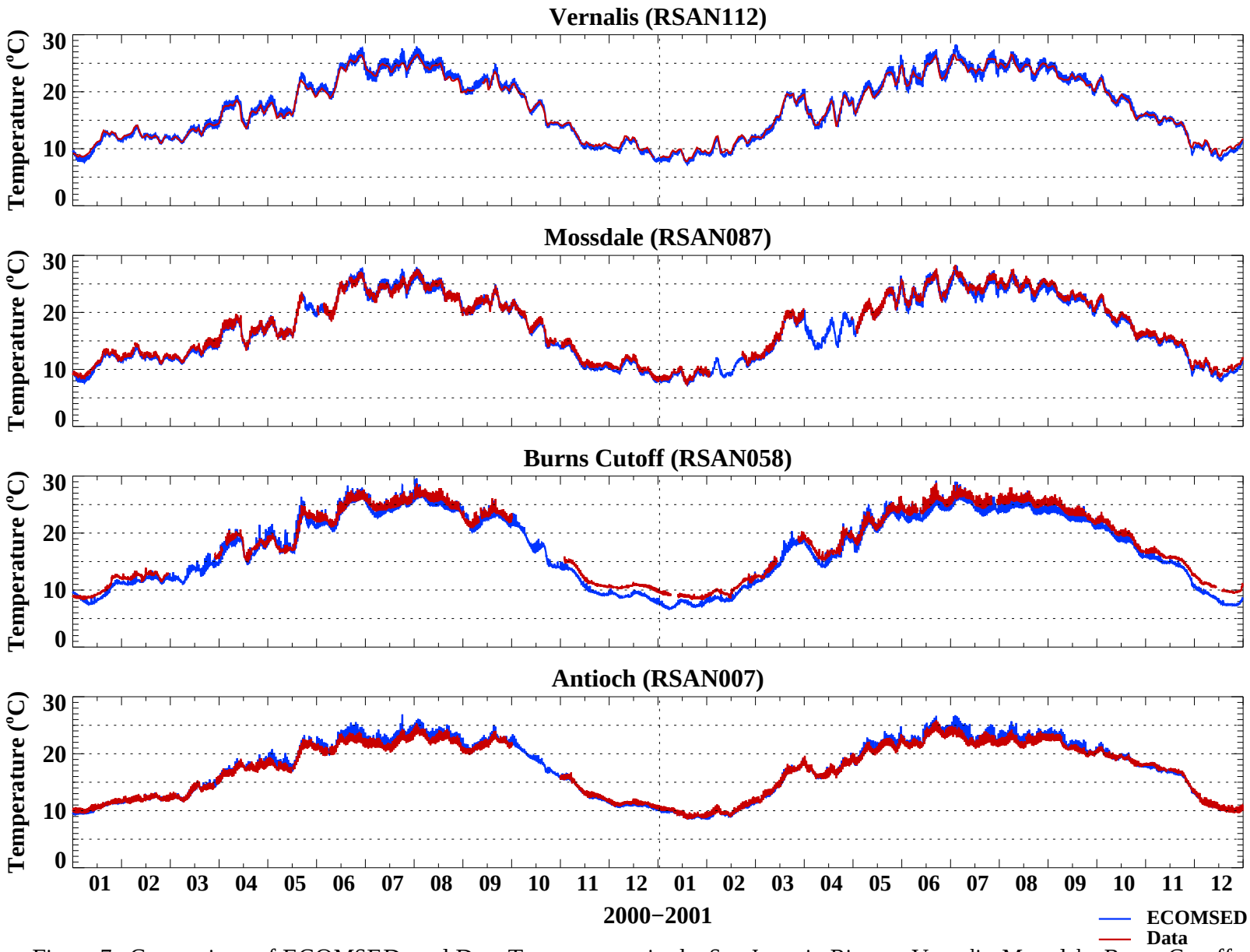

Figure 7. Comparison of ECOMSED, and Data Temperatures in the San Joaquin River at Vernalis, Mossdale, Burns Cutoff, and Antioch, 2000 and 2001

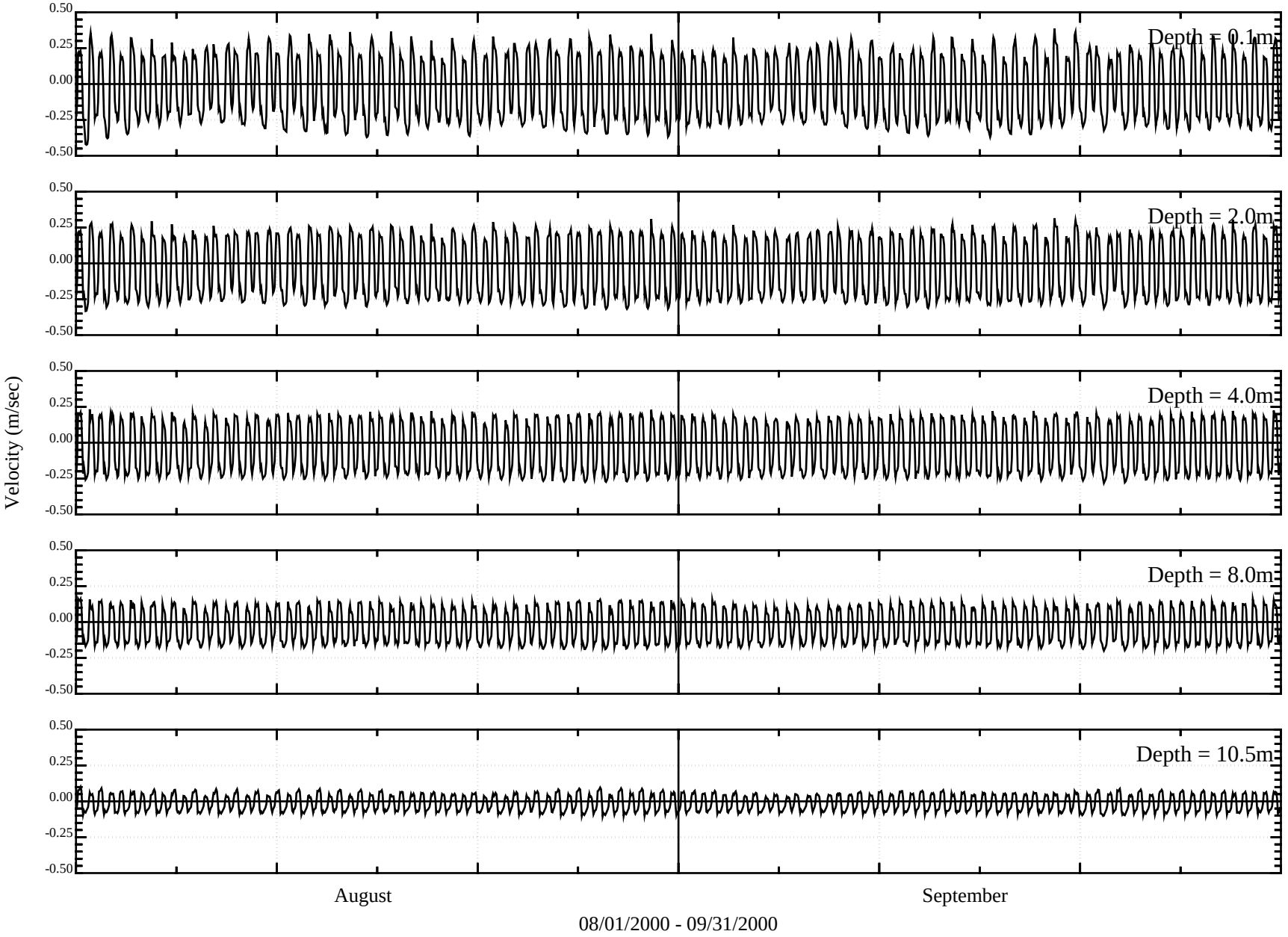

Figure 8. Simulated Velocity Profiles in the San Joaquin River DWSC Downstream of R5, August to September, 2000

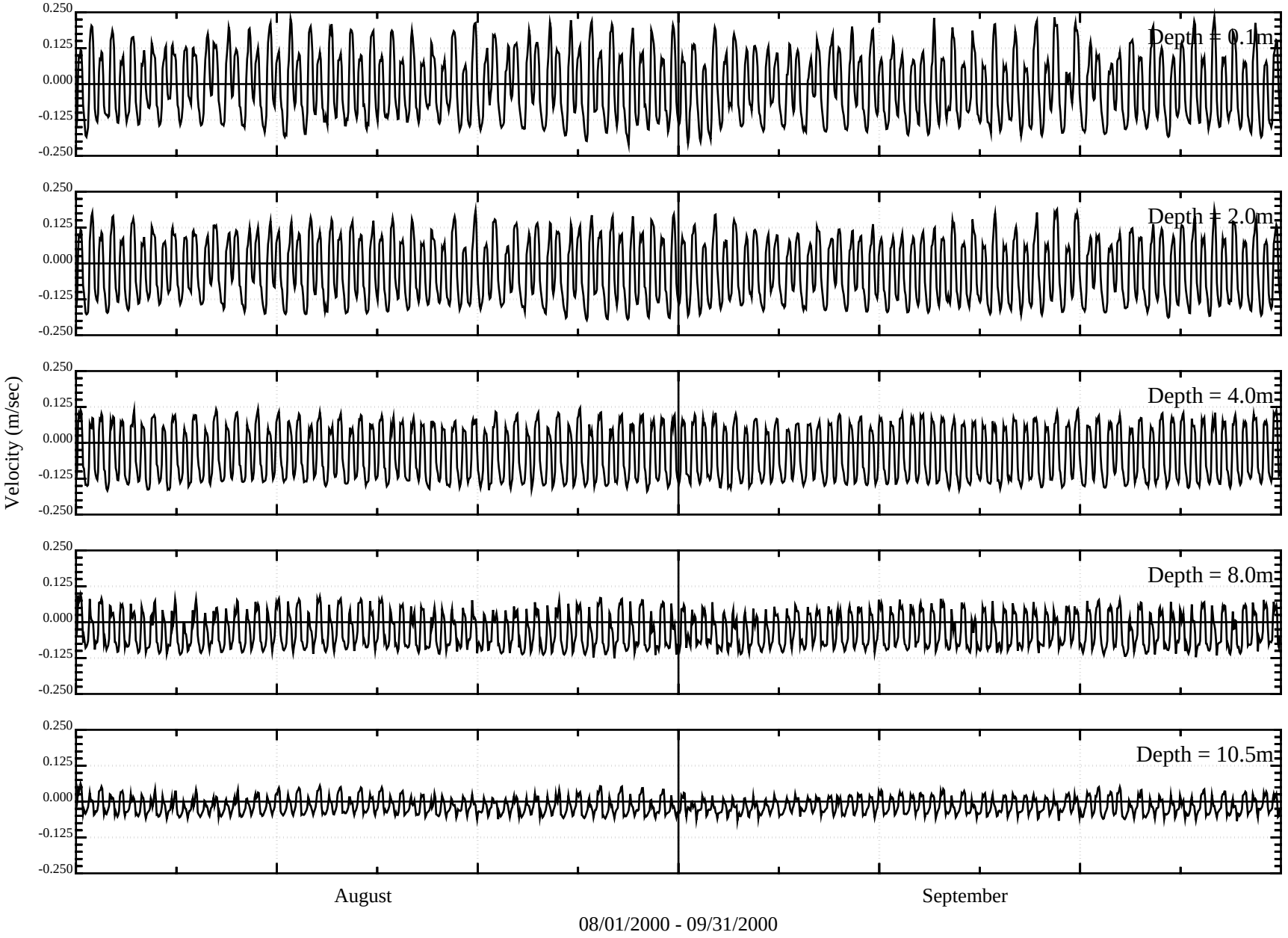

Figure 9. Simulated Velocity Profiles in the San Joaquin River DWSC at R3, Light 48, August to September, 2000

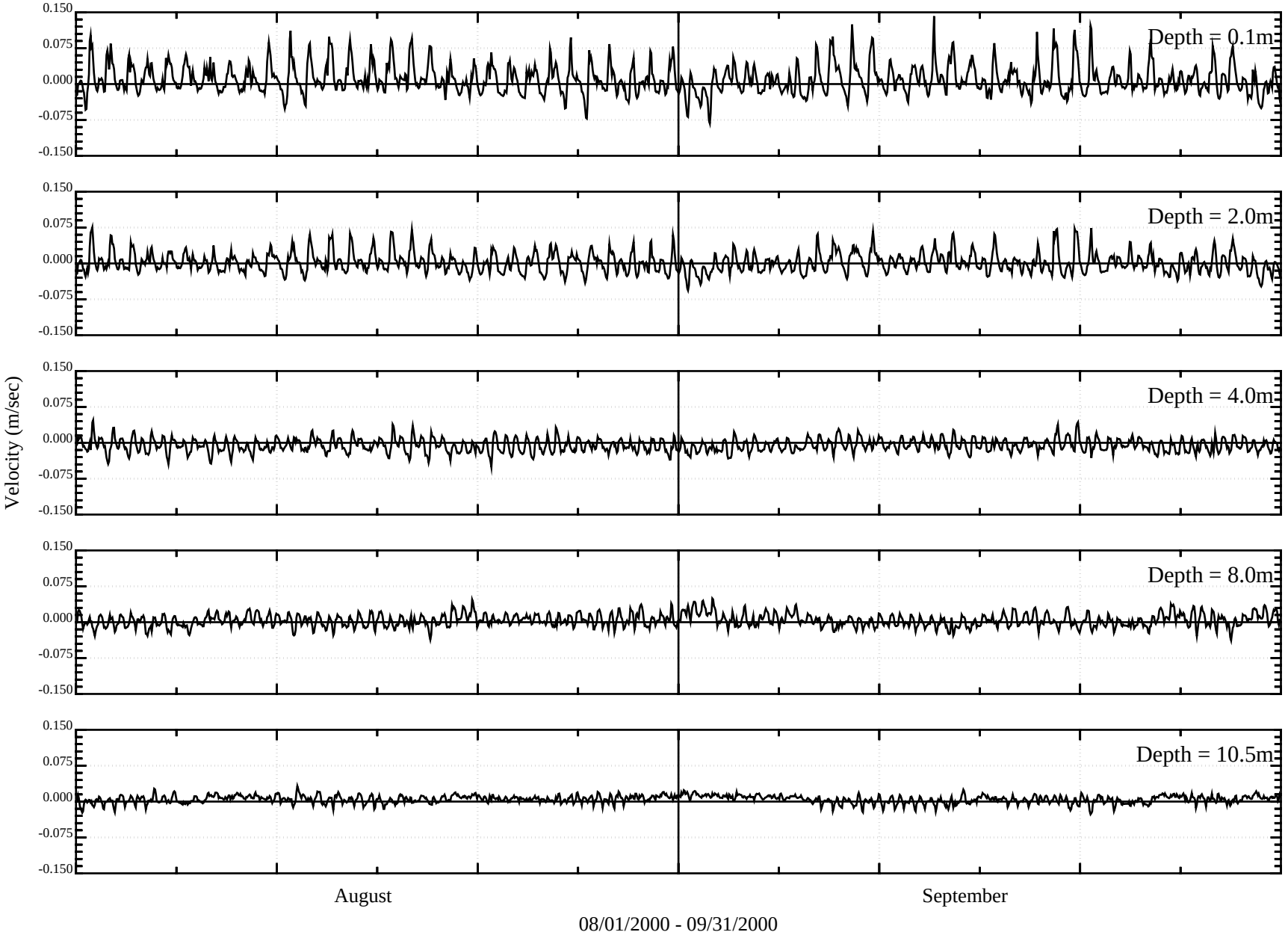

Figure 10. Simulated Velocity Profiles in the San Joaquin River DWSC in the Turning Basin, August to September, 2000

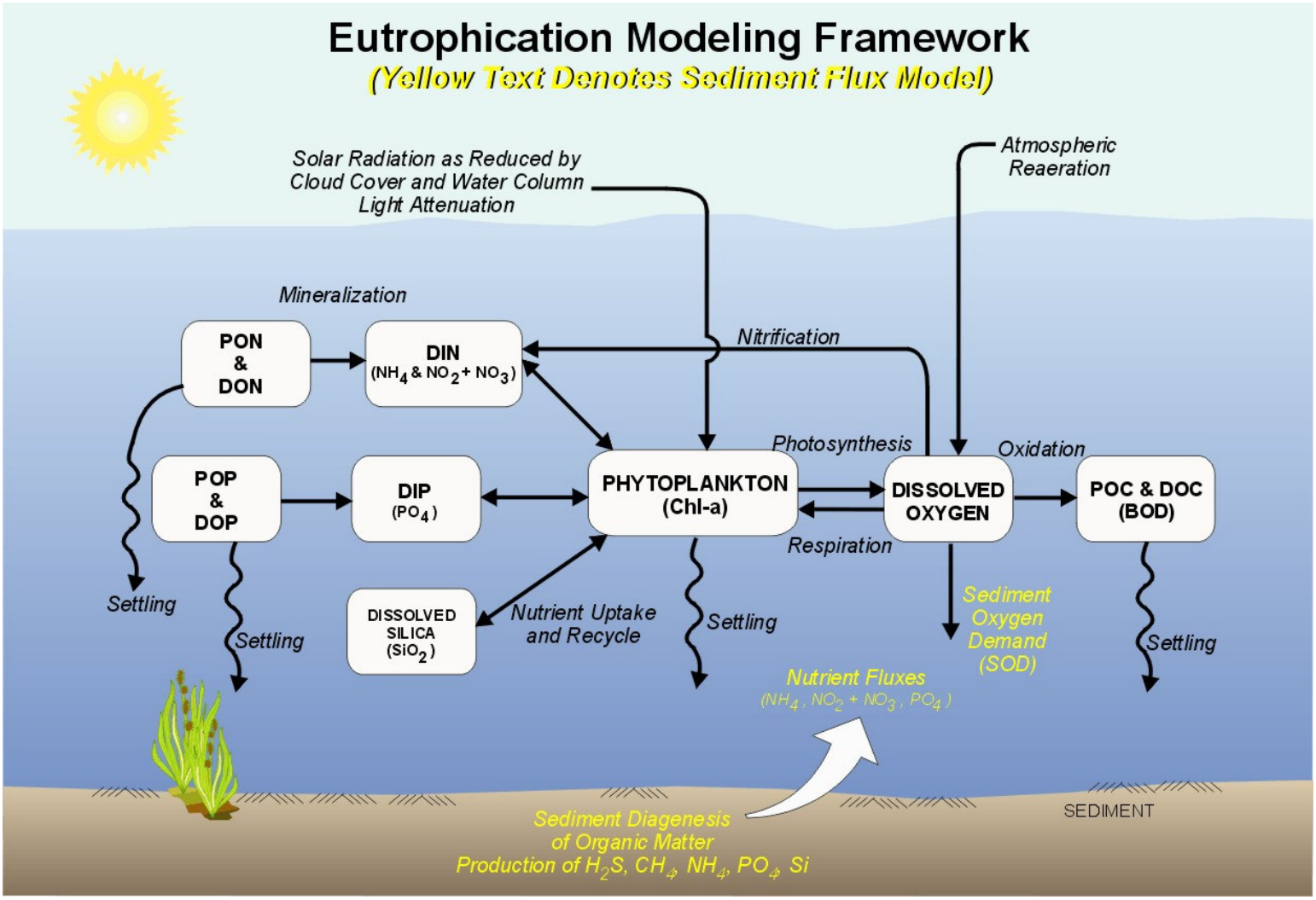

Figure 11. Principal Kinetic Interactions for Nutrient Cycles and Dissolved Oxygen

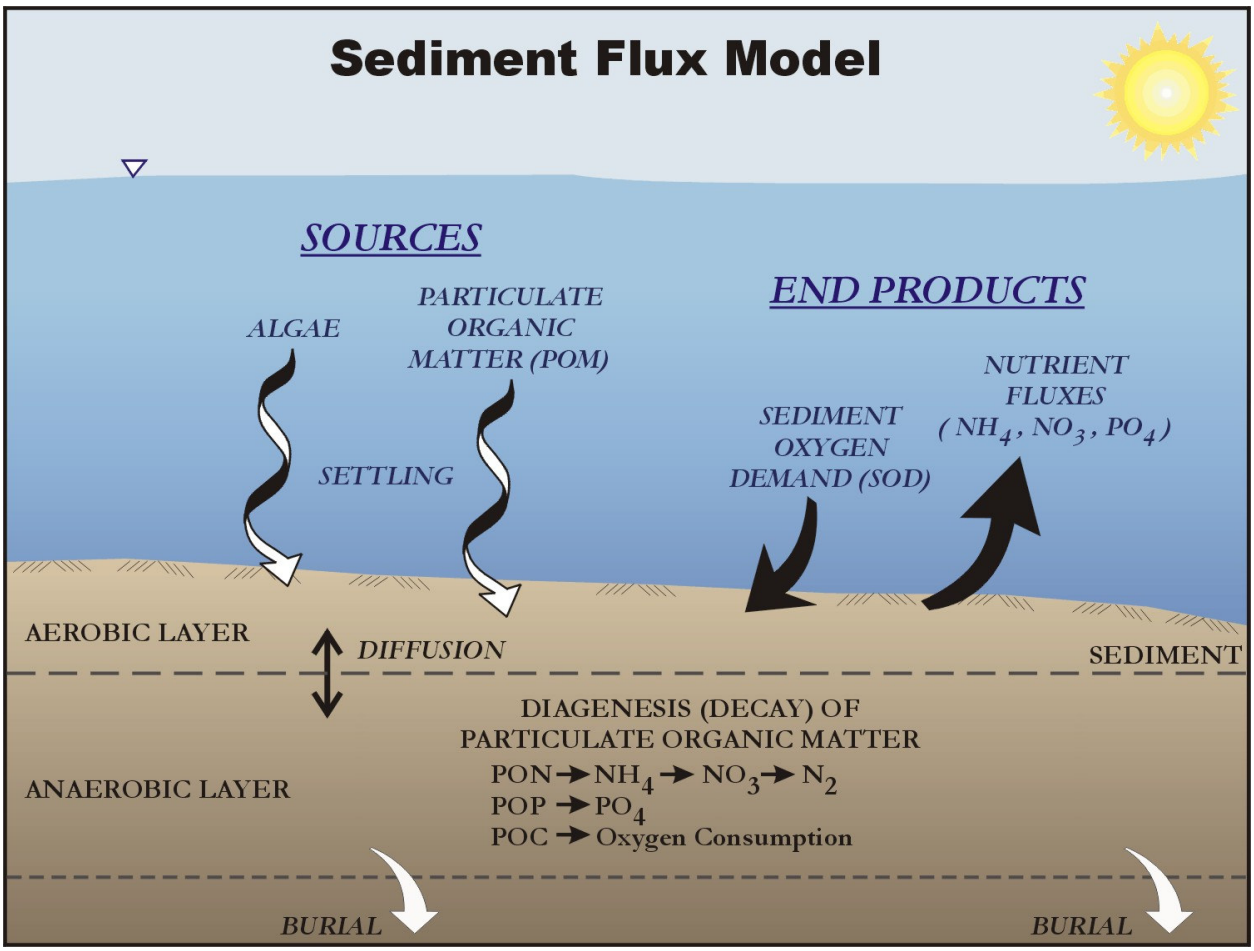

Figure12. Sediment Flux Submodel Kinetic Interactions

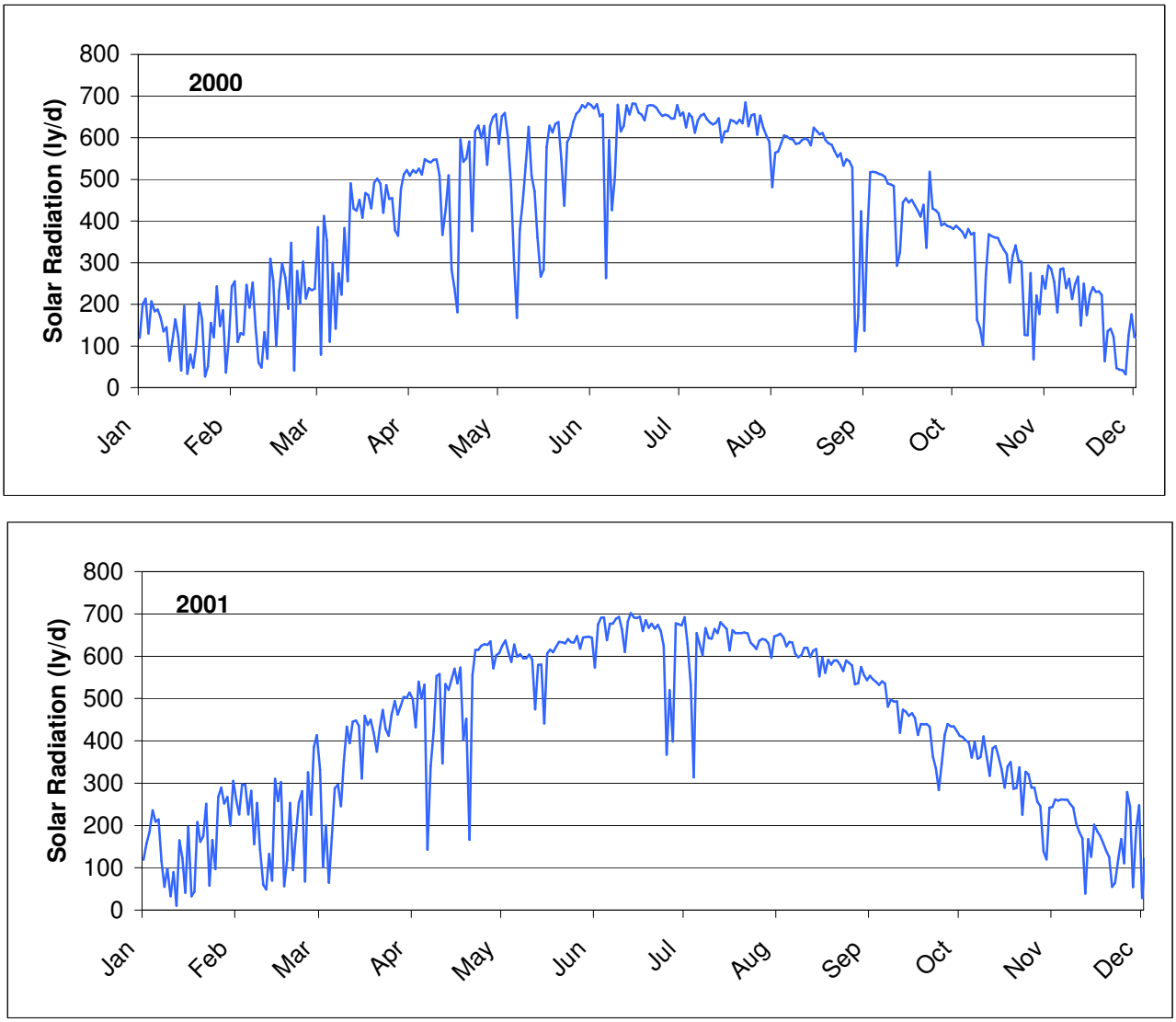

Figure 13. Model Input Solar Radiation Collected at CIMIS Station Lodi West: 2000, 2001

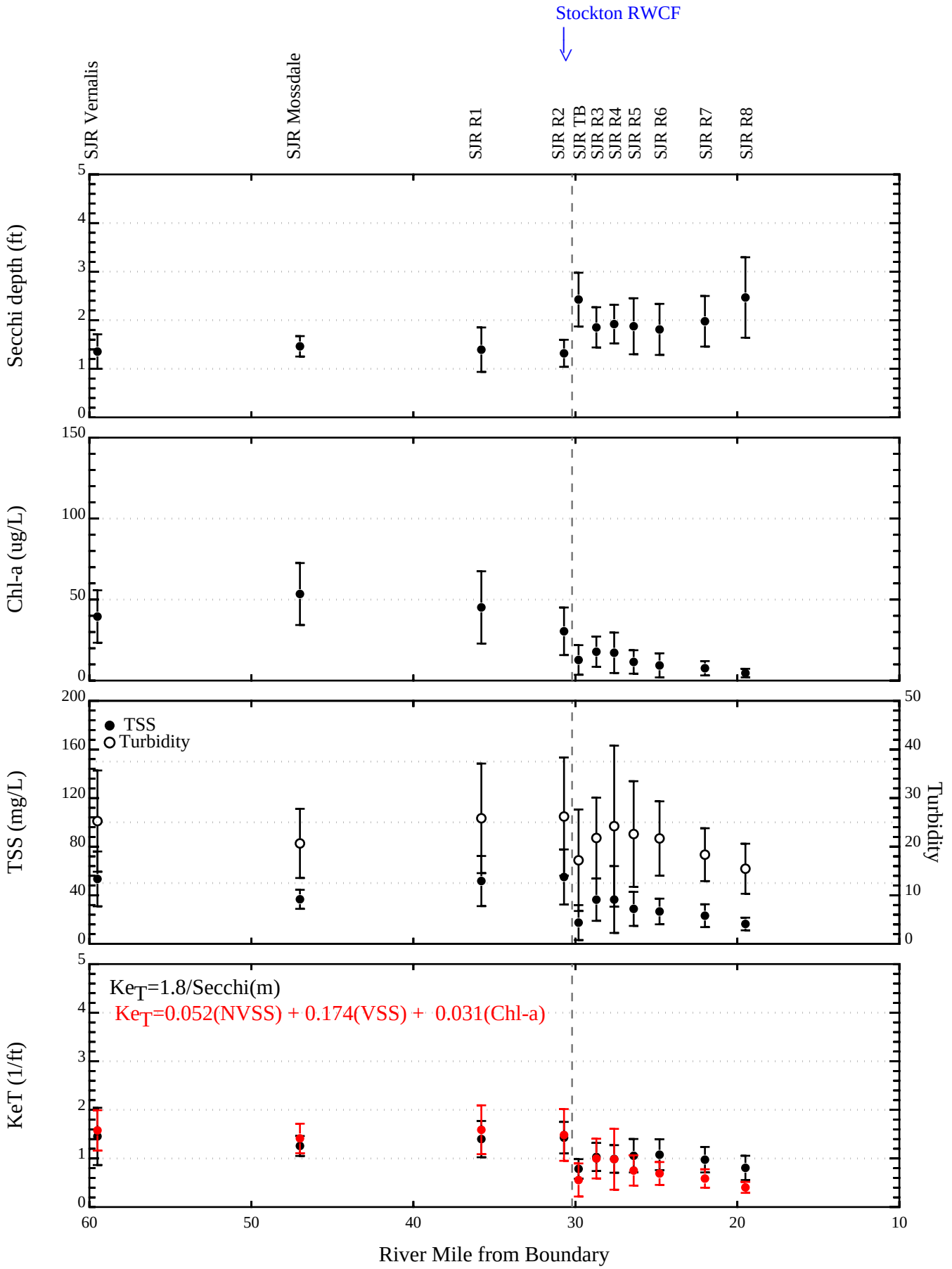

Figure 14. DWSC SJR Light Extinction Coefficient Analysis-Summer

Data From USGS (Kratzer et al.,2004), UCD (Dahlgren et al.,2004), Data Atlas

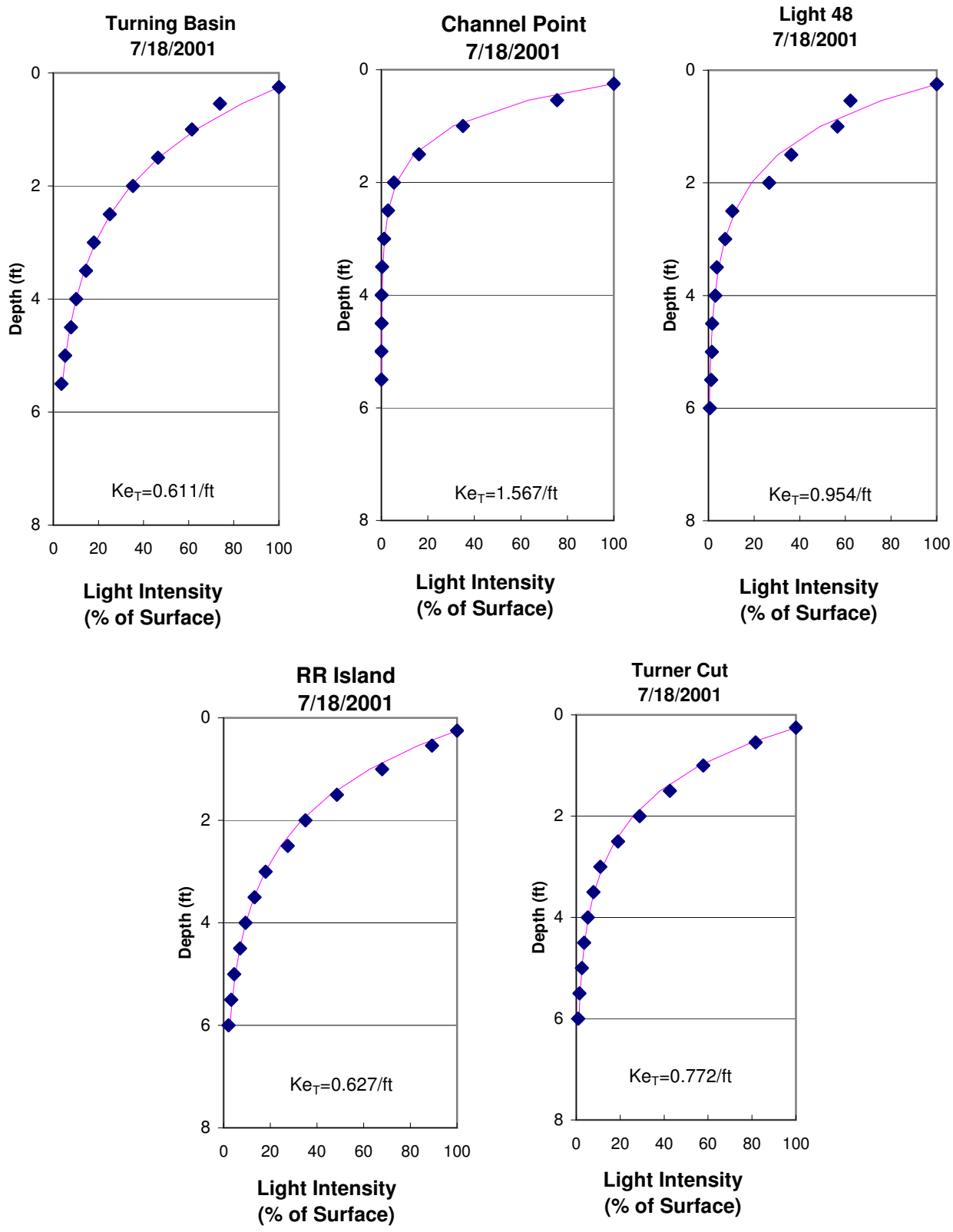

Figure 15. Calculated Light Extinction Coefficients at Locations in the SJR DWSC, July 18, 2001. Source: Lehman, 2005

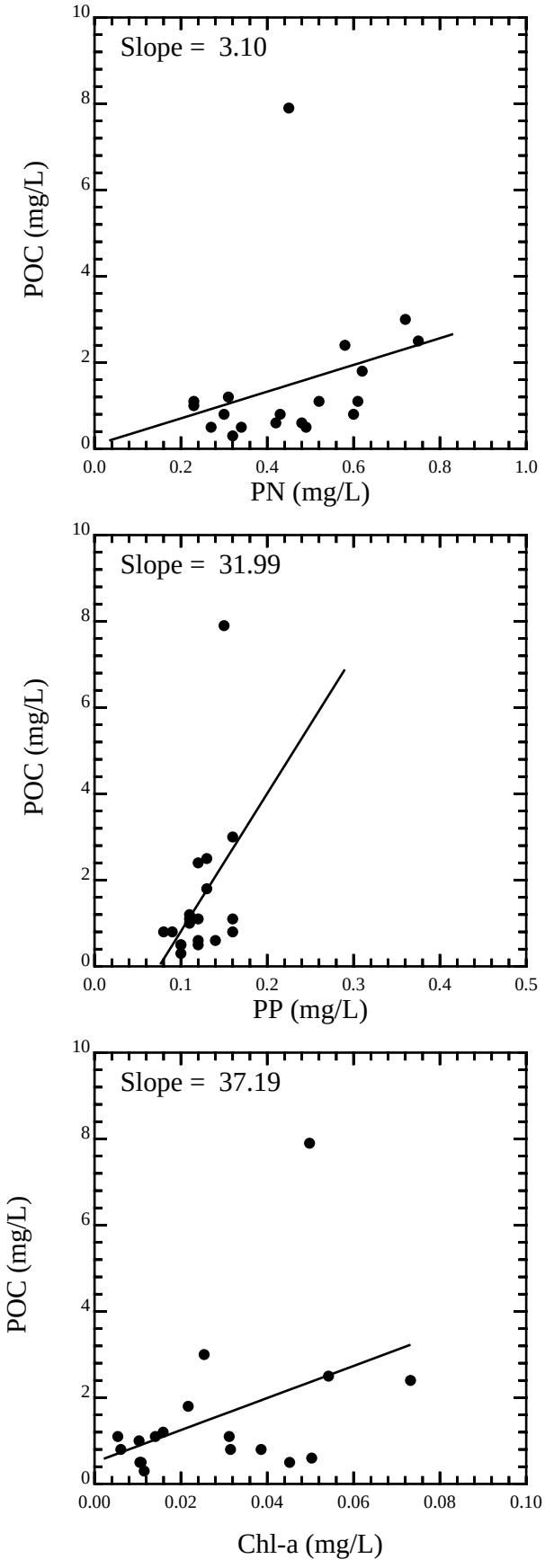

Figure 16. Correlation of POC with PN, PP, & Chlorophyll-a in the SJR near Vernalis

Source: UCD (Dahlgren, 2004), USGS (Kratzer et al., 2004)

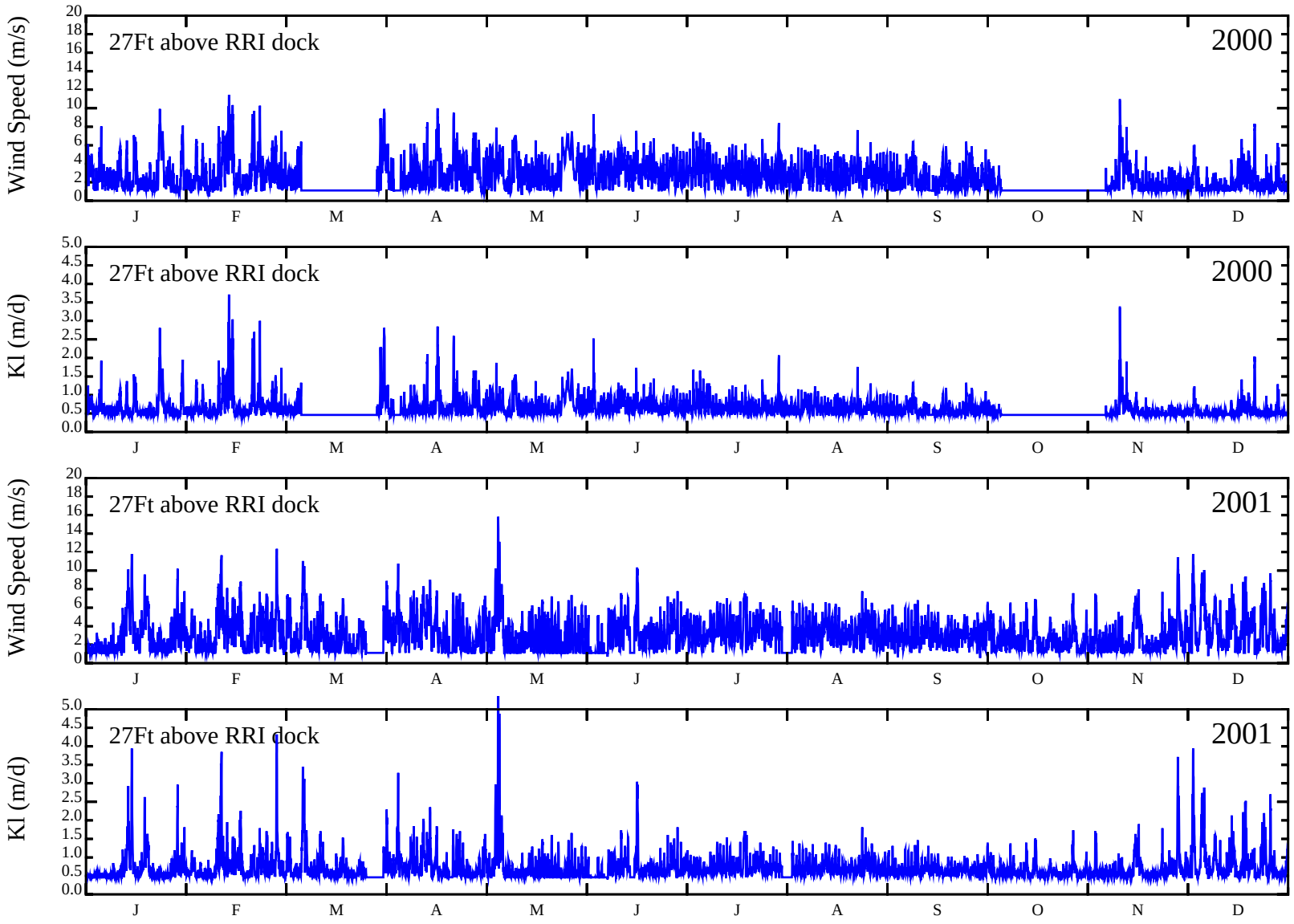

Figure 17. San Joaquin River Hourly Wind Speed and Reaeration (Kl), 2000 & 2001

DATE: 1/11/2006 TIME: 8:55:17

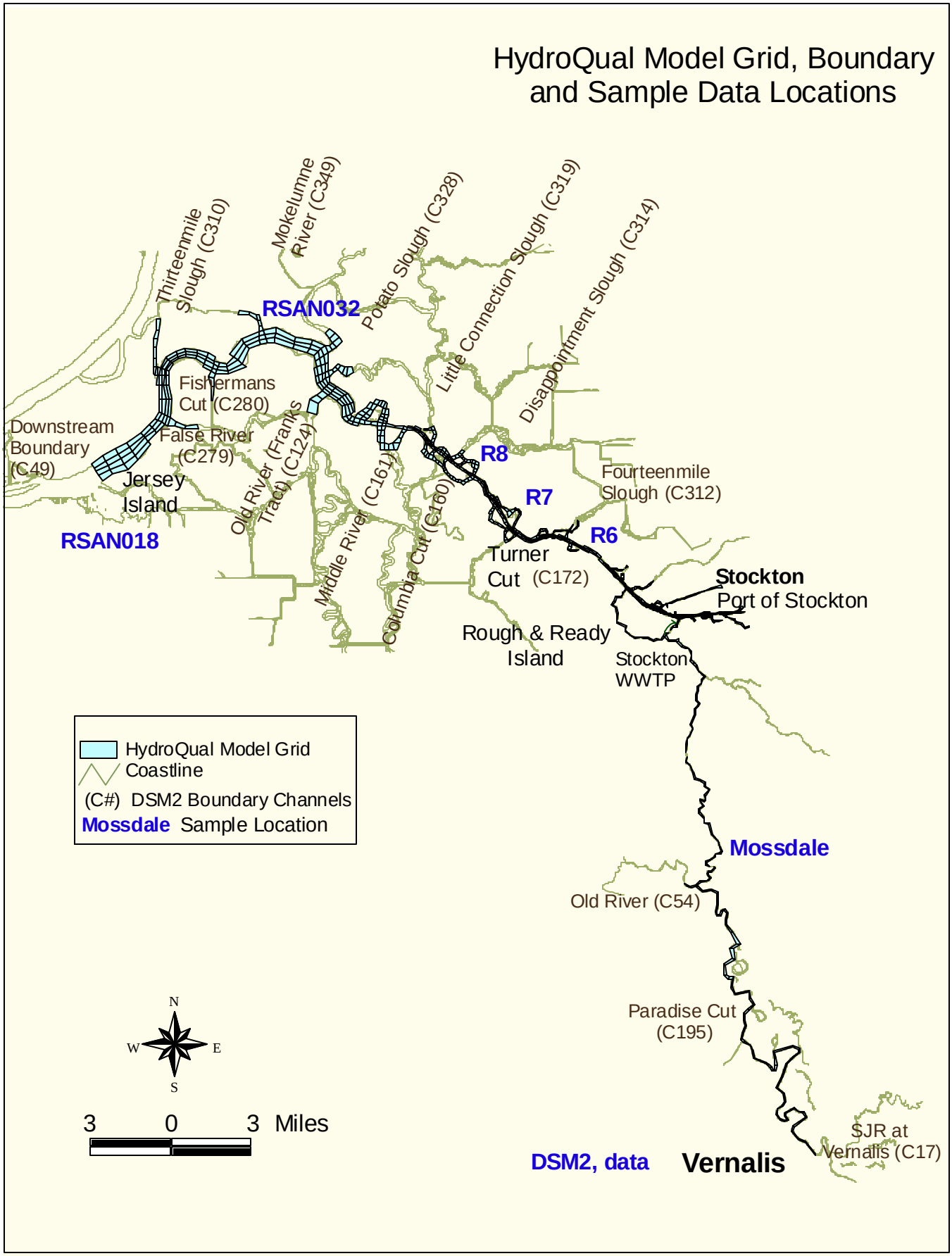

Figure 18. HydroQual Model Grid, Boundary and Sample Data Locations

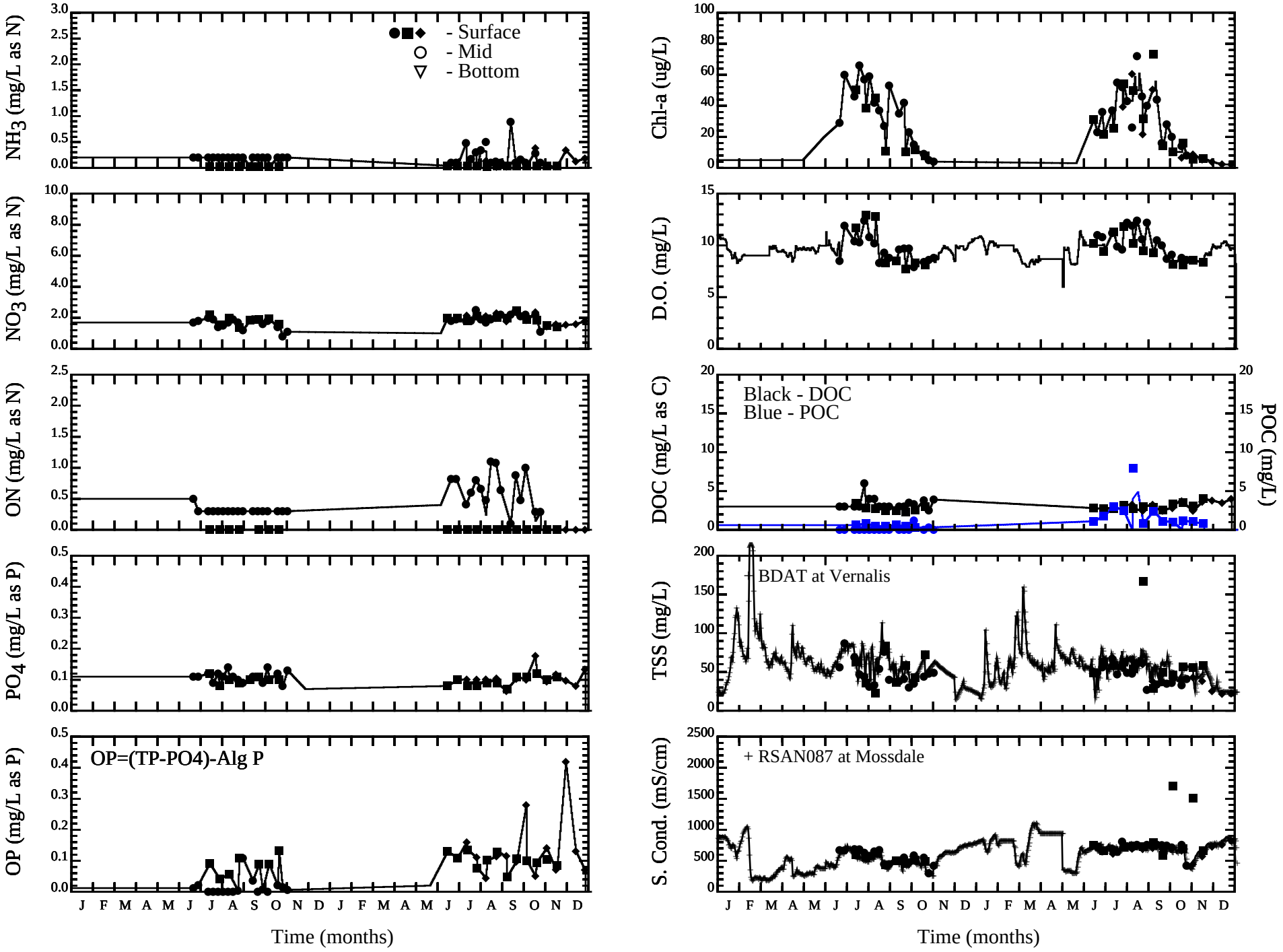

Figure 19. San Joaquin River Data & Model Inputs, 2000 & 2001, Station: Vernalis

Source: J&S Data Atlas

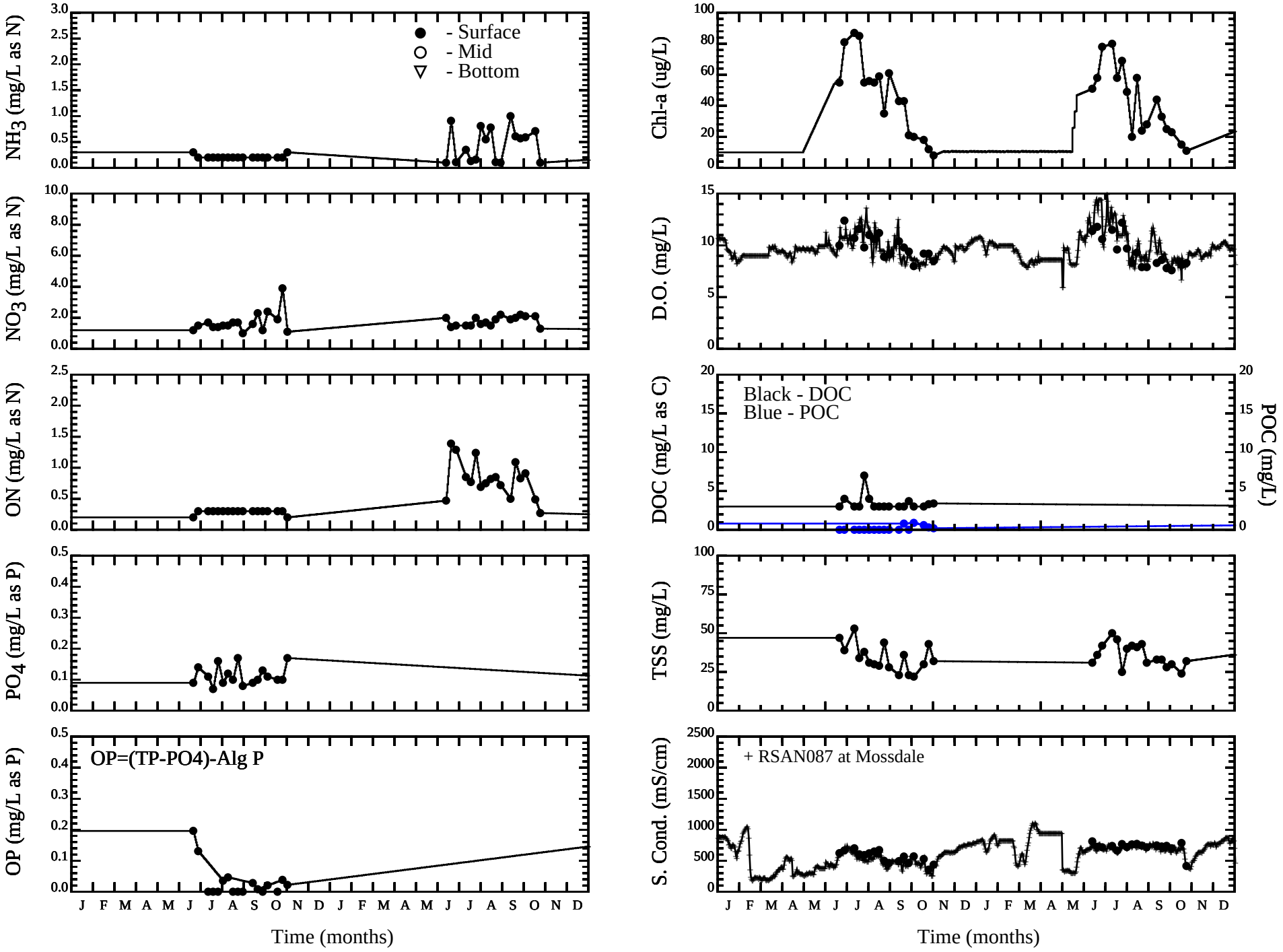

Figure 20. San Joaquin River Data & Model Inputs, 2000 & 2001, Station: Mossdale Bridge

Source: J&S Data Atlas

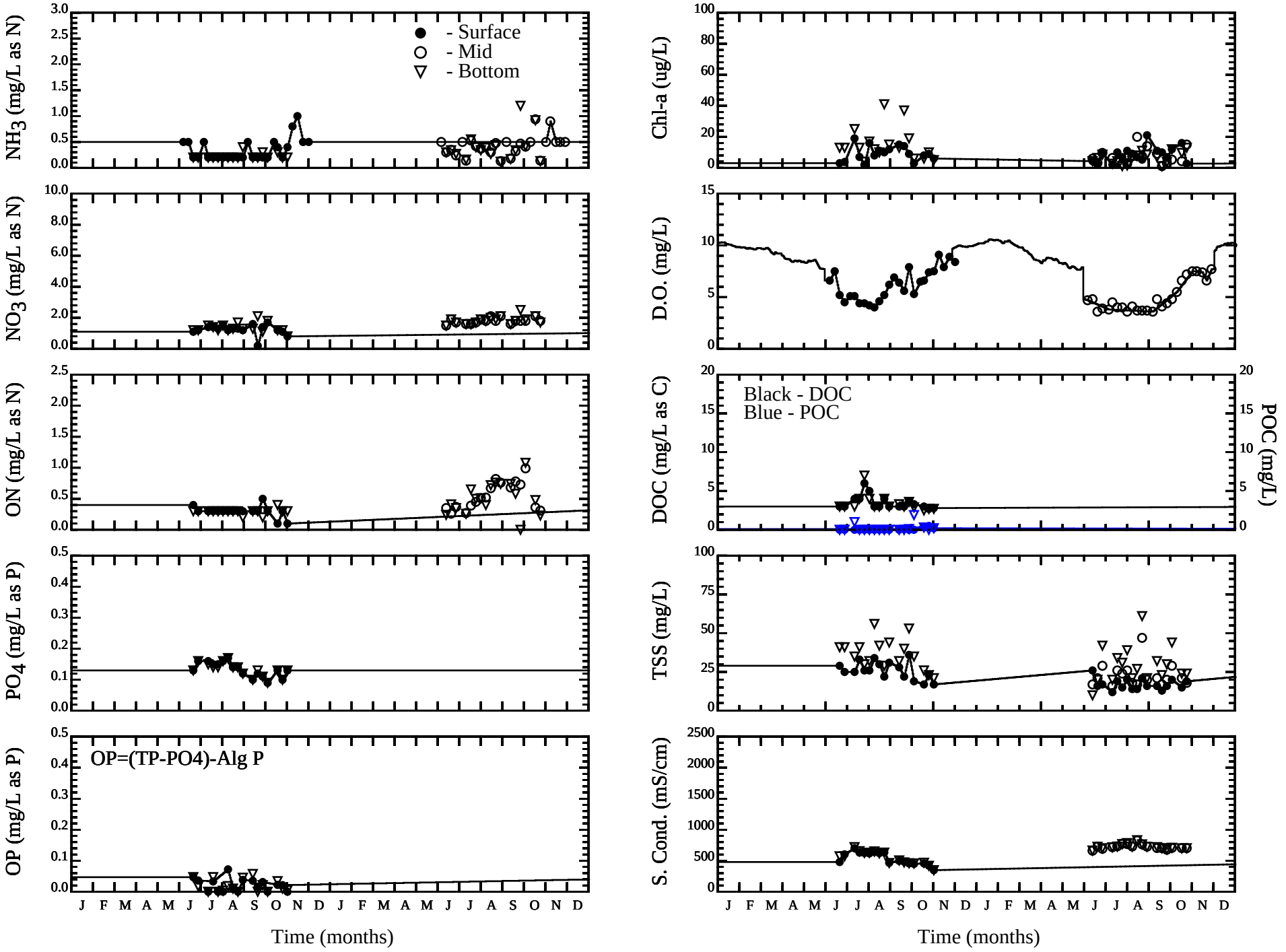

Figure 21. San Joaquin River Data & Model Inputs, 2000 & 2001, Station: R6

Source: J&S Data Atlas

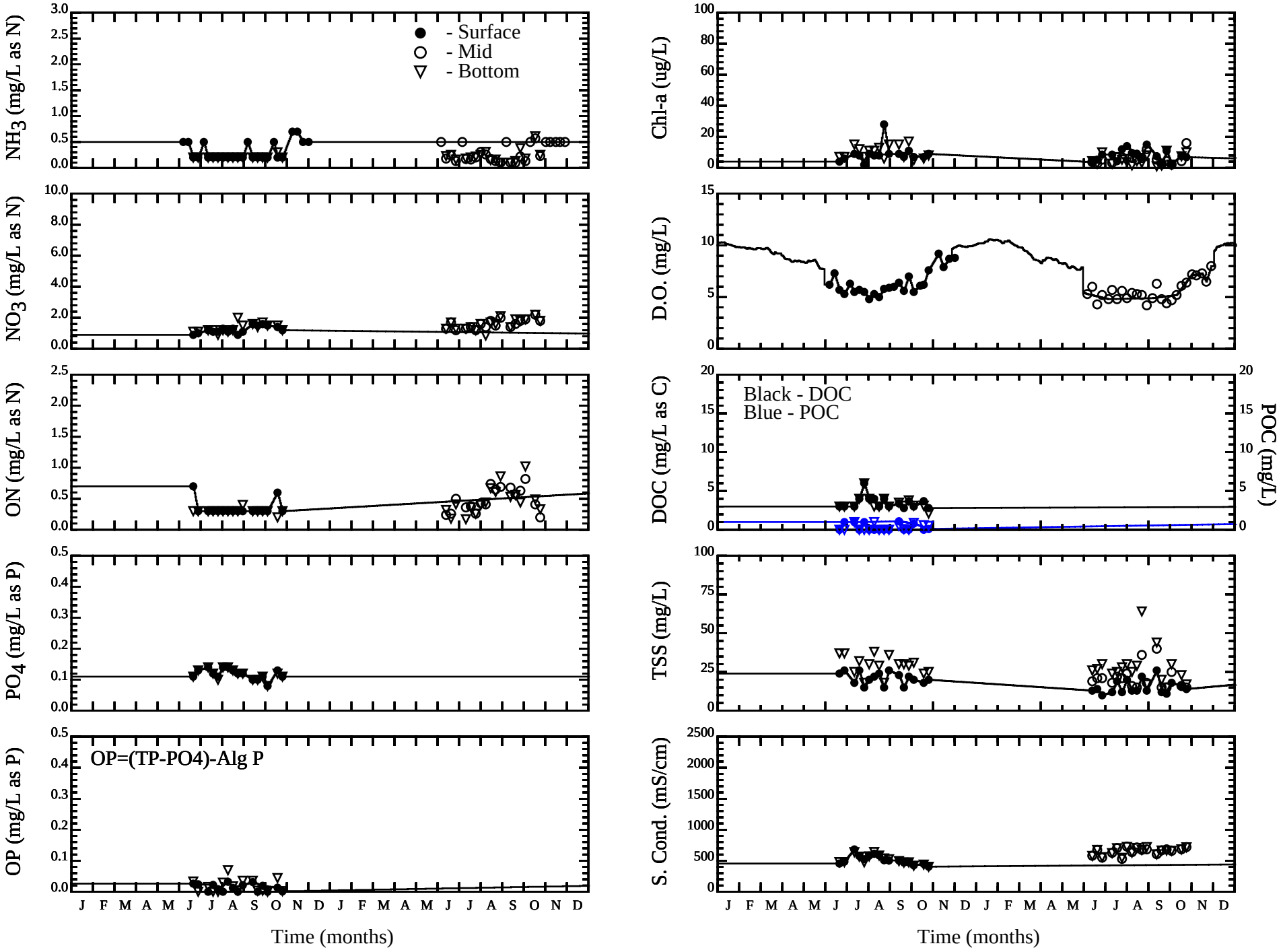

Figure 22. San Joaquin River Data & Model Inputs, 2000 & 2001, Station: R7

Source: J&S Data Atlas

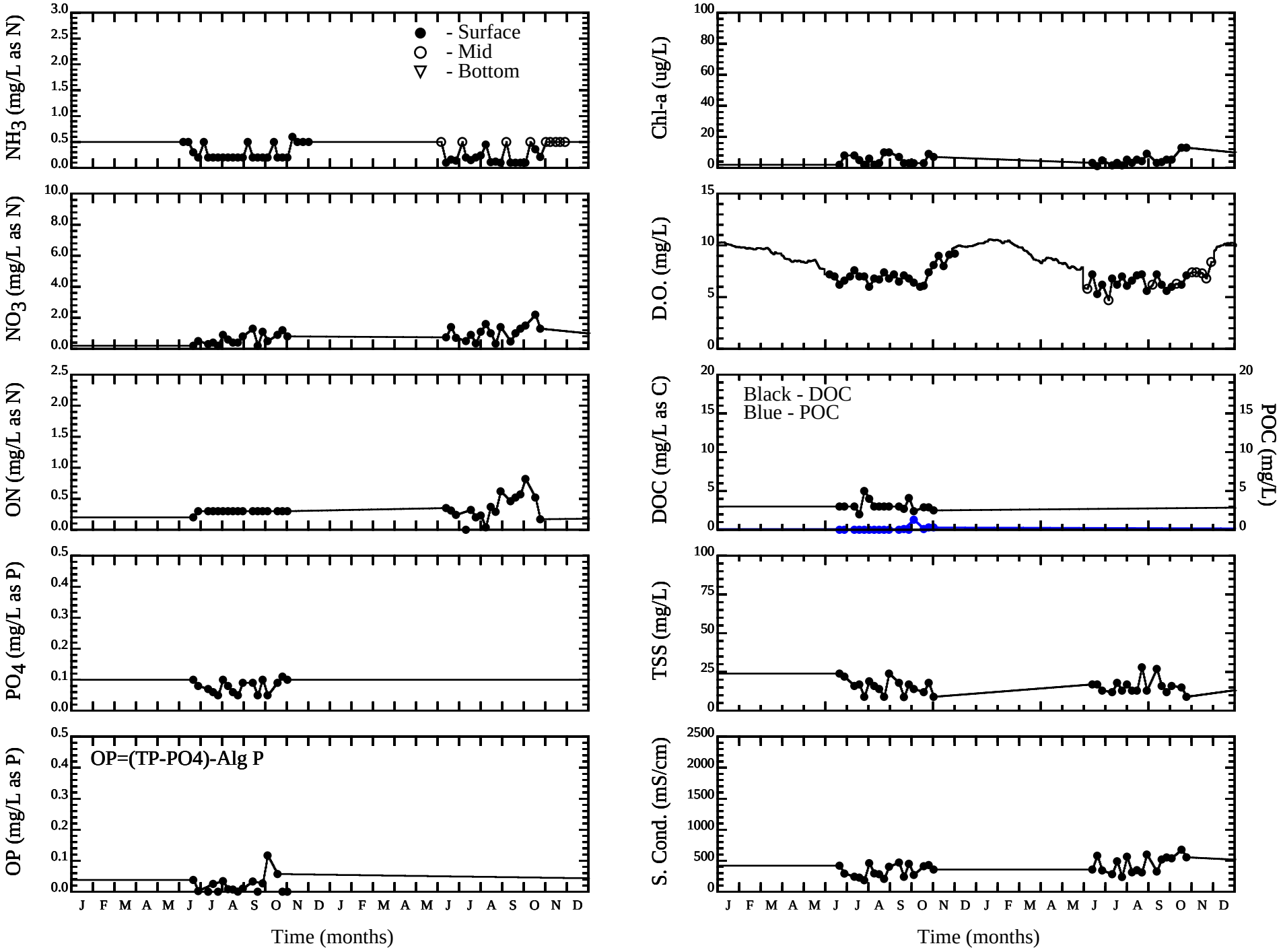

Figure 23. San Joaquin River Data & Model Inputs, 2000 & 2001, Station: R8

Source: J&S Data Atlas

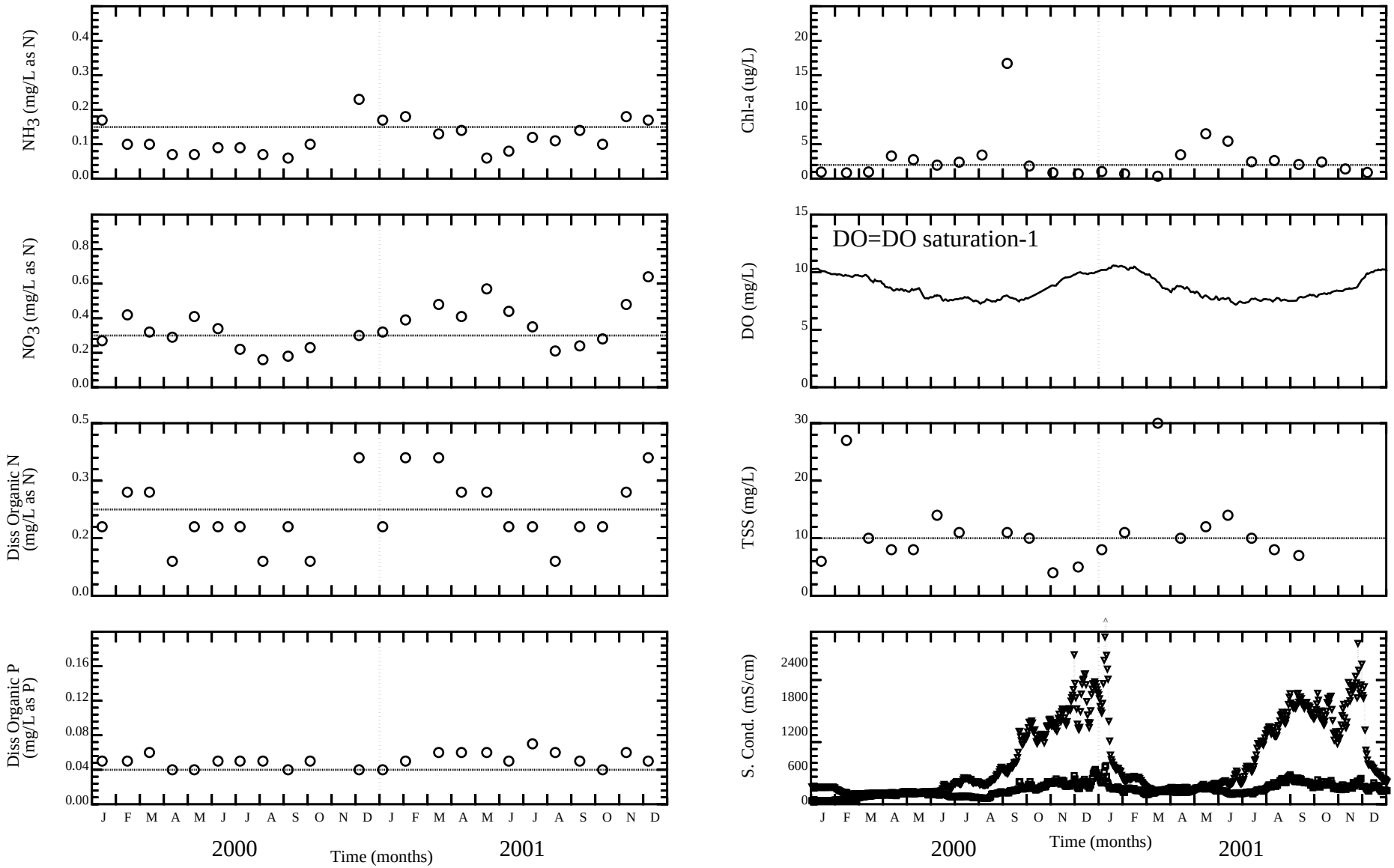

Figure 24 San Joaquin River Potato Point Data and Model Input

Line is Model Input
Symbol is Data

▽ EC at RSAN018 used at downstream boundary (Jersey Pt)
□ EC at RSAN032 used at other boundaries downstream of Potato Pt
○ Data at Potato Pt used at boundaries at and downstream of Potato Pt

DATE: 3/17/2006 TIME: 12:59:17

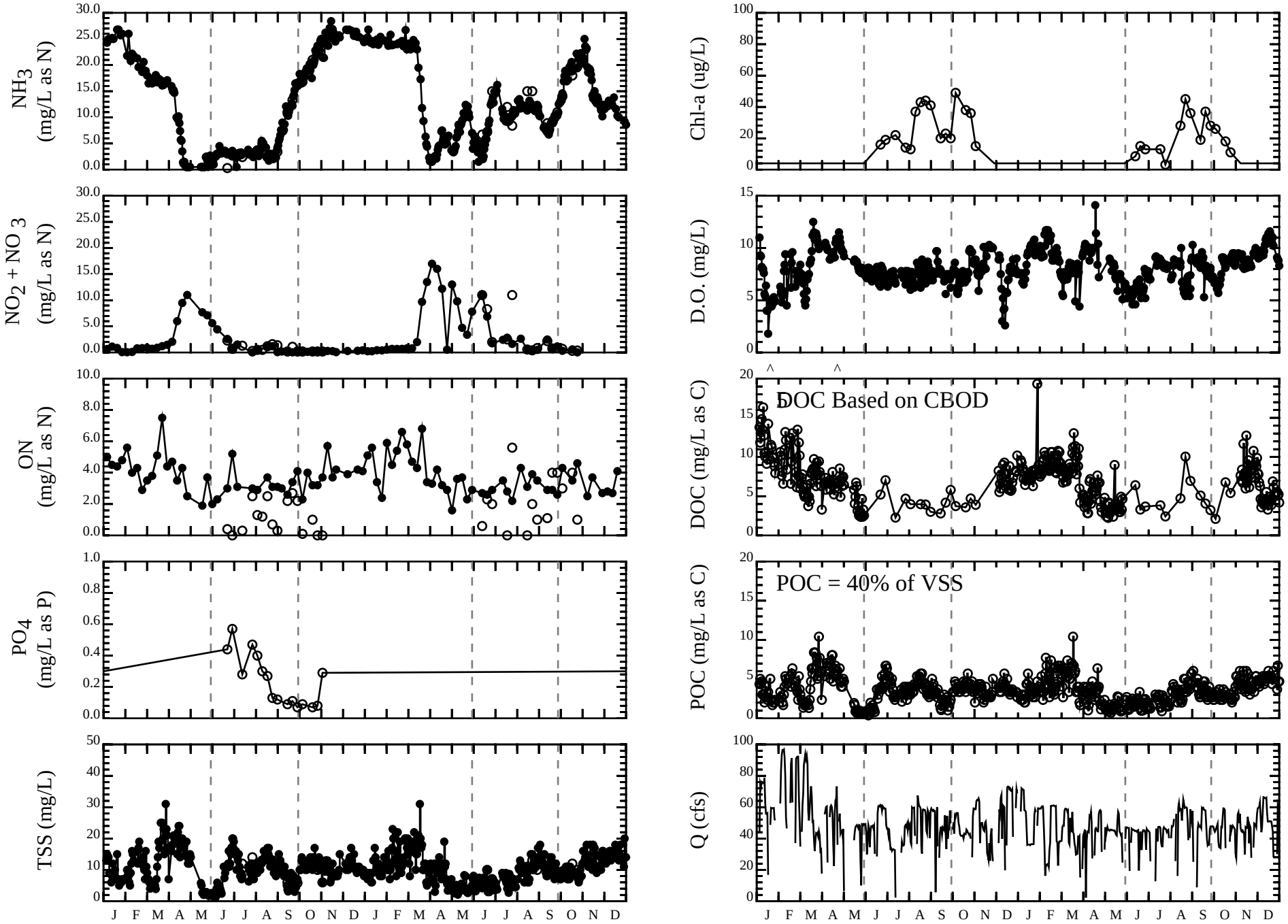

Figure 25. Stockton RWCF Effluent Concentrations, 2000 & 2001

Source: J&S Data Atlas

● -Regular Sampling
○ -Special Summer, Fall Sampling

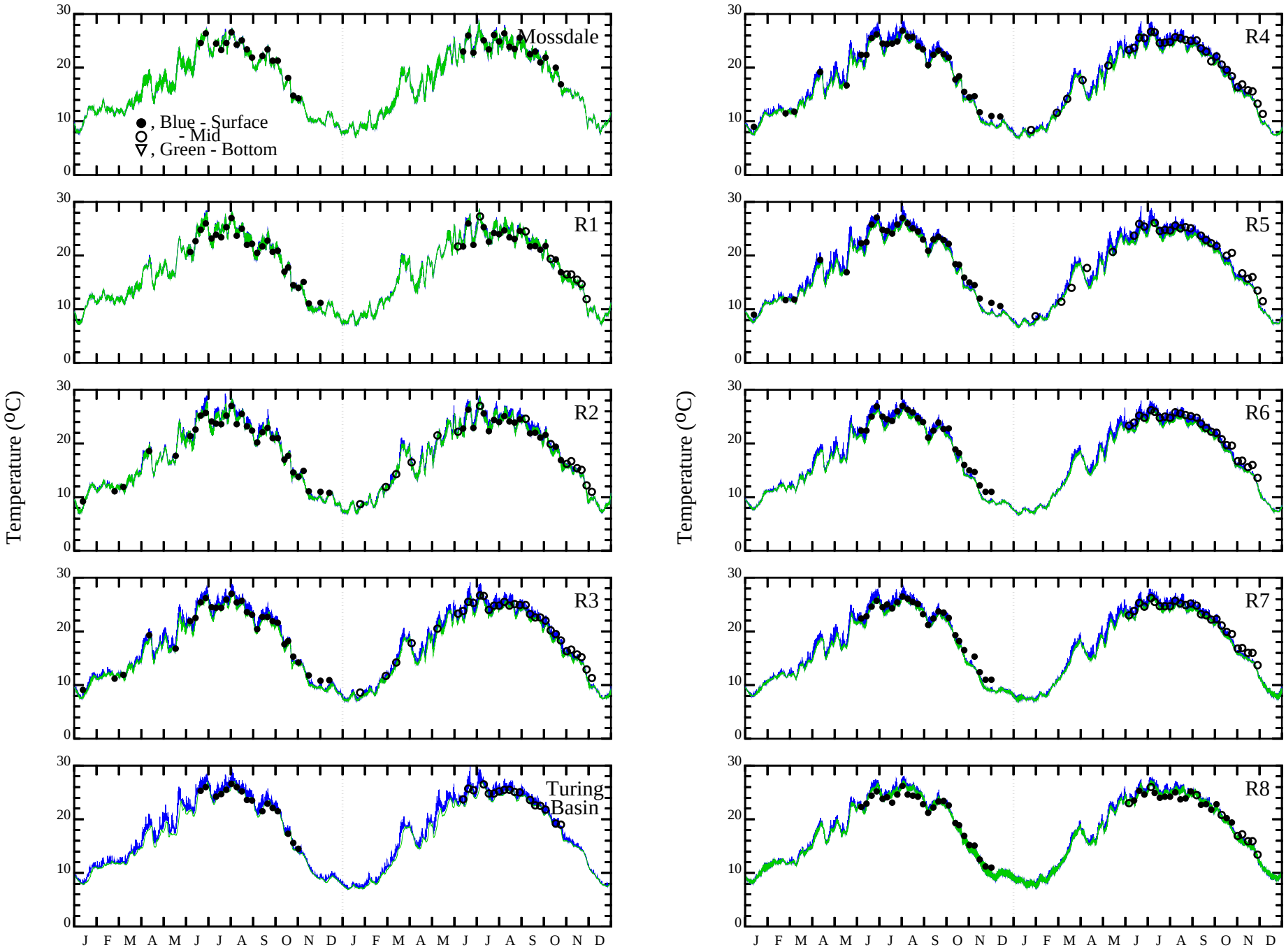

Figure 26. San Joaquin River Temperature Data and Model Calibration, 2000 & 2001

Data Source: J&S Data Atlas, RUN39tc2

Symbols=Data, Line=Model

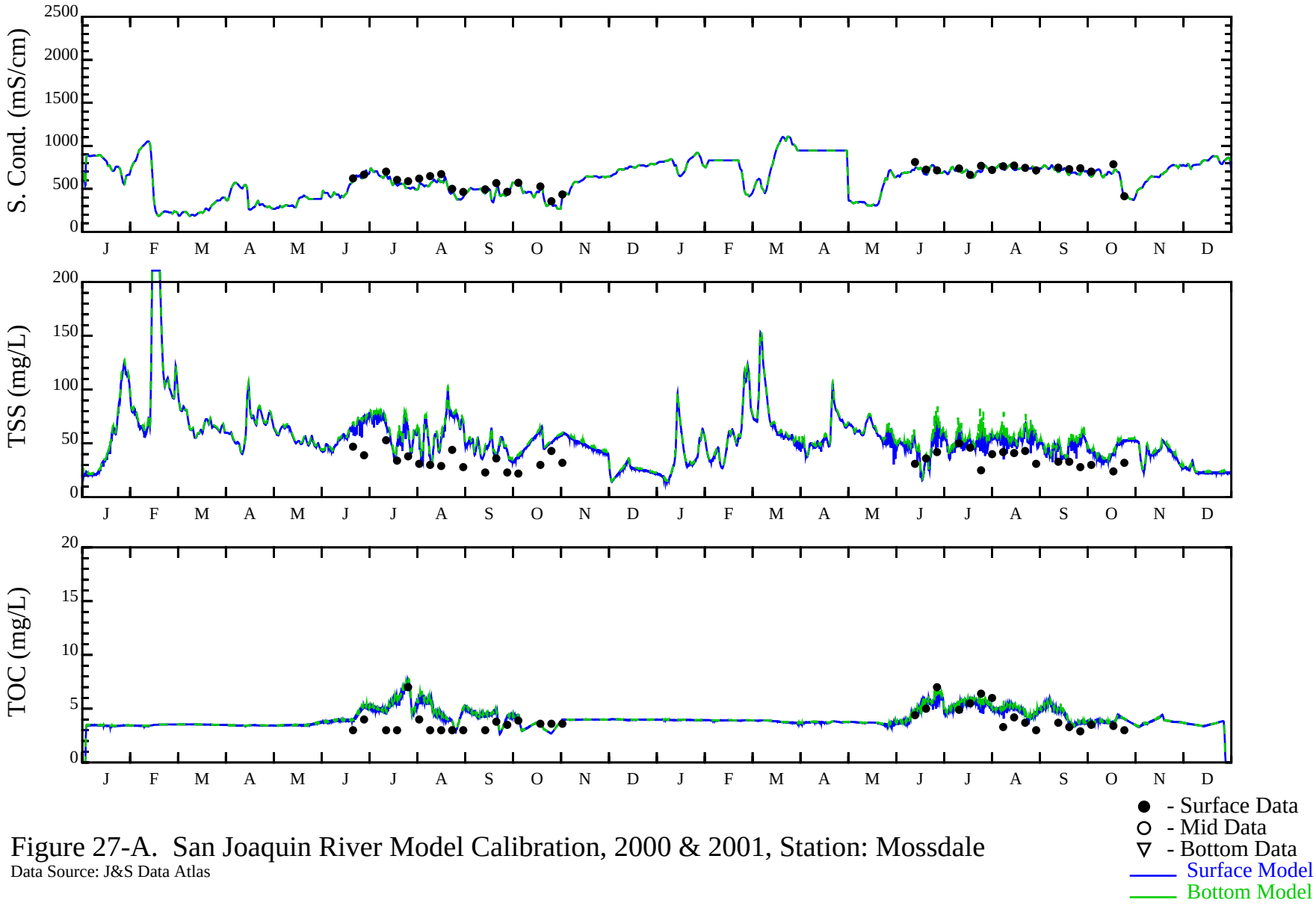

Figure 27-A. San Joaquin River Model Calibration, 2000 & 2001, Station: Mossdale

Data Source: J&S Data Atlas

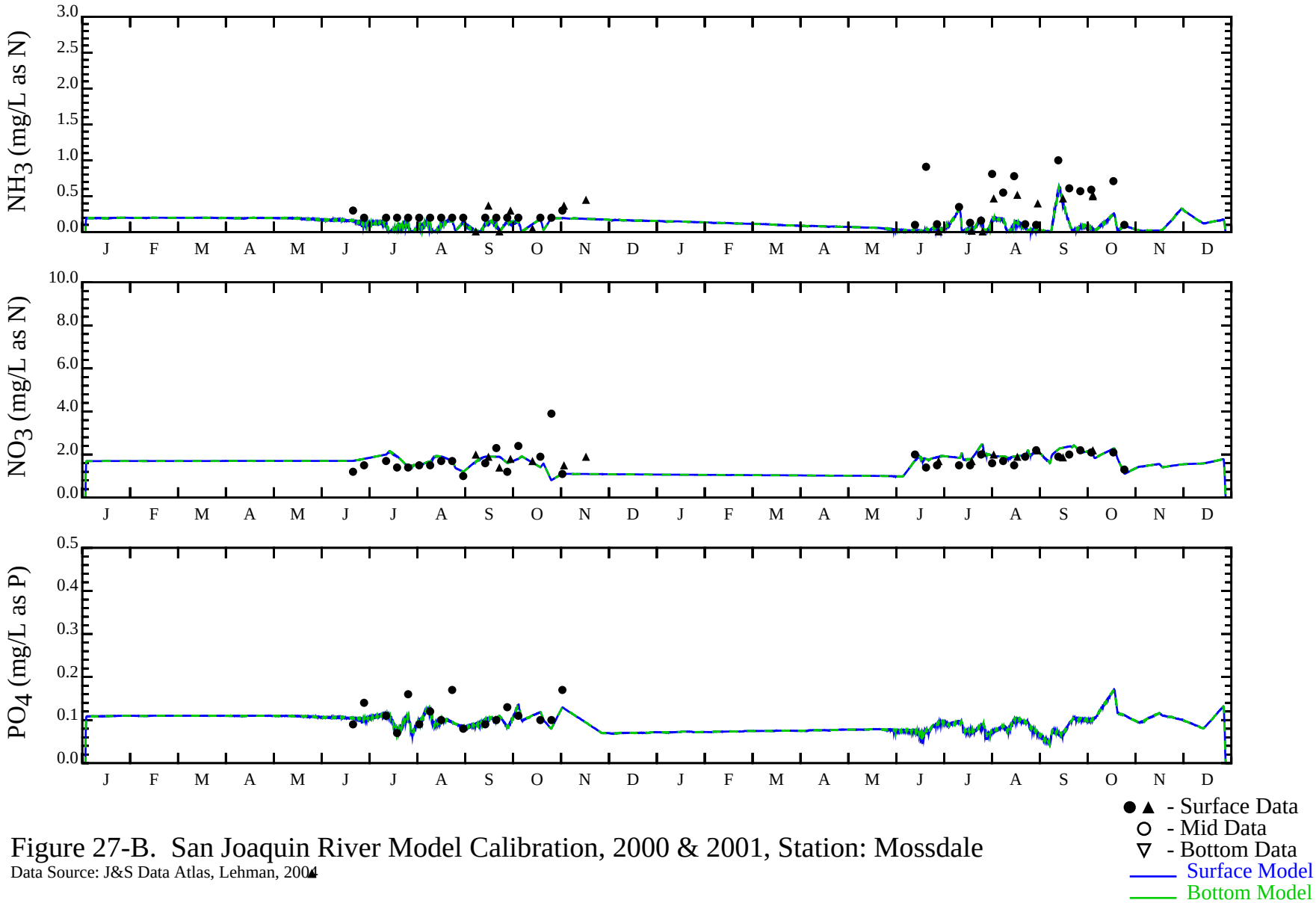

Figure 27-B. San Joaquin River Model Calibration, 2000 & 2001, Station: Mossdale

Data Source: J&S Data Atlas, Lehman, 2004

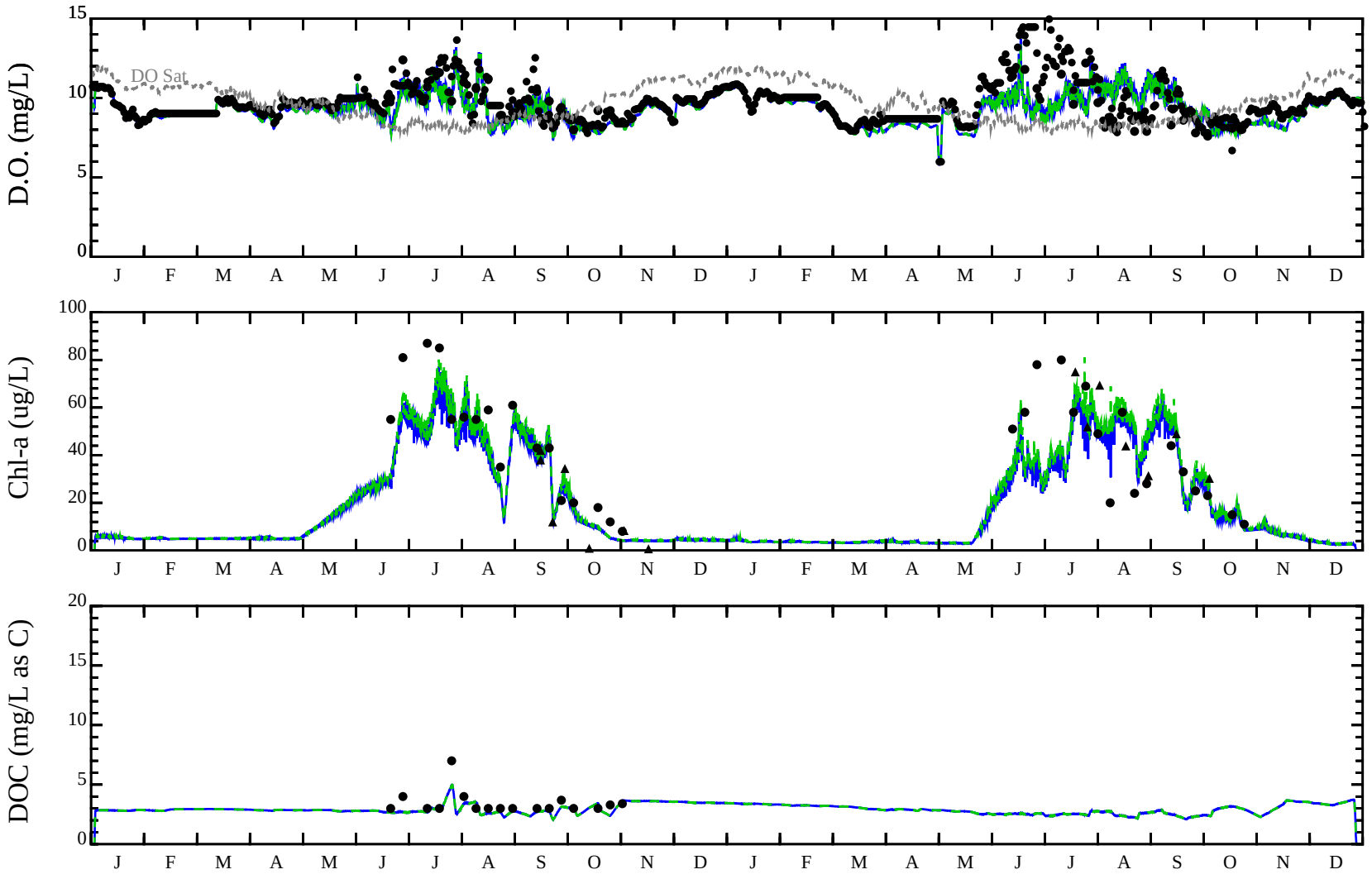

Figure 27-C. San Joaquin River Model Calibration, 2000 & 2001, Station: Mossdale

Data Source: J&S Data Atlas, Lehman, 2004

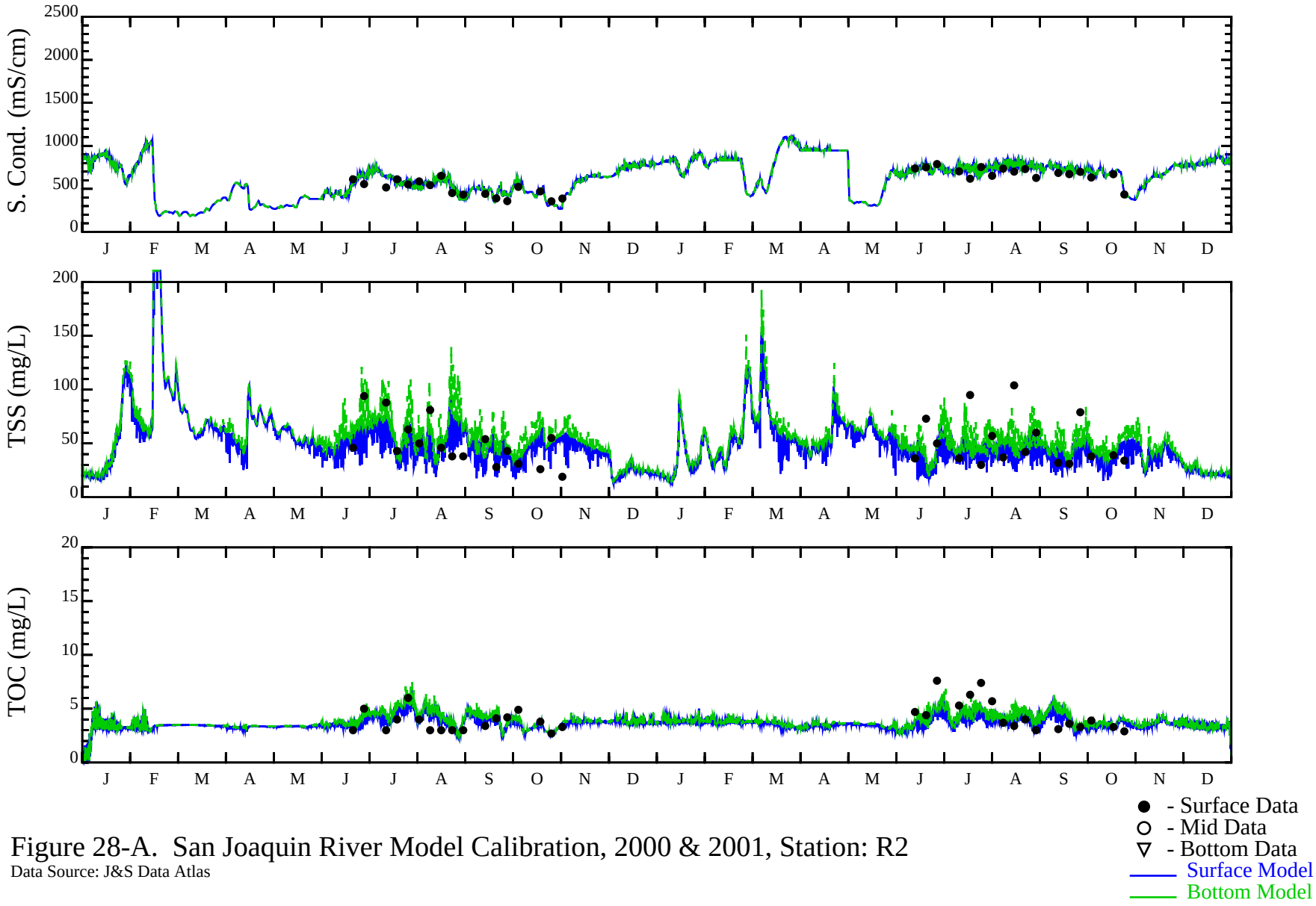

Figure 28-A. San Joaquin River Model Calibration, 2000 & 2001, Station: R2

Data Source: J&S Data Atlas

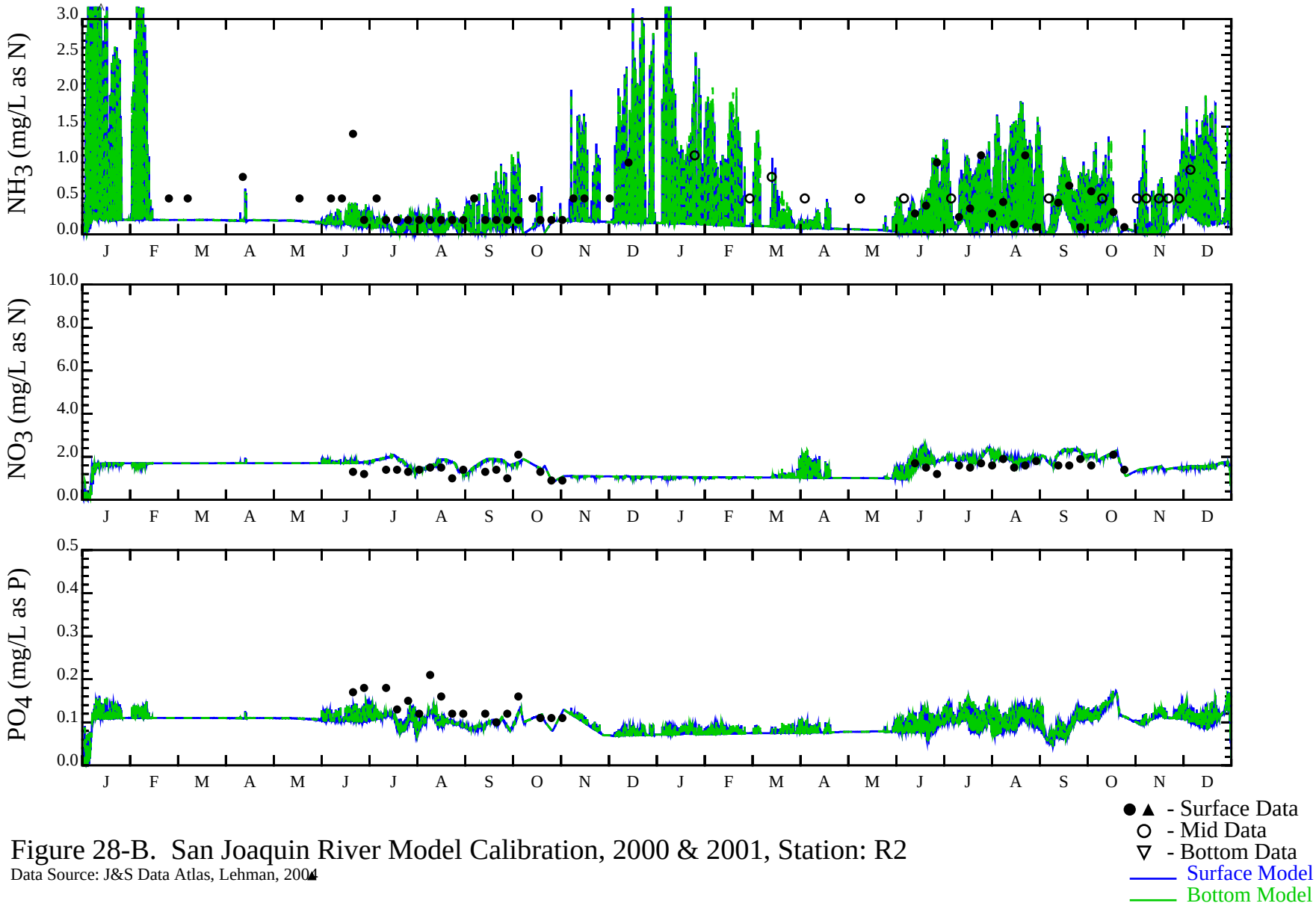

Figure 28-B. San Joaquin River Model Calibration, 2000 & 2001, Station: R2

Data Source: J&S Data Atlas, Lehman, 2004

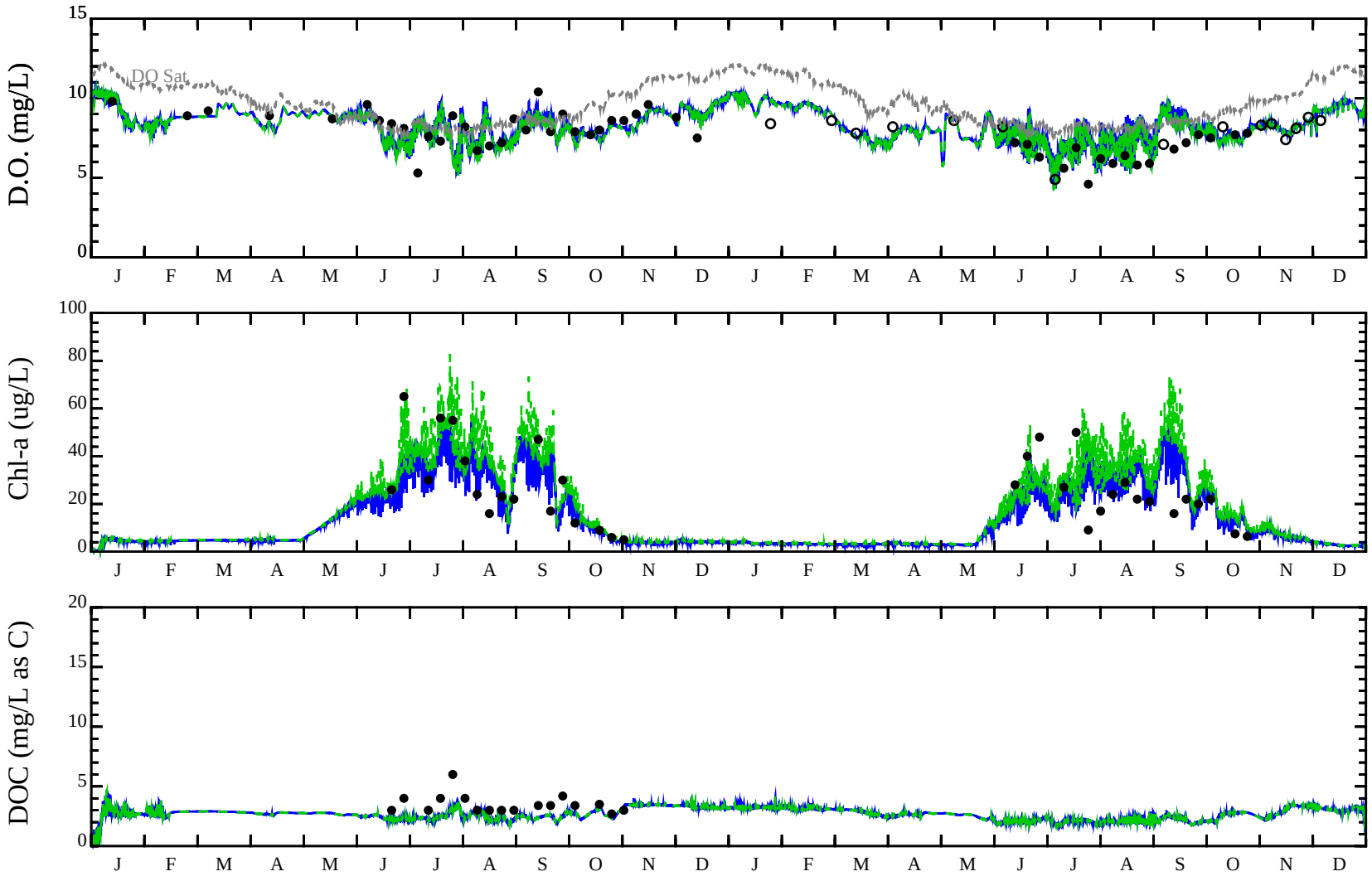

Figure 28-C. San Joaquin River Model Calibration, 2000 & 2001, Station: R2

Data Source: J&S Data Atlas, Lehman, 2004

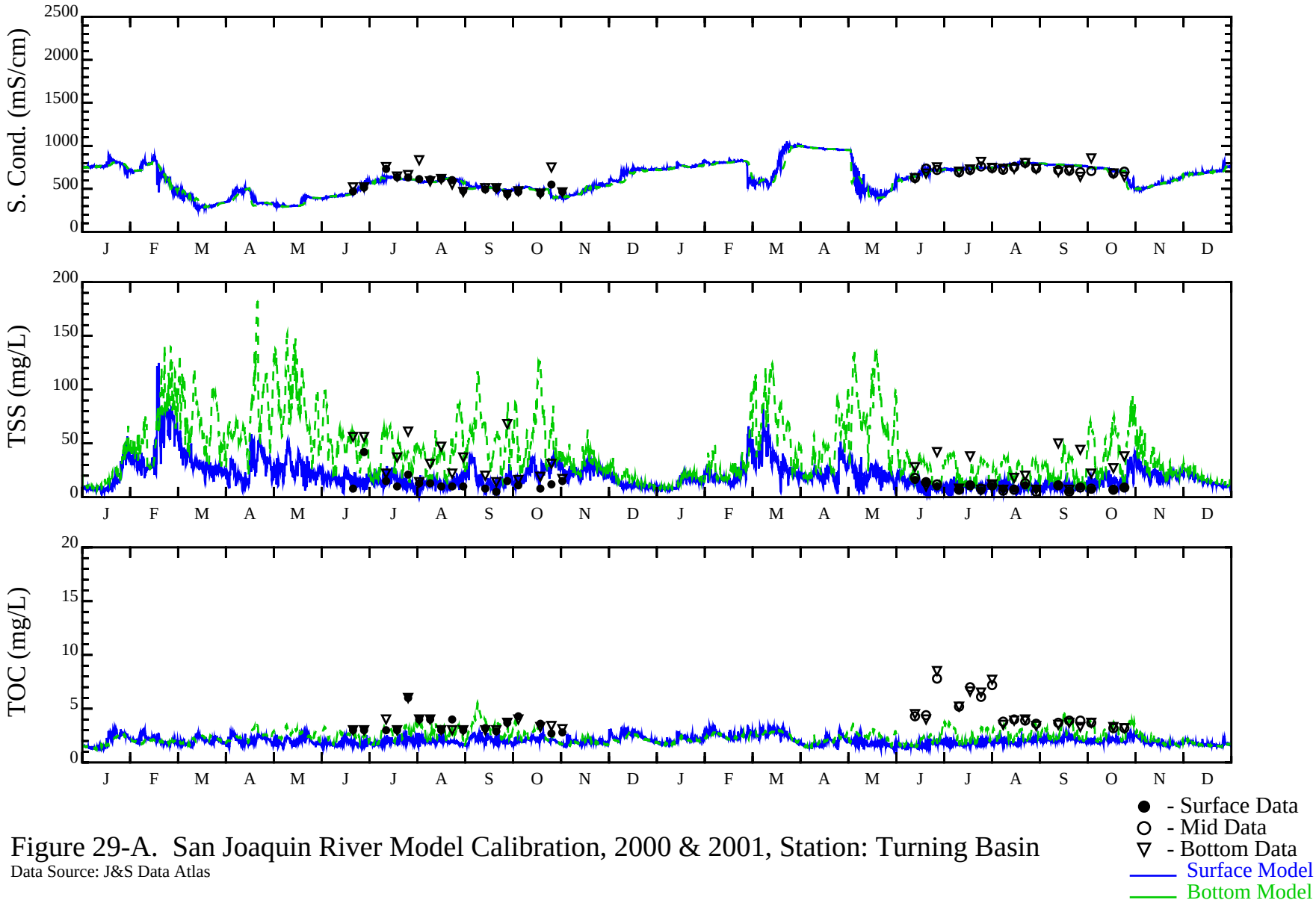

Figure 29-A. San Joaquin River Model Calibration, 2000 & 2001, Station: Turning Basin

Data Source: J&S Data Atlas

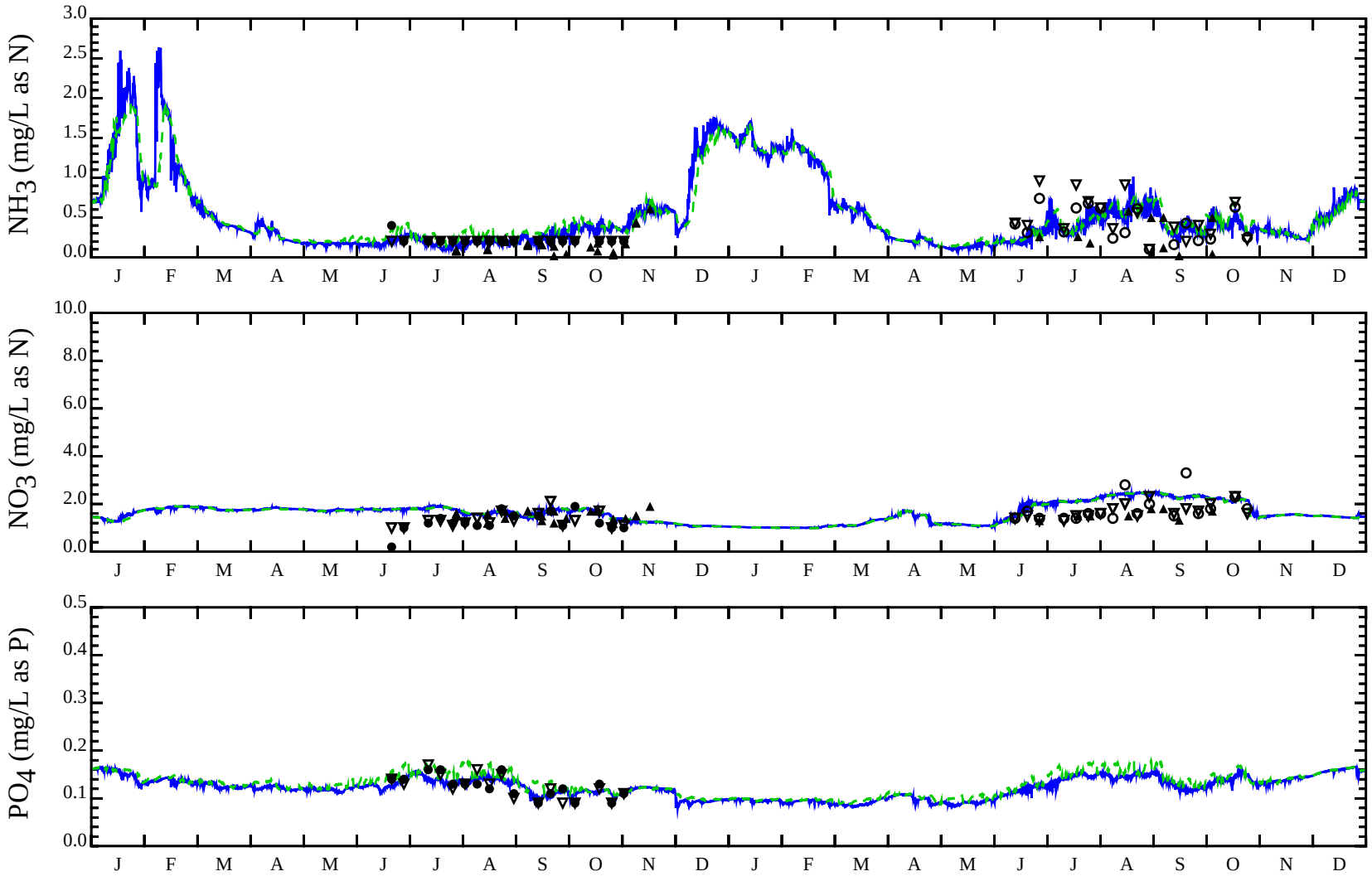

Figure 29-B. San Joaquin River Model Calibration, 2000 & 2001, Station: Turning Basin

Data Source: J&S Data Atlas, Lehman, 2004

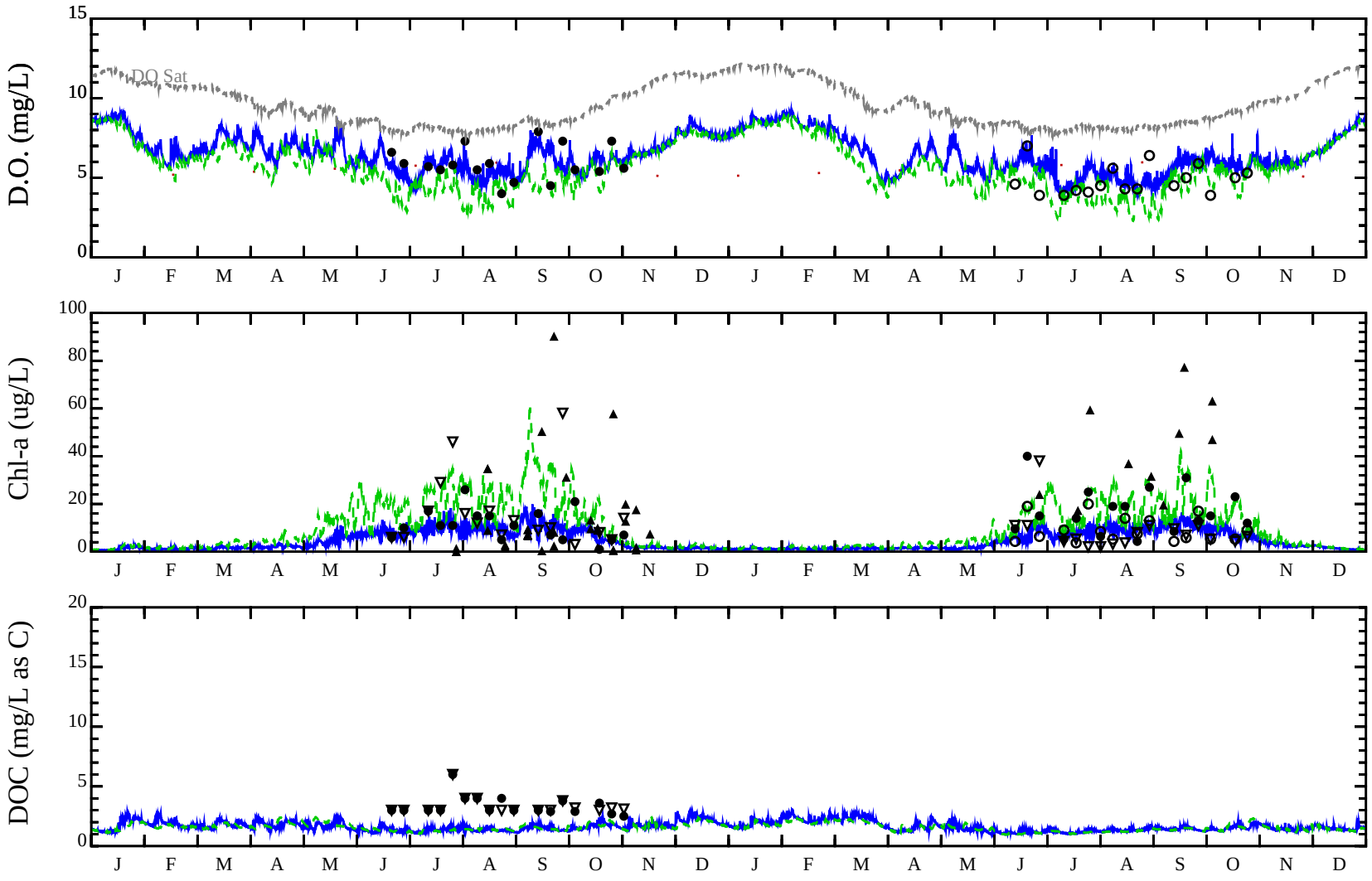

Figure 29-C. San Joaquin River Model Calibration, 2000 & 2001, Station: Turning Basin

Data Source: J&S Data Atlas, Lehman, 2004

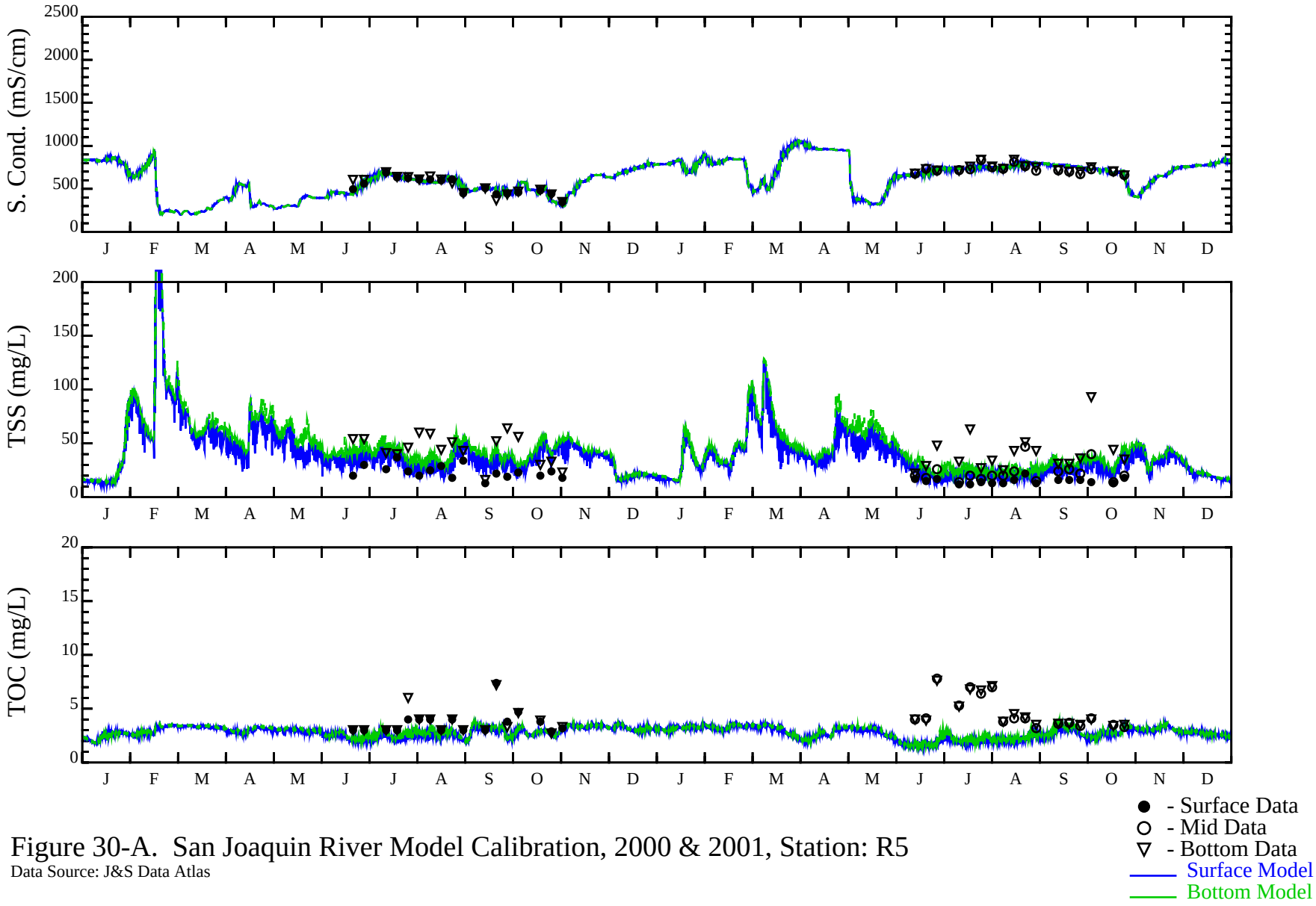

Figure 30-A. San Joaquin River Model Calibration, 2000 & 2001, Station: R5

Data Source: J&S Data Atlas

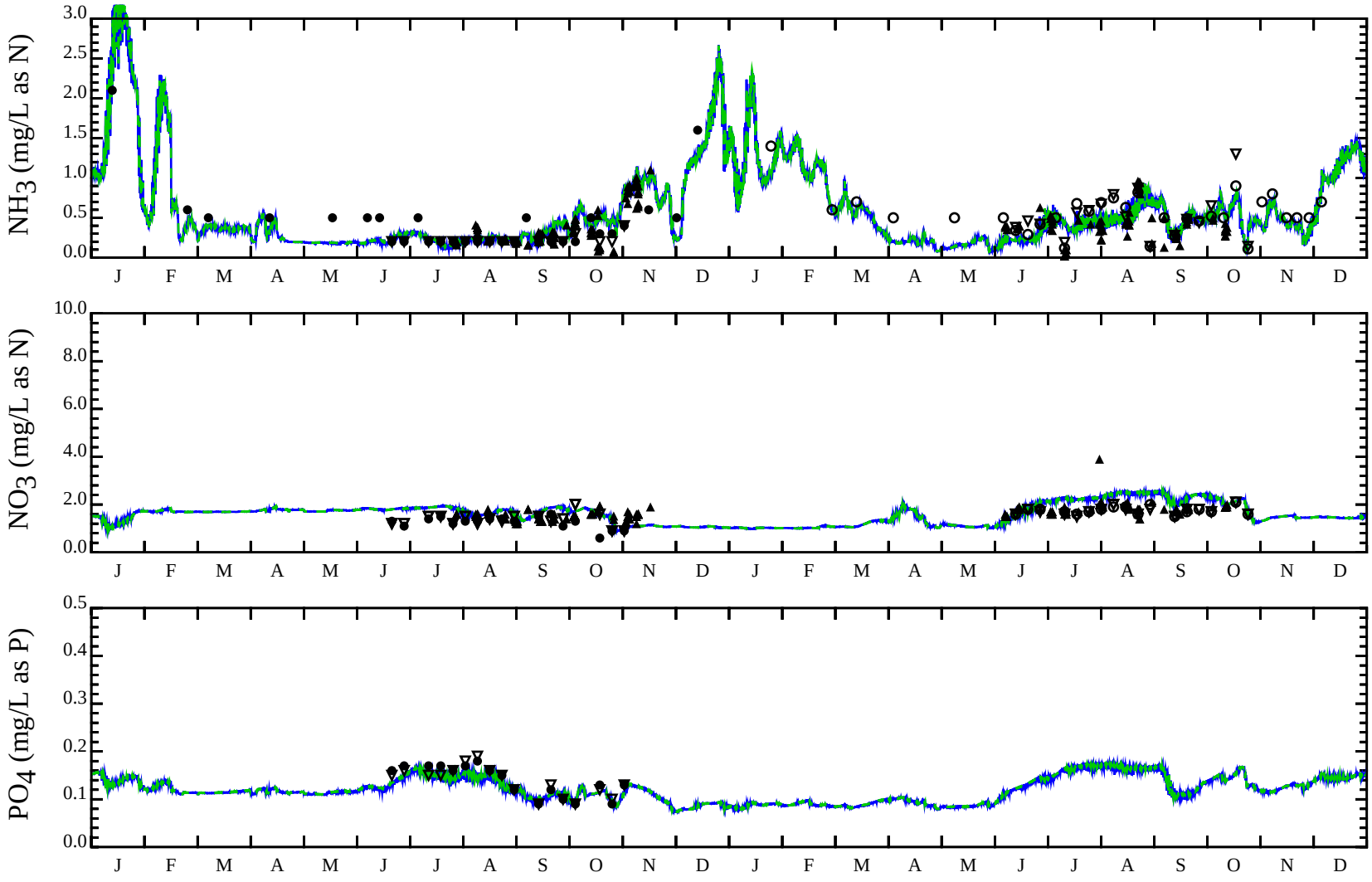

Figure 30-B. San Joaquin River Model Calibration, 2000 & 2001, Station: R5

Data Source: J&S Data Atlas, Lehman, 2004

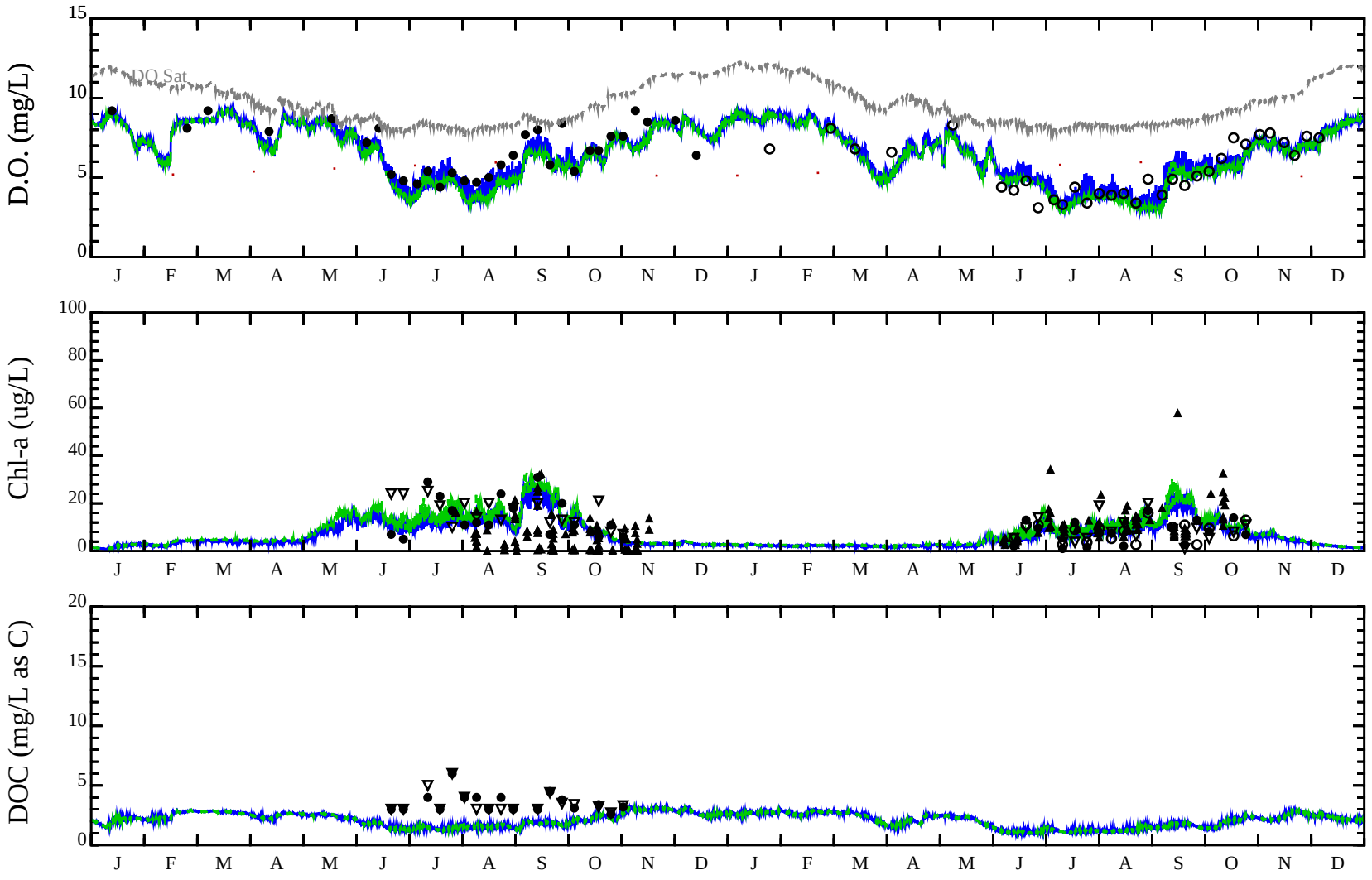

Figure 30-C. San Joaquin River Model Calibration, 2000 & 2001, Station: R5

Data Source: J&S Data Atlas, Lehman, 2004

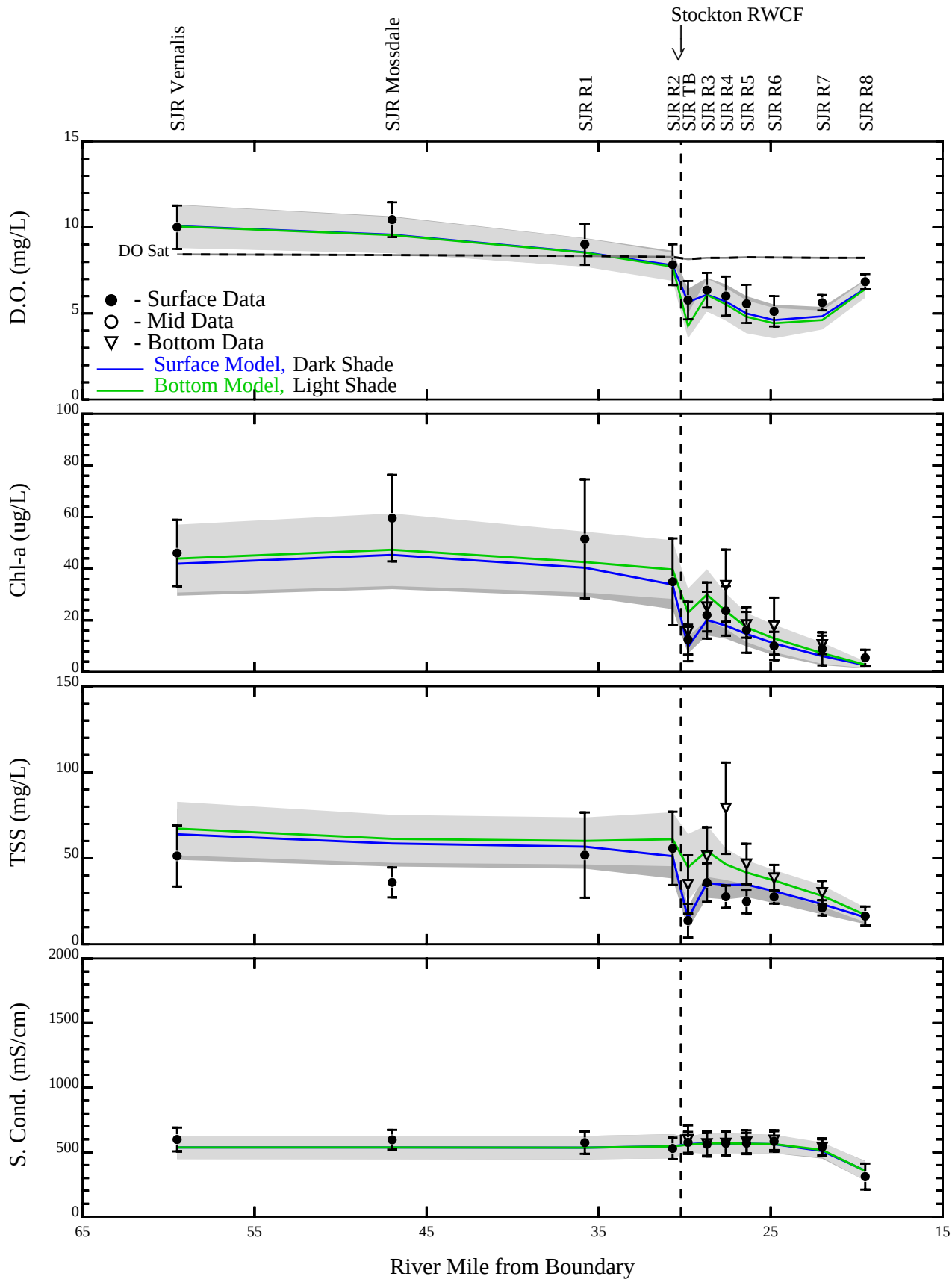

Figure 31. San Joaquin River Spatial Model Calibration and Data, June - October, 2000

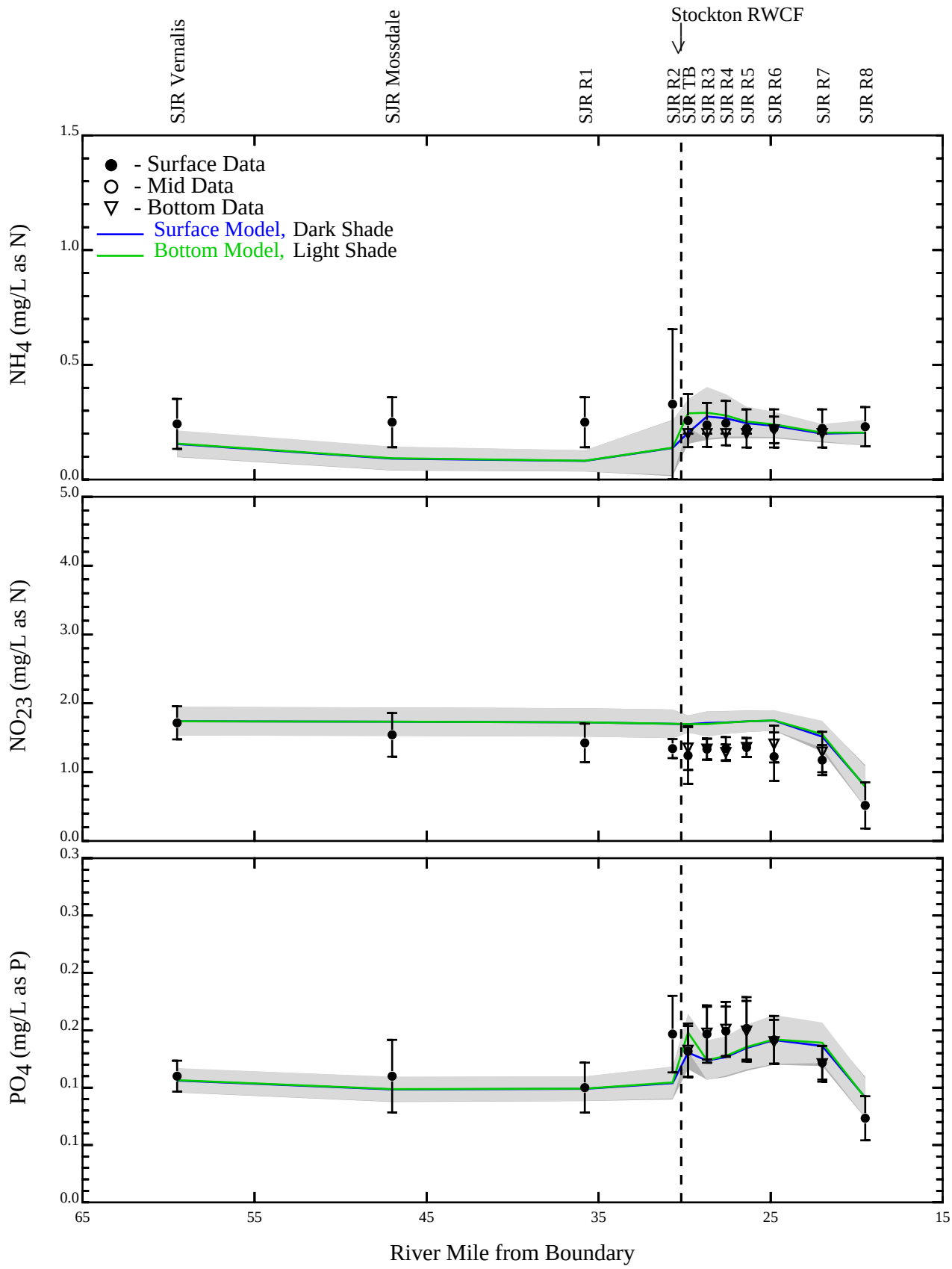

Figure 32. San Joaquin River Spatial Model Calibration and Data, June - October, 2000

Data Source: J&S Data Atlas

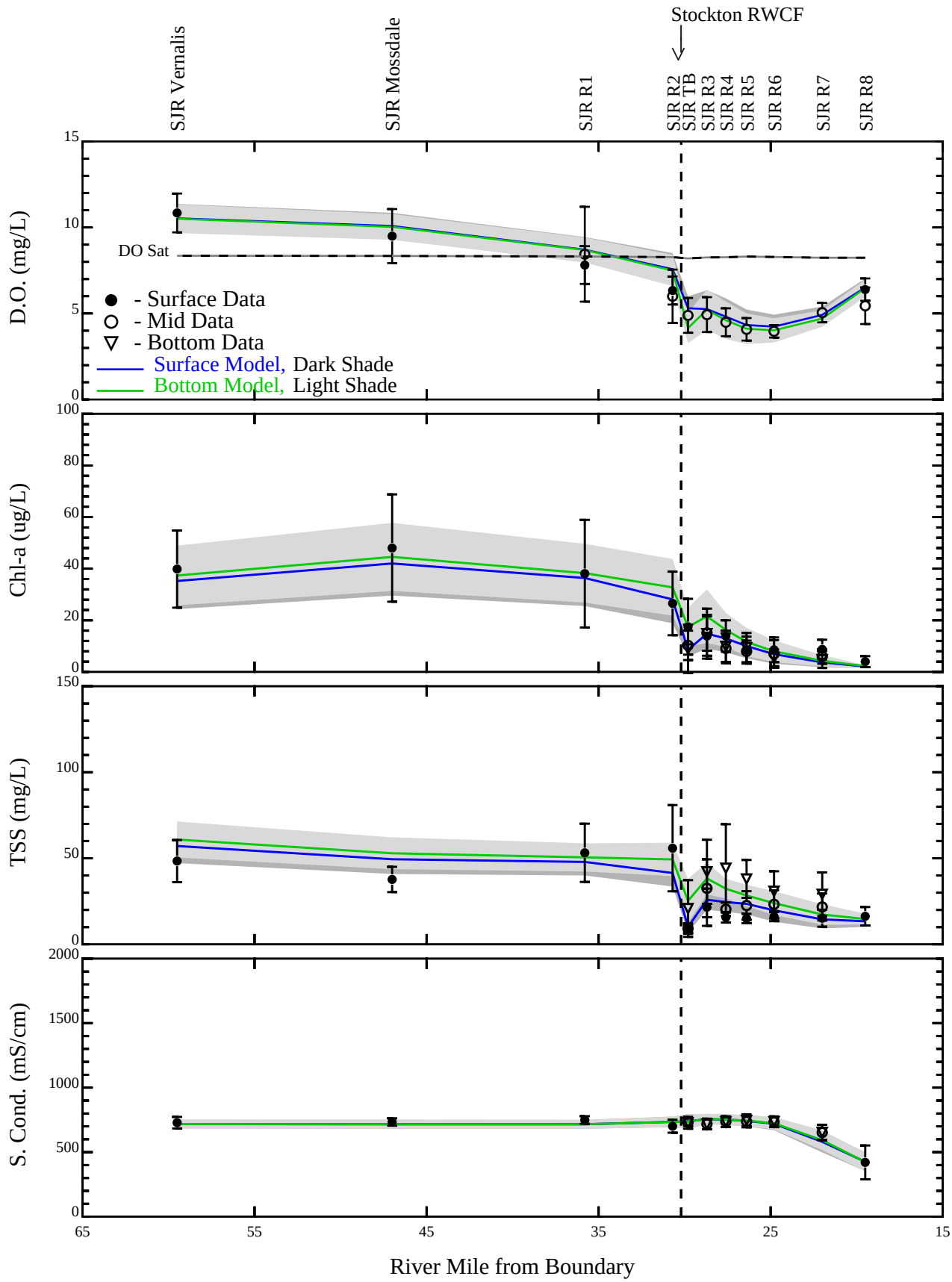

Figure 33. San Joaquin River Spatial Model Calibration and Data, June - October, 2001

DATE: 5/03/2006 TIME: 11:42:26

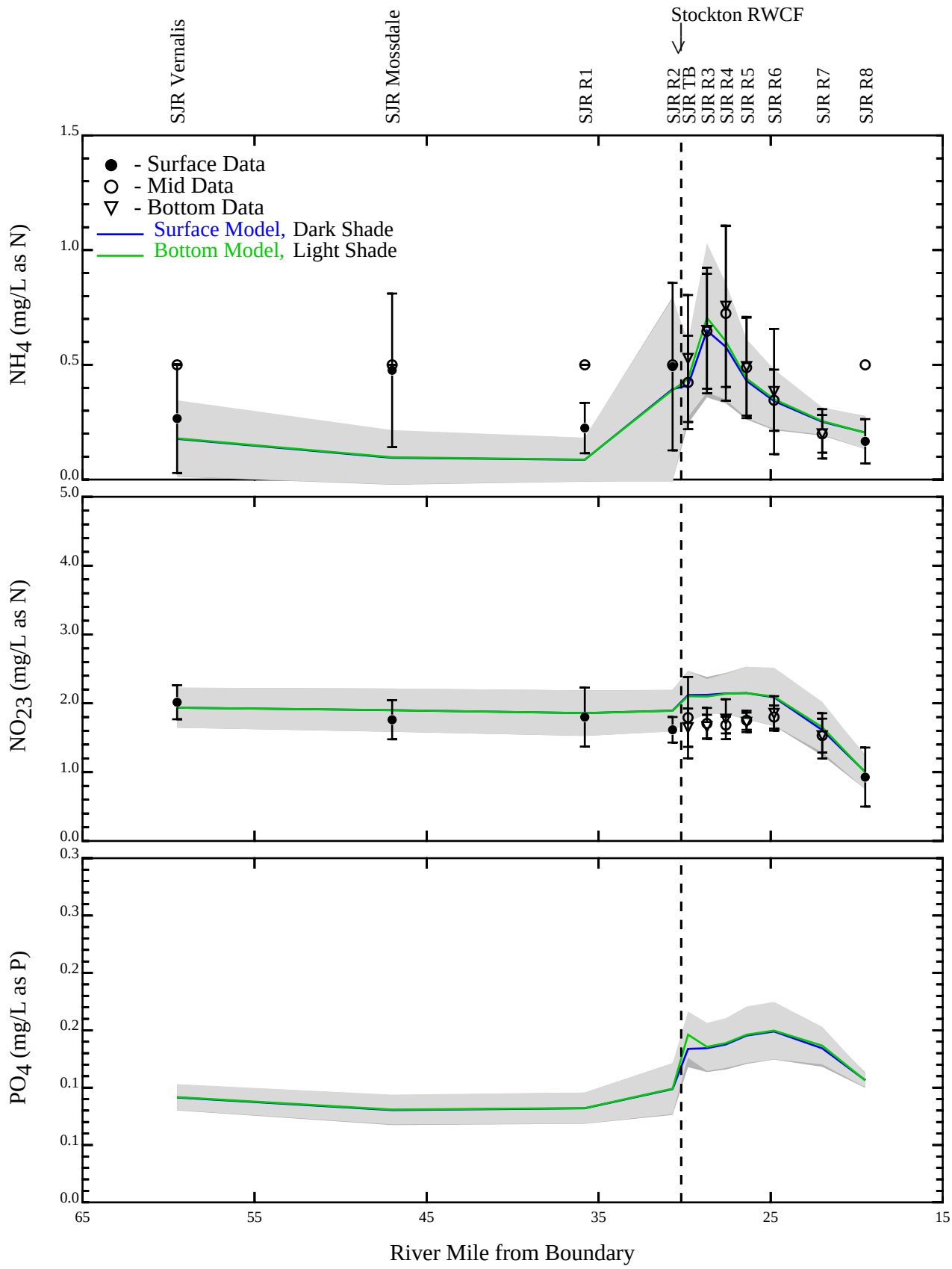

Figure 34. San Joaquin River Spatial Model Calibration and Data, June - October, 2001

DATE: 5/03/2006 TIME: 11:42:26

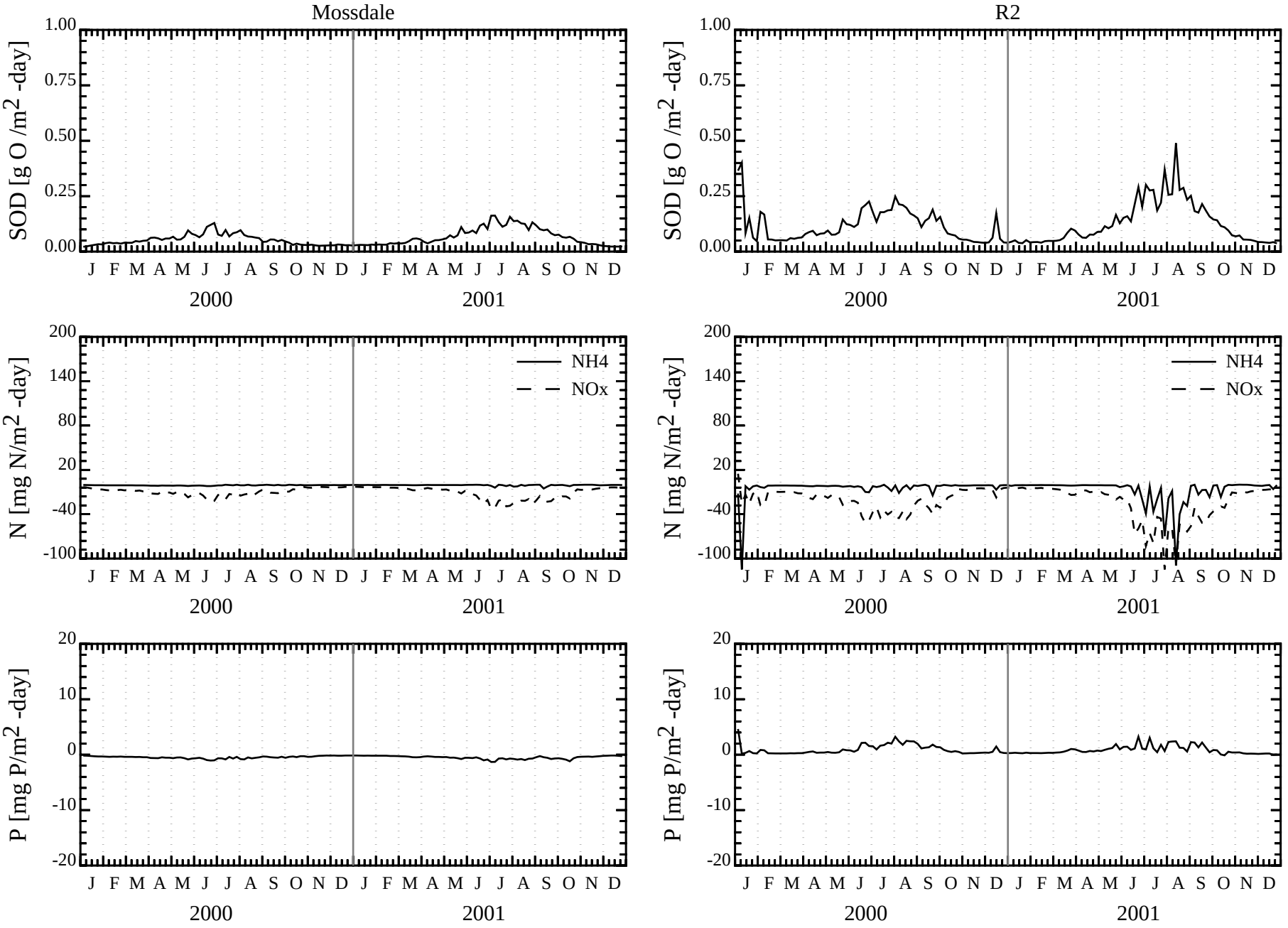

Figure 35. San Joaquin River Sediment Model and SOD Data at Mossdale & R2

Run=39v4Q

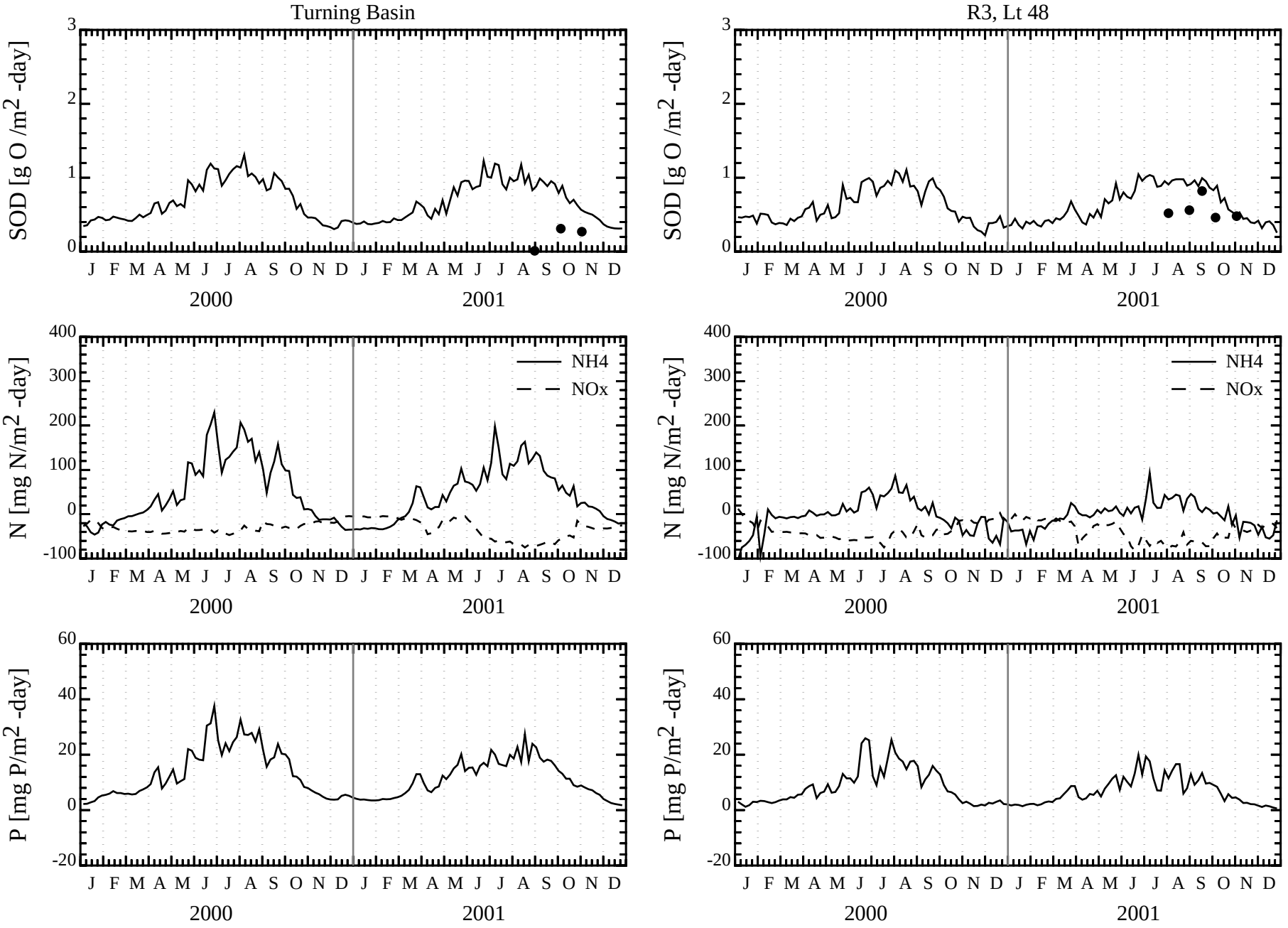

Figure 36. San Joaquin River Sediment Model and SOD Data at Turning Basin & R3, Lt. 48

Run=39v4Q

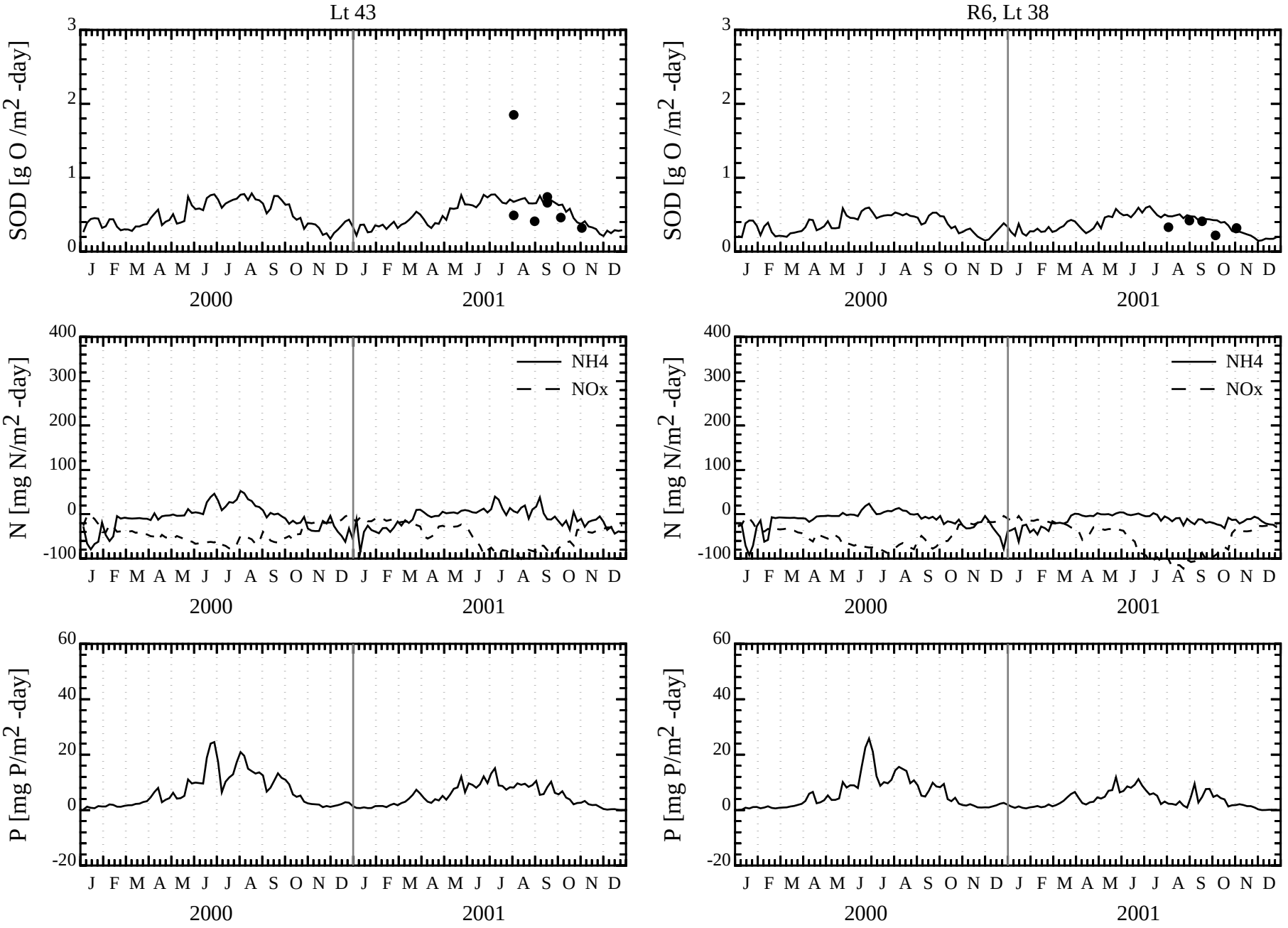

Figure 37. San Joaquin River Sediment Model and SOD Data at Lt. 43 & R2, Lt. 38

Run=39v4Q

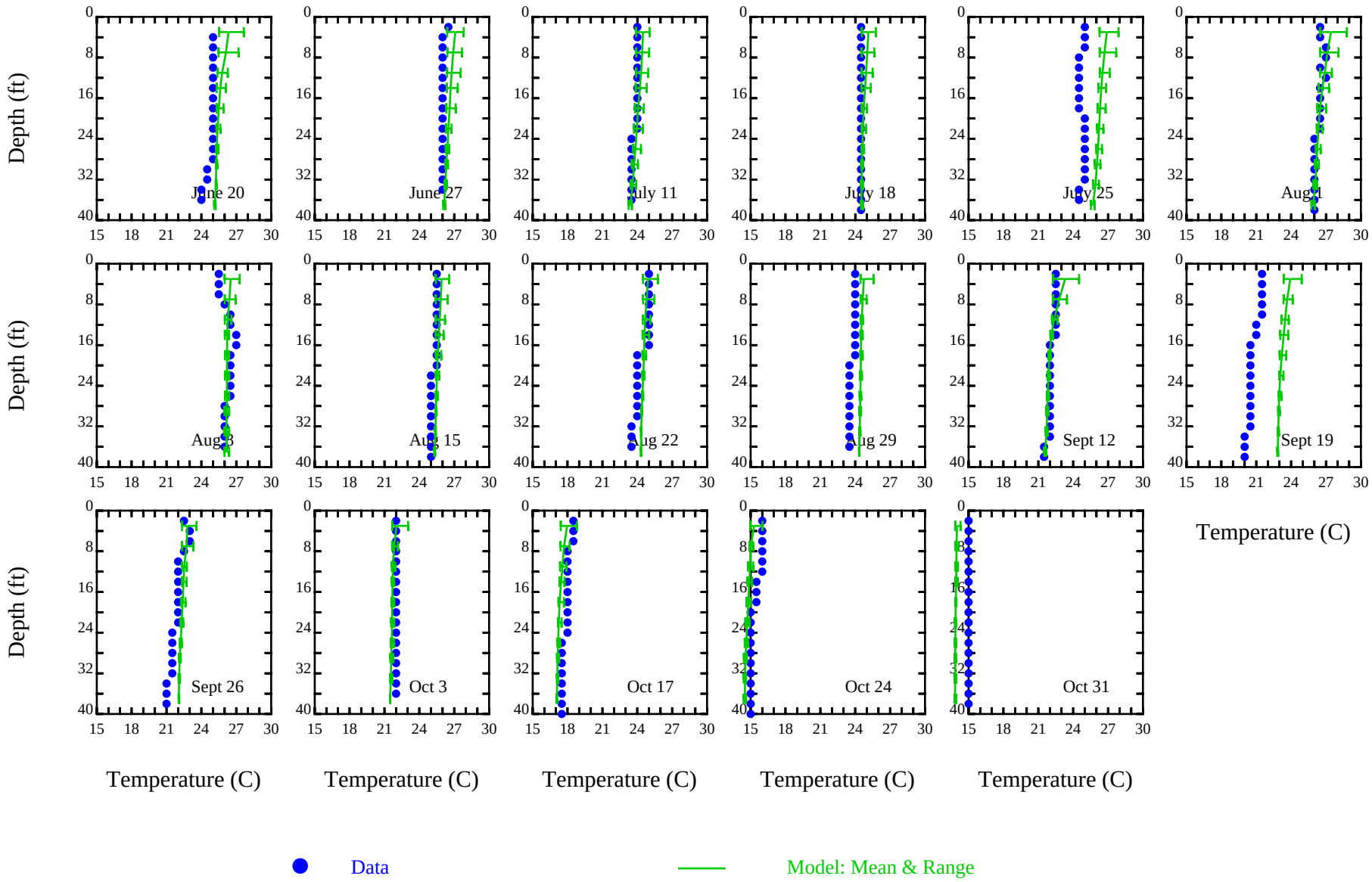

Figure 38. San Joaquin River at Turning Basin Data and Model Temperature Vertical Profiles, June-October 2000

vertdo.gdp, RUN39v4Q

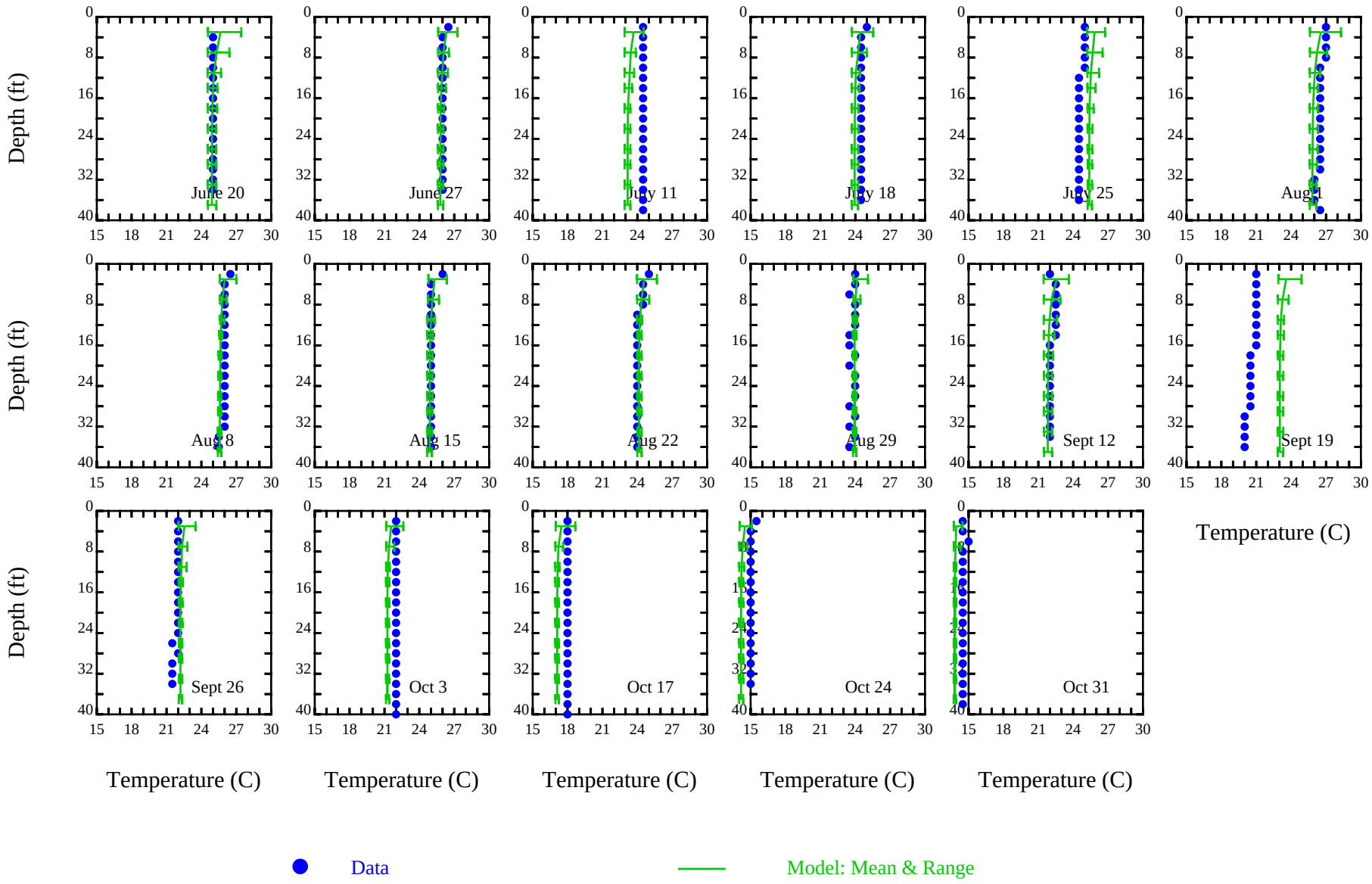

Figure 39. San Joaquin River at R5 Data and Model Temperature Vertical Profiles, June-October 2000

vertdo.gdp, RUN39v4Q

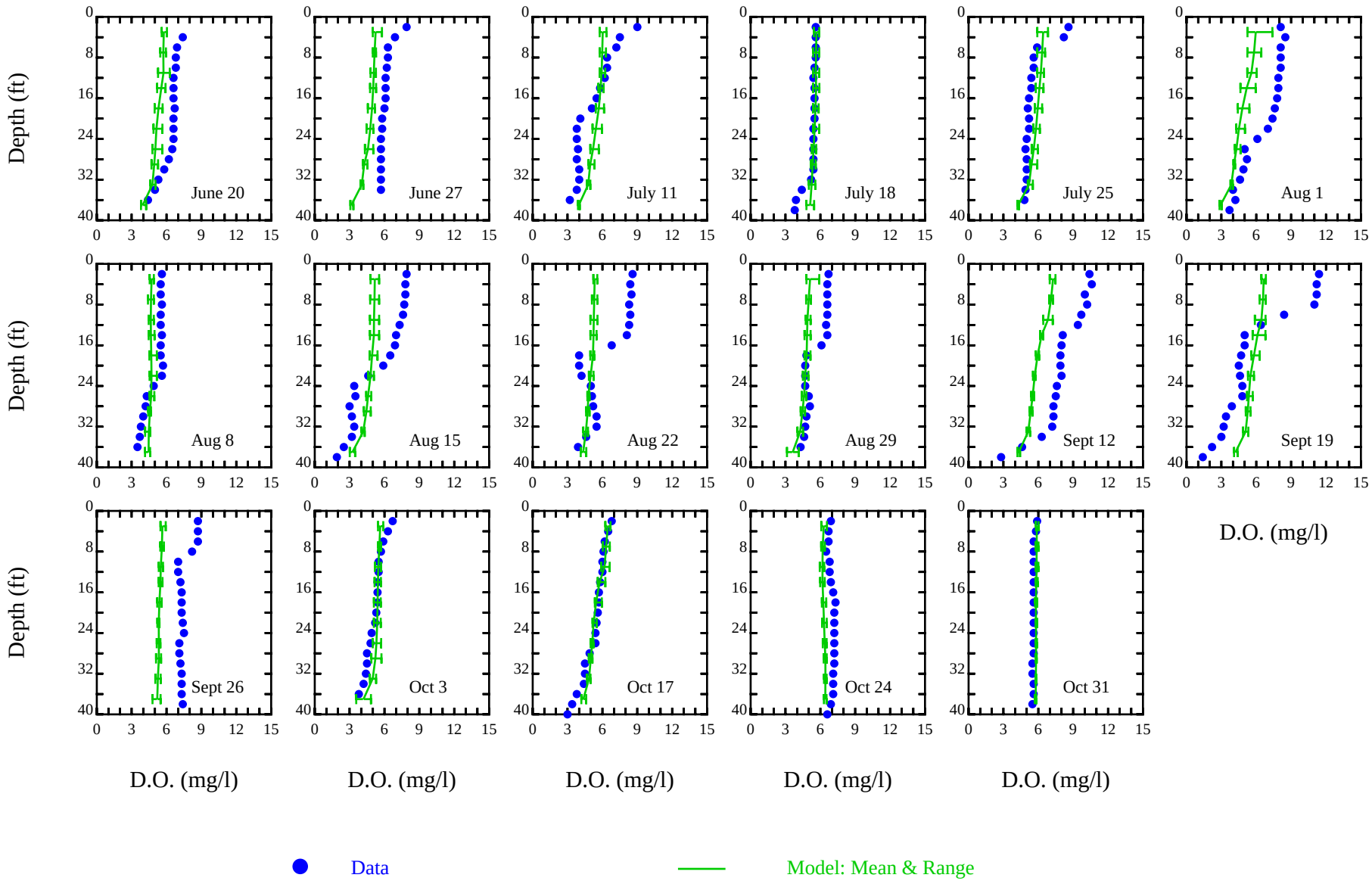

Figure 40. San Joaquin River at Turning Basin Data and Model Dissolved Oxygen Vertical Profiles, June-October 2000

vertdo.gdp, RUN39v4Q

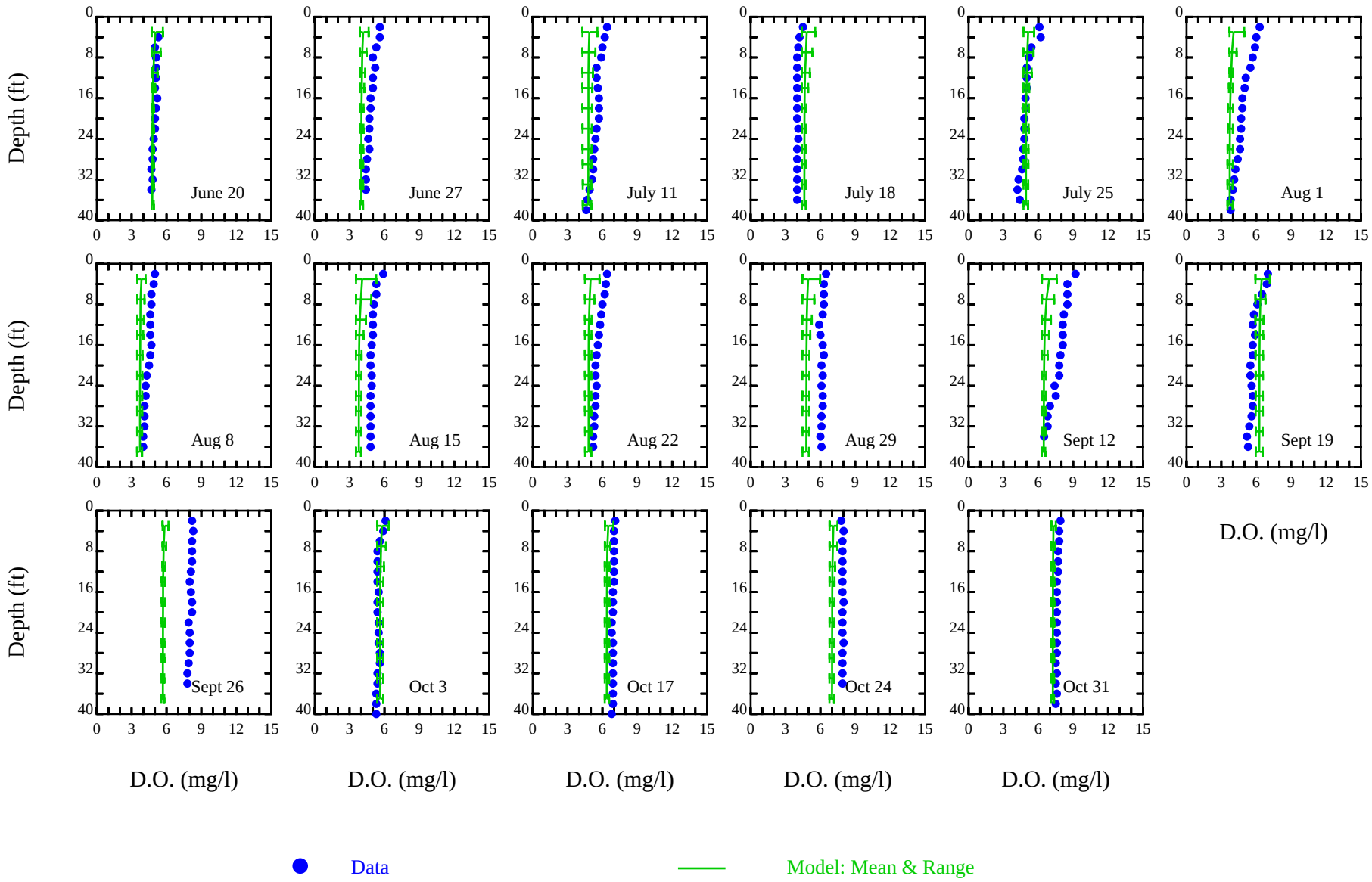

Figure 41. San Joaquin River at R5 Data and Model Dissolved Oxygen Vertical Profiles, June-October 2000

vertdo.gdp, RUN39v4Q

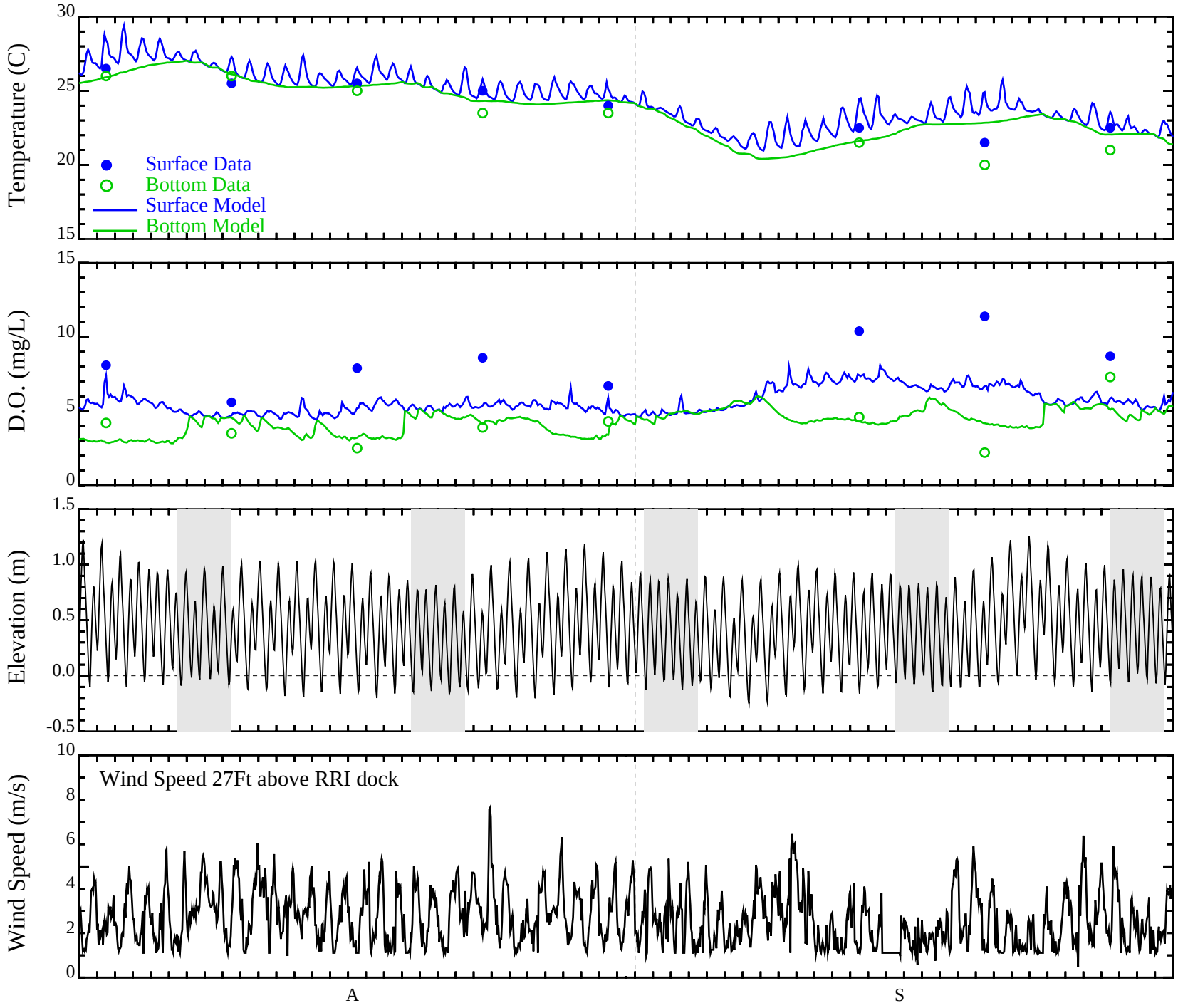

Figure 42. San Joaquin River Stratification, August-September 2000 Station: Turning Basin

Data Source: J&S Data Atlas

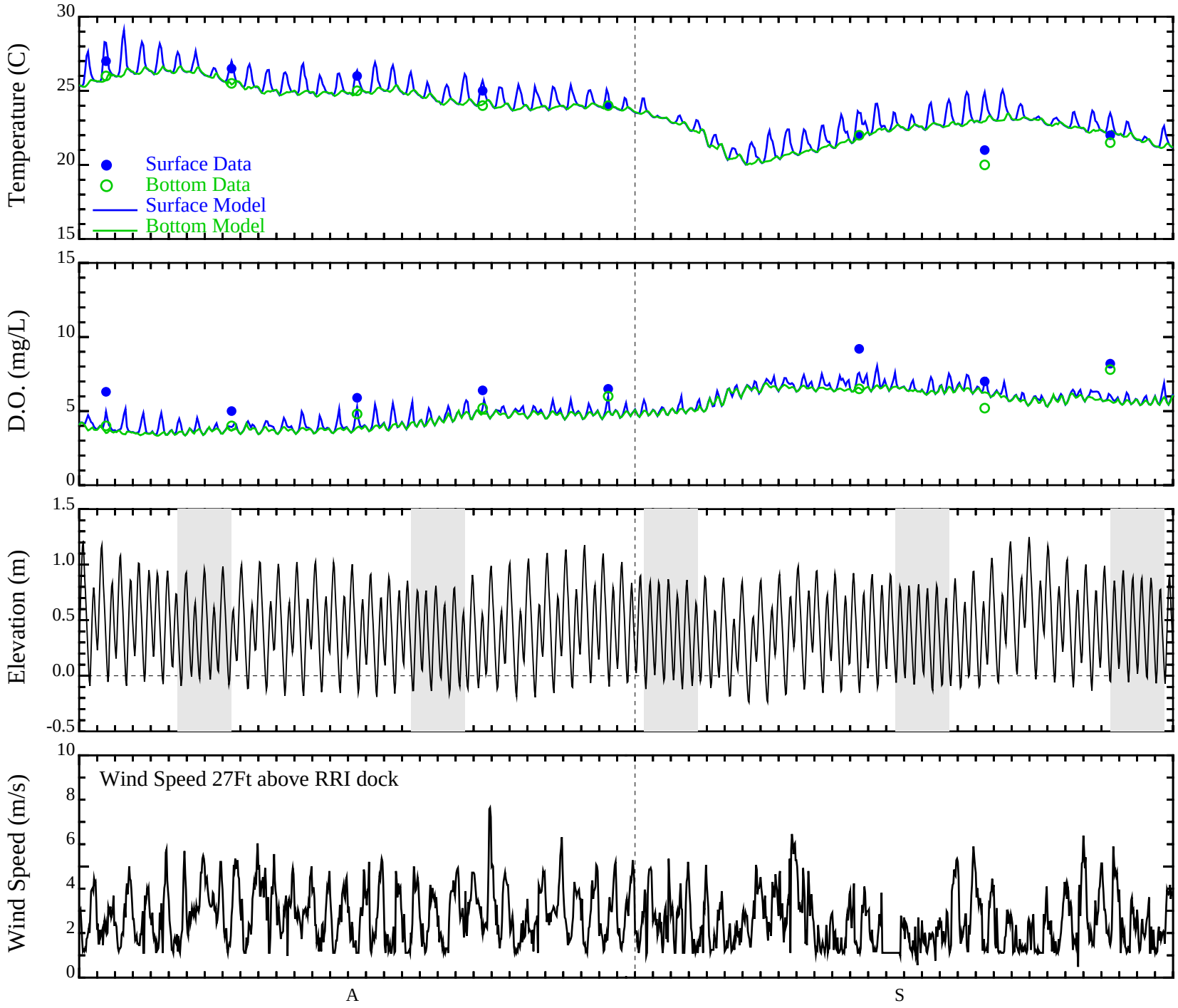

Figure 43. San Joaquin River Stratification, August-September 2000 Station: R5

Data Source: J&S Data Atlas

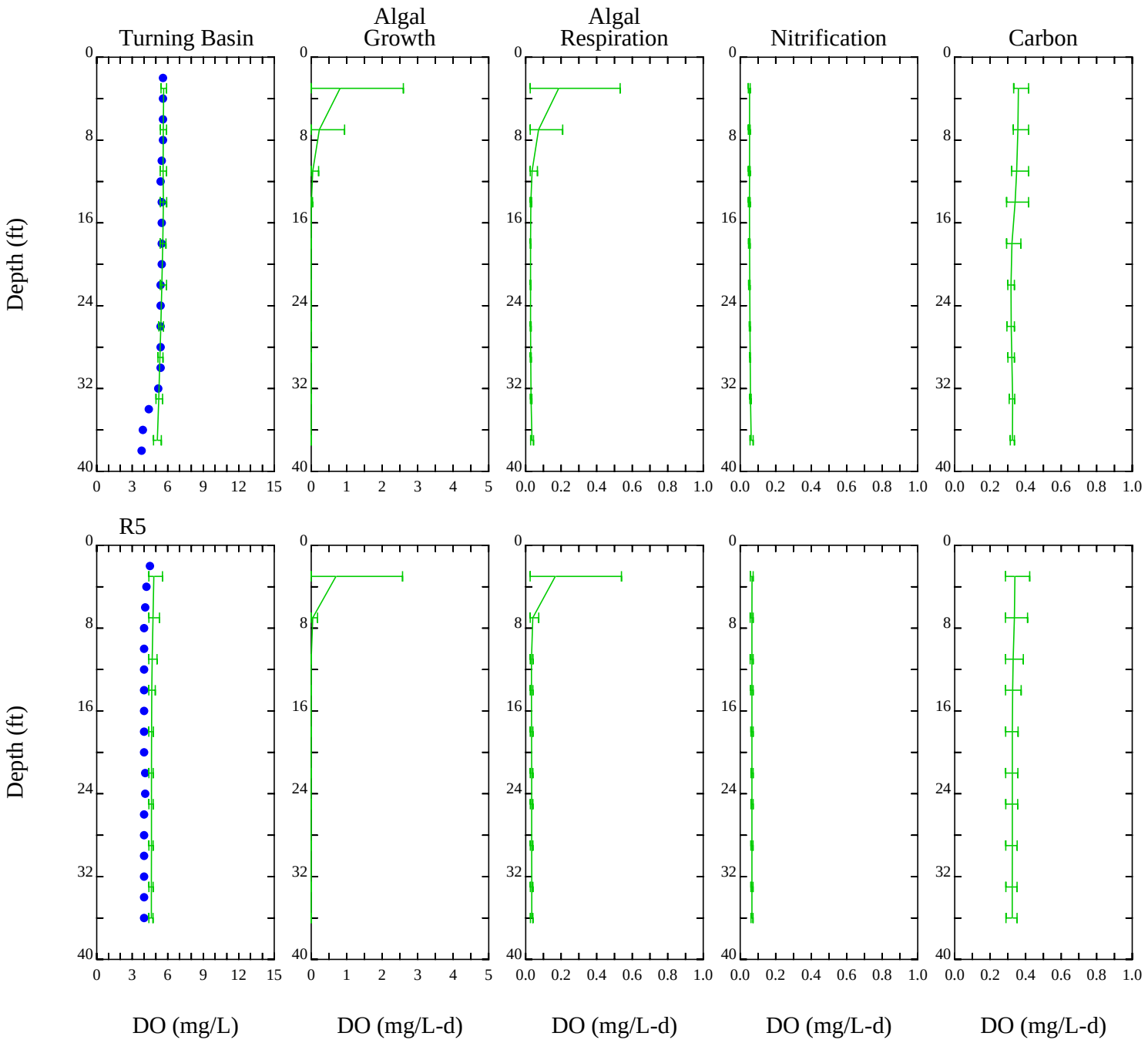

Figure 44. San Joaquin River Dissolved Oxygen Sources & Sinks at Turning Basin and R5: July 18, 2000

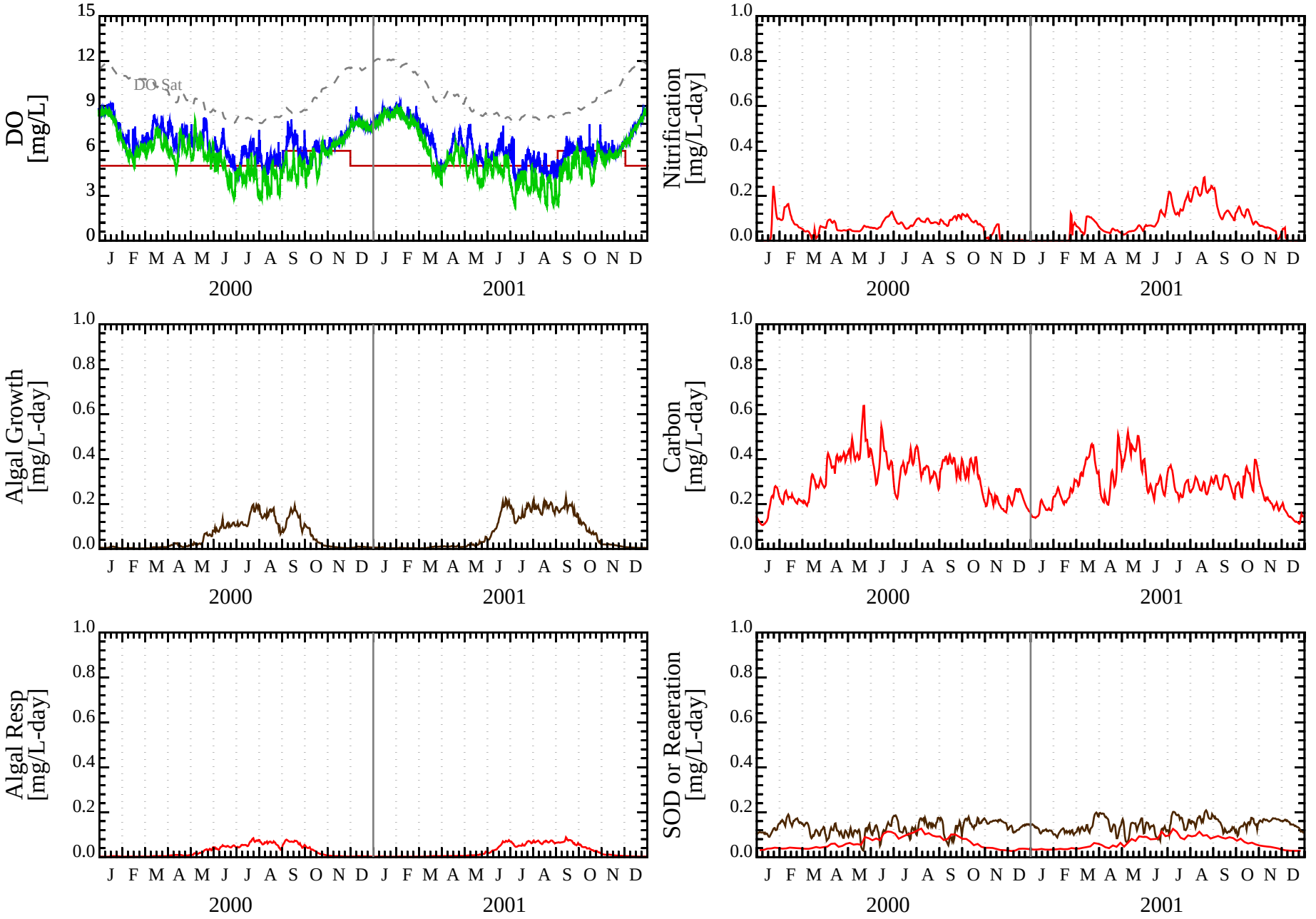

Figure 45. San Joaquin River Depth Averaged Dissolved Oxygen Deficit Components, TB

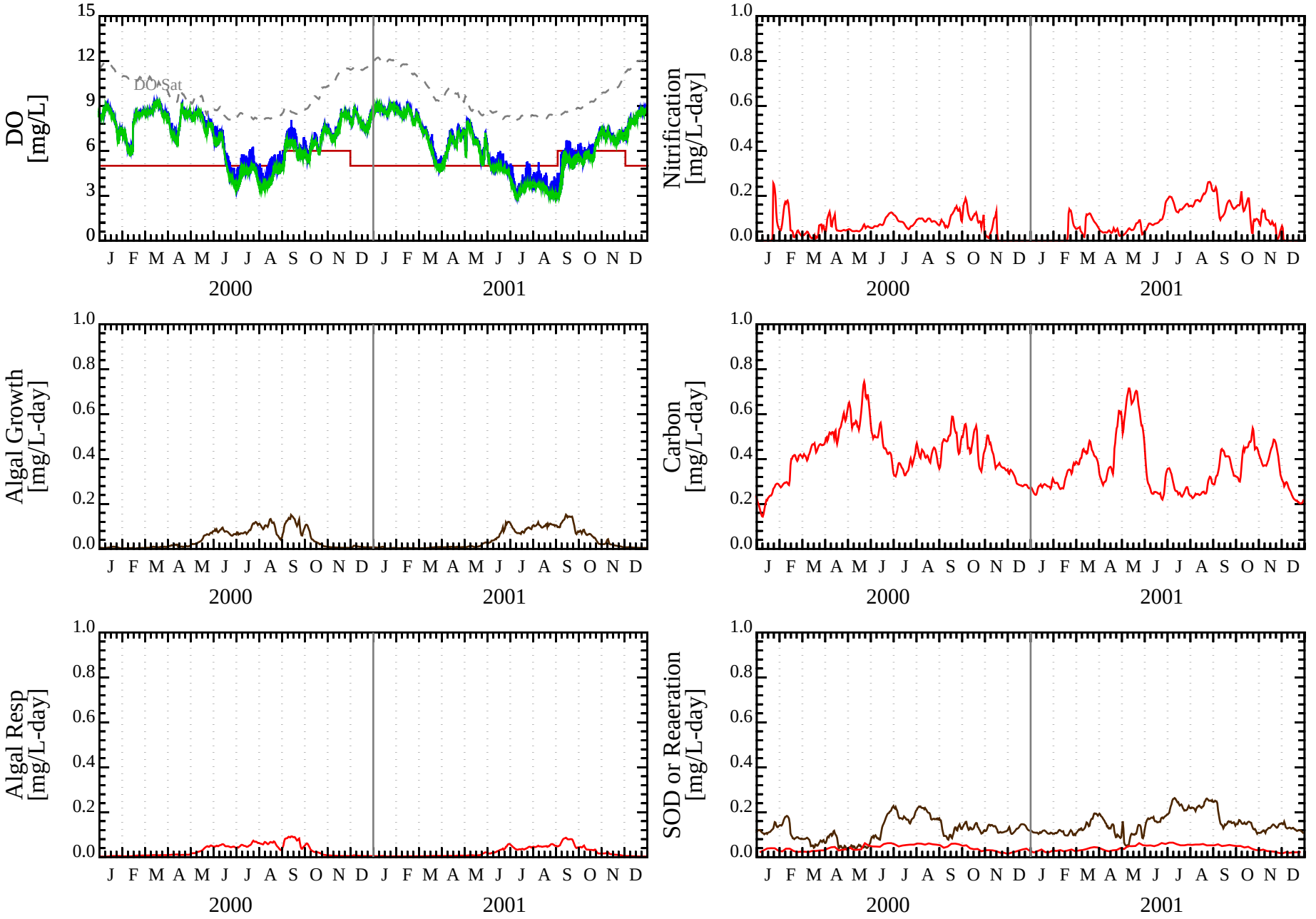

Figure 46. San Joaquin River Depth Averaged Dissolved Oxygen Deficit Components, R5

DATE: 5/01/2006 TIME: 15:44:48

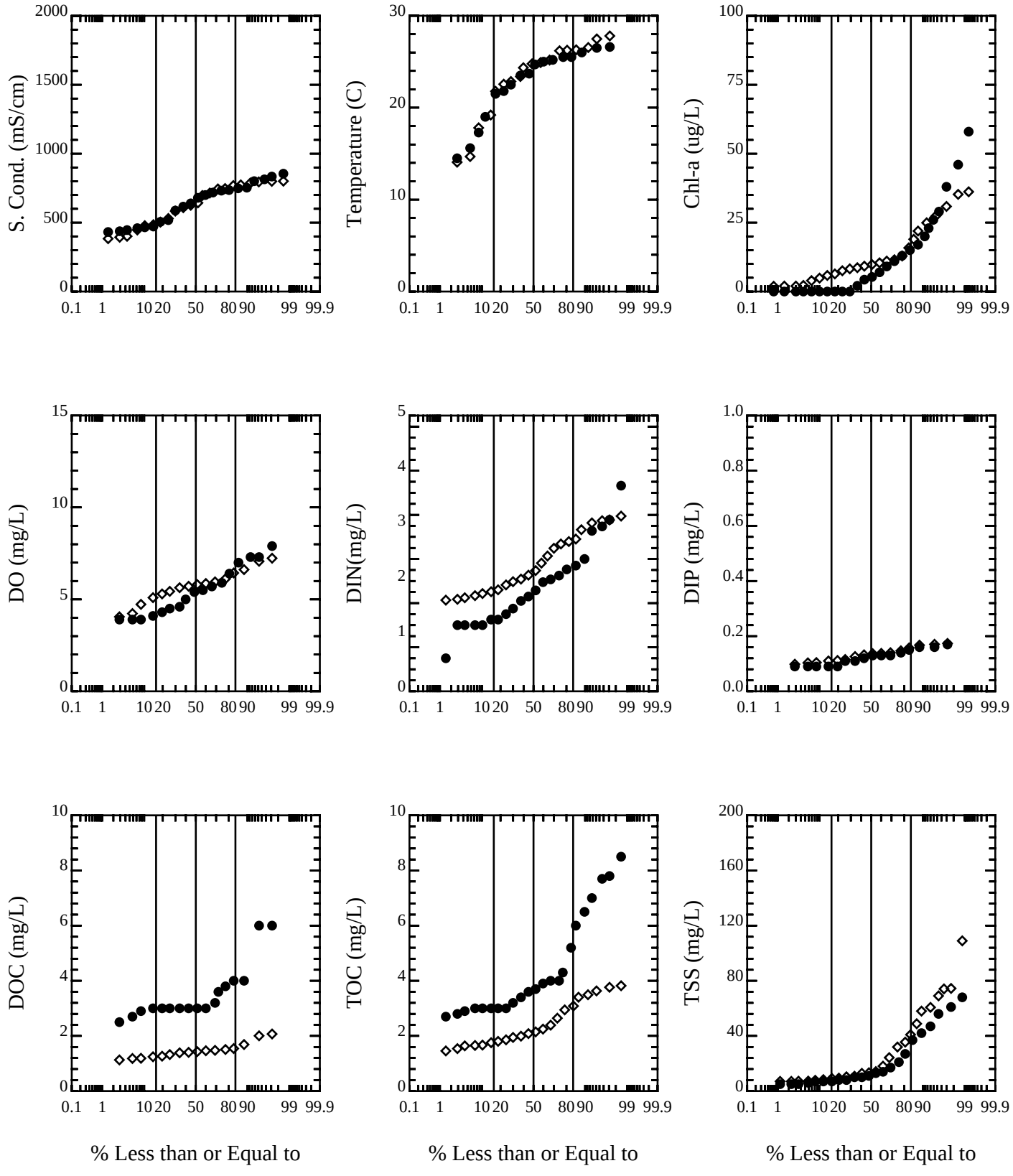

Figure 47. San Joaquin River, Model & Data Comparisons: SJR at Turning Basin

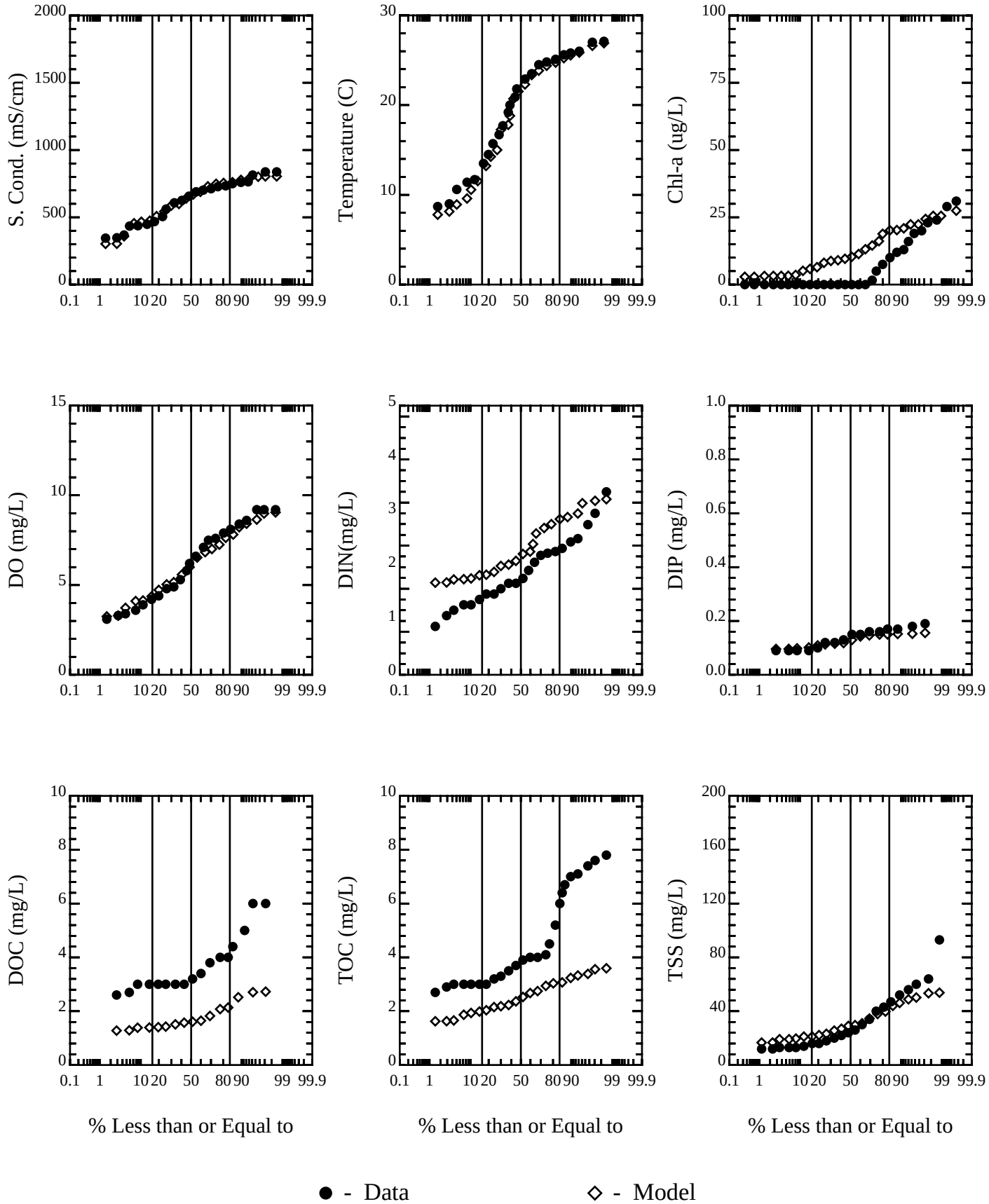

Figure 48. San Joaquin River, Model & Data Comparisons: SJR at R5

APPENDIX A

INTEGRATED EUTROPHICATION AND SEDIMENT NUTRIENT FLUX MODELS

TABLE OF CONTENTS

TABLES

FIGURES

1.0 KINETIC FRAMEWORK FOR THE INTEGRATED EUTROPHICATION MODEL

1.1 INTRODUCTION

This portion of the RCA Users Guide describes an integrated eutrophication/sediment nutrient flux modeling framework, available with the Public Domain release of RCA. In addition, the range in kinetic coefficients used in a number of eutrophication studies performed by HydroQual are provided as a reference.

1.1.1 Conservation of Mass

The modeling framework described in this document is based upon the principle of conservation of mass. The conservation of mass accounts for all of a material entering or leaving a body of water, transport of the material within the water body, and physical, chemical and biological transformations of the material. For an infinitesimal volume oriented along the axis of a three-dimensional coordinate system, a mathematical formulation of the conservation of mass may be written:

$$\frac{\partial c}{\partial t} = \underbrace{\frac{\partial}{\partial x}\left(E_x \frac{\partial c}{\partial x}\right) + \frac{\partial}{\partial y}\left(E_y \frac{\partial c}{\partial y}\right) + \frac{\partial}{\partial z}\left(E_z \frac{\partial c}{\partial z}\right)}_{\text{dispersive transport}} \underbrace{- U_x \frac{\partial c}{\partial x} - U_y \frac{\partial c}{\partial y} - U_z \frac{\partial c}{\partial z}}_{\text{advective transport}} \qquad (1\text{-}1)$$

$$\underbrace{\pm S(x,y,z,t)}_{\text{sources or sinks}} + \underbrace{W(x,y,z,t)}_{\text{external inputs}}$$

where:

c	=	concentration of the water quality variable [M/L^3],
t	=	time [T],
E	=	dispersion (mixing) coefficient due to tides and density and velocity gradients (L^2/T),
U	=	advective velocity (L/T),
S	=	sources and sinks of the water quality variable, representing kinetic interactions (M/L^3-T),
W	=	external inputs of the variable c (M/L^3-T),
x,y,z	=	longitudinal, lateral and vertical coordinates,
M,L,T	=	units of mass, length and time, respectively.

The modeling framework is made up of two components: (1) the transport due to freshwater flow in riverine systems and/or tidal, meteorological and density-driven currents in esturaine and coastal systems, and (2) the kinetic interactions between variables and the external inputs . Freshwater flow and/or density-driven currents and tidally and wind induced mixing are responsible for the movement of the water quality constituents within the waterbody.

External inputs of nutrients and oxygen-demanding material are derived from numerous sources, including: municipal and industrial discharges, combined sewer overflows (CSOs), storm sewer overflows (SSOs), natural surface runoff, and atmospheric deposition to the water surface of the waterbody.

The kinetics control the rates of interactions among the water quality constituents. Ideally, in a modeling effort, they should be independent of location per se, although they may be functions of exogenous variables, such as temperature and light, which may vary with location.

Analytical solutions are not available for partial differential equations of the form of Equation 1-1 except for the simplest cases. Instead, numerical methods are utilized to solve these mass balance equations. A specific method of solution employed in a majority of water quality modeling frameworks is known as the finite difference technique. First, the estuary is divided into finite volumes. Then a finite difference approximation of Equation 1-1 is applied to the i^{th} finite volume or segment, resulting in an equation of the form (see Thomann and Mueller, 1987):

$$V_i \frac{dc_i}{dt} = \sum_{j=1}^{n} R_{ij}\left(c_j - c_i\right) + \sum_{k=1}^{n} Q_{ki}c_k - \sum_{m=1}^{n} Q_{im}c_i \pm S_i + W_i \qquad (1\text{-}2)$$

$i = 1, 2, \ldots n$ (where n = number of segments)

where

V_i = volume of segment i (L^3),
c_i = concentration of the water quality variable in the i^{th} segment, (M/L^3),
R_{ij} = exchange between segment i and j resulting from dispersive mixing, (L^3/T),
Q_{ki} = net advective flow entering segment i from segment k, (L^3/T),
Q_{im} = net advective flow leaving segment i and going to segment m, (L^3/T),
S_i = sources and sinks, in segment i representing kinetic interactions, (M/T),
W_i = external inputs to segment i (M/T).

The exchange coefficients and advective flows are computed from

$$R_{ij} = \frac{E_{ij}\, A_{ij}}{L_{ij}} \qquad (1\text{-}3a)$$

and

$$Q_{ij} = A_{ij}\, U_{ij} \qquad (1\text{-}3b)$$

respectively, where E_{ij} is the dispersion coefficient, representing the overall phenomenon of mixing due to temporal variations in the tidal velocity, lateral and vertical gradients in velocity, and density differences within the water body; A_{ij} is the cross-sectional area of the ij interface; L_{ij} is the characteristic length defined as $(L_i + L_j)/2$; and U_{ij} is the net advective velocity from segment i to j. The term S_i, the sources and sinks of material in segment i, represents the kinetic interactions (physical, chemical and biological) occurring within the segment. These interactions may be functions only of the variable under consideration, for example, the first order decay of organic material. Alternately, they may involve the interactions between other variables, e.g., the first order feed-forward interaction between the oxidation of organic carbon (BOD) and dissolved oxygen, or the more complex interactions between phytoplankton biomass and nutrients, which involve non-linear feed-forward and feed-back interactions. The term W_i represents the external inputs of material into segment i, including point and nonpoint source loads, CSO loads, and/or atmospheric loads.

Mass balance equations in the form of Equation 1-2 are formulated for each segment in the estuary and for each state-variable included in the modeling framework. This results in $n \times m$ simultaneous finite difference equations to be solved, where n is the number of segments and m is the number of state-variables.

1.1.2 Choice of State Variables

An important criterion for the inclusion of variables in a modeling framework is the existence of adequate field data for calibration/verification of the variable, as well as the importance of the variable in the processes being considered. The kinetic framework employed of the integrated eutrophication is based on the LIS 3.0 eutrophication model developed for the Long Island Sound Study (HydroQual, Inc. 1991), the Massachusetts Bays Eutrophication Model (BEM) developed for the Massachusetts Water Resources Authority (MWRA) and the modeling effort of the Chesapeake Bay system (Cerco and Cole, 1995) and utilizes the following 26 state variables:

1. - salinity (S)
2. - phytoplankton carbon - winter assemblage (P_{c1})
3. - phytoplankton carbon - summer assemblage (P_{c2})
4. - phytoplankton carbon - fall assemblage (P_{c3})
5. - refractory particulate organic phosphorus (RPOP)
6. - labile particulate organic phosphorus (LPOP)
7. - refractory dissolved organic phosphorus (RDOP)
8. - labile dissolved organic phosphorus (LDOP)
9. - algal phosphorus + dissolved inorganic phosphorus (PO_4T)
10. - refractory particulate organic nitrogen (RPON)
11. - labile particulate organic nitrogen (LPON)
12. - refractory dissolved organic nitrogen (RDON)
13. - labile dissolved organic nitrogen (LDON)
14. - algal nitrogen + ammonia nitrogen (NH_4T)
15. - nitrite + nitrate nitrogen (NO_2+NO_3)
16. - biogenic silica - unavailable (SiU)
17. - algal silica + available silica (SiT)
18. - refractory particulate organic carbon (RPOC)
19. - labile particulate organic carbon (LPOC)
20. - refractory dissolved organic carbon (RDOC)
21. - labile dissolved organic carbon (LDOC)
22. - algal exudate dissolved organic carbon (ExDOC)
23. - reactive particulate organic carbon (RePOC)
24. - reactive dissolved organic carbon (ReDOC)
25. - dissolved oxygen equivalents (O_2^*)
26. - dissolved oxygen (DO)

The kinetic equations discussed below incorporate these state variables and are designed to simulate the annual cycle of phytoplankton production, its relation to the supply of nutrients and its effect on dissolved oxygen. The calculation is based on formulating the kinetics which govern the interactions of the

biota and the various nutrient forms, and the application of these kinetics to the waterbody within the context of mass conservation equations.

1.2 MODEL KINETICS

1.2.1 General Structure

Salinity is included in the eutrophicaton modeling framework to enable verification that the transport structure of the hydrodynamic model (Blumberg and Mellor, 1987) is transferred to the water quality model properly. For salinity there are no reaction kinetics involved, i.e., they are conservative. There are no direct sources or sinks of salinity, other than via exchange with the model boundaries or via freshwater dilution resulting from wastewater treatment facility discharges, CSOs, etc. and from freshwater rivers draining into the waterbody.

Figure 1-1 presents the principal kinetic interactions for the nutrient cycles and dissolved oxygen. In the phosphorus system kinetics, dissolved inorganic phosphorus (DIP) is utilized by phytoplankton for growth. Phosphorus is returned from the phytoplankton biomass pool to the various dissolved and particulate organic phosphorus pools and to DIP through endogenous respiration and predatory grazing. The various forms of organic phosphorus are converted to DIP at a temperature dependent rate.

The kinetics of the nitrogen species are fundamentally the same as the kinetics of the phosphorus system. Ammonia and nitrite + nitrate are used by phytoplankton for growth. Ammonia is the preferred form of inorganic nitrogen for algal growth, but phytoplankton will utilize nitrite + nitrate nitrogen as ammonia concentrations become depleted. Nitrogen is returned from algal biomass and follows pathways that are similar to those of phosphorus. Organic nitrogen is converted to ammonia at a temperature dependent rate, and ammonia is then converted to nitrite + nitrate (nitrification) at a temperature and oxygen dependent rate. Nitrite + nitrate may be converted to nitrogen gas (denitrification) in the absence of oxygen at a temperature dependent rate.

Available silica is utilized by diatom phytoplankton during growth. Silica is returned to the unavailable silica pool during respiration and predation and must undergo mineralization processes before becoming available for phytoplankton growth.

Dissolved oxygen is coupled to the other state variables. The sources of oxygen considered are reaeration and algal photosynthesis. The sinks of oxygen are algal respiration, oxidation of detrital carbon and carbonaceous material from wastewater treatment plant effluents and nonpoint discharges, nitrification and SOD.

Organic carbon sources include anthropogenic inputs and the by-products of primary production and zooplankton grazing. The kinetic subroutine also incorporates two highly reactive organic carbon pools that can be used to represent organic carbon inputs from combined sewer overflows (CSOs) and/or waste water treatment plants (WWTPs) with poor treatment performance. The sink of organic carbon is via bacterial decomposition or oxidation. Specific details for the above reactions are presented below.

1.2.2 Phytoplankton Growth and Loss Kinetics

The current implementation of RCA permits the user to simulate up to three functional algal groups. They may represent a winter diatom group, a summer mixed assemblage, a fall mixed assemblage or they may represent a winter diatom group, a late spring/summer green group, and a late summer blue-green species (such as *Microcystis* or *Amabena*). The user, however, does have the option of implementing one, two, or three groups. In case, any kinetic framework employed for all three functional algal groups is the same, only the choice of model coefficients is different. It is convenient to express the kinetic source term for phytoplankton, S_P, as the difference between the phytoplankton growth rate, G_P, and the loss rate, D_P. That is:

$$S_p = (G_p - D_p)P \tag{1-4}$$

where P is the phytoplankton biomass (in units of carbon), and where G_P and D_P have units (day^{-1}). The balance between the magnitude of the growth rate and the loss rate (together with the transport and mixing) determines the rate at which phytoplankton mass is created (or lost) in each volume element.

The growth rate of a population of phytoplankton in a natural environment is a complicated function of the species of phytoplankton present and their differing reactions to solar radiation, temperature, and the balance between nutrient availability and nutrient requirements. In order to construct a growth function, a simplified approach is followed. Rather than consider the problem of different species and their associated environmental and nutrient requirements, the population is characterized as a whole by a measurement of the biomass of the phytoplankton present.

For single species, the direct measure of the population size is the number of cells per unit volume. Cell counts of a single species may be obtained fairly readily in a well-controlled laboratory environment. However, in naturally occurring populations, this measure may be somewhat ambiguous. It is often difficult to distinguish between viable and non-viable cells, and colonizing species tend to pose a problem because counts usually do not distinguish individual cells, and the sizes of the colonies are quite variable.

The sum of the numbers of each species, the total count, could be used to characterize biomass, but since cell size varies substantially, the pico-phytoplankton would dominate such an aggregation. To account for this, the total bio-volume, or wet weight of phytoplankton, assuming unit density, can be calculated using characteristic volumes for each identified species. Unfortunately, volumes can vary appreciably as a function of nutrient availability. Conversion to phytoplankton dry weight and carbon involves further species-dependent constants, which are also nutrient dependent, and, therefore, are subject to variation and uncertainty. Thus, although the use of phytoplankton dry weight or carbon concentration is an appealing solution to the issue of aggregation, it suffers from some practical difficulties.

An alternative approach to this problem is to measure a parameter which is characteristic of all phytoplankton, namely, chlorophyll-a (chl-a), and to use this as the aggregated variable. The principal advantages are that the measurement is direct, it integrates cell types and age, and it accounts for cell viability. The principal disadvantages are that it is a community measurement with no differentiation between functional groups (for example, diatoms or blue-green algae), and it is not necessarily a good measurement of standing crop in dry weight or carbon units, since the chlorophyll to dry weight and

chlorophyll to carbon ratios are variable, and non-active chlorophyll (phaeo-pigments) must be measured to determine viable chlorophyll concentrations.

As can be seen from the above discussion, no simple aggregate measurement is entirely satisfactory. From a historical and practical point of view, the availability of extensive chlorophyll-a data for many waterbodies essentially dictates its use as the aggregate measure of the phytoplankton population, or biomass, for calibration and verification purposes. However, for internal computations, the eutrophication model uses phytoplankton carbon as a measure of algal biomass. The reasons for choosing phytoplankton carbon, rather than chl-a as the internal state variable, are twofold. The first reflects the fact that measures of primary production (an important measure of carbon fixation or growth) are made in carbon units. The second reason is that the use of phytoplankton carbon greatly facilitates the model computation of oxygen-demanding material deposited to the sediment bed via settling.

1.2.2.1 Standard Algal Growth Model

At the current time, HydroQual uses one of two algal growth model formulations. The first of these (to be referred to as the "standard" algal growth model formulation) dates back to the early work of DiToro, O'Connor, and Thomann on the Sacramento-San Joaquin River system (DiToro et al., 1971), the Great Lakes (DiToro and Matystik, 1980, DiToro and Connolly, 1980), and the Potomac Estuary (Thomann et al, 1974, Thomann and Fitzpatrick, 1982). The second algal growth model (to be referred to as the Laws and Chalup model) is based on the model developed by Laws and Chalup (1990) and applied by HydroQual (1995) to the Massachusetts Bays system.

To date, the standard model has been applied by HydroQual to more studies than has the Laws and Chalup model, but we feel there is merit in making both versions of the algal growth model available to the user. The details of the standard model will be presented first, followed by the Laws and Chalup model. These in turn will be followed by a description of the nutrient and dissolved oxygen kinetics.

With the choice of biomass units established, i.e., a carbon based system (mg C/L or gm C/m^3), a growth rate, which expresses the rate of production of biomass as a function of the important environmental variables, temperature, light and nutrients, may be developed. The specific growth rate, G_P, is related to G_{Pmax}, the maximum growth rate at optimum light, temperature and nutrients, via the following equation:

$$G_p = G_{Pmax} \cdot \underbrace{G_T(T)}_{\text{temperature}} \cdot \underbrace{G_I(I)}_{\text{light}} \cdot \underbrace{G_N(N)}_{\text{nutrients}} \qquad (1\text{-}5)$$

where
$G_T(T)$ is the effect of temperature, $G_I(I)$ is the light attenuation given by

$$G_I(I) = g(I, f, H, k_e) \qquad (1\text{-}6)$$

and $G_N(N)$ is the nutrient limitation given by

$$G_N(N) = g(DIP, DIN, Si) \qquad (1\text{-}7)$$

where T is the ambient water temperature; I is the incident solar radiation; f is the fraction of daylight; H is the depth of the water column; k_e is the extinction or light attenuation coefficient; and DIP, DIN and Si are the available nutrients required for growth, dissolved inorganic phosphorus (ortho-phosphate), dissolved inorganic nitrogen (ammonia plus nitrite/nitrate) and dissolved available silica, respectively.

Initial estimates of G_{Pmax} are generally based upon the literature and/or previous modeling studies and are subsequently refined during the calibration process. During the simulation, the selected maximum growth rates are temperature corrected using spatially-dependent, time-dependent water column temperature values as computed by the hydrodynamic model. The temperature corrected growth rate is computed using one of the two following equations, which relates $G_{Pmax}(T)$, the growth rate at ambient temperature, T, to $G_{Pmax}(T_{20})$ the growth rate at 20°C (via equation (1-8a)) or to $G_{Pmax}(T_{opt})$, the growth rate at the optimal temperature, T_{opt} (via equations (1-8b) and (1-8c)):

$$G_{P\max}(T) = G_{P\max}(T_{20})\ \theta^{T-20} \qquad (1\text{-}8a)$$

$$G_{P\max}(T) = G_{P\max} e^{-\beta_1 (T_{opt}-T)^2} \qquad T \le T_{opt} \qquad (1\text{-}8b)$$

or

$$G_{P\max}(T) = G_{P\max} e^{-\beta_2 (T_{opt}-T)^2} \qquad T > T_{opt} \qquad (1\text{-}8c)$$

where θ is the Arrenhius temperature coefficient, and β_1 and β_2 are shaping coefficients. When using equations 1-8b and 1-8c to temperature correct G_{Pmax}, T_{opt} has a much lower value for winter diatoms then would be used for the summer mixed assemblage. It is suggested to utilize the Arrenhius formulation when modeling one functional algal group and the shaped formulation when modeling two or more functional groups.

Figure 1-2 presents comparisons of the two temperature correction formulations. In Figure 1-2a, the normalized growth rates are compared for the Arrenhius (normalized to the 20°C growth rate versus the shaped formulation (normalized to the maximum growth rate at the optimum temperature) for a winter temperature optimum of 8°C and a summer temperature optimum of 24°C. Figure 1-2b presents a similar comparison but for "actual" growth rates of 1.7, 2.2, and 3.0 day for the Arrenhius, winter-shaped, and summer-shaped formulations. The temperature corrected growth rate is then adjusted to reflect effects due to ambient light and nutrient levels.

In the natural environment, the light intensity to which the phytoplankton are exposed is not uniformly at the optimum value. At the surface and near-surface of the air-water interface, photo-inhibition can occur due to high light intensities, while at depths below the euphotic zone, light is not available for photosynthesis due to natural and algal related turbidity. The light formulation included in the standard RCA modeling framework extends from a light curve analysis by Steele (1962) and accounts for both the effects of saturating light intensities and light attenuation through the water column. The depth-averaged light attenuated growth rate factor, $G_I(I)$, is presented in Equation 1-9 and is obtained by integrating the specific growth rate over depth:

where:

$$G_I(I) = \frac{e}{k_e H}\left[\exp\left(\frac{-I_o(t)}{I_s}e^{-k_e H}\right) - \exp\frac{-I_o(t)}{I_s}\right] \quad (1\text{-}9)$$

e = 2.718
H = the water column depth or thickness of the water cell or segment (m),
k_e = the total extinction coefficient, $k_{ebase} + k_c P_{chl\text{-}a}$ computed from the sum of the base, non-algal related, light attenuation, k_{ebase}, and the self-shading attenuation due to the ambient phytoplankton population $k_c P_{chl\text{-}a}$ (m^{-1}),
k_c = the algal related extinction coefficient per unit of chlorophyll (m^2/mg chl-a),
$P_{chl\text{-}a}$ = the ambient phytoplankton population as chlorophyll (mg chl-a/L), where $P_{chl\text{-}a} = P_c/a_{cchl}$
P_c = the ambient phytoplankton population as carbon (mg C/L),
a_{cchl} = the ratio of algal carbon to algal chlorophyll (mg C/mg chl-a),
I_o = the incident light intensity at the segment surface (ly/day),
I_s = the saturating light intensity (ly/day).

The value of I_o at the water surface, I_{surf}, may be evaluated at any time, t, within the day using the following formula:

$$I_{surf}(t) = \frac{I_{tot}}{0.635\,f}\sin\left[\frac{\pi(t_d - t_{sunrise})}{f}\right] \quad (1\text{-}10)$$

where
I_{tot} = total daily incident solar radiation (ly/day),
f = fraction of daylight (daylight hours/24),
t_d = time of day,
$t_{sunrise}$ = time of sunrise

To account for the effect of variations of available light as a function of depth, the light intensity, I_o (H), at any depth, H, is related to the incident surface intensity, I_{surf}, via the extinction coefficient, k_e through the formula

$$I_o(H) = I_{surf}\exp^{-k_e H} \quad (1\text{-}11)$$

The effects of various nutrient concentrations on the growth of phytoplankton have been investigated, and the results are quite complex. As a first approximation to the effect of nutrient concentration on the growth rate, it is assumed that the phytoplankton population in question follows Monod growth kinetics with respect to the important nutrients. That is, at an adequate level of nutrient concentration, the growth rate proceeds at the saturated rate for the ambient temperature and light conditions. However, at low nutrient concentration, the growth rate becomes linearly proportional to nutrient concentration. Thus, for a nutrient with concentration N_j in the j^{th} segment, the factor by which the saturated growth rate is reduced in the j^{th} segment is $N_j/(K_m + N_j)$. The constant, K_m, which is called the Michaelis or half-saturation constant, is the nutrient concentration at which the growth rate is half the saturated growth rate. Since there are three nutrients, nitrogen, phosphorus and silica, considered in this

framework, the Michaelis-Menton expression is evaluated for each nutrient and the minimum value is chosen to reduce the saturated growth rate,

$$G_N(N) = \text{Min}\left(\frac{DIN}{K_{mN}+DIN}, \frac{DIP}{K_{mP}+DIP}, \frac{Si}{K_{mSi}+Si}\right) \quad (1\text{-}12)$$

Numerous mechanisms have been proposed which contribute to the death rate of phytoplankton: endogenous respiration, grazing by herbivorous zooplankton, sinking or settling from the water column and parasitization (Fogg, 1965). The first three mechanisms have been included in previous models for phytoplankton dynamics and they have been shown to be of general importance. For this version of the integrated eutrophication model, only endogenous respiration and settling have been explicitly included in the modeling framework. The effect of zooplankton grazing is included indirectly using a first-order temperature corrected algal loss rate.

The endogenous respiration rate of phytoplankton is the rate at which the phytoplankton oxidize their organic carbon to carbon dioxide per unit weight of phytoplankton organic carbon. Respiration is the reverse of the photosynthesis process, and as such, contributes to the loss rate of the phytoplankton population. If the respiration rate of the phytoplankton, as a whole, is greater than the growth rate, there is a net loss of phytoplankton carbon or biomass. The endogenous respiration rate has been shown to be temperature dependent (Riley et al., 1949) and historically has been included in eutrophication models using Equation 1-13a,

$$k_{PR}(T) = k_{PR}(20^oC) \cdot \theta_{PR}^{(T-20)} \quad (1\text{-}13a)$$

where k_{PR} (20°C) is the endogenous respiration rate at 20°C, and k_{PR}(T) is the temperature corrected rate. The units of k_{PR} are day^{-1}.

However, more recently the literature (Laws and Bannister, 1980, Laws and Chalup, 1991) suggests that algal respiration should be divided into two components - basal or resting respiration and respiratory losses associated with photosynthesis. This may be written mathematically as follows:

$$k_{PR}(T) = r_g G_P + r_b \theta_{PR}^{T-20} \quad (1\text{-}13b)$$

where r_g is the fraction of the algal growth (G_P) lost to the energy cost of photosynthesis and r_b is the basal respiration rate. Note, the user can select either form of the respiration rate equation when performing a simulation. If the user wishes to use the first formulation (equation 1-13a) then set r_g equal to zero and use an appropriate value for r_b (~0.1-0.3/day). If the user wises to use the latter form (equation 1-13b) then set r_g to a non-zero value (0.1-0.3) and use a lower value (0.01-0.03/day) for r_b.

The sinking or settling of phytoplankton is an important contribution to the overall mortality of the phytoplankton population, particularly in lakes and coastal oceanic waters. Published values of the sinking velocity of phytoplankton, mostly in quiescent laboratory conditions, range from 0.1 to 18.0 m/day. However, in some instances for certain species, such as dinoflagellates or buoyancy-retulating blue-greens, the settling velocity may be zero or negative. Furthermore, actual settling rates in natural waters are a complex phenomenon, affected by vertical turbulence, density gradients and the physiological state of the

different species of phytoplankton. An important factor determining the physiological state of algae is nutrient availability. Bienfang et al. (1982) measured sinking rate response of four marine diatoms to depletion of nitrate, phosphate and silicate. All four species showed significant increase in sinking rate under conditions of silica depletion; one species showed increased settling rate under nitrate limitation. An analysis of field experiments by Culver and Smith (1989) indicated that low concentrations of nitrate, as well as light availability, affected diatom settling rates. Although the effective settling rate of phytoplankton is greatly reduced in a relatively shallow, well-mixed river or estuary, due to vertical turbulence, it still can contribute to the overall mortality of the algal population. In addition, the settling phytoplankton can be a significant source of nutrients to the sediments and can play an important role in the generation of SOD. For these reasons, a temperature- dependent term representing phyto-plankton settling has been included in the algal mortality expression, and may be written as follows:

$$k_{sP} = \left[\frac{V_{sPb}}{H} + \frac{V_{sPn}}{H} \cdot \left(1 - G_N(N)\right) \right] \cdot \theta_{base}^{(T-20)} \tag{1-14}$$

where k_{sP} is the net effective algal loss rate due to settling (day^{-1}), v_{sPb} is the base settling velocity of phytoplankton (m/day), v_{sPn} is the nutrient dependent settling rate, (m/day), $G_N(N)$ is defined by Equation 1-12, and H is the depth of the segment, (m).

Zooplankton grazing may, depending upon time of the year and zooplankton biomass levels, be an important loss rate for phytoplankton. The loss term used to represent zooplankton grazing is as follows:

$$k_{grz}(T) = k_{grz}(20^{o}C) \cdot \theta_{grz}^{(T-20)} \tag{1-15}$$

where $k_{grz}(T)$ is the temperature corrected loss rate due to zooplankton grazing and $k_{grz}(20°C)$ is the predation rate at 20°C. The units of k_{grz} are day^{-1}.

The total loss rate for phytoplankton is the sum of the three loss rates described above:

$$D_P = k_{PR}(T) + k_{sP} + k_{grz}(T) \tag{1-16}$$

This completes the specification of the growth and death rates for phytoplankton (for the standard algal growth model) in terms of the physical variables: light, temperature and available nutrients. Table 1-1 summarizes the equations and model coefficients used in the standard version of the eutrophicaton model.

TABLE 1-1. STANDARD PHYTOPLANKTON GROWTH EQUATIONS

Phytoplankton Net Growth Rate

$$S_p = \left(G_{P\max} \cdot G_T(T) \cdot G_I(I) \cdot G_N(N) - k_{PR}(T) - k_{sP} - k_{grz}(T)\right) \cdot P_c$$

Temperature Correction

Arrenhius Version

$$G_{Pmax}(T) = G_{Pmax}\ \theta_P^{(T-20)}$$

Optimum Temperature Version

$$G_{Pmax}(T) = G_{Pmax} e^{-\beta_1 (T-T_{opt})^2} \qquad T \le T_{opt}$$

$$G_{Pmax}(T) = G_{Pmax} e^{-\beta_2 (T_{opt}-T)^2} \qquad T > T_{opt}$$

Light Reduction

$$G_I(I) = \frac{e}{k_e H}\left[\exp\left(\frac{-I_o(t)}{I_s} e^{-k_e H}\right) - \exp\frac{-I_o(t)}{I_s}\right]$$

$$k_e = k_{e_{base}} + k_c \cdot a_{cchl} \cdot P_c$$

Nutrient Uptake

$$G_N(N) = \text{Min}\left(\frac{DIN}{K_{mN}+DIN}, \frac{DIP}{K_{mP}+DIP}, \frac{Si}{K_{mSi}+Si}\right)$$

DIN = dissolved inorganic nitrogen = NH_4 + NO_2+NO_3,
DIP = dissolved inorganic phosphorus (PO_4),
Si = available silica

Algal Respiration

$$k_{PR}(T) = k_{PR}(20^oC) \cdot \theta_{PR}^{(T-20)}$$

or

$$k_{PR}(T) = r_g G_P + r_b \theta_{PR}^{(T-20)}$$

Algal Settling

$$k_{sP} = \left[\frac{V_{sPb}}{H} + \frac{V_{sPn}}{H} \cdot \left(1 - G_N(N)\right)\right] \cdot \theta_{base}^{(T-20)}$$

TABLE 1-1. STANDARD PHYTOPLANKTON NET GROWTH EQUATIONS
(Continued)

Zooplankton Grazing

$$k_{grz}(T) = k_{grz}(20^{o}C) \cdot \theta_{grz}^{(T-20)}$$

Exogenous Variables

Description	Notation
Total Extinction Coefficient	k_e
Base Extinction Coefficient	k_{ebase}
Total Daily Surface Solar Radiation	I_o
Temperature	T
Segment Depth	H

Rate Constants

Description	Notation	Winter Diatoms	Summer Assemblage	Units
Maximum Specific Growth Rate at T_{opt}	G_{Pmax}	1.7-2.5	2.0 - 3.0	day^{-1}
Temperature Coefficient	θ_P	1.068	1.068	
Temperature Optimum	T_{opt}	6-12	20 - 25	°C
Shaping parameters	β_1, β_2	0.003-0.006	0.003-0.006	
Phytoplankton Self-Light Attenuation	k_c	0.017	0.017	m^2/mg chl-a
Half-Saturation Constant for Nitrogen	K_{mN}	10.	10.	µgN/L
Half-Saturation Constant for Phosphorus	K_{mP}	1.	1.	µgP/L
Half-Saturation Constant for Silica	K_{mSi}	20.	2.	µgSi/L
Respiration Rate	$k_{PR}(20^oC)$	0.1-0.3	0.1-0.3	day^{-1}
Temperature Coefficient	θ_{PR}	1.047-1.068	1.047-1.068	
Cost of Photosynthesis	r_g	0.2 - 0.3	0.2 - 0.3	
Basal Respiration	r_b	0.01-0.03	0.01-0.03	/day
Base Algal Settling Rate	v_{sPb}	0.2-1.0	0.2-1.0	m/day
Nutrient Dependent Algal Settling Rate	v_{sPn}	0.5-1.0	0.5-1.0	m/day
Temperature Coefficient	θ_{base}	1.029	1.029	
Loss Due to Zooplankton Grazing	$k_{grz}(20^oC)$	0.05-0.10	0.05-0.10	/day
Temperature Coefficient	θ_{grz}	1.10	1.10	
Carbon/Chlorophyll Ratio	a_{cchl}	30-60.	75-100.	mgC/mg chl-a

1.2.2.2 Laws-Chalup Algal Growth Model

The second algal growth model available in this release of RCA draws directly from Laws and Chalup (1990) and an earlier modeling framework developed by Shuter (1979). The following paragraphs provide an overview of the Laws-Chalup model. In the Laws-Chalup model, the carbon in the phytoplankton cell is considered to be found in one of four compartments: structural carbon (S), reservoir or storage carbon (R), carbon associate with the light reactions (photochemical reactions) of photosynthesis (L), or carbon associated with the dark reactions (carbohydrate production and protein and lipid synthesis) of photosynthesis (D). Hence, total cell carbon, C = S + R + L + D. Chlorophyll is assumed to exist only in the L portion of the cell. Nutrients (nitrogen, phosphorus, and silica) are found in the S, L, and D portions of the cell and are assumed to be found in the same ratios in each of these pools. R is assumed to consist entirely of C storage products (carbohydrates and lipids) and hence contains no nutrients. The fraction of C allocated to structural purposes (S/C) is assumed to be constant and independent of growth conditions.

The steady-state gross photosynthetic rate per cell (ρ) is described by

$$\rho = G_{prl}\ L\ I = G_{prd}\ D \tag{1-17}$$

where I is the incident irradiance; G_{prd} is the gross photosynthetic rate per unit D and is a constant; and G_{prl} is the gross rate of photosynthesis per unit L per unit light intensity and is a function of environmental conditions. Respiration losses are assumed to be described by

$$k_{PR} = k_{RB} + k_{RG}\ G_{prd}\ D \tag{1-18}$$

where k_{RB} is the basal respiration rate per cell, i.e., the rate required to maintain the cell in the absence of growth, and k_{RG} is the growth-rate-dependent respiration coefficient (Laws and Bannister, 1980). The substrate for respiration is assumed to come from the R pool.

From the foregoing assumptions, it follows that the rate of nutrient assimilation f_N is constrained by

$$\frac{d}{dt}(S+L+D) = W_{Nx}\ f_N \tag{1-19}$$

where W_{Nx} is the ratio of C to nutrient x (either nitrogen, phosphorus or silica). It also follows that

$$\frac{dC}{dt} = G_{prd}\ D - k_{RB} - k_{RG}\ G_{prd}\ D \tag{1-20}$$

Under conditions of balanced growth it must be true that for any component X of the cell,

$$\mu = \frac{1}{X}\frac{dX}{dt} \tag{1-21}$$

where μ is the growth rate in units of inverse time. Combining Equations (1-20) and (1-21) yields

$$\mu C = G_{prd} D - k_{RB} - k_{RG} G_{prd} D \quad (1\text{-}22)$$

Laws and Chalup also define the assumptions and conditions under which a nutrient saturated version of Equation 1-22 can be developed. The nutrient saturated growth rate, μ_{Pmax}, is of the form

$$\mu_{P\max} = \frac{G_{prd}(1-k_{RG})(1-S/C)I}{I + G_{prd}/G_{prls}} - \frac{k_{RB}}{C} \quad (1\text{-}23)$$

where G_{prls} is the nutrient-saturated value of G_{prl}. Laws and Chalup then account for the relationship between light and G_{prls} by use of Equation (1-24).

$$G_{prls} = \frac{G_{prlo}}{1 + I/I_s} \quad (1\text{-}24)$$

where G_{prlo} is the value of G_{prls} when I = 0, and Is is the value of I when $G_{prls} = 0.5G_{prlo}$.

As described in Section 1.2.2.1 Standard Algal Growth Model, in the natural environment, the light intensity or incident irradiance, I, to which the phytoplankton are exposed is not uniformly at the optimum value. The variations in light exposure that phytoplankton are exposed to due to position in the water column and daily variations to solar radiation that were detailed in Section 1.2.2.1 also apply in the Laws-Chalup growth model. Equations (1-10) and (1-11) are used to determine the diurnal variation in solar radiation at the surface of the water column, given the total solar radiation, and its attenuation through the water column, respectively.

One additional parameterization that is incorporated in the Laws-Chalup formulation is photo-adaptation by phytoplankton. Phytoplankton have been shown to be able to adapt to variations in light intensity (Steemann Nielsen et al., 1962; Steemann Nielsen and Park, 1964; Morel et al. 1987). Experimental data have indicated that phytoplankton may take several hours to two to four days to adapt to changes in light intensity. Therefore, the value of I_s, in Equation 1-24 is permitted to change as a function of the antecedent light history, according to the formula:

$$I_s = \left(I_{tot_{n-3}} + I_{tot_{n-2}} + I_{tot_{n-1}}\right)/3 \quad (1\text{-}25)$$

where:

$I_{tot_{n-3}}$ = total solar radiation three days preceding current model day,
$I_{tot_{n-2}}$ = total solar radiation two days preceding current model day,
$I_{tot_{n-1}}$ = total solar radiation one day preceding current model day.

Note: the use of the photo-adaptation formula is optional. If the user wishes to include photo-adaptation then he or she should set the appropriate I_{sat} in the "Constants" section of the model input to zero. Otherwise, if a non-zero value for I_{sat} is specified then photo-adaptation is ignored the user specified value for I_{sat} is applied in equations (1-9) or (1-24).

The nutrient saturated growth rate is then temperature-corrected using spatially dependent, time-dependent values of ambient water column temperature as computed by the hydrodynamic model. The temperature-corrected growth rate is computed usng either equation 1-8a or equations 1-8b and 1-8c. A principal difference between the winter diatom group and the summer assemblage is that the winter group has a much lower T_{opt} than does the summer assemblage. The nutrient saturated, temperature-corrected growth rate is then adjusted to reflect effects due to nutrient levels, as described earlier (Equation 1-12). Table 1-2 presents the equations used for algal growth for the Law-Chalup version of algal growth.

TABLE 1-2. LAWS-CHALUP PHYTOPLANKTON GROWTH EQUATIONS

Phytoplankton Net Growth Rate

$$S_p = (\mu_{Pmax}(T,I) \cdot G_N(N) - k_{RB} - k_{sP}(T) - k_{grz}(T)) \cdot P_c$$

Specific Growth Rate

$$G_p = \mu_{Pmax}(T,I) \cdot G_N(N)$$

Nutrient Saturated Growth Rate

$$\mu_{Pmax}(T_{opt}, I) = \frac{G_{prd} \cdot (1 - k_{RG}) \cdot (1 - S/C) \cdot I(z,t)}{G_{prd}/G_{prlo} + I(z,t)\ (1 + G_{prd}/I_s G_{prlo})} - k_{RB}$$

Temperature Correction

$$\mu_{Pmax}(T) = \mu_{Pmax}(T_{opt}) \cdot e^{-\beta_1 \cdot (T - T_{opt})^2} \qquad T \le T_{opt}$$

$$\mu_{Pmax}(T) = \mu_{Pmax}(T_{opt}) \cdot e^{-\beta_2 \cdot (T - T_{opt})^2} \qquad T > T_{opt}$$

Light Attenuation

$$I(z,t) = I_{surf}(t)\, e^{-k_e z}$$

Average Light

$$I_{ave} = \frac{I_{surf}(t)}{k_e H}\left(1 - e^{-k_e H}\right)$$

$$k_e = k_{e_{base}} + k_c \cdot a_{ChlC} \cdot P_c$$

$$I_{surf}(t) = \frac{I_{tot}}{0.635 \cdot f} \sin\left(\frac{\pi\left(t_d - t_{sunrise}\right)}{f}\right)$$

$$I_s = \left(I_{tot_{n-3}} + I_{tot_{n-2}} + I_{tot_{n-1}}\right)/3$$

TABLE 1-2. LAWS-CHALUP PHYTOPLANKTON GROWTH EQUATIONS (CONTINUED)

Chlorophyll to Carbon Ratio (a_{ChlC})

$$a_{ChlC} = \frac{1-(1-QF)(1-\mu/\mu_{Pmax})-S/C-(\mu+k_{RB}/C)/\left[(1-k_{RG})G_{prd}\right]}{W_{CChl}}$$

Nutrient Uptake

$$G_N(N) = Min\left(\frac{DIN}{K_{mN}+DIN}, \frac{DIP}{K_{mP}+DIP}, \frac{Si}{K_{mSi}+Si}\right)$$

DIN = dissolved inorganic nitrogen = NH_3 + NO_2 + NO_3
DIP = dissolved inorganic phosphorus
Si = available silica

Endogenous Respiration

$$k_{PR} = \frac{k_{RB}+k_{RG}\cdot\mu}{1-k_{RG}}$$

$$\mu = G_N(N)\cdot\mu_{Pmax}$$

Algal Settling

$$k_{sP}(T) = \left(\frac{v_{sPb}}{H} + \frac{v_{sPn}}{H}\cdot(1-G_N(N))\right)\cdot\theta_{sP}^{(T-20)}$$

Zooplankton Grazing

$$k_{grz}(T) = k_{grz}(20^oC)\cdot\theta_{grz}^{(T-20)}$$

TABLE 1-2. LAWS-CHALUP PHYTOPLANKTON GROWTH EQUATIONS (CONTINUED)

Exogenous Variables

Description	Notation	Units
Total Extinction Coefficient	k_e	m^{-1}
Base Extinction Coefficient	k_{ebase}	m^{-1}
Total Daily Surface Solar Radiation	I_{tot}	langleys/day
Temperature	T	°C
Segment Depth	H	m
Fraction of Daylight	f	day
Time of Day	t_d	day
Time of Sunrise	$t_{sunrise}$	day

Rate Constants

Description	Notation	Winter Diatoms	Summer Assemblage	Units
Gross photosynthetic rate per unit D	G_{prd}	2.5	3.0	day^{-1}
Gross photosynthetic rate per unit L per unit light intensity in the limit of zero irradiance	G_{prlo}	0.28	0.28	m^2/mol quanta
Quotient of nutrient to carbon ratios at relative growth rates of 0 and 1	QF	0.85	0.85	
Effect of Temperature below T_{opt} on growth	β_1	0.004	0.004	
Effect of Temperature above T_{opt}	β_2	0.006	0.006	
Temperature Optimum	T_{opt}	8.	18.	°C
Phytoplankton Self-Shading Attenuation	k_c	0.017	0.017	m^2/mg chl-a
Half-Saturation Constant for Nitrogen	K_{mN}	0.010	0.010	mg N/L
Half-Saturation Constant for Phosphorus	K_{mP}	0.001	0.001	mg P/L
Half-Saturation Constant for Silica	K_{mSi}	0.020	0.005	mg Si/L
Growth Related Respiration Coefficient	k_{RG}	0.28	0.28	
Basal Respiration Rate	k_{RB}	0.03	0.036	day^{-1}
Base Algal Settling Rate	v_{sPb}	0.5	0.3	m/day
Nutrient Dependent Algal Settling Rate	v_{sPn}	1.0	0.7	m/day
Temperature Coefficient	θ_{sP}	1.027	1.027	
Loss Due to Zooplankton Grazing	k_{grz} (20°C)	0.1	0.1	day^{-1}
Temperature Coefficient	θ_{grz}	1.10	1.10	
Nutrient Saturated Carbon/Chlorophyll Ratio in L	W_{CChl}	40.	65.	mg C/mg chl-a
Ratio of Structural to Total Carbon	S/C	0.1	0.1	

1.2.3 Stoichiometry and Uptake Kinetics

A principal component in the mass balance equations for the nutrient systems included in the eutrophication framework is the nutrient uptake kinetics associated with algal growth (as defined via equations (1-5) through (1-25)). In order to quantify the nutrient uptake it is necessary to specify the population stoichiometry in units of nutrient uptake per mass of population synthesized. For carbon as the unit of population biomass, the relevant ratios are the mass of nitrogen, phosphorus and silica per unit mass of carbon.

This version of the integrated eutrophication model includes two variable algal stoichiometry formulations as well as the more traditional constant stoichiometry formulation. The variable stoichiometry formulation allows internal algal nutrient levels to vary as a function of the external nutrient levels. This process is sometimes referred to as "luxury nutrient uptake". That is, when external nutrient levels are in surplus the internal nutrient to carbon ratio increases thereby allowing internal storage of nutrients. The reverse occurs when external nutrient levels are low and are approaching the nutrient half saturation constant. In this case, the internal nutrient to carbon ratios decrease and the algal cell can continue to grow at low external nutrient levels.

1.2.3.1 Algal Stoichiometry and Uptake Kinetics - Standard Algal Growth Model

As mentioned above, two forms of variable nutrient stoichiometry are included in the integrated eutrophication model. The first is based on an emphirical formulation developed for the Chesapeake Bay model (Cerco, 1995). This formulation is presented graphically in Figure 1-3 for the carbon to phosphorus ratio from measurements collected in upper Chesapeake Bay.

A generalized variable stoichiometry formulation, based on the Chesapeake Bay model, may be written for a dissolved nutrient (DIX) as follows:

$$\frac{C}{X} = X_1 + (X_2 - X_1)e^{-X_3 \cdot DIX} \qquad (1\text{-}26)$$

where:

$\frac{C}{X}$ = carbon to nutrient ratio,

X_1 = nutrient saturated, carbon to nutrient ratio,

X_2 = nutrient limited, carbon to nutrient ratio (maximum),

X_3 = coefficient that determines the rate at which the carbon to nutrient ratio changes as a function of the ambient nutrient concentration, DIX,

DIX = dissolved concentration of available nutrient (either DIN, DIP, or DSi).

Table 1-3 lists the range in nitrogen, phosphorus and silica variable-stiochiometry coefficients used in previous modeling studies conducted by HydroQual.

TABLE 1-3. VARIABLE STOICHIOMETRY COEFFICIENTS - STANDARD ALGAL GROWTH MODEL

	Winter Assemblage	Summer Assemblage
Nitrogen		
CRBN1 (mgC/mgN)	5.2-5.67	4-5.67
CRBN2 (mgC/mgN)	6.5-7.20	7.5-10.0
CRBN3 (L/mgN)	10-15	10-15
Phosphorus		
CRBP1 (mgC/mgP)	25-40	25-40
CRBP2 (mgC/mgP)	90	90
CRBP3 (L/mgP)	100-200	40-200
Silica		
CRBS1 (mgC/mgSi)	2.2-3.0	5.-10.
CRBS2 (mgC/mgSi)	8-15	10-25
CRBS3 (L/mgSi)	12-30	5-10

1.2.3.2 Algal Stoichiometry and Uptake Kinetics - Laws-Chalup Algal Growth Model

Lacking extensive measurements of the particulate forms of carbon, nitrogen, phosphorus and biogenic silica, many modeling studies have assumed that phytoplankton are comprised of carbon and nutrients which approximate Redfield ratios; i.e., 106C:16N:1P (atomic), under nutrient saturated conditions. However, while the use of Redfield ratios may be appropriate under nutrient saturated conditions, it has been shown (Anita et al., 1963; Caperon and Meyer, 1972; Chalup and Laws, 1990) that algae change their cellular composition or stoichiometry as a function of nutrient status. This is accounted for in the Laws/Chalup model via the following equations:

$$N_x : C = \left[QF + (1 - QF)\,(\mu / \mu_{P\max}\right] / W_{Cx}$$

$$= 1 / W_{Cx} \quad \text{when } \mu = \mu_{P\max} \tag{1-27}$$

and

$$Chl:C = \frac{1-(1-QF)\,(1-\mu/\mu_{Pmax}) - S/C - (\mu + k_{RB}/C)/\left[(1-k_{RG})\,G_{prd}\right]}{W_{chl}} \quad (1\text{-}28)$$

$$= \left\{1 - S/C - (\mu_{Pmax} + k_{RB}C)/\left[(1-k_{RG})\,G_{prd}\right]\right\}/W_{chl} \text{ when } \mu = \mu_{Pmax}$$

where:

N_x:C = the ratio of nutrient x (nitrogen, phosphorus or silica) to carbon,
QF = quotient of N_x:C values at relative growth rates of 0 and 1,
μ = the nutrient corrected growth rate ($\mu = \mu_{Pmax}\,GN(N)$),
W_{Cx} = the ratio of C to nutrient x in S, L, D,
Chl:C = the ratio of chlorophyll-a to C in P,
W_{Chl} = the ratio of C to chlorophyll-a in P.

The latter equation accounts for changes in the chlorophyll to carbon ratio both as a function of nutrient status and light. Equations 1-27 and 1-28 provide the equilibrium carbon to nutrient and carbon to chlorophyll ratios. However, as has been shown from experimental studies, there is a time period over which it takes the phytoplankton to reach new equilibrium conditions in response to changes in nutrient status and/or available light. This is accounted for by use of the following equations:

$$\frac{dN_x:C^n}{dt} = k_{eq}\left(N_x:C^n_{eq} - N_x:C^n\right) \quad (1\text{-}29)$$

$$N_x:C^{n+1} = N_x:C^n + dt\,\frac{dN_x:C^n}{dt} \quad (1\text{-}30)$$

and

$$\frac{dChl:C^n}{dt} = k_{eq}\left(Chl:C^n_{eq} - Chl:C^n\right) \quad (1\text{-}31)$$

$$Chl:C^{n+1} = Chl:C^n + dt\,\frac{dChl:C^n}{dt} \quad (1\text{-}32)$$

where:

$N_x:C^n$, $N_x:C^{n+1}$ = the nutrient to carbon ratios at time step n and n+1, respectively,
$N_x:C^n_{eq}$ = the equilibrium nutrient to carbon ratio at time step n, as determined from Equation 1-27,
k_{eq} = a constant which determines the time to achieve equilibrium,
$Chl:C^n$, $Chl:C^{n+1}$ = the chlorophyll to carbon ratios at time step n and n+1, respectively,
$Chl:C^n_{eq}$ = the equilibrium chlorophyll to carbon ratio at time step n, as determined from Equation 1-28,
dt = length of time step.

The Laws-Chalup algal growth model evaluates the nutrient to carbon and chlorophyll to carbon ratios to be used form the next time level based on the ratios at the current time level and the equilibrium ratios, determined from Equations 1-27 and 1-28, based upon environmental conditions at the current time level. A value of 1/day was chosen for k_{eq}, based on the literature (Steeman Nielsen and Park, 1964; Anita et al., 1963; Caperon and Meyer, 1972). This corresponds to an equilibrium time of approximately 3 days. This

value has been "hard-wired" in the computer code. Table 1-4 contains the stoichiometric coefficients used in the Massachusetts Bays application of RCA.

TABLE 1-4 VARIABLE STOICHIOMETRY COEFFICIENTS - LAWS-CHALUP ALGAL GROWTH MODEL

	Winter Assemblage	Summer Assemblage
Nitrogen		
W_{CN}	5.67 (6.67[(1)] - 16.2[(2)])	5.67 (6.67[(1)] - 16.2[(2)])
Phosphorus		
W_{CP}	40.(47[(1)] - 114[(2)])	40.(47[(1)] - 114[(2)])
Silica		
W_{csi}	2.5(2.94[(1)] - 7.14[(2)])	7.0(8.2[(1)] - 20.[(2)])
QF quotient of nutrient to carbon ratio at relative growth rates of 0 and 1	0.85[(1)]	0.85[(1)]

(1) maximum C to nutrient ratio at nutrient-limiting conditions using Massachusetts Bays model coefficient of 0.85 for QF

(2) maximum C to nutrient ratio at nutrient-limiting conditions using Laws-Chalup (1990) model coefficient f 0.35 for QF

Figure 1-4 presents a comparison of the carbon to nitrogen ratios obtained using the standard eutrophication variable stoichiometry foundation (Eqn. 1-26) using coefficients used in HydroQual studies versus that proposed by Laws and Chalup (Eqn. 1-27). It is important to note, however, that the coefficient set used by Laws and Chalup was for a single algal species and that a coefficient set that did not produce as sharp a curve was used by HydroQual in its Massachusetts Bay study (1995, 2003).

1.2.3.3 Nutrient Cycling

Once the stoichiometric ratios have been determined, the mass balance equations may be written for the nutrients in much the same way as for the phytoplankton biomass. The principal processes determining the distribution of nutrients among the various pools are: the uptake of inorganic nutrients by phytoplankton for cell growth, the release of organic nutrients by algal respiration and predation processes, and the recycling of organic nutrients to inorganic forms via bacterial hydrolysis and mineralization.

In their work on Lake Huron and Saginaw Bay, Di Toro and Matystick (1980) proposed a nutrient recycle formulation that was a function of the localized phytoplankton population. Drawing from an analysis of available field data and citing the work of others (Hendry, 1977; Lowe, 1976; Henrici, 1938; Menon et al., 1972; and Rao, 1976) that indicated bacterial biomass increased as phytoplankton biomass increased, the mechanism chosen, saturating recycle, was a compromise. This compromise was between the conventional first-order temperature corrected mechanism and a second-order recycle mechanism, in which

the recycle rate is directly proportional to the phytoplankton biomass present, as indicated in pure culture, bacteria seeded laboratory studies (Jewell and McCarty 1971). The various relationships may be written:

$$\text{First} - \text{order recycle}: \quad k(T) = k'(20^{o}C)\,\theta^{T-20} \tag{1-33a}$$

$$\text{Second} - \text{order recycle}: \quad k(T) = k''(20^{o}C)\,\theta^{T-20} \cdot P_c \tag{1-33b}$$

$$\text{Saturating recycle}: \quad k(T) = k'(20^{o}C)\,\theta^{T-20} \cdot \frac{P_c}{K_{mP_c} + P_c} \tag{1-33c}$$

Saturating recycle permits second-order dependency at low phytoplankton concentrations, when $P_c << K_{mPc}$, where K_{mPc} is the half saturation constant for recycle. It also permits first-order recycle when the phytoplankton concentrations greatly exceed the half saturation constant. Basically, this mechanism employs a second order recycle that slows the recycle rate if the algal population is small, but does not permit the rate to increase continuously as phytoplankton concentrations increase. The assumption is that at higher population levels, other factors are limiting the recycle kinetics so that it proceeds at its maximum first-order rate.

1.2.3.4 Organic Carbon

Seven organic carbon state variables are considered: reactive particulate organic (RePOC), reactive dissolved organic (ReDOC), labile dissolved (LDOC), refractory dissolved (RDOC), labile particulate (LPOC), refractory particulate (RPOC) and dissolved algal exudate (ExDOC). Reactive, labile and refractory distinctions are based upon the time scale of oxidation or decomposition. Reactive organic carbon decomposes on a time scale of days to a week or two and is meant to be used for CSO carbon and a portion of the organic carbon discharged from wastewater treatment plants; labile organic carbon decomposes on the time scale of several weeks to a month or two; refractory organic carbon decomposes on the order of months to a year. Reactive and labile organic carbon decompose primarily in the water column or else rapidly in the sediments. Refractory organic carbon decomposes much more slowly, almost entirely in the sediments.

Reactive particulate organic carbon (RePOC) is assumed to have a very high settling rate that is a function of RePOC itself (representing floculation). The underlying assumption is that at elevated concentrations flocculations occurs, thereby enhancing the settling rate of this form of organic carbon. Equation 1-34 is used to determine the settling rates as a function of REPOC (Figure 1-5 illustrates REPOC

$$v = \min\left[v_{max}, v_{min} + (v_{max} - v_{min})\left(\frac{RePOC}{C_{ref}}\right)^{\beta} \right] \tag{1-34}$$

settling rate as a function of REPOC and the two model coefficients β and C_{ref}). Information from settling column tests can be used to guide the selection of appropriate model coefficients, but it is important to (1) remember that settling column tests are usually conducted under quiescent conditions that may not occur in natural systems and (2) the choice of a maximum settling rate should be made remembering that the maximum rate may influence the integration step-size. For example, assuming a maximum rate of 50 m/day

a water column depth of 1 m and a ten layer sigma-level grid would require a time step of about 2.9 minutes or less to ensure numerical stability.

where

v = settling rate, (m/day)
v_{max} = maximum settling rate, (m/day)
v_{min} = maximum settling rate, (m/day)
RePOC = concentration of reactive (CSO) POC, (mg/L)
C_{ref} = reference concentration of RePOC, (mg/L)
β = power exponent for settling function

The principal sources of organic carbon are anthropogenic inputs and natural runoff, and detrital algal carbon, which is produced as a result of predation. Zooplankton take up and redistribute algal carbon to the organic carbon pools via grazing, assimilation, respiration and excretion. Since zooplankton are not directly included in the model, the redistribution of algal carbon by zooplankton is simulated by empirical distribution coefficients. An additional term, representing the excretion of DOC by phytoplankton during photosynthesis, is included in the model. This algal exudate is very reactive and has a time constant similar to the reactive DOC.

The decomposition of organic carbon is assumed to be temperature and bacterial biomass mediated. Since bacterial biomass is not directly included within the model framework, phytoplankton biomass is used as a surrogate variable. Table 1-5 presents the reaction rate terms and range of coefficients for each of the organic carbon pools considered in the model framework.

TABLE 1-5. ORGANIC CARBON REACTION EQUATIONS
(Numbering scheme refers to the variable list in Section 1.1.2)

Refractory Particulate Organic Carbon (RPOC)

$$S_{18} = f_{RPOC} \cdot k_{grz}\,(T) \cdot P_c - k_{18,20}\,\theta_{18,20}^{\,T-20} \cdot RPOC \cdot \frac{P_c}{K_{mP_c} + P_c} - \frac{v_{s18}}{H} \cdot RPOC$$

Labile Particulate Organic Carbon (LPOC)

$$S_{19} = f_{LPOC} \cdot k_{grz}\,(T) \cdot P_c - k_{19,21}\,\theta_{19,21}^{\,T-20} \cdot LPOC \cdot \frac{P_c}{K_{mP_c} + P_c} - \frac{v_{s19}}{H} \cdot LPOC$$

Refractory Dissolve Organic Carbon (RDOC)

$$S_{20} = f_{RDOC} \cdot k_{grz}\,(T) \cdot P_c - k_{18,20}\,\theta_{18,20}^{\,T-20} \cdot RPOC \cdot \frac{P_c}{K_{mP_c} + P_c} - k_{20,0}\,\theta_{20,0}^{\,T-20} \cdot RDOC \cdot \frac{P_c}{K_{mP_c} + P_c} \cdot \frac{DO}{K_{DO} + DO}$$

Labile Dissolved Organic Carbon (LDOC)

$$S_{21} = f_{LDOC} \cdot k_{grz}\,(T) \cdot P_c - k_{19,21}\,\theta_{19,21}^{\,T-20} \cdot LPOC \cdot \frac{P_c}{K_{mP_c} + P_c} - k_{21,0}\,\theta_{21,0}^{\,T-20} \cdot LDOC \cdot \frac{P_c}{K_{mP_c} + P_c} \cdot \frac{DO}{K_{DO} + DO} \cdot \frac{LDOC}{K_{mLDOC} + LDOC} - \frac{5}{4} \cdot \frac{12}{14} \cdot k_{15,0}\,\theta_{15,0}^{\,T-20} \cdot NO_2 + NO_3 \cdot \frac{K_{NO_3}}{K_{NO_3} + DO}$$

TABLE 1-5. ORGANIC CARBON REACTION EQUATIONS
(Numbering scheme refers to the variable list in Section 1.1.2)
(Continued)

Algal Exudate Dissolved Organic Carbon (ExDOC)

$$S_{22} = f_{ExPP} \cdot G_P \cdot P_c - k_{22,0}\theta_{22,0}^{T-20} \cdot ExDOC \cdot \frac{P_c}{K_{mP_c} + P_c} \cdot \frac{DO}{K_{DO} + DO} \cdot \frac{ExDOC}{K_{mLDOC} + ExDOC}$$

Reactive Particulate Organic Carbon (RePOC)

$$S_{23} = -k_{23,24}\theta_{23,24}^{T-20} \cdot RePOC \cdot \frac{P_c}{k_{mp_c} + P_c} - \min\left[v_{24\max}, v_{24\min} + (v_{24\max} - v_{24\min})\left(\frac{RePOC}{C_{ref}}\right)^{\beta}\right] \cdot RePOC$$

Reactive Dissolved Organic Carbon (ReDOC)

$$S_{24} = -k_{23,24}\theta_{23,24}^{T-20} \cdot RePOC \cdot \frac{P_c}{k_{mp_c} + P_c} \cdot k_{24,0}\theta_{24,0}^{T-20} \cdot ReDOC \cdot \frac{P_c}{k_{mp_c} + P_c} \cdot \frac{DO}{K_{DO} + DO} \cdot \frac{ReDOC}{K_{mLDOC} + ReDOC}$$

TABLE 1-5. ORGANIC CARBON REACTION EQUATIONS
(Numbering scheme refers to the variable list in Section 1.1.2)

Description	Notation	Value	Units
Phytoplankton Biomass	P_c	-	mgC/L
Specific Phytoplankton Growth Rate	G_P	Eq. 1-5	day^{-1}
Segment depth	H	-	m
Dissolved Oxygen	DO	-	mgO_2/L
Half Saturation Constant for Phytoplankton Limitation	K_{mPc}	0.05	mgC/L
Fraction of Grazed Organic Carbon Recycle to:			
the LPOC pool	f_{LPOC}	0.30-0.40	
the RPOC pool	f_{RPOC}	0.10-0.15	
the LDOC pool	f_{LDOC}	0.35-0.45	
the RDOC pool	f_{RDOC}	0.10-0.15	
Note: the sum of $f_{LPOC} + f_{RPOC} + f_{LDOC} + f_{RDOC}$ must equal 1.0			
Fraction of Primary Productivity Going to the Algal Exudate DOC pool	f_{ExPP}	0.10-0.15	
Hydrolysis Rate for RPOC	$k_{18,20}$	0.007-0.01	day^{-1}
Temperature Coefficient	$\theta_{18,20}$	1.08	
Settling Rate of RPOC	v_{s18}	0.5-1.0	m/day
Hydrolysis Rate for LPOC	$k_{19,21}$	0.07-0.10	day^{-1}
Temperature Coefficient	$\theta_{19,21}$	1.08	
Settling Rate of LPOC	v_{s19}	0.5-1.0	m/day
Oxidation Rate of RDOC	$k_{20,0}$	0.007-0.01	day^{-1}
Temperature Coefficient	$\theta_{20,0}$	1.08	
Oxidation Rate LDOC	$k_{21,0}$	0.10-0.15	day^{-1}
Temperature Coefficient	$\theta_{21,0}$	1.08	
Oxidation Rate of ReDOC	$k_{22,0}$	0.25-0.35	day^{-1}
Temperature Coefficient	$\theta_{22,0}$	1.047	
Oxidation Rate of ExDOC	$k_{23,0}$	0.1	day^{-1}
Temperature Coefficient	$\theta_{23,0}$	1.08	
Half Saturation for Oxygen Limitation	k_{DO}	0.2	mgO_2/L
Michaelis Constant for LDOC	K_{mLDOC}	0.1	mgC/L
Minimum RePOC settling rate	$v_{24\ min}$	0.5	m/day
Enhanced RePOC settling rate (due to floculation)	v_{24max}	25	m/day
Reference (or normalizing term)	C_{Ref}	10	mgC/day
Power function	β	1.2	

1.2.3.5 Phosphorus

The eutrophication model includes five principal phosphorus forms: labile and refractory dissolved organic (LDOP and RDOP, respectively), labile and refractory particulate organic (LPOP and RPOP, respectively), and DIP. Inorganic phosphorus is utilized by phytoplankton for growth and phosphorus is returned to the various organic and inorganic forms via respiration and predation. A fraction of the phosphorus released during phytoplankton respiration and predation is in the inorganic form and readily available for uptake by other viable algal cells. The remaining fraction released is in the dissolved and particulate organic forms. The organic phosphorus must undergo a mineralization or bacterial decomposition into inorganic phosphorus before it can be used by phytoplankton. Table 1-6 presents the reaction rate terms for each of the five phosphorus forms.

1.2.3.6 Nitrogen

The kinetic structure for nitrogen is similar to that for the phosphorus system. Table 1-7 summarizes the terms used in the nitrogen system kinetics. During algal respiration and death, a fraction of the cellular nitrogen is returned to the inorganic pool in the form of NH_3. The remaining fraction is recycled to the dissolved and particulate organic nitrogen pools. Organic nitrogen undergoes a bacterial decomposition, the end-product of which is NH_4. Ammonia nitrogen, in the presence of nitrifying bacteria and oxygen, is converted to nitrite nitrogen and subsequently nitrate nitrogen (nitrification). Both ammonia and nitrate are available for uptake and are used in cell growth by phytoplankton; however, for physiological reasons, the preferred form is NH_4. The ammonia preference term takes the following form:

$$\alpha_{NH_4} = NH_4 \cdot \frac{NO_2 + NO_3}{\left(K_{mN} + NH_4\right) \cdot \left(K_{mN} + NO_2 + NO_3\right)} + NH_4 \cdot \frac{K_{mN}}{\left(NH_4 + NO_2 + NO_3\right) \cdot \left(K_{mN} + NO_2 + NO_3\right)} \quad (1\text{-}35)$$

The behavior of this equation for a Michaelis value, K_{mN}, of 10 µgN/L, is illustrated on Figure 1-6. The behavior of Equation 1-35 is most sensitive at low values of ammonia or nitrate. For a given concentration of ammonia, as the available nitrate increases above approximately the Michaelis limitation, the preference for ammonia reaches a plateau. Also, as the concentration of available ammonia increases, the plateau occurs at values closer to unity, that is, total preference for ammonia. The process of nitrification in natural waters is carried out by aerobic autotrophs, *Nitrosomonas* and *Nitrobacter*, in particular. It is a two-step process with *Nitrosomonas* bacteria responsible for the conversion of ammonia to nitrite (NO_2) and *Nitrobacter* responsible for the subsequent conversion of nitrite to nitrate (NO_3). Essential to this reaction process are aerobic conditions. In order to reduce the number of state variables required in the modeling framework, it was decided to incorporate nitrite and nitrate together as a single state variable. Therefore, the process of nitrification is assumed to be approximated by a first-order reaction rate that is a function of the water column dissolved oxygen concentration and ambient temperature.

TABLE 1-6. PHOSPHORUS REACTION RATES
(Numbering scheme refers to the variable list in Section 1.1.2)

Refractory Particulate Organic Phosphorus (RPOP)

$$S_5 = a_{PC} \cdot f_{RPOP} \cdot \left(k_{PR}(T) + k_{grz}(T)\right) \cdot P_c - k_{5,7}\,\theta_{5,7}^{T-20} \cdot RPOP \cdot \frac{P_c}{K_{mP_c} + P_c}$$

$$- \frac{v_{s5}}{H} \cdot RPOP$$

Labile Particulate Organic Phosphorus (LPOP)

$$S_6 = a_{PC} \cdot f_{LPOP} \cdot \left(k_{PR}(T) + k_{grz}(T)\right) \cdot P_c - k_{6,8}\,\theta_{6,8}^{T-20} \cdot LPOP \cdot \frac{P_c}{K_{mP_c} + P_c}$$

$$- \frac{v_{s6}}{H} \cdot LPOP$$

Refractory Dissolved Organic Phosphorus (RDOP)

$$S_7 = a_{PC} \cdot f_{RDOP} \cdot \left(k_{PR}(T) + k_{grz}(T)\right) \cdot P_c + k_{5,7}\,\theta_{5,7}^{T-20} \cdot RPOP \cdot \frac{P_c}{K_{mP_c} + P_c}$$

$$- k_{7,9}\theta_{7,9}^{T-20} \cdot RDOP \cdot \frac{P_c}{K_{mP_c} + P_c}$$

Labile Dissolved Organic Phosphorus (LDOP)

$$S_8 = a_{PC} \cdot f_{LDOP} \cdot \left(k_{PR}(T) + k_{grz}(T)\right) \cdot P_c + k_{6,8}\,\theta_{6,8}^{T-20} \cdot LPOP \cdot \frac{P_c}{K_{mP_c} + P_c}$$

$$- k_{8,9}\,\theta_{8,9}^{T-20} \cdot LPOP \cdot \frac{P_c}{K_{mP_c} + P_c}$$

TABLE 1-6. PHOSPHORUS REACTION RATES
(Continued)

Dissolved Inorganic Phosphorus (DIP)

$$S_9 = a_{PC} \cdot f_{DIP} \cdot \left(k_{PR}(T) + k_{grz}(T)\right) \cdot P_c + \left(k_{7,9}\,\theta_{7,9}^{\,T-20} \cdot RDOP + k_{8,9}\,\theta_{8,9}^{\,T-20} \cdot LDOP\right) \cdot \frac{P_c}{K_{mP_c} + P_c} - a_{PC} \cdot \left(1 - f_{ExPP}\right) \cdot G_P \cdot P_c$$

TABLE 1-6. PHOSPHORUS REACTION RATES
(Continued)

Description	Notation	Value	Units
Phytoplankton Biomass	P_c	-	mgC/L
Temperature Corrected Algal Respiration Rate	$k_{PR}(T)$	Eq. 1-11a	day^{-1}
Temperature Corrected Grazing Rate	$k_{grz}(T)$	Eq. 1-13	day^{-1}
Specific Phytoplankton Growth Rate	G_P	Eq. 1-5	day^{-1}
Phosphorus to Carbon Ratio	a_{PC}	Table 1-2	mgP/mgC
Fraction of Primary Productivity Going to the Algal Exudate DOC pool	f_{ExPP}	0.1	
Fraction of Respired and Grazed Algal Phosphorus Recycled to			
the LPOP pool	f_{LPOP}	0.25-0.35	
the RPOP pool	f_{RPOP}	0.10-0.15	
the LDOP pool	f_{LDOP}	0.10-0.15	
the RDOP pool	f_{RDOP}	0.100.15	
the DIP pool	f_{DIP}	0.20-0.45	
Note: the sum of $f_{LPOP} + f_{RPOP} + f_{LDOP} + f_{RDOP} + f_{DIP}$ must equal 1.0			
RPOP Hydrolysis Rate at 20°C	$k_{5,7}$	0.007-0.01	day^{-1}
Temperature Coefficient	$\theta_{5,7}$	1.08	
RPOP Settling Rate	v_{s5}	0.5-1.0	m/day
LPOP Hydrolysis Rate at 20°C	$k_{6,8}$	0.085-0.10	day^{-1}
Temperature Coefficient	$\theta_{6,8}$	1.08	
LPOP Settling Rate	v_{s6}	0.5-1.0	m/day
RDOP Mineralization Rate at 20°C	$k_{7,9}$	0.01-0.02	day^{-1}
Temperature Coefficient	$\theta_{7,9}$	1.08	
LDOP Mineralization Rate at 20°C	$k_{8,9}$	0.1-0.2	day^{-1}
Temperature Coefficient	$\theta_{8,9}$	1.08	

TABLE 1-7. NITROGEN REACTION RATES
(Numbering scheme refers to the variable list in Section 1.1.2)

Refractory Particulate Organic Nitrogen (RPON)

$$S_{10} = a_{NC} \cdot f_{RPON} \cdot \left(k_{PR}(T) + k_{grz}(T)\right) \cdot P_c - k_{10,12}\,\theta_{10,12}^{\,T-20} \cdot RPON \cdot \frac{P_c}{K_{mP_c} + P_c} - \frac{V_{s10}}{H} \cdot RPON$$

Labile Particulate Organic Nitrogen (LPON)

$$S_{11} = a_{NC} \cdot f_{LPON} \cdot \left(k_{PR}(T) + k_{grz}(T)\right) \cdot P_c - k_{11,13}\,\theta_{11,13}^{\,T-20} \cdot LPON \cdot \frac{P_c}{K_{mP_c} + P_c} - \frac{V_{s11}}{H} \cdot LPON$$

Refractory Dissolved Organic Nitrogen (RDON)

$$S_{12} = a_{NC} \cdot f_{RDON} \cdot \left(k_{PR}(T) + k_{grz}(T)\right) \cdot P_c + k_{10,12}\,\theta_{10,12}^{\,T-20} \cdot RPON \cdot \frac{P_c}{K_{mP_c} + P_c} - k_{12,14}\,\theta_{12,14}^{\,T-20} \cdot RDON \cdot \frac{P_c}{K_{mP_c} + P_c}$$

Labile Dissolved Organic Nitrogen (LDON)

$$S_{13} = a_{NC} \cdot f_{LDON} \cdot \left(k_{PR}(T) + k_{grz}(T)\right) \cdot P_c + k_{11,13}\,\theta_{11,13}^{\,T-20} \cdot LPON \cdot \frac{P_c}{K_{mP_c} + P_c} k_{13,14}\,\theta_{13,14}^{\,T-20} \cdot LDON \cdot \frac{P_c}{K_{mP_c} + P_c}$$

TABLE 1-7. NITROGEN REACTION RATES
(Continued)

Ammonia Nitrogen (NH_4)

$$S_{14} = a_{NC} \cdot f_{NH_4} \cdot \left(k_{PR}(T) + k_{grz}(T)\right) \cdot P_c + \left(k_{12,14}\,\theta_{12,14}^{\,T-20} \cdot RDON + k_{13,14}\,\theta_{13,14}^{\,T-20} \cdot LDON\right) \cdot \frac{P_c}{K_{mP_c} + P_c} - a_{NC} \cdot \alpha_{NH_4} \cdot \left(1 - f_{ExPP}\right) \cdot G_P \cdot P_c - k_{14,15}\,\theta_{14,15}^{\,T-20} \cdot NH_4 \cdot \frac{DO}{K_{nitr} + DO}$$

Nitrite + Nitrate Nitrogen (NO_2+ NO_3)

$$S_{15} = k_{14,15}\,\theta_{14,15}^{\,T-20} \cdot NH_4 \cdot \frac{DO}{K_{nitr} + DO} - a_{NC} \cdot \left(1 - \alpha_{NH_4}\right) \cdot \left(1 - f_{ExPP}\right) \cdot G_P \cdot P_c - k_{15,0}\,\theta_{15,0}^{\,T-20} \cdot NO_2 + NO_3 \cdot \frac{K_{NO_3}}{K_{NO_3} + DO}$$

TABLE 1-7. NITROGEN REACTION RATES
(Continued)

Description	Notation	Value	Units
Phytoplankton Biomass	P_c	-	mgC/L
Temperature Corrected Algal Respiration Rate	$k_{PR}(T)$	cf Eq. 1-11a	day^{-1}
Temperature Corrected Grazing Rate	$k_{grz}(T)$	cf Eq. 1-13	day^{-1}
Specific Phytoplankton Growth Rate	G_P	cf Eq. 1-5	day^{-1}
Nitrogen to Carbon Ration	a_{NC}	cf Table 1-2	mgN/mgC
Fraction of Primary Productivity Going to the Algal Exudate DOC pool	f_{ExPP}	0.1	
Fraction of Respired and Grazed Algal Nitrogen Recycled to			
The LPON pool	f_{LPON}	0.30-0.35	
the RPON pool	f_{RPON}	0.10-0.15	
the LDON pool	f_{LDON}	0.125-0.15	
the RDON pool	f_{RDON}	0.125-0.20	
the NH_4 pool	f_{NH4}	0.15-0.35	
Note: the sum of $f_{LPON} + f_{RPON} + f_{LDON} + f_{RDON} + f_{NH4}$ must equal 1.0			
RPON Hydrolysis Rate at 20°C	$k_{10,12}$	0.007-0.01	day^{-1}
Temperature Coefficient	$\theta_{10,12}$	1.08	
RPON Settling Rate	v_{s10}	0.5-1.0	m/day
LPON Hydrolysis Rate at 20°C	$k_{11,13}$	0.05-0.07	day^{-1}
Temperature Coefficient	$\theta_{11,13}$	1.08	
LPON Settling Rate	v_{s11}	0.5-1.0	m/day
RDON Mineralization Rate at 20°C	$k_{12,14}$	0.0080.01	day^{-1}
Temperature Coefficient	$\theta_{12,14}$	1.08	
LDON Mineralization Rate at 20°C	$k_{13,14}$	0.085-0.10	day^{-1}
Temperature Coefficient	$\theta_{13,14}$	1.08	
Nitrification Rate at 20°C	$k_{14,15}$	0.05-0.10	day^{-1}
Temperature Coefficient	$\theta_{14,15}$	1.08	
Half Saturation Constant for Oxygen Limitation	K_{nitr}	1.0	$mg0_2/L$
Denitrification Rate at 20°C	$K_{15,0}$	0.05-0.4	day^{-1}
Temperature Coefficient	$\theta_{15,0}$	1.045	
Michaelis Constant for Denitrification	K_{NO_3}	0.1	$mg0_{2/L}$

Denitrification refers to the reduction of NO_3 to N_2 and other gaseous products such as N_2O and NO. This process is carried out by a large number of heterotrophic, facultative anaerobes. Under normal aerobic conditions found in the water column, these organisms utilize oxygen to oxidize organic material. However, under the anaerobic conditions found in the sediment bed or during extremely low oxygen conditions in the water column, these organisms are able to use NO_3 as the electron acceptor. The process of denitrification is included in the modeling framework simply as a sink of nitrate. This can always occur in the anaerobic sediment layer. In the water column, however, denitrification should only occur under extremely low dissolved oxygen conditions. This is accomplished computationally by modifying the linear first-order denitrification rate by the expression $K_{NO3}/(K_{NO3} + DO)$. This expression is similar to the Michaelis-Menton expression; for concentrations of dissolved oxygen greater than 1 mg/L, the expression reduces denitrification to near zero, whereas for dissolved oxygen levels less than 0.1mg/L, this expression permits denitrification to occur. Table 1-7 presents the state-variable equations for the six nitrogen forms utilized in the model framework.

1.2.3.7 Silica

Two silica state-variables are considered: available (Si) and unavailable or particulate biogenic (SiU). Available silica is dissolved and is utilized by diatoms during growth for their cell structure. Unavailable or particulate biogenic silica is produced from diatom respiration and diatom grazing by zooplankton. Particulate biogenic silica undergoes mineralization to available silica or settles to the sediment from the water column. Table 1-8 presents the state-variable equations for the two silica forms utilized in the model framework.

1.2.3.8 Dissolved Oxygen

A by-product of photosynthetic carbon fixation is the production of dissolved oxygen. The rate of oxygen production and nutrient uptake is proportional to the growth rate of the phytoplankton, since its stoichiometry is fixed. An additional source of oxygen from algal growth occurs when the available ammonia nutrient source is exhausted and the phytoplankton begin to utilize the available nitrate. This additional oxygen source can be seen by comparing equations 1-36a and 1-36b (Morel, 1983).

$$106\ CO_2 + 16\ NH_4^+ + H_2PO_4^- + 106\ H_2O \Rightarrow \text{Protoplasm} + 106\ O_2 + 15H^+ \quad (1\text{-}36a)$$

$$106\ CO_2 + 16\ NO_3^- + H_2PO_4^- + 122\ H_2O + 17H+ \Rightarrow \text{Protoplasm} + 138\ O_2 \quad (1\text{-}36b)$$

The above equations present the stoichiometric description of the photosynthetic process assuming ammonium (Equation 1-36a) or nitrate (Equation 1-36b) as the nitrogen source and assuming algal biomass to have Redfield stoichiometry:

TABLE 1-8. SILICA REACTION EQUATIONS

Biogenic Silica (BSi)

$$S_{16} = \left(k_{PR}(T) + k_{grz}(T)\right) \cdot P_c - k_{16,17}\,\theta_{16,17}^{T-20} \cdot BSi \cdot \frac{P_c}{K_{mP_c} + P_c} - \frac{v_{s16}}{H} \cdot BSi$$

Available Silica (Si)

$$S_{17} = k_{16,17}\,\theta_{16,17}^{T-20} \cdot BSi \cdot \frac{P_c}{K_{mP_c} + P_c} - (1 - f_{ExPP}) \cdot a_{sc} \cdot G_P \cdot P_c$$

Description	Notation	Value	Units
Phytoplankton Biomass	P_c	—	mgC/L
Temperature Corrected Algal Respiration Rate	$k_{PR}(T)$	Eq. 1-11a	day^{-1}
Temperature Corrected Grazing Rate	$k_{grz}(T)$	Eq. 1-13	day^{-1}
Specific Phytoplankton Growth Rate	G_p	Eq. 1-5	day^{-1}
Silica to Carbon Ration	a_{sc}	Table 1-2	mgSi/mgC
Fraction of Primary Productivity Going to the Algal Exudate pool	f_{ExPP}	0.1	
Mineralization Rate of Biogenic Silica	$k_{16,17}$	0.1-0.25	day^{-1}
Temperature Coefficient	$\theta_{16,17}$	1.08	
Silica Settling Rate	V_{s16}	0.5-1.0	m/day

$$\text{Biomass} = C_{106}\ H_{263}\ O_{110}\ N_{16}\ P_1 \tag{1-37}$$

Oxygen-deficient or under-saturated waters are replenished via atmospheric reaeration. The reaeration coefficient is a function of the average tidal velocity, wind and temperature, and is computed using Equations 1-38a and 1-38b:

$$k_a\ (20^oC) = \underset{\text{wind}}{K_L / H} \tag{1-38a}$$

$$k_a\ (T) = \underset{\text{temperature}}{k_a\ (20^oC)\theta_a^{T-20}} \tag{1-38b}$$

where

k_a = the surface mass transfer coefficient (m/day),
H = depth (m),
θ_a = temperature coefficient.

Dissolved oxygen saturation is a function of both temperature and salinity and is determined via Equation 1-39 (Standard Methods, 1992):

$$\begin{aligned} DO_{sat} = \exp\ [&-139.34411 + 1.575701 \cdot 10^5 / T \\ &-6.642308 \cdot 10^7 / T^2 + 1.243800 \cdot 10^{10} / T^3 \\ &-8.621949 \cdot 10^{11} / T^4 - S(1.7674 \cdot 10^{-2} \\ &-10.754 / T + 2140.7 / T^2)] \end{aligned} \tag{1-39}$$

where

S = salinity (psu),
T = temperature (°K).

Dissolved oxygen is diminished in the water column as a result of algal respiration, which is the reverse process of photosynthesis; as a result of nitrification:

$$NH_4^+ + 2O_2 \Rightarrow NO_3^- + H_2O + 2H^+ \tag{1-40}$$

as a result of the oxidation of carbonaceous material (including detrital phytoplankton):

$$CH_2O + O_2 \Rightarrow CO_2 + H_2O \quad (1\text{-}41)$$

and, if dissolved oxygen concentrations are sufficiently low, as a result of denitrification:

$$5CH_2O + 4NO_3^- + \Rightarrow 5CO_2 + 2N_2 + 7H_2O \quad (1\text{-}42)$$

Table 1-9 presents a summary of the dissolved oxygen mass balance equation and associated coefficients incorporated in the integrated eutrophication model.

TABLE 1-9. DISSOLVED OXYGEN AND O_2^* REACTION RATES

Sulfide Oxygen Equivalents (O_2^*)

$$S_{24} = K_{O_2^*}\,\theta_{O_2^*}^{T-20} \cdot O_2^* \cdot \frac{P_c}{K_{mP_c} + P_c} \cdot \frac{DO}{K_{DO_{O_2^*}} + DO}$$

Dissolved Oxygen (DO)

$$\begin{aligned} S_{25} = {} & a_{OC} \cdot \alpha_{NH_4} \cdot G_P \cdot P_c + \left(a_{NO_3} c\right) \cdot \left(1-\alpha_{NH_4}\right) \cdot G_P \cdot P_c \\ & + k_a \theta_a^{T-20} \cdot \left(DO_{sat} - DO\right) - a_{OC} \cdot k_{PR}\,(T) \cdot P_c \\ & - 2 \cdot a_{ON} \cdot k_{14,15} \theta_{14,15}^{T-20} \cdot NH_4 \cdot \frac{DO}{K_{nitr} + DO} \\ & - a_{OC} \cdot \left[k_{20,0}\,\theta_{20,0}^{T-20} \cdot RDOC + k_{21,0}\,\theta_{21,0}^{T-20} \cdot LDOC \cdot \frac{LDOC}{K_{m_{LDOC}} + LDOC} \right. \\ & + k_{22,0}\,\theta_{22,0}^{T-20} \cdot Re\,DOC \cdot \frac{Re\,DOC}{K_{mLDOC} + Re\,DOC} \\ & \left. + k_{23,0}\,\theta_{23,0}^{T-20} \cdot ExDOC \cdot \frac{ExDOC}{K_{mLDOC} + ExDOC} \right] \cdot \frac{P_c}{K_{mPc} + P_c} \cdot \frac{DO}{K_{DO} + DO} \\ & - k_{o_2^*}\,\theta_{o_2^*}^{T-20} \cdot O_2^* \cdot \frac{P_c}{K_{mPc} + P_c} \cdot \frac{DO}{K_{DO_{O_2^*}} + DO} \end{aligned}$$

TABLE 1-9. DISSOLVED OXYGEN AND O_2^* REACTION RATES
(continued)

Description	Notation	Value	Units
	Rate Constants		
Oxygen to Carbon Ratio	a_{OC}	32/12	$mgO_2/mg\ C$
Oxygen to Nitrogen Ratio	a_{ON}	32/14	$mgO_2/mg\ N$
Oxygen to Carbon Ratio for Nitrate Uptake	α_{NO_3C}	$\frac{48}{14} a_{NC}$	$mgO_2/mg\ C$
Reaeration Rate at 20°C	k_a	Eq. 1.19a	day^{-1}
Temperature Coefficient	θ_a	1.024	none
Oxygen Transfer Coefficient	k_L	0.75-1.8	m/day
Dissolved Oxygen Saturation	DO_{sat}	Eq. 1.20	mgO_2/L
Oxidation Rates and Temperature Coefficients			
for RDOC	$k_{20,0}$ $\theta_{20,0}$	0.008-0.01 1.08	day^{-1}
for LDOC	$k_{21,0}$ $\theta_{21,0}$	0.10-0.15 1.047	day^{-1}
for ReDOC	$k_{22,0}$ $\theta_{22,0}$	0.25-0.3 1.047	day^{-1}
for ExDOC	$k_{23,0}$ $\theta_{23,0}$	0.1-0.125 1.08	day^{-1}
Oxidation Rate of Dissolved Sulfide	$k_{o_2^*}$	0.15-0.5	day^{-1}
Temperature Coefficient	$\theta_{o_2^*}$	1.08	
Half Saturation for Oxygen Limitation	$k_{DO_{o_2^*}}$	0.2	mgO_2/L

1.2.4 Specification of Input Variables Associated with the Eutrophication Model

As described earlier, the user has the choice of two algal growth formulation - the standard formulation and the Laws-Chalup formulation. The user can also select whether to simulate one, two, or three algal groups. In addition, the user can select from various options to specify the reaeration coefficient and the extinction coefficient. These selections are provided for via the first three constants specified in Card Group L (more specifically in L10). These constants are described below.

Constant Number	Name	Description
1	AGOPT	algal growth model option = 0, use standard or traditional algal growth kinetics = 1, use Laws-Chalup formulation
2	ACTALG	number of algal groups to simulate = 1, just one group (state-variable #2) will be simulated = 2, two groups will be simulated (using state-variables #2 and #3) = 3, three algal groups will be simulated (using state-variables #2 through #4)
3	KAOPT	reaeration formulation option = 0, use spatially constant k_L ($k_a = k_L$/depth) = 1, use spatially variable k_L = 2, use velocity shear and oxygen diffusivity = 3, use wind shear formulation
4	KEOPT	extinction coefficient option = 0, k_e is a constant (spatially and temporally invariant = 1, k_e is a spatially variable but constant in time(using 2-d parameter array) = 2, k_e is spatially invariant but varies in time (using time-variable function) = 3, k_e is spatially variable and can vary in time, (using 2-d parameter array and one time-variable function) = 4, k_e is spatially and temporally variable (requires separate input file)

TABLE 1-10. KINETIC CONSTANTS USED FOR STANDARD EUTROPHICATION ALGAL GROWTH MODEL

If <AGOPT> = 0 then the following constants (9 through 99) are used by the eutrophication model and must be specified by the user. If the user is simulating only one phytoplankton group then constants 41-99 can be ignored; if the user is simulating two group then constants 73-99 can be ignored.

Number	Name	Description	Units
9	TOPT1	optimal growth temperature for algal group #1	deg C
10	K1BETA1	temperature correction effect on growth rate below <TOPT1>	$(\text{deg C})^{-2}$
11	K1BETA2	temperature correction effect on growth rate above <TOPT1>	$(\text{deg C})^{-2}$
12	K1C	saturated phytoplankton growth rate (at temperature = <TOPT1>)	/day
13	K1T	temperature coefficient	
14	IS1	saturating algal light intensity	ly/day
15	KMN1	half saturation constant for nitrogen	mg N/L
16	KMP1	half saturation constant for phosphorous	mg P/L
17	KMS1	half saturation constant for silica	mg Si/L
18	K1RB	basal/resting respiration rate -or- endogenous respiration rate at 20 deg C	/day
19	K1RT	temperature coefficient	
20	K1RG	growth-rate-dependent respiration coefficient	
21	K1GRZC	death rate due to grazing	/day
22	K1GRZT	temperature coefficient	
23	CCHL1	carbon to chlorophyll ratio	mg C/mg Chla
24	CRBP11	carbon to phosphorus ratio - non-P limited	mg C/mg P
25	CRBP12	carbon to phosphorus ratio - P limited	mg C/mg P
26	CRBP13	coefficient determining range of P limitation	L/mg P
27	CRBN11	carbon to nitrogen ratio - non-N limited	mg C/mg N
28	CRBN12	carbon to nitrogen ratio - N limited	mg C/mg N
29	CRBN13	coefficient determining range of N limitation	L/mg N
30	CRBS11	carbon to silica ratio - non-Si limited	mg C/mg Si
31	CRBS12	carbon to silica ratio - Si limited	mg C/mg Si
32	CRBS13	coefficient determining range of Si limitation	L/mg Si
33	XKC1	chlorophyll self-shading extinction coefficient	m^2/mg Chla
34	VSBAS1	base algal settling rate	m/day
35	VSNTR1	nutrient stressed algal settling rate	m/day

TABLE 1-10. KINETIC CONSTANTS USED FOR STANDARD EUTROPHICATION ALGAL GROWTH MODEL (Continued)

41	TOPT2	optimal growth temperature for algal group #2	deg C
42	K2BETA1	temperature correction effect on growth rate below <TOPT2>	$(\text{deg C})^{-2}$
43	K2BETA2	temperature correction effect on growth rate above <TOPT2>	$(\text{deg C})^{-2}$
44	K2C	saturated phytoplankton growth rate (at temperature = <TOPT2>)	/day
45	K2T	temperature coefficient	
46	IS2	saturating algal light intensity	ly/day
47	KMN2	half saturation constant for nitrogen	mg N/L
48	KMP2	half saturation constant for phosphorous	mg P/L
49	KMS2	half saturation constant for silica	mg Si/L
50	K2RB	basal/resting respiration rate -or- endogenous respiration rate at 20 deg C	/day /day
51	K2RT	temperature coefficient	
52	K2RG	growth-rate-dependent respiration coefficient	
53	K2GRZC	death rate due to grazing	/day
54	K2GRZT	temperature coefficient	
55	CCHL2	carbon to chlorophyll ratio	mg C/mg Chla
56	CRBP21	carbon to phosphorus ratio - non-P limited	mg C/mg P
57	CRBP22	carbon to phosphorus ratio - P limited	mg C/mg P
58	CRBP23	coefficient determining range of P limitation	L/mg P
59	CRBN21	carbon to nitrogen ratio - non-N limited	mg C/mg N
60	CRBN22	carbon to nitrogen ratio - N limited	mg C/mg N
61	CRBN23	coefficient determining range of N limitation	L/mg N
62	CRBS21	carbon to silica ratio - non-Si limited	mg C/mg Si
63	CRBS22	carbon to silica ratio - Si limited	mg C/mg Si
64	CRBS23	coefficient determining range of Si limitation	L/mg Si
65	XKC2	chlorophyll self-shading extinction coefficient	m^2/mg Chla
66	VSBAS2	base algal settling rate	m/day
67	VSNTR2	nutrient stressed algal settling rate	m/day

TABLE 1-10. KINETIC CONSTANTS USED FOR STANDARD EUTROPHICATION ALGAL GROWTH MODEL (Continued)

73	TOPT3	optimal growth temperature for algal group #3	deg C
74	K3BETA1	temperature correction effect on growth rate below <TOPT1>	$(\text{deg C})^{-2}$
75	K3BETA2	temperature correction effect on growth rate above <TOPT1>	$(\text{deg C})^{-2}$
76	K3C	saturated phytoplankton growth rate (at temperature = <TOPT1>)	/day
77	K3T	temperature coefficient	
78	IS3	saturating algal light intensity	ly/day
79	KMN3	half saturation constant for nitrogen	mg N/L
80	KMP3	half saturation constant for phosphorous	mg P/L
81	KMS3	half saturation constant for silica	mg Si/L
82	K1RB	basal/resting respiration rate -or- endogenous respiration rate at 20 deg C	/day /day
83	K3RT	temperature coefficient	
84	K3RG	growth-rate-dependent respiration coefficient	
85	K3GRZC	death rate due to grazing	/day
86	K3GRZT	temperature coefficient	
87	CCHL3	carbon to chlorophyll ratio	mg C/mg Chla
88	CRBP31	carbon to phosphorus ratio - non-P limited	mg C/mg P
89	CRBP32	carbon to phosphorus ratio - P limited	mg C/mg P
90	CRBP33	coefficient determining range of P limitation	L/mg P
91	CRBN31	carbon to nitrogen ratio - non-N limited	mg C/mg N
92	CRBN32	carbon to nitrogen ratio - N limited	mg C/mg N
93	CRBN33	coefficient determining range of N limitation	L/mg N
94	CRBS31	carbon to silica ratio - non-Si limited	mg C/mg Si
95	CRBS32	carbon to silica ratio - Si limited	mg C/mg Si
96	CRBS33	coefficient determining range of Si limitation	L/mg Si
97	XKC3	chlorophyll self-shading extinction coefficient	m^2/mg Chla
98	VSBAS3	base algal settling rate	m/day
99	VSNTR3	nutrient stressed algal settling rate	m/day
105	KMPHYT	half saturation constant for phytoplankton	mg C/L

TABLE 1-11. KINETIC CONSTANTS USED FOR LAWS-CHALUP EUTROPHICATION ALGAL GROWTH MODEL

If <AGOPT> = 1 then the following constants (6 through 95) are used by the eutrophication model and must be specified by the user. If the user is simulating only one phytoplankton group, then constants 41-95 can be ignored; if the user is simulating only two groups, then constants 73-95 can be ignored.

9	TOPT1	optimal growth temperature for algal group #1	deg C
10	K1BETA1	temperature correction effect on growth rate below <TOPT1>	$(\text{deg C})^{-2}$
11	K1BETA2	temperature correction effect on growth rate above <TOPT1>	$(\text{deg C})^{-2}$
12	GPRE1	gross photosynthetic rate per unit cell (associated with photosynthetic dark reactions)	/day
13	GPR01	gross photosynthetic rate per unit cell per unit light intensity under nutrient-saturated conditions and zero irradiance	m^2/mol quanta
14	IS1	saturating algal light intensity	ly/day
15	KMN1	half saturation constant for nitrogen	mg N/L
16	KMP1	half saturation constant for phosphorous	mg P/L
17	KMS1	half saturation constant for silica	mg Si/L
18	K1RB	basal or resting respiration rate	/day
19	K1RT	temperature coefficient for basal/endogenous respiration	
20	K1RG	growth-rate-dependent respiration coefficient	
21	K1GRZC	death rate due to grazing	/day
22	K1GRZT	temperature coefficient	
23	FSC1	fraction of C allocated to structural purposes	
24	WCCHL1	carbon to chlorophyll ratio	mg C/mg Chla
25	WCP1	carbon to phosphorus ratio - non-P limited	mg C/mg P
26	WCN1	carbon to nitrogen ratio - non-N limited	mg C/mg N
27	WCS1	carbon to silica ratio - non-Si limited	mg C/mg Si
28	QF1	quotient of nutrient-limited nutrient:C ratios at relative growth rates of 0 and 1	
29	XKC1	chlorophyll self-shading extinction coefficient	m^2/mg Chla
30	VSBAS1	base algal settling rate	m/day
31	VSNTR1	nutrient stressed algal settling rate	m/day

TABLE 1-11. KINETIC CONSTANTS USED FOR LAWS-CHALUP EUTROPHICATION ALGAL GROWTH MODEL (Continued)

41	TOPT2	optimal growth temperature for algal group #2	deg C
42	K2BETA1	temperature correction effect on growth rate below <TOPT2>	$(\text{deg C})^{-2}$
43	K2BETA2	temperature correction effect on growth rate above <TOPT2>	$(\text{deg C})^{-2}$
44	GPRE2	gross photosynthetic rate per unit cell (associated with photosynthetic dark reactions)	/day
45	GPR02	gross photosynthetic rate per unit cell per unit light intensity under nutrient-saturated conditions and zero irradiance	m^2/mol quanta
46	IS2	saturating algal light intensity	ly/day
47	KMN2	half saturation constant for nitrogen	mg N/L
48	KMP2	half saturation constant for phosphorous	mg P/L
49	KMS2	half saturation constant for silica	mg Si/L
50	K2RB	basal or resting respiration rate	/day
51	K2RT	temperature coefficient for basal/endogenous respiration	
52	K2RG	growth-rate-dependent respiration coefficient	
53	K2GRZC	death rate due to grazing	/day
54	K2GRZT	temperature coefficient	
55	FSC2	fraction of C allocated to structural purposes	
56	WCCHL2	carbon to chlorophyll ratio	mg C/mg Chla
57	WCP2	carbon to phosphorus ratio - non-P limited	mg C/mg P
58	WCN2	carbon to nitrogen ratio - non-N limited	mg C/mg N
59	WCS2	carbon to silica ratio - non-Si limited	mg C/mg Si
60	QF2	quotient of nutrient-limited nutrient: C ratios at relative growth rates of 0 and 1	
61	XKC2	chlorophyll self-shading extinction coefficient	m^2/mg Chla
62	VSBAS2	base algal settling rate	m/day
63	VSNTR2	nutrient stressed algal settling rate	m/day

TABLE 1-11. KINETIC CONSTANTS USED FOR LAWS-CHALUP EUTROPHICATION ALGAL GROWTH MODEL (Continued)

73	TOPT3	optimal growth temperature for algal group #3	deg C
74	K3BETA1	temperature correction effect on growth rate below <TOPT1>	$(\text{deg C})^{-2}$
75	K3BETA2	temperature correction effect on growth rate above <TOPT1>	$(\text{deg C})^{-2}$
76	GPRE3	gross photosynthetic rate per unit cell (associated with photosynthetic dark reactions)	/day
77	GPR03	gross photosynthetic rate per unit cell per unit light intensity under nutrient-saturated conditions and zero irradiance	m^2/mol quanta
78	IS3	saturating algal light intensity	ly/day
79	KMN3	half saturation constant for nitrogen	mg N/L
80	KMP3	half saturation constant for phosphorous	mg P/L
81	KMS3	half saturation constant for silica	mg Si/L
82	K3RB	basal or resting respiration rate	/day
83	K3RT	temperature coefficient for basal/endogenous	
84	K3RG	growth-rate-dependent respiration coefficient respiration	
85	K3GRZC	death rate due to grazing	/day
86	K3GRZT	temperature coefficient	
87	FSC3	fraction of C allocated to structural purposes	
88	WCCHL3	carbon to chlorophyll ratio	mg C/mg Chla
89	WCP3	carbon to phosphorus ratio - non-P limited	mg C/mg P
90	WCN3	carbon to nitrogen ratio - non-N limited	mg C/mg N
91	WCS3	carbon to silica ratio - non-Si limited	mg C/mg Si
92	QF3	quotient of nutrient-limited nutrient: C ratios at relative growth rates of 0 and 1	
93	XKC3	chlorophyll self-shading extinction coefficient	m^2/mg Chla
94	VSBAS3	base algal settling rate	m/day
95	VSNWTR3	nutrient stressed algal settling rate	m/day
105	KMPHYT	half saturation constant for phytoplankton	mg C/L

TABLE 1-12. REMAINING KINETIC CONSTANTS USED FOR INTEGRATED EUTROPHICATION MODEL

		Recycle Fractions - Fraction of Grayed/Respired Algal Biomass Going to....	
106	FRPOP	refractory particulate organic phosphorous	
107	FLPOP	labile particulate organic phosphorous	
108	FRDOP	refractory dissolved organic phosphorous	
109	FLDOP	labile dissolved organic phosphorous	
110	FPO4	dissolved inorganic phosphorous	
111	FRPON	refractory particulate organic nitrogen	
112	FLPON	labile particulate organic nitrogen	
113	FRDON	refractory dissolved organic nitrogen	
114	FLDON	labile dissolved organic nitrogen	
115	FNH4	ammonia	
116	FRPOC	refractory particulate organic carbon	
117	FLPOC	labile particulate organic carbon	
118	FRDOC	refractory dissolved organic carbon	
119	FLDOC	labile dissolved organic carbon	
		Phosphorus Hydrolysis/Mineralization Rates at 20 deg C	
120	K57C	hydrolysis rate of RPOP to RDOP	/day
121	K57T	temperature coefficient	
122	K68C	hydrolysis rate of LPOP to LDOP	/day
123	K68T	temperature coefficient	
124	K79C	mineralization rate of RDOP to PO4	/day
125	K79T	temperature coefficient	
126	K89C	mineralization rate of LDOP to PO4	/day
127	K89T	temperature coefficient	
		Nitrogen Hydrolysis/Mineralization Rates at 20 deg C	
128	K1012C	hydrolysis rate of RPON to RDON	/day
129	K1012T	temperature coefficient	
130	K1113C	hydrolysis rate of LPON to LDON	/day
131	K1113T	temperature coefficient	
132	K1214C	mineralization rate of RDON to NH4	/day
133	K1214T	temperature coefficient	
134	K1314C	mineralization rate of LDON to NH4	/day
135	K1314T	temperature coefficient	

TABLE 1-12. REMAINING KINETIC CONSTANTS USED FOR INTEGRATED EUTROPHICATION MODEL (Continued)

		Nitrification/Denitification Rates	
136	K1415C	nitrification rate at 20 deg C	/day
137	K1415T	temperature coefficient	
138	KNIT	half saturation constant for nitrification oxygen limitation	mg O2/L
139	K150C	denitrification rate at 20 deg C	/day
140	K150T	temperature coefficient	
141	KNO3	Michaelis constant for denitrification oxygen limitation	mg O2/L
		Silica Mineralization Rates at 20 deg C	
142	K1617C	mineralization rate of biogenic Si to available dissolved Si	/day
143	K1617T	temperature coefficient	
		Carbon Hydrolysis/Oxidation Rates at 20 deg C	
144	K1820C	hydrolysis rate of RPOC to RDOC	/day
145	K1820T	temperature coefficient	
146	K1921C	hydrolysis rate of LPOC to LDOC	/day
147	K1921T	temperature coefficient	
148	K200C	oxidation rate of RDOC	/day
149	K200T	temperature coefficient	
150	K210C	oxidation rate of LDOC	/day
151	K210T	temperature coefficient	
152	KMLDOC	Michaelis constant for LDOC	mg C/L
153	KDOC	half saturation constant for organic carbon	mg O2/L
154	K220C	algal exudate DOC oxidation rate	/day
155	K220T	temperature coefficient	
156	FLOCEX	fraction of primary productivity going to labile organic carbon via exudation	
157	K2324C	hydrolysis rate of REPOC to REDOC	/day
158	K2324T	temperature coefficient	
159	K240C	reactive DOC oxidation rate	/day
160	K240T	temperature coefficient	
161	CTOPCSO	carbon to phosphorus ratio of CSO solids	mg C/mg P
162	CTONCSO	carbon to nitrogen ratio of CSO solids	mg C/mg N
163	K250C	oxidation rate for aqueous sod	/day
164	K250T	temperature coefficient	

TABLE 1-12. REMAINING KINETIC CONSTANTS USED FOR INTEGRATED EUTROPHICATION MODEL (Continued)

165	KO2EQ	half saturation constant for O_2^*	mg O_2/L
166	KLMIN	if <KAOPT> = 0, then $K_{lmin} = K_l$ if <KAOPT> > 0, then K_{lmin} = minimum value for K_l	m/day
167	DIFUS	diffusivity of oxygen across the air-water interface	m^2/day
168	KAT	temperature correction coefficient for atmospheric reaeration	
169	VSBAST	temperature correction	
170	VSPOM	particulate organic matter settling rate	m/day
171	VSPMT	temperature correction	
172	VSSEDT	temperature correction for deposition to sediment	
173	BVCSO	power coefficient for CSO solid settling rate (>=1)	unitless
174	CRCSO	critical REPOC concentration for CSO settling function	mg C/L
175	VMINCSO	minimum settling rate for CSO solids Vcso =min (VMAXCSO + VMINCSO + (VMAXCSO - VMINCSO) * (REPOC/CRCSO)**BVCSO)	m/day
176	VMAXCSO	maximum settling rate for CSO solids	m/day
177	KADPO4	partition coefficient for sorbed phosphorus	L/mg ss
178	KADSI	partition coefficient for sorbed silica	L/mg ss
179	VSPIM	settling rate for phosphorus/silica sorbed to suspended solids	m/day
180	KECONST	base (chl-a corrected) extinction coefficient (used when <KEOPT> = 0,2)	/m

1.2.4.1 Parameters, Constants, and Time Functions

The parameters, constants, and time functions required by the kinetics of this model are specified according to the formatting described for input Group L in the RCA Users Guide. Table 1-13 lists the required two dimensional segment parameters. No three dimensional parameters are included in the kinetic routine. Required time variable functions are described in Table 1-14.

TABLE 1-13. 2-D PARAMETERS

Number	Name	Description	Units
1	KL	transfer coefficient for reaeration	m/day
2	VSNET1	settling efficiency from water column to the bed for algal group number 1 (the winter diatom group)	
3	VSNET2	settling efficiency from water column to the bed for algal group number 2 (the summer mixed assemblage)	m/day
4	VSNET3	settling efficiency from water column to bed for algal group number 3	m/day
5	VSNET4	settling efficiency from water column to the bed for non-living particulate organic matter (POM)	m/day
6	KEBS	base extinction coefficient (when KEOPT - 1 or 3)	m^{-1}

Note: by settling efficiency, it is meant the "stickiness" of a particle settling from the water column to the sediment bed; range 0 to 1. If VSNET = 1, all of the particles settling from the water column to the bed, stick to the bed and become incorporated in the sediment. If VSNET = 0.5, only half of the particles settling from the water column to the bed become incorporated in the sediment; the remainder are assumed to become "resuspended" and may be transported elsewhere. If VSNET = 0, none of the particles settle to the bed, i.e., no deposition in this segment.

TABLE 1-14. TIME-VARIABLE FUNCTIONS

Number	Name	Description	Units
1	ITOTSF	total daily solar radiation	ly/day
2	F	fraction of daylight	day
3	WIND	wind speed	m/sec
4	KETVF	extinction coefficient (when KEOPT = 2 or 3)	m^{-1}

Table 1-15 presents a sample input deck for the standard eutrophication model coefficient set, which includes one kinetic subroutine specific file, i.e., the sediment nutrient flux subroutine input data set.

TABLE 1-15. SAMPLE EUTROPHICATION INPUT DATASET

```
C N2DPARAM
         6
C    Scale1     Scale2     Scale3     Scale4
     0.3048        1.0        1.0        1.0
kL
     0.0000     0.0000     0.0000
     0.0000     0.7870     0.0000
     0.0000     0.0000     0.0000
Vsnet1 - algal group 1
     0.0000     0.0000     0.0000
     0.0000     1.0000     0.0000
     0.0000     0.0000     0.0000
Vsnet2 - algal group 2
     0.0000     0.0000     0.0000
     0.0000     1.0000     0.0000
     0.0000     0.0000     0.0000
Vsnet3 - algal group 3
     0.0000     0.0000     0.0000
     0.0000     1.0000     0.0000
     0.0000     0.0000     0.0000
Vsnet4 - pom
     0.0000     0.0000     0.0000
     0.0000     1.0000     0.0000
     0.0000     0.0000     0.0000
KEbs
     0.0000     0.0000     0.0000
     0.0000     0.0000     0.0000
     0.0000     0.0000     0.0000
C N3DPARAM
    1                                  number of 3D parameters
C    SCALE1
   1.0E-20
SS (mg/L)
       0.01       0.01       0.01
       0.01       0.01       0.01
       0.01       0.01       0.01           Layer #1
       0.01       0.01       0.01
       0.01       0.01       0.01
       0.01       0.01       0.01           Layer #2
C     NCONS
        180                                    number of constants
      AGOPT     ACTALG      KAOPT      KEOPT     Unused     Unused     Unused     Unused
         0.         2.         1.         2.
      TOPT1    K1BETA1    K2BETA2       K1C        K1T        IS1       KMN1       KMP1
       3.50       .004       .006      2.500      1.068    150.000      0.010      0.001
       KMS1       K1RB       K1RT       K1RG      K1GZC      K1GZT      CCHL1      CPR11
      0.020      0.075      1.047        0.0      0.100       1.10       30.0       40.0
      CPR12      CPR13      CNR11      CNR12      CNR13      CSR11      CSR12      CSR13
        0.0        0.0      5.670        0.0        0.0        5.0       10.0        0.0
       XKC1     VSBAS1     VSNTR1    Unused     Unused     Unused     Unused     Unused
      0.017        0.2        0.5
      TOPT2    K2BETA1    K2BETA2       K2C        K2T        IS2       KMN2       KMP2
       22.        .004       .006      2.400      1.068      350.      0.010      0.001
       KMS2       K2RB       K2RT       K2RG      K2GZC      K2GRT      CCHL2      CPR21
      0.002      0.075      1.047        0.0      0.120      1.100       80.0       40.0
      CPR22      CPR23      CNR21      CNR22      CNR23      CSR21      CSR22      CSR23
        0.0        0.0      5.670        0.0        0.0        8.0        0.0        0.0
       XKC2     VSBAS2     VSNTR2    Unused     Unused     Unused     Unused     Unused
      0.017        0.5        0.2
      TOPT3    K3BETA1    K3BETA2       K3C        K3T        IS3       KMN3       KMP3
         0.         0.         0.         0.         0.         0.         0.         0.
       KMS3       K3RB       K3RT       K3RG      K3GZC      K3GRT      CCHL3      CPR31
         0.         0.         0.         0.         0.         0.         0.         0.
      CPR32      CPR33      CNR31      CNR32      CNR33      CSR31      CSR32      CSR33
```

TABLE 1-15. SAMPLE EUTROPHICATION INPUT DATASET (Cont.)

```
        0.        0.        0.        0.        0.        0.        0.        0.
      XKC3    VSBAS3    VSNTR3    Unused    Unused    Unused    Unused    Unused
        0.        0.        0.
     KMPHY     FRPOP     FLPOP     FRDOP     FLDOP      FPO4     FRPON     FLPON
     0.050     0.100     0.250     0.100     0.100     0.450     0.001     0.399
     FRDON     FLDON      FNH4     FRPOC     FLPOC     FRDOC     FLDOC      K57C
     0.125     0.125     0.350     0.001     0.449     0.100     0.450     0.010
      K57T      K68C      K68T      K79C      K79T      K89C      K89T    K1012C
     1.080     0.070     1.080     0.020     1.080     0.090     1.080     0.010
    K1012T    K1113C    K1113T    K1214C    K1214T    K1314C    K1314T    K1415C
     1.080     0.050     1.080     0.010     1.080     0.075     1.080     0.040
    K1415T      KNIT     K150C     K150T      KNO3    K1617C    K1617T    K1820C
     1.040     1.500     0.050     1.045     0.010      0.10     1.080     0.010
    K1820T    K1921C    K1921T    K200C     K200T     K210C     K210T    KMLDOC
     1.080     0.070     1.080     0.010     1.080     0.150     1.047     0.100
      KDOC     K220C     K220T    FLOCEX    K2324C    K2324T     K24OC     K24OT
     0.200     0.120     1.047       0.0      0.35     1.047     0.100     1.080
   CTOPCSO   CTONCSO     K25OC     K25OT     KO2EQ     KLMIN     DIFUS       KAT
        35.       6.0     0.150     1.080     0.100       2.0      0.00     1.024
    VSBAST     VSPOM     VSPMT    VSSEDT     BVCSO     CRCSO    KADPO4    KADSI
     1.000     0.750      1.00       1.0       2.0       10.       6.0       6.0
     VSPIM   KECONST
       0.0       0.0
C    NOTVF   TVPWLOPT
         4         1                    number of time functions
C    PNAME     NOBRK   TWARPTVF
      ITOT        13      DAYS          TOTAL DAILY RADIATION
      118.        0.      168.        11.       218.       59.       318.       90.
      418.      120.      468.       151.       518.      181.       468.      212.
      418.      243.      318.       273.       218.      304.       168.      335.
      118.      365.
C    PNAME     NOBRK   TWARPTVF
     F DAY        13      DAYS          FRACTION OF DAYLIGHT
      0.37        0.      0.42        31.       0.46       59.       0.52       90.
      0.58      120.      0.61       151.       0.63      181.       0.59      212.
      0.54      243.      0.49       273.       0.43      304.       0.40      335.
      0.37      365.
C    PNAME     NOBRK   TWARPTVF
      Wind         2      DAYS          Wind Speed (m/sec)
      000.        0.      000.      9999.
C    PNAME     NOBRK   TWARPTVF
        KE        13      DAYS          Extinction coefficient (/m)
      0.70        0.      0.65        31.       0.60       59.       0.55       90.
      0.73      120.      0.96       151.       1.12      181.       0.74      212.
      0.57      243.      0.57       273.       0.51      304.       0.63      335.
      0.67      365.
C NOKINFIL                          Number of kinetic subroutine specific files
         1
sed.inp
```

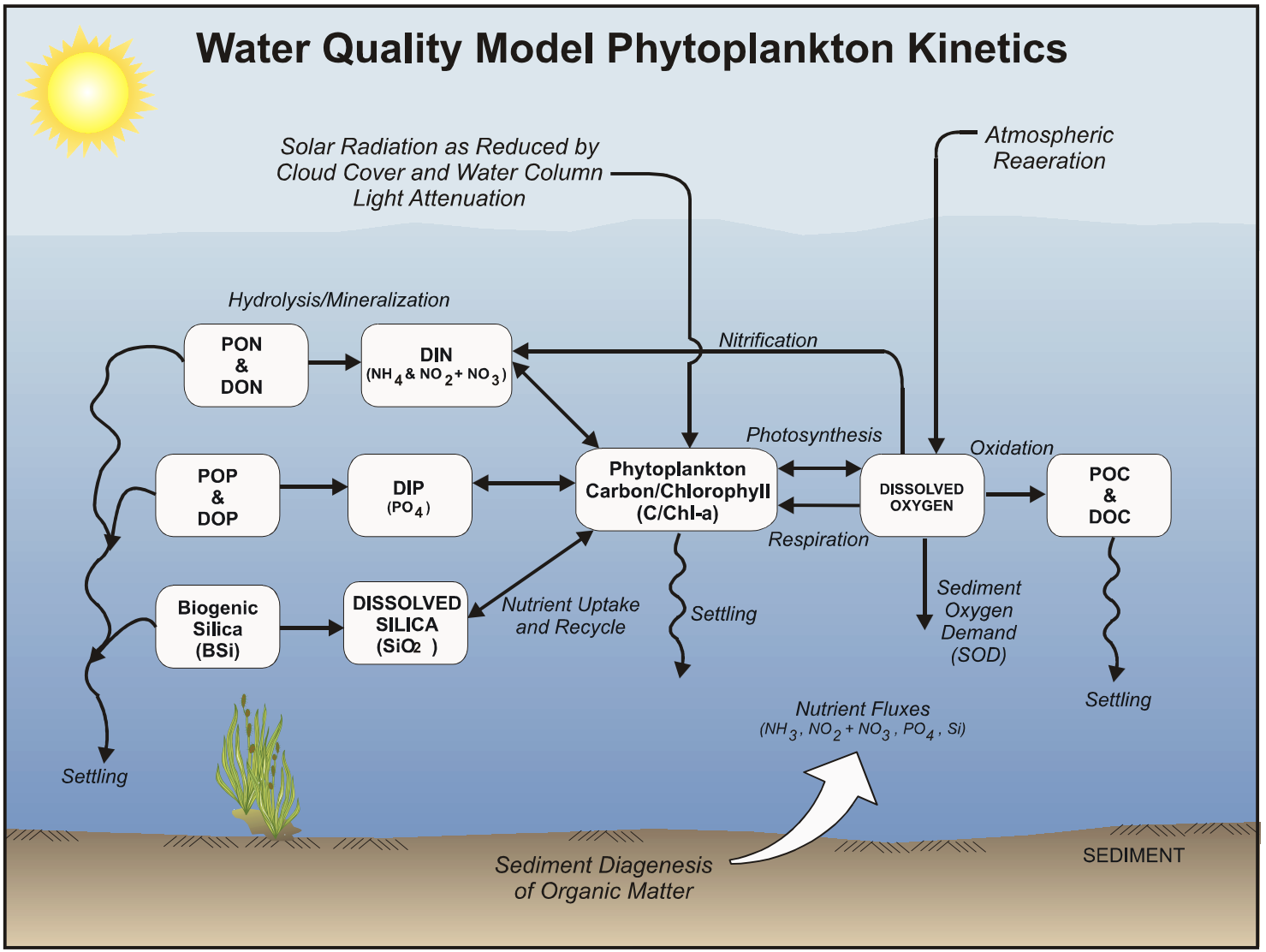

Figure 1-1. Principal Kinetic Interactions for Nutrient Cycles and Dissolved Oxygen

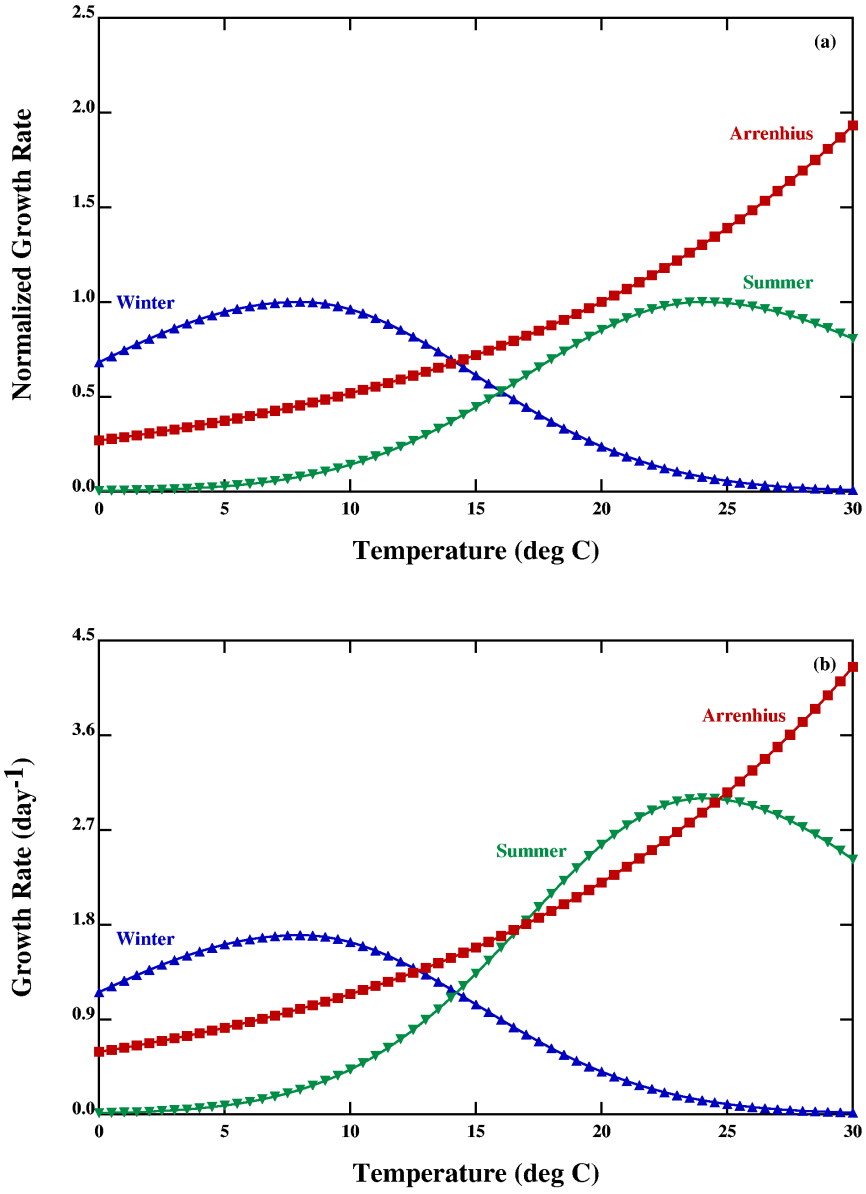

Figure 1-2. Growth Rate as a Function of Temperature

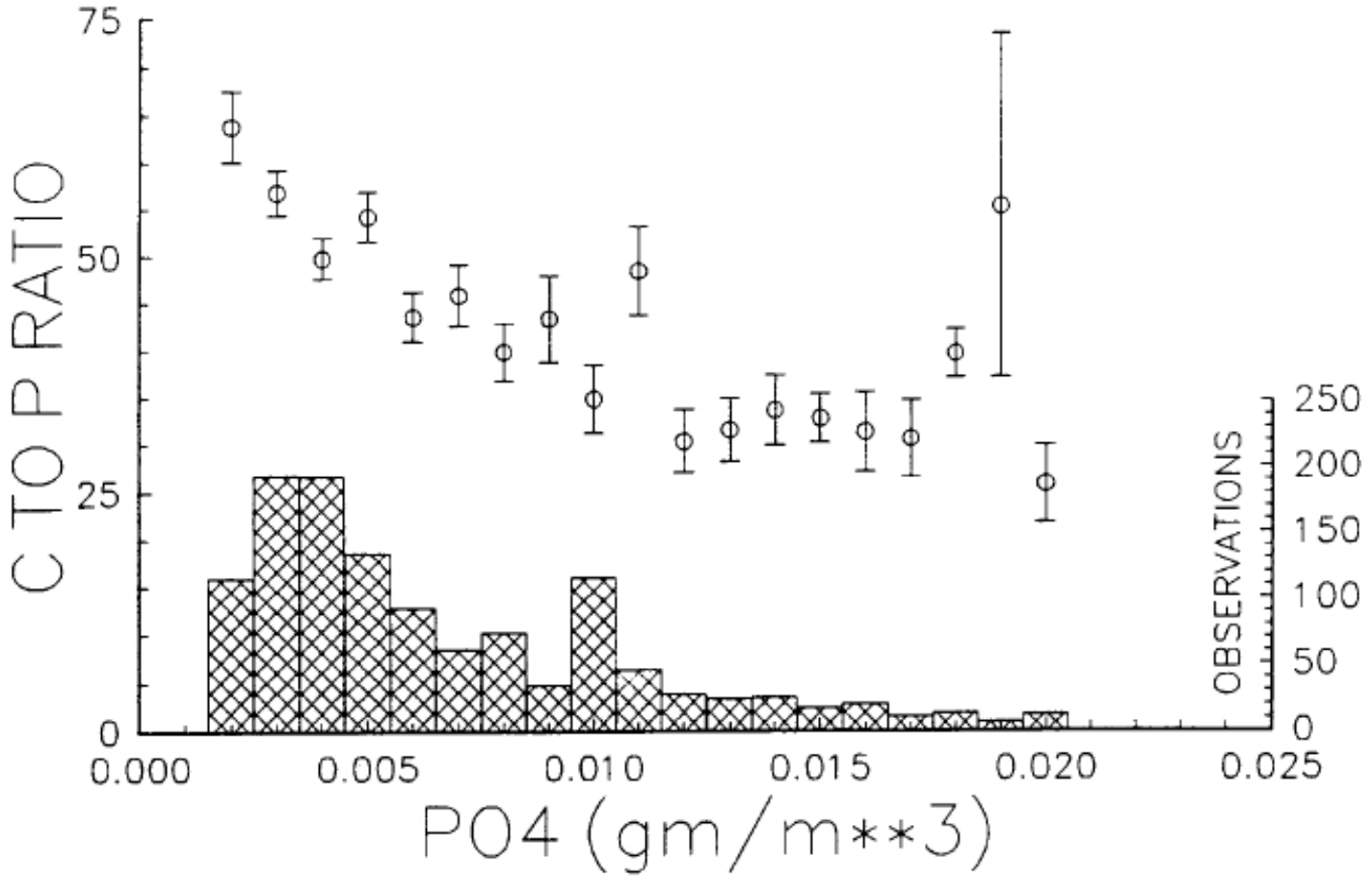

Figure 1-3. Carbon-to-phosphorus ratio (mean and standard error) of seston in Upper Chesapeake Bay. Bars show number of observations.

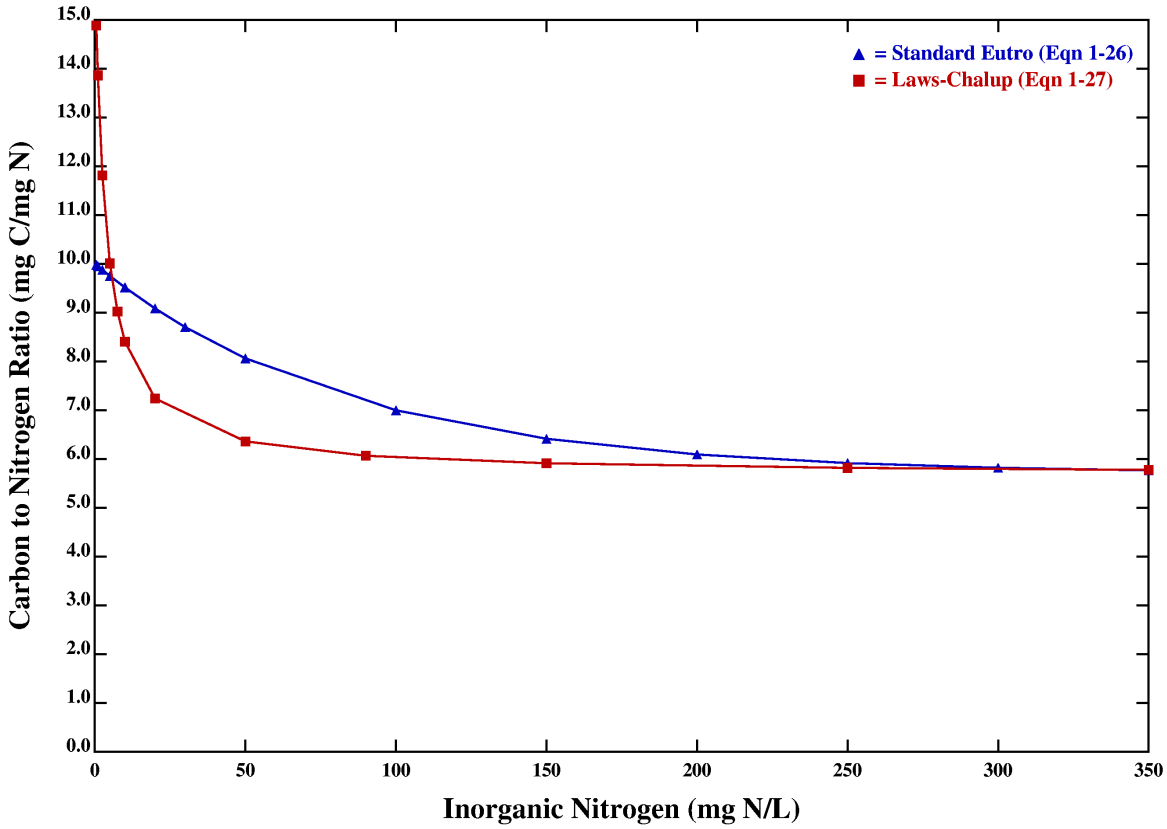

Figure 1-4. Carbon to nitrogen ratios as a function of the concentration of dissolved inorganic nitrogen.

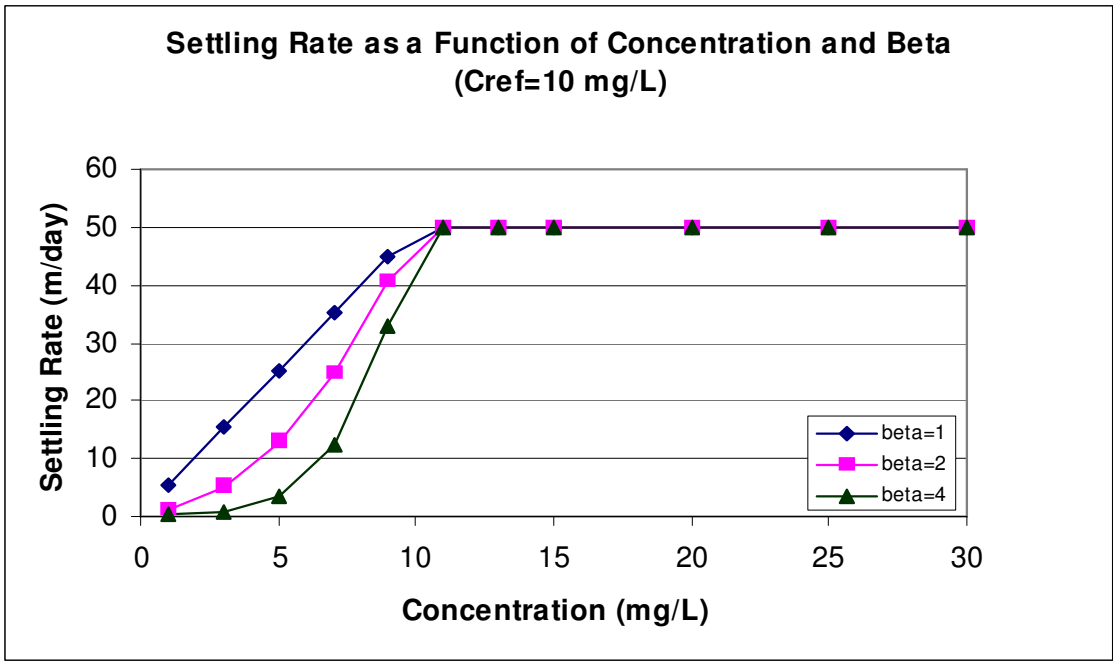

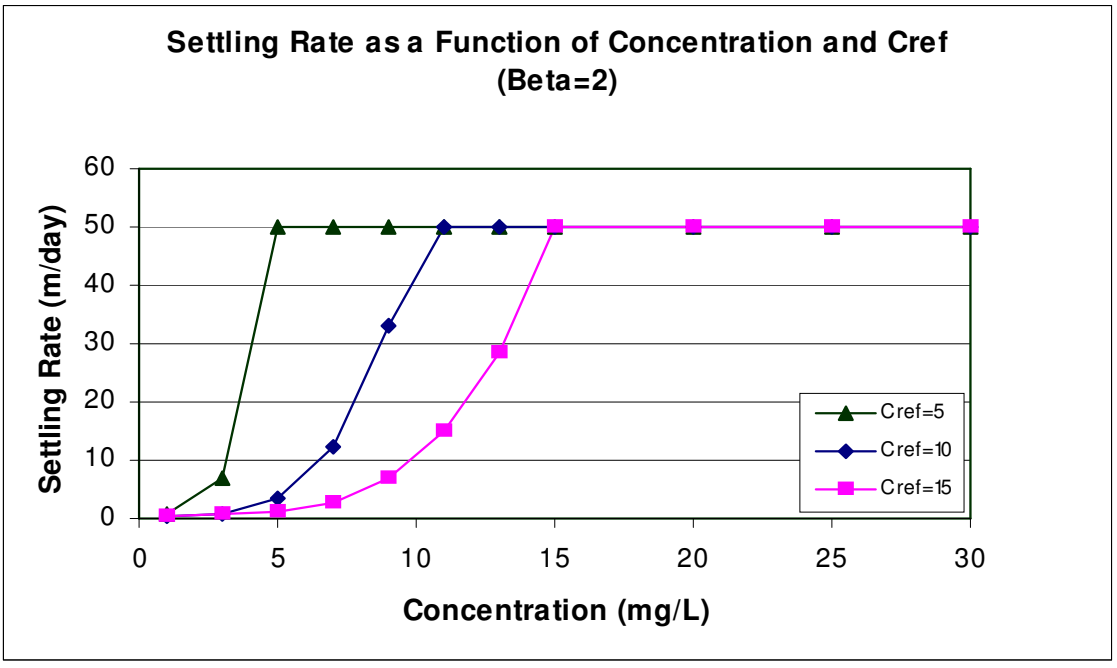

Figure 1-5. Settling Rate as a Function of Concentration and β (Beta) and C_{ref}

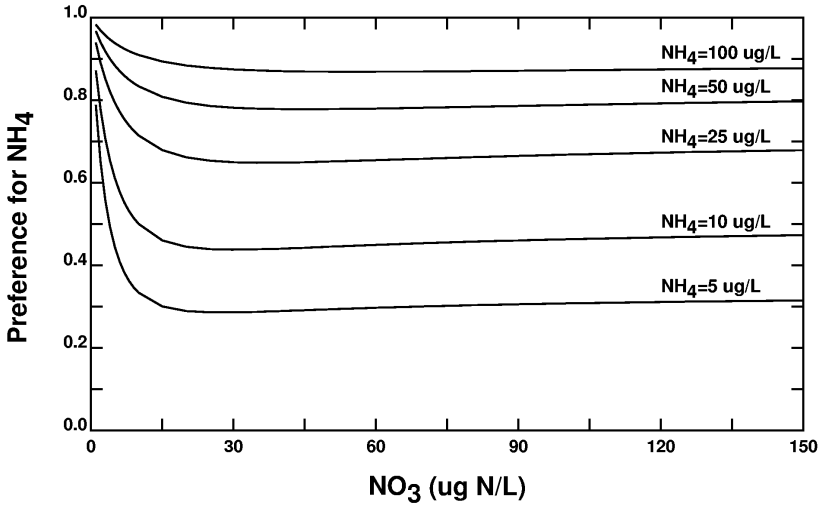

Figure 1-6. Behavior of the Ammonia Preference Structure for Various Concentrations of NH_3 and NO_2+NO_3.

2.0 FRAMEWORK FOR THE SEDIMENT FLUX SUBMODEL

2.1 Overview of Model Framework

The sediment receives fluxes of particulate organic carbon (POC), particulate organic nitrogen (PON), and particulate organic phosphorus (POP). This is collectively referred to as particulate organic matter (POM). Mineralization, which is termed diagenesis, produces soluble end-products. These can react in the aerobic and anaerobic layers of the sediment. The difference between the resulting aerobic layer dissolved concentration and the overlying water concentration determines the flux to or from the sediment. The magnitude of the flux is determined by the surface mass transfer coefficient.

2.2 Diagenesis

The water column model state-variables that are deposited to the sediment include: detrital algae, labile and refractory POC, labile and refractory PON, and labile and refractory POP. The fluxes of these state variables make up the incoming sources of particulate organic matter to the sediment. Carbon, nitrogen, and phosphorus are treated analogously.

The multi-class G model (Westrich and Berner 1984) is used as the basis for the diagenesis of POM. Each class represents a portion of the organic material that reacts at a specific rate. The reaction rates for each class are approximately an order of magnitude smaller than the previous class. For this application three G classes are chosen. The three classes represent three scales of reactivity: reactive (~20 day half life); refractory (~1 year half life); and inert (i.e., conservative). Particulate organic matter is also allowed to be removed by burial.

The kinetic equations for particulate organic carbon, nitrogen, and phosphorus are analogous. Let $G_{POC,i}$ be the concentration of POC in the i^{th} diagenesis class (i=1, 2, or 3). The kinetic equation for diagenesis is:

$$H\frac{dG_{POC,i}}{dt} = -k_{GPOC,i}\,\theta_{GPOC,i}^{T-20}\,G_{POC,i}\,H + J_{GPOC,i}(t) \qquad (2\text{-}1)$$

where:

H	=	depth of the active sediment layer [m],
$G_{POC,i}$	=	concentration of particulate organic carbon in reactivity class i, (g/m^3)
$k_{GPOC,i}$	=	first order reaction rate coefficient ($k_{GPOC,3} = 0$), (/day),

$\theta_{GPOC,i}$ = temperature coefficient,
$J_{GPOC,i}(t)$ = POC flux of the i^{th} G class to the sediment from the overlying water, (g/m^2-day).

The water column sources that contribute to each reactivity class are:

$$J_{GPOC.1} = f_{G1} J_{POC}$$
$$J_{GPOC,2} = f_{G2} J_{POC}$$
$$J_{GPOC,3} = f_{G3} J_{POC}$$

where:

f_{G1} = fraction of water column POC that is in reactivity class G_1
f_{G2} = fraction of water column POC that is in reactivity class G_2
f_{G3} = fraction of water column POC that is in reactivity class G_3
J_{POC} = total flux of POC from the overlying water column to the sediment bed

Carbon diagenesis flux, J_C, is computed from the rates of mineralization of the labile and refractory G classes. (Note: it is assumed that G_3 carbon is inert; therefore, it does not contribute to carbon diagenesis):

$$J_C = \sum_{i=1}^{2} k_{GPOC,i}\ \theta_{GPOC,i}^{(T-20)}\ G_{POC,i}\ H \qquad (2\text{-}2)$$

Nitrogen and phosphorus are completely analogous.

$$J_N = \sum_{i=1}^{2} k_{GPON,i}\ \theta_{GPON,i}^{(T-20)}\ G_{PON,i}\ H \qquad (2\text{-}3)$$

$$J_P = \sum_{i=1}^{2} k_{GPOP,i}\ \theta_{GPOP,i}^{(T-20)}\ G_{POP,i}\ H \qquad (2\text{-}4)$$

The reaction rates and temperature coefficients are analogous to those listed above for carbon.

2.3 The General Sediment Model Equations

The sediment model is constructed from a mass balance equation in the aerobic layer, denoted as layer 1, and the anaerobic layer, layer 2 (with the overlying water column concentrations denoted using the subscript 0). The equations are expressed in terms of the total concentration of the chemical. The distribution between particulate and dissolved fractions is modeled using a linear partitioning model. The mass balance equations of the model can be expressed in a general form which is quite convenient for numerical solution. The layer 1 and 2 equations are:

$$H_1 \frac{dC_{T1}}{dt} = K_{L01}\left(f_{d1}C_{T1} - C_{d0}\right) + w_{12}\left(f_{p2}C_{T2} - f_{p1}C_{T1}\right) + K_{L12}\left(f_{d2}C_{T2} - f_{d1}C_{T1}\right) - k_1 H_1 C_{T1} + J_{T1} \quad (2\text{-}5)$$

$$H_2 \frac{dC_{T2}}{dt} = -w_{12}\left(f_{p2}C_{T2} - f_{p1}C_{T1}\right) - K_{L12}\left(f_{d2}C_{T2} - f_{d1}C\right) - k_2 H_2 C_{T2} - w_2 C_{T2} + J_{T2} \quad (2\text{-}6)$$

where:

C_{T1} = total concentration in layer 1 [M/L^3],
C_{T2} = total concentration in layer 2 [M/L^3],
f_{d1} = dissolved fraction in layer 1, $\frac{1}{1+ m_2\pi_2}$
f_{p1} = 1 - f_{d1} = particulate fraction in layer 1,
f_{d2} = $\frac{1}{1+ m_2\pi_2}$ dissolved fraction in layer 2,
C_{p2} = $f_{p2}\, C_{T2}$ = particulate concentration in layer 2 [M/L^3],
C_{d0} = dissolved concentration,
J_{T1} = total source into layer 1 [M/L^2-T],
J_{T2} = total source into layer 2 [M/L^2-T],
H_1 = depth of layer 1 [L],
H_2 = depth of layer 2 [L],
K_{L01} = aqueous mass transfer coefficient between layer 1 and the overlying water [L/T],
K_{L12} = aqueous mass transfer coefficient between layer 1 and layer 2 [L/T],
w_{12} = particle mixing velocity between layer 1 and layer 2 [L/T],
w_2 = sedimentation velocity out of layer 2 [L/T],

k_1 = first order decay rate coefficient removal process in layer 1 [T^{-1}],
k_2 = first order decay rate coefficient removal process in layer 2 [T^{-1}].

The dissolved and particulate concentrations and fractions are:

$C_{d1} = f_{d1} C_{T1}$ = dissolved concentration in layer 1 [M/L^3],

$$f_{d1} = \frac{1}{1 + m_1 \pi_1}$$

C_{p1} = $f_{p1}\, C_{T1}$ = particulate concentrations in layer 1 [M/L^3],

C_{d2} = $f_{d2}\, C_{T2}$ = dissolved fraction in layer 2 [M/L^3],

f_{p2} = 1 - f_{d2} = particulate fraction in layer 2,

where:

m_1 = solids concentration in layer 1 (aerobic layer) [M/L^3],
m_2 = solids concentration in layer 2 (anerobic layer) [M/L^3],
π_1 = partition coefficient in layer 1 [L^3/M],
π_2 = partition coefficient in layer 2 [L^3/M].

2.3.1 Surface Mass Transfer Coefficient and Reaction Velocities

The surface mass transfer coefficient, K_{L01}, quantifies the mixing between layer 1 and the overlying water. The critical observation is that it can be related to the sediment oxygen demand, SOD. The SOD is the mass flux of dissolved oxygen into the sediment. Thus, it can be calculated from the mass transfer equation:

$$D_1 \frac{d[O_2]}{dz}\Big|_{z=0} \approx D_1 \frac{[O_2(0)] - [O_2(H_1)]}{H_1} = \frac{D_1}{H_1}[O_2(0)] \qquad (2\text{-}7)$$

where a straight line approximation to the derivative is used. The second equality follows from $[O_2(H_1)] = 0$, since H_1 is the depth of zero oxygen concentration. Therefore, the surface mass transfer coefficient can be expressed as:

$$K_{L01} = \frac{D_1}{H_1} = \frac{SOD}{[O_2(0)]} = s \tag{2-8}$$

which is the ratio of SOD and overlying water oxygen concentration. For notational simplicity this ratio is termed s.

The reaction rate in the aerobic layer is formulated as a conventional first order reaction with reaction rate constant k_1. The term in the layer 1 equation is k_1H_1. The depth of the aerobic zone follows from the definition of the surface mass transfer coefficient: $s = D_1/H_1$. Hence $k_1H_1 = k_1D_1/s$. The reaction velocity, which has units [L/T], is defined as:

$$\kappa_1 = \sqrt{D_1 k_1} \tag{2-9}$$

The square root is used to conform to the parameter group that appears in the spatially continuous form of the model. With these definitions the reaction rate - aerobic layer depth product becomes:

$$K_1H_1 = \frac{\kappa_1^2}{s} \tag{2-10}$$

For convenience of nomenclature only, the reaction velocity in layer 2 may be defined as:

$$\kappa_2 = K_2H_2 \tag{2-11}$$

It has units of [L/T]. However, it is not equivalent to the aerobic layer reaction velocities which include diffusion coefficient as well as a reaction rate constant.

With these definitions the layer 1 and 2 equations become:

$$\begin{aligned} H_1 \frac{dC_{T1}}{dt} &= s\left(f_{d1}C_{T1} - C_{d0}\right) + w_{12}\left(f_{p2}C_{T2} - f_{p1}C_{T1}\right) \\ &\quad + K_{L12}\left(f_{d2}C_{T2} - f_{d1}C_{T1}\right) - \frac{\kappa_1^2}{s} C_{T1} + J_{T1} \end{aligned} \tag{2-12}$$

$$H_2 \frac{dC_{T2}}{dt} = w_{12}\left(f_{d2}C_{T2} - f_{p1}C_{T1}\right) - K_{L12}\left(f_{d2}C_{T2} - f_{d1}C_{T1}\right) - \kappa_2 C_{T2} - w_2 C_{T2} + J_{T2} \quad (2\text{-}13)$$

2.3.2 Particulate Phase Mixing

The rate of mixing of sediment particles by macrobenthos (bioturbation) has been quantified by estimating an apparent particle diffusion coefficient. The variation has been found to be proportional to the biomass of the benthos (Matisoft, 1982). In addition, it has been found that the benthic biomass is correlated to the carbon input to the sediment (Maughan, 1986, Robbins et al., 1989). In order to make the model self consistent - that is to use only internally computed variables in the parameterization - it seems reasonable to assume that benthic biomass is proportional to the labile carbon in the sediment, which is calculated by the model as $G_{POC,1}$. The temperature dependency of particle mixing has been accounted for by using an Arrhenius formulation.

A series of experiments have examined the relationship between particle mixing due to benthic organisms and the overlying water oxygen concentration. There is a general dependency of mixing rate on DO, with the lower rates occurring at the lower DO concentration. This dependency is modeled using a Michaelis Menton expression. The particle mixing mass transfer coefficient that results is:

$$w_{12}^{*} = D_p \frac{\theta_{Dp}^{(T-20)}}{H_2} \frac{G_{POC,1}}{G_{POC,R}} \frac{[O_2(0)]}{K_{M,Dp} + [O_2(0)]} \quad (2\text{-}14)$$

with units [L/T]. The superscript * is used to denote this formulation from the final expression for w_{12} that is developed below. The parameter values are:

D_p = Diffusion coefficient for particle (m^2/d),
θ_{Dp} = Temperature coefficient for D_p
$G_{POC,R}$ = Reference concentration for $G_{POC,1}$ (mg/m^3),
$K_{M,Dp}$ = Particle mixing half saturation constant for oxygen (mg/L).

2.3.3 Benthic Stress

In addition to the reduction in particle mixing velocity due to the instantaneous oxygen concentration, it has been found necessary to include a more lasting effect. In particular, if anoxia occurs the benthic fauna population is reduced or eliminated. This is modeled using a first order differential

equation that accumulates stress, S, when overlying water dissolved oxygen is below the particle mixing half saturation constant for oxygen, $K_{M,Dp}$. Thus:

$$\frac{dS}{dt} = - k_s S + \frac{K_{M,Dp}}{K_{M,Dp} + [O_2(O)]} \quad (2\text{-}15)$$

where:

S = Accumulated benthic stress [T],

k_s = First order decay coefficient for accumulated stress [T^{-1}].

The behavior of this formulation can be understood by evaluating the limiting steady state stresses at the two oxygen extremes:

$$[O_2(0)] \to 0 \quad k_s S \to 1 \quad (1 - k_s S) \to 0$$

$$[O_2(0)] \to \infty \quad k_s S \to 0 \quad (1 - k_s S) \to 1$$

Note that as $[O_2(0)]$ approaches zero at the onset of anoxia, the term (1 - k_sS) is the proper variable to quantify the degree of benthic stress. The expression is unitless and requires no additional parameter - for example a half saturation constant for benthic stress. The final formulation for the particle mixing velocity which includes the benthic stress is:

$$w_{12} = w^*_{12} \min \{(1 - k_s S)\} \quad (2\text{-}16)$$

where w^*_{12} is defined above. The stress is continued at its minimum value through the end of the year, in order to conform to the observation that once the benthos has been suppressed by low oxygen, it does not recover until the next year.

2.3.4 Dissolved Phase Mixing

Dissolved phase mixing between layers 1 and 2 is via passive molecular diffusion which is enhanced by the mixing activities of the benthic organisms (bio-irrigation). This is modeled by increasing the diffusion coefficient by a factor of 10 over the molecular diffusion coefficient.

$$K_{L12} = \frac{D_d \theta_{Dd}^{(T-20)}}{H_2} \quad (2\text{-}17)$$

D_d = Pore water diffusion coefficient (m^2/day),
θ_{Dd} = Temperature coefficient for D_d.

2.3.5 Solids Burial

The deposition of solids to the sediment causes an increase in the depth of the sediment relative to a fixed datum. If the sediment surface is regarded as the point of reference, then the increase in the depth of sediment is a loss of mass due to burial from the active sediment layer.

w_2 = Sedimentation velocity (m/d)

2.3.6 Active Layer Depth

The active layer depth is chosen to represent the depth of organism mixing. Particles buried below this depth can longer be recycled to the aerobic layer. They are permanently buried.

H_2 = Depth of the anaerobic layer (m)

Table 2-1. Sediment Model Coefficients

Description	Notation	Value	Units
Aerobic layer solids concentration	m_1	0.2-1.2	kg/L
Anaerobic layer solids concentration	m_2	0.2-1.2	kg/L
Particle mixing diffusion coefficient	D_p	0.00006	m^2/d
Sedimentation velocity	w_2	0.25-0.75	cm/yr
Pore water diffusion coefficient	D_d	0.0005-0.0050	m^2/d
Temperature coefficient	θ_{Dp}	1.08-1.10	
Temperature coefficient	θ_{Dd}	1.10-1.117	
Water-sediment diffusion coefficient	D_{d0}	0.001	m^2/d
Temperature coefficient	θ_{Dd0}	1.08	
Reaction velocity for nitrification-saltwater	κ_{nh4}	0.1313	m/d
Reaction velocity for nitrification-freshwater	κ	0.20	m/d
Ammonia partition coefficient	π_{nh4}	1.0	L/kg
Temperature coefficient	θ_{nh4}	1.123	
Nitrification half saturation constant for ammonia	k_{mnh4}	728.	mg N/L
Temperature coefficient	θ_{kmnh4}	1.125	
Nitrification half saturation constant for oxygen	k_{mnh4o2}	0.37	mg O_2/L
Aerobic denitrification velocity-saltwater	κ_{1no3}	1.25	m/d
Aerobic denitrification velocity-freshwater	κ_{1no3}	0.20	m/d
Anaerobic layer reaction velocity	κ_{2no3}	0.25	m/d
Temperature coefficient	θ_{no3}	1.08	
Reaction velocity for dissolved sulfide oxidation in the aerobic layer	κ_{d1}	0.2	m/d
Reaction velocity for particulate sulfide oxidation in the aerobic layer	κ_{p1}	0.4	m/d
Partition coefficient for sulfide in the aerobic layer	π_{1s}	100.	L/kg
Partition coefficient for sulfide in the anaerobic layer	π_{2s}	100.	L/kg
Temperature coefficient	θ_{dp1}	1.08	
Sulfide oxidation normalization constant for oxygen	k_{mhso2}	4.	mg O_2/L
First order reaction rate	k_{si}	0.5-0.75	/day
Silica saturation concentration	c_{sisat}	40000.	µg Si/L
Incremental partition coefficient for silica in the aerobic layer	$\Delta\pi_{1si}$	10.	
Partition coefficient for silica in the anaerobic layer	π_{2si}	100.	L/kg
Depth of sediment layer	h_{20}	0.1	m
Temperature coefficient	θ_{si}	1.10	

Table 2-1. Sediment Model Coefficients (Continued)

Description	Notation	Value	Units
Particulate biogenic silica half saturation constant for dissolution	k_{mpsi}	5.0E+07	mg Si/m^3
Overlying water oxygen concentration at which aerobic layer incremental partitioning starts to decrease	$O_{2critsi}$	2.0	mg O_2/L
Partition coefficient for phosphate in the anaerobic layer	$\pi_1 PO_{4n}$	20-1000	L/kg
Enhanced aerobic layer partition coefficient under fully oxic conditions	$\pi_1 PO_{4m}$	20-300	L/kg
Overlying water oxygen concentration at which aerobic layer incremental partitioning starts to decrease	O_{2crit}	2	mg O_2/L
Particle mixing half saturation constant for oxygen	k_{mo2Dp}	4.0	mg O_2/L
Temperature which benthic community begins to recover after an anoxic event	tempbnth	10.0	˚C
Rate at which benthic stress is dissipated	$k_{bnthstr}$	0.03	/d
Scale factor for enhancement of dissolved phase mixing due to benthic activity	k_{lbnth}	0.0	
Minimum particle mixing coefficient	D_{pmin}	3.0E-06	m2/d
Reaction velocity for methane oxidation in the aerobic layer	κ_{ch4}	0.2	m/d
Temperature coefficient	θ_{ch4}	1.08	
Reaction Rate Constant for Diagenesis -G1	$k_{GPOM,1}$	0.035	/day
Reaction Rate Constant for Diagenesis -G2	$k_{GPOM,2}$	0.0018	/day
Reaction Rate Constant for Diagenesis -G3	$k_{GPOM,3}$	0.0-1.0E-6	/day
Temperature Coefficient for Diagenesis - G1	θ_{G1}	1.10	
Temperature Coefficient for Diagenesis - G2	θ_{G2}	1.15	
Temperature Coefficient for Diagenesis - G3	θ_{G3}	1.17	

Table 2-1. Sediment Model Coefficients (Continued)

Source	Distribution of Water Water Column POM Fractions To Each Class		
	G1	G2	G3
Algal Carbon	0.6	0.2	0.2
Labile Particulate Organic Carbon	1.0	0.0	0.0
Refractory Particulate Organic Carbon	0.0	0.5	0.5
Algal Nitrogen	0.6	0.2	0.2
Labile Particulate Organic Nitrogen	1.0	0.0	0.0
Refractory Particulate Organic Nitrogen	0.0	0.6	0.4
AlgalPhosphorus	0.6	0.2	0.2
Labile Particulate Organic Phosphorus	1.0	0.0	0.0
Refractory Particulate Organic Phosphorus	0.0	0.5	0.5

GROUP P: SEDIMENT MODEL INPUT

P1. Print Options

```
                  80
Comment
FORMAT (A80)
```

Comment = Comment line (ignored by RCA)

```
          10          20          30          40
ISEDPRNT  IPRNTSED  TWARPSED    IGDSEDOPT
FORMAT ()
```

ISEDPRNT = sediment print control
- = 0, do not print sediment input
- = 1, print sediment input

IPRNTSED = print interval to save sediment computations (nominal = seconds)

TWARPSED = time-warp or units used for IPRNTSED. Normally IPRNTSED is input in units of seconds. The user may, however, use different units.
- = SECS or secs
- = MINS or mins
- = HRS or hrs
- = DAYS or days

IGDSEDOPT = global dump averaging option
- = 0, no averaging
- = 1, perform averaging

P2. Sediment Depths

```
                  80
Comment
FORMAT (A80)
```

Comment = Comment line (ignored by RCA)

```
       10                  80
HSED(1,1)   ... HSED(NX,1)
    .
    .
    .
       10                  80
HSED(1,NY)  ... HSED(NX,NY)
FORMAT (8F10.3)
```

HSED(ISED) = sediment layer depth (cm)

P3. Sediment Initial Conditions

```
                80
Comment
FORMAT (A80)
```

Comment = Comment line (ignored by RCA)

```
      10
SCALEIC
FORMAT (F10.2)
```

SCALEIC = scale factor for each sediment variable initial conditions

```
          10              20                  80
SCARAY(1,1)  SCARAY(2,1)  ...  SCARAY(NX,1)
    .
    .
    .
          10                  80
SCARAY(1,NY)  ...  SCARAY(NX,NY)
FORMAT (8E10.2)
```

SCARAY(IX,IY) = sediment initial condition for segment (IX,IY)

The comment line SCALEIC and SCARAY are repeated for each of the following variables used in the sediment nutrient flux model. The order of the initial conditions required for the sediment nutrient flux model is as follows:

CTEMP (IX,IY)	=	Initial sediment temperature (ºC)
CPOP (IX,IY, 1)	=	G_1 Particulate Organic Phosphorus, POP ,(mg/m^3)
CPON (IX,IY, 1)	=	G_1 Particulate Organic Nitrogen, PON, (mg/m^3)
CPOC (IX,IY, 1)	=	G_1 Particulate Organic Carbon, POP, (mg/m^3)
CPOP (IX,IY, 2)	=	G_2 POP (mg/m^3)
CPON (IX,IY, 2)	=	G_3 PON, (mg/m^3)
CPOC (IX,IY, 2)	=	G_2 POC, (mg/m^3)
CPOP (IX,IY, 3)	=	G_3 POP, (mg/m^3)
CPON (IX,IY, 3)	=	G_3 PON, (mg/m^3)
CPOC (IX,IY, 3)	=	G_3 POC, (mg/m^3)
PO4T2 (IX,IY)	=	Layer 2 orthophosphate, PO_4, (mg/m^3)
NH4T2 (IX,IY)	=	Layer 2 ammonia, NH_4, (mg/m^3)
NO3T2 (IX,IY)	=	Layer 3 nitrate, NO_3, (mg/m^3)
H2ST2 (IX,IY)	=	Layer 2 hydrogen sulfide (in oxygen equivalents), H_2S, (mg O_2/m^3)
SIT2 (IX,IY)	=	Layer 2 silica, (mg/m^3)
BNTHSTRS (IX,IY)	=	Benthic stress
PO4T1 (IX,IY)	=	Layer 1 orthophosphate, PO_4, (mg/m^3)
NH4T1 (IX,IY)	=	Layer 1 ammonia, NH_4, (mg/m^3)

NO3T1 (IX,IY) = Layer 1 nitrate NO_3, (mg/m^3)
SIT1 (IX,IY) = Layer 1 silica, (mg/m^3)
H2ST1 (IX,IY) = Layer 1 hydrogen sulfide (in oxygen equivalents), H_2S, ($mg O_2/m^3$)
CH4T1 (IX,IY) = Layer 1 total methane (in oxygen equivalents), CH_4, (mgO_2/m^3)
CH4T2(IX,IY) = Layer 2 Total Methane (in oxygen equivalents), CH_4, (mgO_2/m^3)
SO4T2 (IX,IY) = Layer 2 total sulfate (in oxygen equivalents), SO_4, (mgO_2/m^3)

P4. Temperature Diffusion Coefficient, G Component Fractions and Diagenesis Rates

80
Comment
FORMAT (A80)

Comment = Comment line (ignored by RCA)

10
DIFFT
FORMAT (F10.0)

DIFFT = Water column-sediment layer temperature diffusion coefficient (cm^2/sec)

80
Comment
FORMAT (A80)

Comment = Comment line (ignored by RCA)

10
SALTSW
FORMAT(F10.0)

SALTSW = salinity concentration for determining whether saltwater or freshwater nitrification and denitrification rates are applied. (If salinity is greater than SALTSW then saltwater values are applied.

80
Comment
FORMAT (A80)

Comment = Comment line (ignored by RCA)

10 20 30
FRPPH1(1) FRPPH1(2) FRPPH1(3)

80
Comment
FORMAT (A80)

Comment = Comment line (ignored by RCA)

10 20 30
FRPPH2(1) FRPPH2(2) FRPPH2(3)

80
Comment
FORMAT (A80)

Comment = Comment line (ignored by RCA)

10 20 30
FRPPH3(1) FRPPH3(2) FRPPH3(3)
FORMAT(3F10.0)

FRPPHI(I) = fractions of algal phosphorus going to G_1, G_2, G_3 sediment organic phosphorus for algal group I.

80
Comment
FORMAT (A80)

Comment = Comment line (ignored by RCA)

10 20 30
FRPOP(1) FRPOP(2) FRPOP(3)
FORMAT(3F10.0)

FRPOP(I) = fraction of non-algal/detrital POP going to G_1, G_2, G_3 sediment organic phosphorus

80
Comment
FORMAT (A80)

Comment = Comment line (ignored by RCA)

10 20 30
FRNPH1(1) FRNPH1(2) FRNPH1(3)

80
Comment
FORMAT (A80)

Comment = Comment line (ignored by RCA)

10 20 30
FRNPH2(1) FRNPH2(2) FRNPH2(3)

80
Comment
FORMAT (A80)

Comment = Comment line (ignored by RCA)

10 20 30
FRNPH3(1) FRNPH3(2) FRNPH3(3)
FORMAT(3F10.0)

FRNPHI(I) = fraction of algal nitrogen going to G_1, G_2, and G_3 sediment organic nitrogen for algal group I

80
Comment
FORMAT (A80)

Comment = Comment line (ignored by RCA)

10 20 30
FRPON(1) FRPON(2) FRPON(3)
FORMAT(3F10.0)

FRPON(I) = fraction of non-algal/detrital PON going to G_1, G_2, and G_3 sediment organic nitrogen

80
Comment
FORMAT (A80)

Comment = Comment line (ignored by RCA)

10 20 30
FRCPH1(1) FRCPH1(2) FRCPH1(3)

80
Comment
FORMAT (A80)

Comment = Comment line (ignored by RCA)

10 20 30
FRCPH2(1) FRCPH2(2) FRCPH2(3)

80
Comment
FORMAT (A80)

Comment = Comment line (ignored by RCA)

10 20 30
FRCPH3(1) FRCPH3(2) FRCPH3(3)
FORMAT(3F10.0)

FRCPHI(I) = fraction of algal carbon going to G_1, G_2, and G_3 sediment organic carbon from algal group I

80
Comment
FORMAT (A80)

Comment = Comment line (ignored by RCA)

10 20 30
FRPOC(1) FRPOC(2) FRPOC(3)
FORMAT(3F10.0)

FRPOC(I) = fraction of non-algal/detrital POC going to G_1, G_2, and G_3 sediment organic carbon

80
Comment

FORMAT (A80)

Comment = Comment line (ignored by RCA)

10	20	30	40	50	60
KPDIAG(1)	DPTHTA(1)	KPDIAG(2)	DPTHTA(2)	KPDIAG(3)	DPTHTA(3)

FORMAT(6F10.0)

KPDIAG(I) = diagenesis reaction rates for POP G_1, G_2 and G_3, respectively, (1/day)
DPTHTA(I) = temperature coefficients for POP G_1, G_2 and G_3, respectively

10	20	30	40	50	60
KNDIAG(1)	DNTHTA(1)	KNDIAG(2)	DNTHTA(2)	KNDIAG(3)	DNTHTA(3)

FORMAT(6F10.0)

KNDIAG(I) = diagenesis reaction rates for PON G_1, G_2 and G_3, respectively, (1/day)
DNTHTA(I) = temperature coefficients for PON G_1, G_2 and G_3, respectively

10	20	30	40	50	60
KCDIAG(1)	DCTHTA(1)	KCDIAG(2)	DCTHTA(2)	KCDIAG(3)	DCTHTA(3)

FORMAT(6F10.0)

KCDIAG(I) = diagenesis reaction rates for POC G_1, G_2 and G_3, respectively, (1/day)
DCTHTA(I) = temperature coefficients for POC G_1, G_2 and G_3, respectively

10	20
KSI	THTASI

FORMAT(2F10.0)

KSI = Diagenesis reaction rate for Si, (1/day)
THTASI = Temperature coefficient for Si

P5. Sedimentation and Particle Mixing Rates

80
Comment

FORMAT (A80)

Comment = Comment line (ignored by RCA)

10	20		80
VECTOR(1,1)	VECTOR(2,1)	...	VECTOR(NX,1)
.			
.			
.			
10			80
VECTOR(1,NY)		...	VECTOR(NX,NY)

FORMAT(8E10.2)

Comment and VECTOR(IX,IY) are repeated for the following variables:

VSED(IX,IY) = sedimentation velocity, (cm/yr)
VPMIX(IX,IY) = solid-phase mixing rate, (m^2/day) - D_p
VDMIX(IX,IY) = dissolved-phase mixing rate, (m^2/day) - D_d

P6. Sediment Model Constants

80
Comment

FORMAT (A80)

Comment = Comment line (ignored by RCA)

10	20	30
M1M2OPT	PIESIOPT	PIEPO4OPT

FORMAT(3F10.0)

M1M2OPT = M1,M2 input option
= 0, M1 and M2 are spatially constant
= 1, M1 and M2 are spatially variable
PIESIOPT = PIESI input option
= 0, Si partition coefficients are spatially constant
= 1, Si partition coefficients are spatially variable
PIEPO4OPT = PIEPO4 input option
= 0, PO_4 partition coefficients are spatially constant
= 1, PO_4 partition coefficients are spatially variable

If MIM20PT = 0 (spatially constant M1 and M2)

80
Comment

FORMAT (A80)

Comment = Comment line (ignored by RCA)

10	20	30	40
M1	M2	THTADp	THTADd

FORMAT(4F10.0)

M1 = aerobic layer solids concentration, (kg/l)
M2 = anaerobic layer solids concentration, (kg/l)
THTADp = temperature coefficient for D_p
THTADd = temperature coefficient for D_d

If MIM20PT = 1 (spatially variable M1 and M2)

80
Comment

FORMAT (A80)

Comment = Comment line (ignored by RCA)

10
SCALE

FORMAT (F10.0)

SCALE = scale factor

10	20		80
M1(1,1)	M1(2,1)	. . .	M1(NX,1)
.			
.			
.			
M1(1,NY)	M1(2,NY)	. . .	M1(NX,NY)

FORMAT(8F10.0)

M1(IX,IY) = aerobic layer solids concentration for sediment segment IX,IY (kg/L)

10
SCALE

FORMAT (F10.0)

SCALE = scale factor

			80
M2(1,1)	M2(2,1)	. . .	M2(NX,1)
.			
.			
.			
M2(1,NY)	M2(2,NY)	. . .	M2(NX,NY)

FORMAT(8F10.0)

M2(IX,IY) = an aerobic layer solids concentration for sediment segment IX,IY (kg/L)

80
Comment

FORMAT (A80)

Comment = Comment line (ignored by RCA)

10	20
THTADp	THTADd

FORMAT (2F10.0)

THTADp = temperature coefficient for D_p
THTADd = temperature coefficient for D_d

80
Comment

FORMAT (A80)

Comment = Comment line (ignored by RCA)

10	20
Dd0	THTADd0

FORMAT(2F10.0)

Dd0 = minimum pore water diffusion coefficient (m^2/day)
THTADd0 = temperature coefficient for Dd0

80
Comment

FORMAT (A80)

Comment = Comment line (ignored by RCA)

10	20	30	40	50	60
KAPPNH4S	PIENH4	THTANH4S	KMNH4	THTAKMNH4	KMNH4O2

FORMAT(6F10.0)

KAPPNH4S = nitrification velocity in saltwater, (m/d)
PIENH4 = partition coefficient for nitrogen, (L/kg)
THTANH4S = nitrification temperature coefficient in saltwater
KMN4 = ammonia half saturation constant, (mg N/L)
THTAKMN4 = temperature coefficient
KMNH402 = oxygen half saturation constant, (mg O_2/L)

```
                  80
Comment
FORMAT (A80)
```

Comment = Comment line (ignored by RCA)

```
          10              20
KAPPNH4F    THTANH4F
FORMAT(2F10.0)
```

KAPPNH4F = nitrification velocity in freshwater, (m/d)
THTANH4F = nitrification temperature coefficient in freshwater

```
                  80
Comment
FORMAT (A80)
```

Comment = Comment line (ignored by RCA)

```
          10          20          30
KAPP1NO3S   K2NO3S   THTANO3S
FORMAT(3F10.0)
```

KAPP1NO3S = aerobic denitrification velocity in seawater, (m/d)
K2NO3S = anaerobic layer denitrification rate for seawater, (1/d)
THTANO3S = diagenesis temperature coefficient in seawater

```
                  80
Comment
FORMAT (A80)
```

Comment = Comment line (ignored by RCA)

```
          10          20          30
KAPP1NO3F   K2NO3F   THTANO3F
FORMAT(3F10.0)
```

KAPP1NO3F = aerobic denitrification velocity in freshwater, (m/d)
K2NO3F = anaerobic layer denitrification rate for freshwater, (1/d)
THTANO3F = diagenesis temperature coefficient in freshwater

```
                  80
Comment
FORMAT (A80)
```

Comment = Comment line (ignored by RCA)

10	20	30	40	50	60
KAPPD1	KAPPP1	PIE1S	PIE2S	THTAPD1	KMHSO2

FORMAT(6F10.0)

KAPPD1 = reaction velocity for dissolved sulfide oxidation in the aerobic layer, (m/day)
KAPPP1 = reaction velocity for particulate sulfide oxidation in the aerobic layer, (m/day)
PIE1S = partition coefficient for sulfide in the aerobic layer, (L/kg)
PIE2S = partition coefficient for sulfide in the aerobic layer, (L/kg)
THTAPD1 = temperature coefficient for sulfide oxidation

KMHSO2 = sulfide oxidation normalization constant for oxygen, (mgO_2/L)

If PIESIOPT =0 (PIE1SI and PIE2SI are spatially constant)

80
Comment

FORMAT (A80)

Comment = Comment line (ignored by RCA)

10	20	30	40	50	60	70	80
CSISAT	PIE1SI	PIE2SI	KSI	THTASI	KMPSI	OCRITSI	JSIDETR

FORMAT(8F10.0)

CSISAT = silica saturation concentration, (mg Si/L)
PIEISI = partition coefficient for silica in aerobic layers, (L/kg)
PIE2SI = partition coefficient for silica in anaerobic layer, (L/kg)
KSI = first order reaction rate, (1/day)
THTASI = temperature coefficient
KMPSI = half saturation constant, (mg Si/g)
O2CRITSI = overlying water oxygen concentration at which aerobic layer incremental, partitioning starts to decrease (mg O_2/L)
JSIDETR = flux of detrital silica, (mg Si/m^2 - d)

If PIESIOPT =1 (PIE1SI and PIE2SI are spatially variable)

80
Comment

FORMAT (A80)

Comment = Comment line (ignored by RCA)

10
SCALE
FORMAT (F10.0)

SCALE = scale factor

10 20 80
PIE1SI(1,1) PIE1SI(2,1) . . . PIE1SI(NX,1)
.
.
.
10 80
PIE1SI(1,NY) . . . PIE1SI(NX,NY)

80
Comment
FORMAT (A80)

Comment = Comment line (ignored by RCA)

10
SCALE
FORMAT (F10.0)

SCALE = scale factor

10 20 80
PIE2SI(1,1) PIE2SI(2,1) . . . PIE2SI(NX,1)
.
.
.
10 80
PIE2SI(1,NY) . . . PIE2SI(NX,NY)

PIE1SI(IX,IY) = aerobic layer Si partition coefficient (L/kg)
PIE2SI(IX,IY) = anaerobic layer Si partition coefficient (L/kg)

80
Comment
FORMAT (A80)

Comment = Comment line (ignored by RCA)

10	20	30	40	50	60
CSISAT	KSI	THTASI	KMPSI	O2CRITSI	JSIDETR

CSISAT = silica saturation concentration, (mg Si/L)
KSI = first order reaction rate, (1/day)
THTASI = temperature coefficient
KMPSI = half saturation constant, (mg Si/g)
O2CRITSI = overlying water oxygen concentration at which aerobic layer incremental, partitioning starts to decrease (mg O_2/L)
JSIDETR = flux of detrital silica, (mg Si/m^2 - d)

If PIEPO4OPT =0 (PIE1PO4M and PIE1PO4N are spatially constant)

80
Comment

FORMAT (A80)

Comment = Comment line (ignored by RCA)

10	20	30	40
PIE1PO4M	PIE1PO4N	O2CRIT	KMO2DP

FORMAT(4F10.0)

PIE1PO4M = incremental partition coefficient for phosphate in aerobic layer, (L/kg)
PIE1PO4N = partition coefficient for phosphate in the anaerobic layer, (L/kg)
O2CRIT = overlying water oxygen concentration at which aerobic layer incremental partitioning starts to decrease, (mg O_2/L)
KMO2DP = half saturation constant, (mg Si/g)

If PIEPO4OPT = 1 (PIE1PO4 and PIE2PO4 are spatially variable)

80
Comment

FORMAT (A80)

Comment = Comment line (ignored by RCA)

10
SCALE

FORMAT (F10.0)

SCALE = scale factor

10	20	80
PIE1PO4(1,1)	PIE1PO4(2,1) . . .	PIE1PO4(NX,1)
.		
.		
.		
10		80
PIE1PO4(1,NY)	. . .	PIE1PO4(NX,NY)

80
Comment

FORMAT (A80)

Comment = Comment line (ignored by RCA)

10
SCALE

FORMAT (F10.0)

SCALE = scale factor

10	20	80
PIE2PO4(1,1)	PIE2PO4(2,1) . . .	PIE2PO4(NX,1)
.		
.		
.		
10		80
PIE2PO4(1,NY)	. . .	PIE2PO4(NX,NY)

PIE1PO4(IX,IY) = aerobic layer PO4 partition coefficient (L/kg)
PIE2PO4(IX,IY) = anaerobic layer PO4 partition coefficient (L/kg)

80
Comment

FORMAT (A80)

Comment = Comment line (ignored by RCA)

10	20
02CRIT	KMO2DP

O2CRIT = overlying water oxygen concentration at which aerobic layer incremental partitioning starts to decrease (mg O_2/L)
KMO2Dp = half saturation constant for particle mixing (mgO_2/L)

80
Comment

FORMAT (A80)

Comment = Comment line (ignored by RCA)

10	20	30	40
TEMPBNTH	KBNTHSTR	KLBNTH	DPMIN

FORMAT(4F10.0)

TEMPBNTH = benthic temperature switch (°C)
KBNTHSTR = benthic stress decay rate constant (1/day)
KLBNTH = benthic stress enhancement constant
DPMIN = minimum value for physical benthic mixing, (m^2/day)

80
Comment

FORMAT (A80)

Comment = Comment line (ignored by RCA)

10	20	30	40	50
KAPPCH4	THTACH4	KMCH402	KMSO4	SO4OMG

FORMAT(5F10.0)

KAPPCH4 = reaction velocity for methane production (??/day)
THTACH4 = temperature coefficient for methane production
KMCH4O2 = half saturation coefficient for methane production (mg O2/L)
KMS04 = half saturation coefficient for sulfate (mg/L)
SO4OMG = overlying water sulfate concentration (mg s/L)

Table 2-2 presents a sample input deck for the sediment model coefficient set.

TABLE 2-2. SAMPLE INPUT DECK FOR THE SEDIMENT MODEL COEFFICIENT SET

```
C ISEDPRNT  IPRNTSED  TWARPSED IGDSEDOPT
          0    864000      SECS         1
C  Sediment depths (cm)
       0.       0.00       0.0       0.0
       0.      10.00      10.0       0.0
       0.      10.00      10.0       0.0
       0.       0.00       0.0       0.0
C  scale factor / temperature initial conditions (Deg C)
 0.100E+01
       0.0       0.0       0.0       0.0
       0.0       3.2       3.2       0.0
       0.0       3.2       3.2       0.0
       0.0       0.0       0.0       0.0
C  scale factor / G1 POP initial conditions (mg P/m**3)
 0.100E+01
       0.0       0.0       0.0       0.0
       0.0     1320.     1320.       0.0
       0.0     1320.     1320.       0.0
       0.0       0.0       0.0       0.0
C  scale factor / G1 PON initial conditions (mg N/m**3)
 0.100E+01
       0.0       0.0       0.0       0.0
       0.0    12400.    12400.       0.0
       0.0    12400.    12400.       0.0
       0.0       0.0       0.0       0.0
C  scale factor / G1 POC initial conditions (mg C/m**3)
 0.100E+01
       0.0       0.0       0.0       0.0
       0.0    61400.    61400.       0.0
       0.0    61400.    61400.       0.0
       0.0       0.0       0.0       0.0
C  scale factor / G2 POP initial conditions (mg P/m**3)
 0.100E+01
       0.0       0.0       0.0       0.0
       0.0     8680.     8680.       0.0
       0.0     8680.     8680.       0.0
       0.0       0.0       0.0       0.0
C  scale factor / G2 PON initial conditions (mg N/m**3)
 0.100E+01
       0.0       0.0       0.0       0.0
       0.0    92700.    92700.       0.0
       0.0    92700.    92700.       0.0
       0.0       0.0       0.0       0.0
C  scale factor / G2 POC initial conditions (mg C/m**3)
 0.100E+01
       0.0       0.0       0.0       0.0
       0.0   410000.   410000.       0.0
       0.0   410000.   410000.       0.0
       0.0       0.0       0.0       0.0
C  scale factor / G3 POP initial conditions (mg P/m**3)
 0.100E+01
       0.0       0.0       0.0       0.0
       0.0    58100.    58100.       0.0
       0.0    58100.    58100.       0.0
       0.0       0.0       0.0       0.0
C  scale factor / G3 PON initial conditions (mg N/m**3)
 0.100E+01
       0.0       0.0       0.0       0.0
       0.0   480000.   480000.       0.0
       0.0   480000.   480000.       0.0
       0.0       0.0       0.0       0.0
C  scale factor / G3 POC initial conditions (mg C/m**3)
 0.100E+01
       0.0       0.0       0.0       0.0
       0.0  4210000.  4210000.       0.0
       0.0  4210000.  4210000.       0.0
       0.0       0.0       0.0       0.0
C  scale factor / Biogenic Si initial conditions (mg Si/m**3)
 0.100E+01
       0.0       0.0       0.0       0.0
       0.0  5470000.  5470000.       0.0
       0.0  5470000.  5470000.       0.0
       0.0       0.0       0.0       0.0
C  scale factor / Layer 2 Total Inorganic PO4 (mg P/m**3)
 0.100E+01
       0.0       0.0       0.0       0.0
       0.0    11500.    11500.       0.0
       0.0    11500.    11500.       0.0
       0.0       0.0       0.0       0.0
C  scale factor / Layer 2 Total NH4 (mg N/m**3)
 0.100E+01
       0.0       0.0       0.0       0.0
       0.0     8770.     8770.       0.0
```

TABLE 2-2. SAMPLE INPUT DECK FOR THE SEDIMENT MODEL COEFFICIENT SET (Cont.).

```
      0.0     8770.     8770.       0.0
       0.0       0.0       0.0       0.0
C  scale factor / Layer 2 Nitrate (mg N/m**3)
 0.100E+01
       0.0       0.0       0.0       0.0
       0.0      250.      250.       0.0


       0.0      250.      250.       0.0
       0.0       0.0       0.0       0.0
C  scale factor / Layer 2 Total Sulfide (as O2 equivalents) (mg O2/m**3)
 0.100E+01
       0.0       0.0       0.0       0.0
       0.0     1180.     1180.       0.0
       0.0     1180.     1180.       0.0
       0.0       0.0       0.0       0.0
C  scale factor / Layer 2 Total Inorganic Si (mg Si/m**3)
 0.100E+01
       0.0       0.0       0.0       0.0
       0.0    22700.    22700.       0.0
       0.0    22700.    22700.       0.0
       0.0       0.0       0.0       0.0
C  scale factor / Benthic Stress initial conditions
 0.100E+01
       0.       0.00       0.0       0.0
       0.      11.00      11.0       0.0
       0.      11.00      11.0       0.0
       0.       0.00       0.0       0.0
C  scale factor / Layer 1 Total Inorganic PO4 (mg P/m**3)
 0.100E+01
       0.0       0.0       0.0       0.0
       0.0    16000.    16000.       0.0
       0.0    16000.    16000.       0.0
       0.0       0.0       0.0       0.0
C  scale factor / Layer 1 Total Inorganic NH4 (mg N/m**3)
 0.100E+01
       0.        0.0       0.0       0.0
       0.       35.0       35.       0.0
       0.       35.0       35.       0.0
       0.        0.0       0.0       0.0
C  scale factor / Layer 1 NO3 (mg N/m**3)
 0.100E+01
       0.        0.0       0.0       0.0
       0.       343.      343.       0.0
       0.       343.      343.       0.0
       0.        0.0       0.0       0.0
C  scale factor / Layer 1 Total Inorganic Si (mg Si/m**3)
 0.100E+01
       0.        0.0       0.0       0.0
       0.      8000.     8000.       0.0
       0.      8000.     8000.       0.0
       0.        0.0       0.0       0.0
C  scale factor / Layer 1 Sulfide (in oxygen equivalents) (mg O2/m**3)
 0.100E+01
       0.        0.0       0.0       0.0
       0.       0.02      0.02       0.0
       0.       0.02      0.02       0.0
       0.        0.0       0.0       0.0
C  scale factor / Layer 1 Methane (in oxygen equivalents) (mg O2/m**3)
 0.100E+01
       0.        0.0       0.0       0.0
       0.       0.02      0.02       0.0
       0.       0.02      0.02       0.0
       0.        0.0       0.0       0.0
C  scale factor / Layer 2 Methane (in oxygen equivalents) (mg O2/m**3)
 0.100E+01
       0.        0.0       0.0       0.0
       0.        5.0       5.0       0.0
       0.        5.0       5.0       0.0
       0.        0.0       0.0       0.0
C  scale factor / Layer 2 Sulfate (in oxygen equivalents) (mg O2/m**3)
 0.100E+01
       0.        0.0       0.0       0.0
       0.        0.9       0.9       0.0
       0.        0.9       0.9       0.0
       0.        0.0       0.0       0.0
C    Difft
   0.00180
C   SALTSW
      0.00                            SALTSW
C FRPPH1-G1 FRPPH1-G2 FRPPH1-G3    fractions to G1, G2, G3 P for Algal Group 1
     0.650     0.200     0.150     FRPPH1 (G1,G2,G3)
C FRPPH2-G1 FRPPH2-G2 FRPPH2-G3    fractions to G1, G2, G3 P for Algal Group 2
```

TABLE 2-2. SAMPLE INPUT DECK FOR THE SEDIMENT MODEL COEFFICIENT SET (Cont.).

```
     0.650     0.200     0.150     FRPPH2 (G1,G2,G3)
C FRPPH3-G1 FRPPH3-G2 FRPPH3-G3    fractions to G1, G2, G3 P for Algal Group 3
     0.650     0.200     0.150     FRPPH2 (G1,G2,G3)
C FRPOP-G1  FRPOP-G2  FRPOP-G3    fractions to G1, G2, G3 P for detrital POP
     0.650     0.200     0.150     FRPOP (G1,G2,G3)
C FRNPH1-G1 FRNPH1-G2 FRNPH1-G3    fractions to G1, G2, G3 N for Algal Group 1
     0.650     0.250     0.100     FRNPH1 (G1,G2,G3)
C FRNPH2-G1 FRNPH2-G2 FRNPH2-G3    fractions to G1, G2, G3 N for Algal Group 2
     0.650     0.250     0.100     FRNPH2 (G1,G2,G3)
C FRNPH3-G1 FRNPH3-G2 FRNPH3-G3    fractions to G1, G2, G3 N for Algal Group 3
     0.650     0.250     0.100     FRNPH2 (G1,G2,G3)
C FRPON-G1  FRPON-G2  FRPON-G3    fractions to G1, G2, G3 N for detrital PON
     0.650     0.250     0.100     FRPON (G1,G2,G3)
C FRCPH1-G1 FRCPH1-G2 FRCPH1-G3    fractions to G1, G2, G3 C for Algal Group 1
     0.650     0.200     0.150     FRCPH1 (G1,G2,G3)
C FRCPH2-G1 FRCPH2-G2 FRCPH2-G3    fractions to G1, G2, G3 C for Algal Group 2
     0.650     0.200     0.150     FRCPH2 (G1,G2,G3)
C FRCPH3-G1 FRCPH3-G2 FRCPH3-G3    fractions to G1, G2, G3 C for Algal Group 3
     0.650     0.200     0.150     FRCPH2 (G1,G2,G3)
C FRPOC-G1  FRPOC-G2  FRPOC-G3    fractions to G1, G2, G3 C for detrital POC
     0.650     0.200     0.150     FRPOC (G1,G2,G3)
C KPDIAGG1   THETAG1  KPDIAGG2   THETAG2  KPDIAGG3   THETAG3    POP Diag Rates
 0.0350000     1.100 0.0018000     1.150 0.0000010     1.170
C KNDIAGG1   THETAG1  KNDIAGG2   THETAG2  KNDIAGG3   THETAG3    PON Diag Rates
 0.0350000     1.100 0.0018000     1.150 0.0000010     1.170
C KCDIAGG1   THETAG1  KCDIAGG2   THETAG2  KCDIAGG3   THETAG3    POC Diag Rates
 0.0350000     1.100 0.0018000     1.150 0.0000010     1.170
C  KSiDiag     THETA                                      Biogenic Diag Rate
     0.500     1.100
C   Sedimentation or Burial Rates  (cm/yr)
C Scale Factor
 0.100E+01
       0.       0.00       0.0       0.0
       0.      0.250      0.25       0.0
       0.      0.250      0.25       0.0
       0.       0.00       0.0       0.0
C   Particle or solid phase mixing rate (m2/day)
C Scale Factor
 0.100E+01
       0.0       0.0       0.0       0.0
       0.0 0.120E-03 0.120E-03       0.0
       0.0 0.120E-03 0.120E-03       0.0
       0.0       0.0       0.0       0.0
C   Dissolved phase mixing rate (m2/day)
C Scale Factor
 0.100E+01
       0.0       0.0       0.0       0.0
       0.0 0.100E-02 0.100E-02       0.0
       0.0 0.100E-02 0.100E-02       0.0
       0.0       0.0       0.0       0.0
C  M1M2OPT  PIESIOPT PIEPO4OPT   (0=spatially constant,1=variable)
         0         0         0
C       M1        M2   ThetaDp   ThetaDd
     0.500     0.500    1.1500    1.1500
C      Ddo  ThetaDdo
    0.0010    1.0800
C KappNH4S    PIENH4 ThetaNH4S     KMNH4 ThtaKmNH4   KMNH4O2    (saltwater values)
    0.1313    1.0000    1.0800  728.0000    1.1250    0.7400
C KappNH4F ThetaNH4F    (freshwater values)
    0.2000    1.0800
C KappNO3S    K2NO3S ThetaNO3S    (saltwater values)
    0.0500    0.1000    1.3000
C KappNO3F    K2NO3F ThetaNO3F    (freshwater values)
    0.1000    0.2500    1.0800
C   Kappd1    Kappp1     PIE1S     PIE2S  ThetaPD1    KMHSO2
    0.2000    0.4000  100.0000  100.0000    1.0800    4.0000
C   CSiSat    PIE1Si    PIE2Si       KSi   ThetaSi     KMPSi  O2CritSi   JsiDetr
40000.0000    15.000    100.00    0.5000    1.1000   5.0E+07    2.0000      060.
C  PIEPO4M  PIE1PO4N    O2Crit    KMO2Dp
      20.0      20.0      2.00      4.00
C TempBnth  KBnthStr    K1Bnth     Dpmin
   10.0000    0.0300    0.0000    0.0000
C  KappCh4  ThetaCh4   KMCH4O2     KMSO4
      0.20      1.08      0.20      0.10
```

3.0 REFERENCES

Bienfang, P.K., P.J. Harrison and L.M. Quarmby, 1982. "Sinking Rate Response to Depletion of Nitrate, Phosphate and Silicate in Four Marine Diatoms," Marine Biology, 67, 295-302.

Blumberg, A.F. and G.L. Mellor, 1987. "A Description of a Three-Dimensional Coastal Ocean Circulation Model," in: Three-Dimensional Coastal Ocean Models, N. Heaps, ed., pp. 1-16, American Geophysical Union.

Cerco, C.F., and T. Cole (1995). "Users Guide to the CE-QUAL-ICM three dimensional eutrophication model: release version 1.0," Technical Report EL-95-15, U.S. Army Engineer Waterways Experiment Station, Vicksburg, MS.

Culver, M.E. and W.O. Smith, Jr., 1989. "Effects of Environmental Variation on Sinking Rates of Marine Phytoplankton," J. Phycol. 25, 262-270.

Di Toro, D.M., D.J. O'Connor, and R.V. Thomann, 1971. "A Dynamic Model of the Pytoplankton Population in the Sacramento San Joaquin Delta," Adv. Chem. Ser. 106, American Chemical Society, Washington D.C., 131-180.

Di Toro, D.M. and W. F. Matystick, 1980. "Mathematical Models of Water Quality in Large Lakes, Part 1: Lake Huron and Saginaw Bay," EPA/600/3-80/056, 28-30.

DiToro, D. M. and J. P. Connolly, 1980. Mathematical Models of Water Quality in Large Lakes, Part 2: Lake Erie. EPA-600/3-80-065.

Hendry, G.S., 1977. "Relationships Between Bacterial Levels and Other Characteristics of Recreational Lakes in the District of Muskoka," Interim Microbiology Report, Laboratory Service Branch, Ontario Ministry of the Environment.

Henrici, A.T., "Seasonal Fluctuation of Lake Bacteria in Relation to Plankton Production," J. Bacteriol., 35, 129-139.

Hutchinson, G.E., 1967. "A Treatise on Limnology," In Introduction to Lake Biology and Limnoplankton. Vol. II, Wiley, New York, 306-354.

HydroQual, Inc., 1995. A Water Quality Model for Massachusetts and Cape Cod Bays: Calibration of the Bays Eutrophication Model (BEM). Prepared for the Massachusetts Water Resources Authority (MWRA) under subcontract to Normandeau and Associates.

HydroQual, Inc., 1996. Water Quality Modeling Analysis of Hypoxia in Long Island Sound Using LIS 3.0. Prepared for the Management Committee of the Long Island Sound Estuary Study and New England Interstate Water Pollution Control Commission.

HydroQual, Inc., 2003. Sensitivity of the Bays Eutrophication Model (BEM) to Changes in Algal Model Coefficients. Prepared for the Massachusetts Water Resources Authority (MWRA) under subcontract to Battelle.

Hyer, P.V., C.S. Fang, E.P. Ruzecki and W.J. Hargis, 1971. "Hydrography and Hydrodynamics of Virginia Estuaries, Studies of the Distribution of Salinity and Dissolved Oxygen in the Upper York System," Virginia Institute of Marine Science.

Laws, E.A and M.S. Chalup, 1990. A Microalgal Growth Model. Limnol. Oceanogr. 35:597-608.

Lund, J.W.G., 1965. "The Ecology of the Freshwater Phytoplankton," Biol. Rev., 40, 231-293.

Menon, A.S., W.A. Gloschenko and N.M. Burns, 1972. "Bacteria-Phytoplankton Relationships in Lake Erie," Proc. 15th Conf. Great Lakes Res., 94, Inter. Assoc. Great Lakes Res., 101.

Morel, F.M., 1983. Principles of Aquatic Chemistry, John Wiley and Sons, New York, New York.

Rao, S.S., 1976. "Observations on Bacteriological Conditions in the Upper Great Lakes 1968-1974," Scientific Series, No. 64, Inland Waters Directorate CCIW Branch, Burlington, Canada.

Raymont, J.E.G., 1963. Plankton and Productivity in the Oceans, Pergamon, New York, 93-466.

Rhee, G.Y., 1973. "A Continuous Culture Study of Phosphate Uptake, Growth Rate and Ploy phosphates in Secendemus sp," J. Phycol, 9, 495-506.

Riley, G.A., H. Stommel and D.F. Bumpus, 1949. "Quantitative Ecology of the Plankton of the Western North Atlantic, " Bull, Bingham Oceanogr, Coll., 12(3), 1-169.

Steele, J.H., 1962. "Environmental Control of Photosynthesis in the Sea," Limnol. Oceanogr., 7, 13;7-150.

Strickland, J.D.H., 1965. Chemical Oceanography, Production of Organic Matter in the Primary Stages of the Marine Food Chain. Vol. 1., J.P. Riley and G. Skivow, Eds., Academic Press, New York, 503pp.

Thomann, R.V., D.M. DiToro, and D.J. O'Connor, 1974. Preliminary Model of Potomac Estuary Phytoplankton. J. Envir. Engr. Div., ASCE, 100, EE3.

Thomann, R.V. and J. J. Fitzpatrick, 1982. Calibration and Verification of a Mathematical Model of the Eutrophication of the Potomac Estuary. Prepared for the Department of Environmental Services, Government of the District of Columbia. Hydroscience, Westwood, NJ.

Thomann, R.V. and J.A. Mueller, 1987. Principles of Surface Water Quality Modeling and Control, Harper & Row, Publishers, Inc.

APPENDIX B

HYDRODYNAMIC MODEL VALIDATION FIGURES

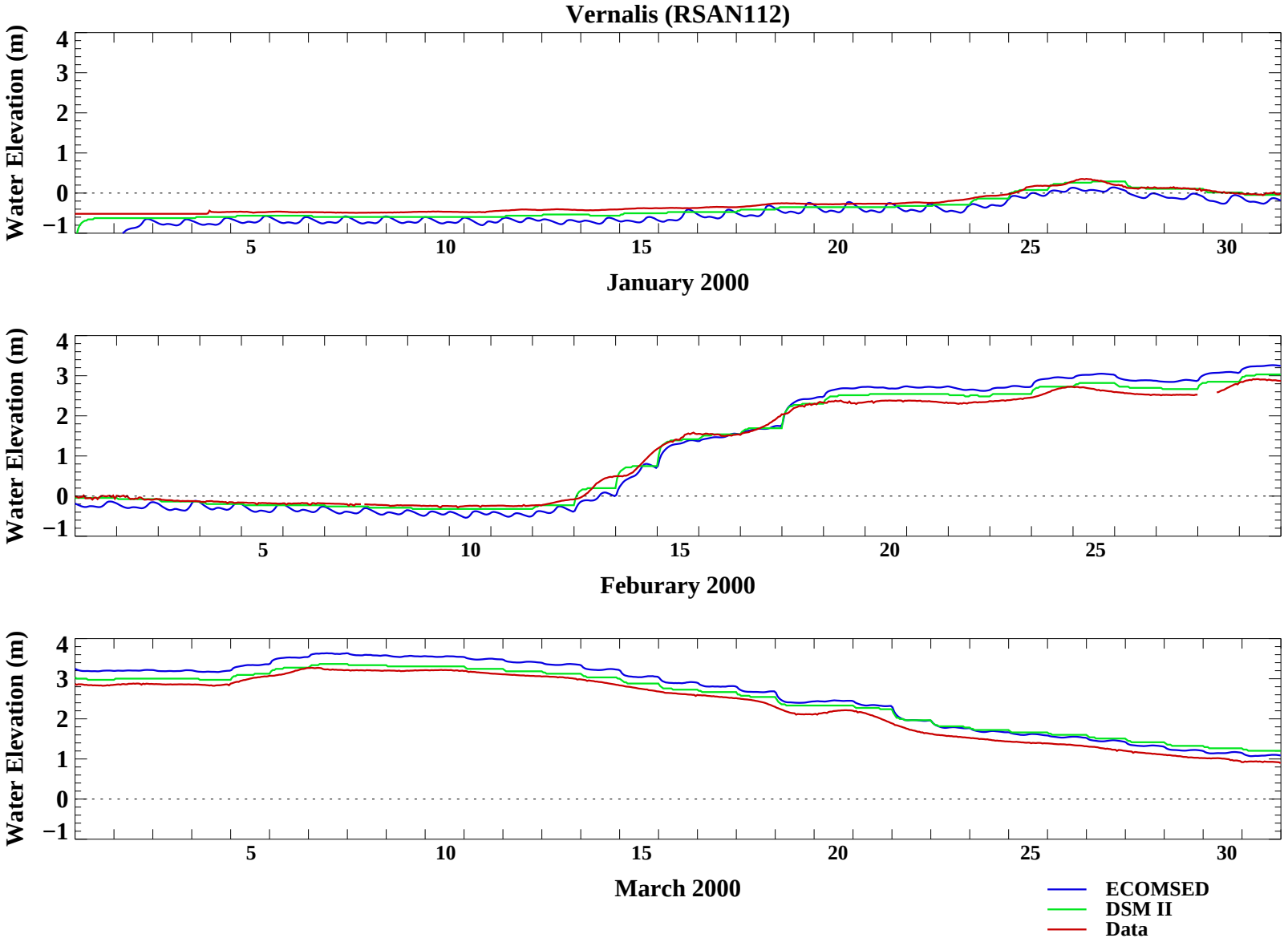
Vernalis (RSAN112)
Water Elevation (m)
4
3
2
1
0
−1
5
10
15
20
25
30
January 2000
Water Elevation (m)
Feburary 2000
Water Elevation (m)
March 2000
ECOMSED
DSM II
Data

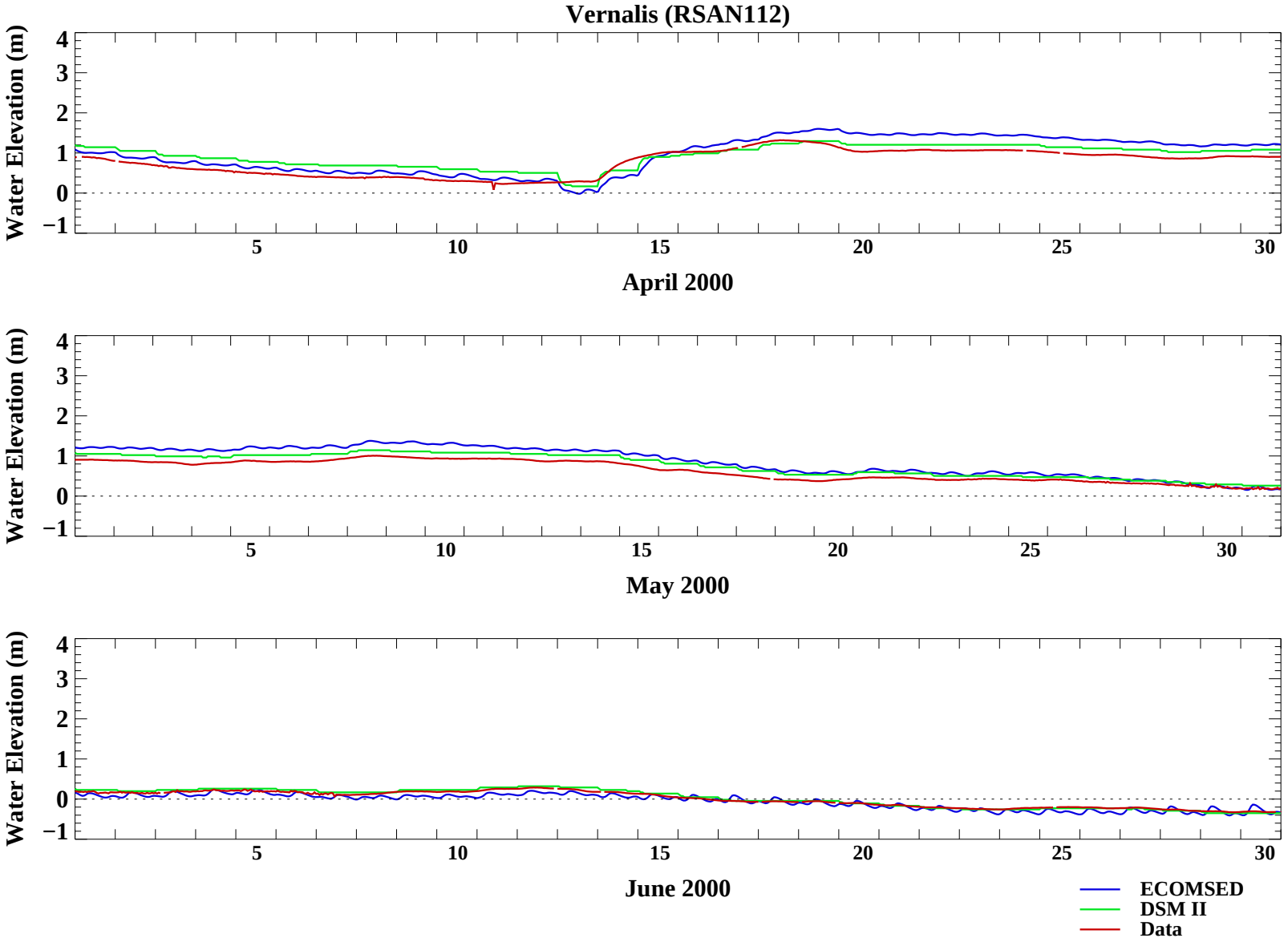
Vernalis (RSAN112)
Water Elevation (m)
4
3
2
1
0
−1
5
10
15
20
25
30
April 2000
May 2000
June 2000
ECOMSED
DSM II
Data

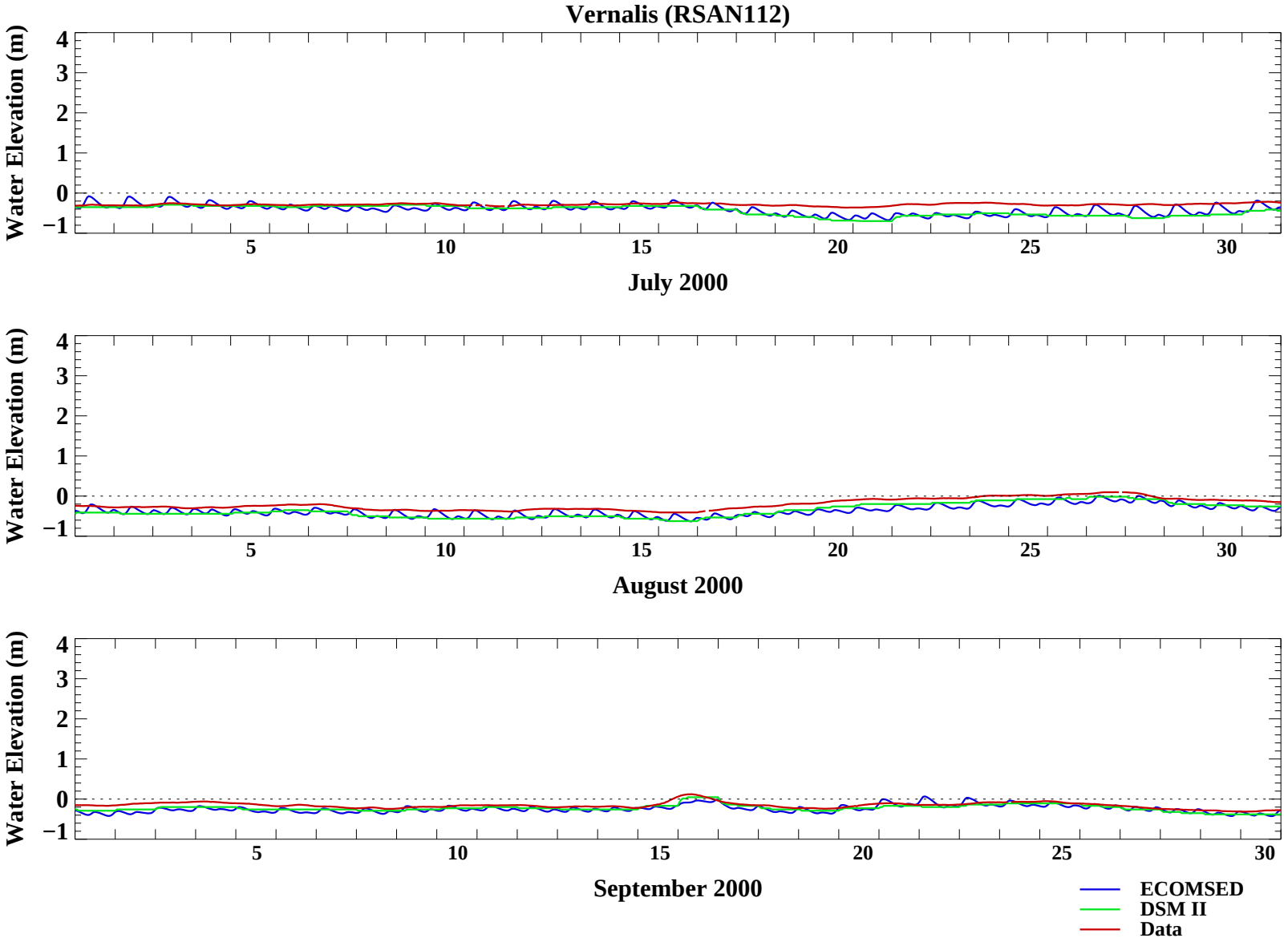
Vernalis (RSAN112)
Water Elevation (m)
4
3
2
1
0
−1
5
10
15
20
25
30
July 2000
August 2000
September 2000
ECOMSED
DSM II
Data

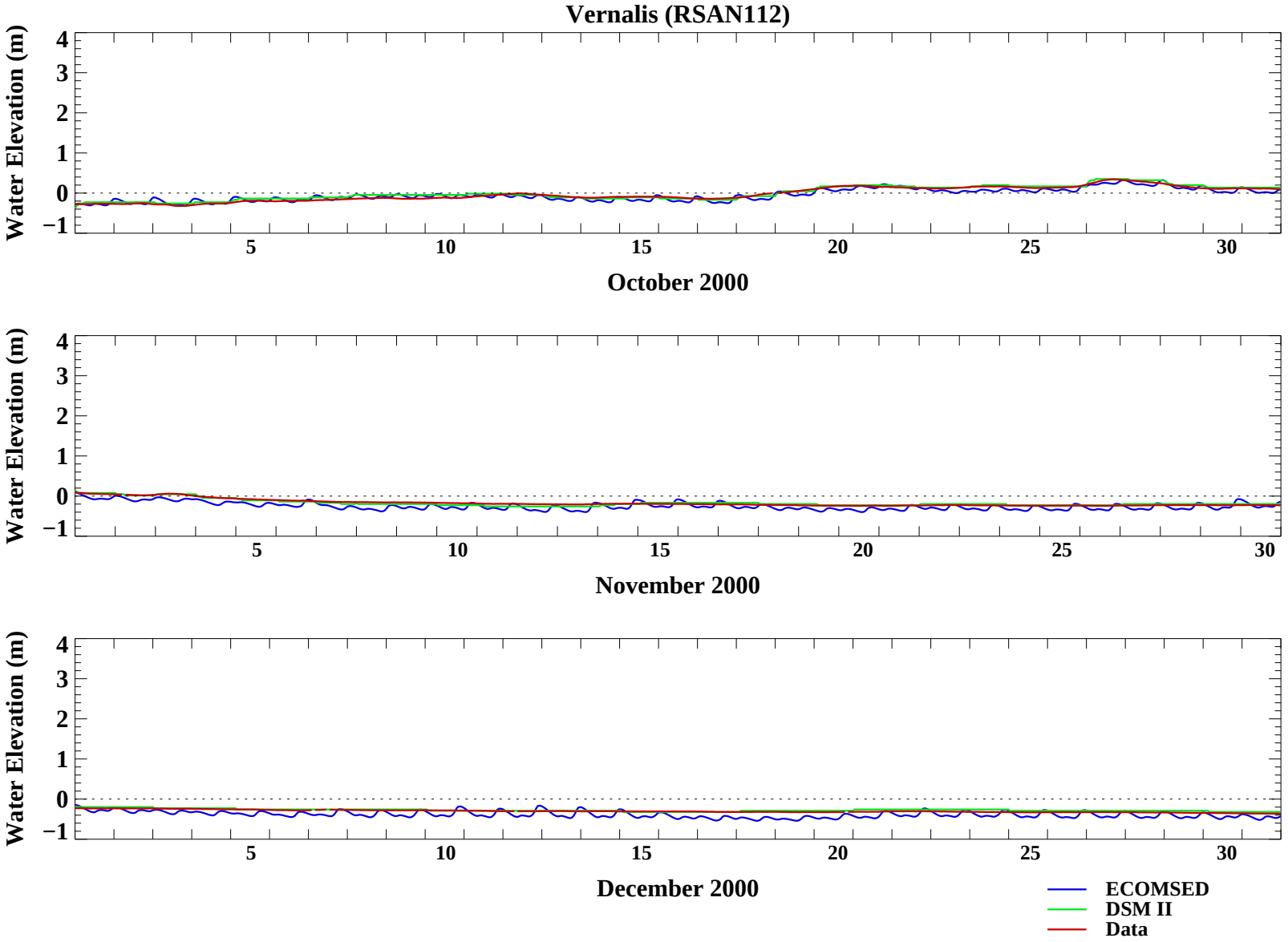
Vernalis (RSAN112)
Water Elevation (m)
4
3
2
1
0
−1
5
10
15
20
25
30
October 2000
November 2000
December 2000
ECOMSED
DSM II
Data

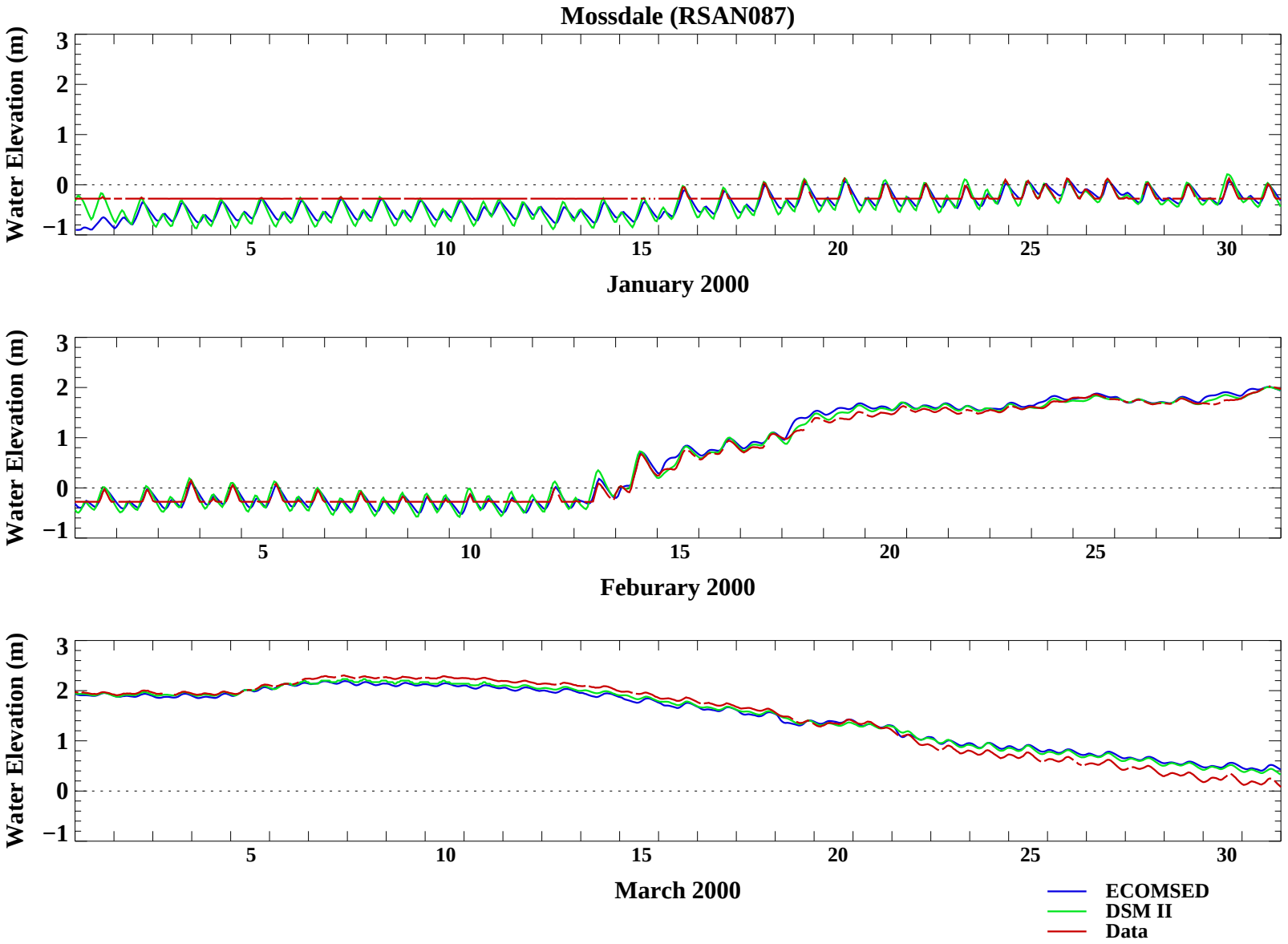
Mossdale (RSAN087)
Water Elevation (m)
3
2
1
0
−1
5
10
15
20
25
30
January 2000
Water Elevation (m)
3
2
1
0
−1
5
10
15
20
25
Feburary 2000
Water Elevation (m)
3
2
1
0
−1
5
10
15
20
25
30
March 2000
ECOMSED
DSM II
Data

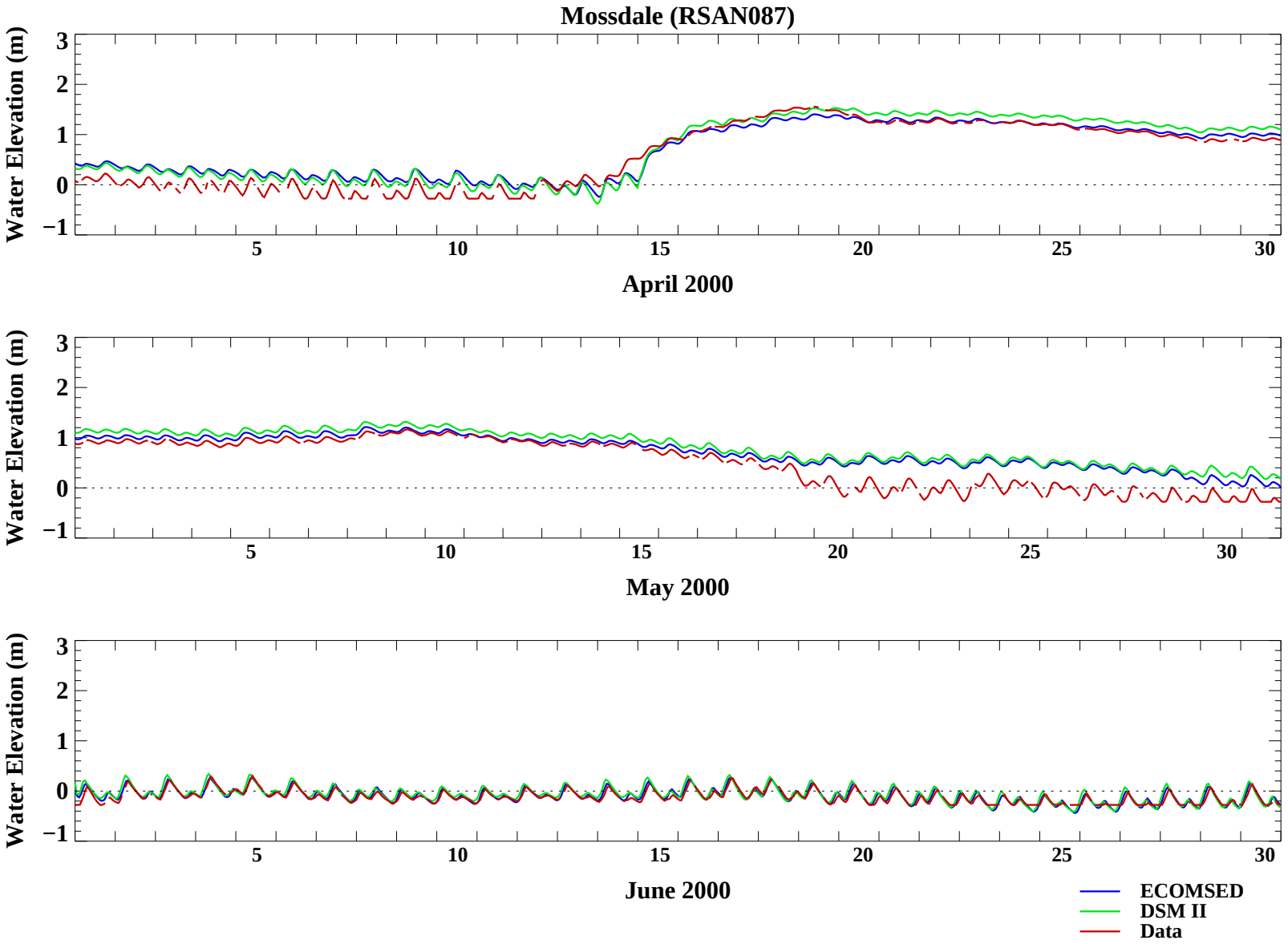
Mossdale (RSAN087)
Water Elevation (m)
3
2
1
0
−1
5
10
15
20
25
30
April 2000
Water Elevation (m)
May 2000
Water Elevation (m)
June 2000
ECOMSED
DSM II
Data

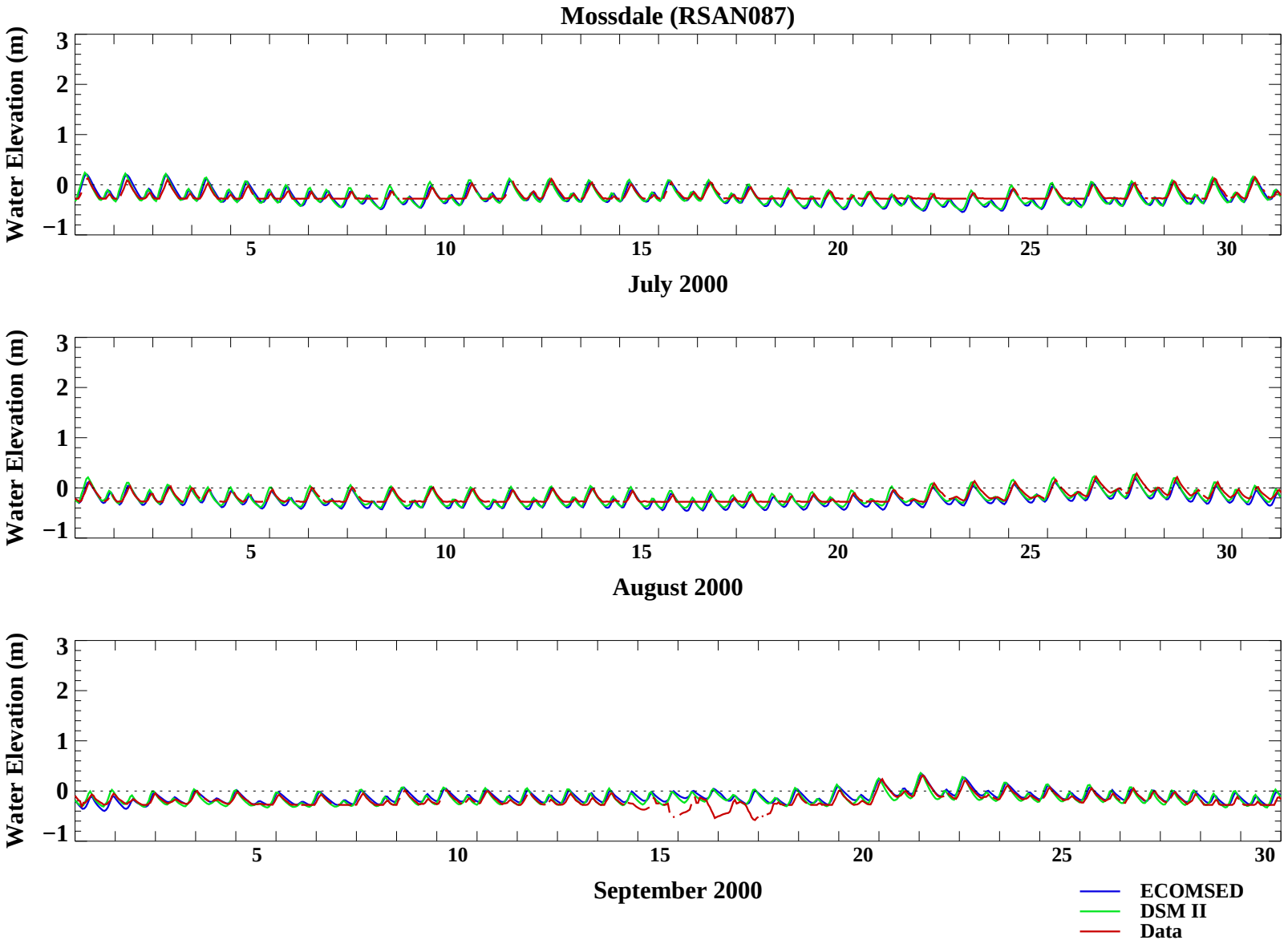
Mossdale (RSAN087)
Water Elevation (m)
3
2
1
0
−1
5
10
15
20
25
30
July 2000
Water Elevation (m)
August 2000
Water Elevation (m)
September 2000
ECOMSED
DSM II
Data

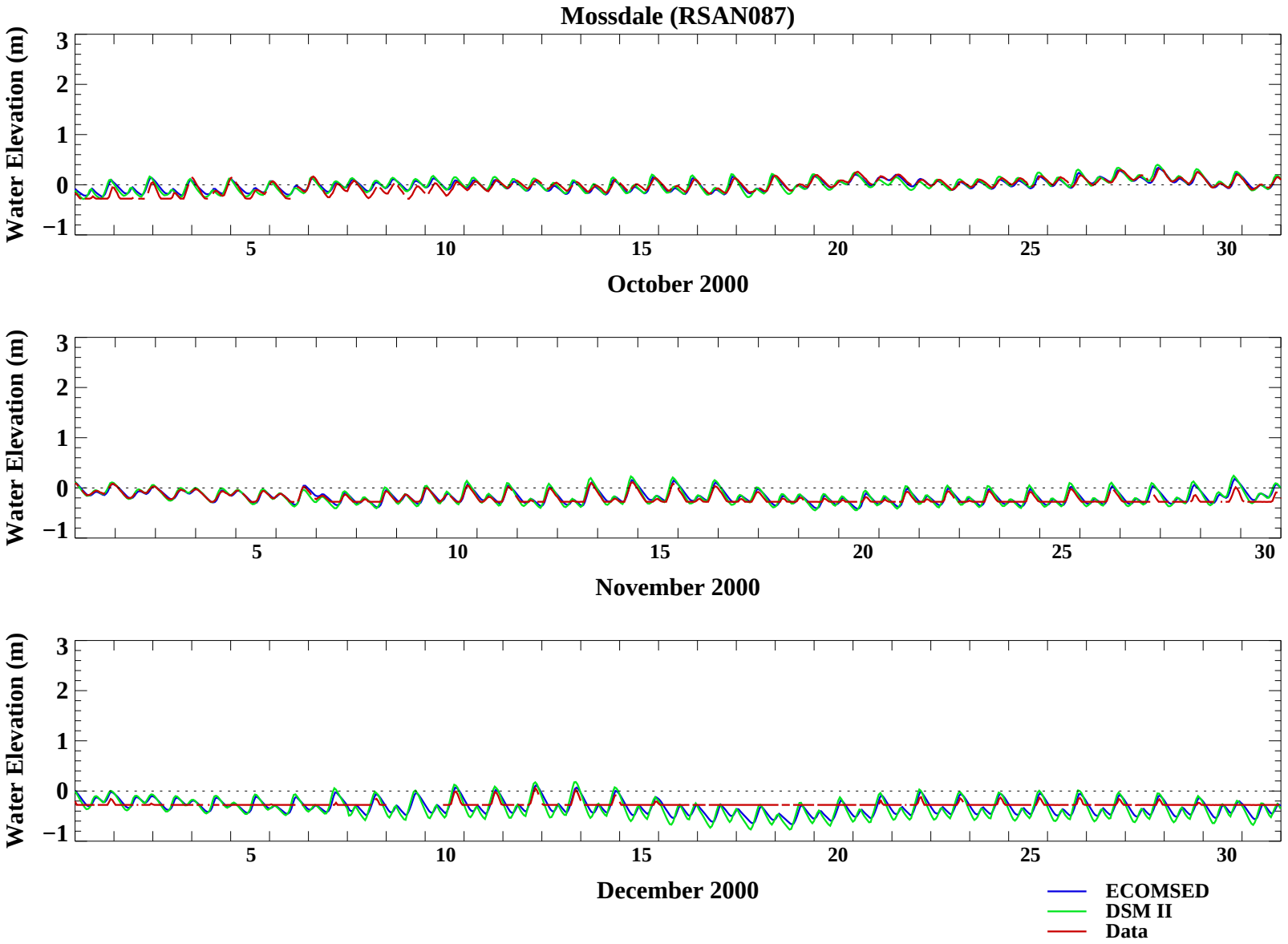
Mossdale (RSAN087)
Water Elevation (m)
3
2
1
0
−1
5
10
15
20
25
30
October 2000
November 2000
December 2000
ECOMSED
DSM II
Data

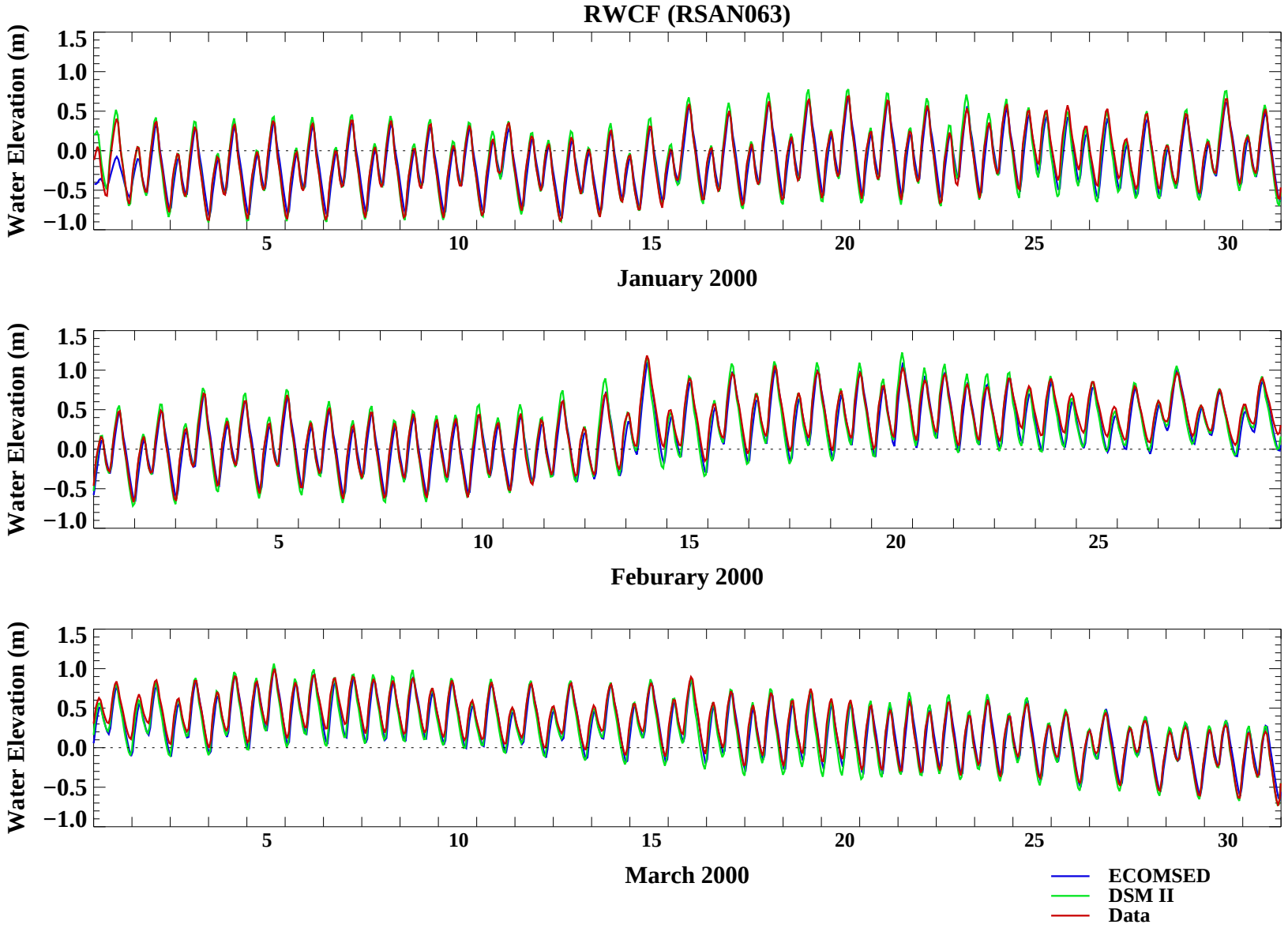
RWCF (RSAN063)
Water Elevation (m)
1.5
1.0
0.5
0.0
−0.5
−1.0
5
10
15
20
25
30
January 2000
Water Elevation (m)
Feburary 2000
Water Elevation (m)
March 2000
ECOMSED
DSM II
Data

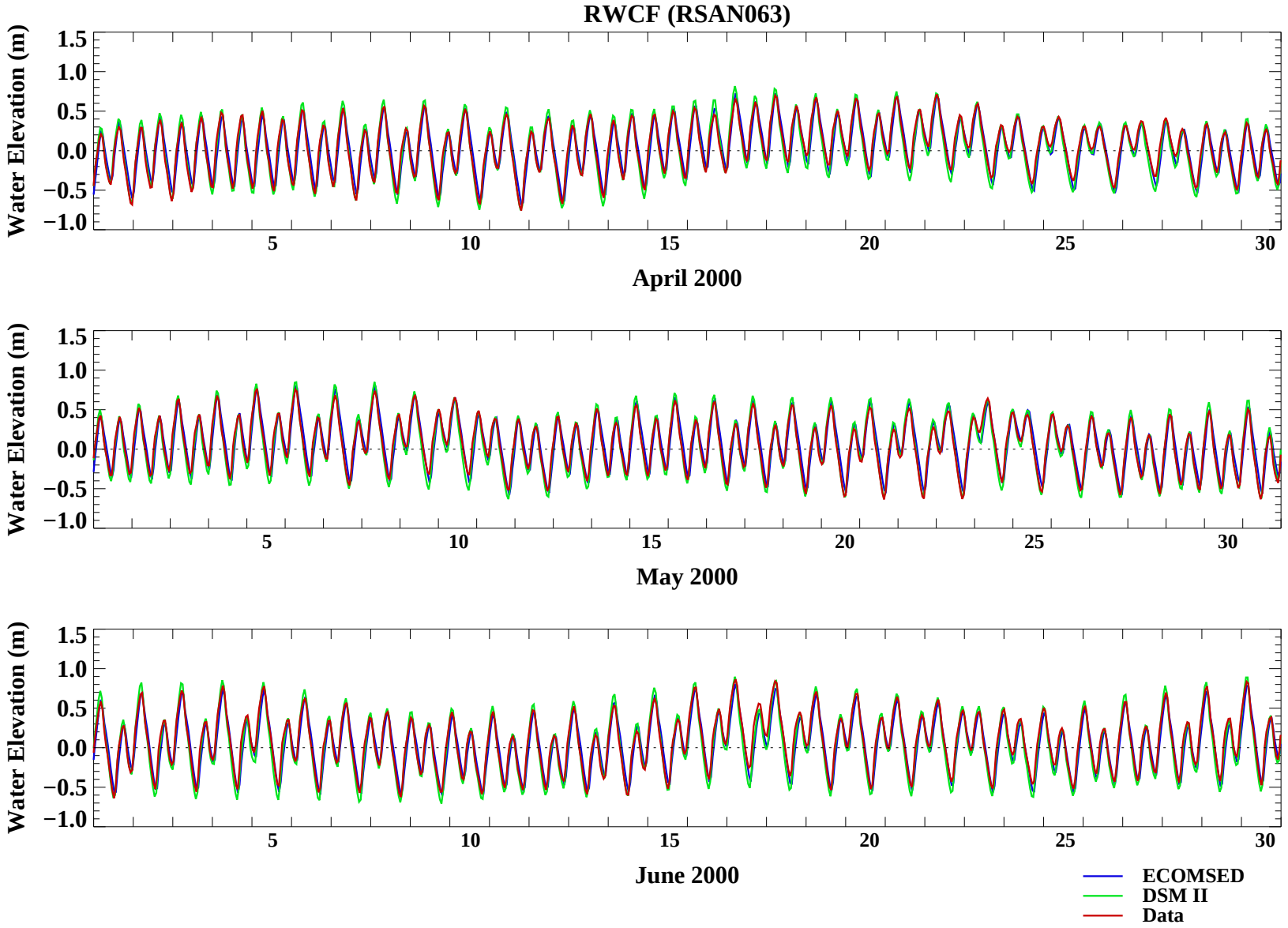
RWCF (RSAN063)
Water Elevation (m)
1.5
1.0
0.5
0.0
−0.5
−1.0
5
10
15
20
25
30
April 2000
May 2000
June 2000
ECOMSED
DSM II
Data

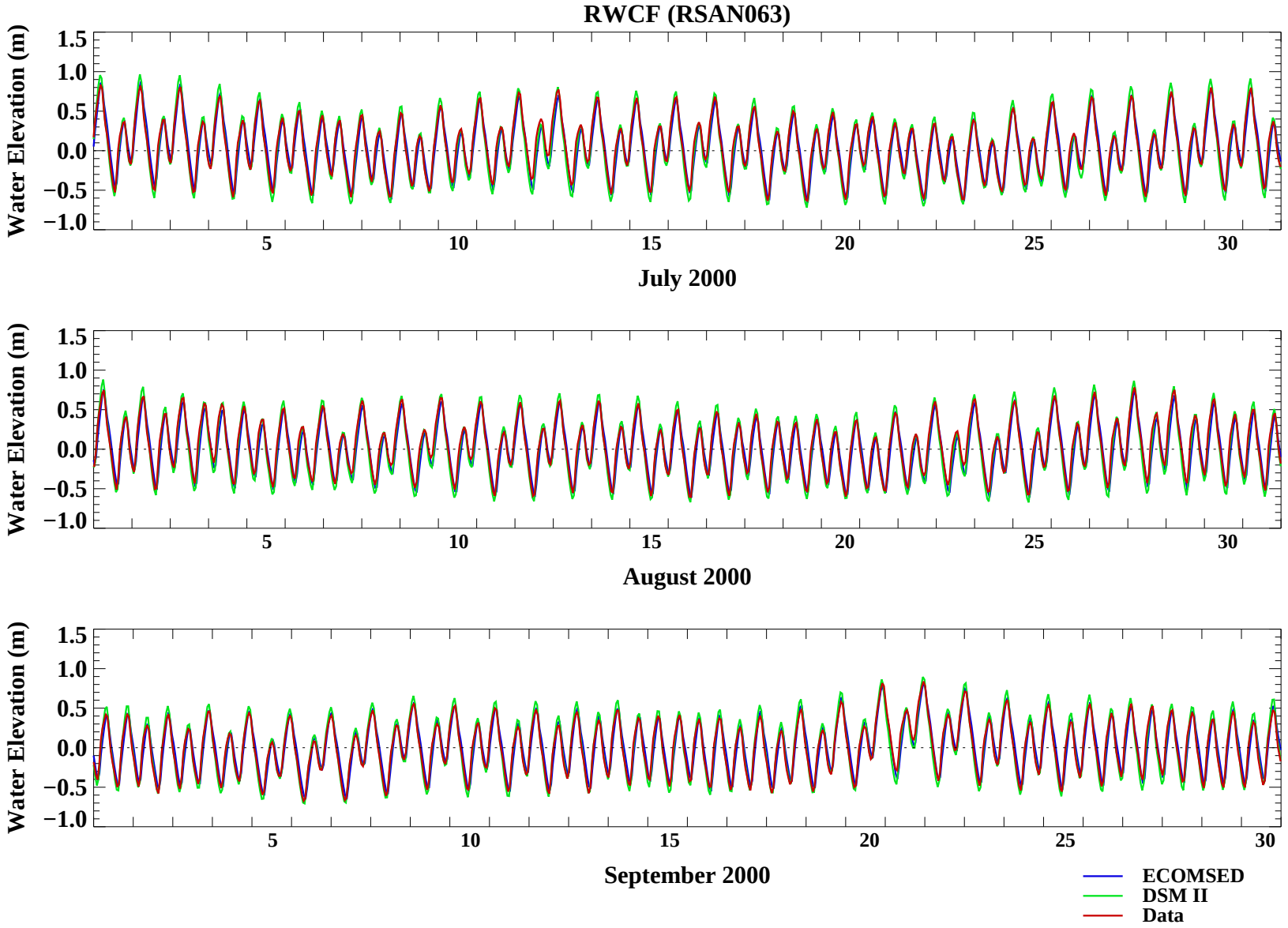
RWCF (RSAN063)
Water Elevation (m)
1.5
1.0
0.5
0.0
−0.5
−1.0
5
10
15
20
25
30
July 2000
August 2000
September 2000
ECOMSED
DSM II
Data

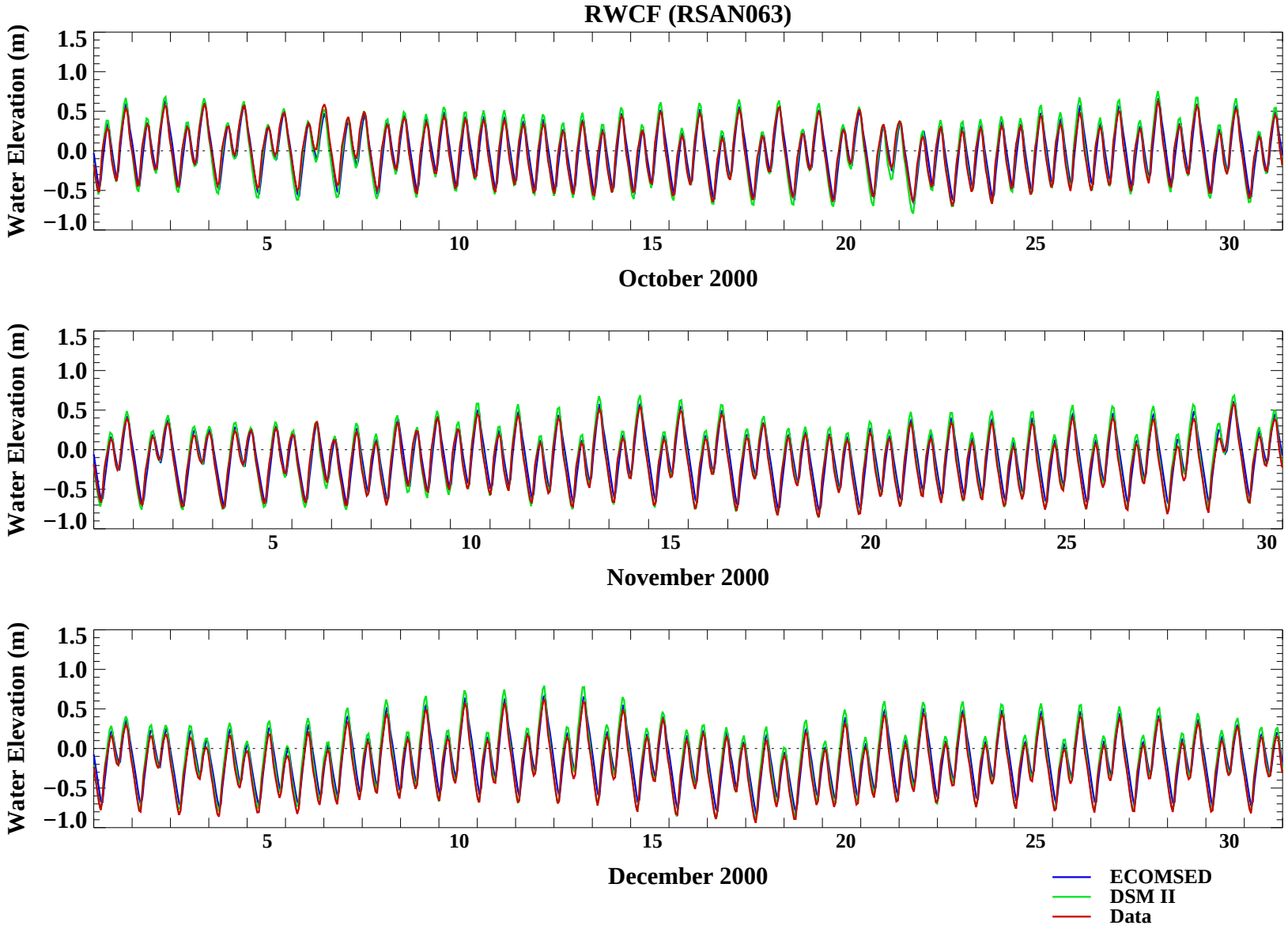
RWCF (RSAN063)
Water Elevation (m)
1.5
1.0
0.5
0.0
−0.5
−1.0
5
10
15
20
25
30
October 2000
November 2000
December 2000
ECOMSED
DSM II
Data

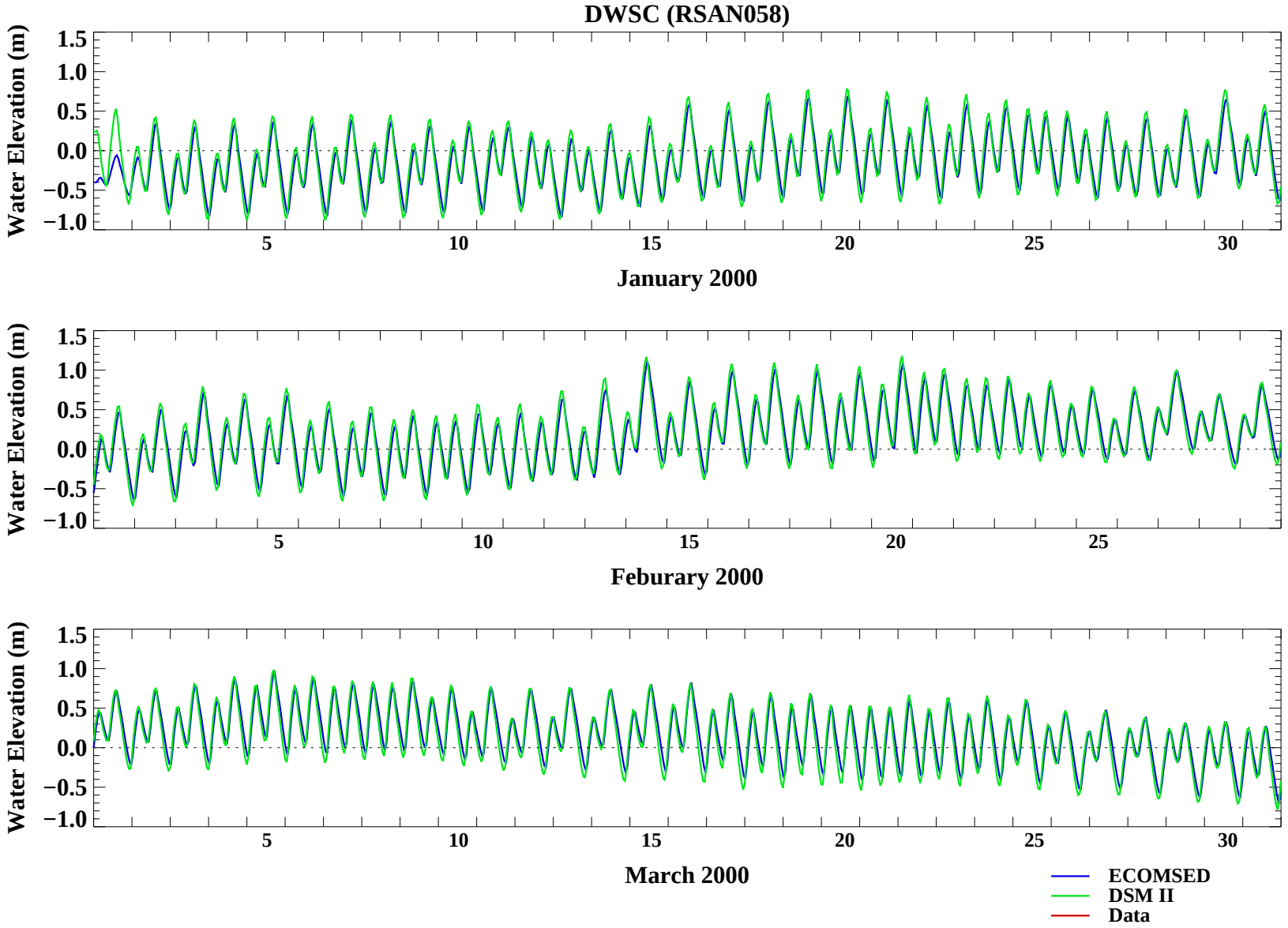
DWSC (RSAN058)
Water Elevation (m)
1.5
1.0
0.5
0.0
−0.5
−1.0
5
10
15
20
25
30
January 2000
Water Elevation (m)
1.5
1.0
0.5
0.0
−0.5
−1.0
5
10
15
20
25
Feburary 2000
Water Elevation (m)
1.5
1.0
0.5
0.0
−0.5
−1.0
5
10
15
20
25
30
March 2000
ECOMSED
DSM II
Data

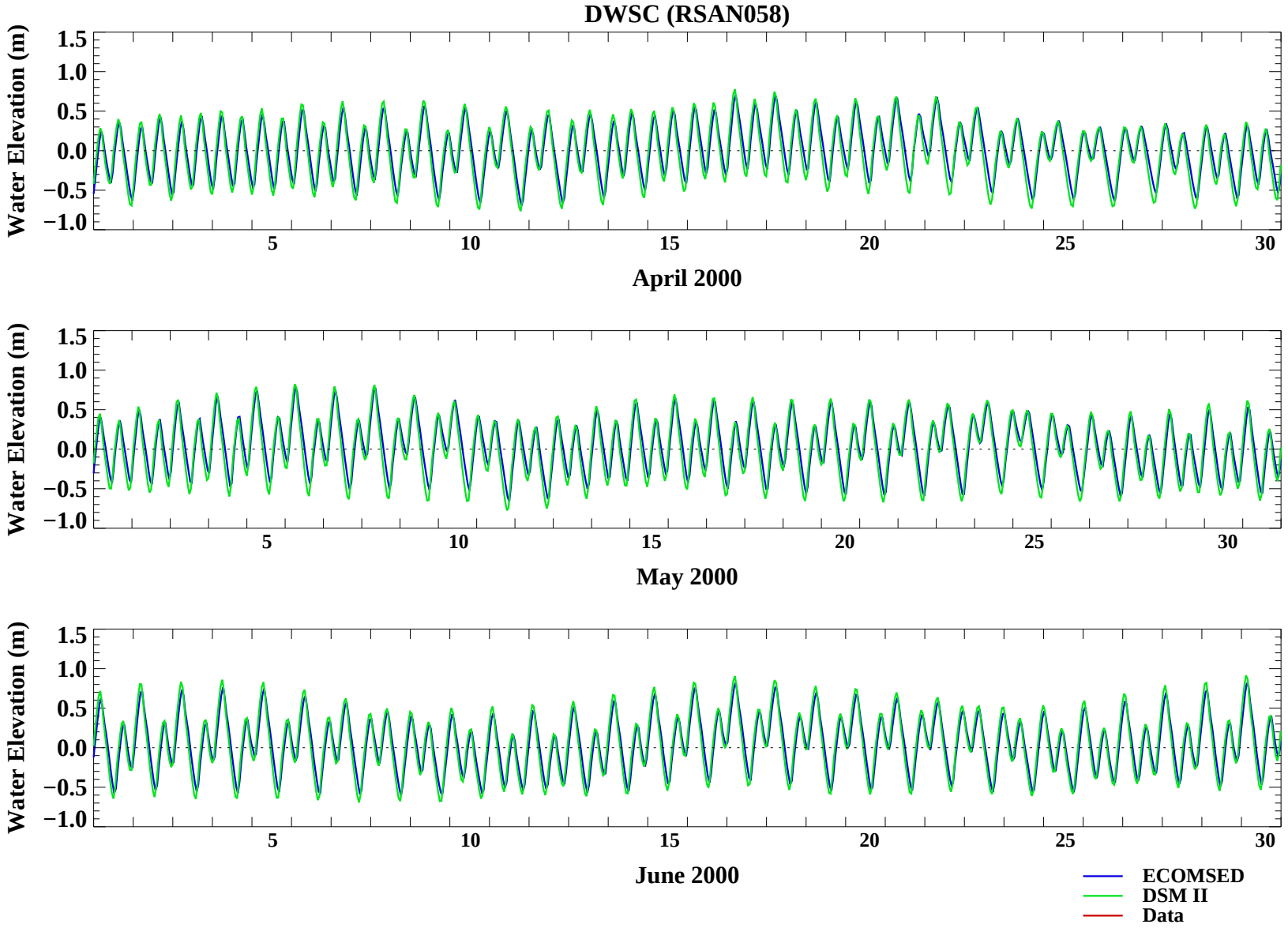
DWSC (RSAN058)
Water Elevation (m)
1.5
1.0
0.5
0.0
−0.5
−1.0
5
10
15
20
25
30
April 2000
May 2000
June 2000
ECOMSED
DSM II
Data

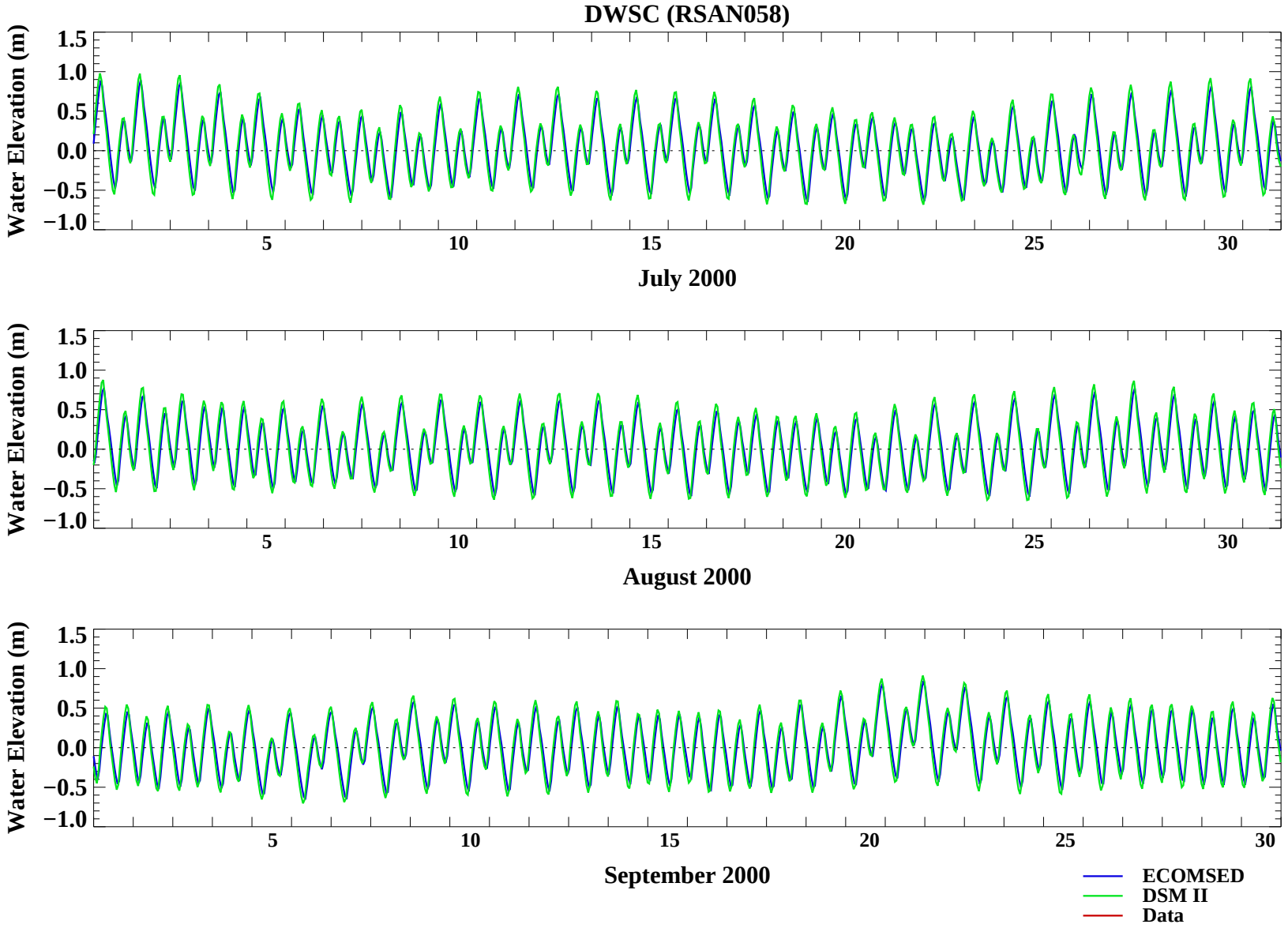
DWSC (RSAN058)
Water Elevation (m)
1.5
1.0
0.5
0.0
−0.5
−1.0
5
10
15
20
25
30
July 2000
August 2000
September 2000
ECOMSED
DSM II
Data

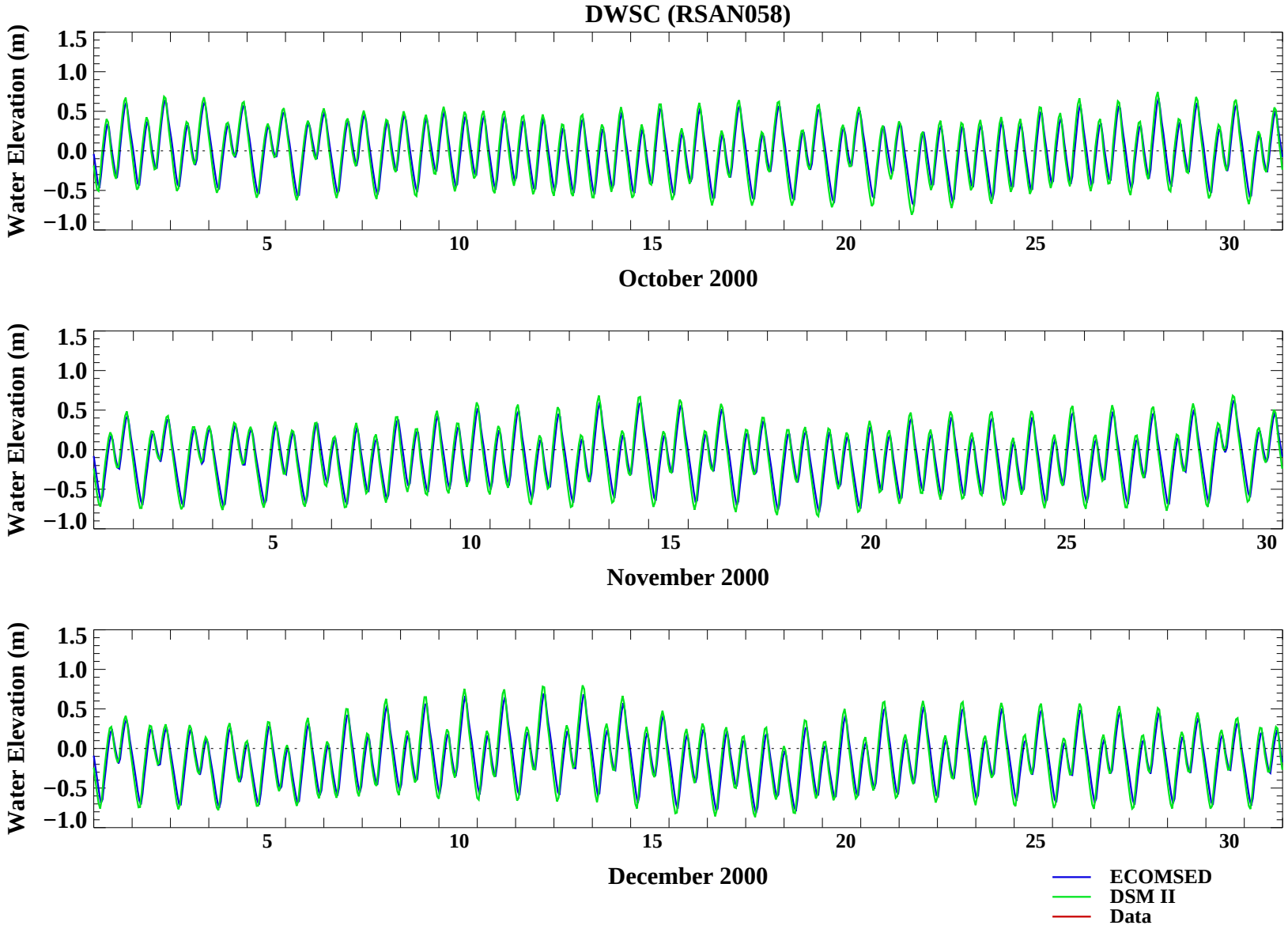
DWSC (RSAN058)
Water Elevation (m)
1.5
1.0
0.5
0.0
−0.5
−1.0
5
10
15
20
25
30
October 2000
November 2000
December 2000
ECOMSED
DSM II
Data

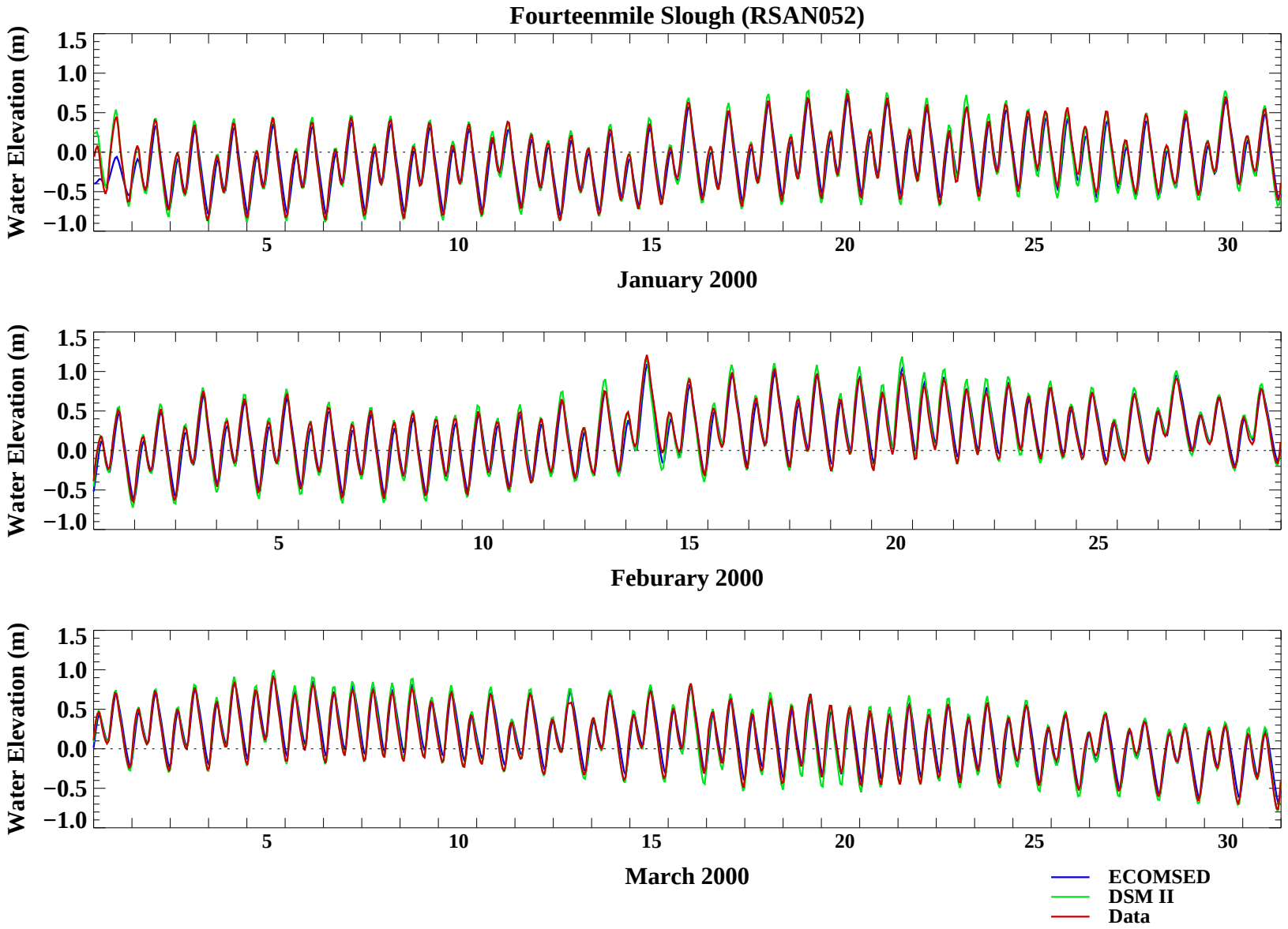
Fourteenmile Slough (RSAN052)
Water Elevation (m)
1.5
1.0
0.5
0.0
−0.5
−1.0
5
10
15
20
25
30
January 2000
Water Elevation (m)
1.5
1.0
0.5
0.0
−0.5
−1.0
5
10
15
20
25
Feburary 2000
Water Elevation (m)
1.5
1.0
0.5
0.0
−0.5
−1.0
5
10
15
20
25
30
March 2000
ECOMSED
DSM II
Data

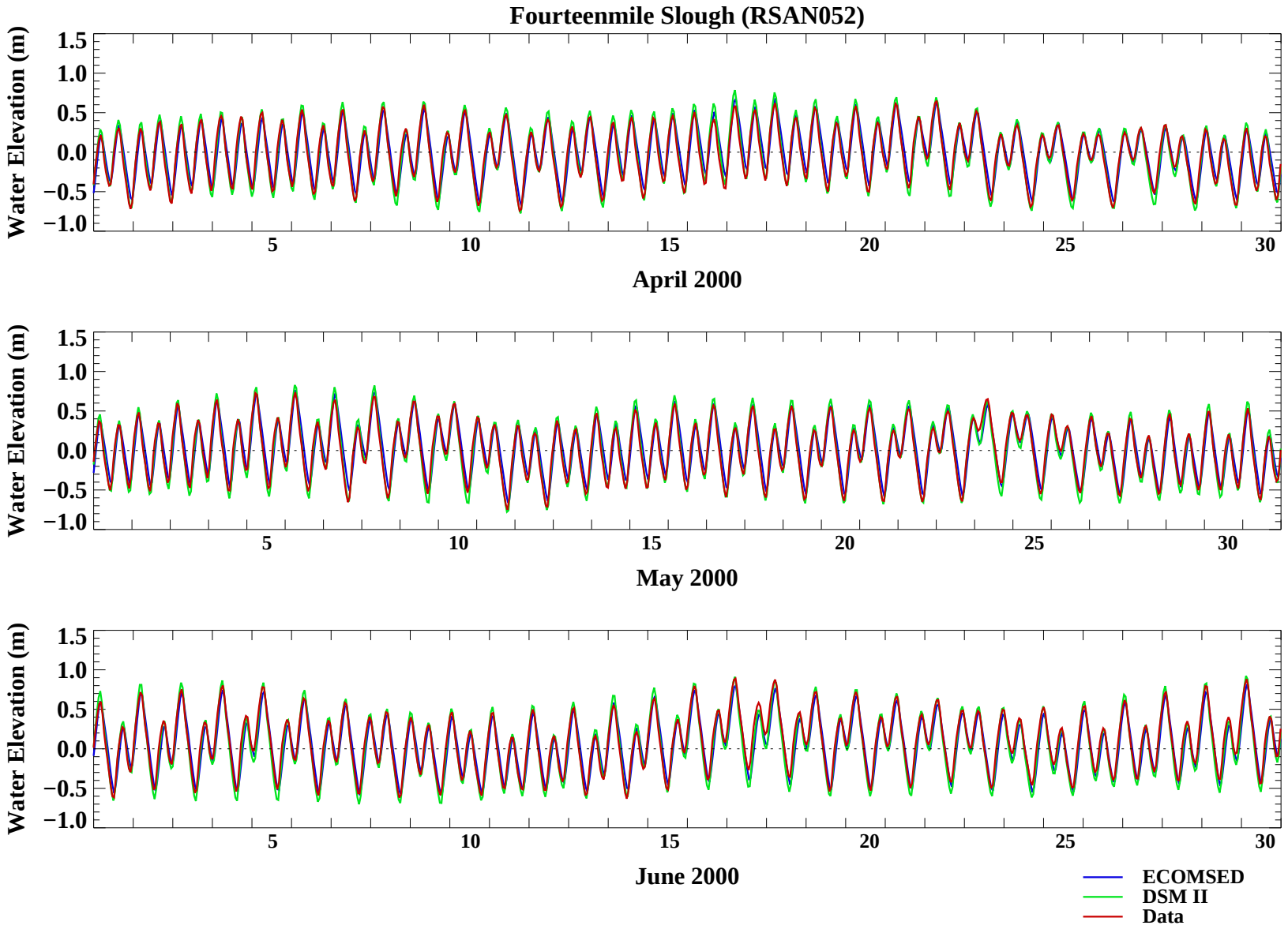
Fourteenmile Slough (RSAN052)
Water Elevation (m)
1.5
1.0
0.5
0.0
−0.5
−1.0
5
10
15
20
25
30
April 2000
May 2000
June 2000
ECOMSED
DSM II
Data

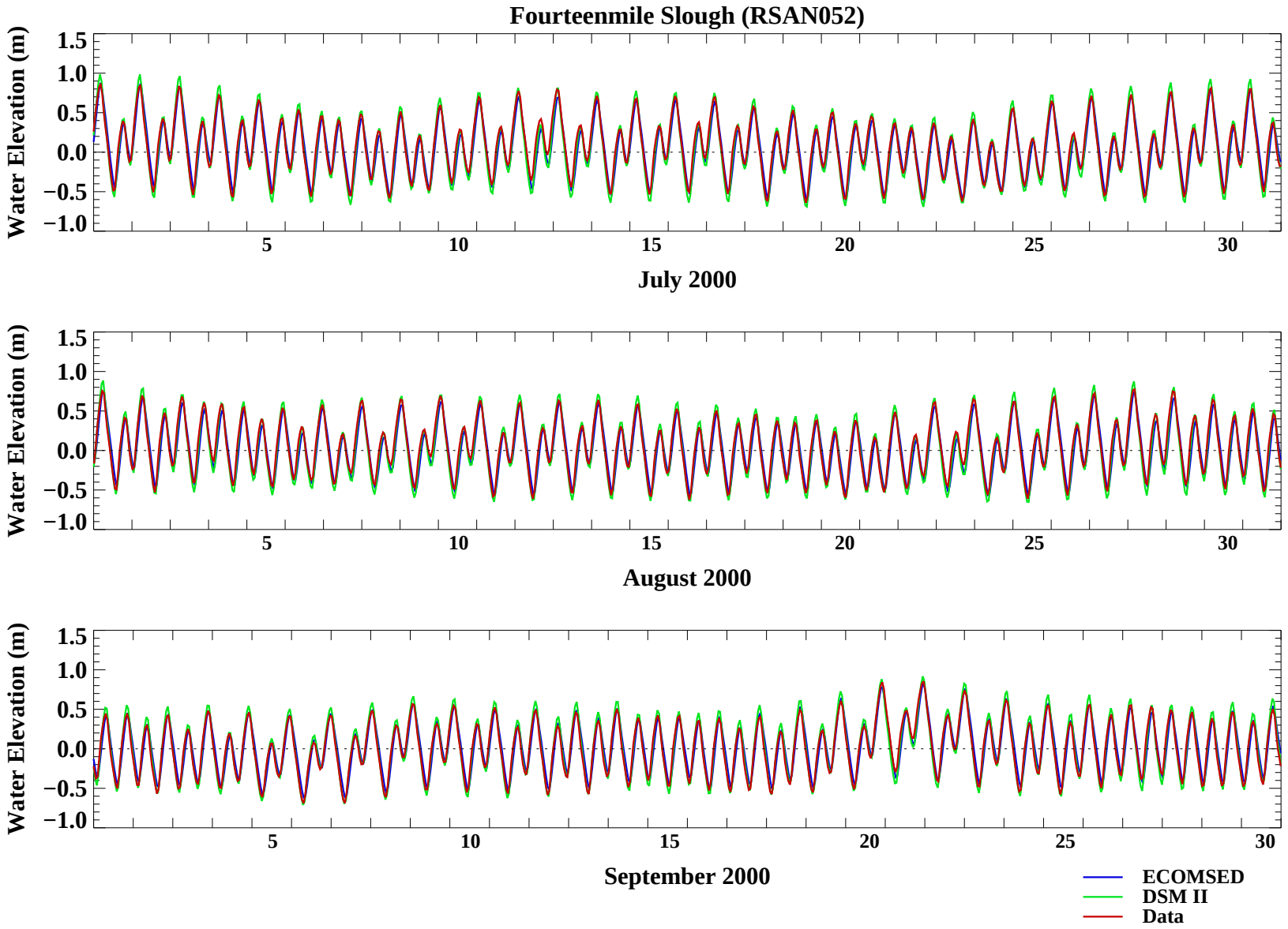
Fourteenmile Slough (RSAN052)
Water Elevation (m)
1.5
1.0
0.5
0.0
−0.5
−1.0
5
10
15
20
25
30
July 2000
August 2000
September 2000
ECOMSED
DSM II
Data

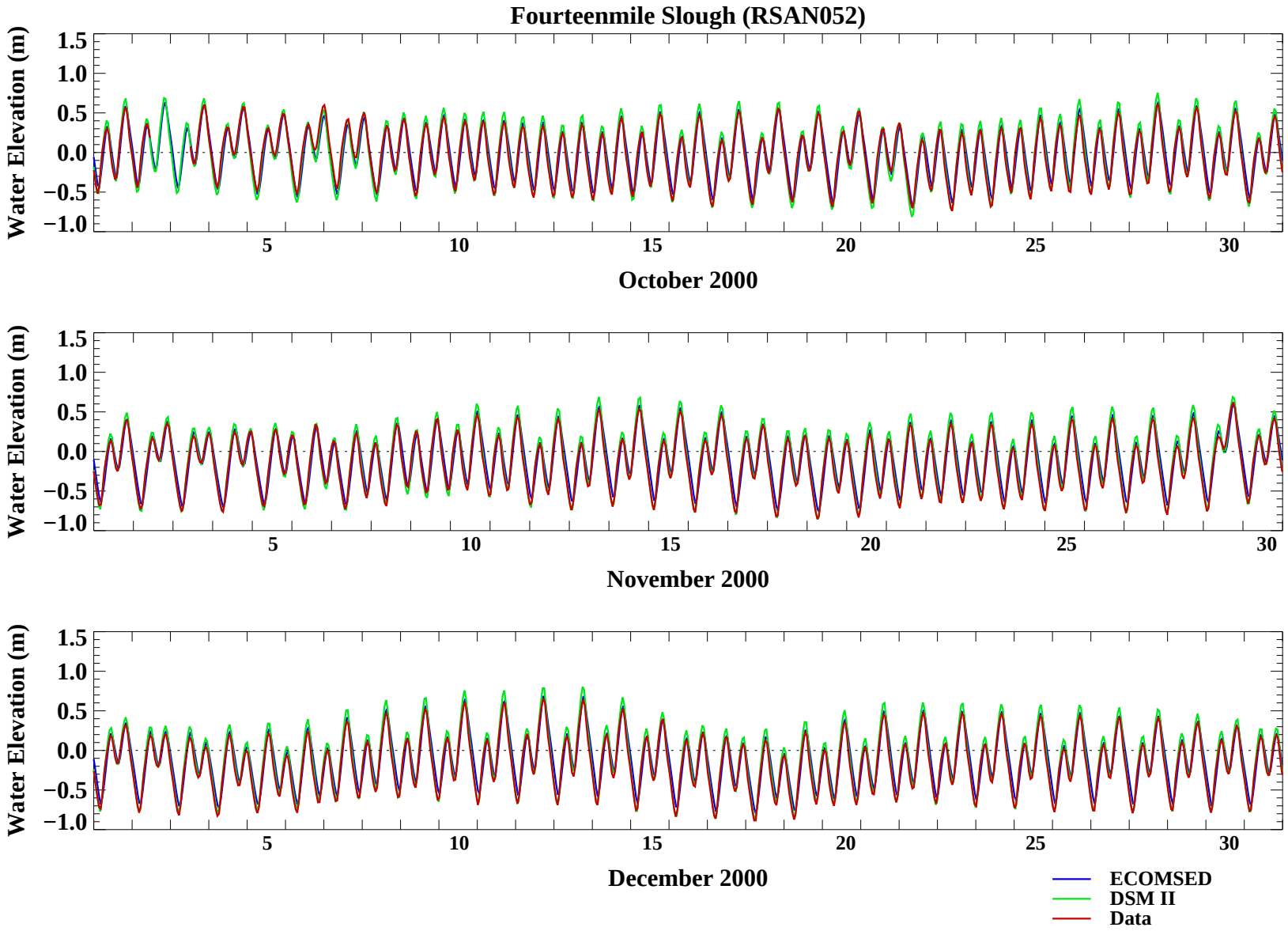
Fourteenmile Slough (RSAN052)
Water Elevation (m)
1.5
1.0
0.5
0.0
−0.5
−1.0
5
10
15
20
25
30
October 2000
November 2000
December 2000
ECOMSED
DSM II
Data

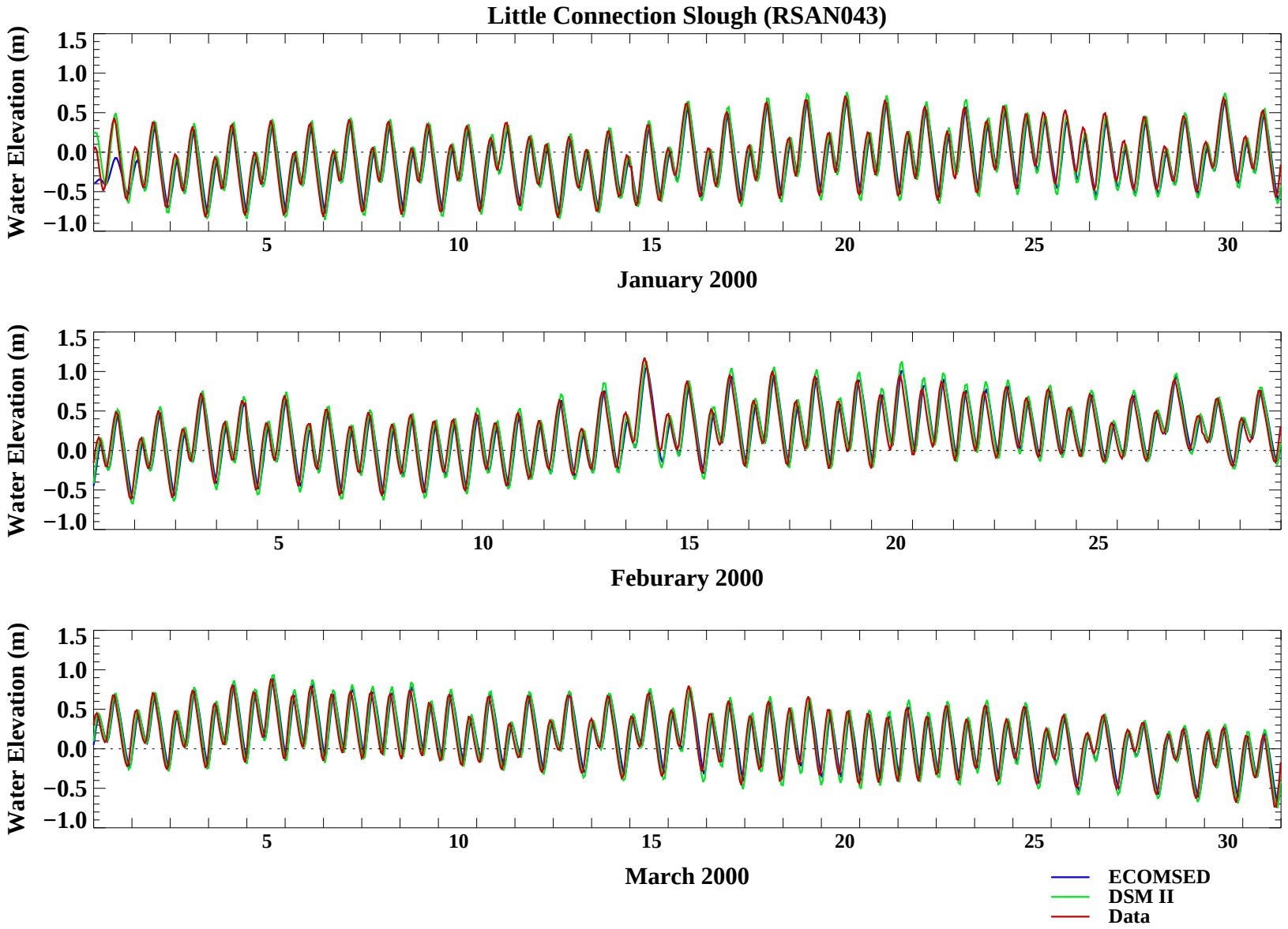
Little Connection Slough (RSAN043)
Water Elevation (m)
1.5
1.0
0.5
0.0
−0.5
−1.0
5
10
15
20
25
30
January 2000
Water Elevation (m)
Feburary 2000
Water Elevation (m)
March 2000
ECOMSED
DSM II
Data

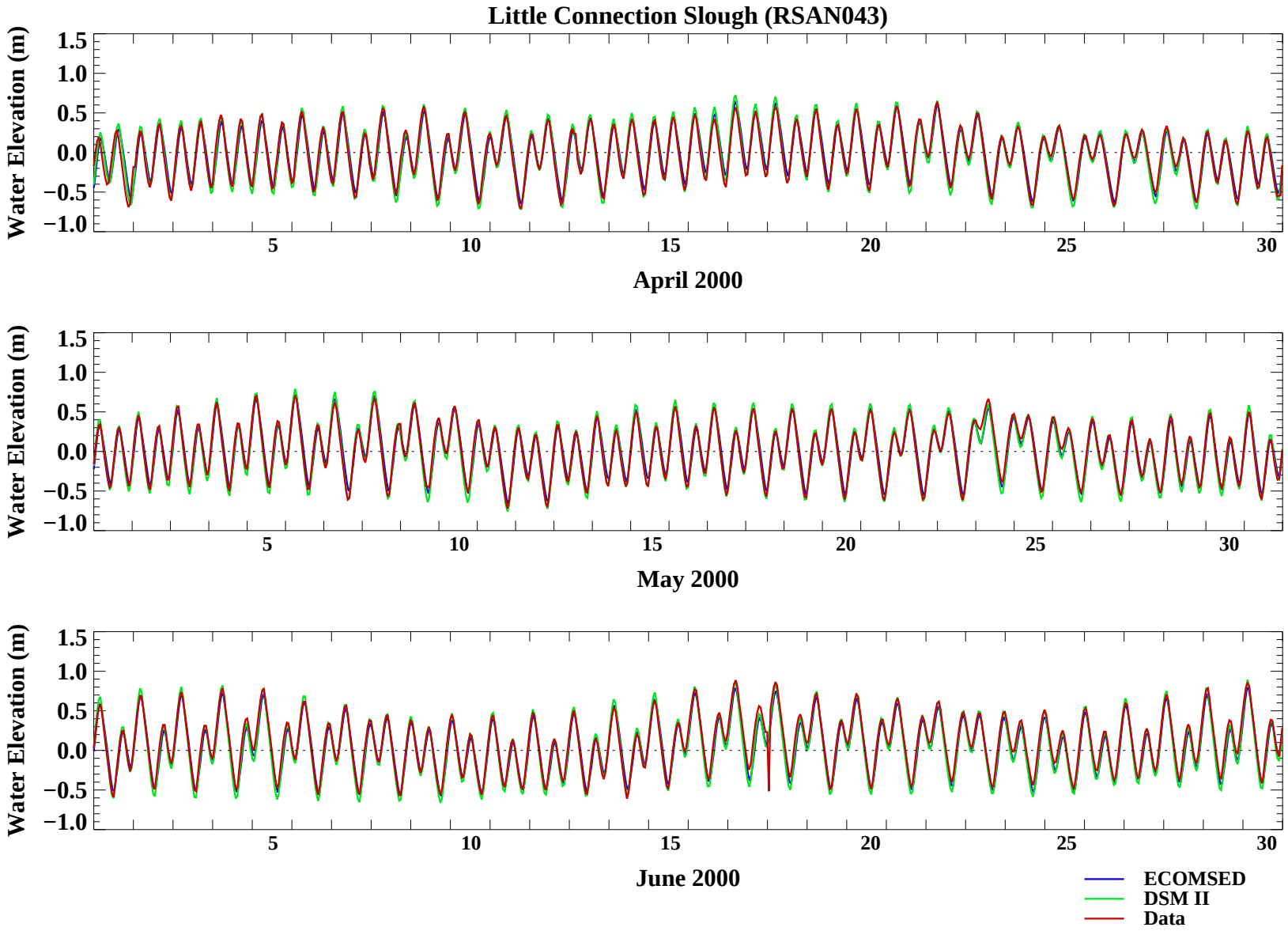
Little Connection Slough (RSAN043)
Water Elevation (m)
1.5
1.0
0.5
0.0
−0.5
−1.0
5
10
15
20
25
30
April 2000
May 2000
June 2000
ECOMSED
DSM II
Data

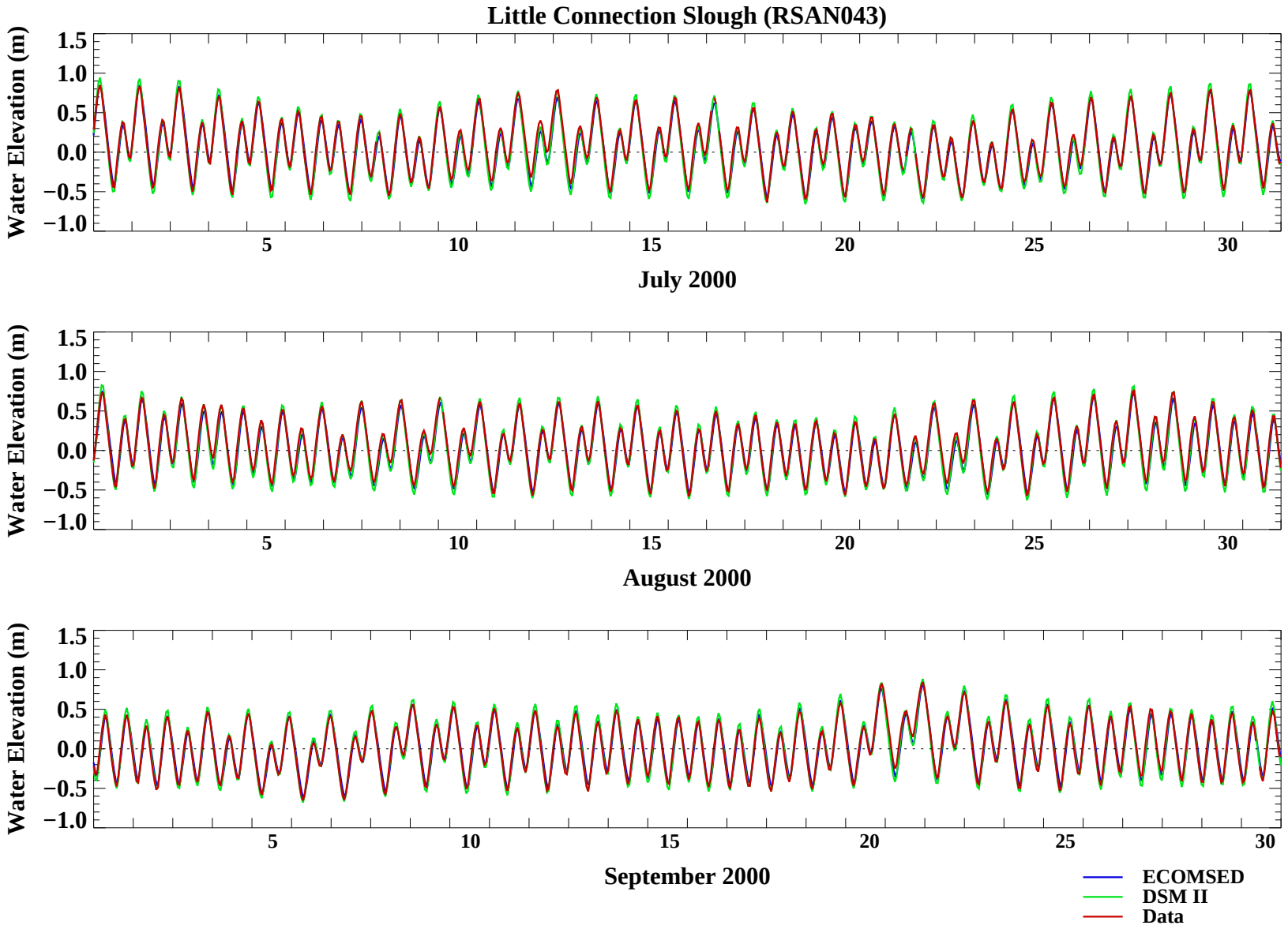
Little Connection Slough (RSAN043)
Water Elevation (m)
1.5
1.0
0.5
0.0
−0.5
−1.0
5
10
15
20
25
30
July 2000
August 2000
September 2000
ECOMSED
DSM II
Data

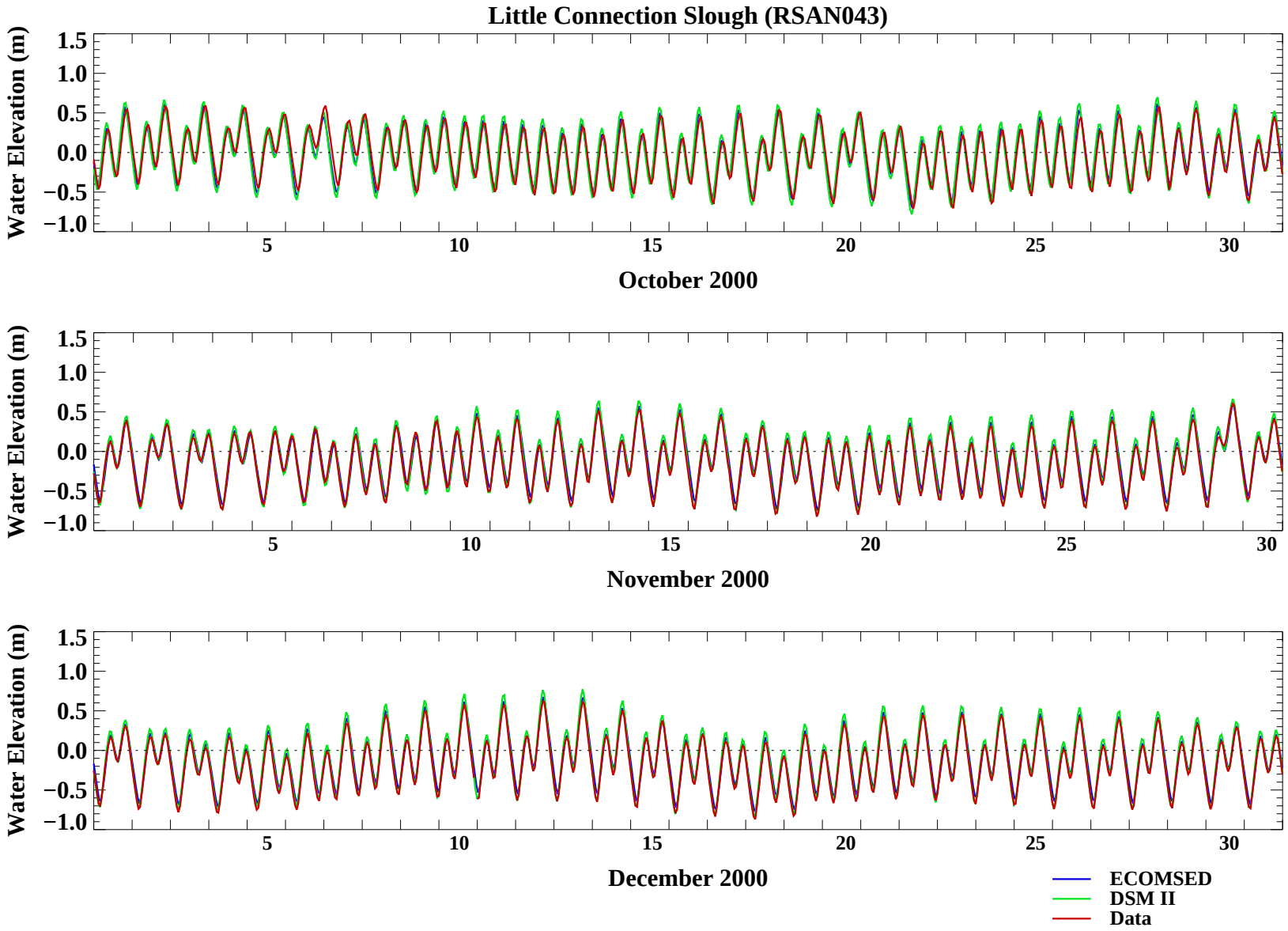
Little Connection Slough (RSAN043)
Water Elevation (m)
1.5
1.0
0.5
0.0
−0.5
−1.0
5
10
15
20
25
30
October 2000
November 2000
December 2000
ECOMSED
DSM II
Data

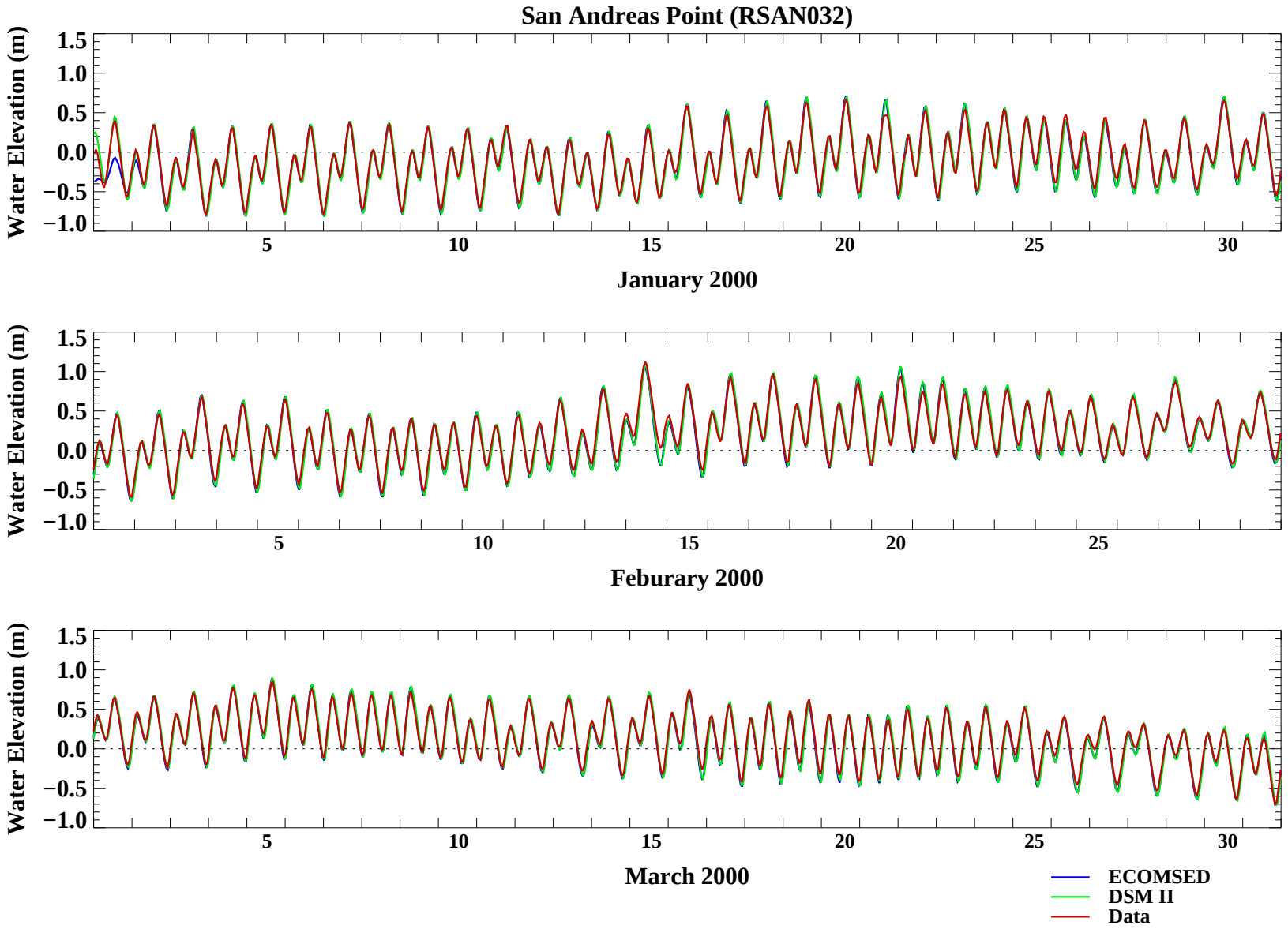
San Andreas Point (RSAN032)
Water Elevation (m)
1.5
1.0
0.5
0.0
−0.5
−1.0
5
10
15
20
25
30
January 2000
Water Elevation (m)
Feburary 2000
Water Elevation (m)
March 2000
ECOMSED
DSM II
Data

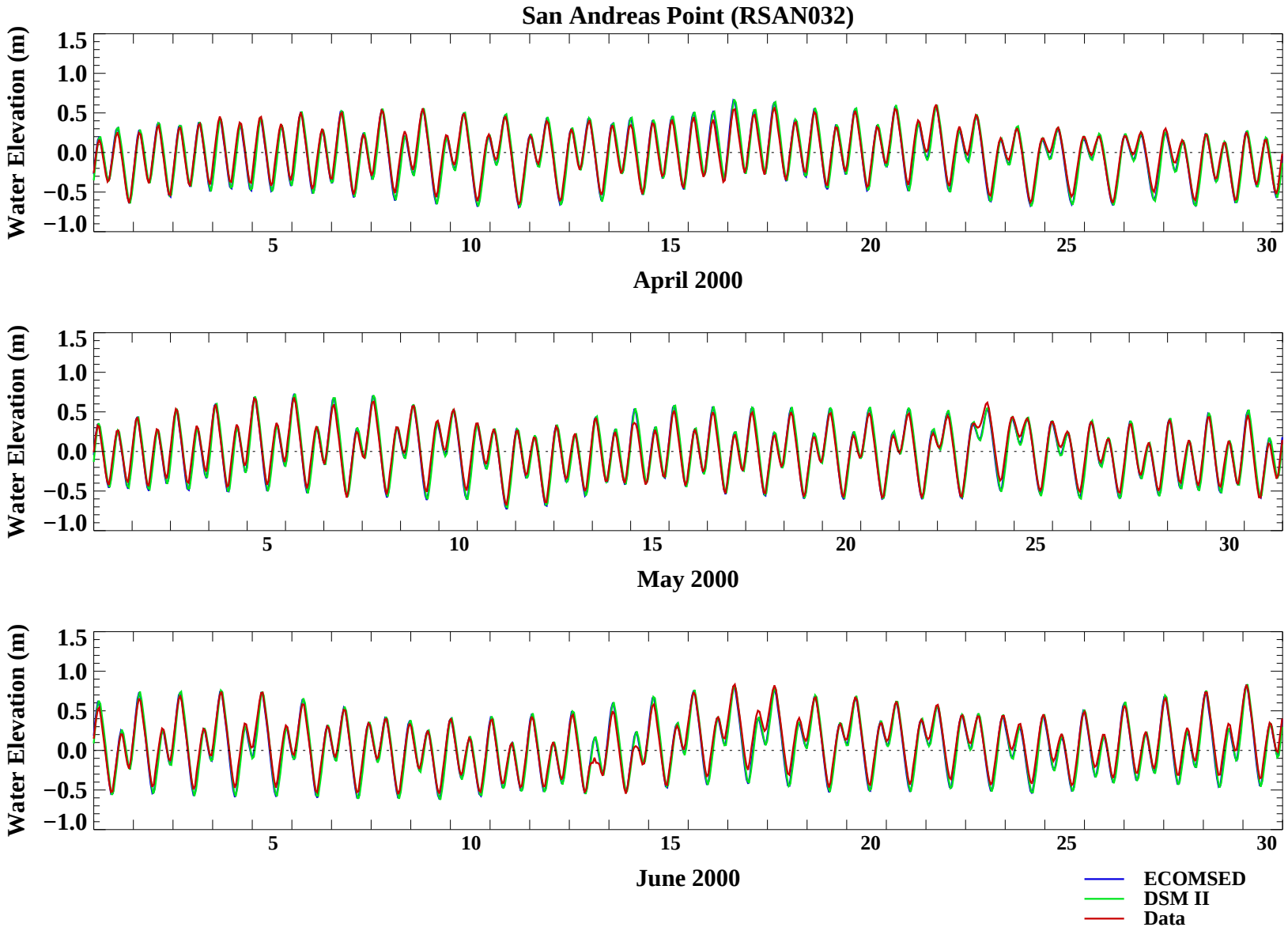
San Andreas Point (RSAN032)
Water Elevation (m)
1.5
1.0
0.5
0.0
−0.5
−1.0
5
10
15
20
25
30
April 2000
May 2000
June 2000
ECOMSED
DSM II
Data

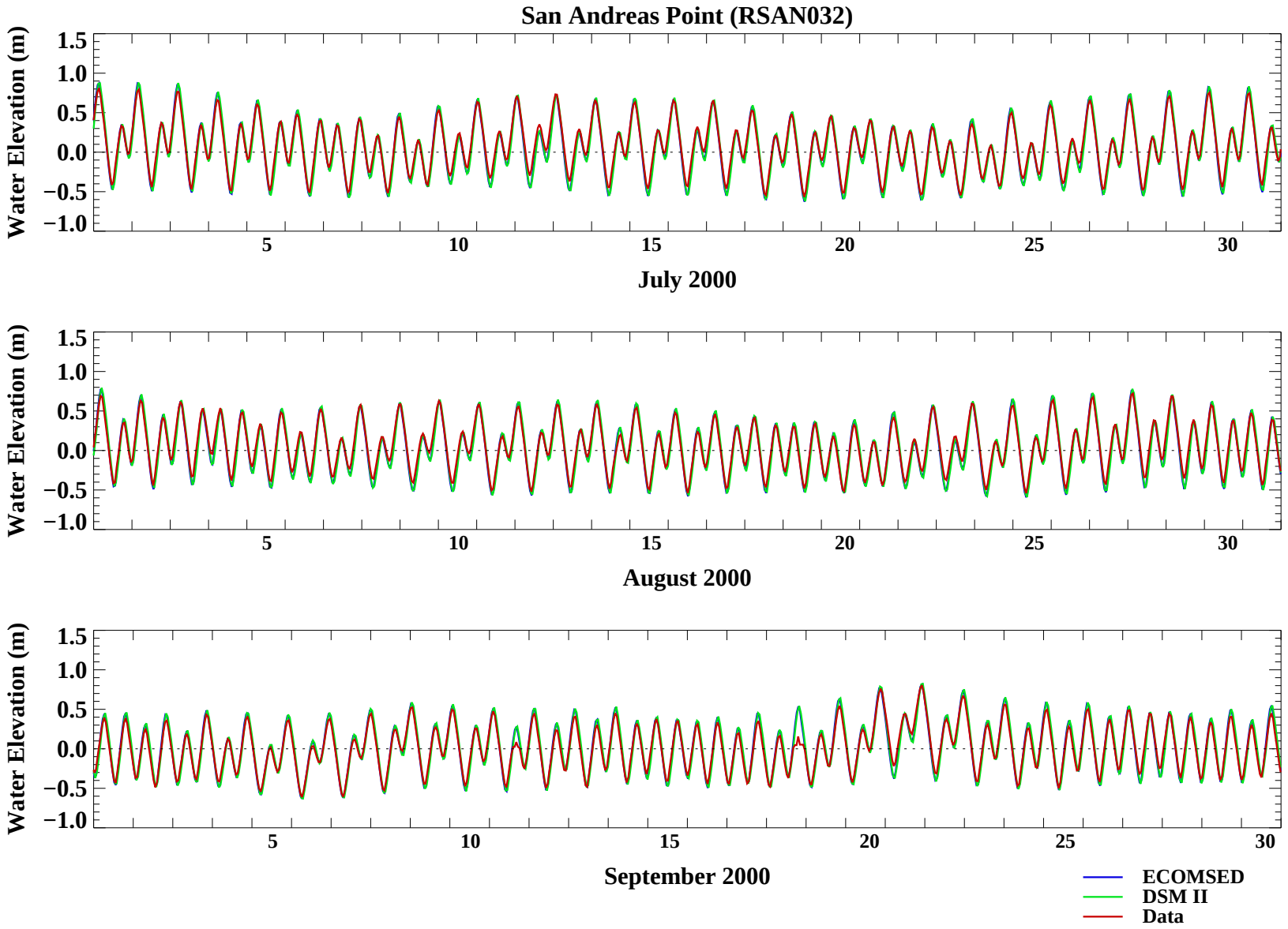
San Andreas Point (RSAN032)
Water Elevation (m)
1.5
1.0
0.5
0.0
−0.5
−1.0
5
10
15
20
25
30
July 2000
August 2000
September 2000
ECOMSED
DSM II
Data

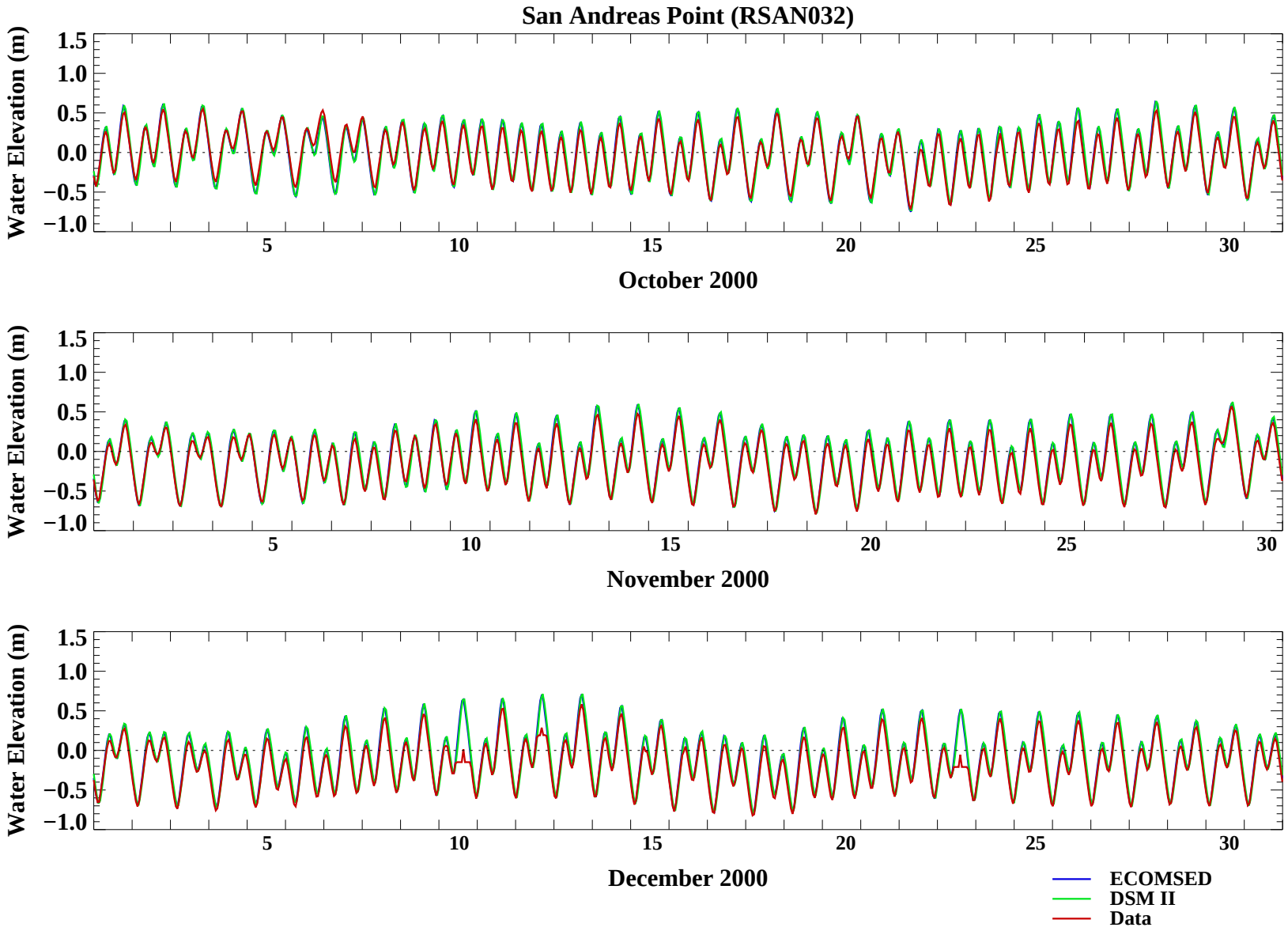
San Andreas Point (RSAN032)
Water Elevation (m)
1.5
1.0
0.5
0.0
−0.5
−1.0
5
10
15
20
25
30
October 2000
November 2000
December 2000
ECOMSED
DSM II
Data

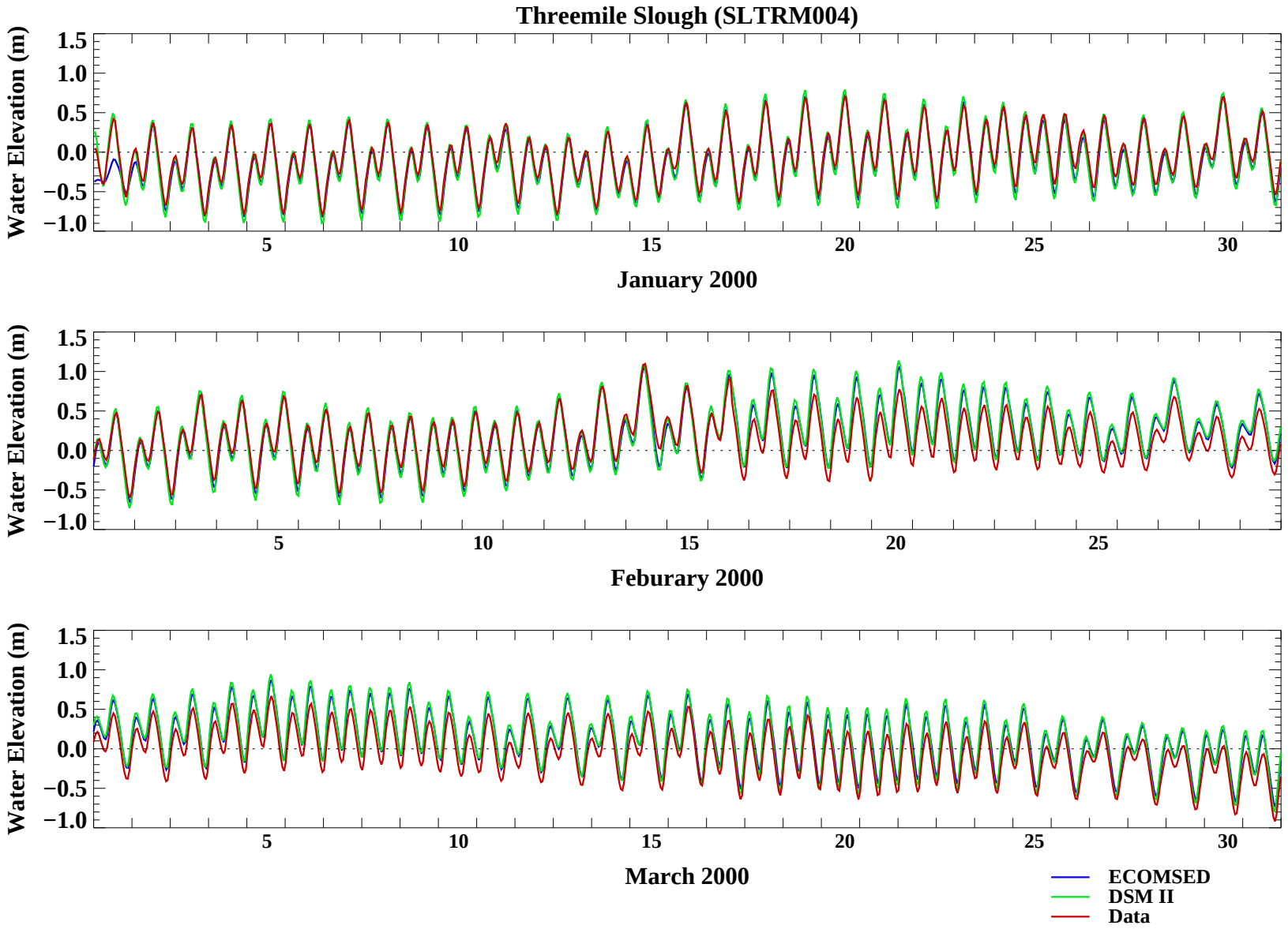
Threemile Slough (SLTRM004)
Water Elevation (m)
1.5
1.0
0.5
0.0
−0.5
−1.0
5
10
15
20
25
30
January 2000
Water Elevation (m)
Feburary 2000
Water Elevation (m)
March 2000
ECOMSED
DSM II
Data

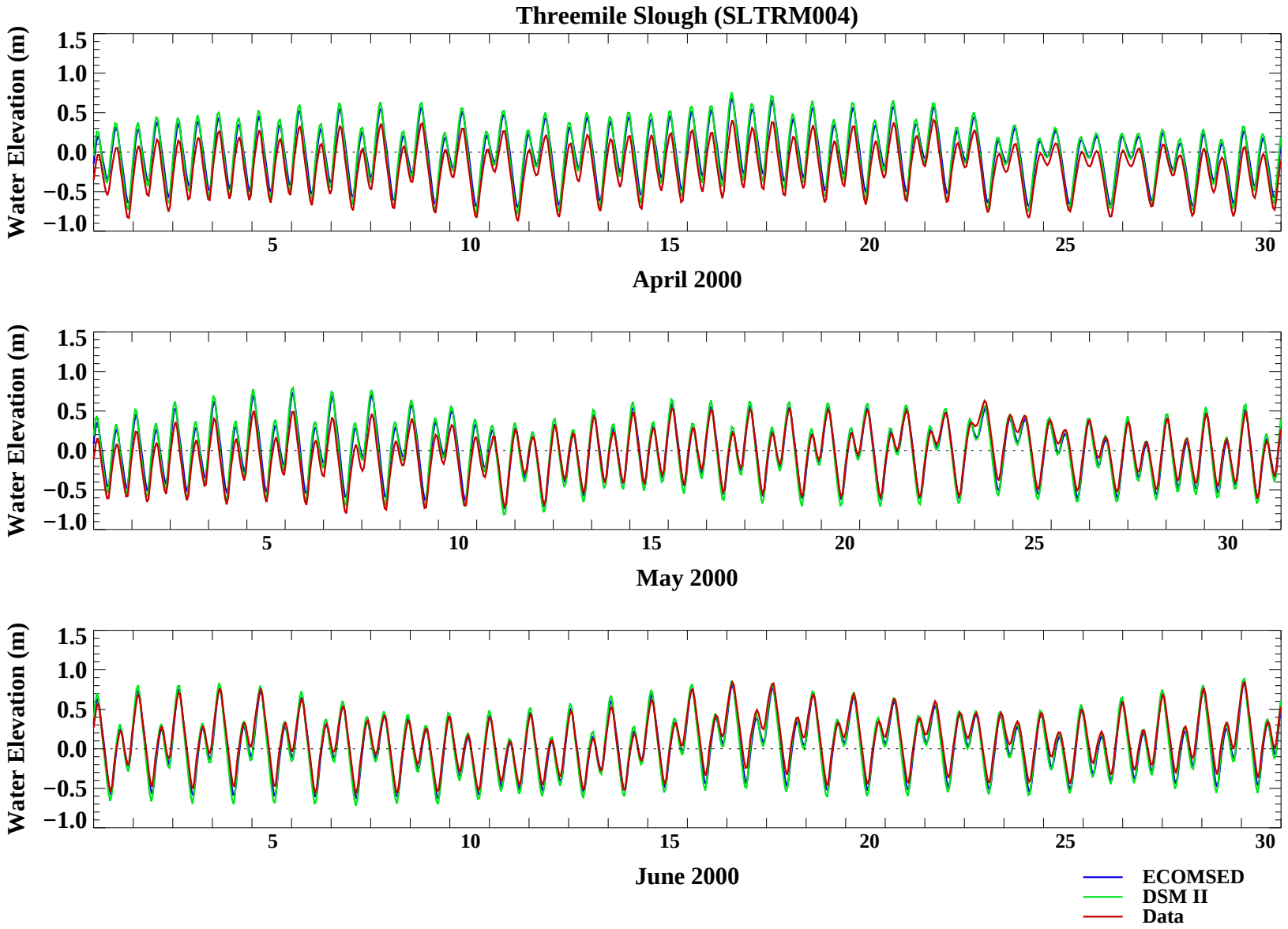
Threemile Slough (SLTRM004)
Water Elevation (m)
1.5
1.0
0.5
0.0
−0.5
−1.0
5
10
15
20
25
30
April 2000
May 2000
June 2000
ECOMSED
DSM II
Data

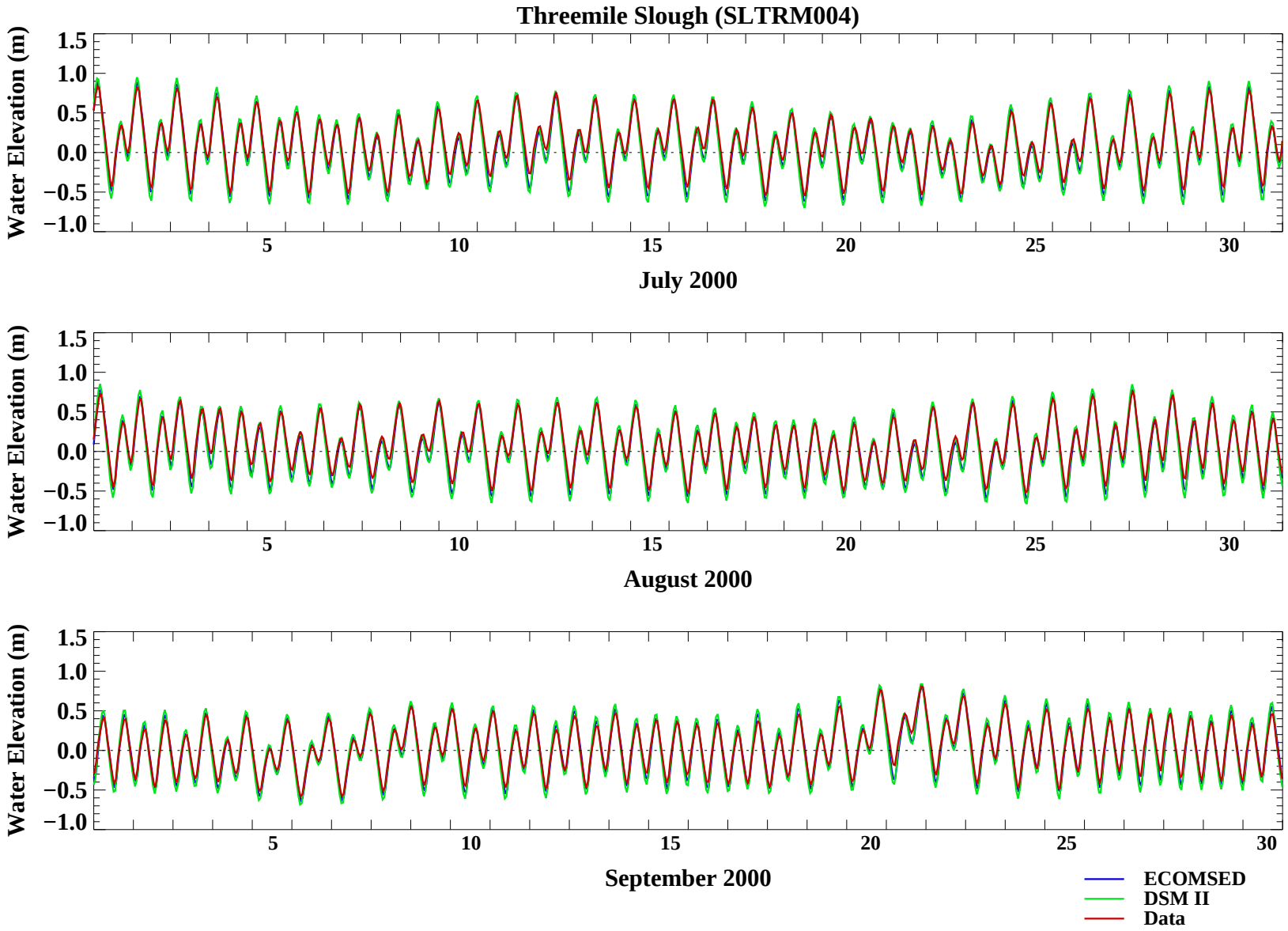
Threemile Slough (SLTRM004)
Water Elevation (m)
1.5
1.0
0.5
0.0
−0.5
−1.0
5
10
15
20
25
30
July 2000
August 2000
September 2000
ECOMSED
DSM II
Data

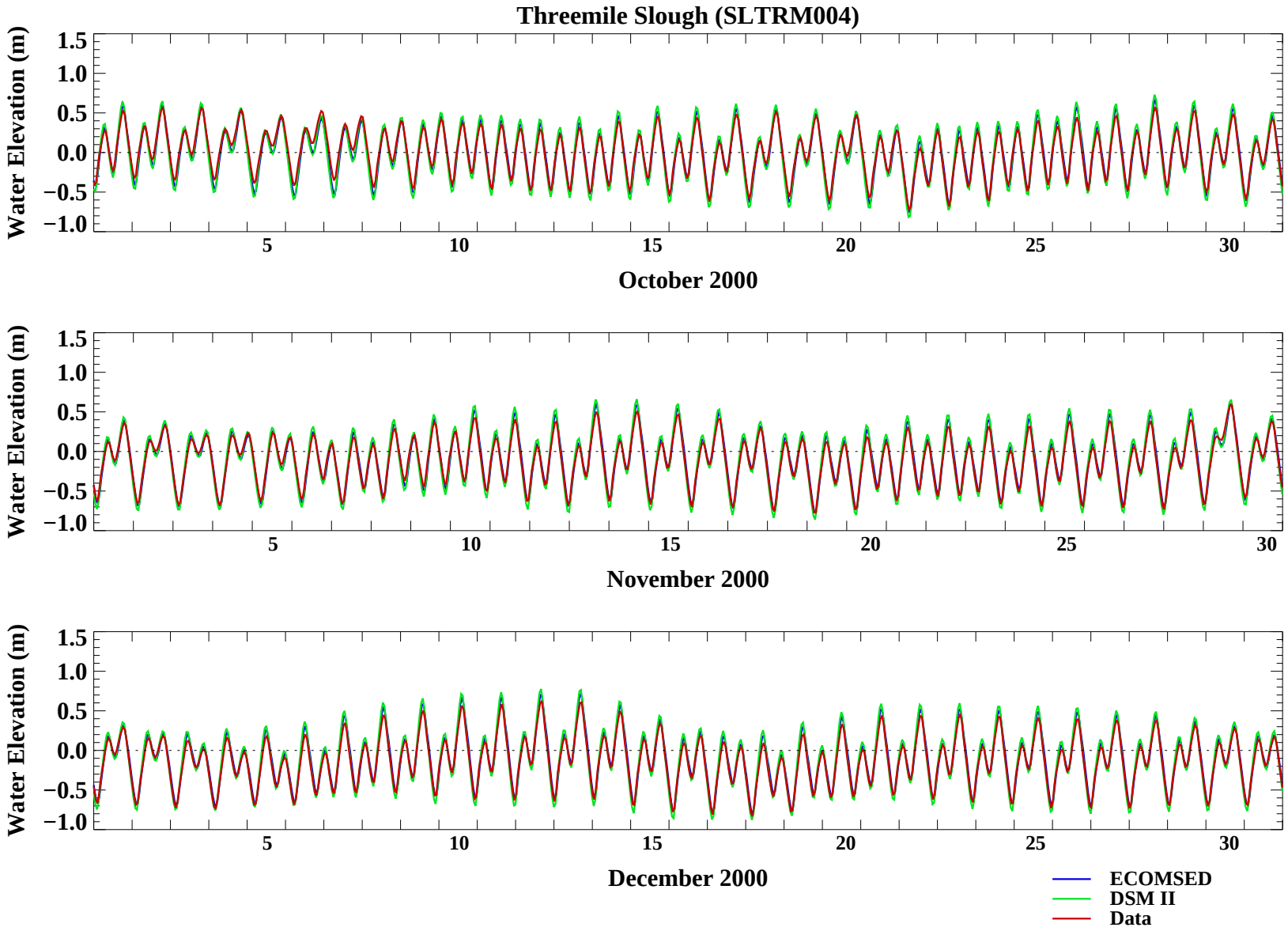
Threemile Slough (SLTRM004)
Water Elevation (m)
1.5
1.0
0.5
0.0
−0.5
−1.0
5
10
15
20
25
30
October 2000
November 2000
December 2000
ECOMSED
DSM II
Data

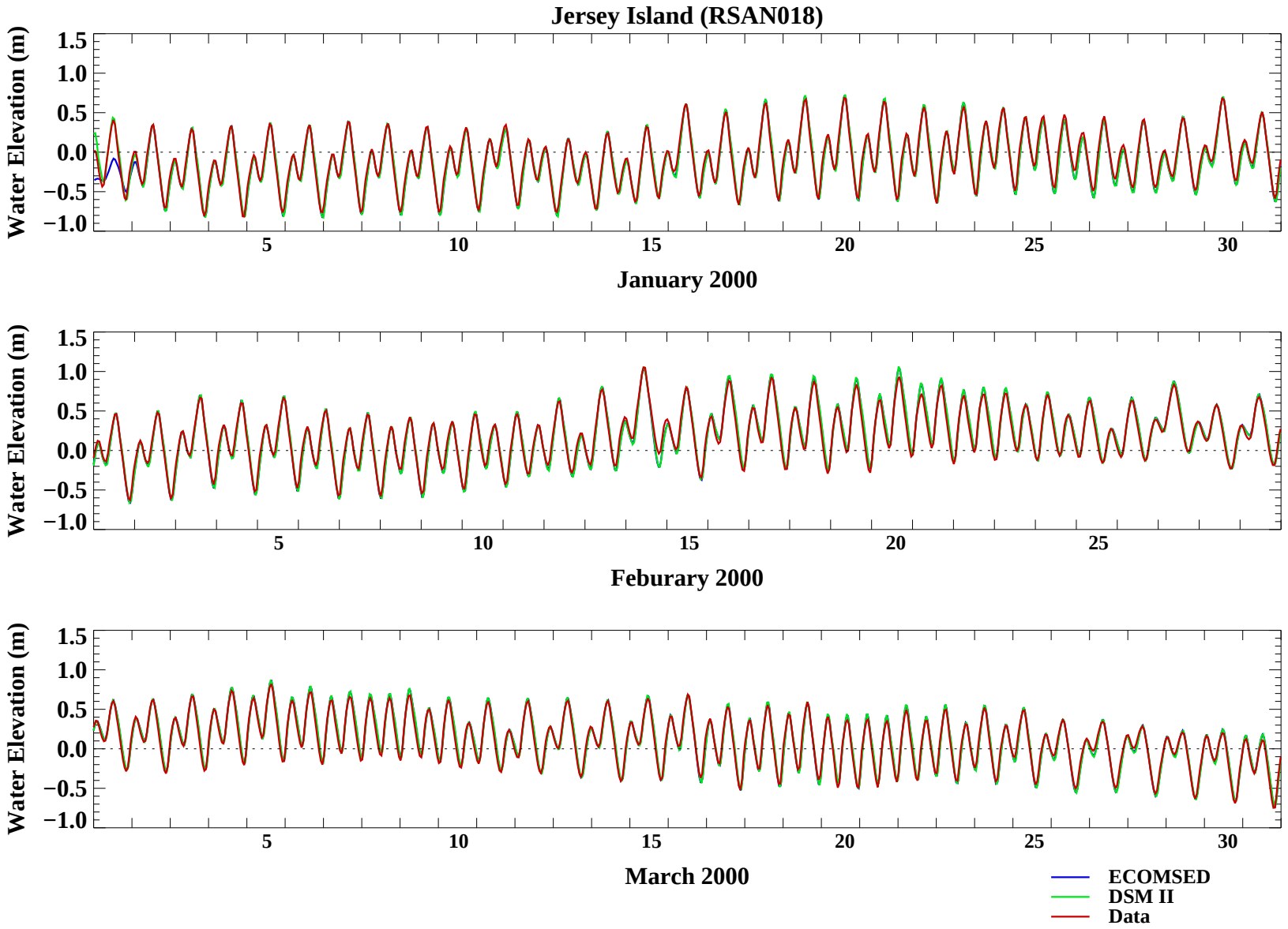
Jersey Island (RSAN018)
Water Elevation (m)
1.5
1.0
0.5
0.0
−0.5
−1.0
5
10
15
20
25
30
January 2000
Water Elevation (m)
Feburary 2000
Water Elevation (m)
March 2000
ECOMSED
DSM II
Data

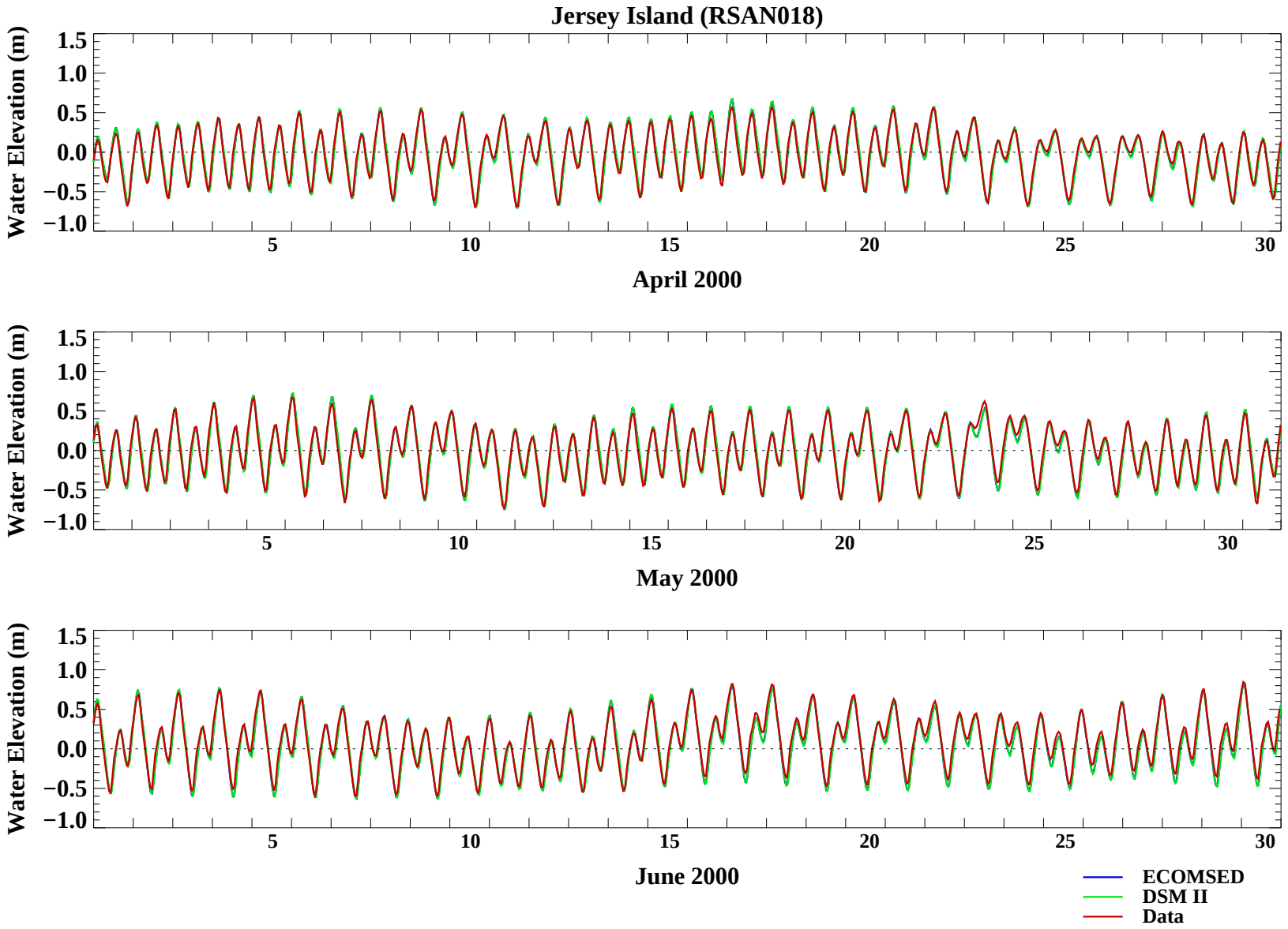
Jersey Island (RSAN018)
Water Elevation (m)
1.5
1.0
0.5
0.0
−0.5
−1.0
5
10
15
20
25
30
April 2000
May 2000
June 2000
ECOMSED
DSM II
Data

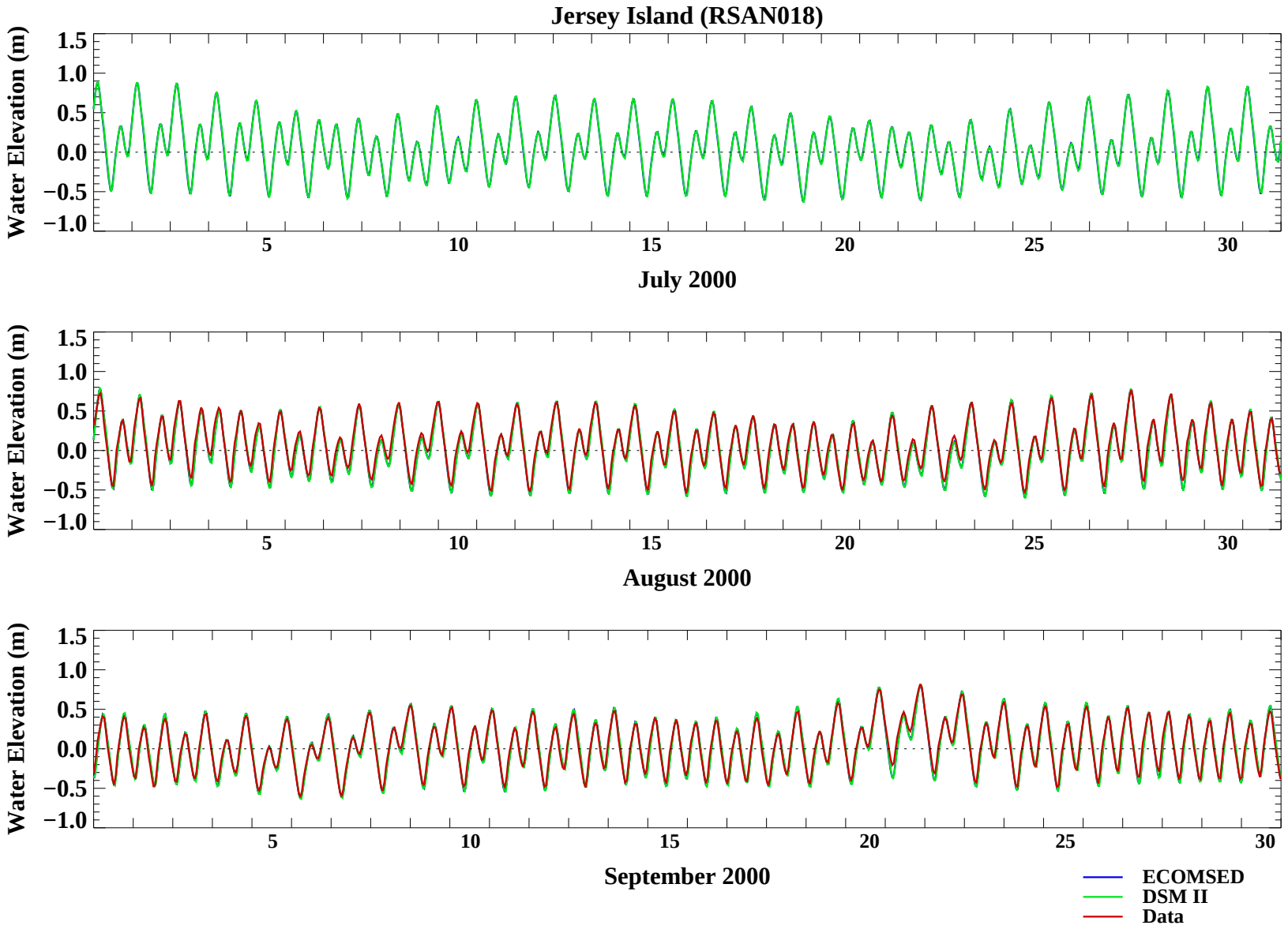
Jersey Island (RSAN018)
Water Elevation (m)
1.5
1.0
0.5
0.0
−0.5
−1.0
5
10
15
20
25
30
July 2000
August 2000
September 2000
ECOMSED
DSM II
Data

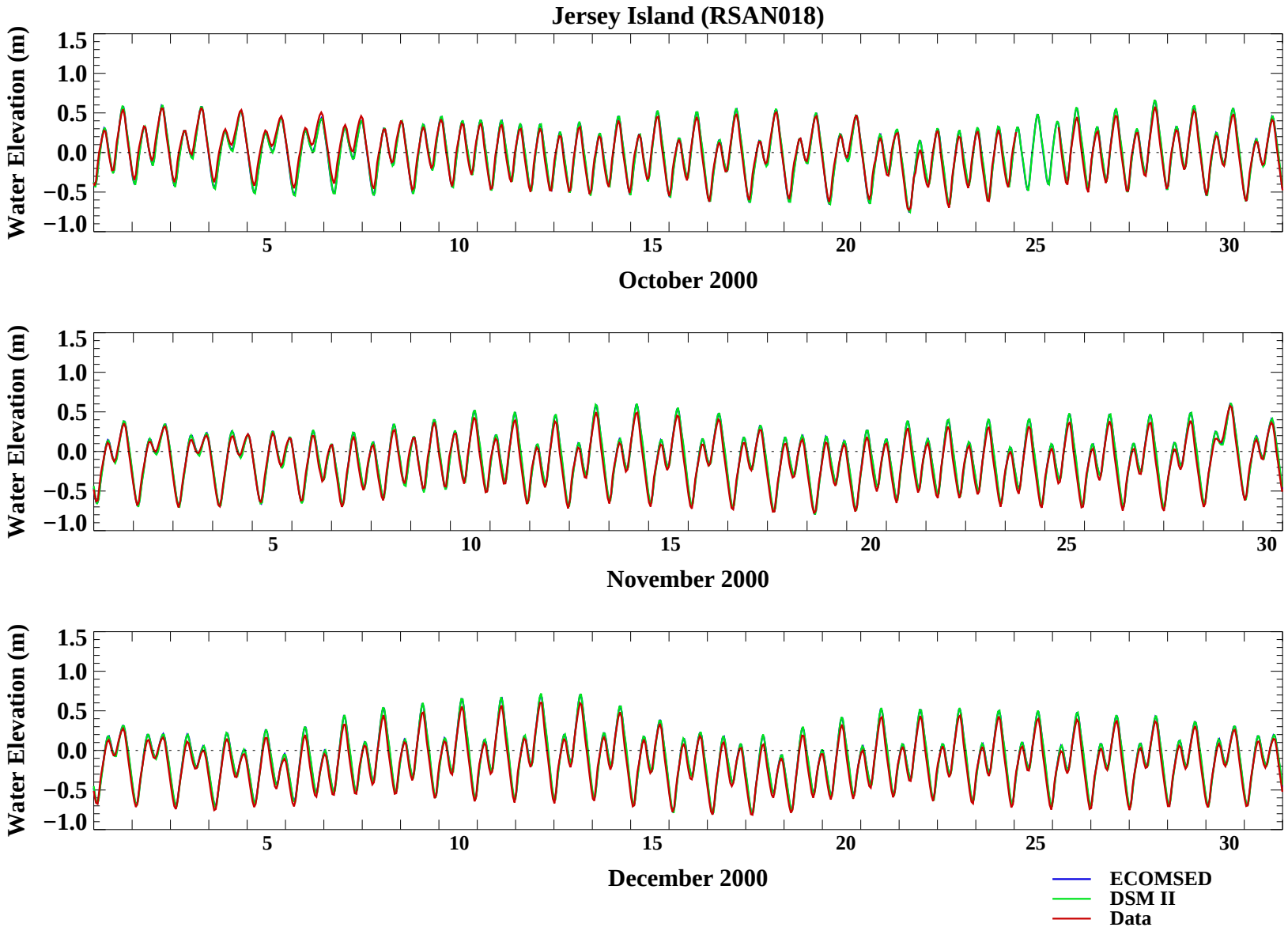
Jersey Island (RSAN018)
Water Elevation (m)
1.5
1.0
0.5
0.0
−0.5
−1.0
5
10
15
20
25
30
October 2000
November 2000
December 2000
ECOMSED
DSM II
Data

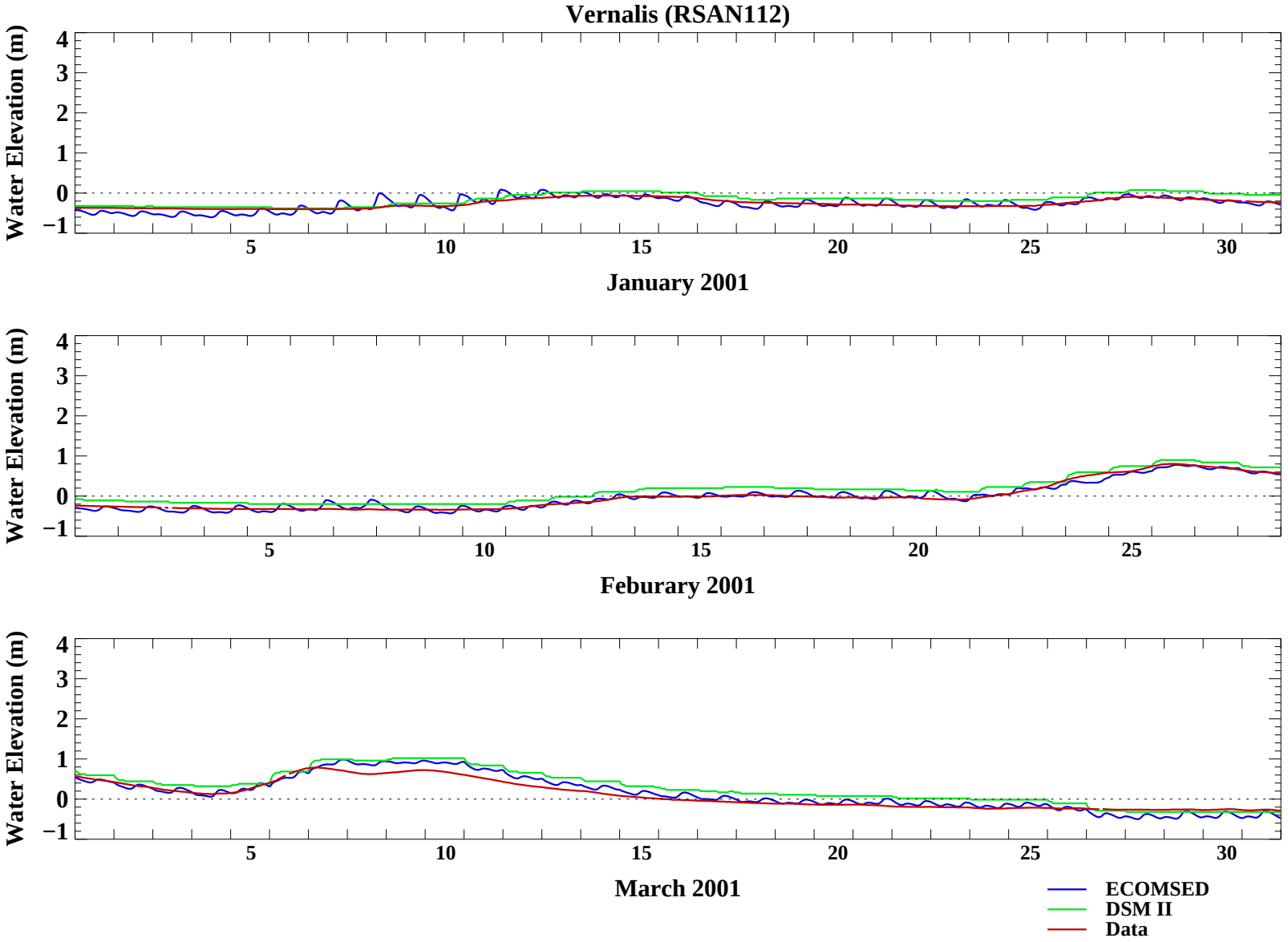
Vernalis (RSAN112)
Water Elevation (m)
4
3
2
1
0
−1
5
10
15
20
25
30
January 2001
Water Elevation (m)
Feburary 2001
Water Elevation (m)
March 2001
ECOMSED
DSM II
Data

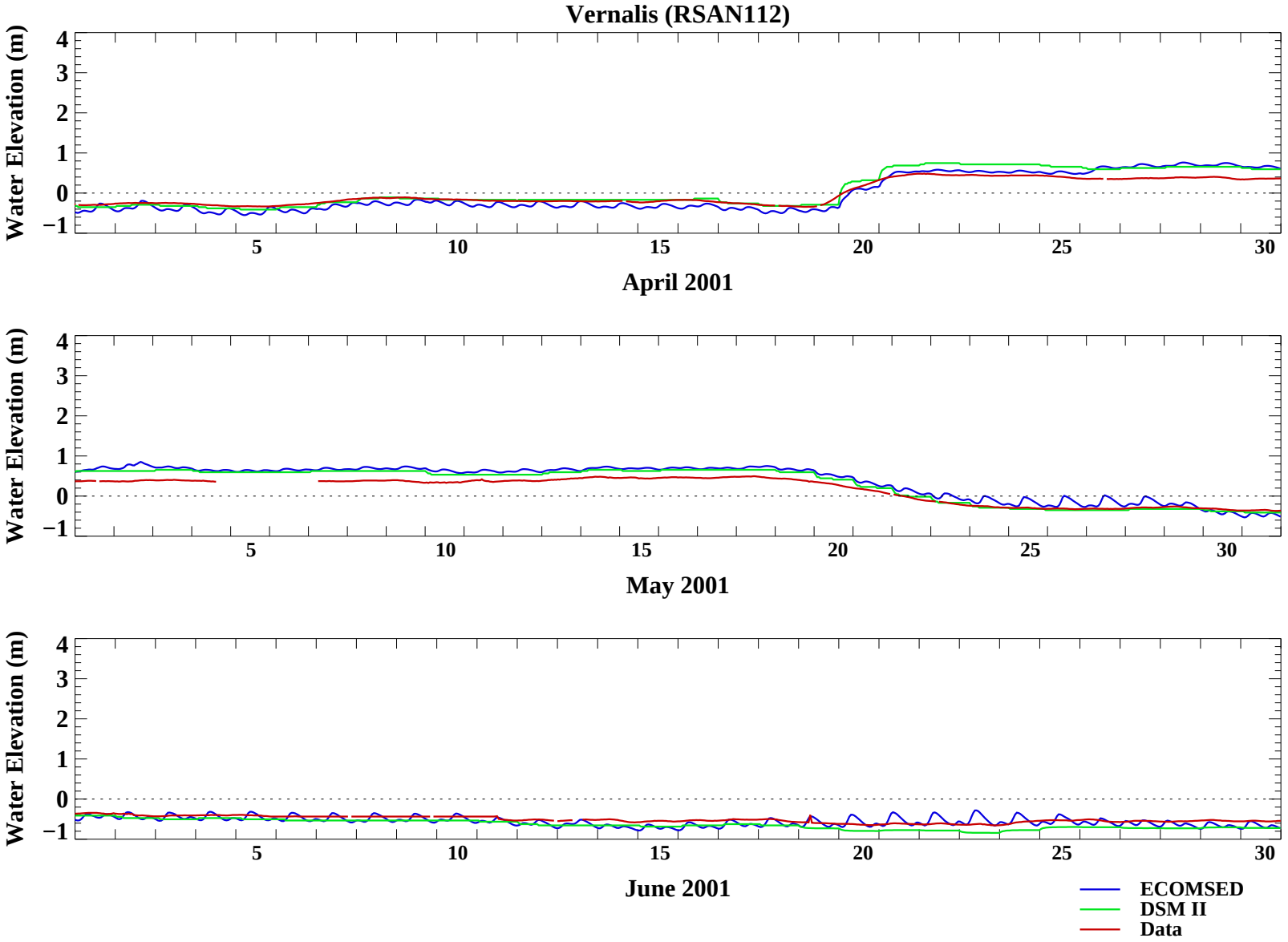
Vernalis (RSAN112)
Water Elevation (m)
4
3
2
1
0
−1
5
10
15
20
25
30
April 2001
Water Elevation (m)
May 2001
Water Elevation (m)
June 2001
ECOMSED
DSM II
Data

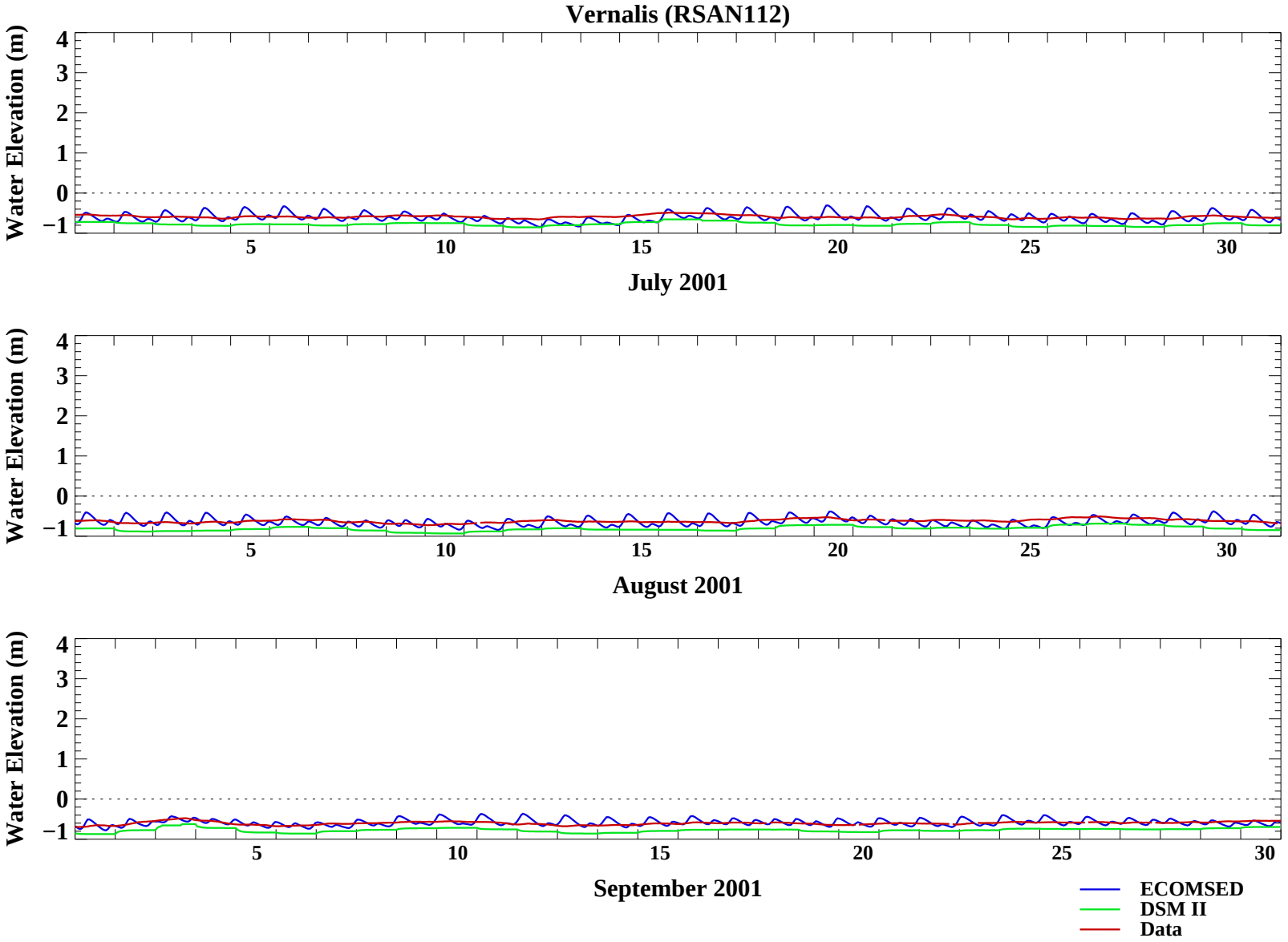
Vernalis (RSAN112)
Water Elevation (m)
4
3
2
1
0
−1
5
10
15
20
25
30
July 2001
August 2001
September 2001
ECOMSED
DSM II
Data

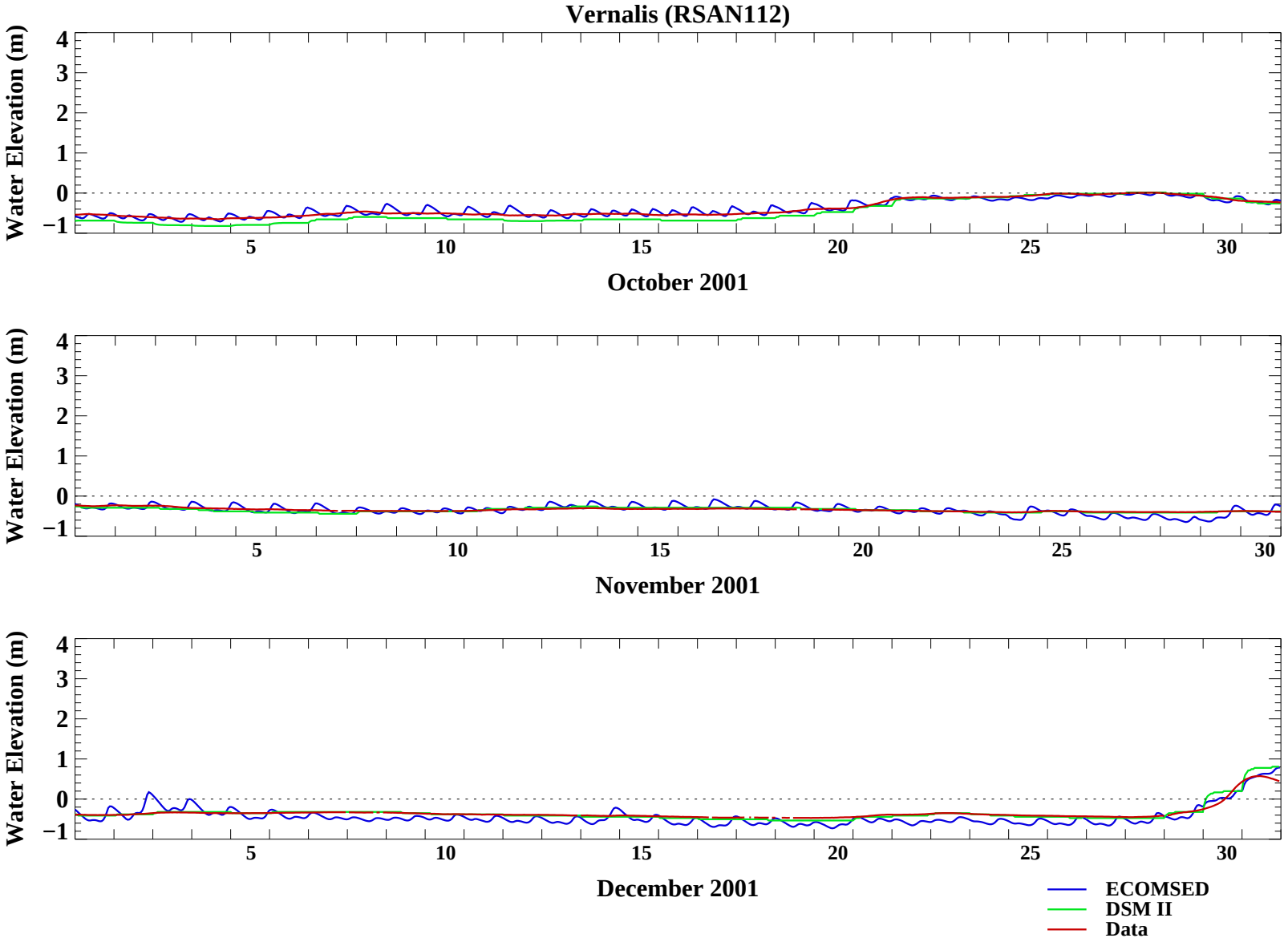
Vernalis (RSAN112)
Water Elevation (m)
4
3
2
1
0
−1
5
10
15
20
25
30
October 2001
Water Elevation (m)
November 2001
Water Elevation (m)
December 2001
ECOMSED
DSM II
Data

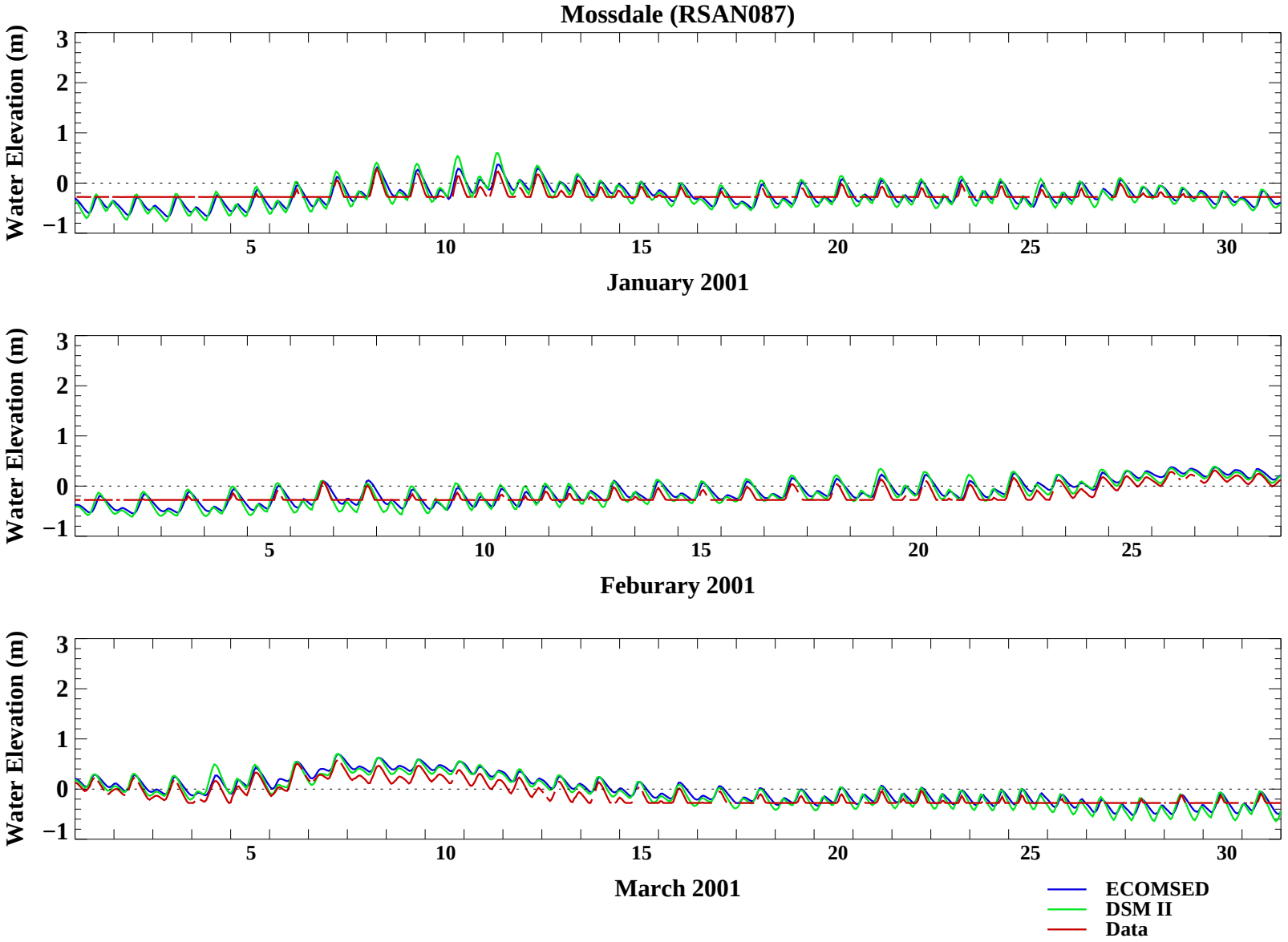
Mossdale (RSAN087)
Water Elevation (m)
3
2
1
0
−1
5
10
15
20
25
30
January 2001
Water Elevation (m)
3
2
1
0
−1
5
10
15
20
25
Feburary 2001
Water Elevation (m)
3
2
1
0
−1
5
10
15
20
25
30
March 2001
ECOMSED
DSM II
Data

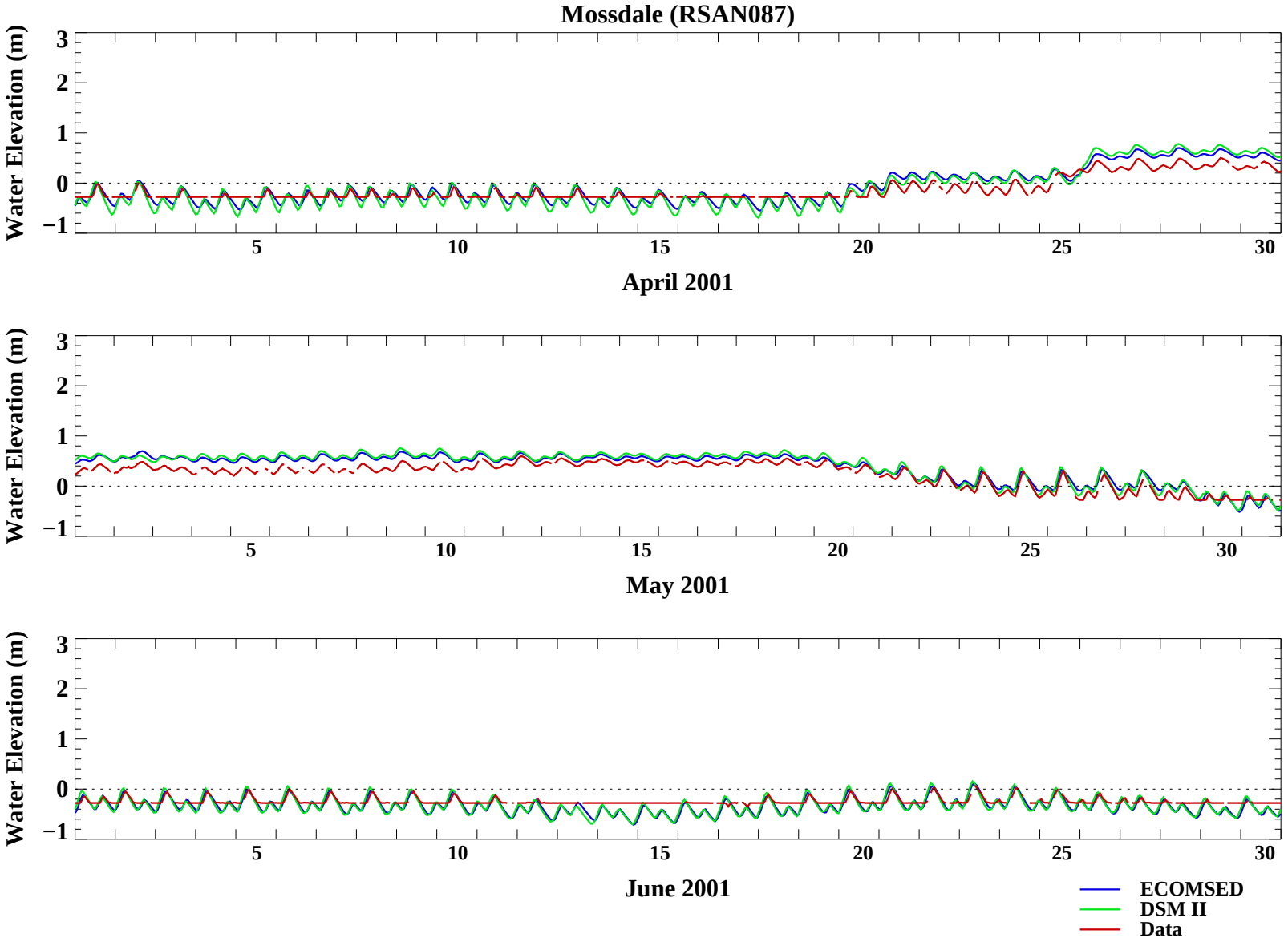
Mossdale (RSAN087)
Water Elevation (m)
3
2
1
0
−1
5
10
15
20
25
30
April 2001
May 2001
June 2001
ECOMSED
DSM II
Data

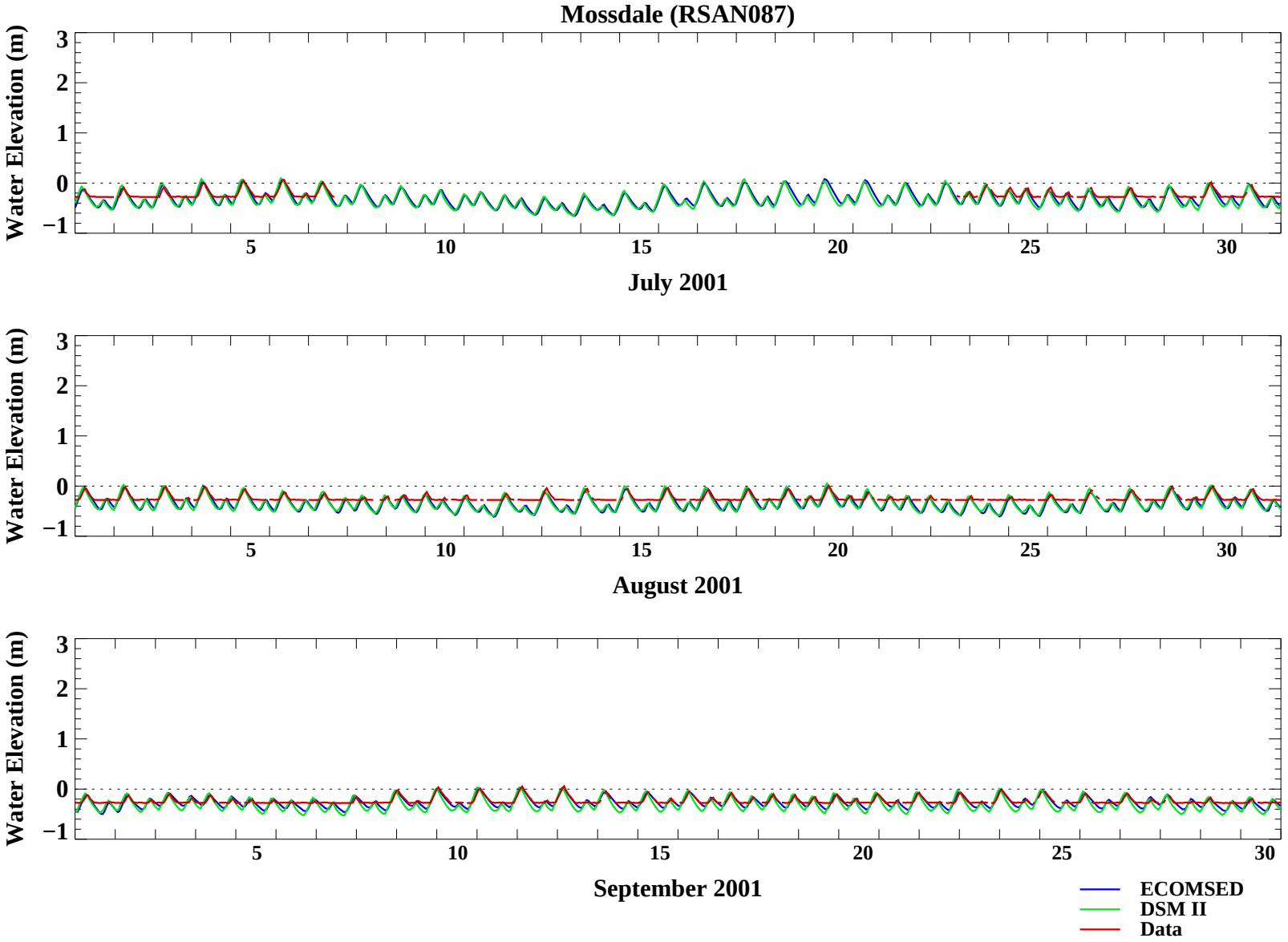
Mossdale (RSAN087)
Water Elevation (m)
3
2
1
0
−1
5
10
15
20
25
30
July 2001
Water Elevation (m)
August 2001
Water Elevation (m)
September 2001
ECOMSED
DSM II
Data

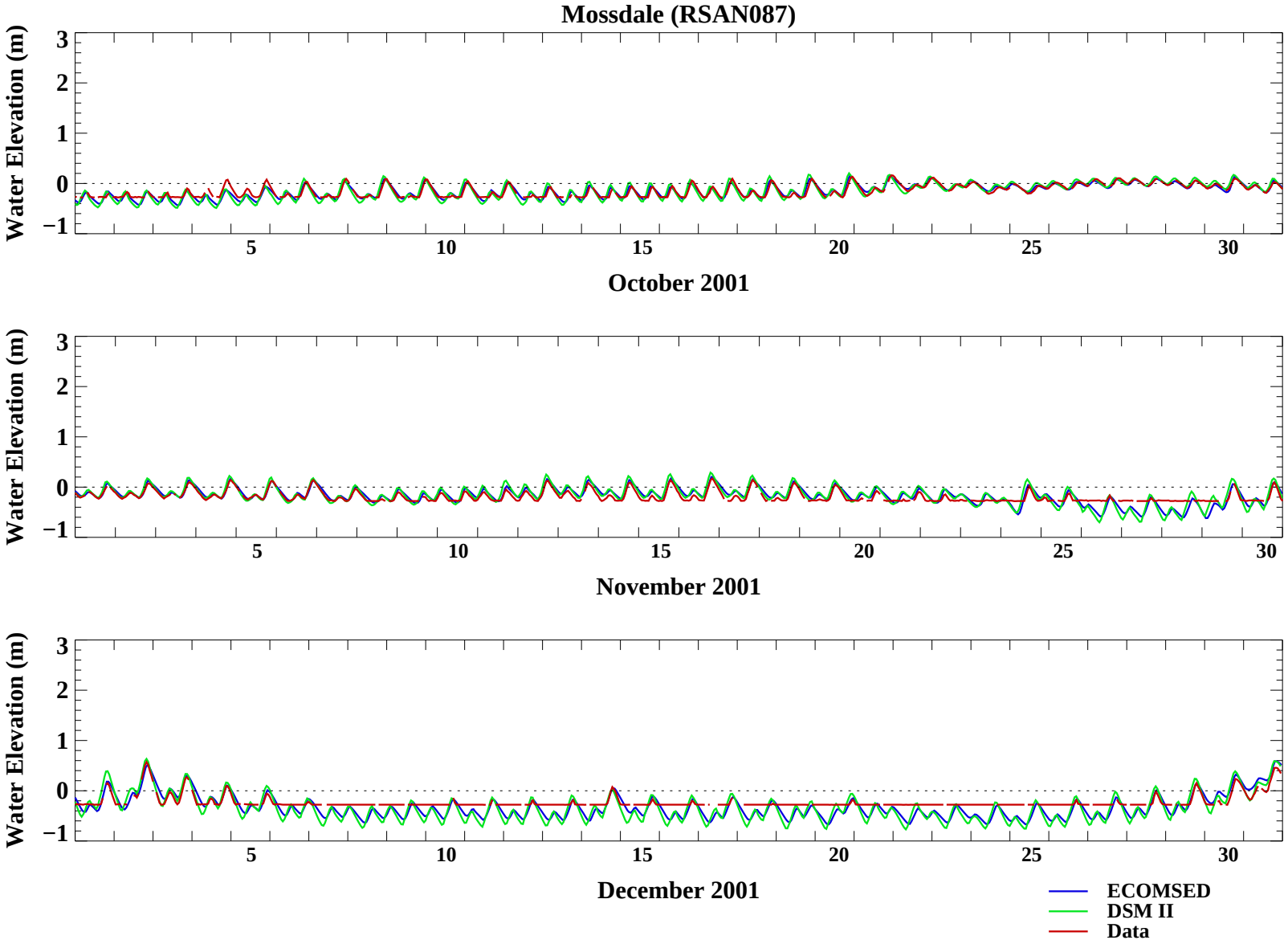
Mossdale (RSAN087)
Water Elevation (m)
3
2
1
0
−1
5
10
15
20
25
30
October 2001
November 2001
December 2001
ECOMSED
DSM II
Data

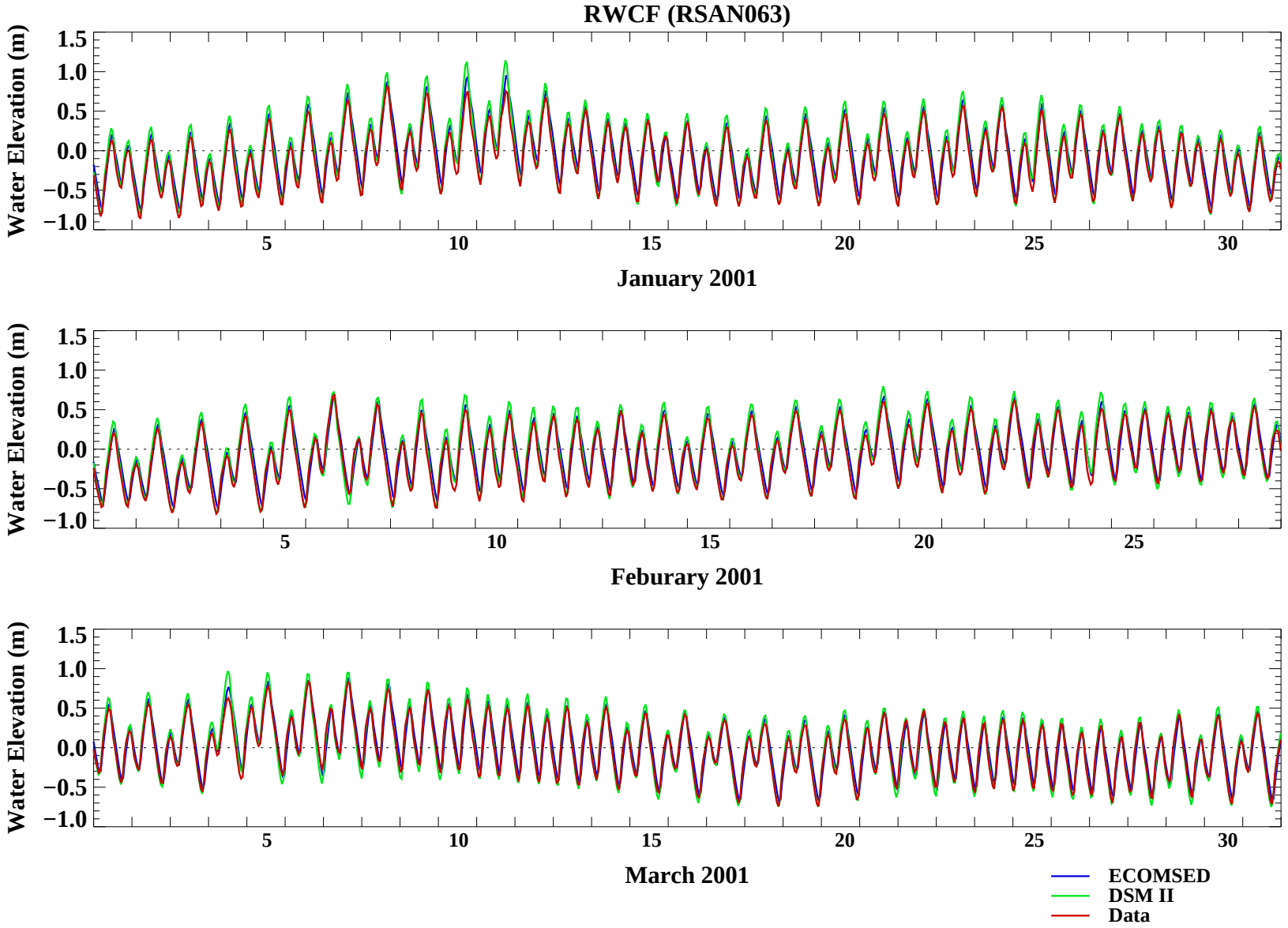
RWCF (RSAN063)
Water Elevation (m)
1.5
1.0
0.5
0.0
−0.5
−1.0
5
10
15
20
25
30
January 2001
Water Elevation (m)
Feburary 2001
Water Elevation (m)
March 2001
ECOMSED
DSM II
Data

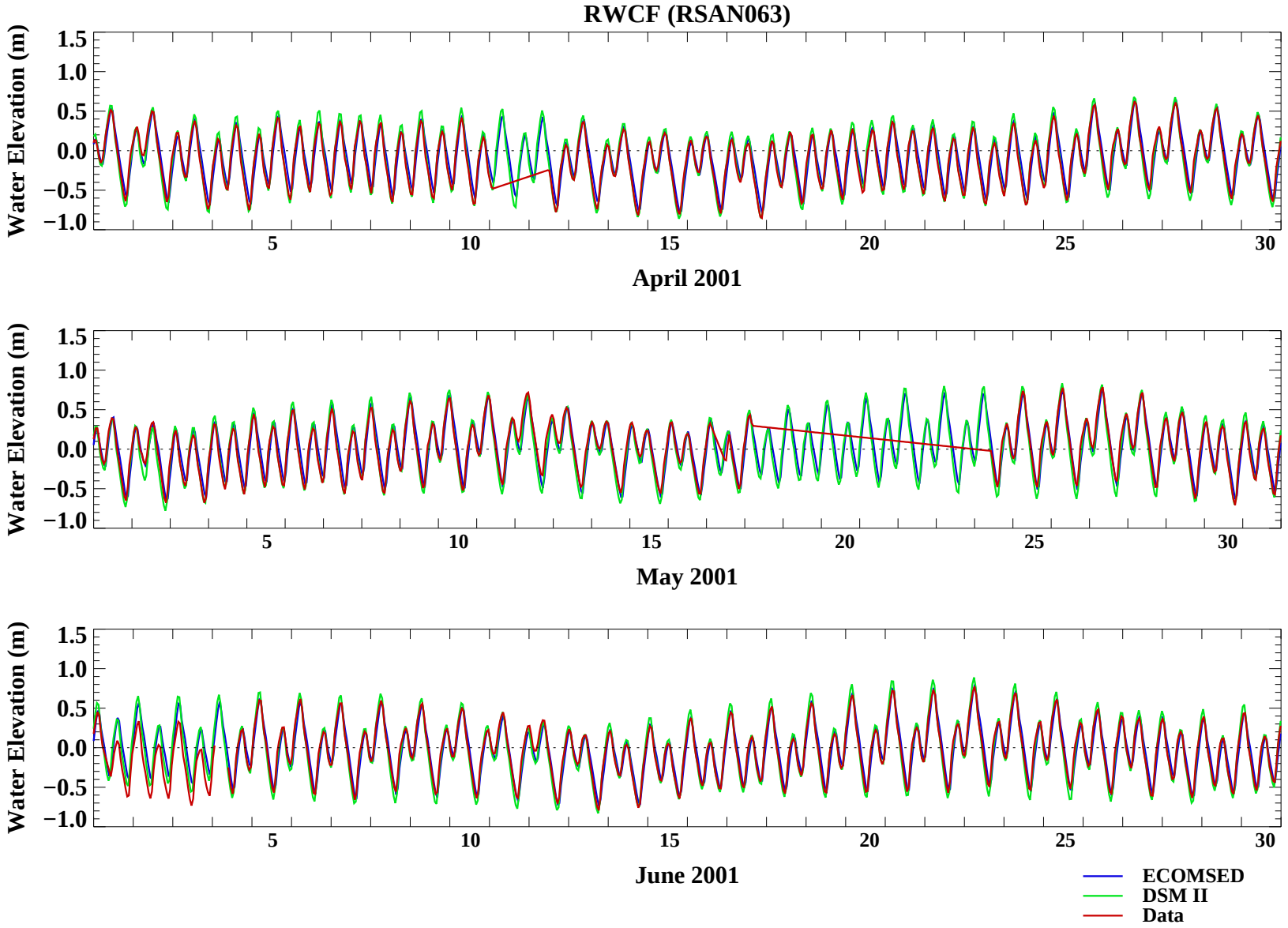
RWCF (RSAN063)
Water Elevation (m)
1.5
1.0
0.5
0.0
−0.5
−1.0
5
10
15
20
25
30
April 2001
May 2001
June 2001
ECOMSED
DSM II
Data

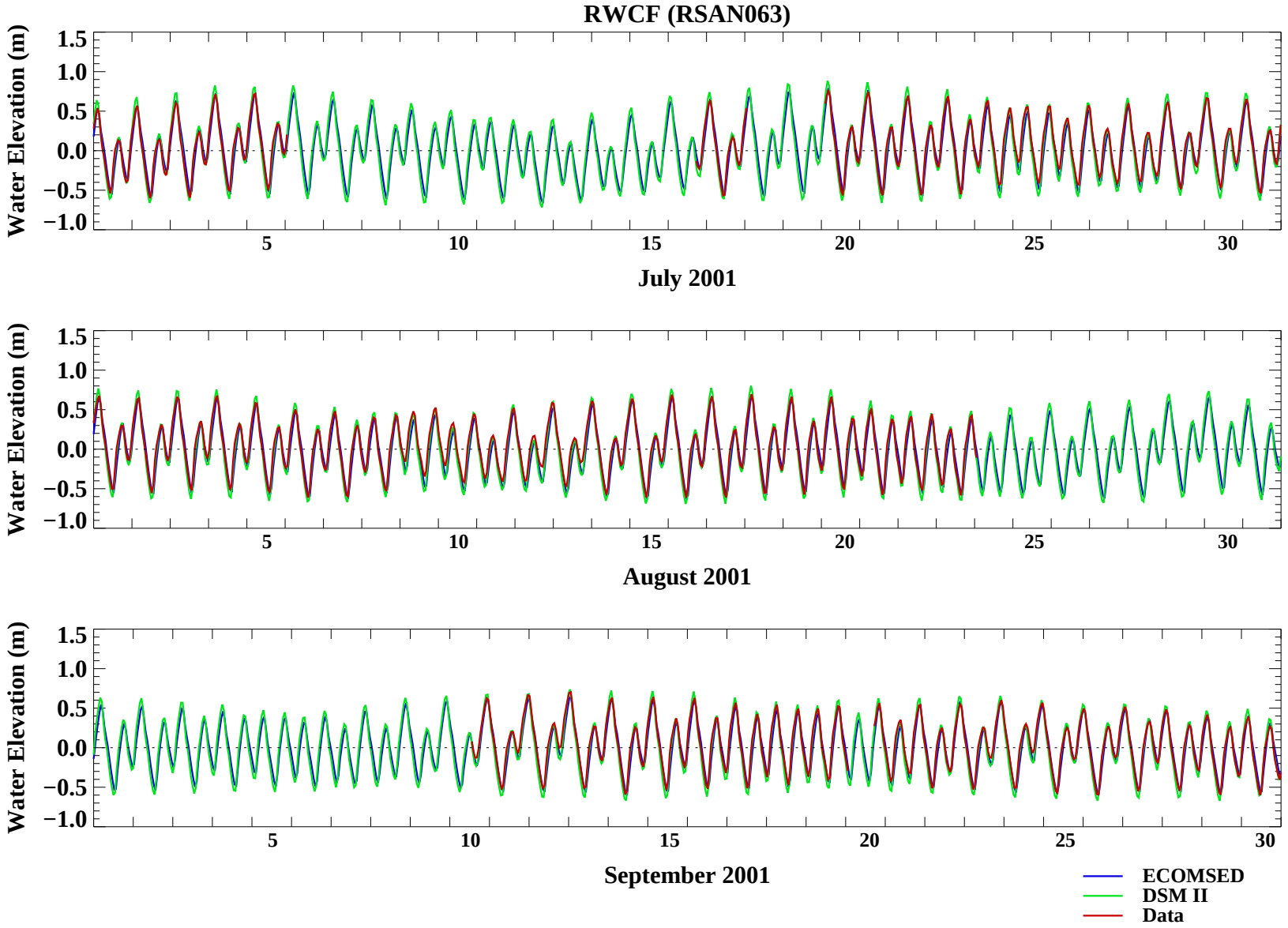
RWCF (RSAN063)
Water Elevation (m)
1.5
1.0
0.5
0.0
−0.5
−1.0
5
10
15
20
25
30
July 2001
August 2001
September 2001
ECOMSED
DSM II
Data

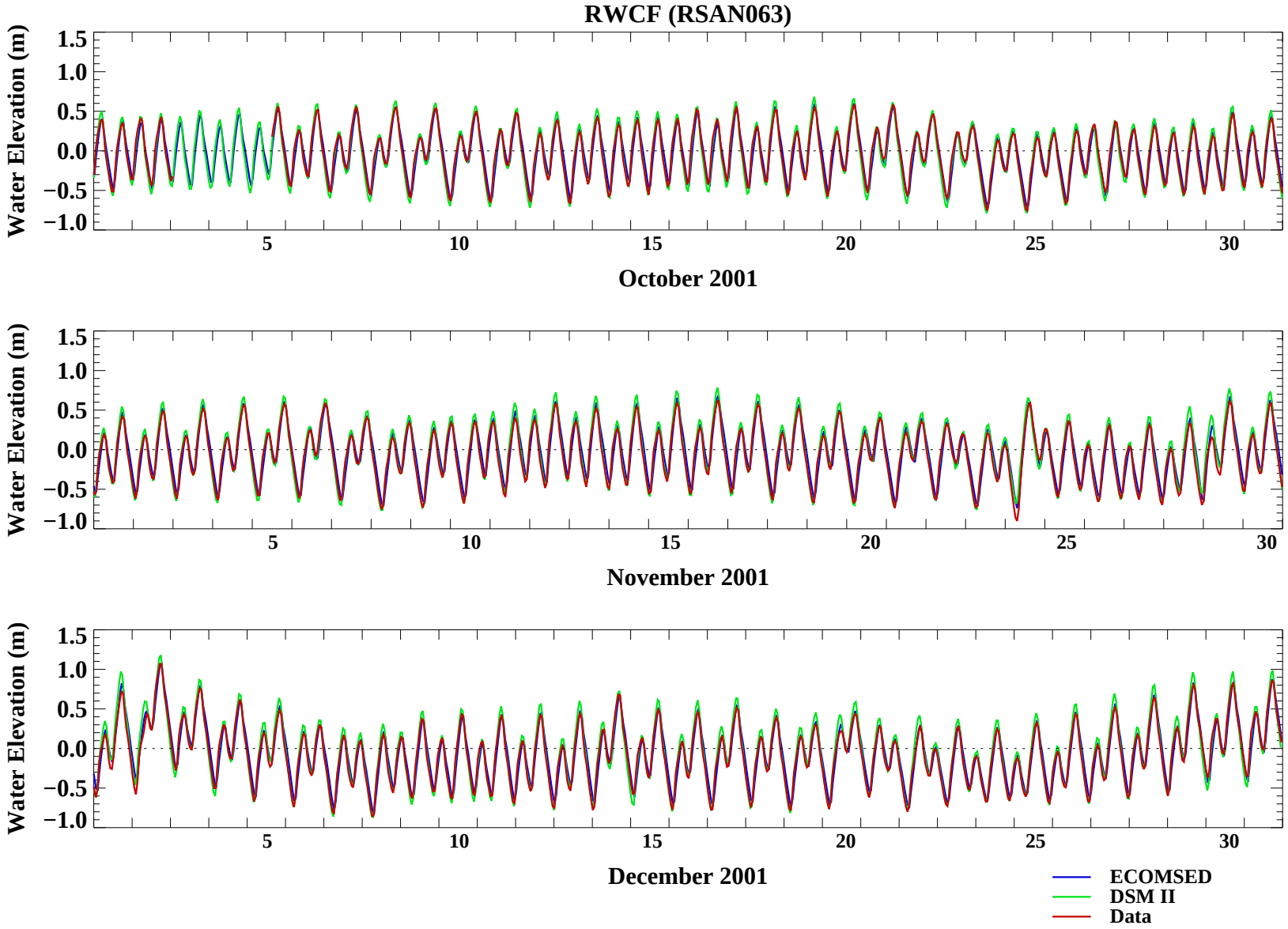
RWCF (RSAN063)
Water Elevation (m)
1.5
1.0
0.5
0.0
−0.5
−1.0
5
10
15
20
25
30
October 2001
November 2001
December 2001
ECOMSED
DSM II
Data

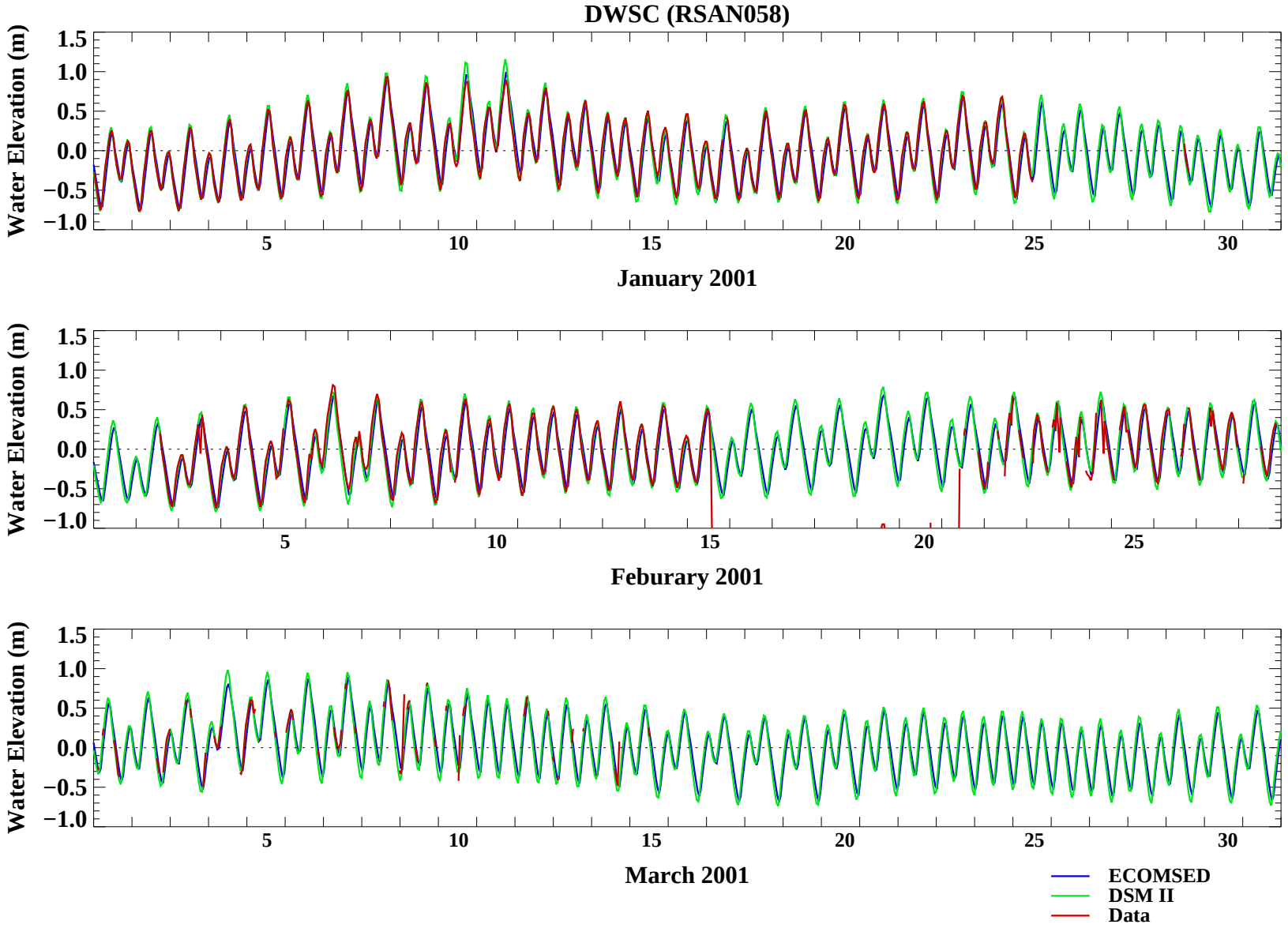
DWSC (RSAN058)
Water Elevation (m)
1.5
1.0
0.5
0.0
−0.5
−1.0
5
10
15
20
25
30
January 2001
Water Elevation (m)
Feburary 2001
Water Elevation (m)
March 2001
ECOMSED
DSM II
Data

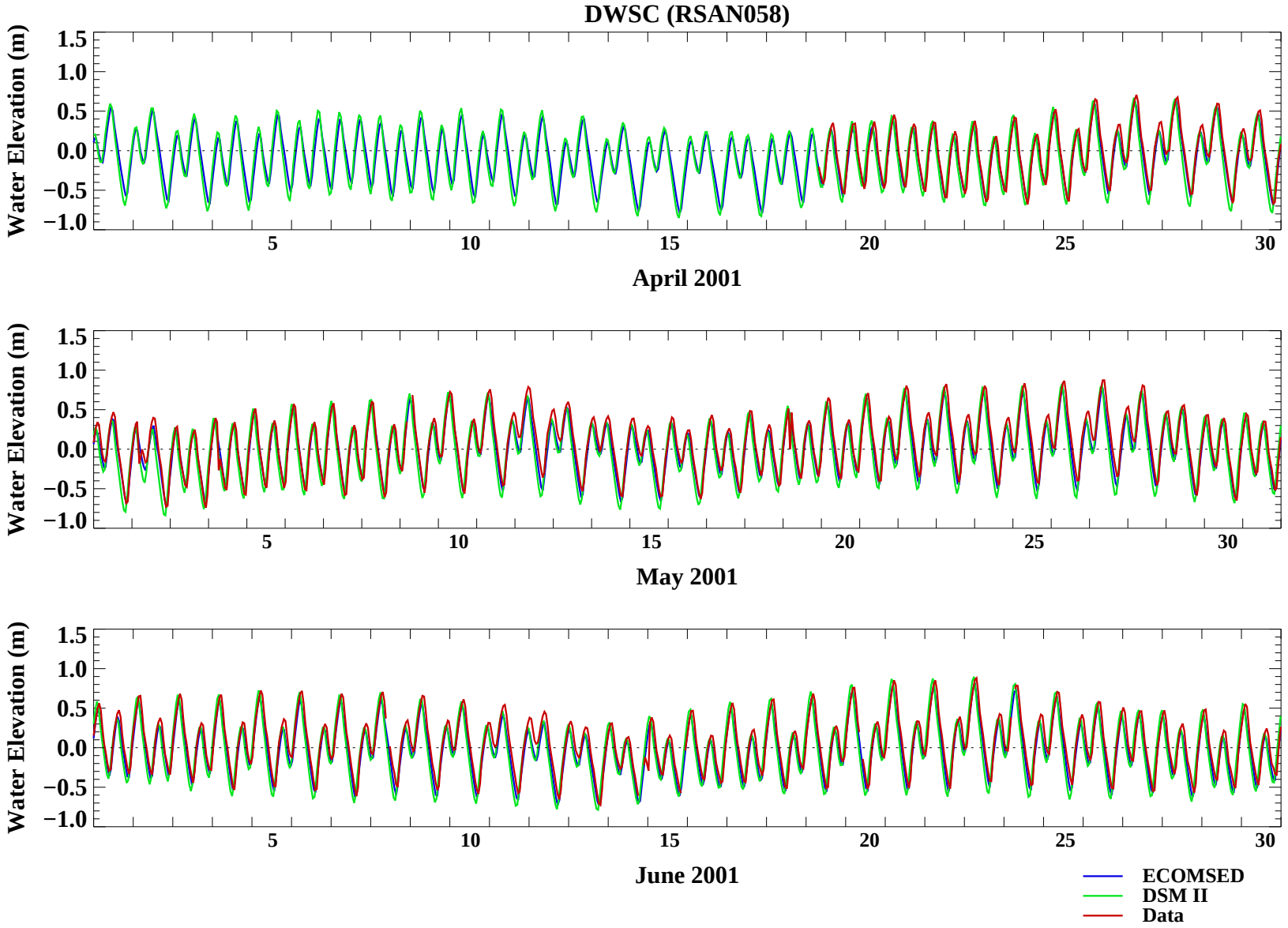
DWSC (RSAN058)
Water Elevation (m)
1.5
1.0
0.5
0.0
−0.5
−1.0
5
10
15
20
25
30
April 2001
May 2001
June 2001
ECOMSED
DSM II
Data

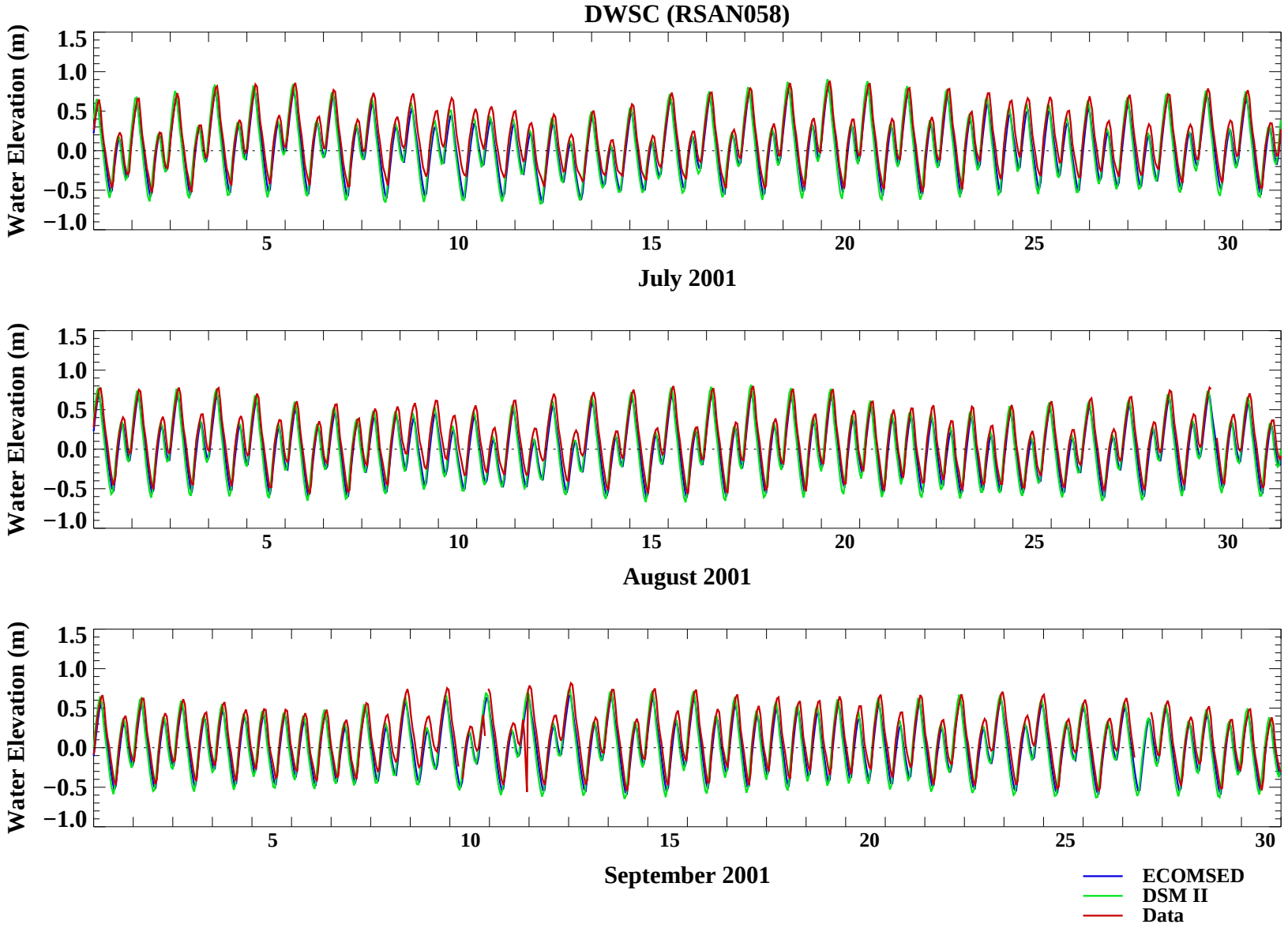
DWSC (RSAN058)
Water Elevation (m)
1.5
1.0
0.5
0.0
−0.5
−1.0
5
10
15
20
25
30
July 2001
August 2001
September 2001
ECOMSED
DSM II
Data

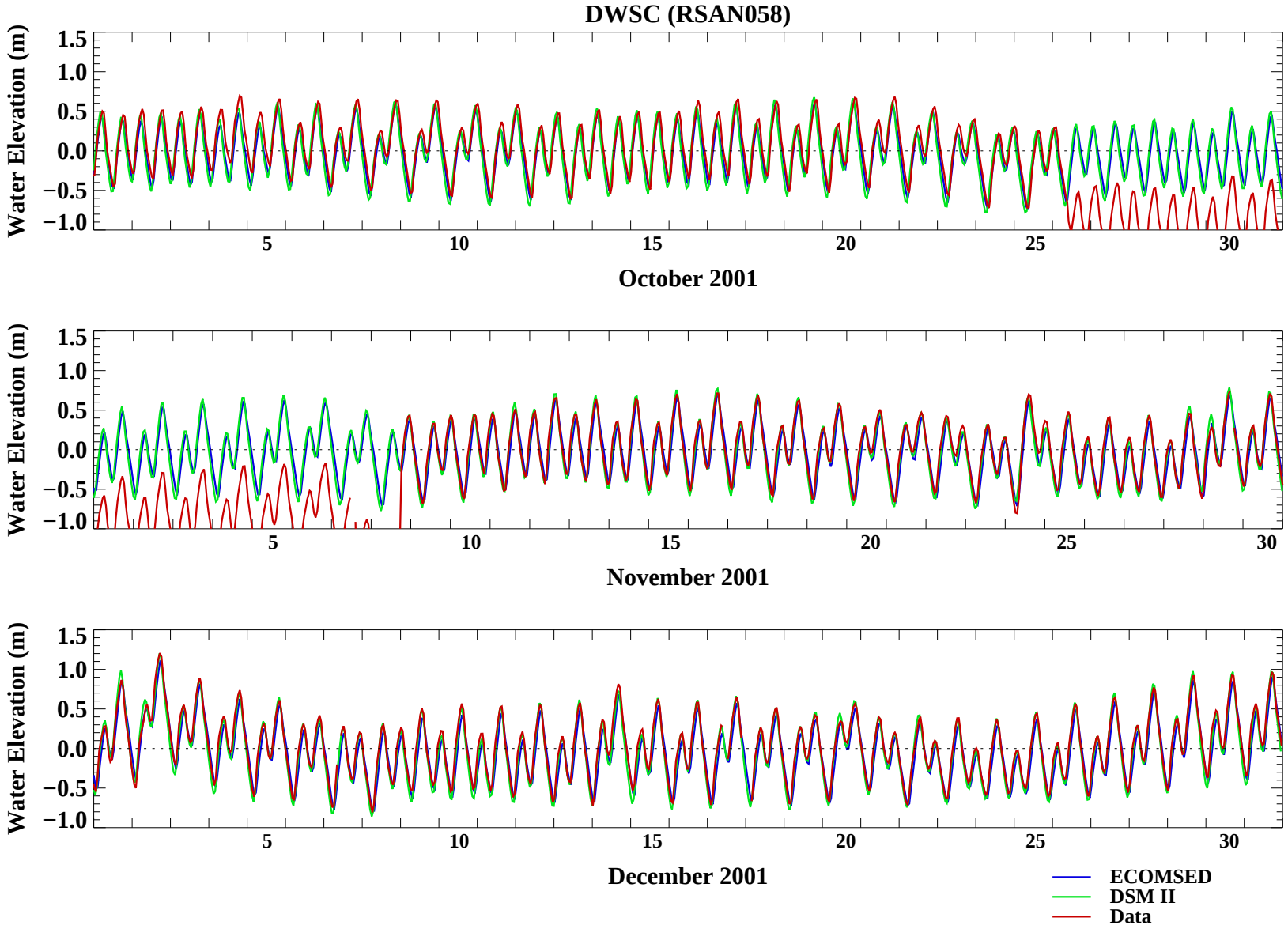
DWSC (RSAN058)
Water Elevation (m)
1.5
1.0
0.5
0.0
−0.5
−1.0
5
10
15
20
25
30
October 2001
November 2001
December 2001
ECOMSED
DSM II
Data

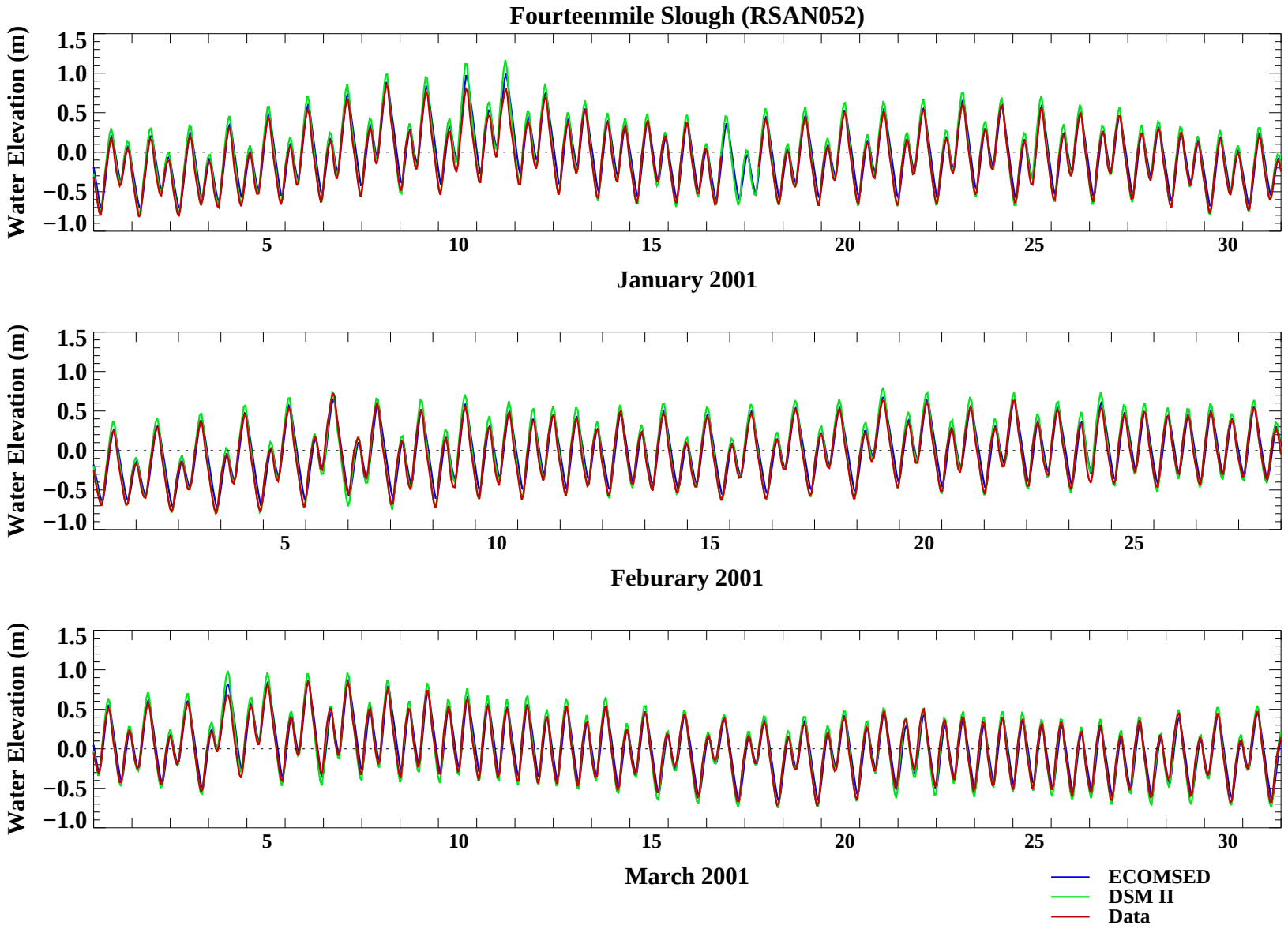
Fourteenmile Slough (RSAN052)
Water Elevation (m)
1.5
1.0
0.5
0.0
−0.5
−1.0
5
10
15
20
25
30
January 2001
Water Elevation (m)
Feburary 2001
Water Elevation (m)
March 2001
ECOMSED
DSM II
Data

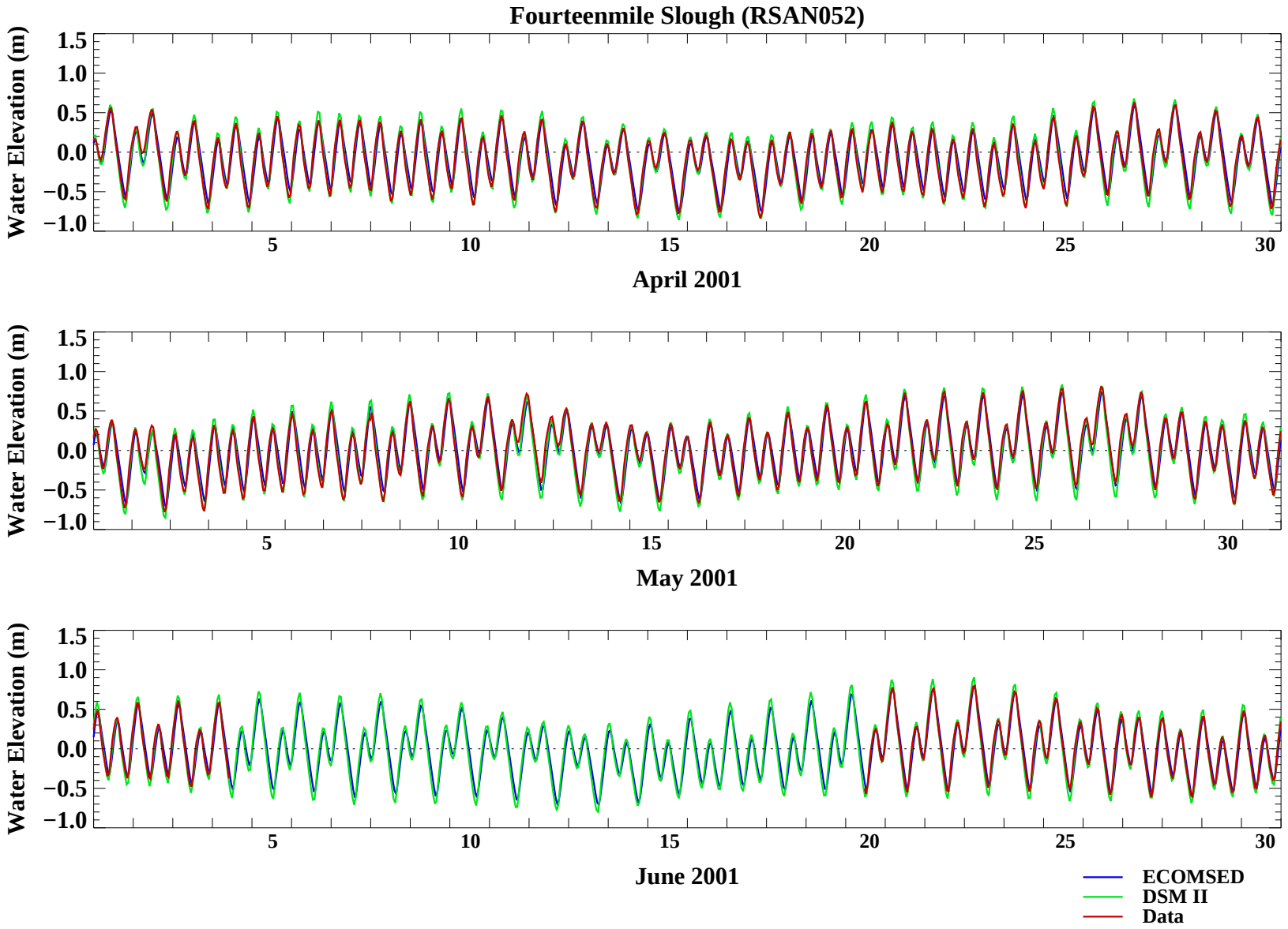
Fourteenmile Slough (RSAN052)
Water Elevation (m)
1.5
1.0
0.5
0.0
−0.5
−1.0
5
10
15
20
25
30
April 2001
May 2001
June 2001
ECOMSED
DSM II
Data

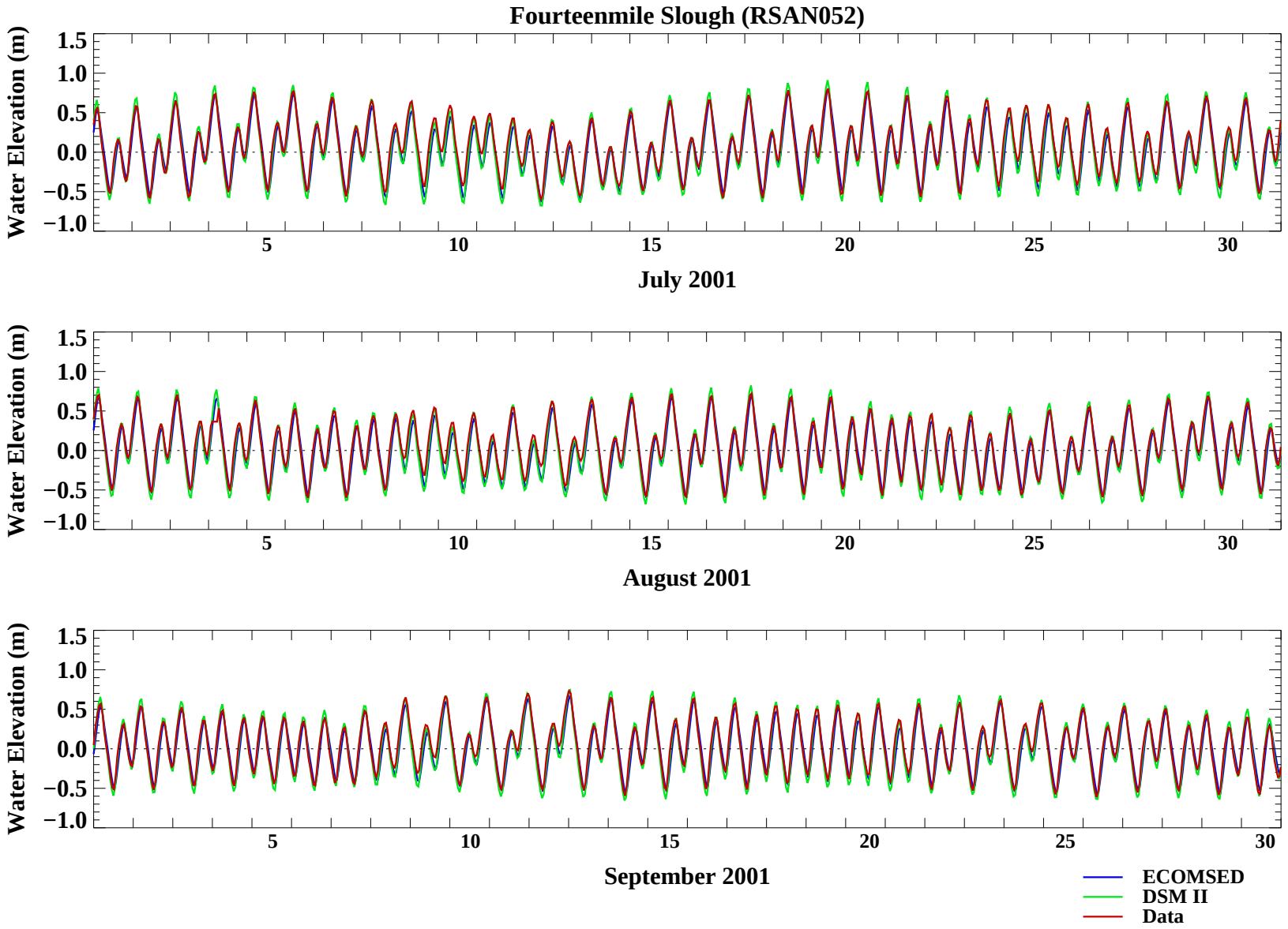
Fourteenmile Slough (RSAN052)
Water Elevation (m)
1.5
1.0
0.5
0.0
−0.5
−1.0
5
10
15
20
25
30
July 2001
August 2001
September 2001
ECOMSED
DSM II
Data

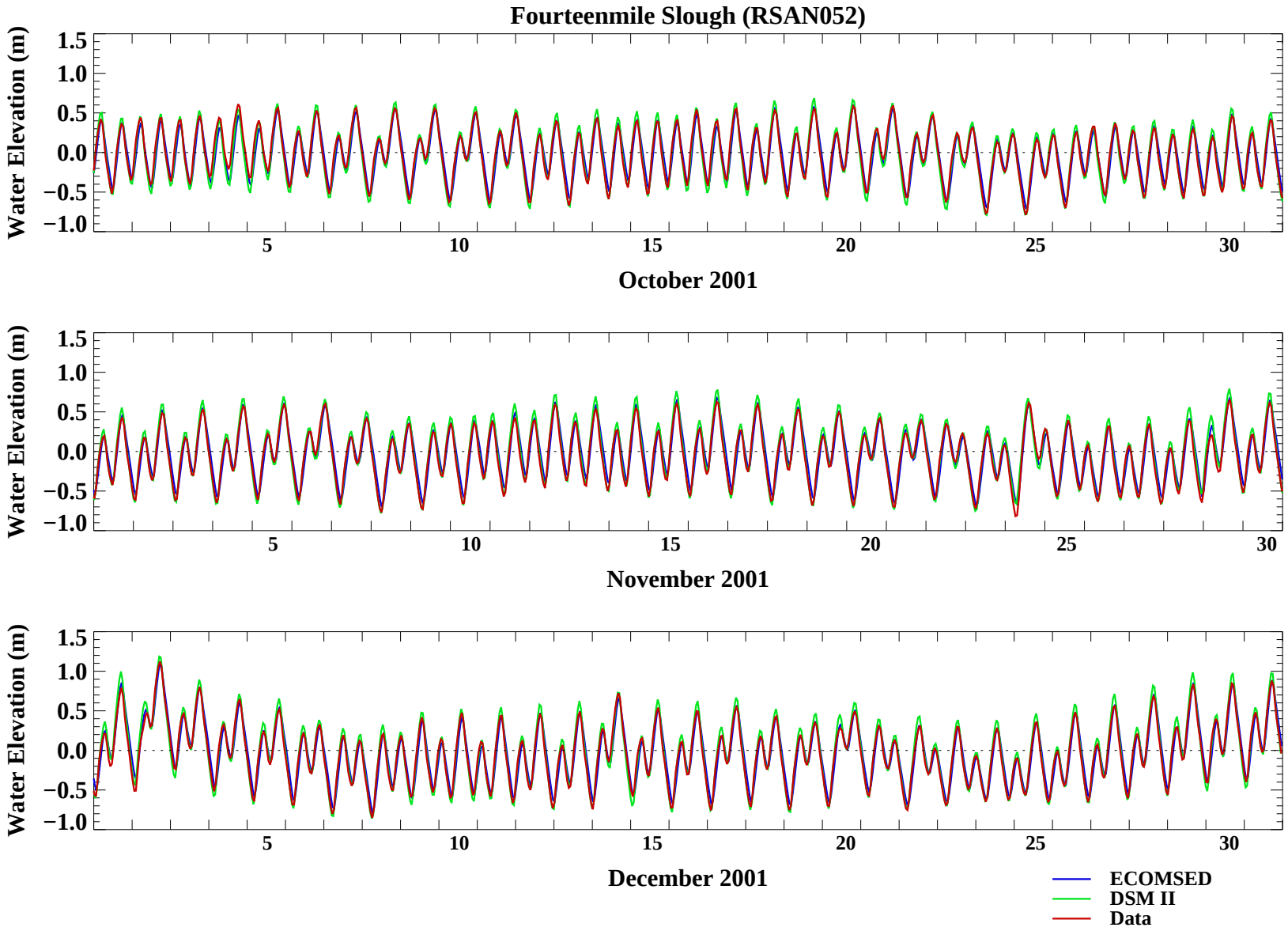
Fourteenmile Slough (RSAN052)
Water Elevation (m)
1.5
1.0
0.5
0.0
−0.5
−1.0
5
10
15
20
25
30
October 2001
November 2001
December 2001
ECOMSED
DSM II
Data

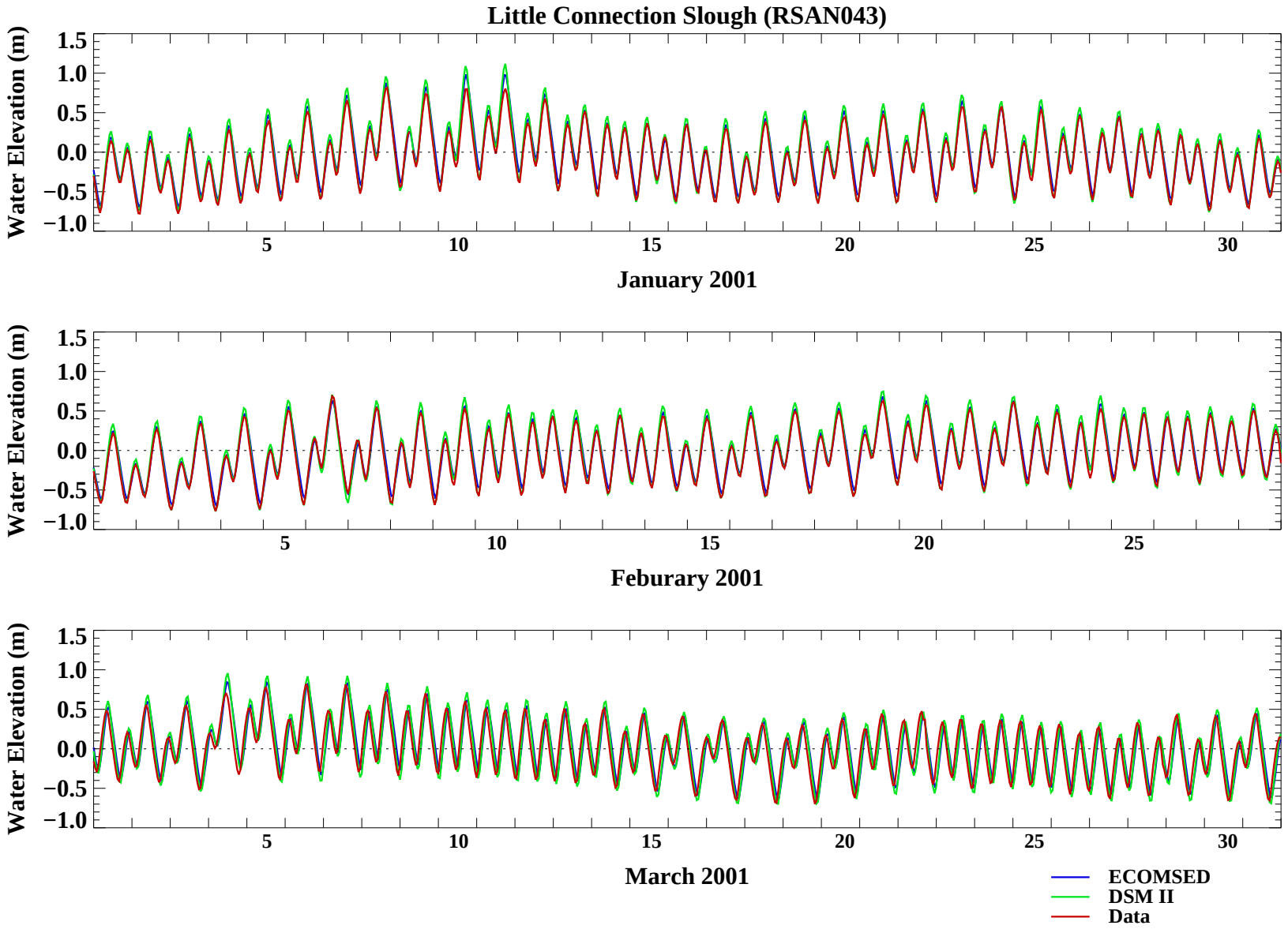
Little Connection Slough (RSAN043)
Water Elevation (m)
1.5
1.0
0.5
0.0
−0.5
−1.0
5
10
15
20
25
30
January 2001
Water Elevation (m)
Feburary 2001
Water Elevation (m)
March 2001
ECOMSED
DSM II
Data

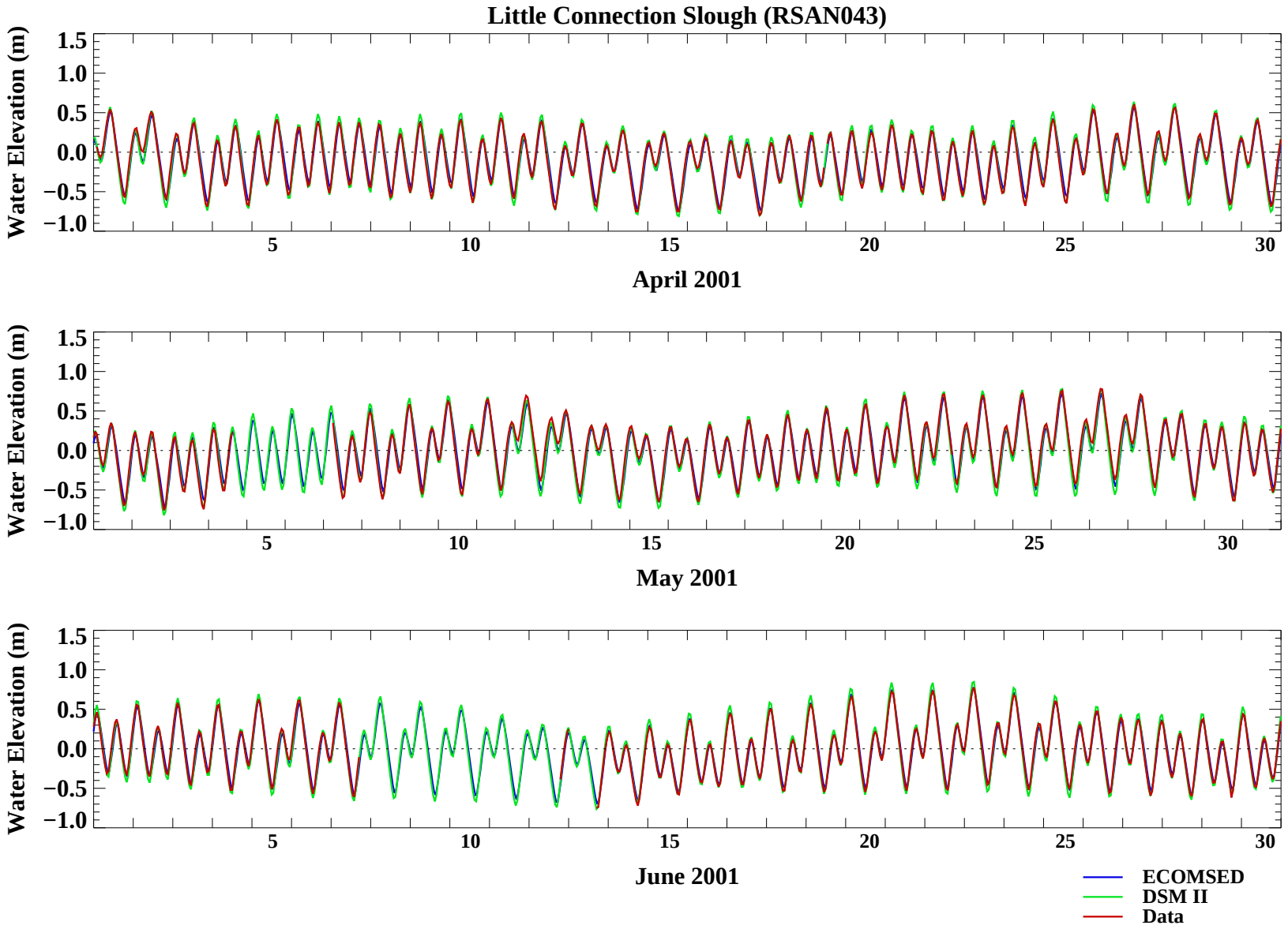
Little Connection Slough (RSAN043)
Water Elevation (m)
1.5
1.0
0.5
0.0
−0.5
−1.0
5
10
15
20
25
30
April 2001
May 2001
June 2001
ECOMSED
DSM II
Data

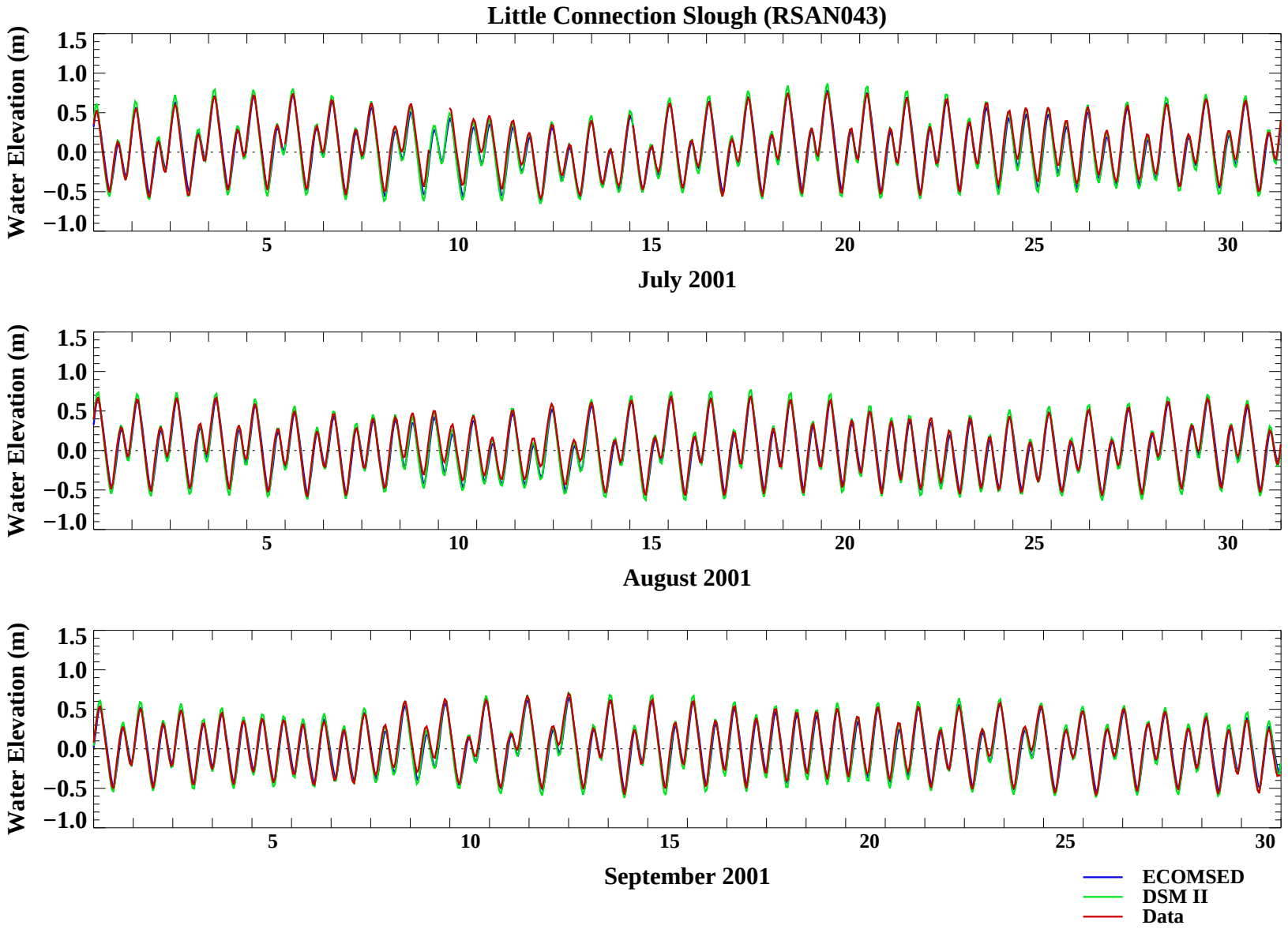
Little Connection Slough (RSAN043)
Water Elevation (m)
1.5
1.0
0.5
0.0
−0.5
−1.0
5
10
15
20
25
30
July 2001
August 2001
September 2001
ECOMSED
DSM II
Data

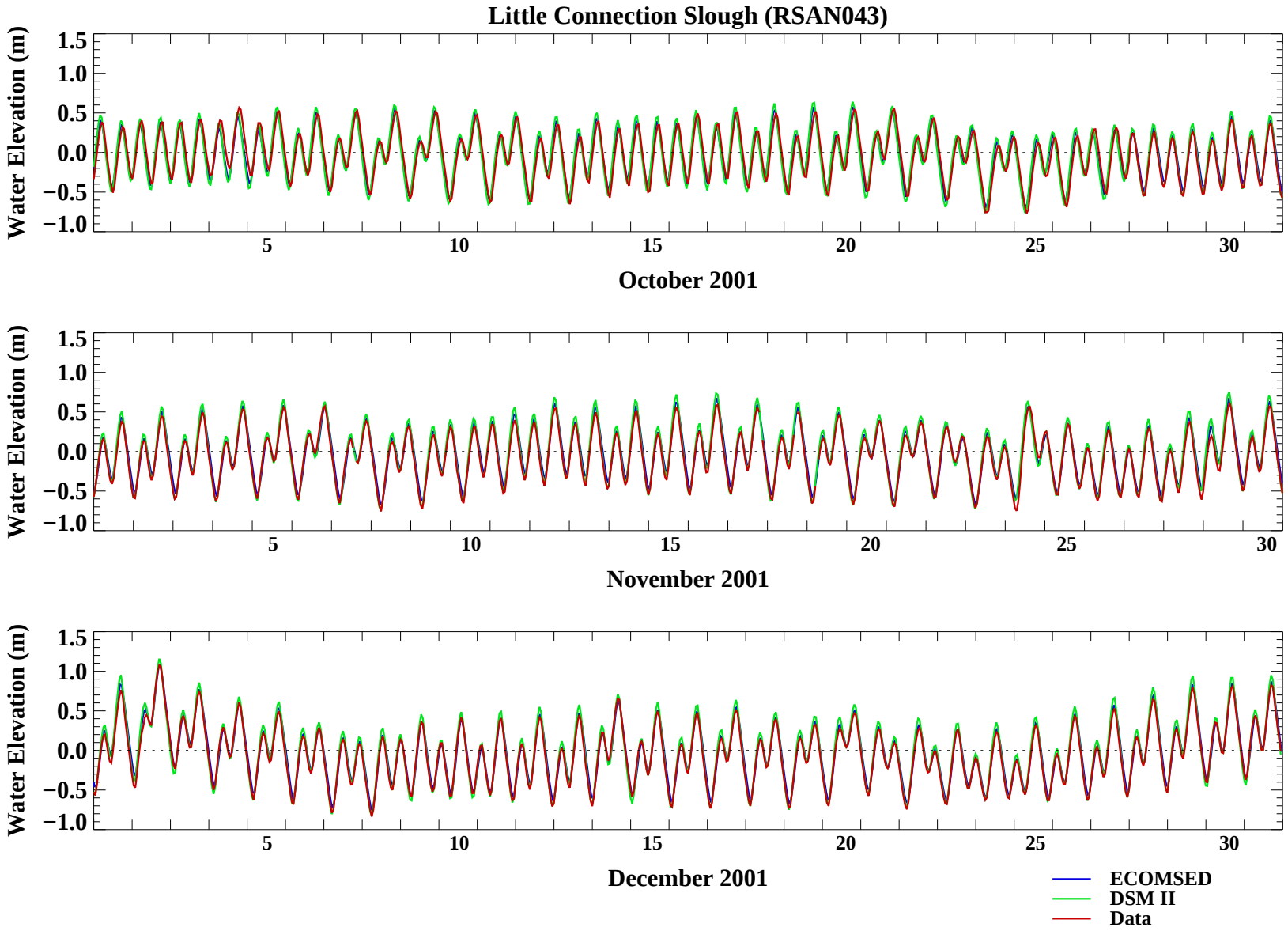
Little Connection Slough (RSAN043)
Water Elevation (m)
1.5
1.0
0.5
0.0
−0.5
−1.0
5
10
15
20
25
30
October 2001
November 2001
December 2001
ECOMSED
DSM II
Data

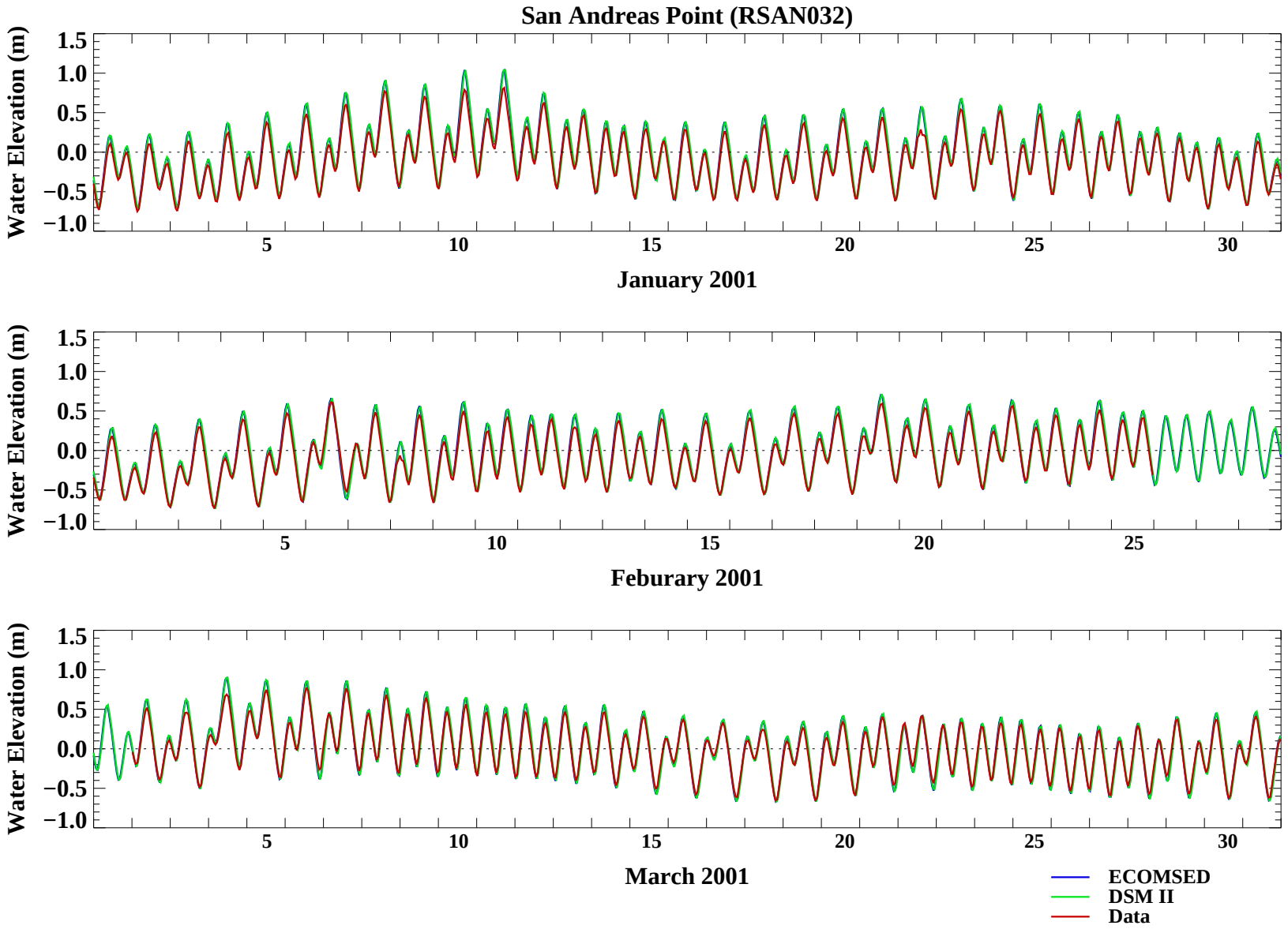
San Andreas Point (RSAN032)
Water Elevation (m)
1.5
1.0
0.5
0.0
−0.5
−1.0
5
10
15
20
25
30
January 2001
Water Elevation (m)
Feburary 2001
Water Elevation (m)
March 2001
ECOMSED
DSM II
Data

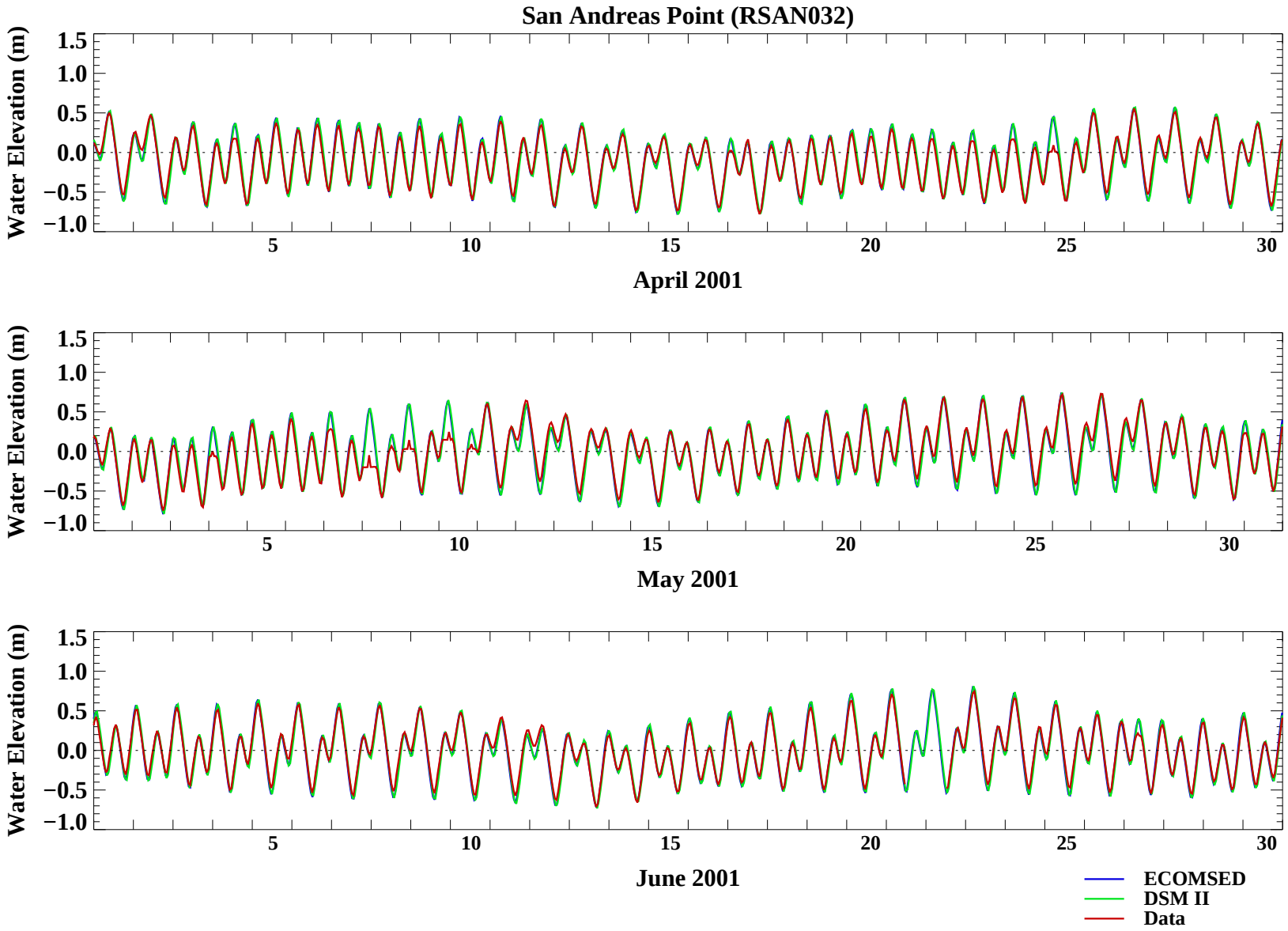
San Andreas Point (RSAN032)
Water Elevation (m)
1.5
1.0
0.5
0.0
−0.5
−1.0
5
10
15
20
25
30
April 2001
May 2001
June 2001
ECOMSED
DSM II
Data

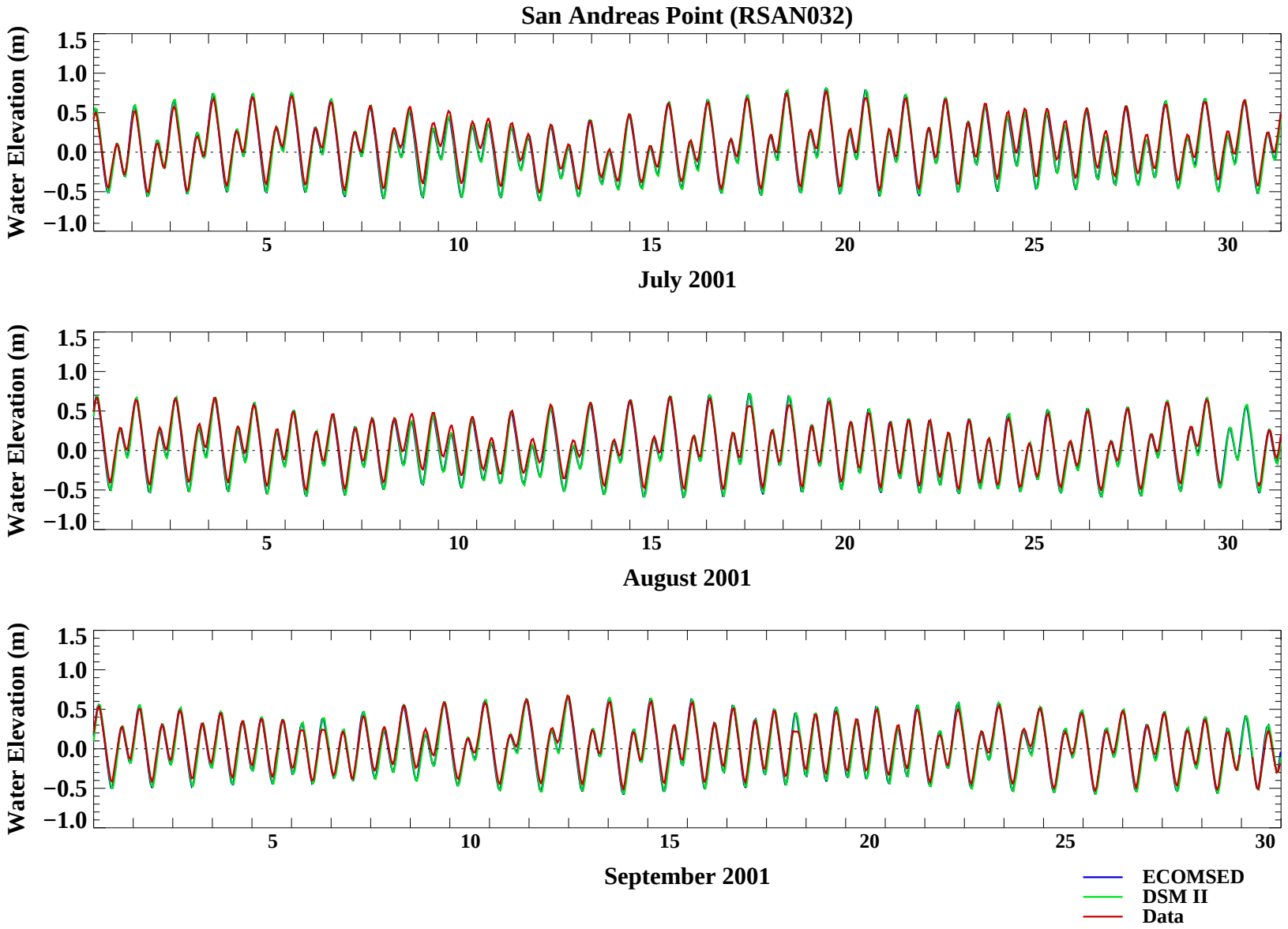
San Andreas Point (RSAN032)
Water Elevation (m)
1.5
1.0
0.5
0.0
−0.5
−1.0
5
10
15
20
25
30
July 2001
August 2001
September 2001
ECOMSED
DSM II
Data

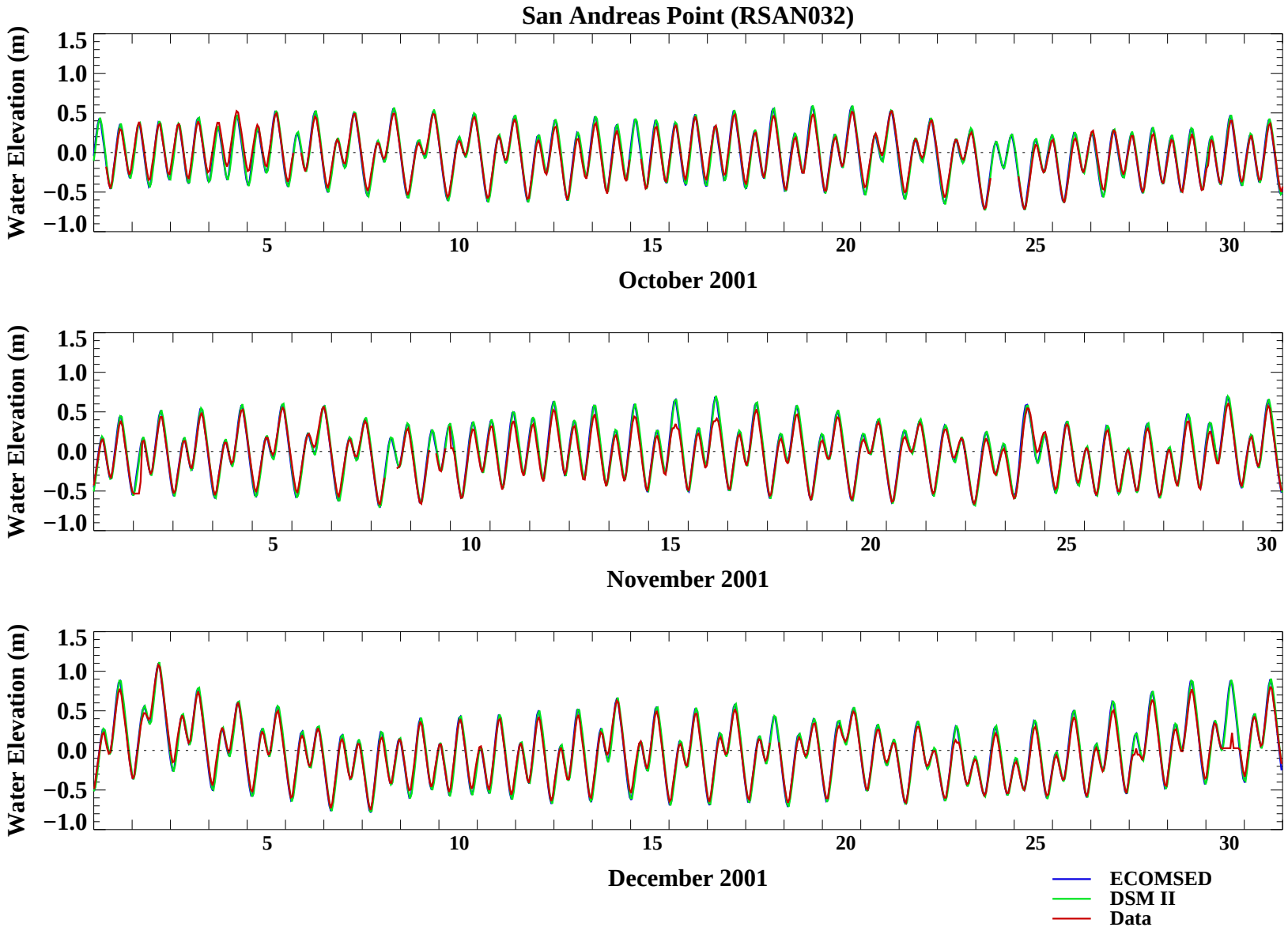
San Andreas Point (RSAN032)
Water Elevation (m)
1.5
1.0
0.5
0.0
−0.5
−1.0
5
10
15
20
25
30
October 2001
November 2001
December 2001
ECOMSED
DSM II
Data

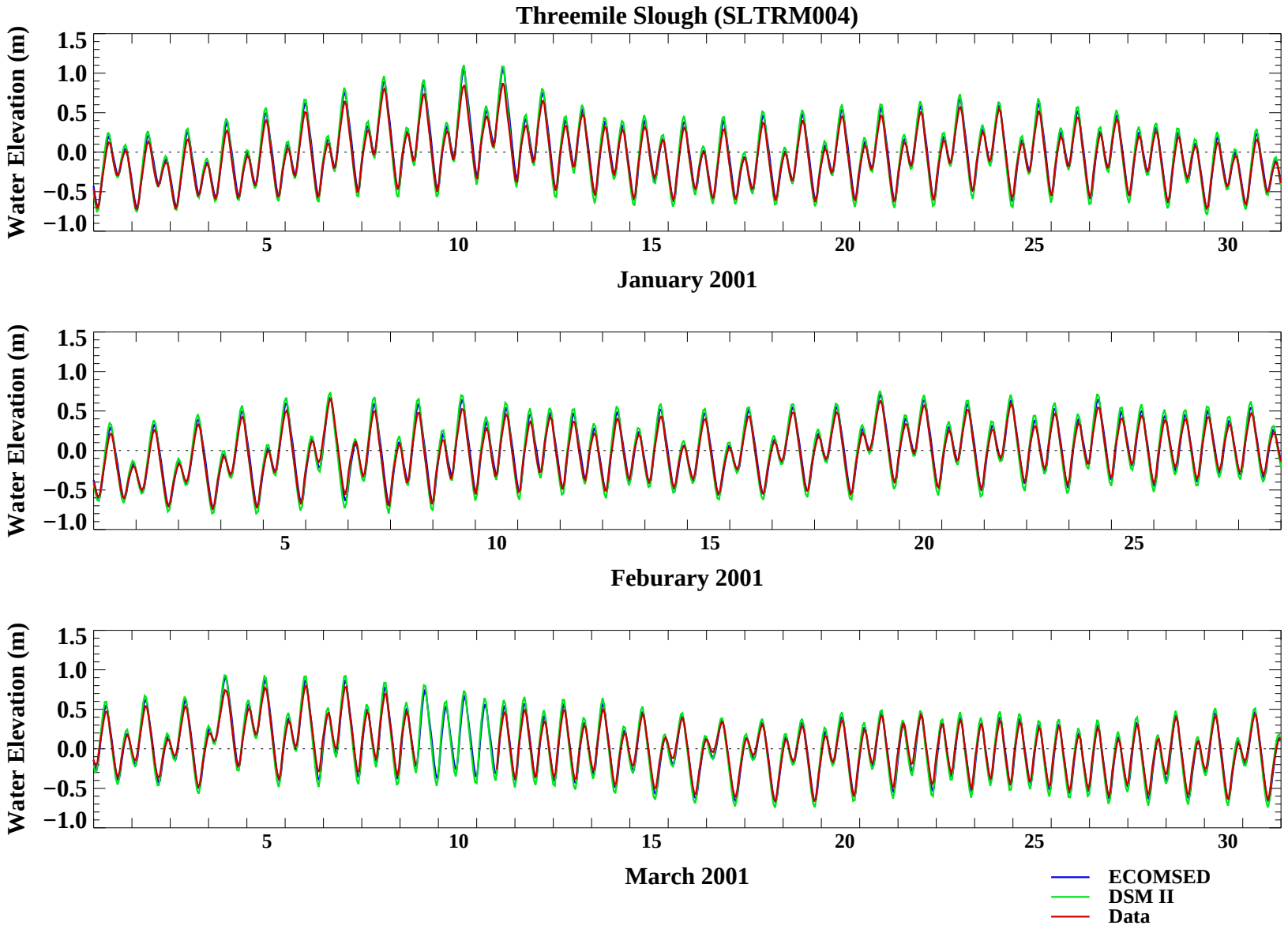
Threemile Slough (SLTRM004)
Water Elevation (m)
1.5
1.0
0.5
0.0
−0.5
−1.0
5
10
15
20
25
30
January 2001
Water Elevation (m)
Feburary 2001
Water Elevation (m)
March 2001
ECOMSED
DSM II
Data

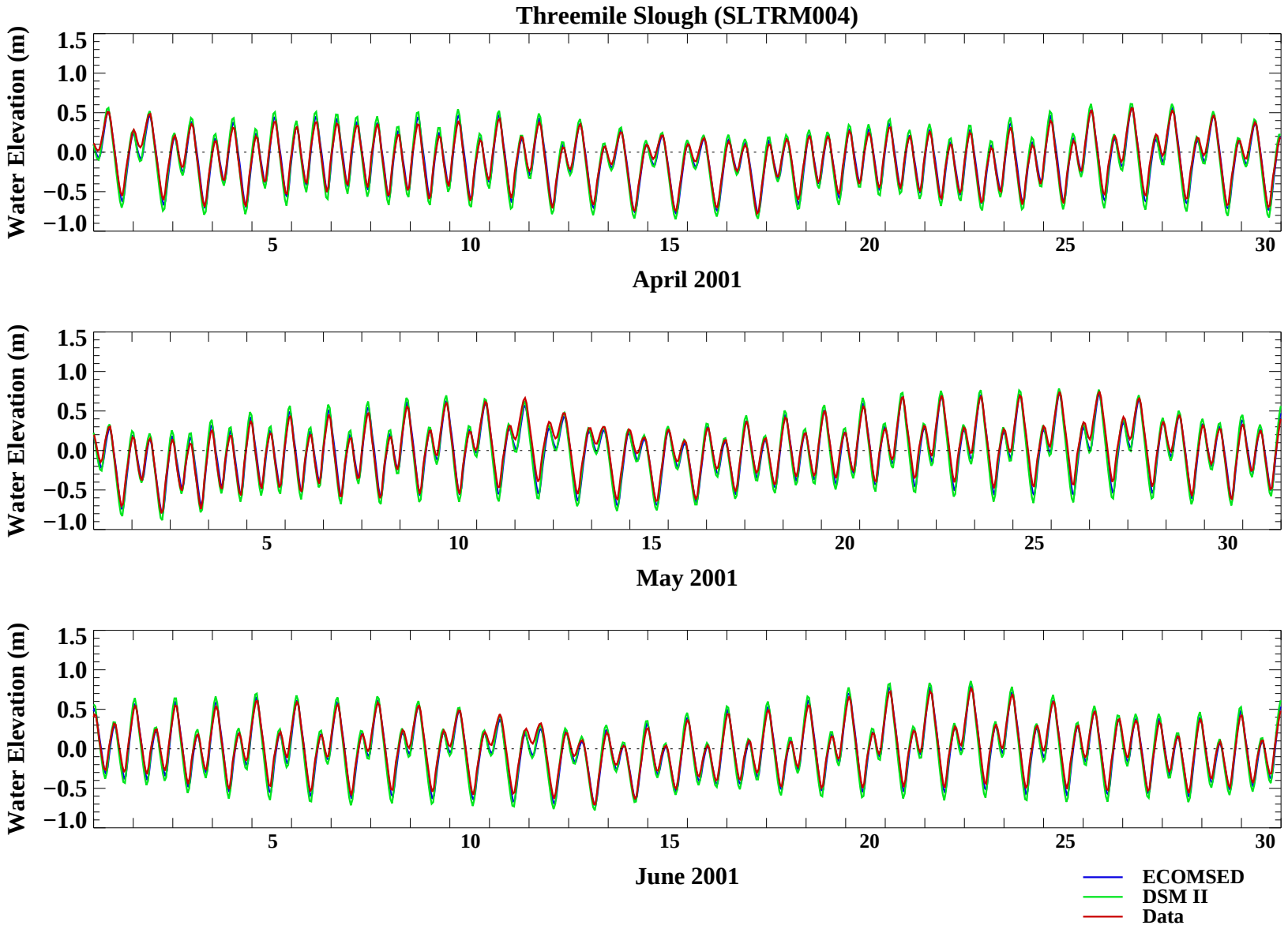
Threemile Slough (SLTRM004)
Water Elevation (m)
1.5
1.0
0.5
0.0
−0.5
−1.0
5
10
15
20
25
30
April 2001
May 2001
June 2001
ECOMSED
DSM II
Data

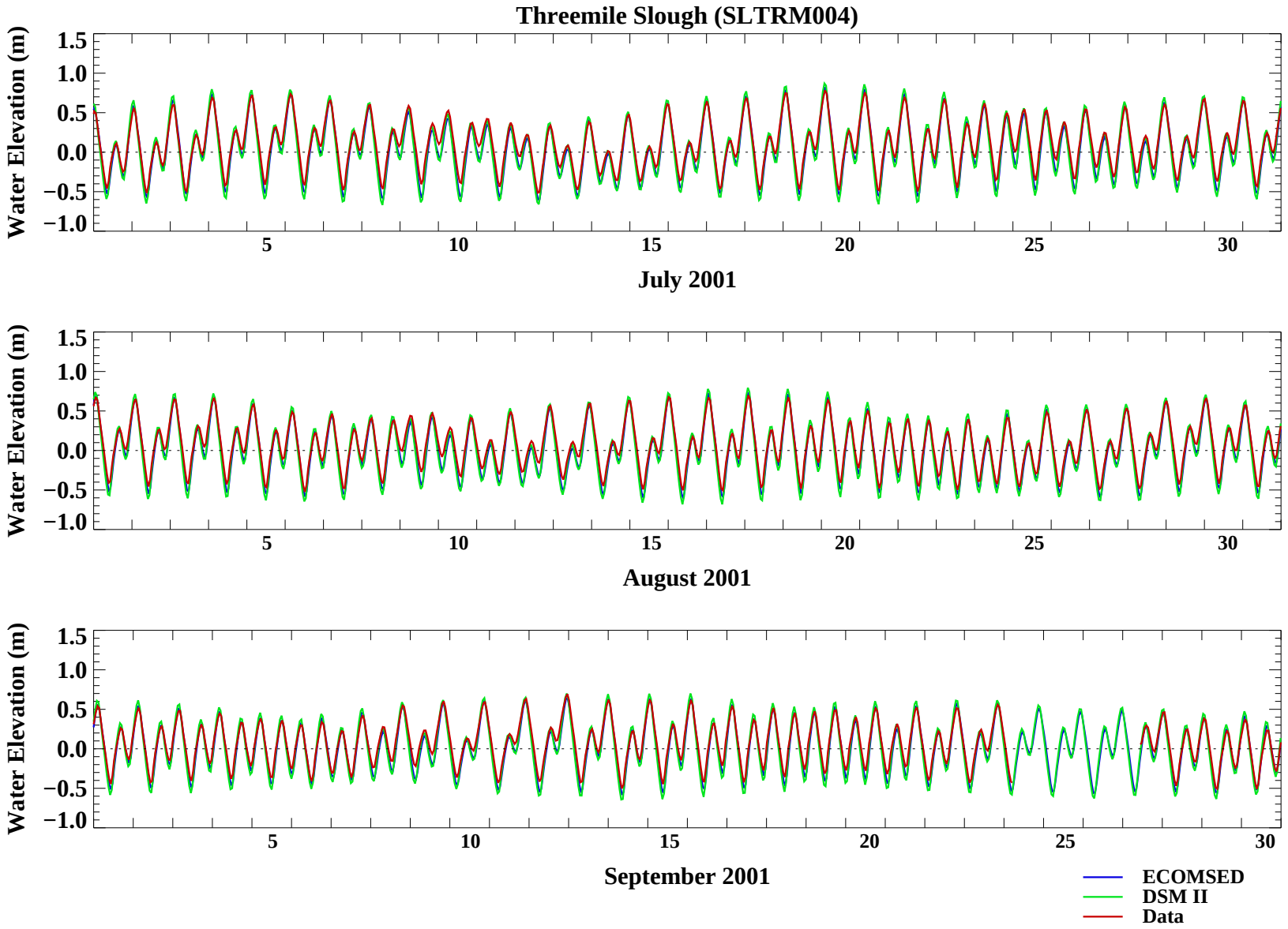
Threemile Slough (SLTRM004)
Water Elevation (m)
1.5
1.0
0.5
0.0
−0.5
−1.0
5
10
15
20
25
30
July 2001
August 2001
September 2001
ECOMSED
DSM II
Data

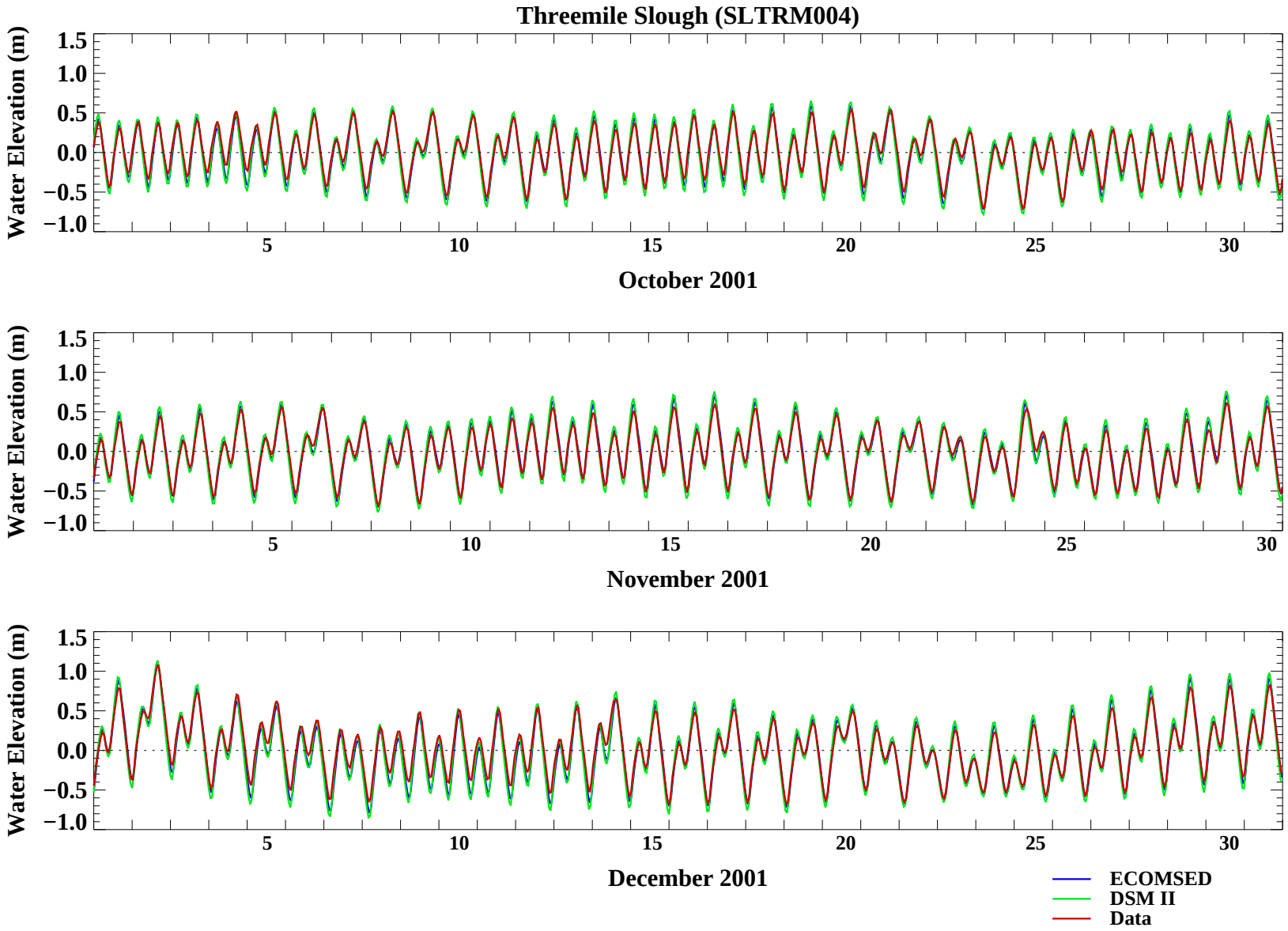
Threemile Slough (SLTRM004)
Water Elevation (m)
1.5
1.0
0.5
0.0
−0.5
−1.0
5
10
15
20
25
30
October 2001
November 2001
December 2001
ECOMSED
DSM II
Data

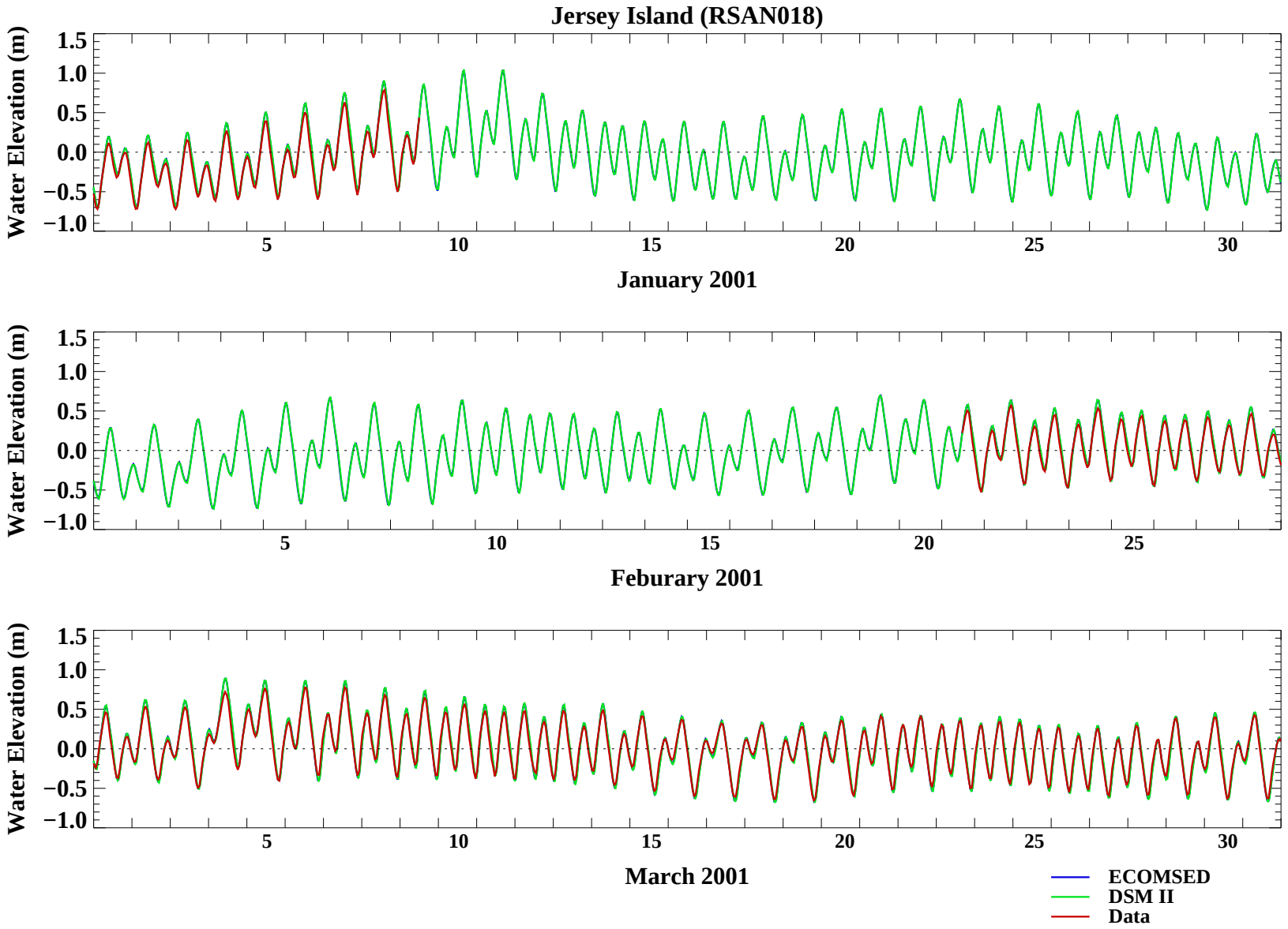
Jersey Island (RSAN018)
Water Elevation (m)
1.5
1.0
0.5
0.0
−0.5
−1.0
5
10
15
20
25
30
January 2001
Water Elevation (m)
Feburary 2001
Water Elevation (m)
March 2001
ECOMSED
DSM II
Data

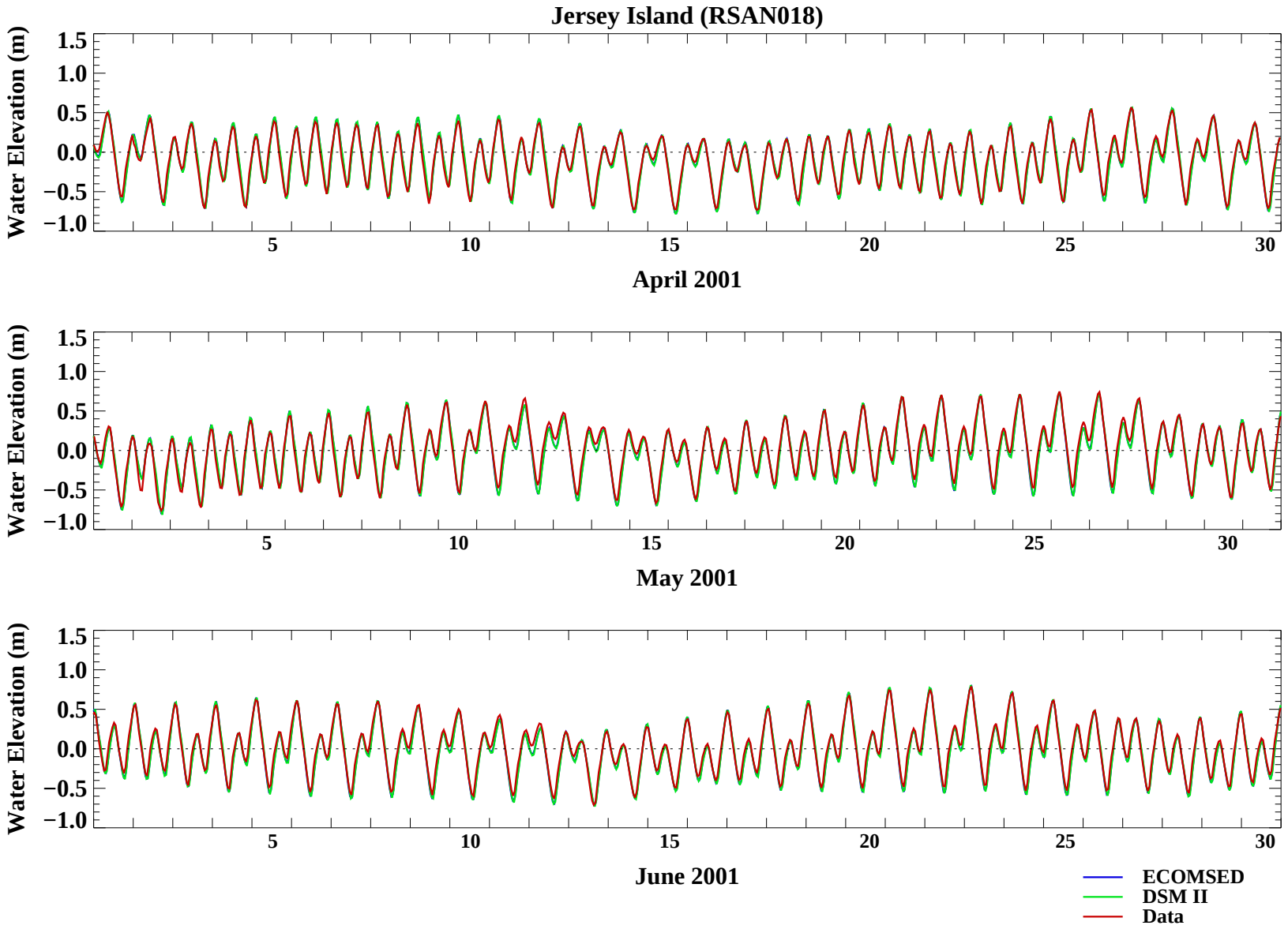
Jersey Island (RSAN018)
Water Elevation (m)
1.5
1.0
0.5
0.0
−0.5
−1.0
5
10
15
20
25
30
April 2001
May 2001
June 2001
ECOMSED
DSM II
Data

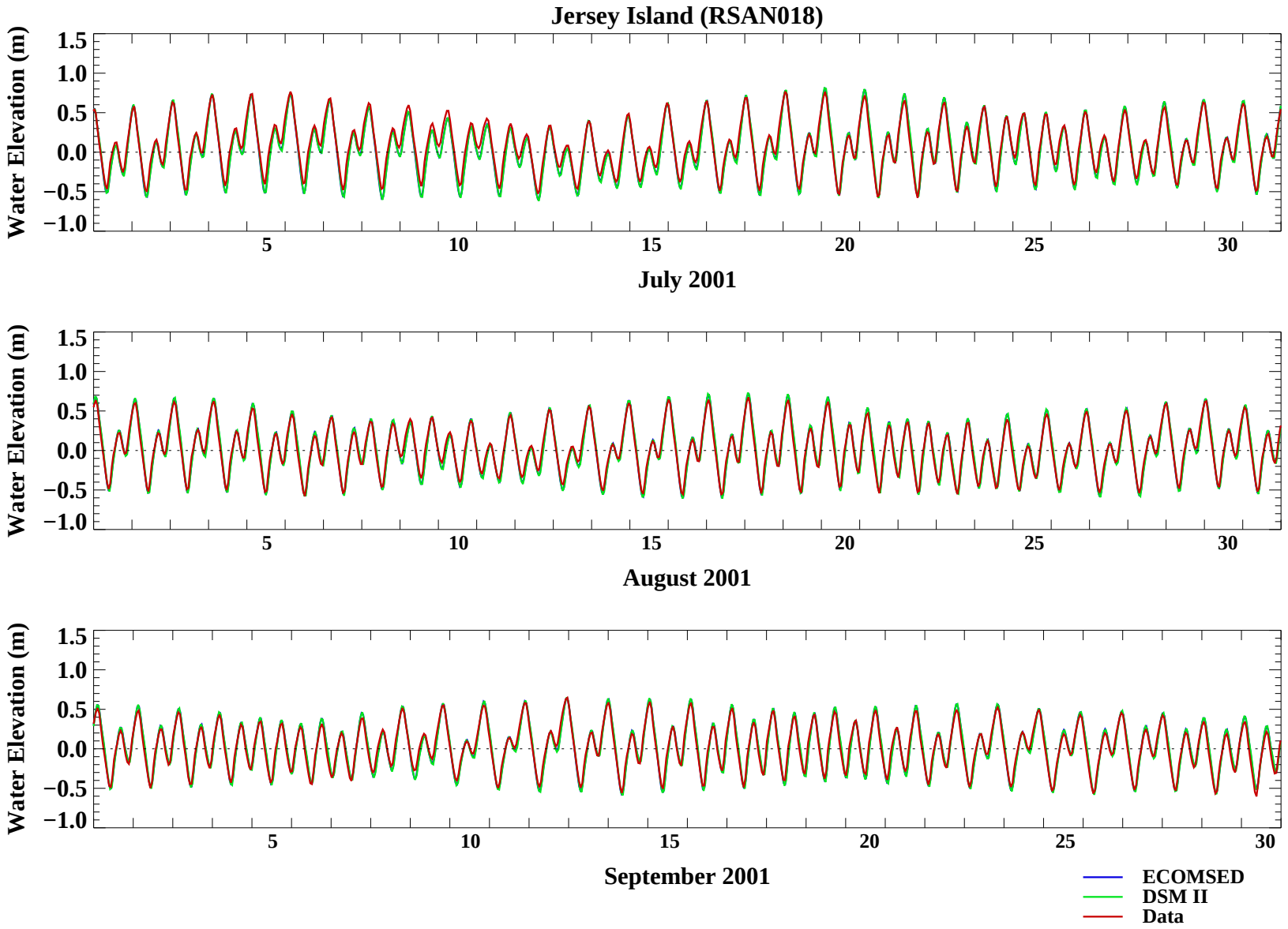
Jersey Island (RSAN018)
Water Elevation (m)
1.5
1.0
0.5
0.0
−0.5
−1.0
5
10
15
20
25
30
July 2001
August 2001
September 2001
ECOMSED
DSM II
Data

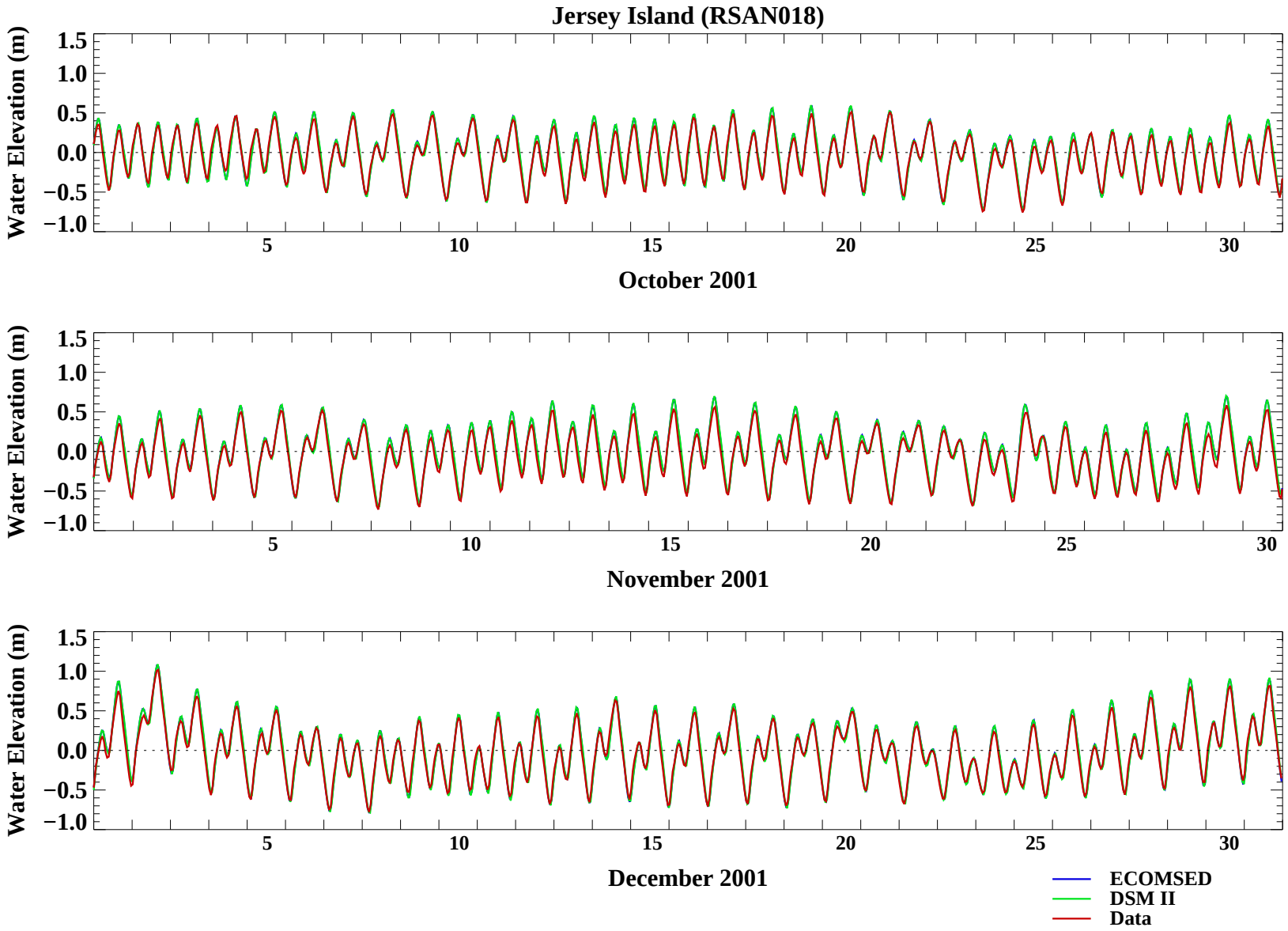
Jersey Island (RSAN018)
Water Elevation (m)
1.5
1.0
0.5
0.0
−0.5
−1.0
5
10
15
20
25
30
October 2001
November 2001
December 2001
ECOMSED
DSM II
Data

APPENDIX C

WATER QUALITY MODEL CALIBRATION FIGURES

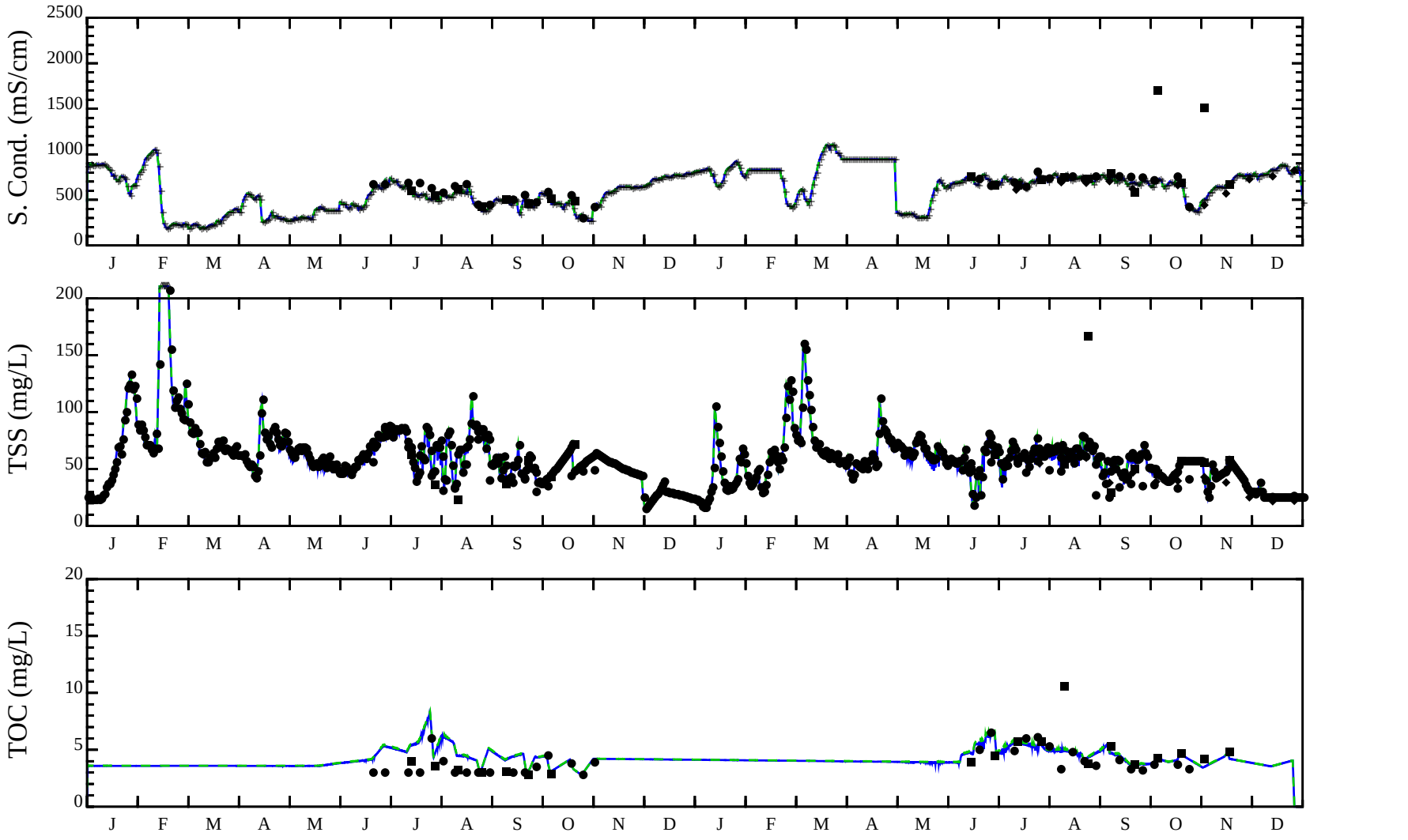

Figure C1-A. San Joaquin River Model Calibration, 2000 & 2001, Station: Vernalis

UCD (Dahlgren, 2004) - filled diamond
USGS (Kratzer et al., 2004) - filled square
Lehman, 2004 - filled triangle
All other data from J&S Data Atlas, (DO & Conductivity denoted by + is at Mossdale RSAN087)

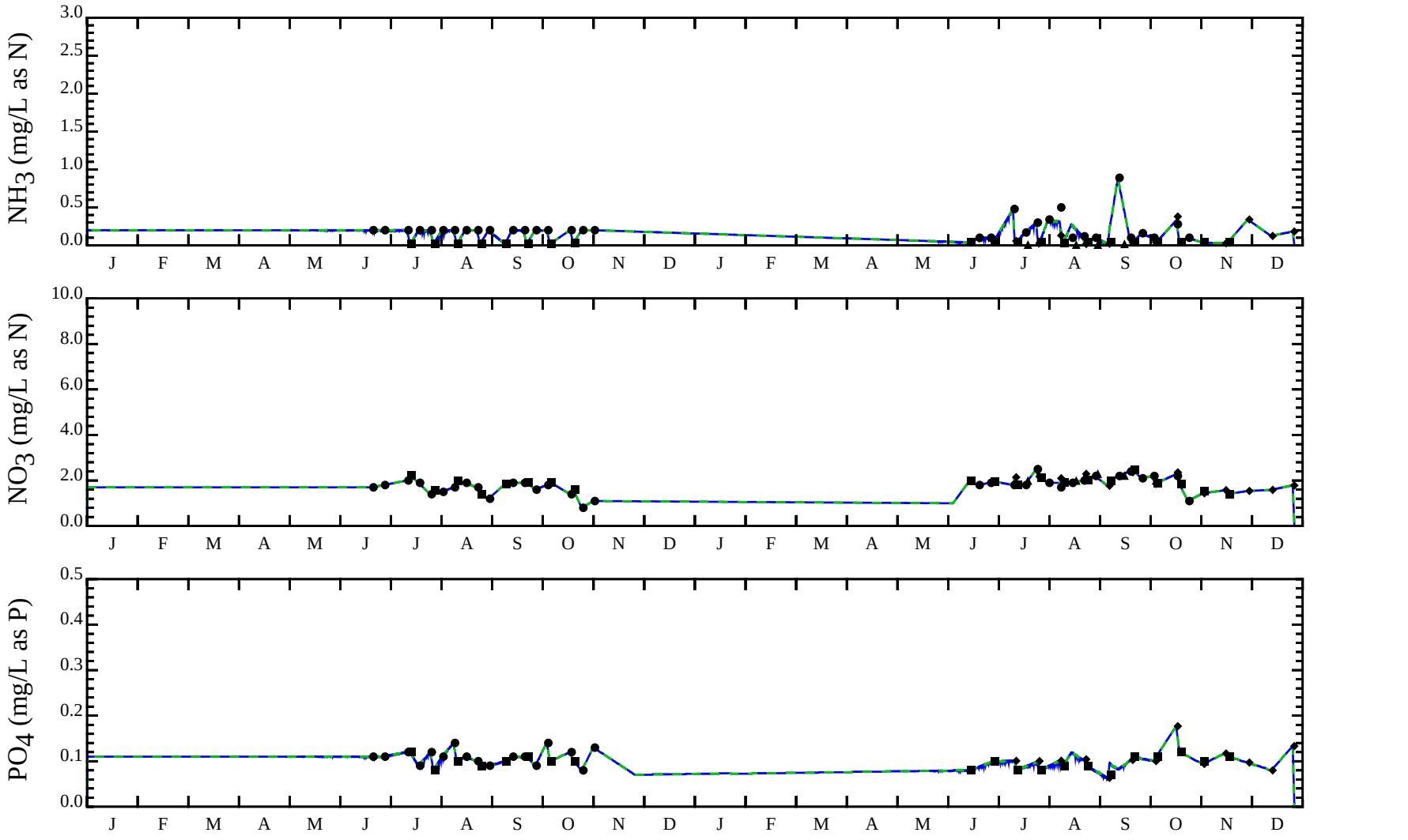

Figure C1-B. San Joaquin River Model Calibration, 2000 & 2001, Station: Vernalis

UCD (Dahlgren, 2004) - filled diamond
USGS (Kratzer et al., 2004) - filled square
Lehman, 2004 - filled triangle
All other data from J&S Data Atlas, (DO & Conductivity denoted by + is at Mossdale RSAN087)

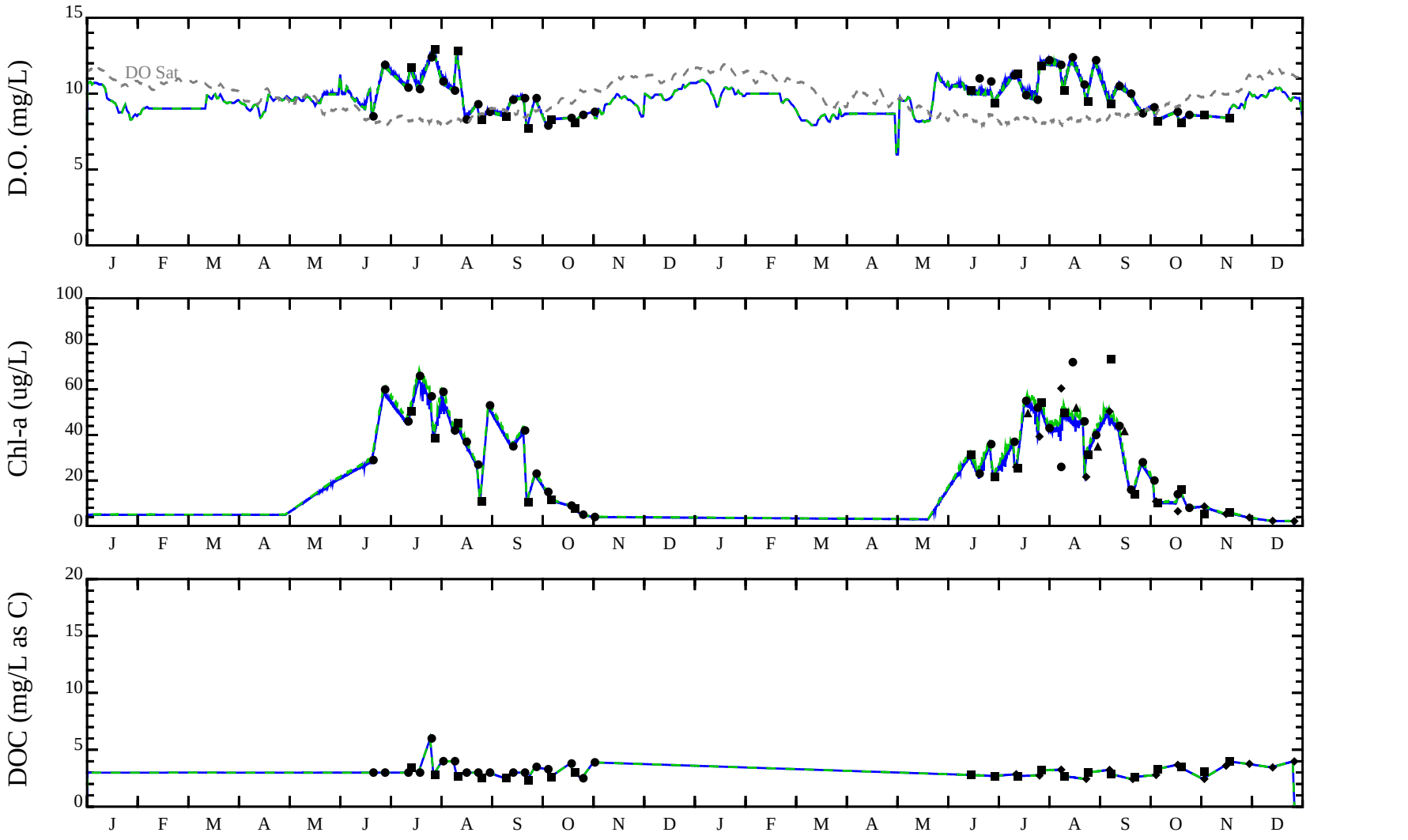

Figure C1-C. San Joaquin River Model Calibration, 2000 & 2001, Station: Vernalis

UCD (Dahlgren, 2004) - filled diamond
USGS (Kratzer et al., 2004) - filled square
Lehman, 2004 - filled triangle
All other data from J&S Data Atlas, (DO & Conductivity denoted by + is at Mossdale RSAN087)

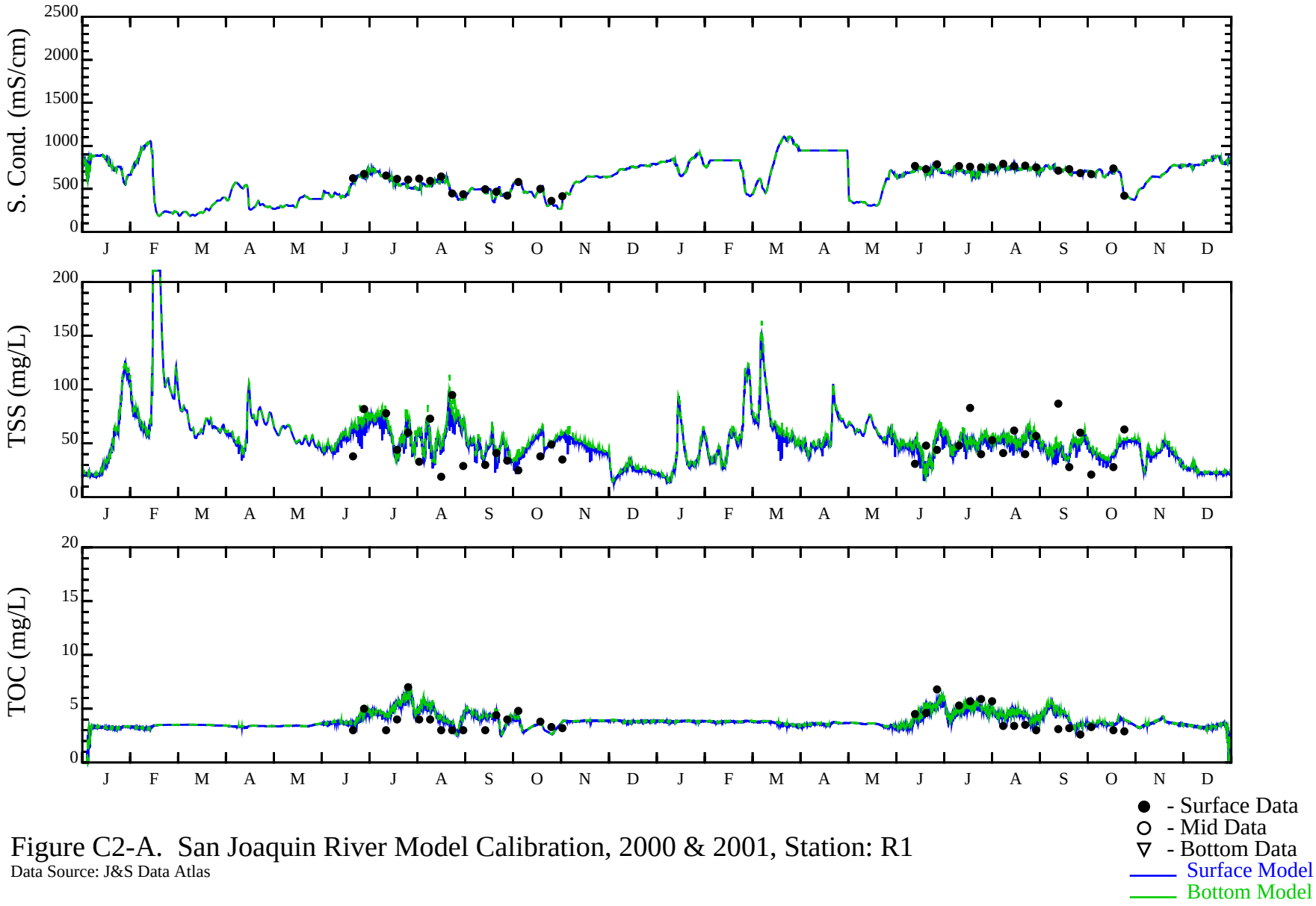

Figure C2-A. San Joaquin River Model Calibration, 2000 & 2001, Station: R1

Data Source: J&S Data Atlas

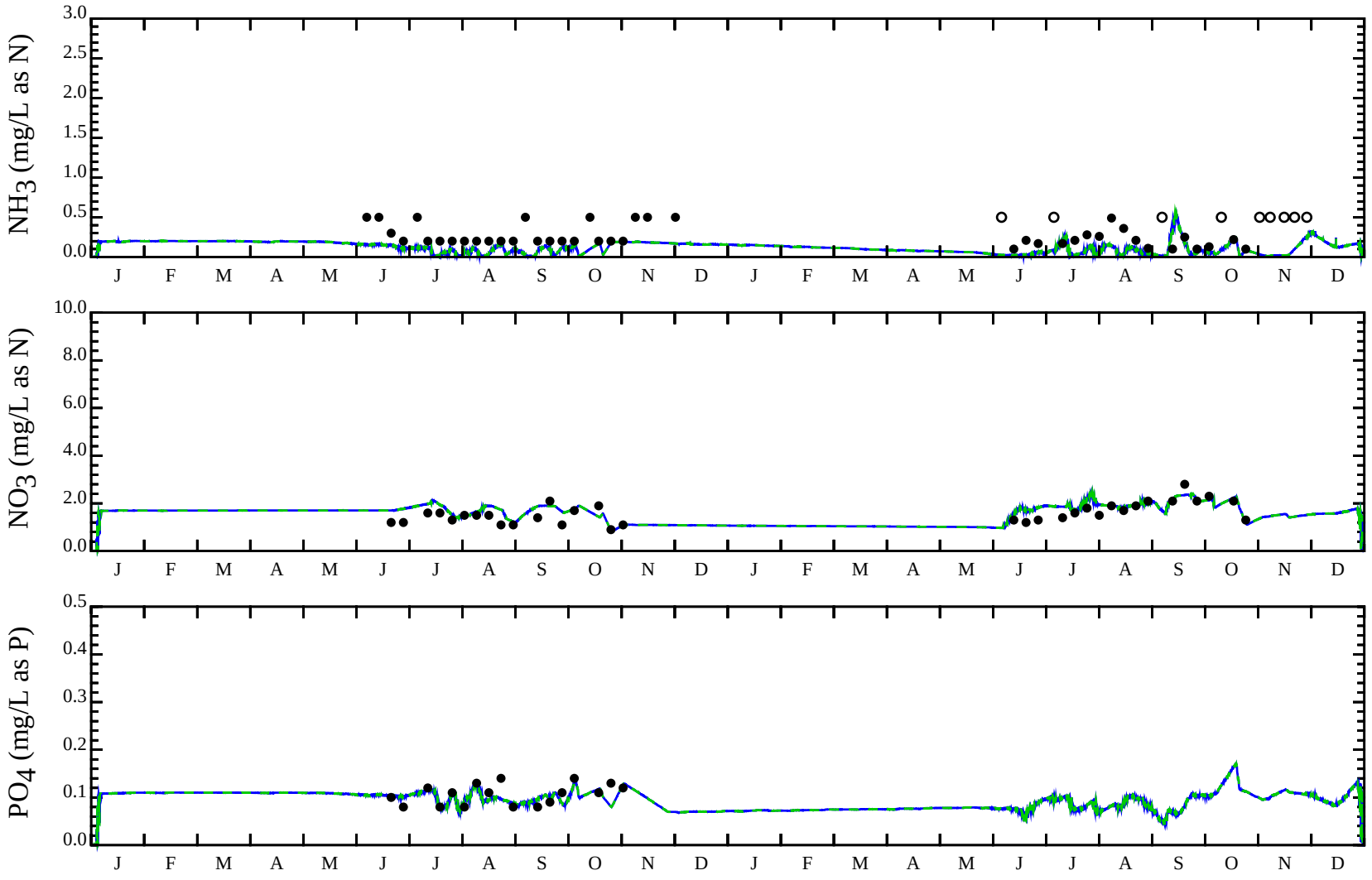

Figure C2-B. San Joaquin River Model Calibration, 2000 & 2001, Station: R1

Data Source: J&S Data Atlas, Lehman, 2004

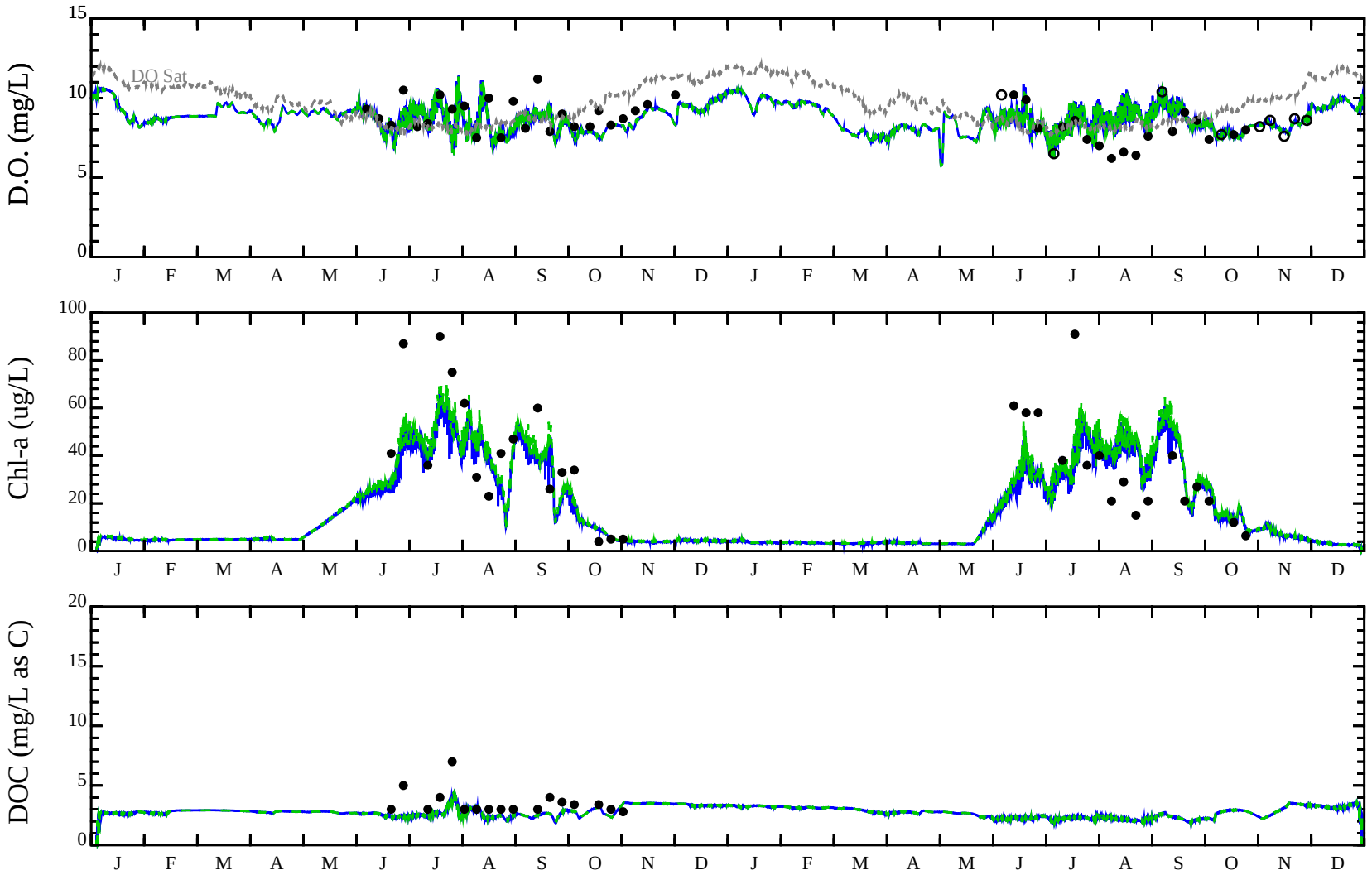

Figure C2-C. San Joaquin River Model Calibration, 2000 & 2001, Station: R1

Data Source: J&S Data Atlas, Lehman, 2004

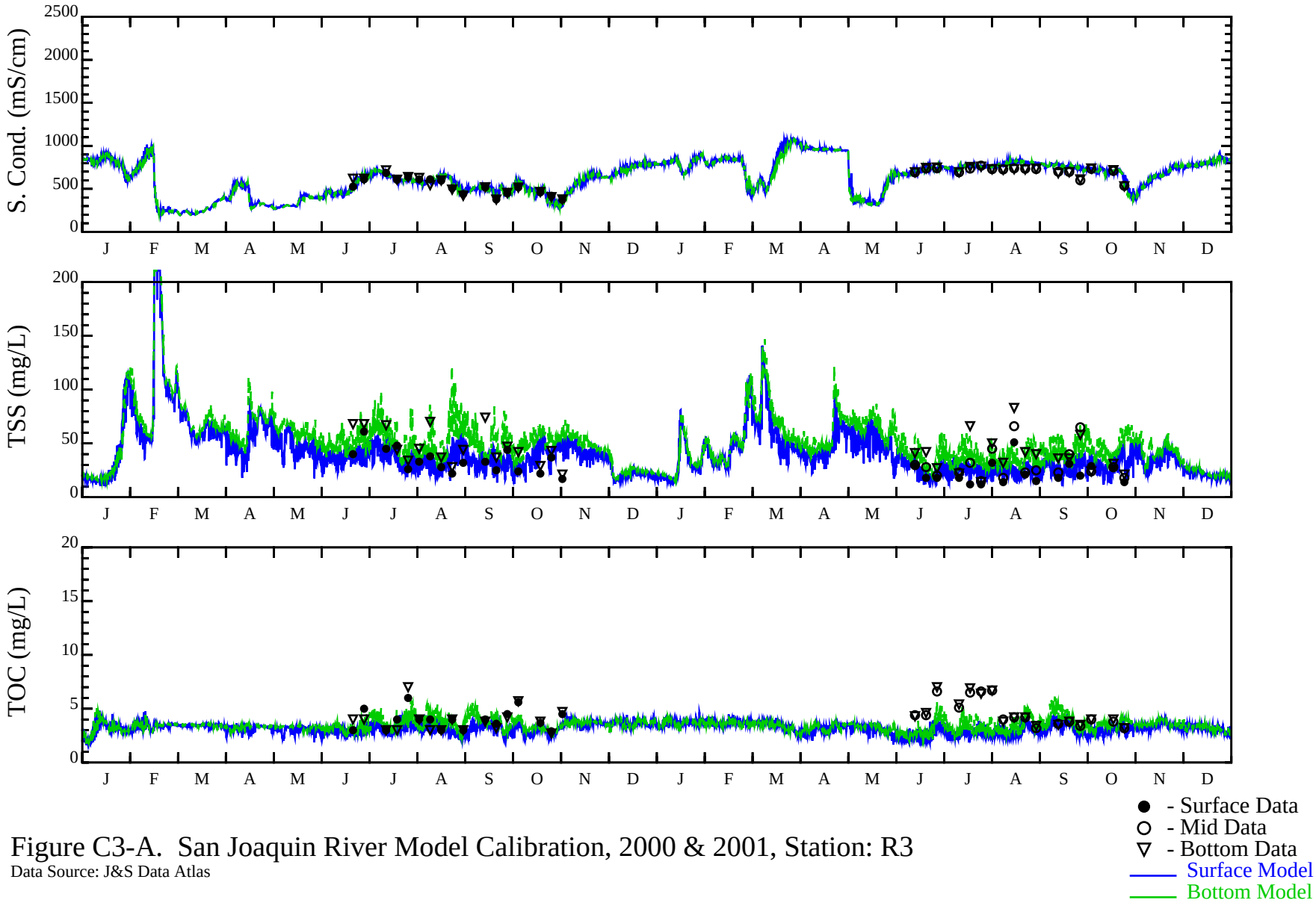

Figure C3-A. San Joaquin River Model Calibration, 2000 & 2001, Station: R3

Data Source: J&S Data Atlas

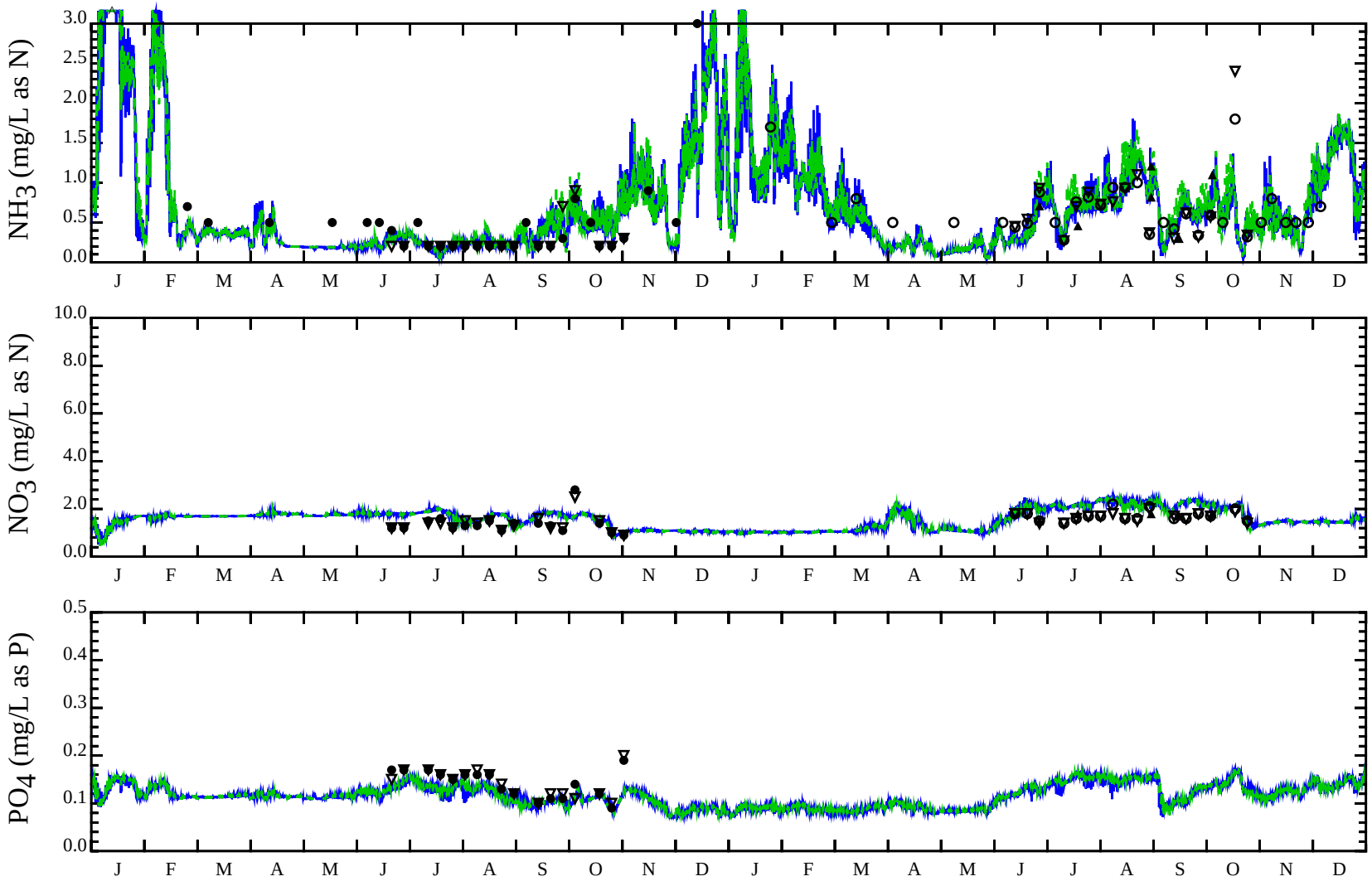

Figure C3-B. San Joaquin River Model Calibration, 2000 & 2001, Station: R3

Data Source: J&S Data Atlas, Lehman, 2004

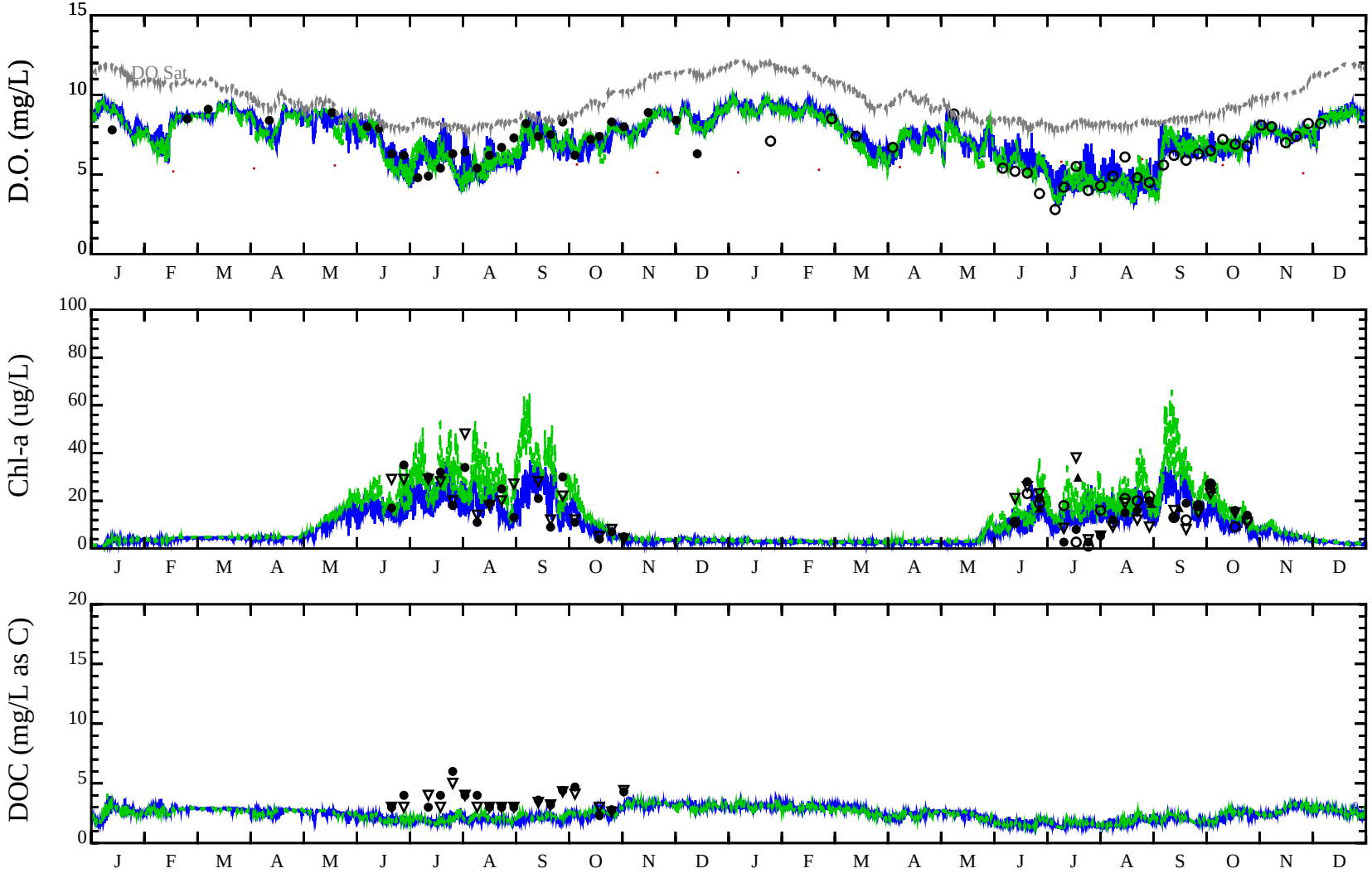

Figure C3-C. San Joaquin River Model Calibration, 2000 & 2001, Station: R3

Data Source: J&S Data Atlas, Lehman, 2004

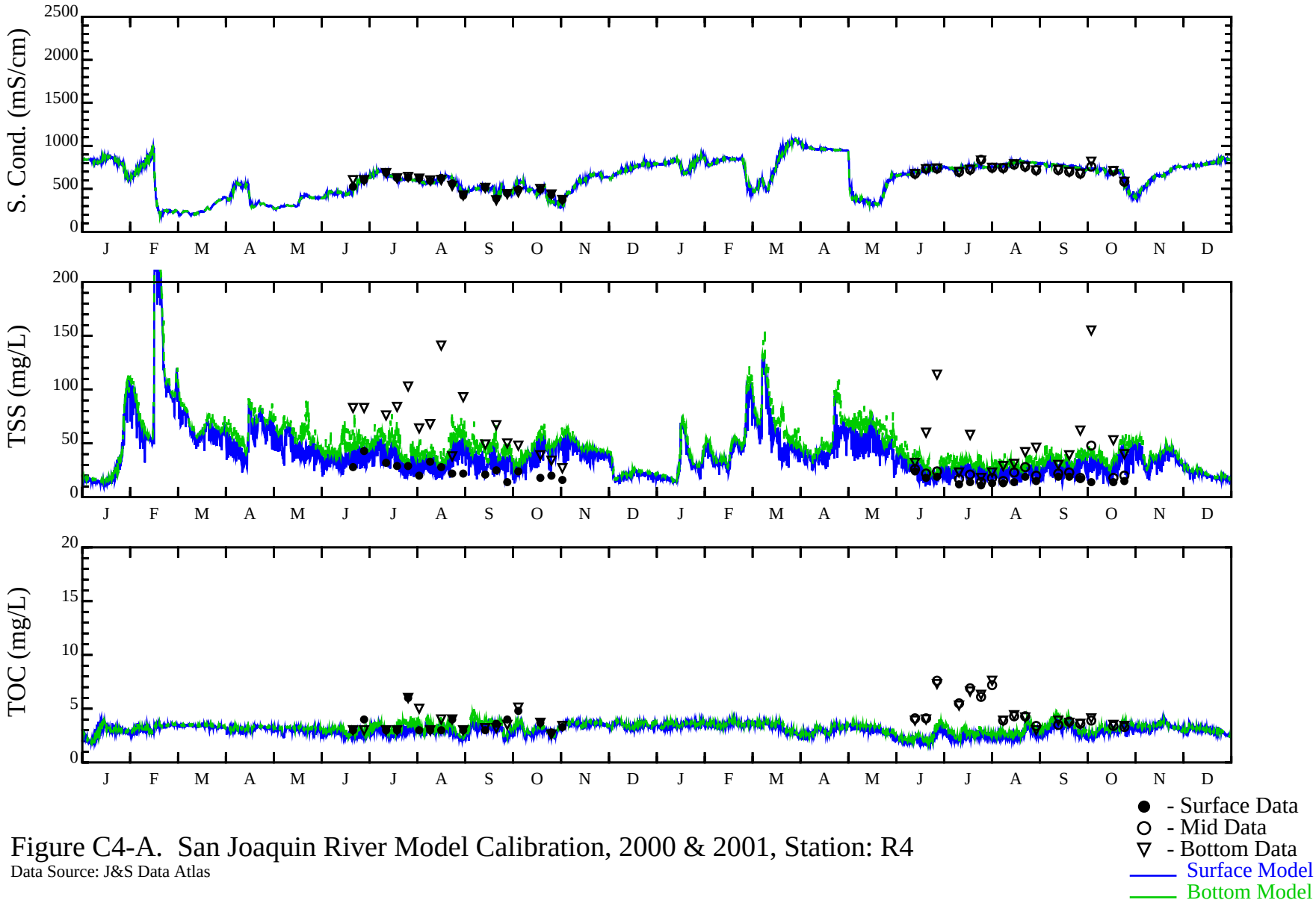

Figure C4-A. San Joaquin River Model Calibration, 2000 & 2001, Station: R4

Data Source: J&S Data Atlas

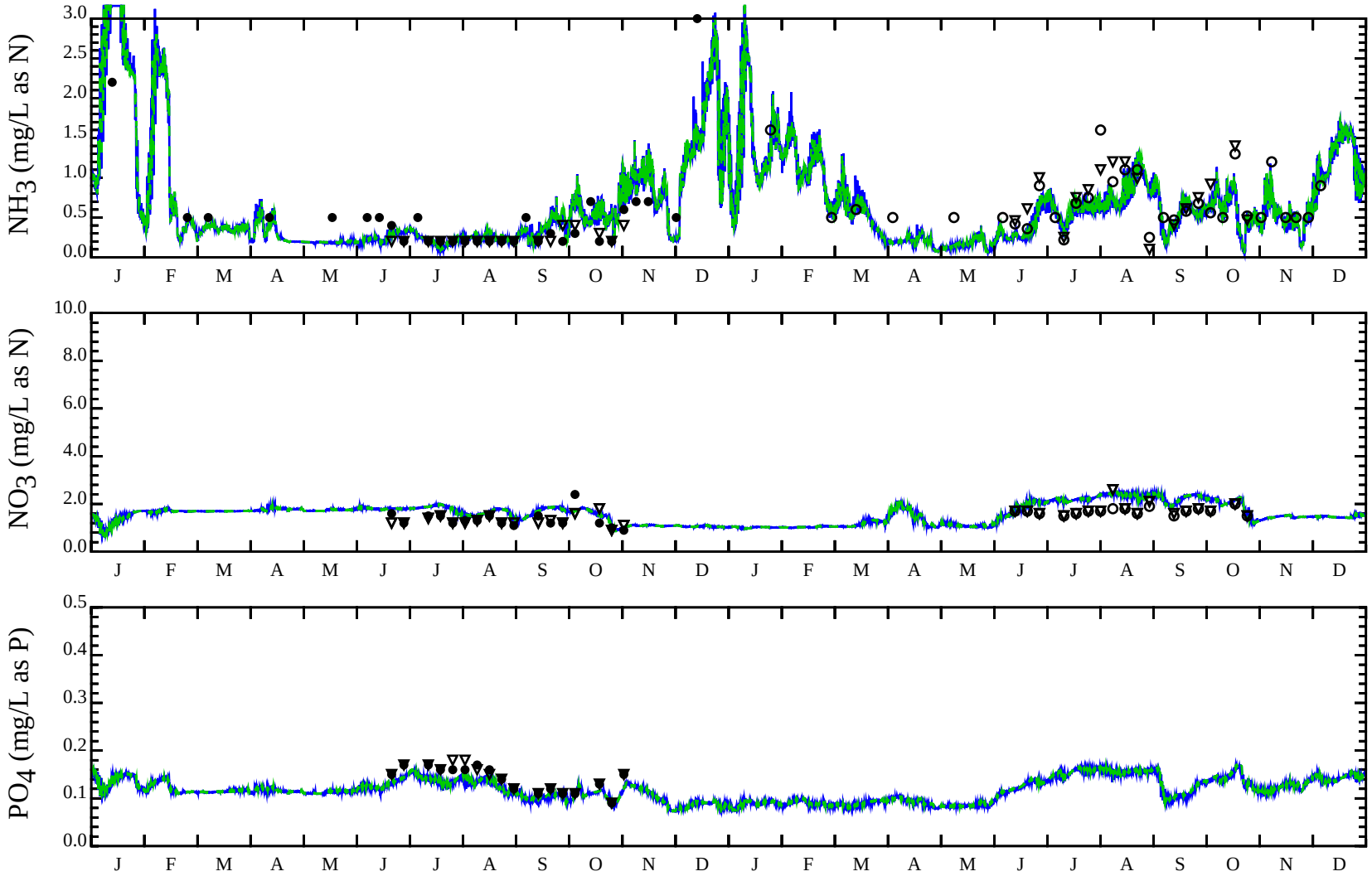

Figure C4-B. San Joaquin River Model Calibration, 2000 & 2001, Station: R4

Data Source: J&S Data Atlas, Lehman, 2004

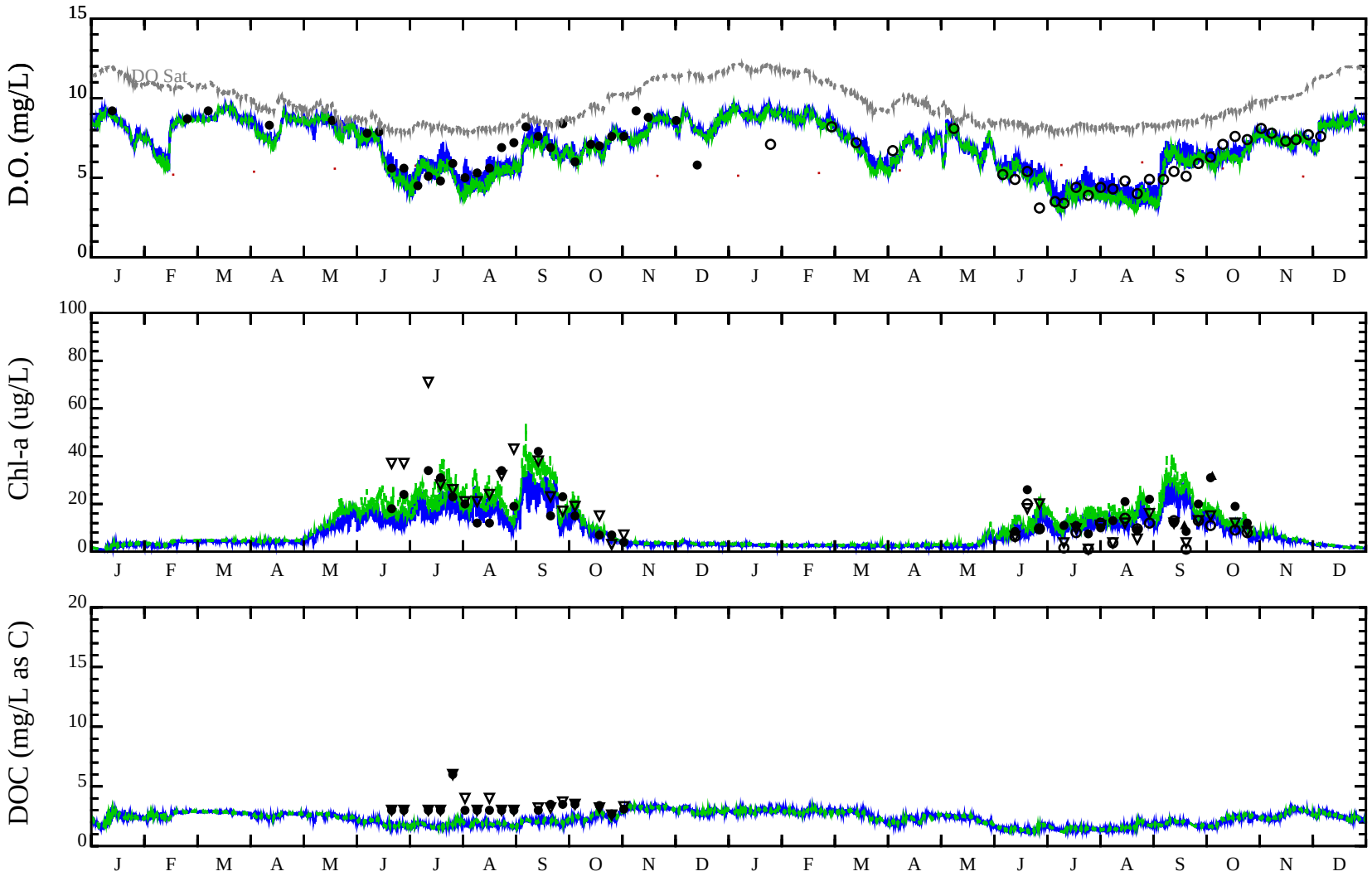

Figure C4-C. San Joaquin River Model Calibration, 2000 & 2001, Station: R4

Data Source: J&S Data Atlas, Lehman, 2004

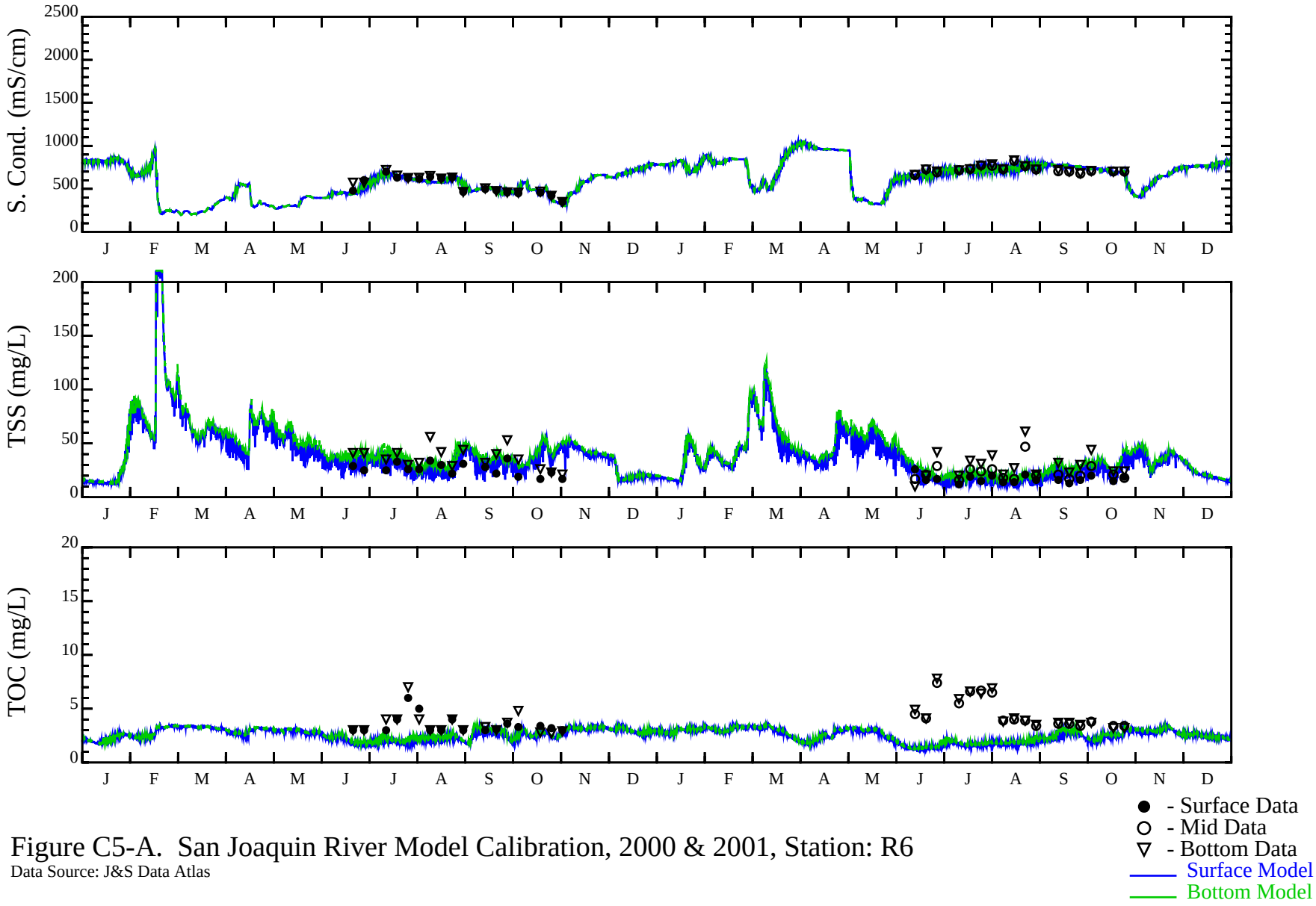

Figure C5-A. San Joaquin River Model Calibration, 2000 & 2001, Station: R6

Data Source: J&S Data Atlas

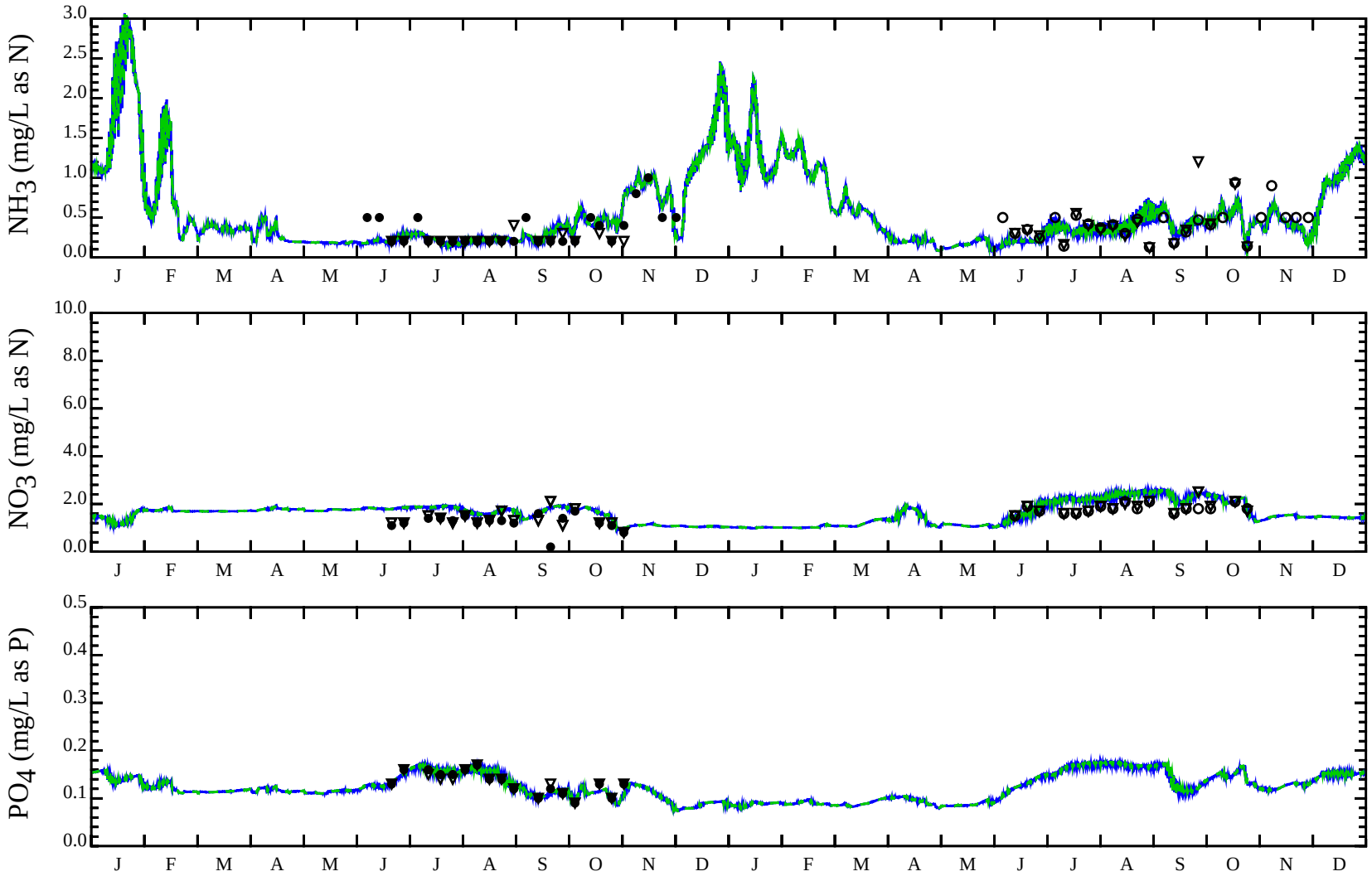

Figure C5-B. San Joaquin River Model Calibration, 2000 & 2001, Station: R6

Data Source: J&S Data Atlas, Lehman, 2004

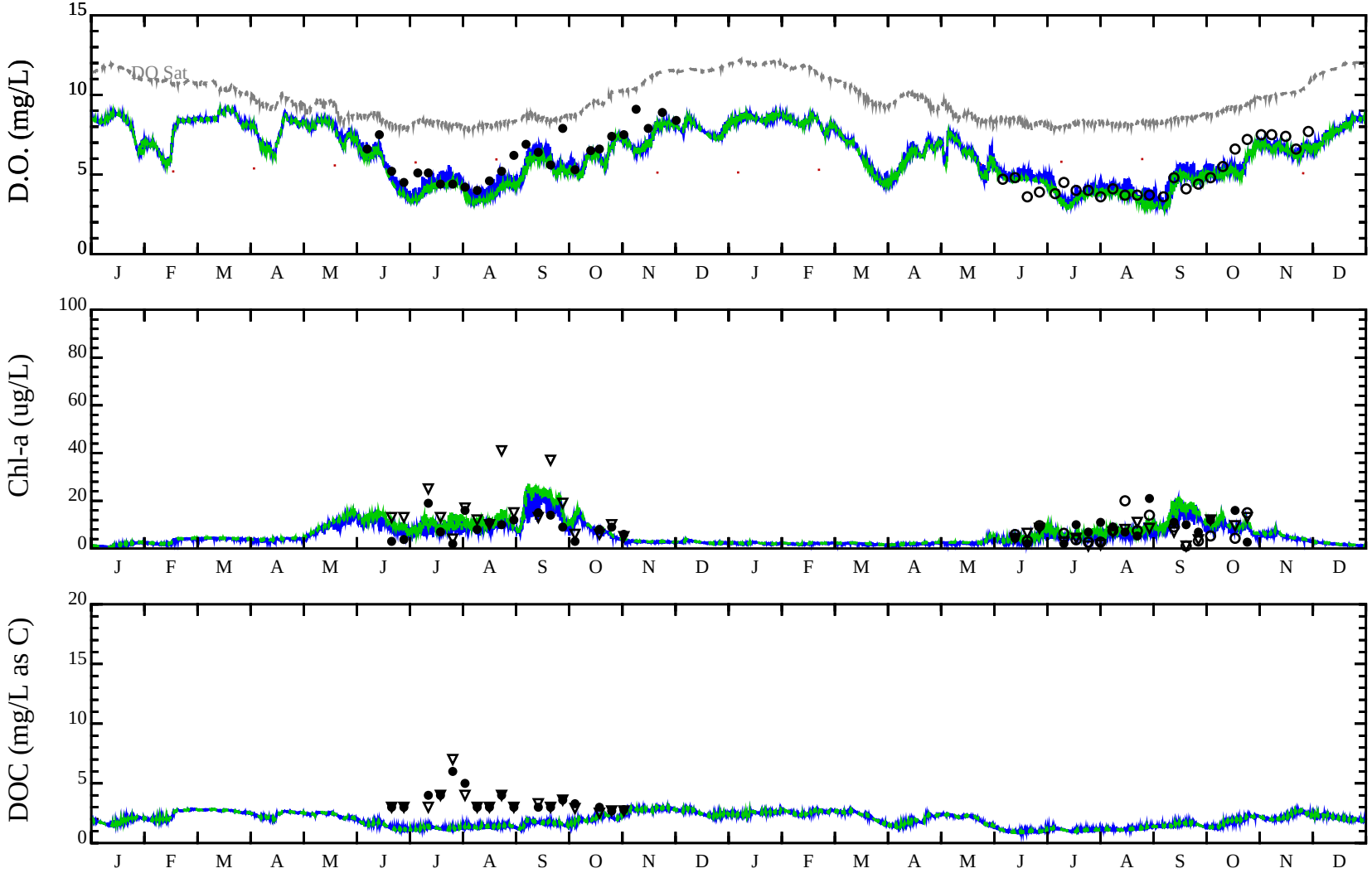

Figure C5-C. San Joaquin River Model Calibration, 2000 & 2001, Station: R6

Data Source: J&S Data Atlas, Lehman, 2004

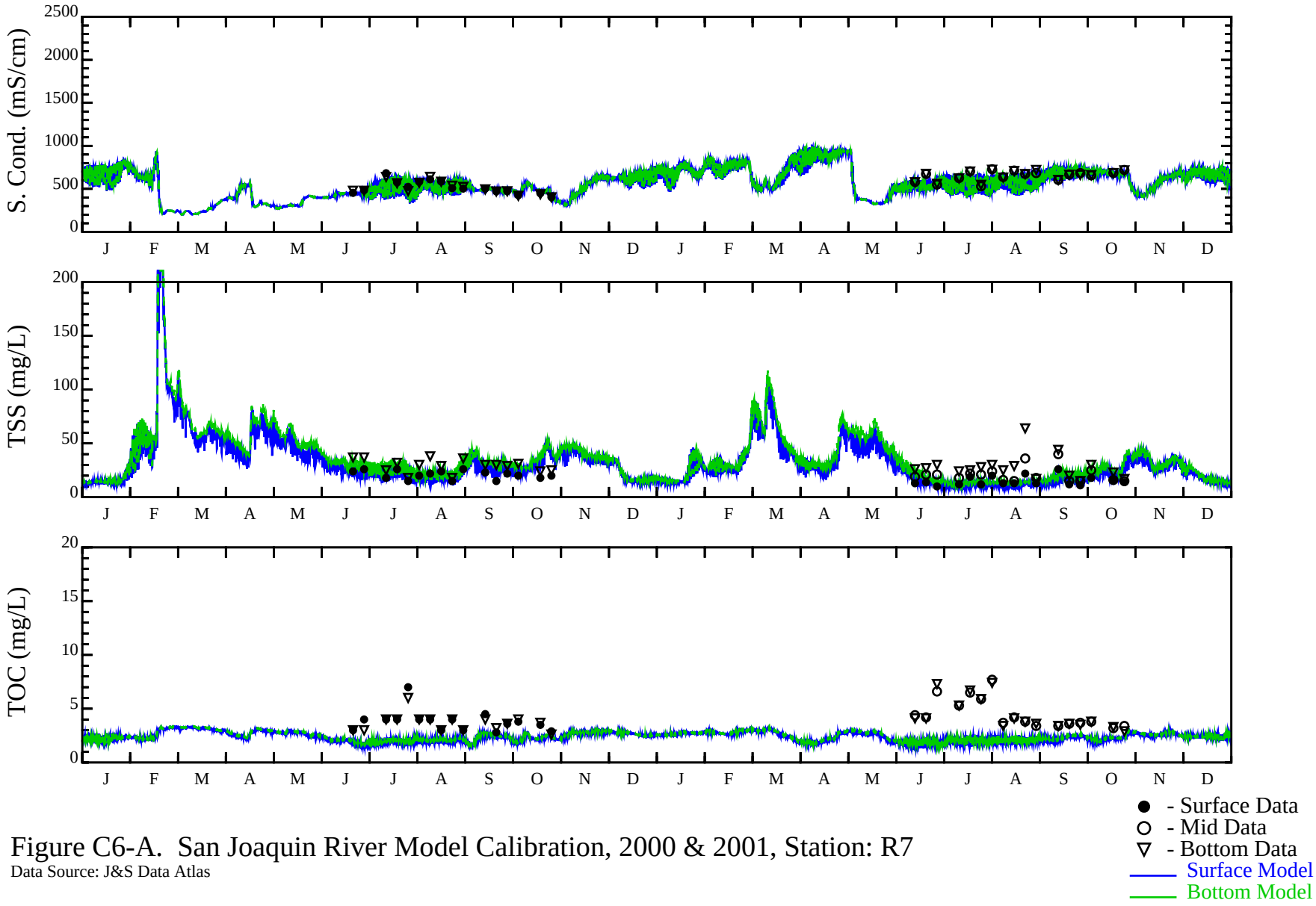

Figure C6-A. San Joaquin River Model Calibration, 2000 & 2001, Station: R7

Data Source: J&S Data Atlas

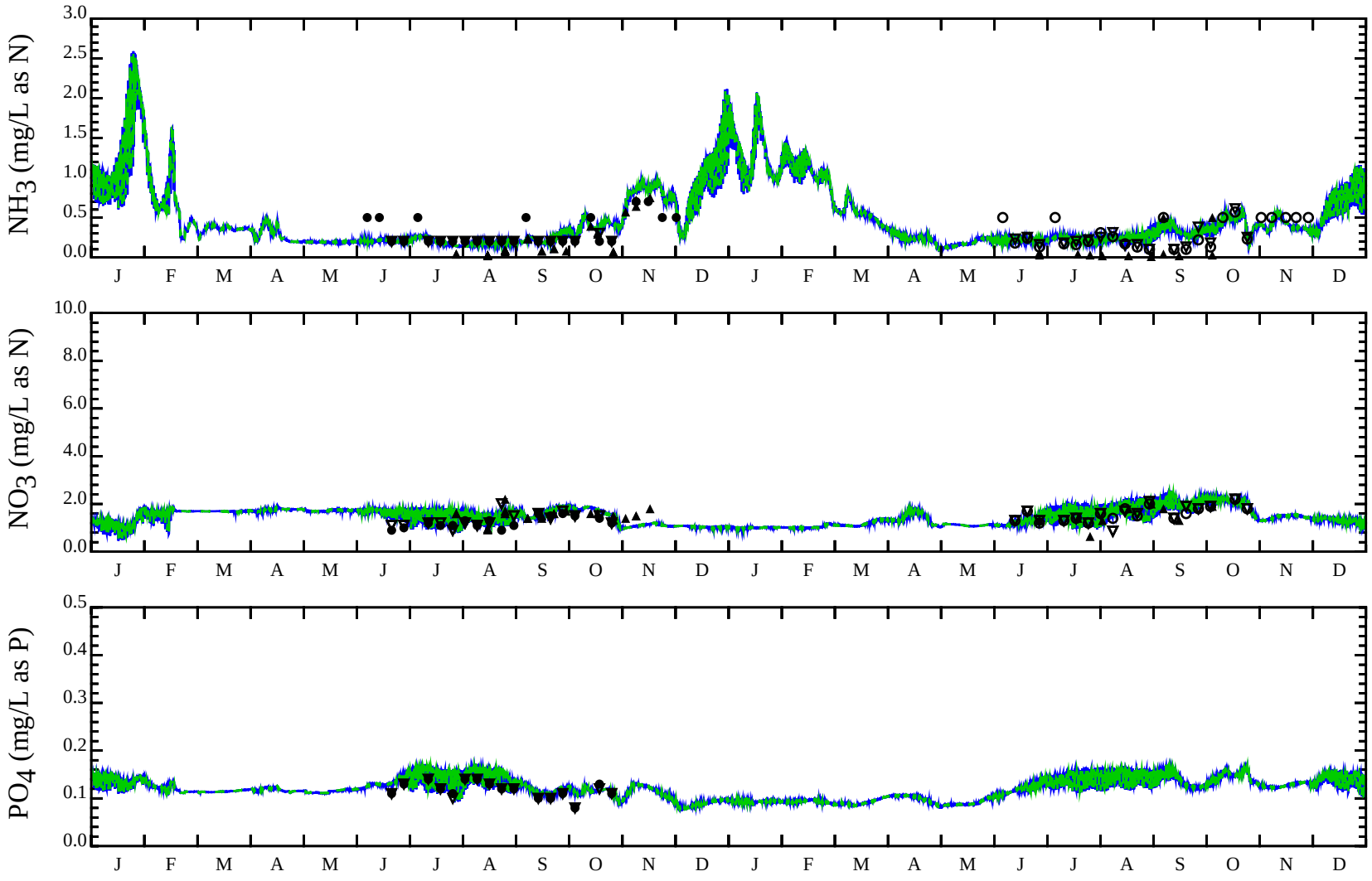

Figure C6-B. San Joaquin River Model Calibration, 2000 & 2001, Station: R7

Data Source: J&S Data Atlas, Lehman, 2004

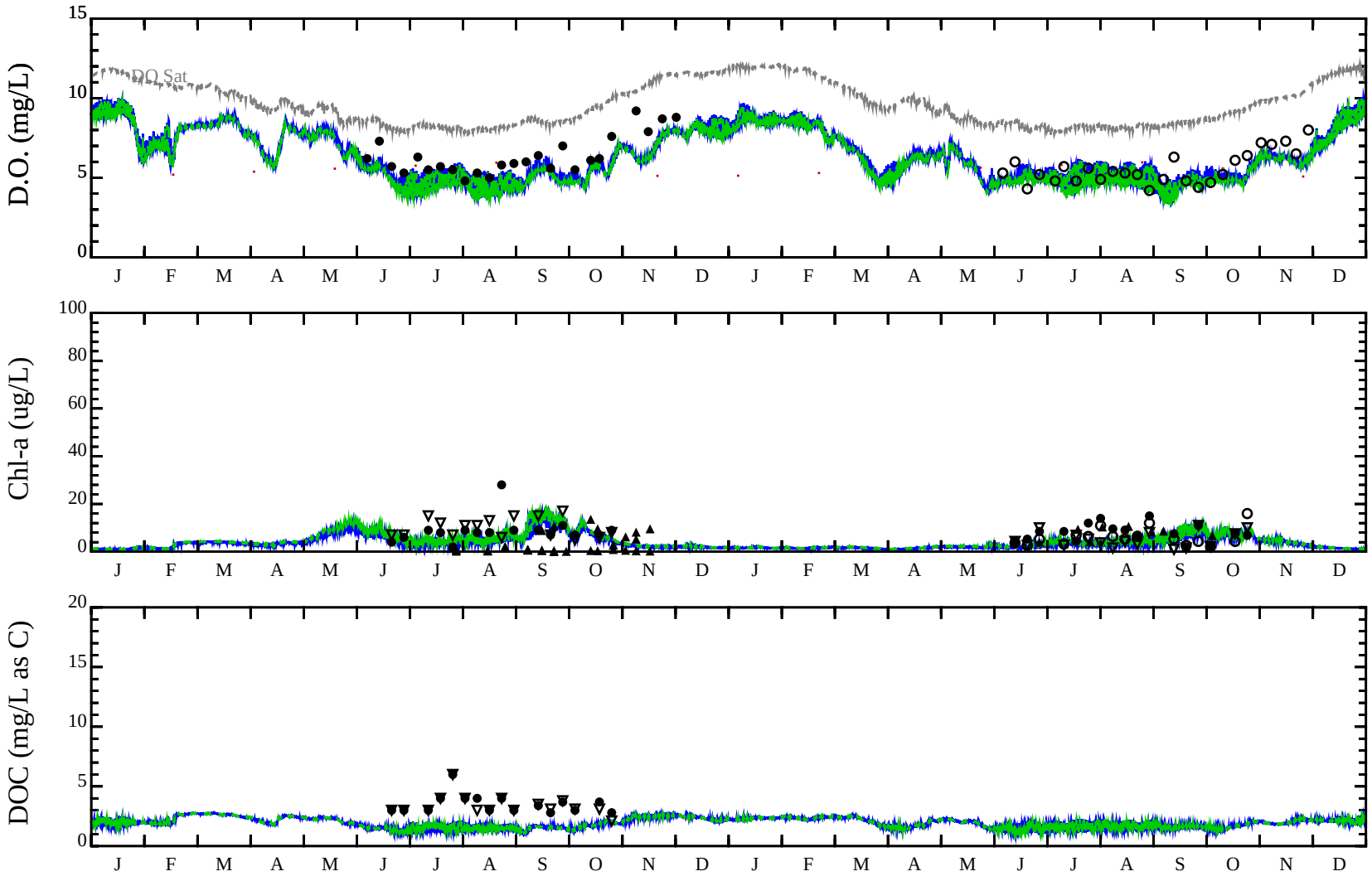

Figure C6-C. San Joaquin River Model Calibration, 2000 & 2001, Station: R7

Data Source: J&S Data Atlas, Lehman, 2004

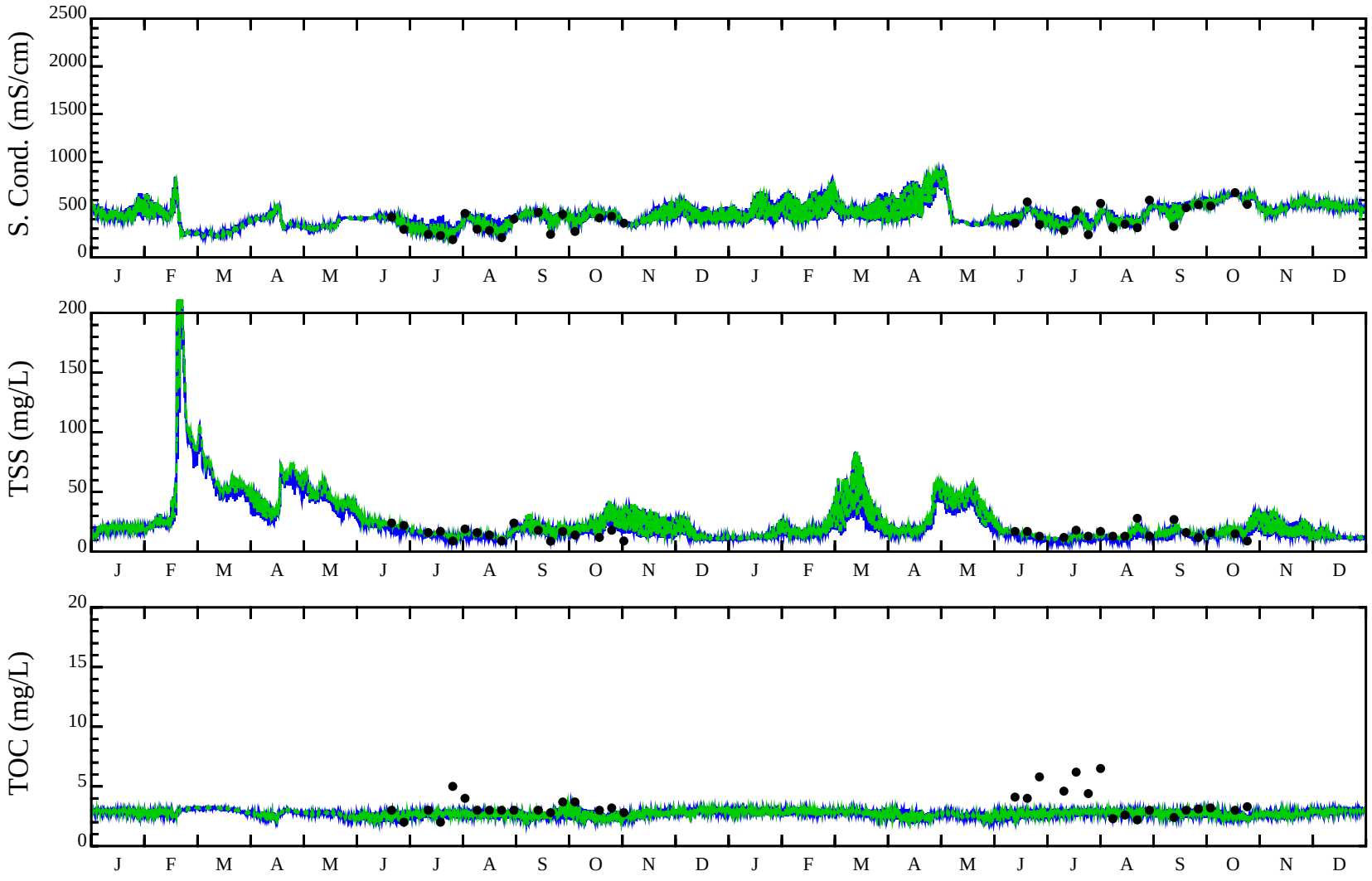

Figure C7-A. San Joaquin River Model Calibration, 2000 & 2001, Station: R8

Data Source: J&S Data Atlas

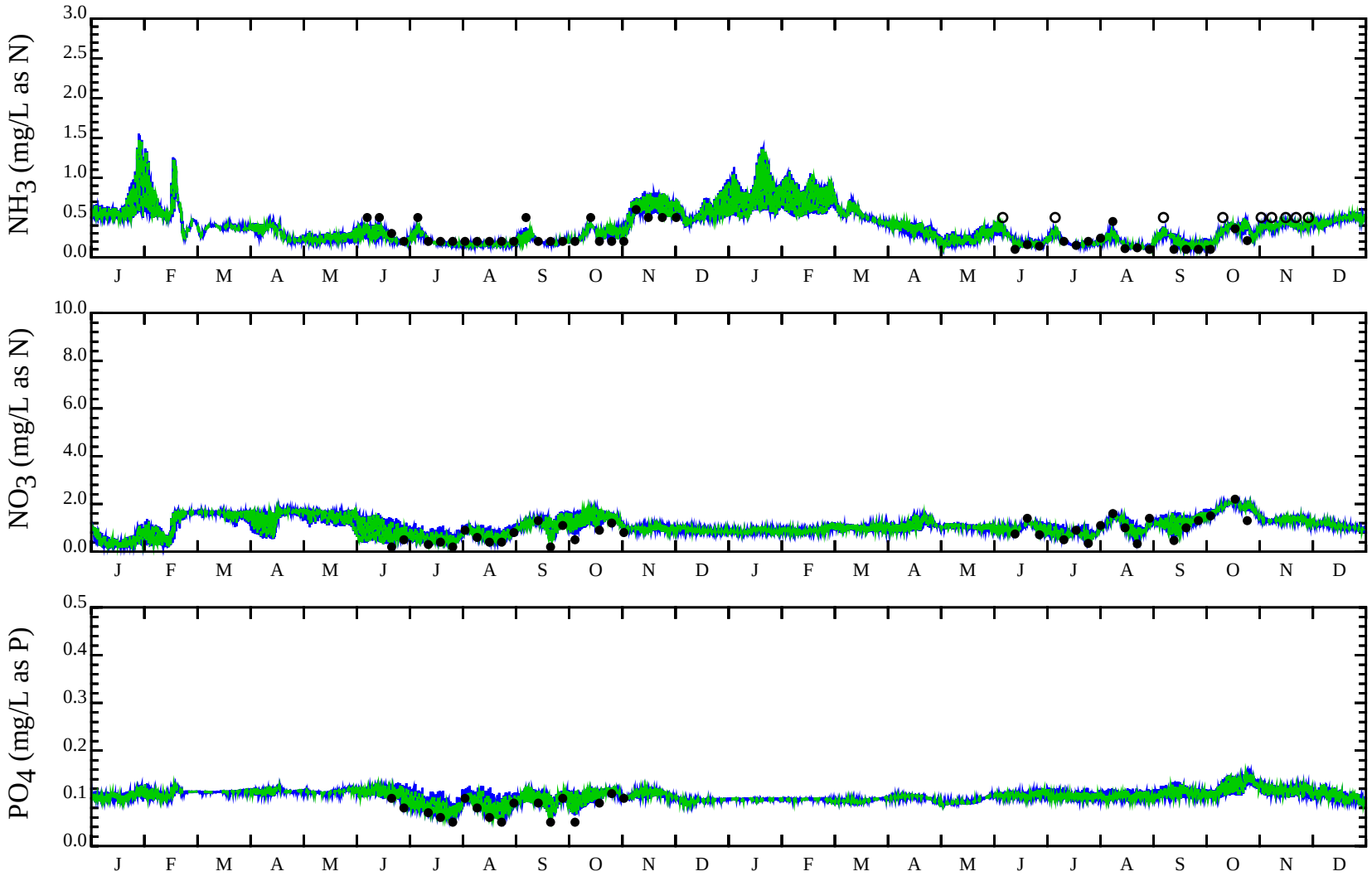

Figure C7-B. San Joaquin River Model Calibration, 2000 & 2001, Station: R8

Data Source: J&S Data Atlas, Lehman, 2004

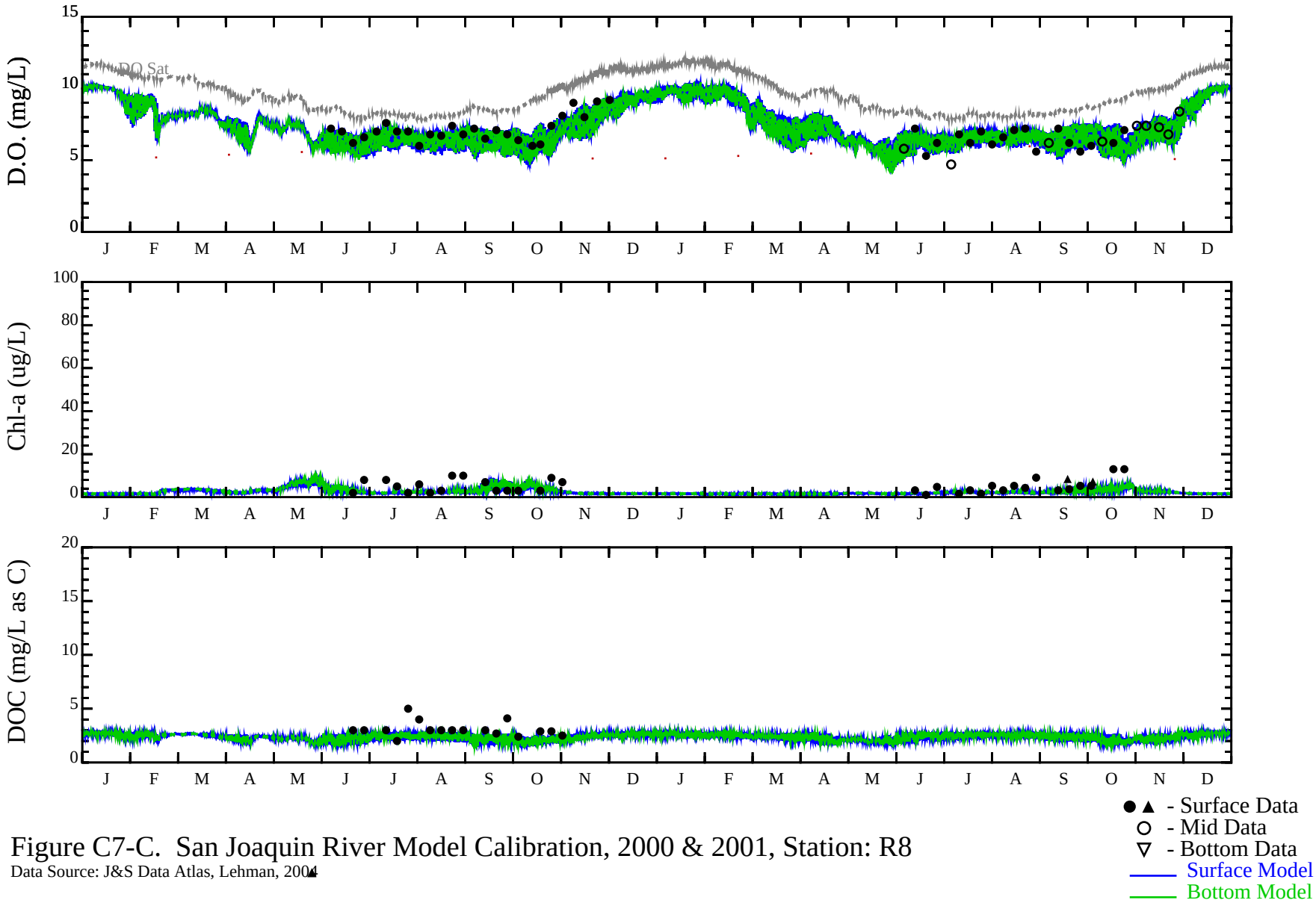

Figure C7-C. San Joaquin River Model Calibration, 2000 & 2001, Station: R8

Data Source: J&S Data Atlas, Lehman, 2004

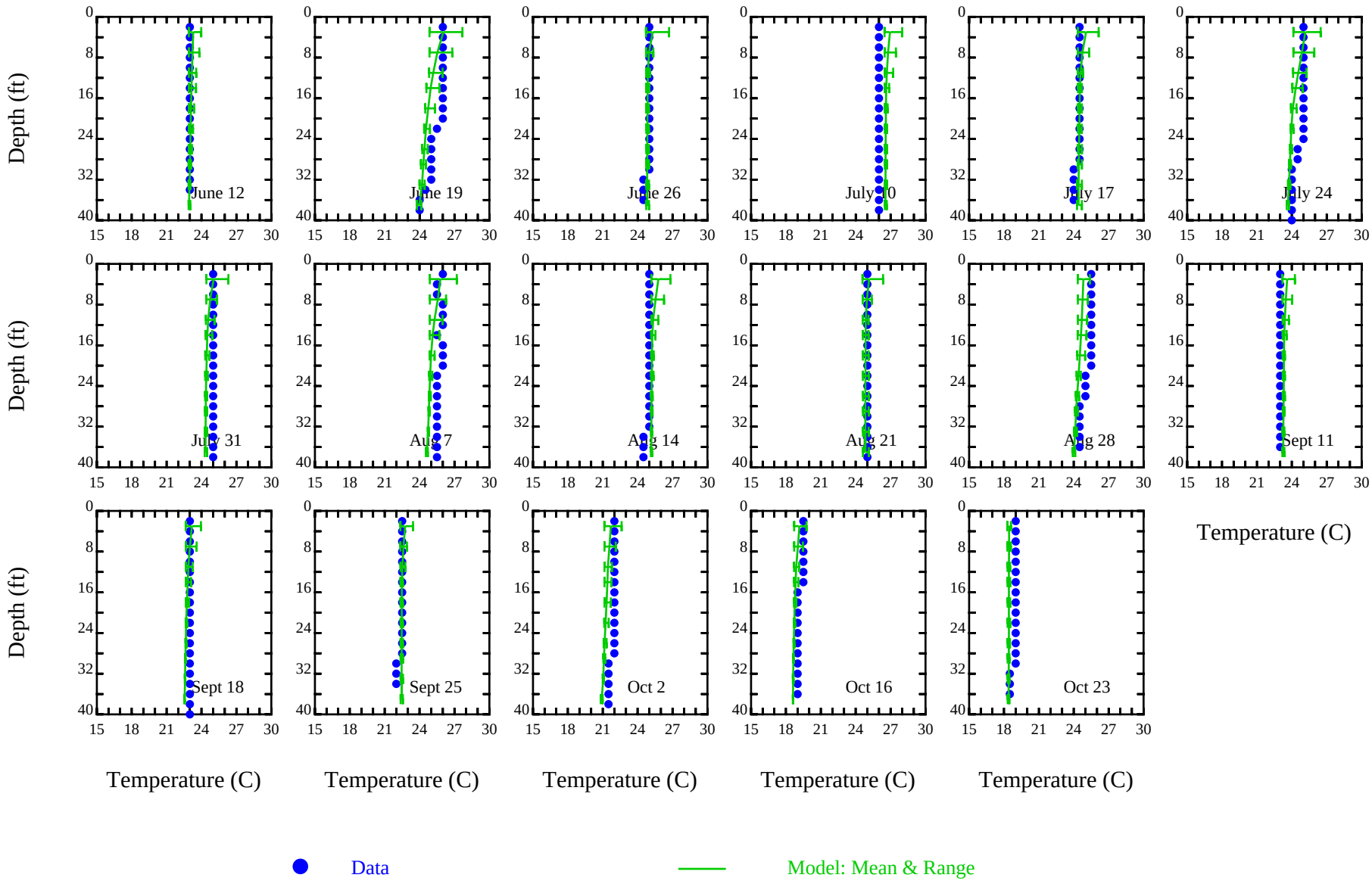

Figure C8. San Joaquin River at Turning Basin Data and Model Temperature Vertical Profiles, June-October 2001

vertdo.gdp, RUN39v4Q

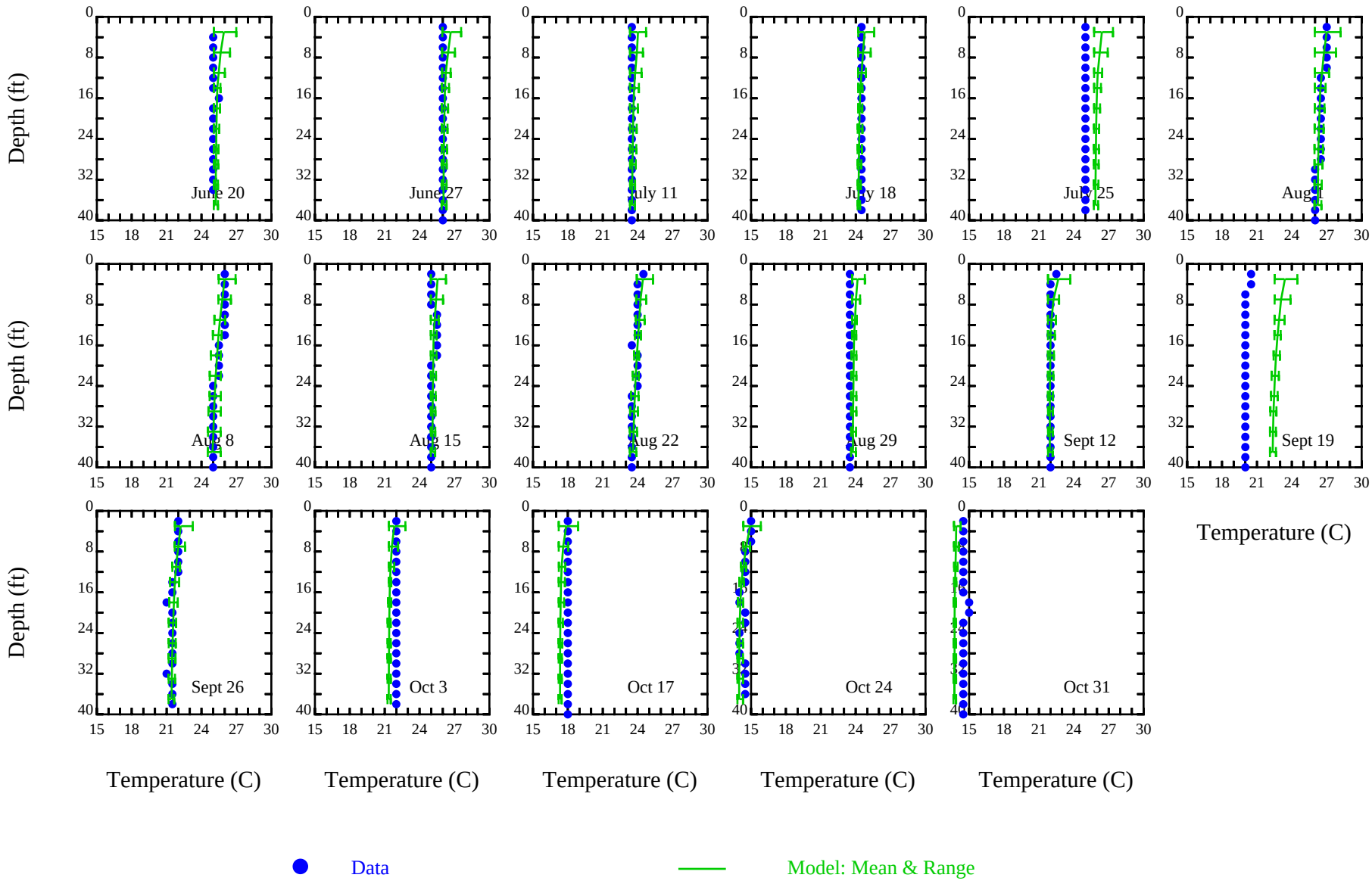

Figure C9. San Joaquin River at R3 Data and Model Temperature Vertical Profiles, June-October 2000

vertdo.gdp, RUN39v4Q

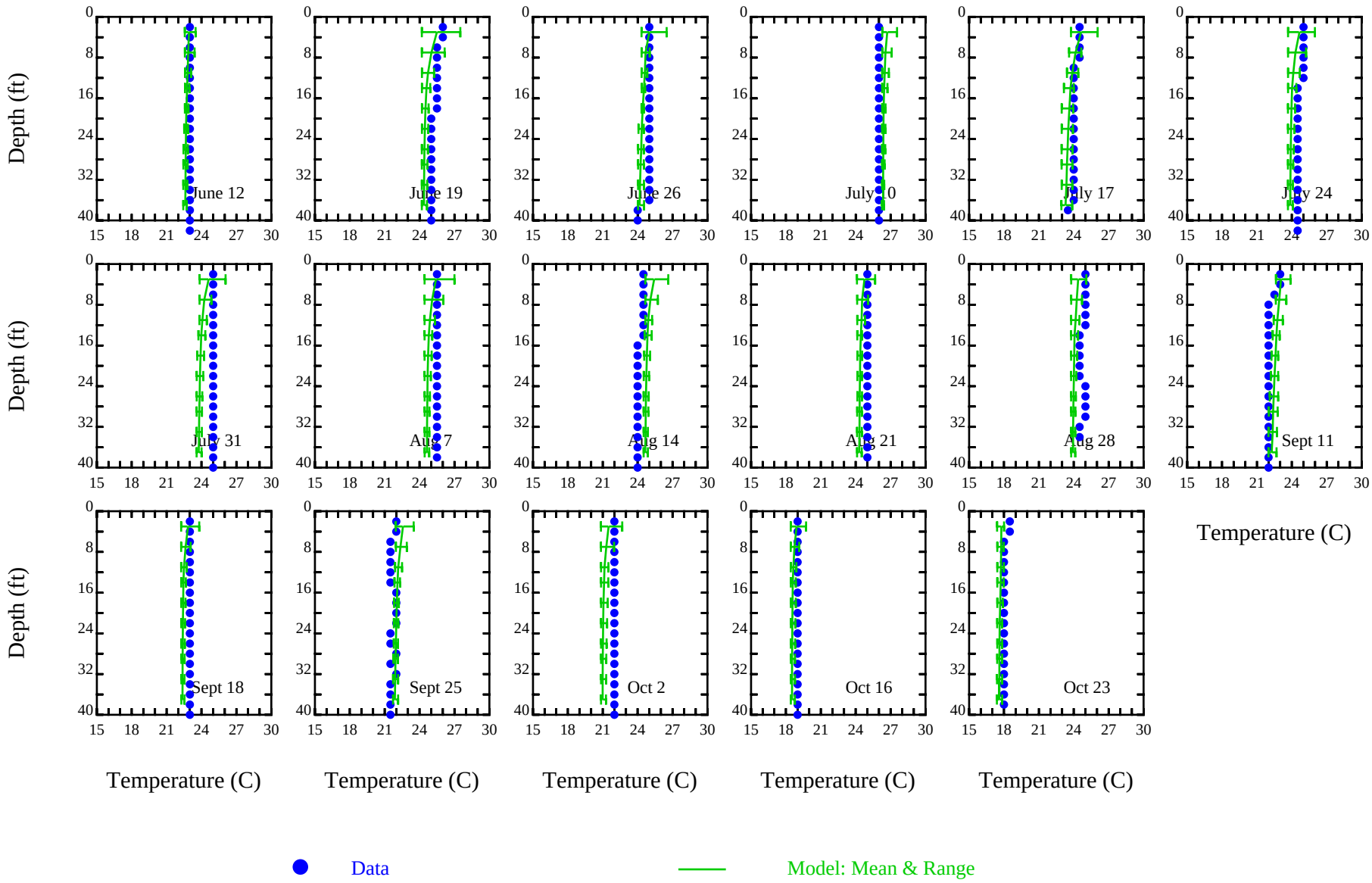

Figure C10. San Joaquin River at R3 Data and Model Temperature Vertical Profiles, June-October 2001

vertdo.gdp, RUN39v4Q

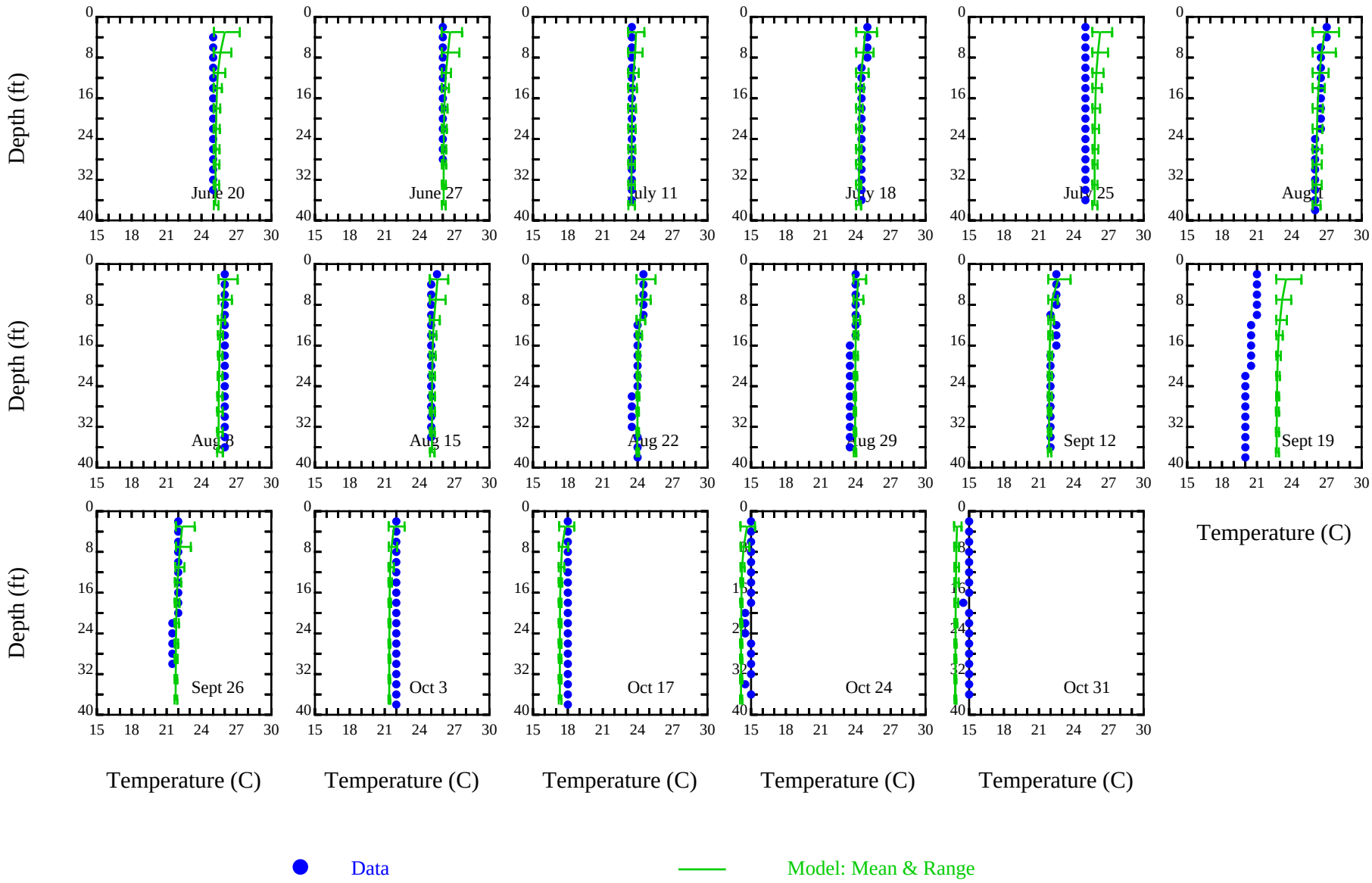

Figure C11. San Joaquin River at R4 Data and Model Temperature Vertical Profiles, June-October 2000

vertdo.gdp, RUN39v4Q

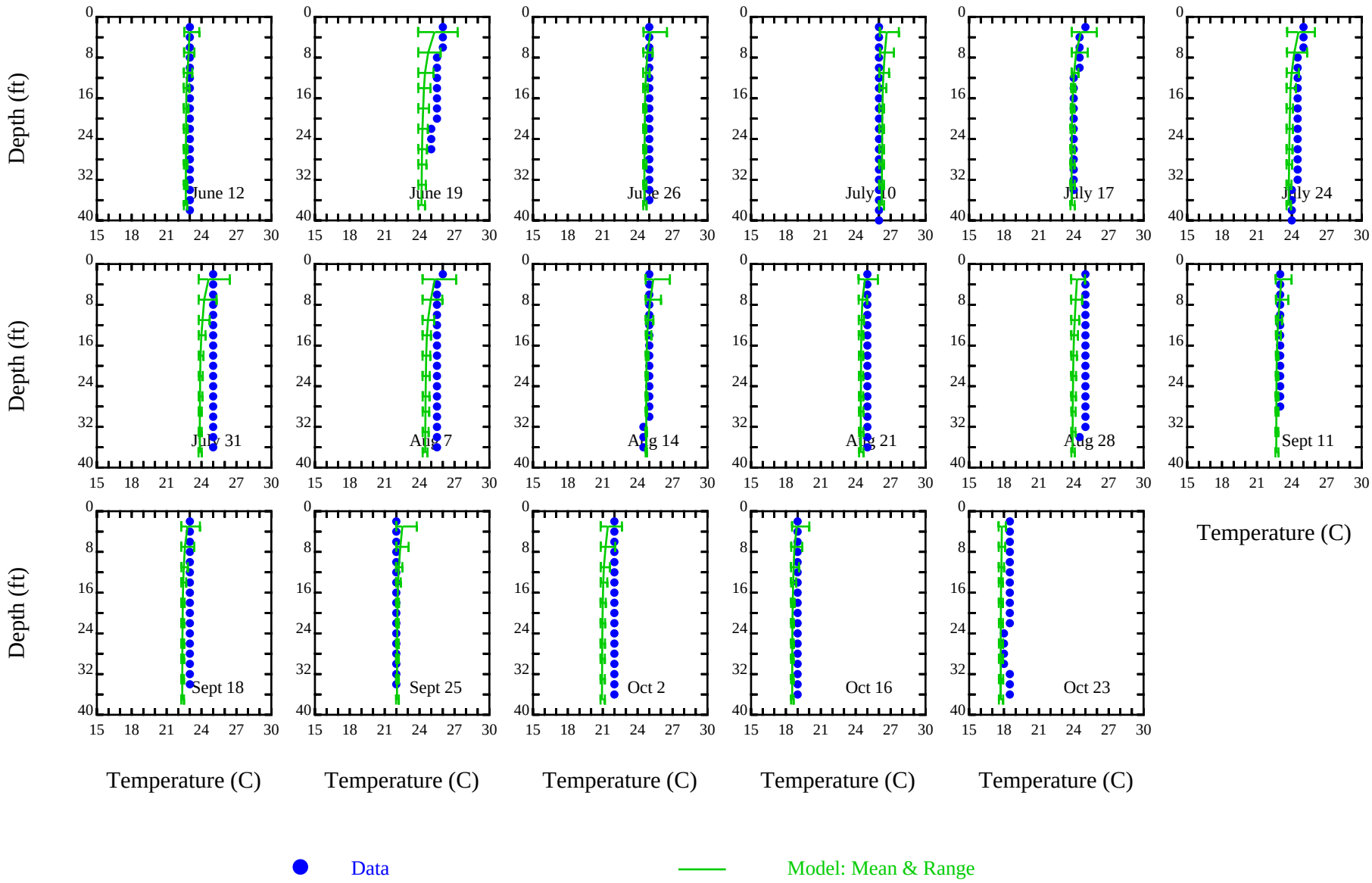

Figure C12. San Joaquin River at R4 Data and Model Temperature Vertical Profiles, June-October 2001

vertdo.gdp, RUN39v4Q

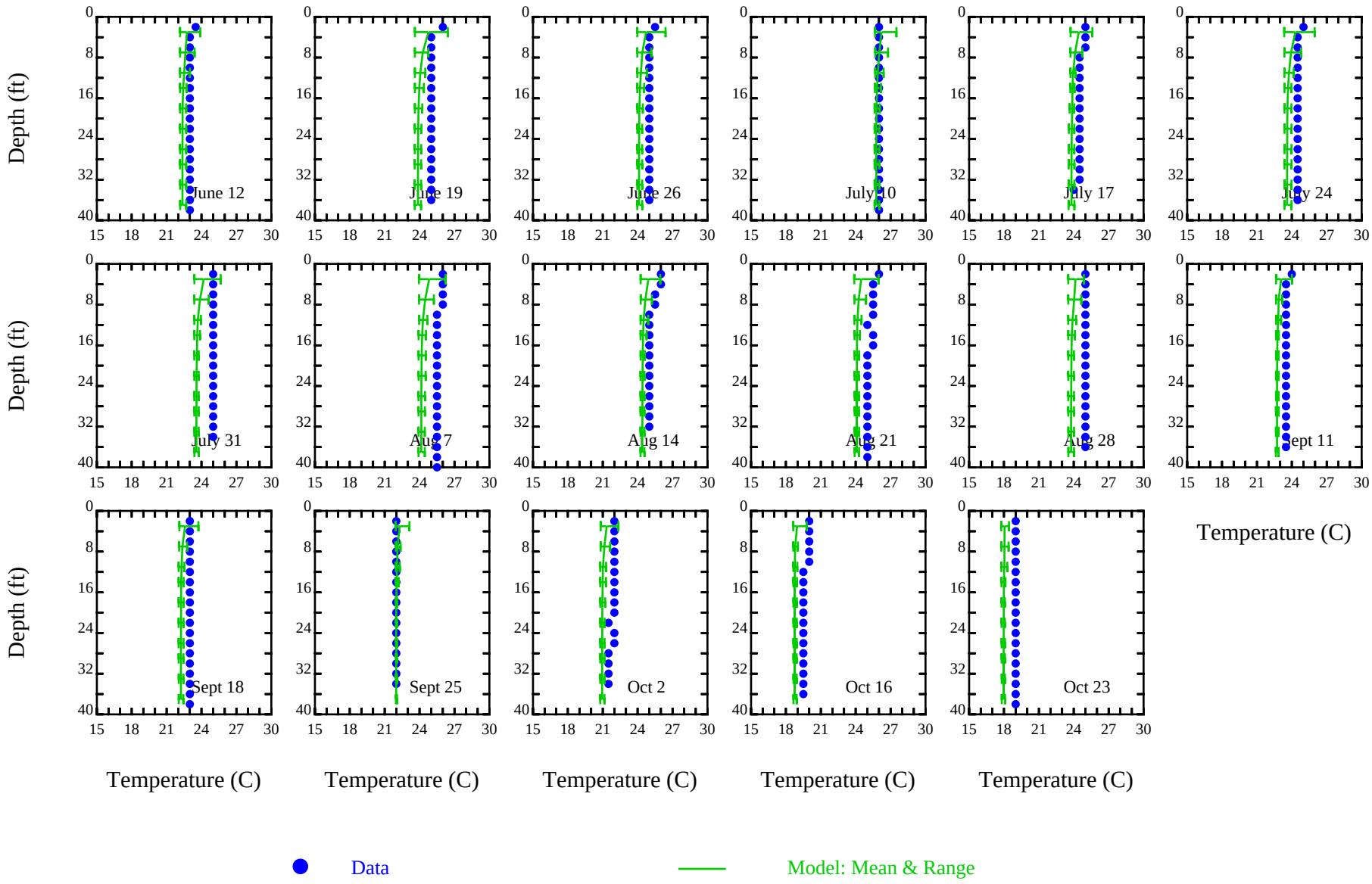

Figure C13. San Joaquin River at R5 Data and Model Temperature Vertical Profiles, June-October 2001

vertdo.gdp, RUN39v4Q

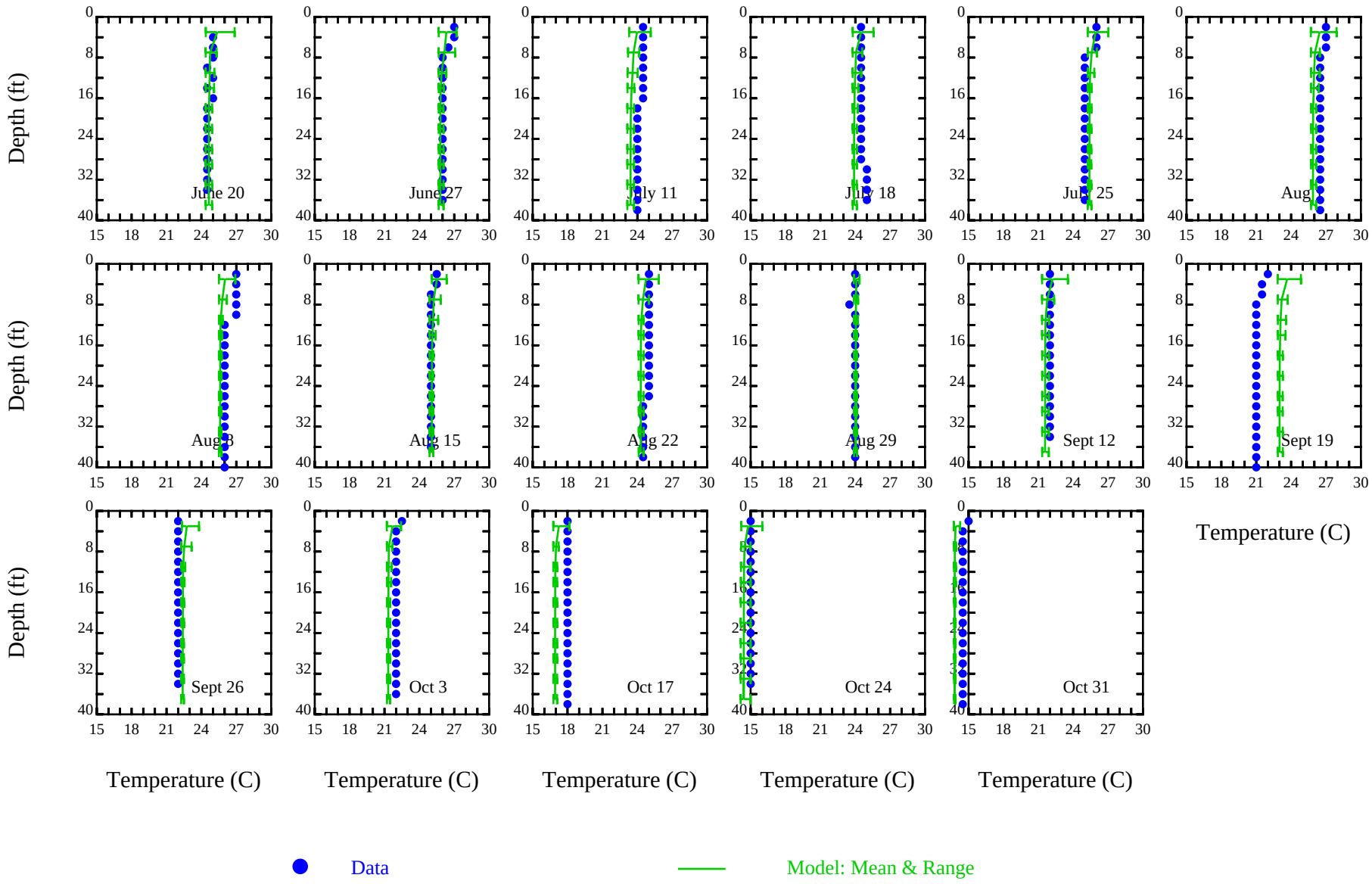

Figure C14. San Joaquin River at R6 Data and Model Temperature Vertical Profiles, June-October 2000

vertdo.gdp, RUN39v4Q

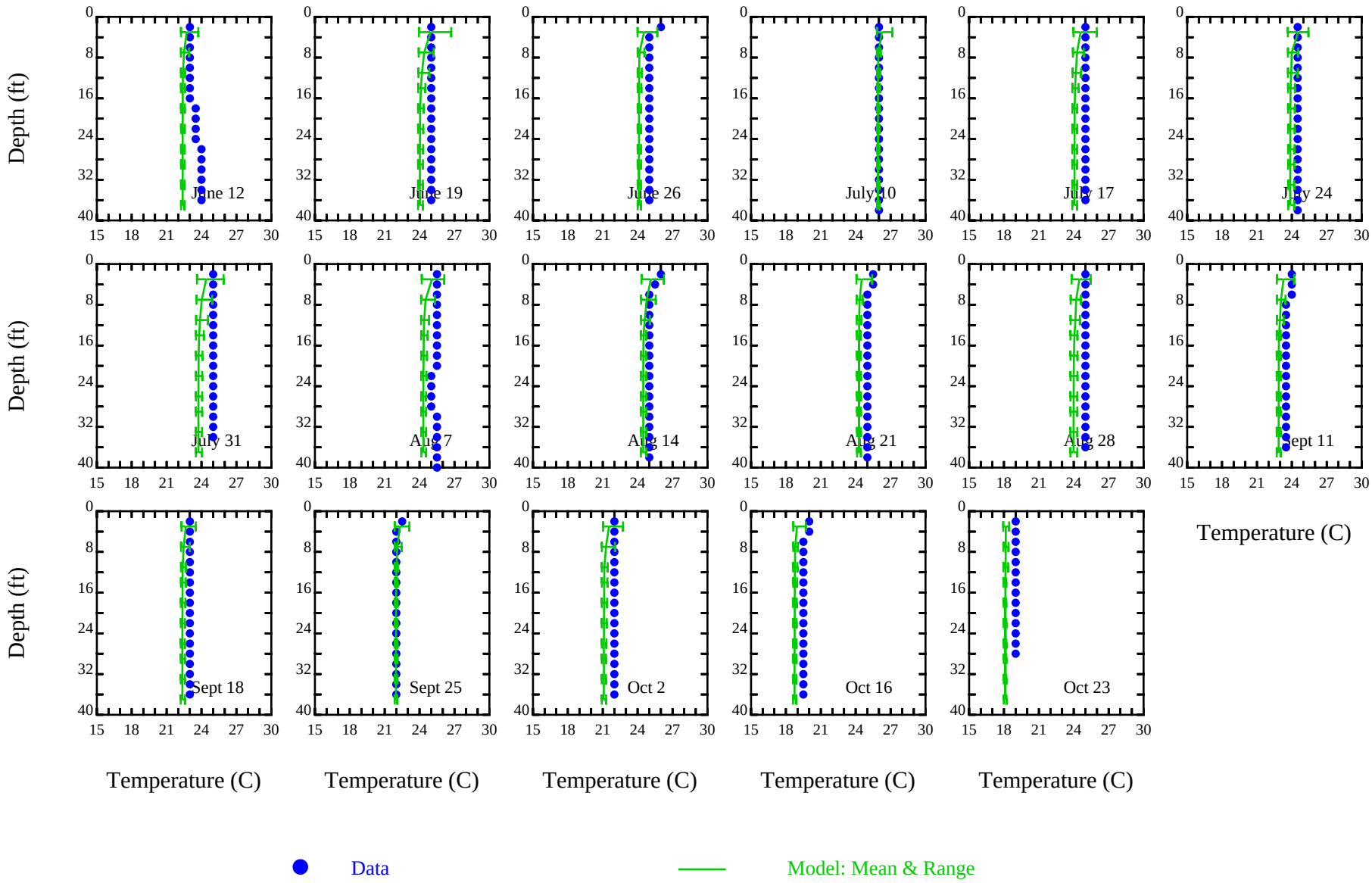

Figure C15. San Joaquin River at R6 Data and Model Temperature Vertical Profiles, June-October 2001

vertdo.gdp, RUN39v4Q

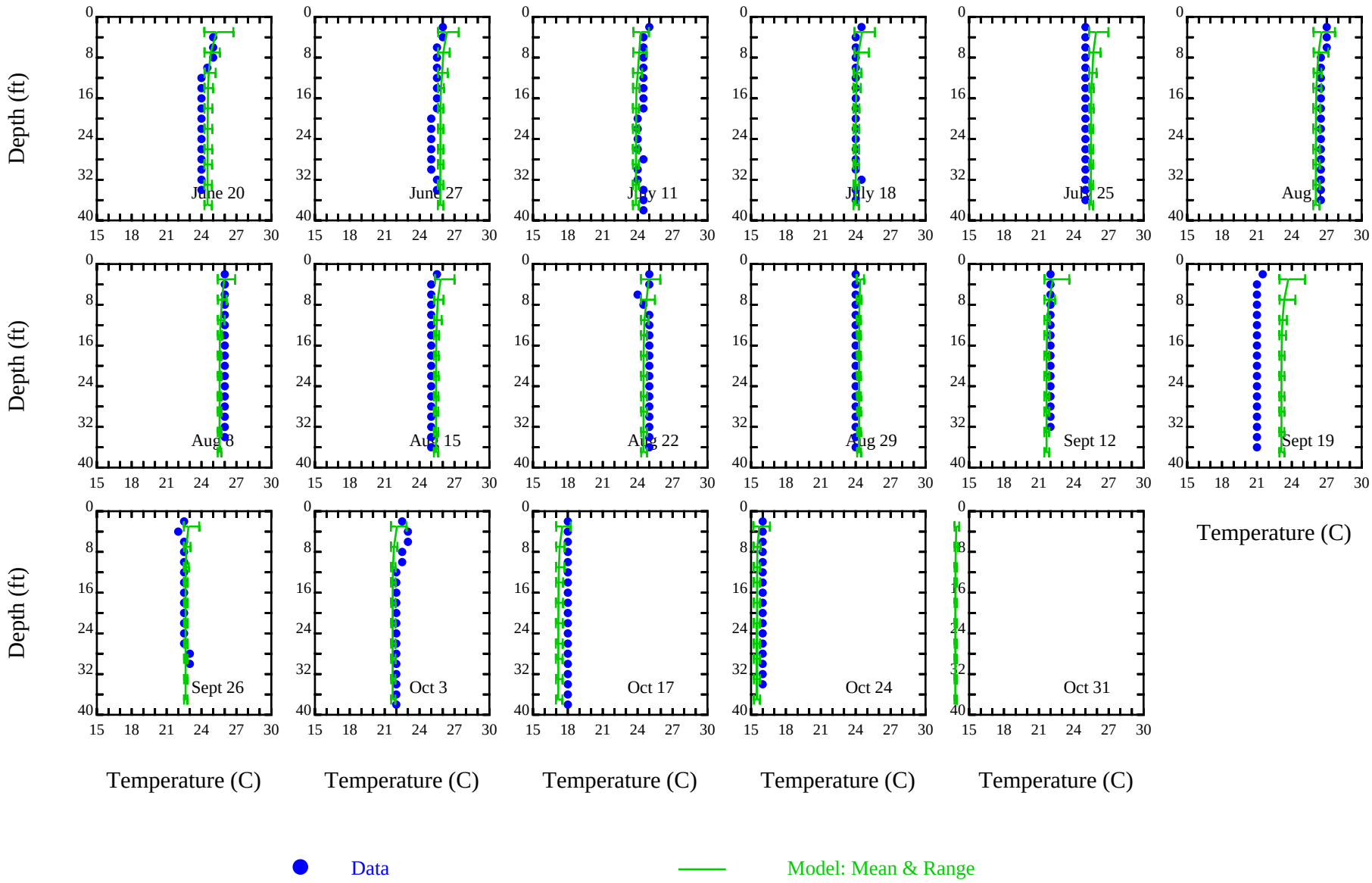

Figure C16. San Joaquin River at R7 Data and Model Temperature Vertical Profiles, June-October 2000

vertdo.gdp, RUN39v4Q

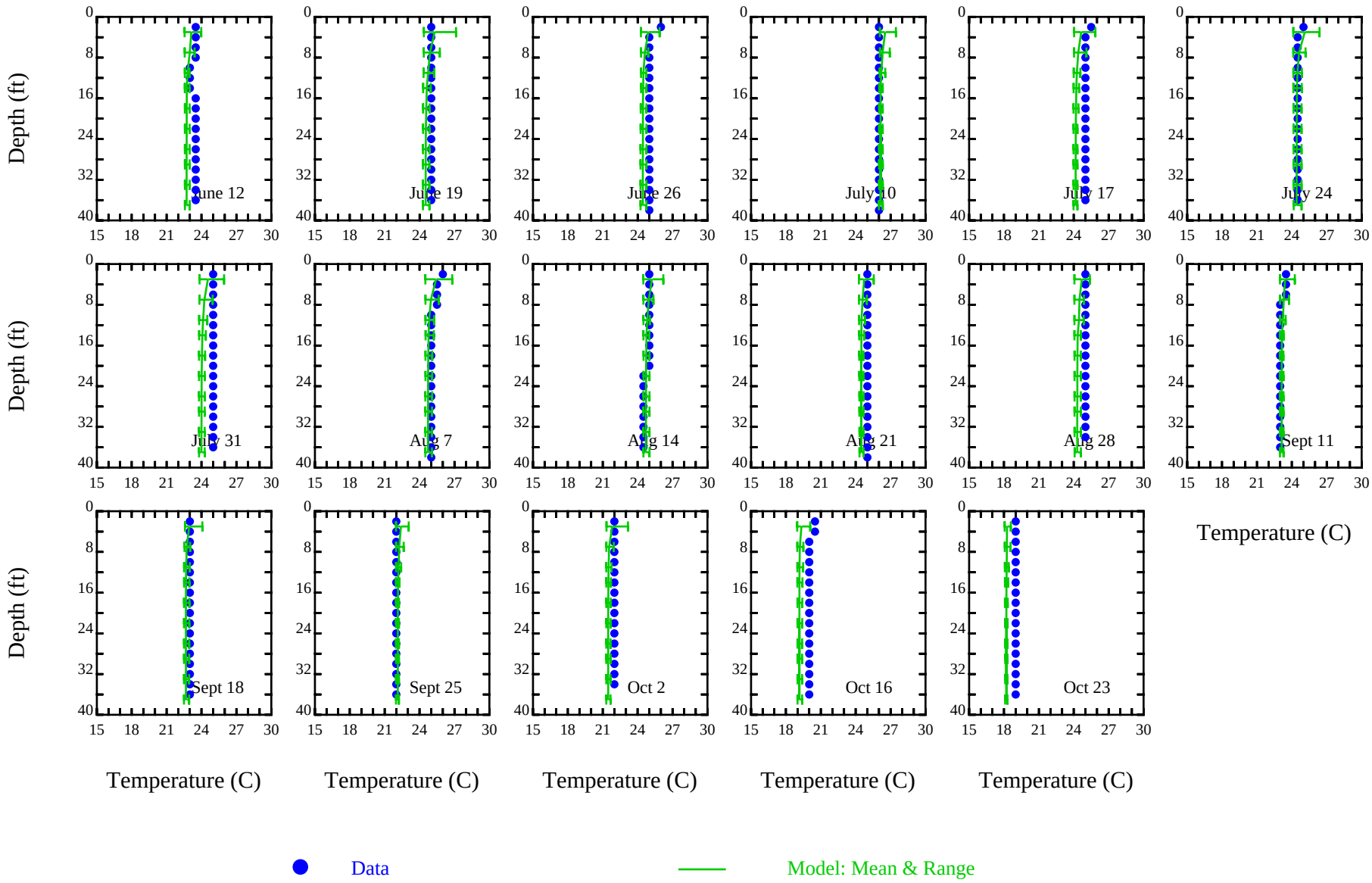

Figure C17. San Joaquin River at R7 Data and Model Temperature Vertical Profiles, June-October 2001

vertdo.gdp, RUN39v4Q

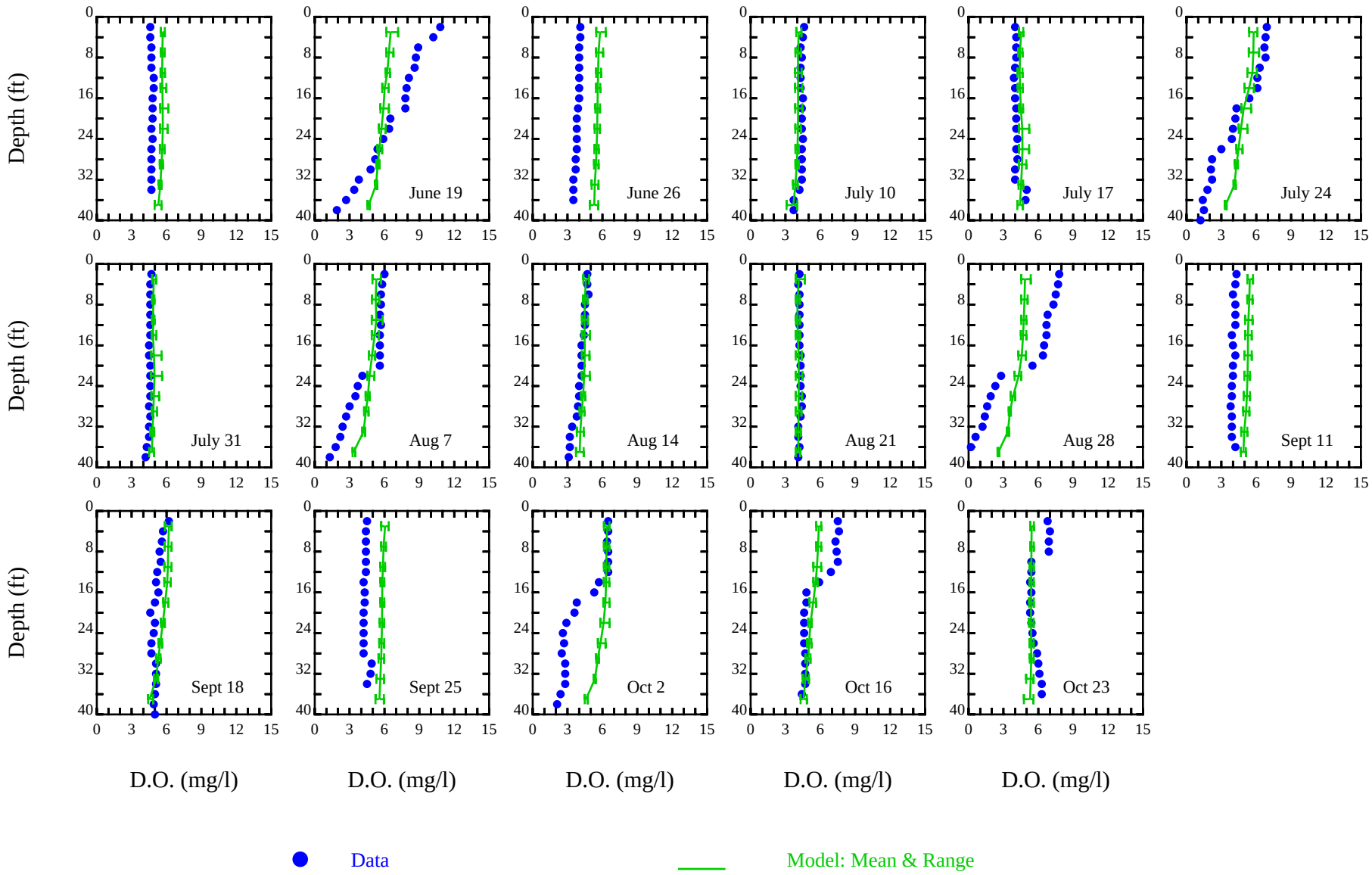

Figure C18. San Joaquin River at Turning Basin Data and Model Dissolved Oxygen Vertical Profiles, June-October 2001

vertdo.gdp, RUN39v4Q

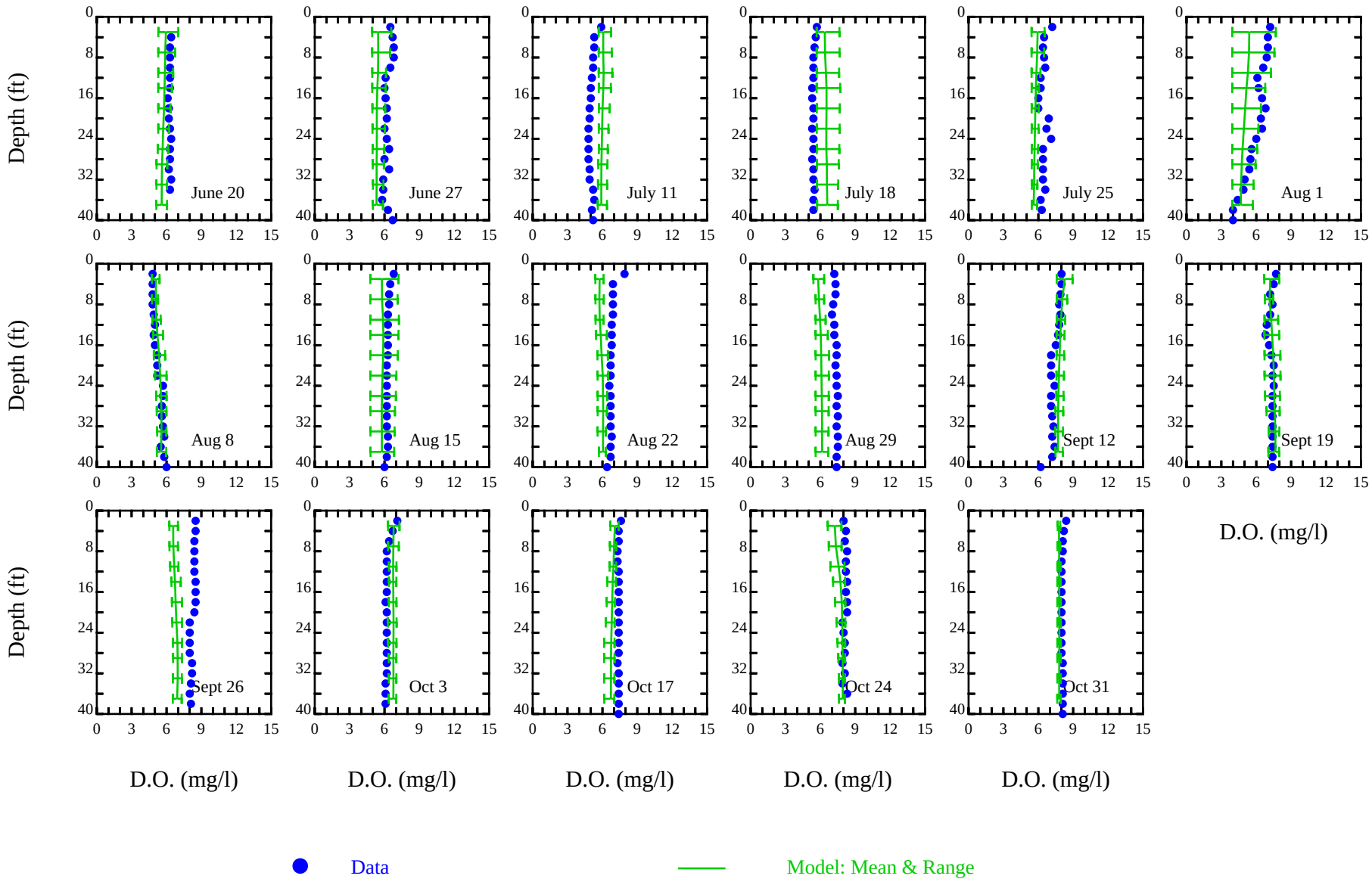

Figure C19. San Joaquin River at R3 Data and Model Dissolved Oxygen Vertical Profiles, June-October 2000

vertdo.gdp, RUN39v4Q

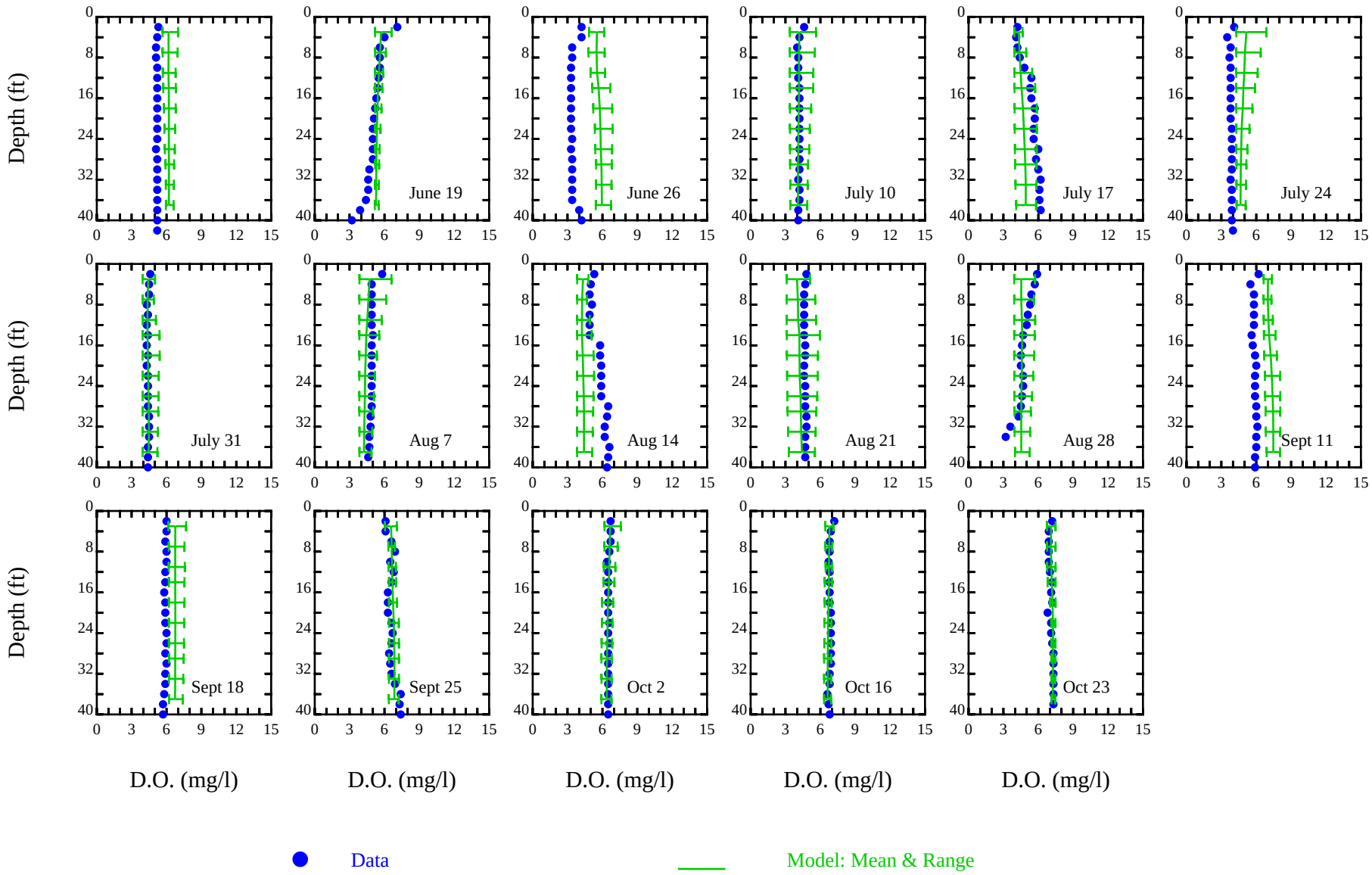

Figure C20. San Joaquin River at R3 Data and Model Dissolved Oxygen Vertical Profiles, June-October 2001

vertdo.gdp, RUN39v4Q

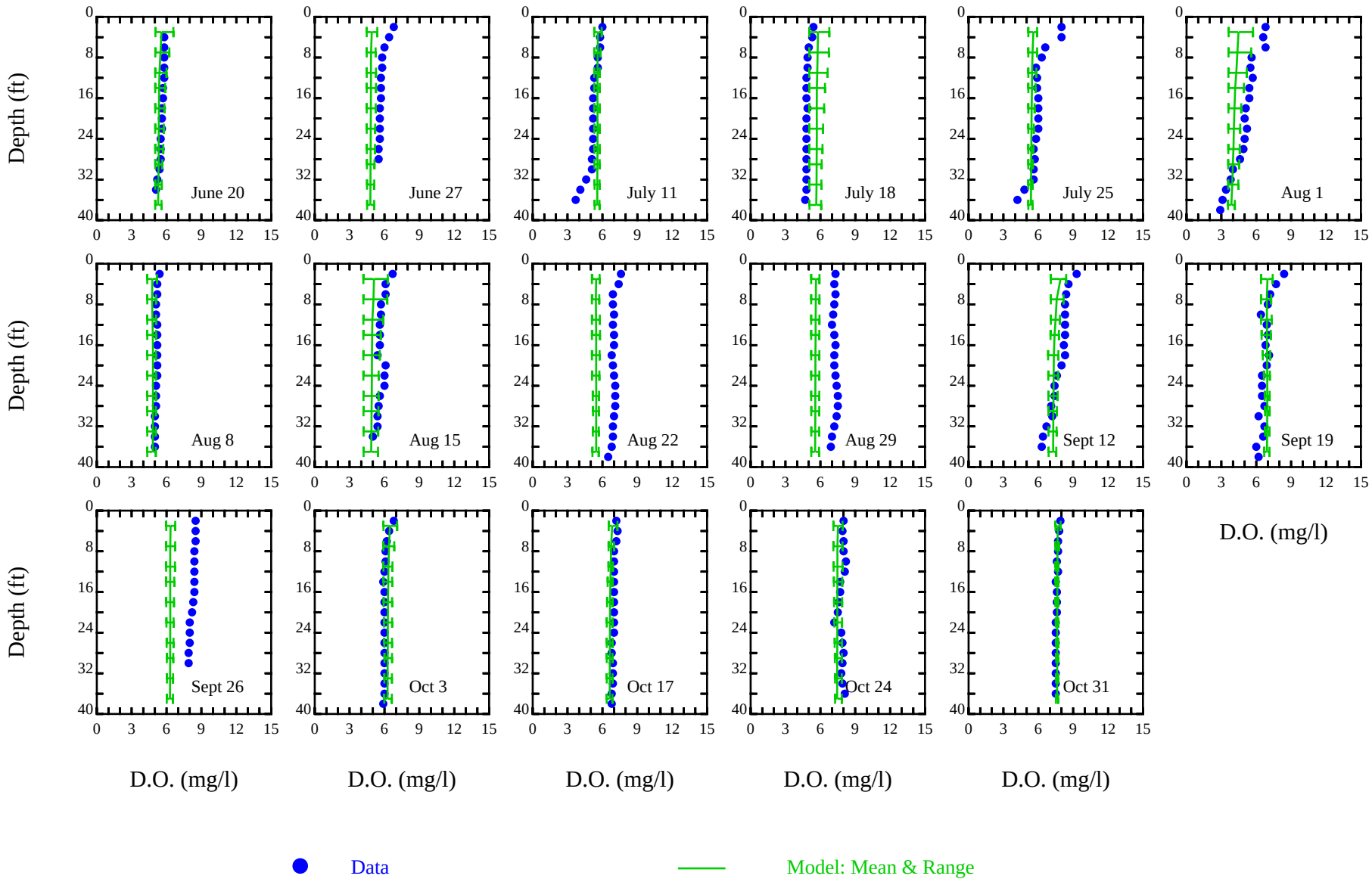

Figure C21. San Joaquin River at R4 Data and Model Dissolved Oxygen Vertical Profiles, June-October 2000

vertdo.gdp, RUN39v4Q

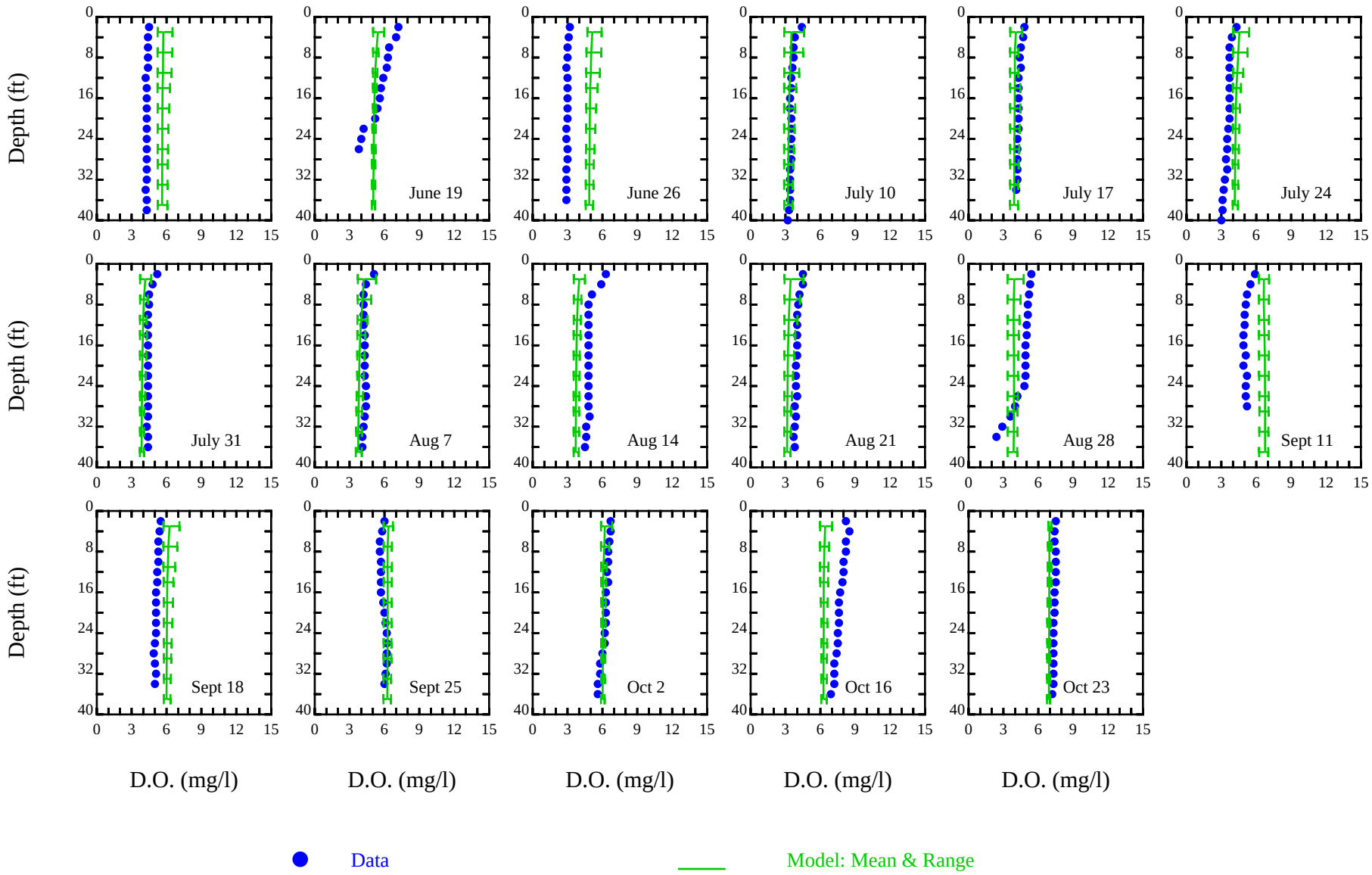

Figure C22. San Joaquin River at R4 Data and Model Dissolved Oxygen Vertical Profiles, June-October 2001

vertdo.gdp, RUN39v4Q

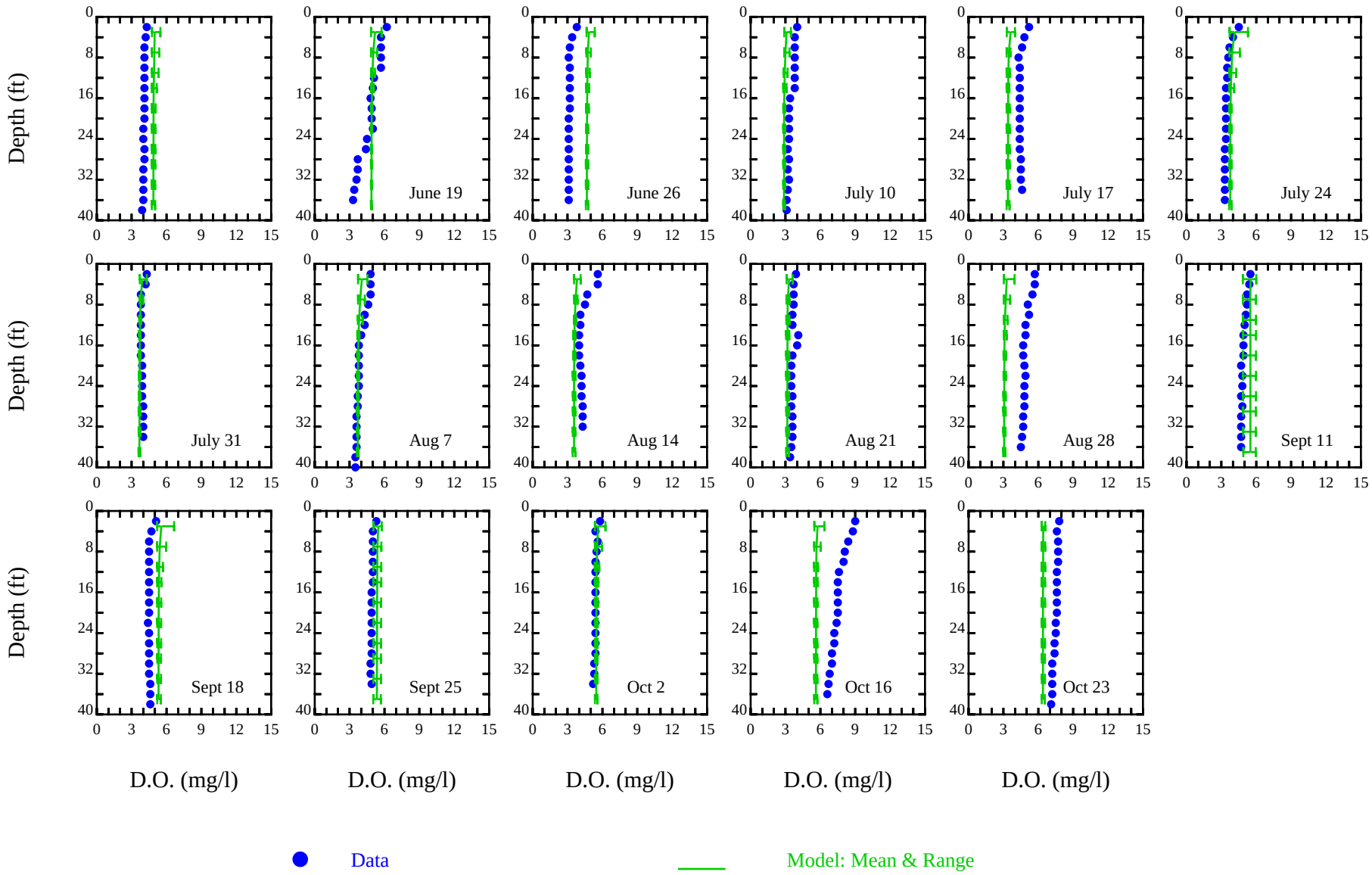

Figure C23. San Joaquin River at R5 Data and Model Dissolved Oxygen Vertical Profiles, June-October 2001

vertdo.gdp, RUN39v4Q

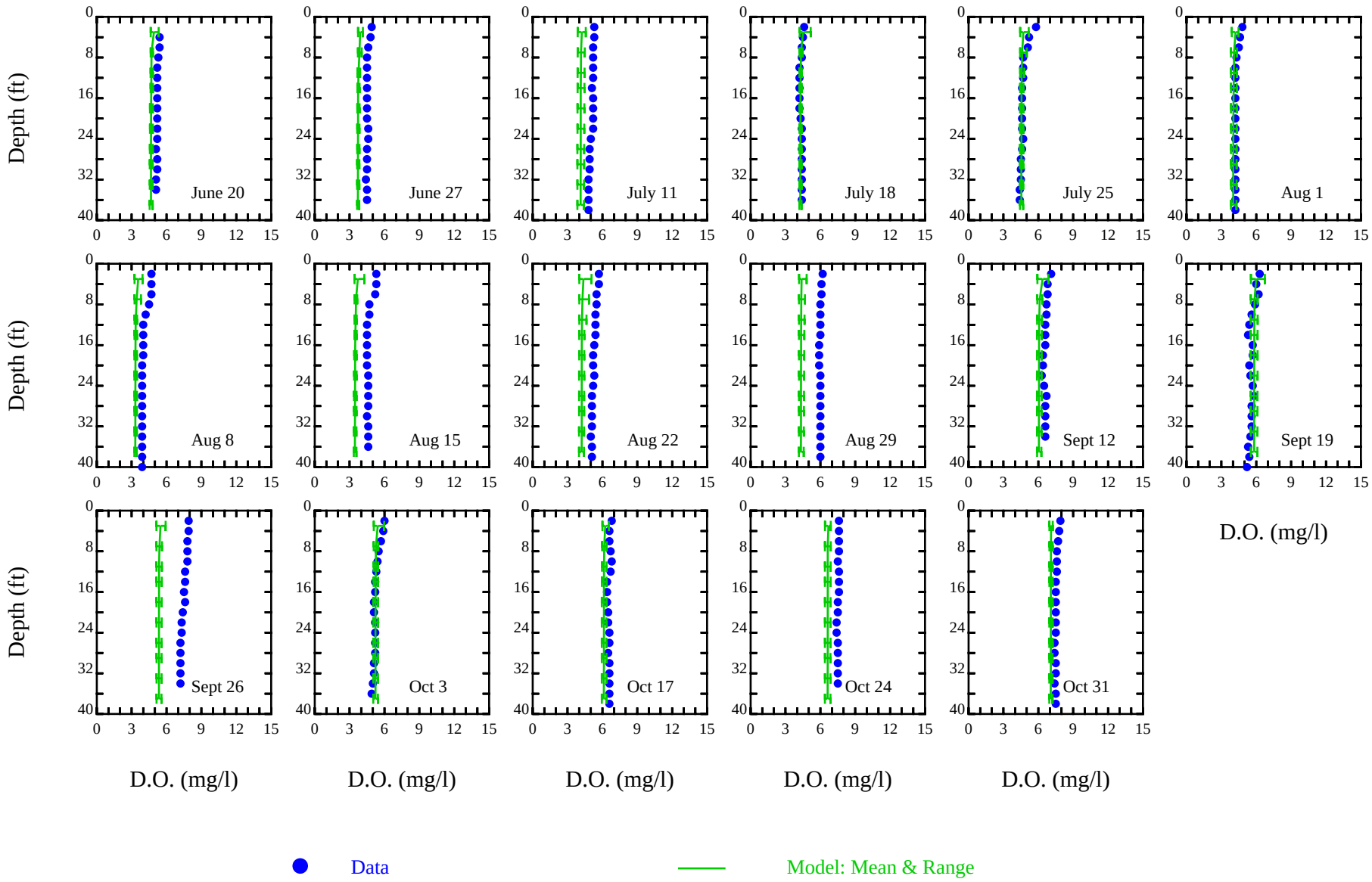

Figure C24. San Joaquin River at R6 Data and Model Dissolved Oxygen Vertical Profiles, June-October 2000

vertdo.gdp, RUN39v4Q

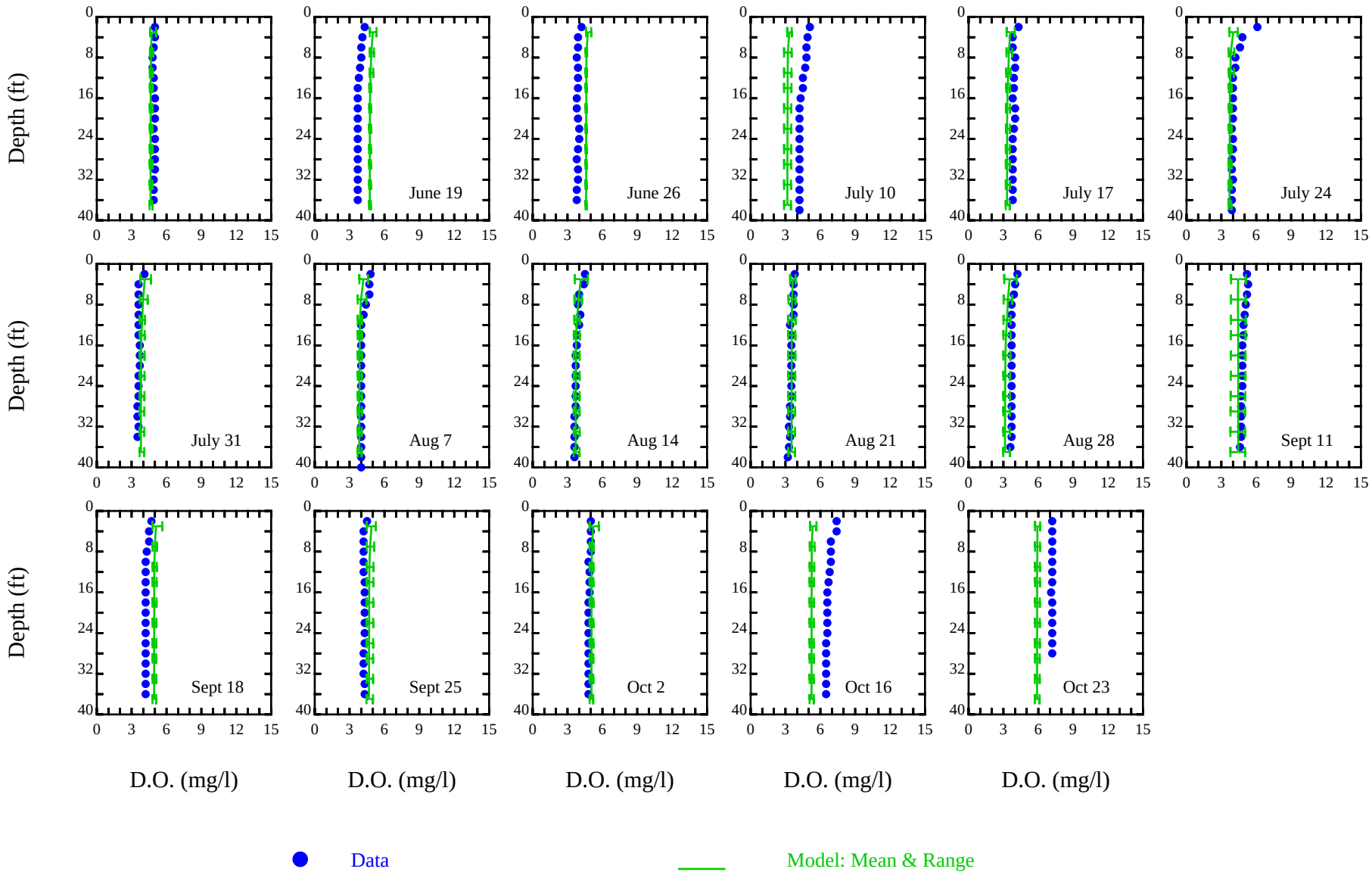

Figure C25. San Joaquin River at R6 Data and Model Dissolved Oxygen Vertical Profiles, June-October 2001

vertdo.gdp, RUN39v4Q

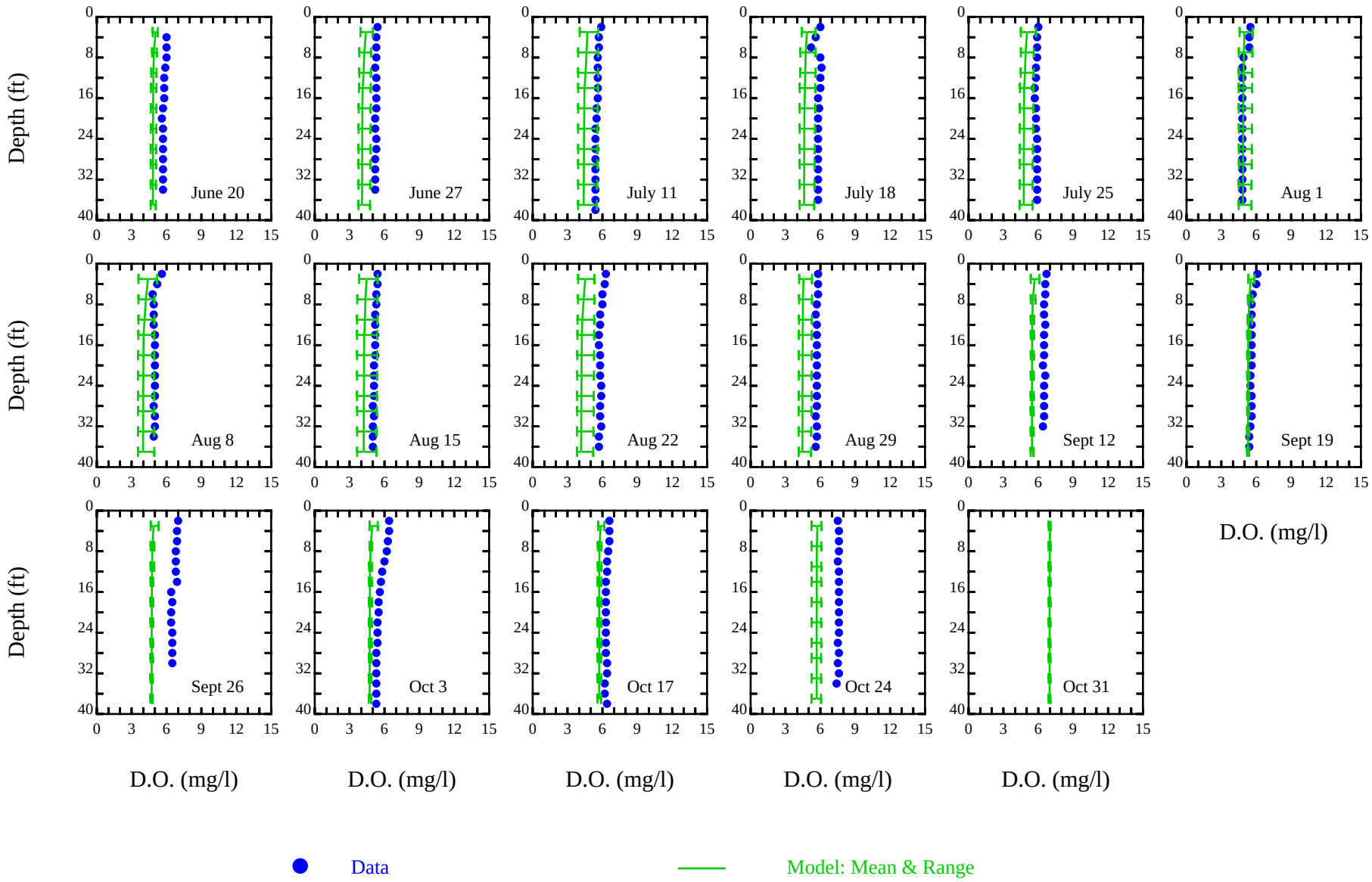

Figure C26. San Joaquin River at R7 Data and Model Dissolved Oxygen Vertical Profiles, June-October 2000

vertdo.gdp, RUN39v4Q

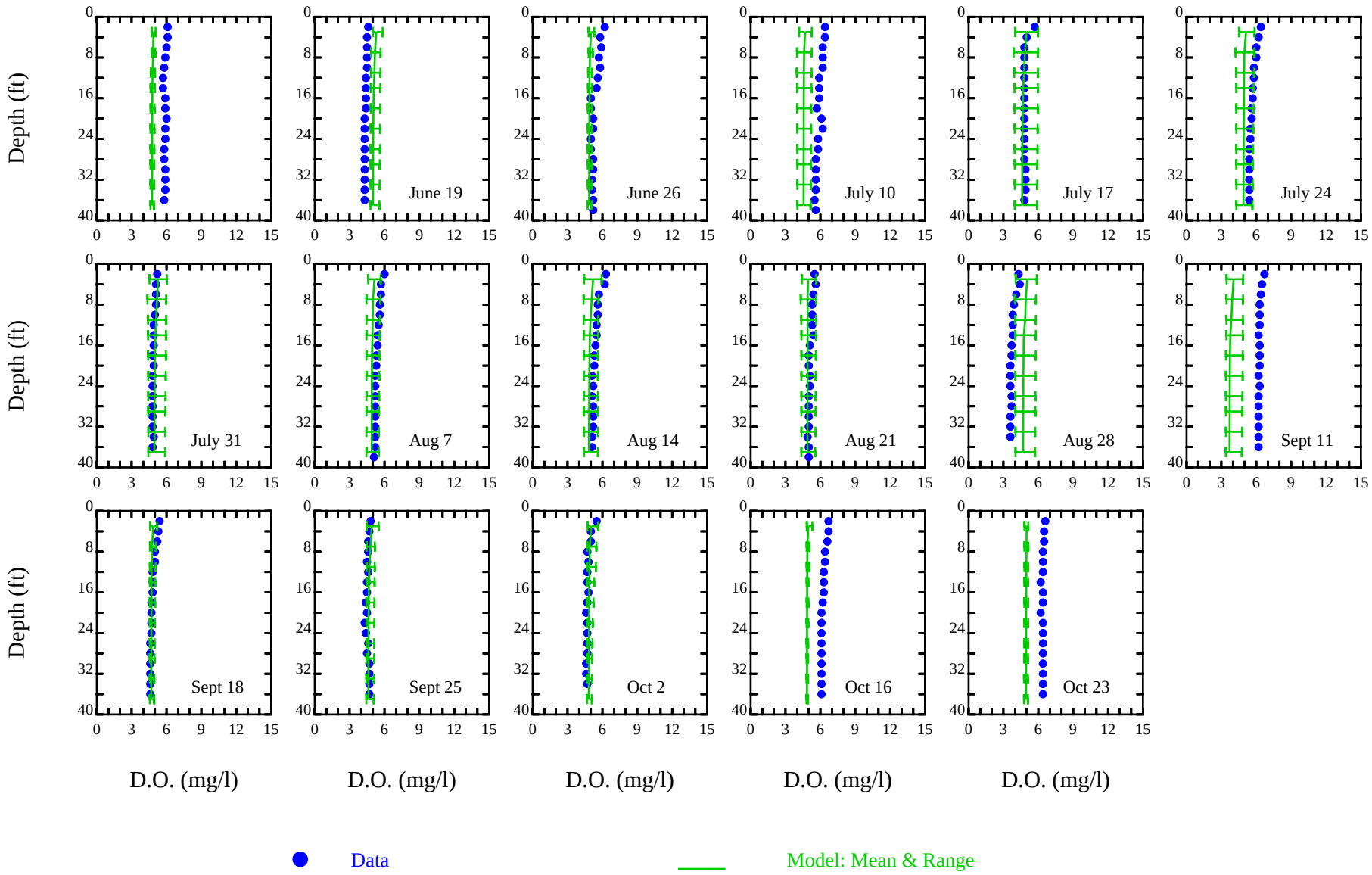

Figure C27. San Joaquin River at R7 Data and Model Dissolved Oxygen Vertical Profiles, June-October 2001

vertdo.gdp, RUN39v4Q

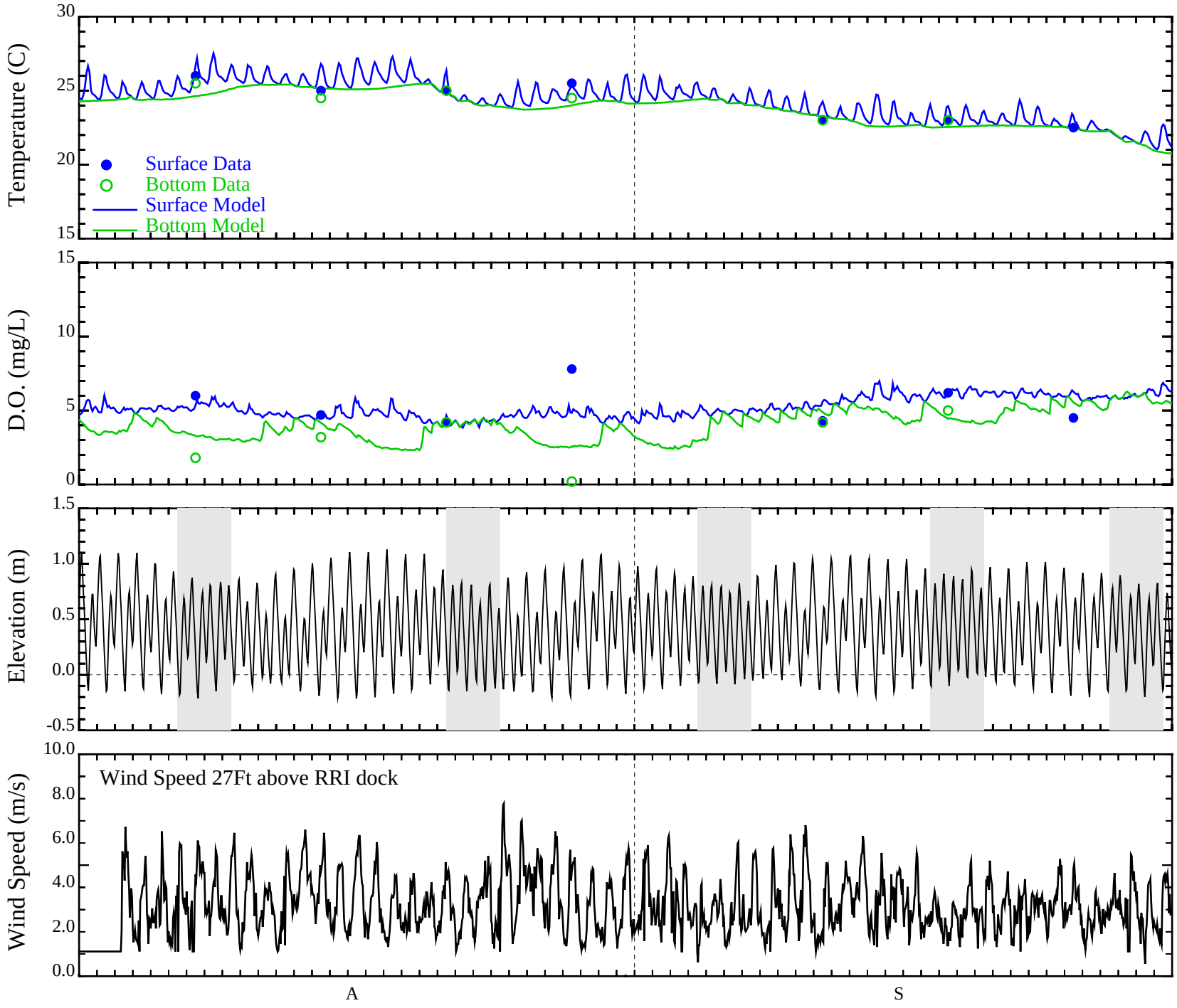

Figure C28. San Joaquin River Stratification, August-September 2001 Station: Turning Basin

Data Source: J&S Data Atlas

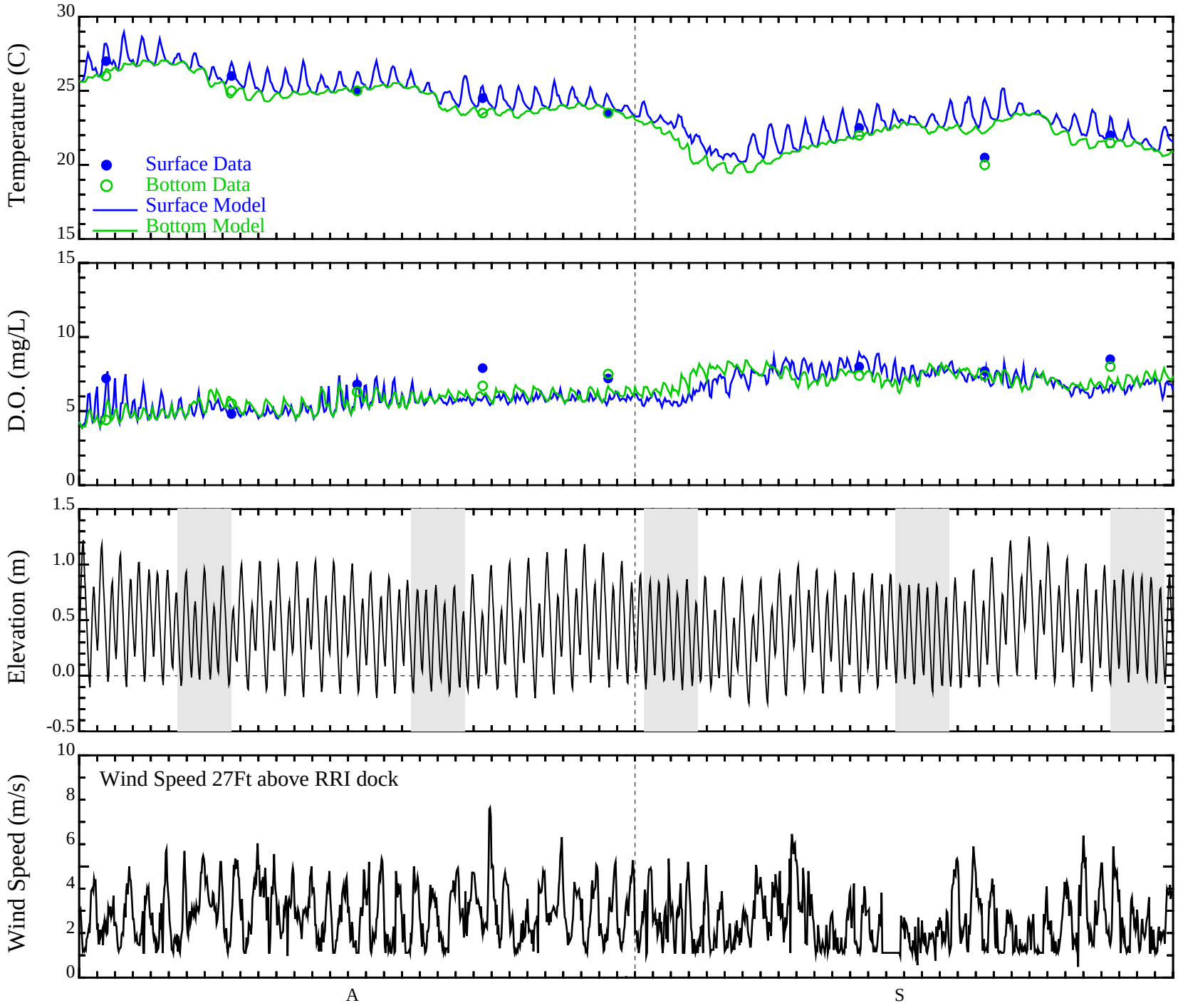

Figure C29. San Joaquin River Stratification, August-September 2000 Station: R3

Data Source: J&S Data Atlas

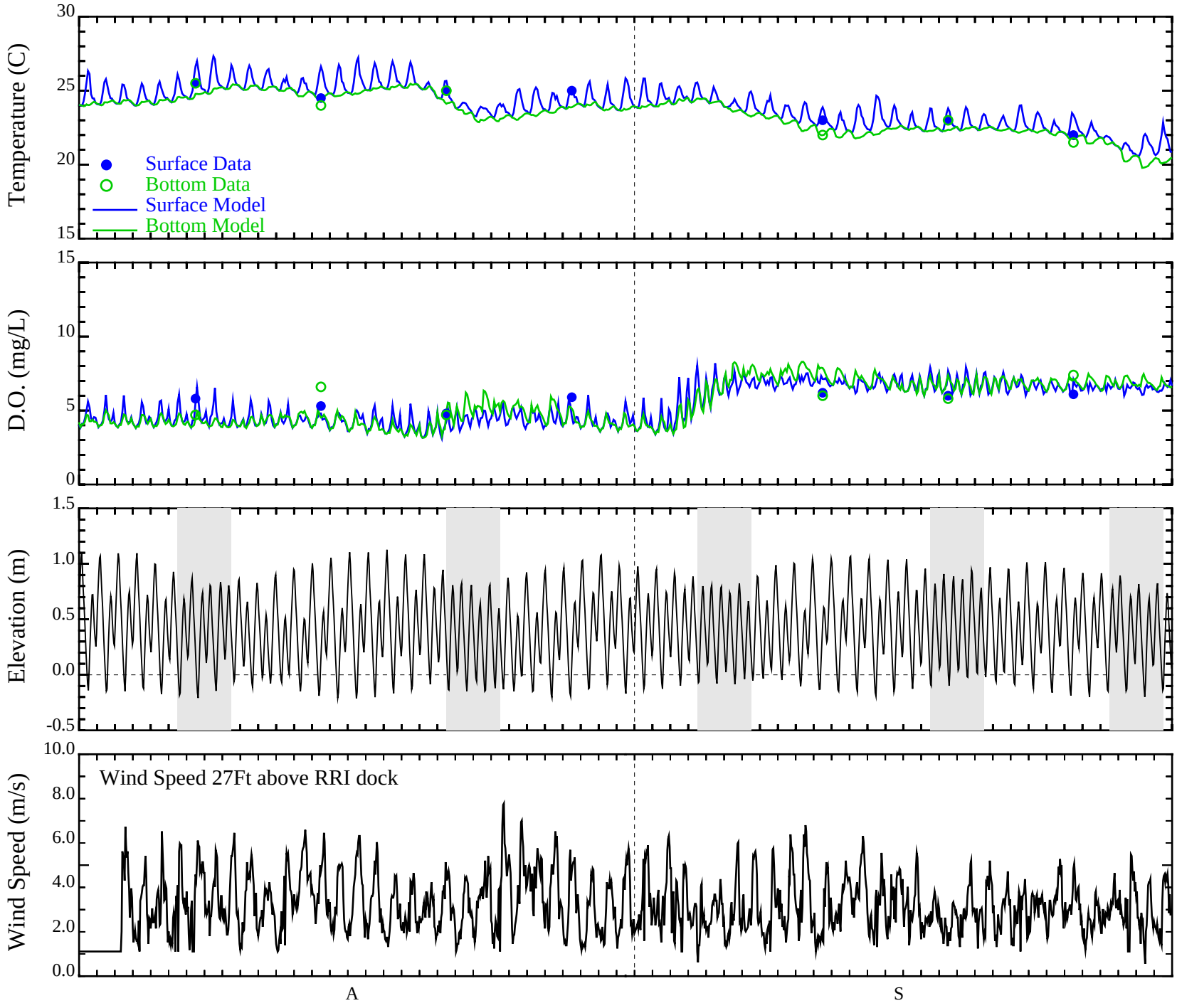

Figure C30. San Joaquin River Stratification, August-September 2001 Station: R3

Data Source: J&S Data Atlas

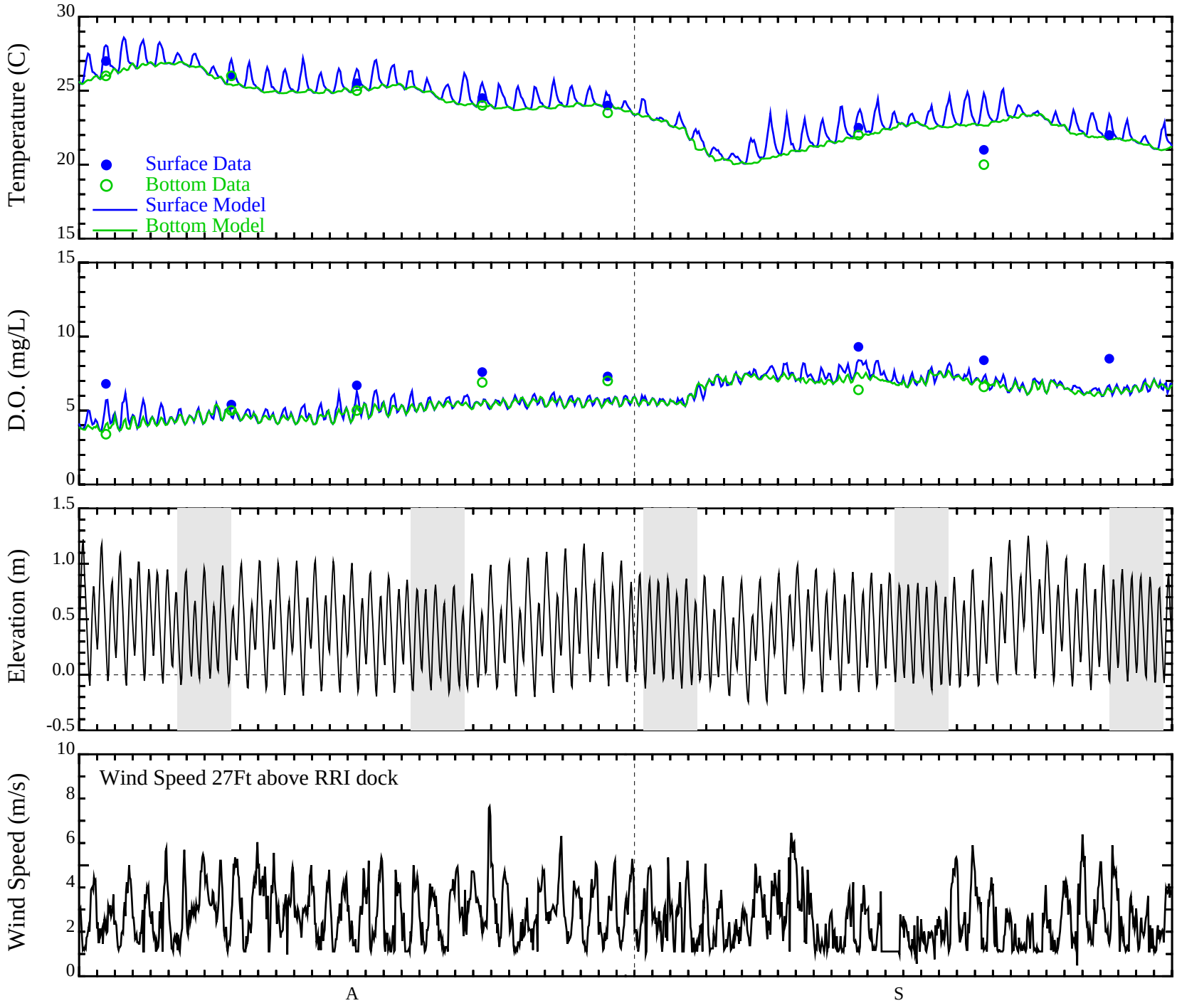

Figure C31. San Joaquin River Stratification, August-September 2000 Station: R4

Data Source: J&S Data Atlas

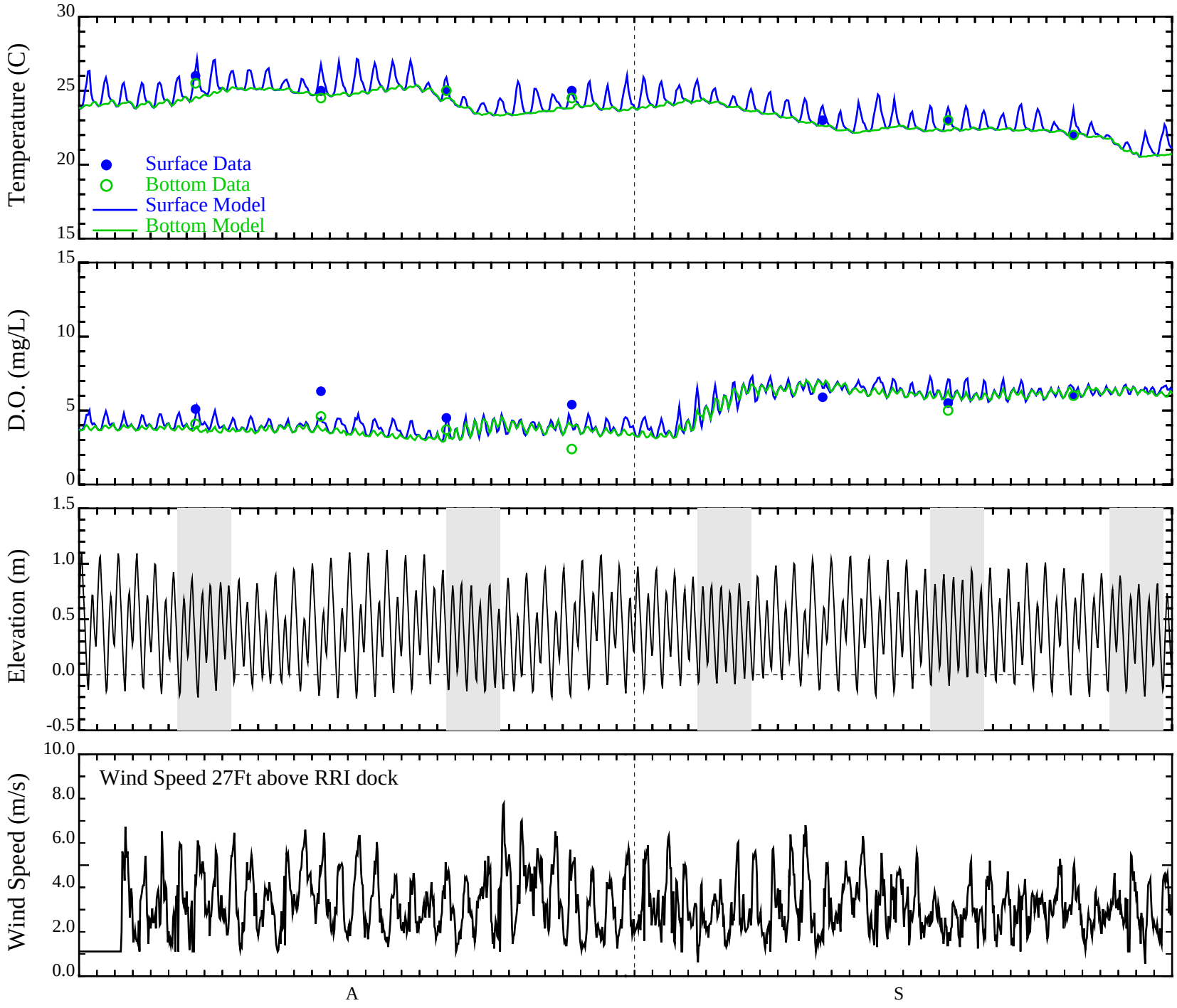

Figure C32. San Joaquin River Stratification, August-September 2001 Station: R4

Data Source: J&S Data Atlas

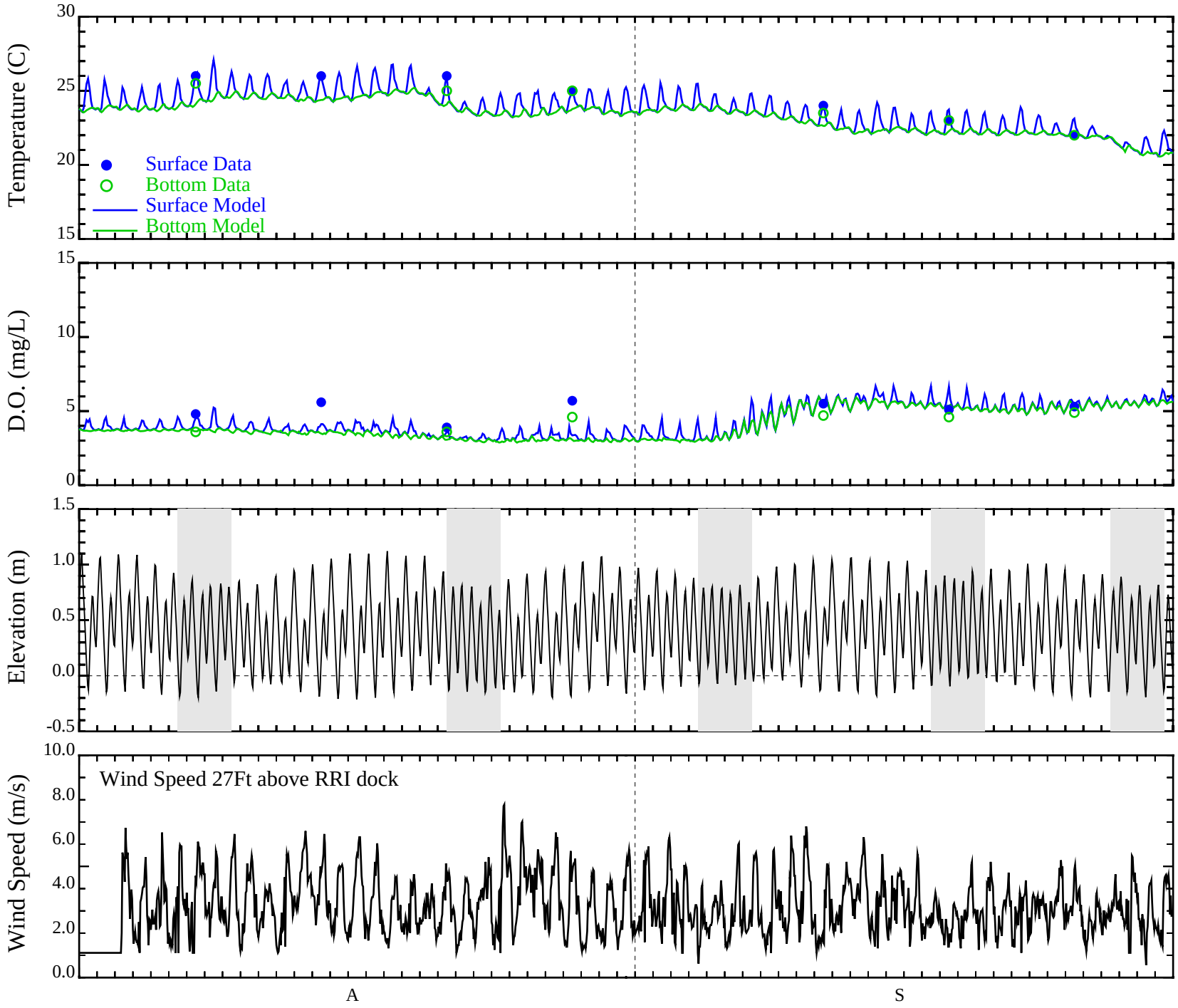

Figure C33. San Joaquin River Stratification, August-September 2001 Station: R5

Data Source: J&S Data Atlas

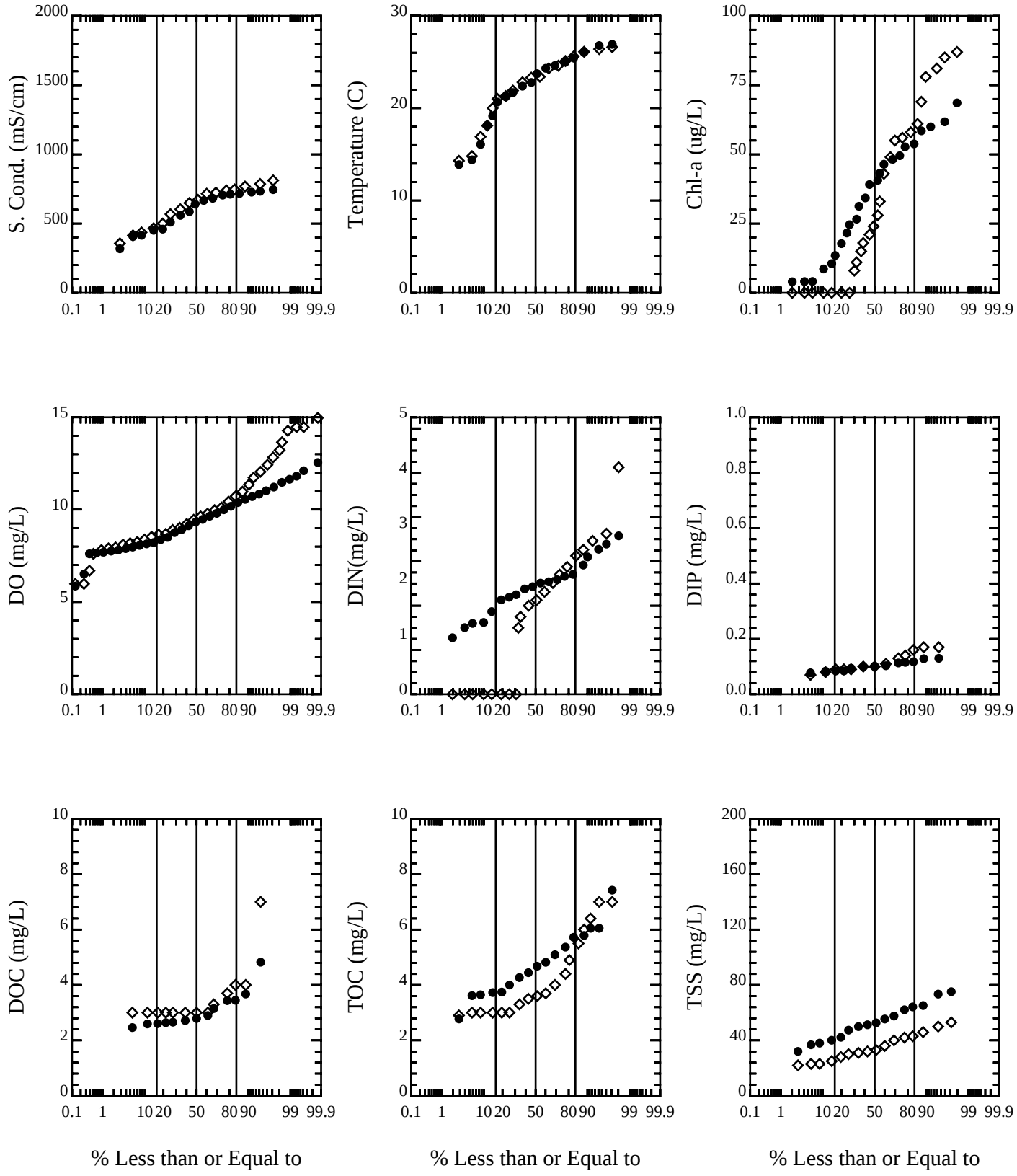

Figure C34. San Joaquin River, Model & Data Comparisons: SJR at Mossdale

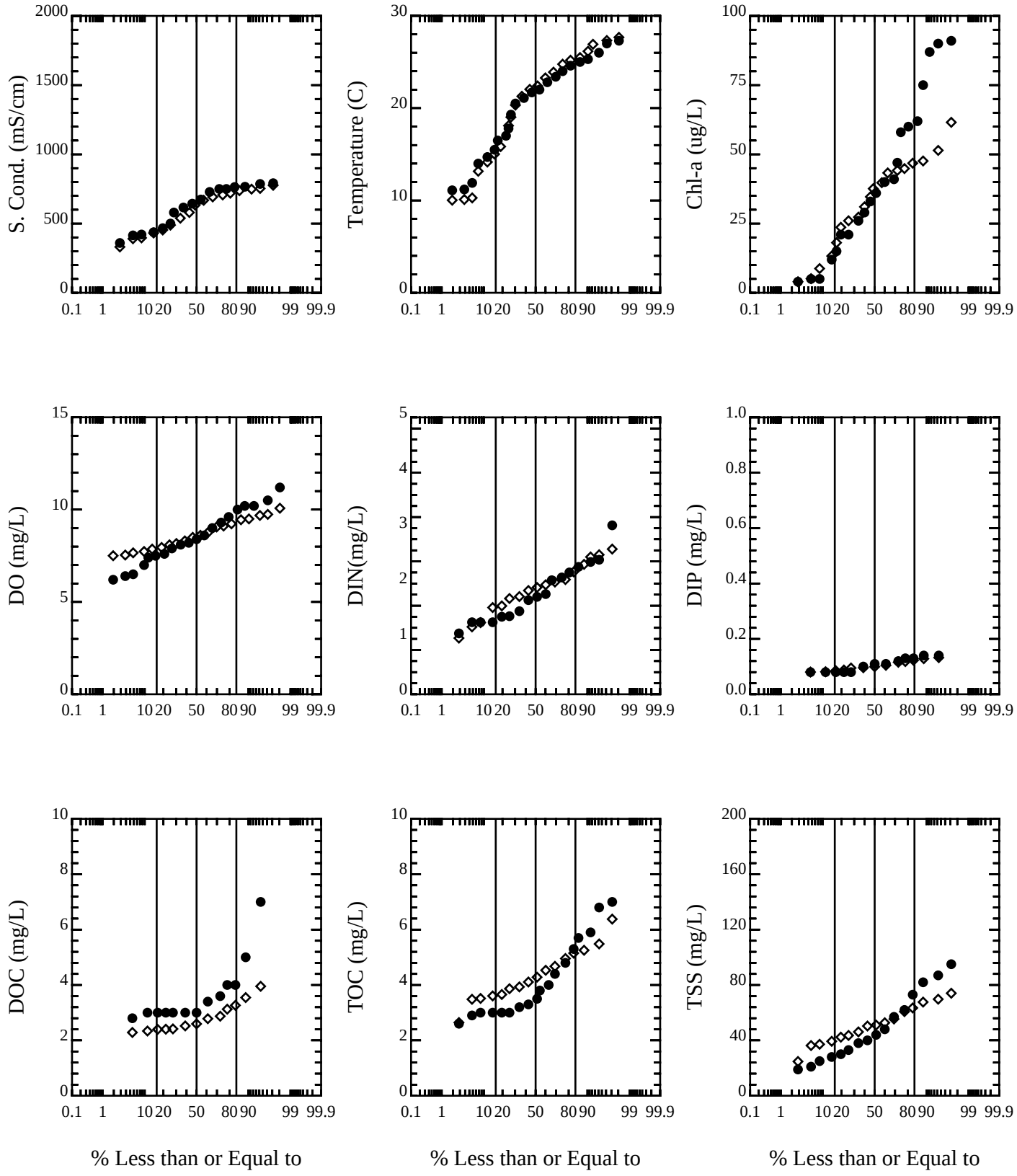

Figure C35. San Joaquin River, Model & Data Comparisons: SJR at R1

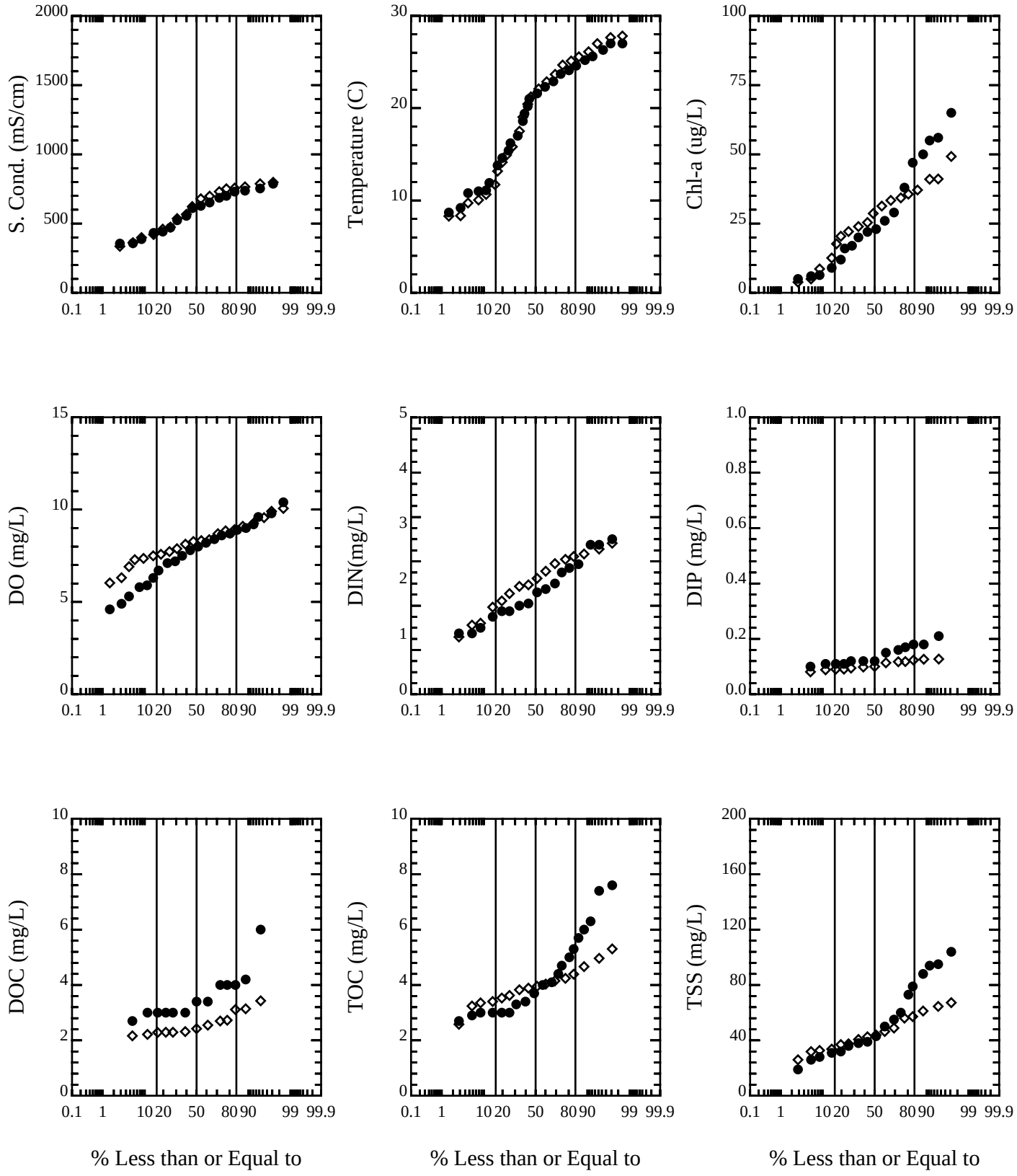

Figure C36. San Joaquin River, Model & Data Comparisons: SJR at R2

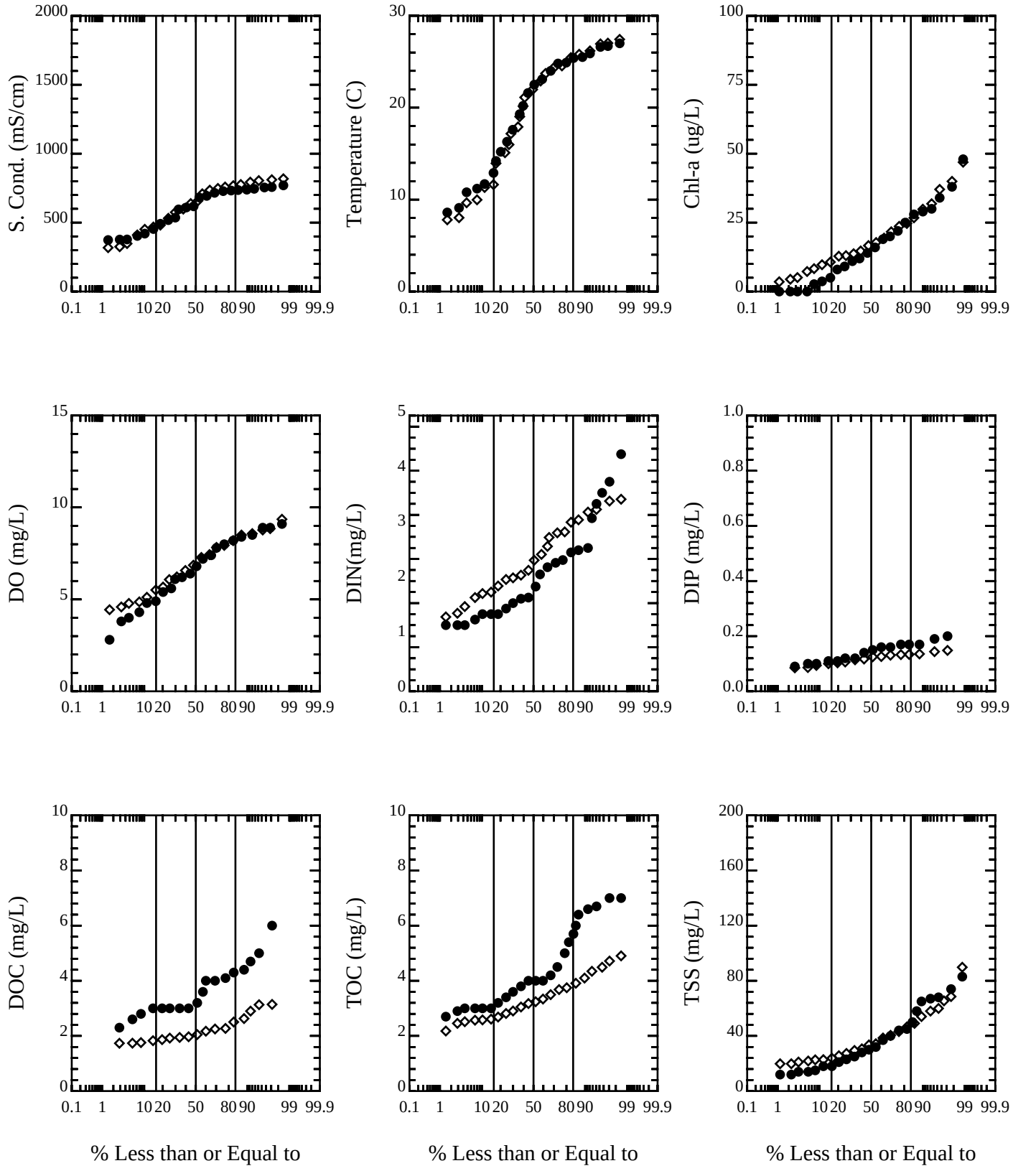

Figure C37. San Joaquin River, Model & Data Comparisons: SJR at R3

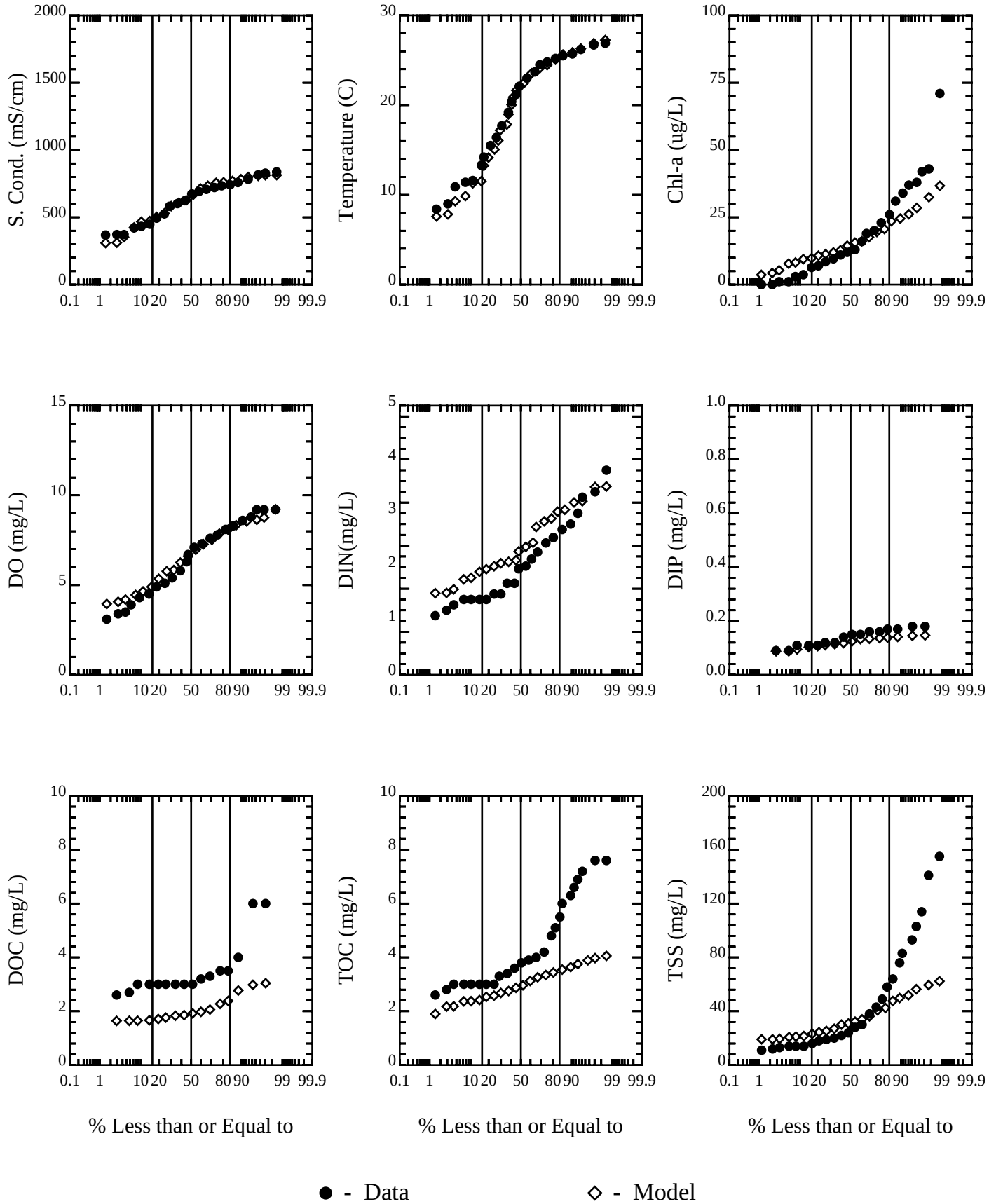

Figure C38. San Joaquin River, Model & Data Comparisons: SJR at R4

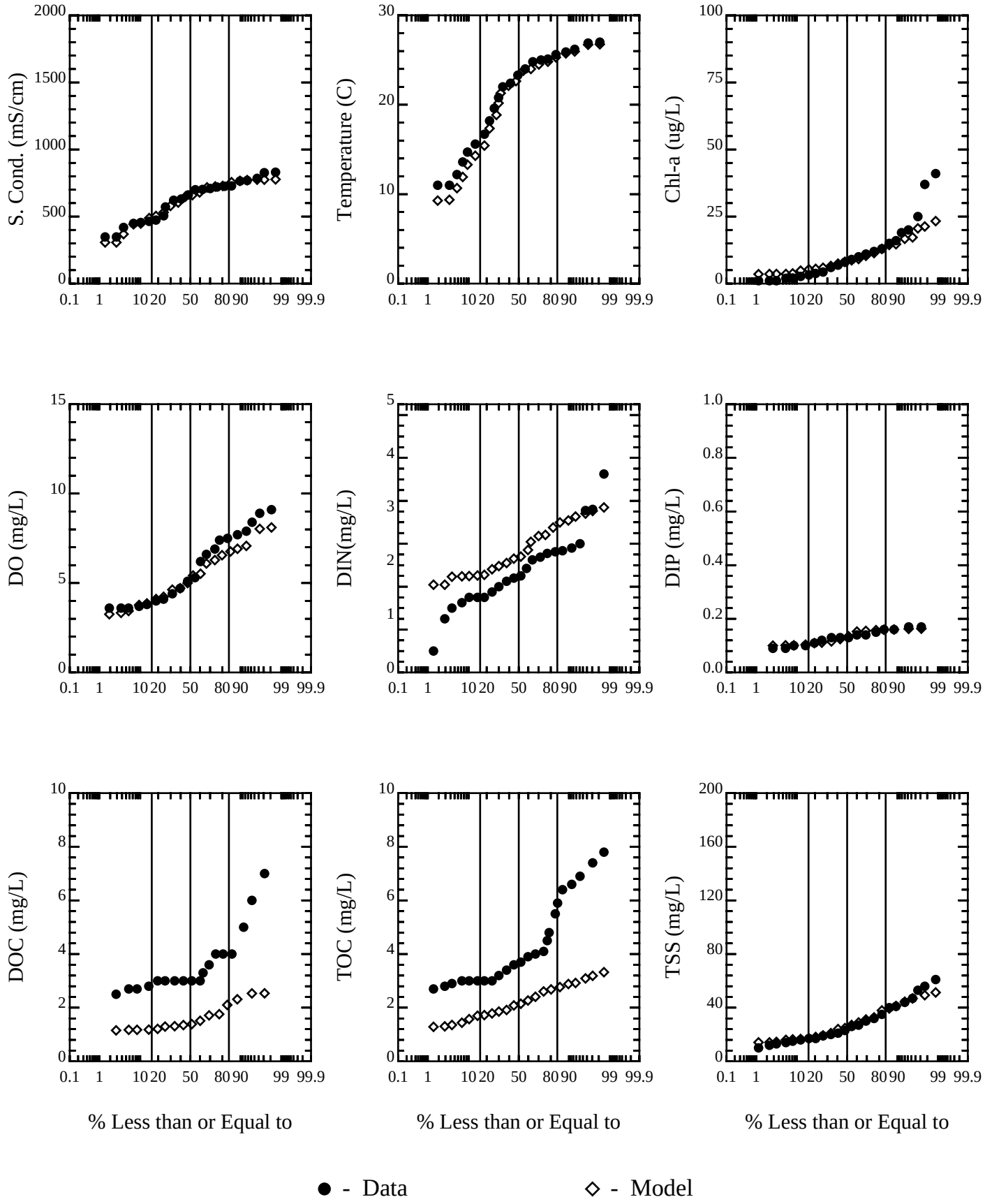

Figure C39. San Joaquin River, Model & Data Comparisons: SJR at R6

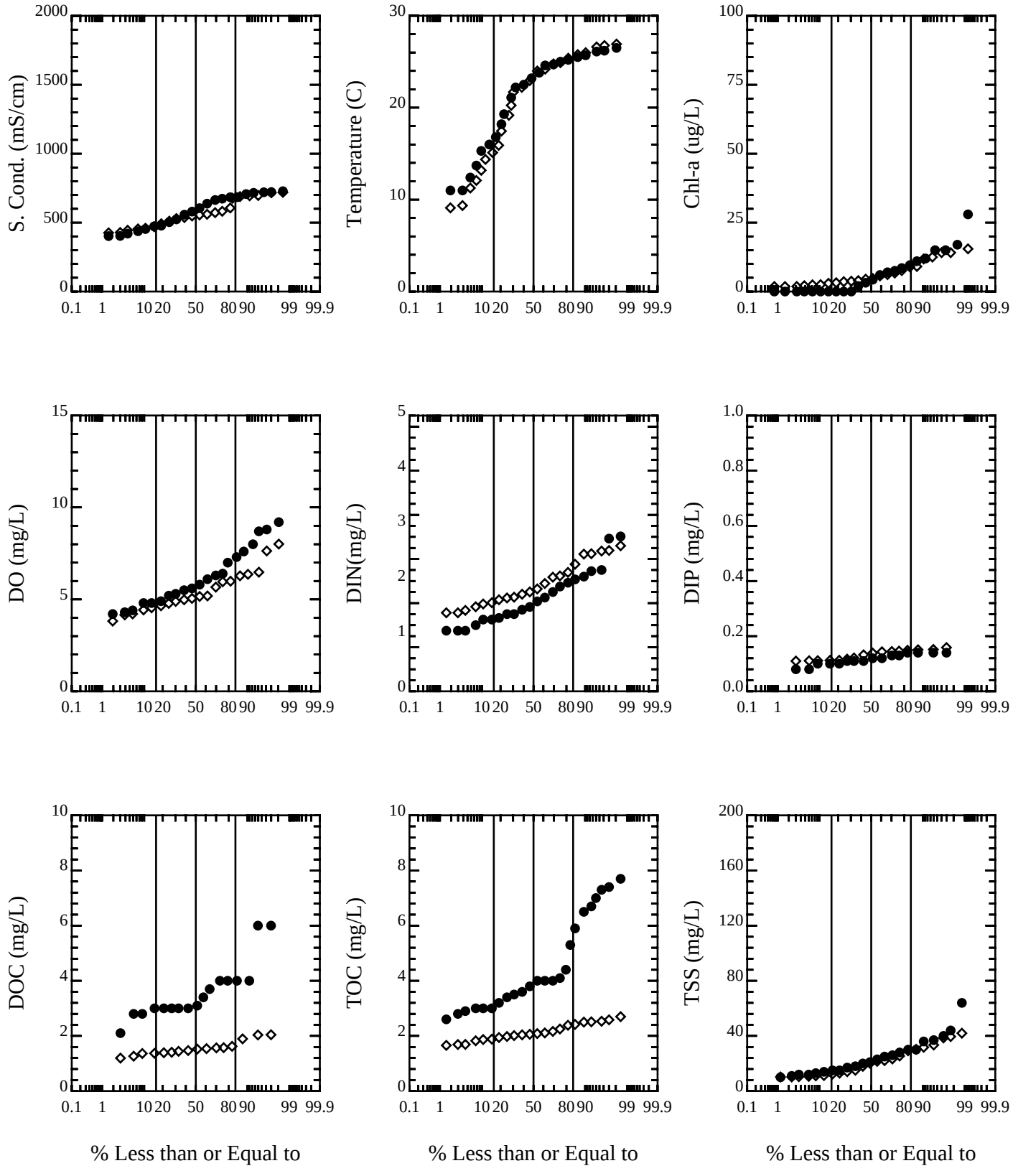

Figure C40. San Joaquin River, Model & Data Comparisons: SJR at R7

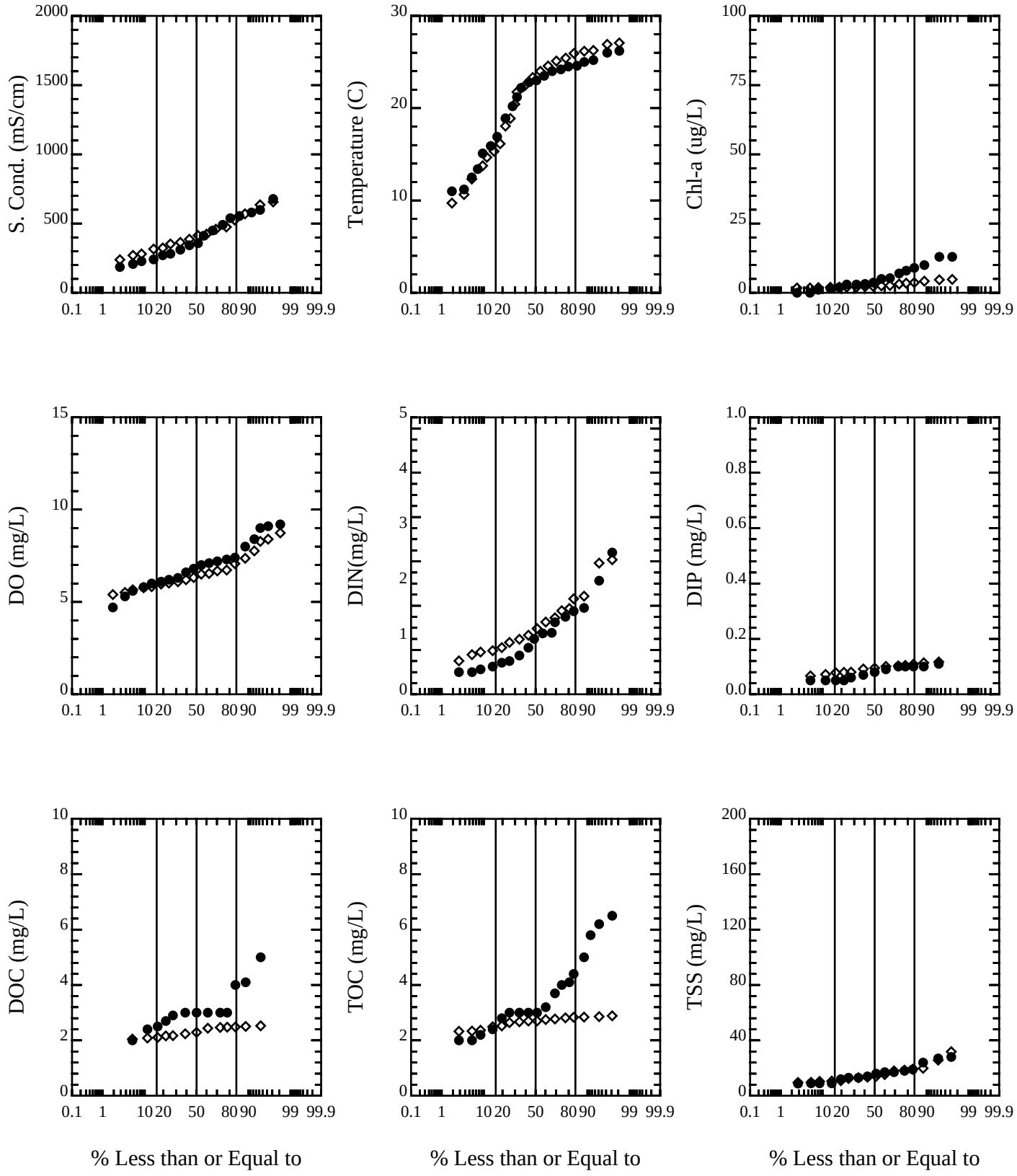

Figure C41. San Joaquin River, Model & Data Comparisons: SJR at R8